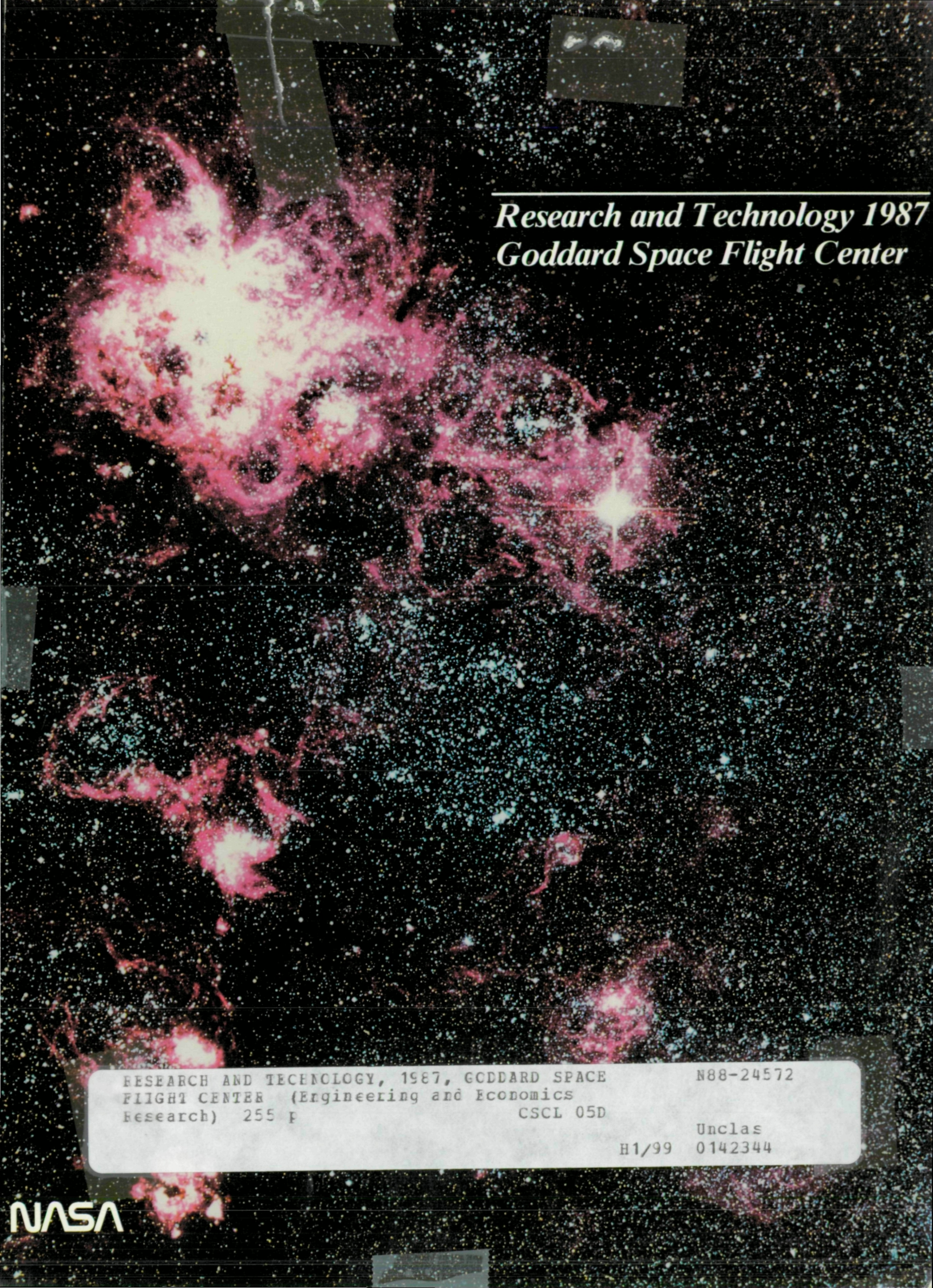

Research and Technology 1987
Goddard Space Flight Center

RESEARCH AND TECHNOLOGY, 1987, GODDARD SPACE FLIGHT CENTER (Engineering and Economics Research) 255 p
N88-24572
CSCL 05D
Unclas
H1/99 0142344

NASA

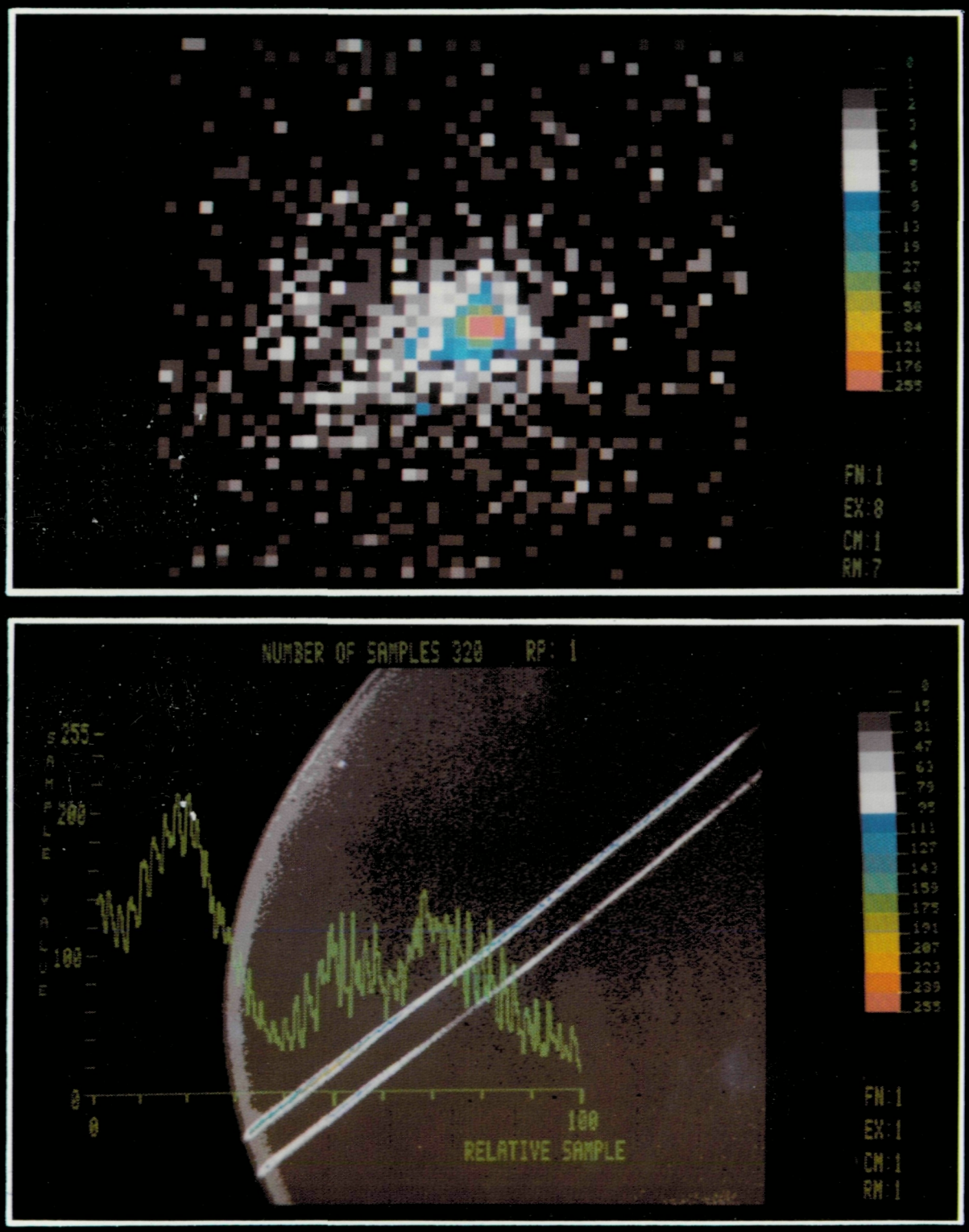

Cover photo: Supernova 1987a and the 30 Doradus Nebula. Photograph taken by European Southern Observatory. Top photo: Magnified FES image of SN 1986a. Bottom photo: Low-resolution ultraviolet spectra of SN 1987a taken with the IUE. Two consecutive exposures were made on the same image to save time.

ORIGINAL CONTAINS
COLOR ILLUSTRATIONS

Research and Technology

1987 Annual Report of the Goddard Space Flight Center

Foreword

The year 1987 will undoubtedly be remembered by scientists as the year of the large supernova. A century from now there will be only a sketchy memory of other present day events such as the discovery of high-temperature superconductivity, the various global military actions, or the social concerns that face our contemporary society. But 1987 is marked by this infrequent colossal cosmic event, and I feel fortunate to have joined Goddard during the time when it has focused some of its energy toward understanding the physics of an exploding star.

It is fitting to use the *1987 Annual Research and Technology Report* to highlight our efforts. Supernova 1987a has presented astronomers with the opportunity to observe the events of the disintegration of a nearby star in the Magellanic Cloud. The photo on the cover was taken at an observatory in Australia where the viewing was optimal.

Goddard's IUE satellite was ideally timed to make observations from space in the ultraviolet part of the electromagnetic spectrum. All of us were delighted to see this Center host the numerous meetings and planning sessions for debating the scientific issues and developing the strategy for measuring and observing. While no one anticipated a supernova, we were ready when the opportunity came. To me, this is the spirit of great research. NASA has a fine reputation for developing both big and little projects, organizing them, and carrying them out, but we infrequently credit the high caliber of our action-oriented scientists and engineers who can be depended upon for an intelligent, rapid response to natural phenomena.

In this same sense, our activities in the Antarctic in measuring the ozone hole is another fine example. With the experience of the Nimbus missions and the upcoming UARS mission, it was natural for GSFC to be involved in this worldwide event.

The middle part of my government career was spent at Goddard. In those early days of the sixties, we were pioneering every realm of space. On my return to NASA, I see dramatic change. We have opened more doors than we can possibly look into. We must now chart a course with wisdom and vision that matches our talents and resources with the technical questions and challenges of our times.

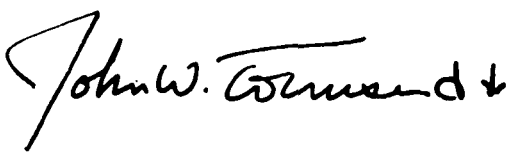

John W. Townsend, Jr.
Director

Contents

	Page
SPACE AND EARTH SCIENCES	1
Supernova	1
Stars and Sun	10
High Energy Astrophysics	24
Planetary and Interplanetary	36
Atmospheres	55
Climatology and General Terrestrial	59
Ocean	99
Terrestrial	110
Biology	118
TECHNOLOGY	127
Sensors and Space Technology	127
Techniques	150
User Space Data Systems	153
Space Communication Systems	168
System and Software Engineering	192
FLIGHT PROJECTS AND MISSION DEFINITION STUDIES	219
Flight Projects	219
Hubble Space Telescope	220
Space Station	234
INSTITUTIONAL TECHNOLOGY	239
Institutional Technology	239
INDEX	245

Space and Earth Sciences

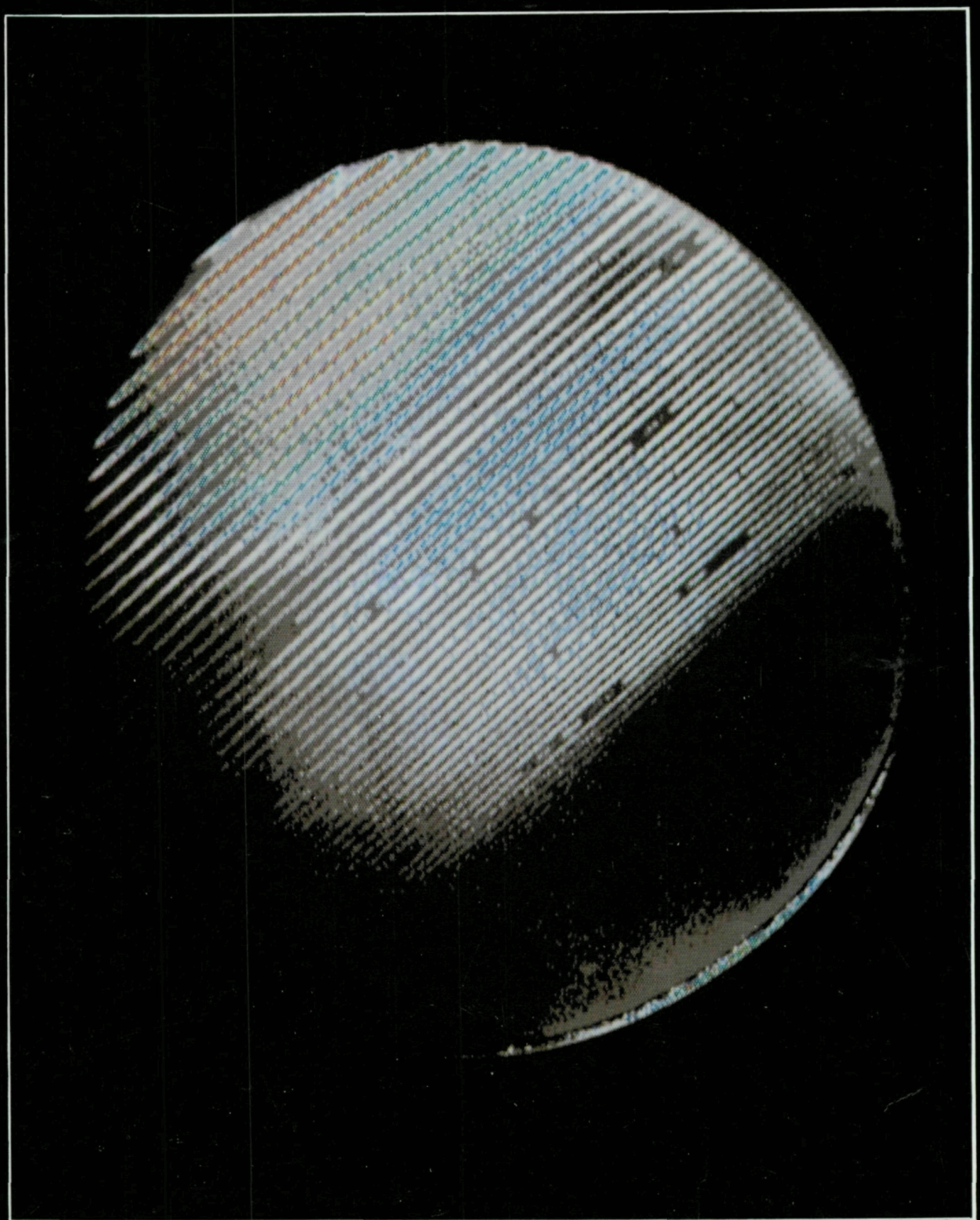

Supernovae—cosmological beacons that flare a million-fold brighter than the progenitor star as the star destroys itself.

SUPERNOVA

Chinese court astrologers patiently cataloged the appearance and disappearance of guest stars and what their visitation in the heavens portended to the rulers. As the study of the celestial sphere gradually evolved, astronomers came to understand what these guest stars were. Some proved to be comets, like Comet Halley that recently made its once-every-76-year passage close to the Sun. Other guest stars were nearby novae, thought to be dense, accreting members of binary systems that flare a thousand-fold in brightness due to surface nuclear explosions. The remaining guest stars were most likely supernovae, true cosmological beacons that flare a million-fold brighter than the progenitor star as the star destroys itself. Today astronomers have found, at the positions of some well-documented guest stars, rapidly expanding shells, like the Crab Nebula, which is linked to the Chinese guest star of 1054 A.D.

SN 1987a occurred in our nearest galaxy, the Large Magellanic Cloud, which is 160,000 light years distant. It is so close that SN 1987a was visible to the unaided human eye. The last supernova with such visibility occurred in 1604. Johannes Kepler used the best astronomical instruments then available to obtain rough positions and visual estimates of brightness. Major advances in instrumentation have allowed astronomers access to virtually all parts of the electromagnetic spectrum. For example, the International Ultraviolet Explorer (IUE), has been utilized to study numerous supernovae. Within a few years, the Hubble Space Telescope will provide astronomers with opportunities to observe fainter, more distant supernovae.

The first supernova that was recognized as such, s Andromeda, occurred about a century ago in M31, the Andromeda Galaxy, a nearby spiral galaxy. Since then, hundreds of supernovae have been found in more distant galaxies, but they were so faint that only limited observations were possible. SN 1987a was detected very soon after occurrence, and even some information is known about the progenitor star. Astronomers are using every tool available to gain data to understand the nature of SN 1987a.

At least two types of supernovae are known to occur by virtue of similarities in the visible wavelength spectra. One group, Type Ia, is thought to be due to white dwarf progenitor stars that accrete much material in a close binary system. The other group (Type Ib and Type II) is thought to be from hot, massive stars that burn their hydrogen fuel very rapidly, lasting only for millions of years. When the core of hydrogen is exhausted, the massive star collapses. The first group of supernovae occurs in all galaxies. The second group occurs in galaxies that show evidence of recent star formation, namely spiral galaxies and irregular galaxies.

SN 1987a occurred in an irregular galaxy at the position of a previously surveyed young massive star, Sanduleak -69 202. Careful astrometric studies by astronomers using IUE show that Sanduleak -69 202 is no longer detected in the ultraviolet. This result supports supernova models that predict that the progenitor star was about 15 to 30 times the mass of our Sun.

However, SN 1987a is peculiar in some important ways. Astronomers know that Type I supernovae have characteristic light curves and well-defined maximum absolute luminosities. Each Type II supernova demonstrates a

◀ *High-resolution ultraviolet spectra of SN 1987a taken with the IUE.*

different maximum absolute luminosity and an individual light curve. SN 1987a, which is classifiable as a Type II, is no exception. Its maximum visible brightness was about 30 times fainter than most Type II's; at radio wavelengths, its emission was very faint, and it faded within days. The ultraviolet spectrum dropped by a thousandfold within a few days.

Astronomers are learning rapidly that the Type II supernova's maximum brightness and light curve are characterized by the history of the outer envelope: how much material flowed outward in a massive stellar wind and how much remained. Theorists are modeling how the progenitor star may have evolved and are using the SN 1987a observations to check the models.

SN 1987a has a mysterious nearby companion. Speckle interferometry detected a second, bright component separated by several thousand times the distance from the Earth to the Sun. Observations in the infrared from the ground and Kuiper Airborne Observatory may tell us whether this was due to the stellar wind.

SN 1987a was noted by naked-eye observation within hours of the actual event. Two separate neutrino monitors recorded a burst of neutrinos at what is now thought to be the time of stellar collapse. SN 1987a is thus the first astronomical object detected in neutrino astronomy.

SN 1987a offers astronomers a truly unique opportunity to follow changes in a supernova as it evolves through its initial stages and how the physical changes may influence the supernova remnant that will eventually form. Based upon models and our knowledge derived from supernova remnants like the Crab Nebula, most astronomers expect to find a spinning neutron star, or pulsar, within. Such a pulsar with its compressed magnetic fields and rapidly spinning behavior would act as a central powerhouse, lighting the supernova interior for centuries to come. By mid-September 1987, SN 1987a was gradually decreasing in brightness at visible wavelengths, yet ultraviolet emissions were slowly increasing, and X rays have been detected by the Ginga Satellite. The supernova is slowly becoming transparent, and sounding rocket and balloon payloads are being prepared to study the X-ray and far-ultraviolet portions of the spectrum. We can anticipate that astronomers will study SN 1987a and its surroundings with space- and ground-based instruments for decades to come.

Dr. Theodore Gull

SUPERNOVA 1987a

The supernova detected on February 24 in the Large Magellanic Cloud, which is our sister galaxy some 160,000 light years away, is the brightest supernova observed since Johannes Kepler's observation of a galactic supernova in 1604. The discovery was made by Ian Shelton, who was observing at the University of Toronto's Chilean station at the Las Campanas Observatory. Shelton's and other observations nearly pinpoint the exact time of the initial brightening.

From the preexplosion photographic image of the location of the supernova and the far-ultraviolet International Ultraviolet Explorer (IUE) spectra of the same position, George Sonneborn, Robert Kirshner, and Bruce Altner determined that the progenitor of the supernova was a B3 Ia star cataloged as Sanduleak -69 202. This is the first time in history that the precursor of a supernova has been identified, thus providing an opportunity to significantly enhance our understanding of the supernova phenomenon.

There are two basic types of supernovae, Type I and Type II. The classification is based on the spectrum produced by the supernova. If the hydrogen Balmer lines are absent, a supernova is considered a Type I; if the Balmer lines are present, it is classified as a Type II. However, this classification is largely morphological; it is probably more useful to classify supernovae by the physical processes involved.

A Type I supernova is thought to occur when a massive white dwarf star in a binary star system has a thermonuclear runaway in its interior and detonates itself. Since a massive white dwarf star contains little hydrogen, the spectrum does not exhibit hydrogen. According to the contemporary theory, such a runaway conflagration occurs when gaseous matter is transferred from a normal companion star to the white dwarf at a critical rate, destabilizing the white dwarf's delicate internal balance of density, pressure, and temperature.

A Type II supernova occurs when the highly evolved iron core of a massive supergiant star collapses. The converted potential energy of the implosion gives rise to a catastrophic explosion that violently blows away its extended atmosphere. The atmosphere contains a large quantity of hydrogen gas; hence, its spectrum is rich in Balmer lines.

The spectrum of Supernova 1987a observed with ground-based telescopes showed strong hydrogen Balmer lines from the beginning. Its emission and absorption characteristics are known to astronomers as P Cygni features, so named after the prototype star P Cygni that exhibits similar spectral features. The shortest wavelength edge of absorption showed that the ejected gas was expanding at a velocity of at least 17,000 km/s. According to the conventional classification scheme, it appeared to be Type II. The immediate appearance of the Balmer emission lines also indicated that the hydrogen atmosphere surrounding the progenitor was probably not very extensive. The rapid change of the far-ultraviolet flux observed with the IUE, which declined about three orders of magnitude in just a few days, also agreed with the possibility that the progenitor's atmosphere was relatively small.

The visual light brightness of the supernova has been observed continuously, since its discovery, with the Fine Error Sensor (FES), also known as the startracker, of the IUE. It brightened from the initial visual magnitude of 4.5 on February 24 to the maximum brightness of 3.0 magnitude on about May 20. Its brightness since then has declined steadily. After about June 25, the rate of decline has become asymptotic, which looks linear in a magnitude versus time plot (see figure). An asymptotic decline is expected when the energy source for the supernova remnant becomes primarily radioactive decay of nickel-56 and cobalt-56.

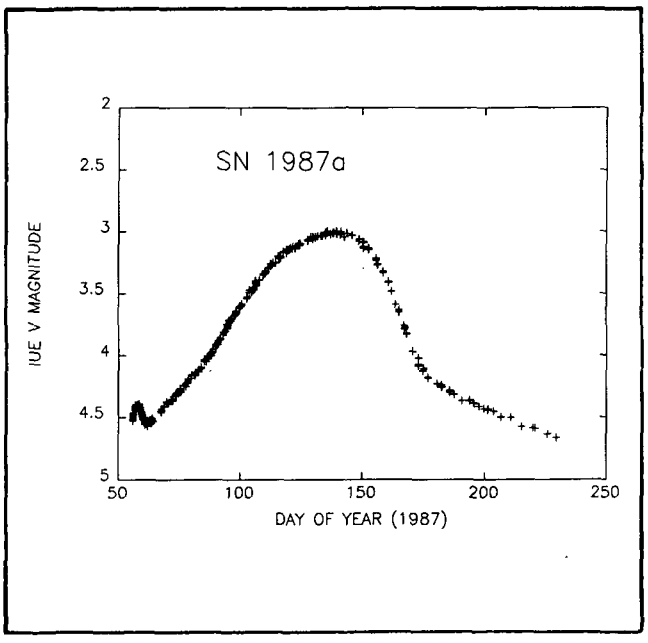

The visual light curve of SN 1987a observed with the FES of the IUE. Day 1 corresponds to January 1 Universal Time. The greater the magnitude, the fainter the object.

As of mid-August, the IUE ultraviolet spectrum of the supernova obtained by Kirshner and Sonneborn showed emission lines of circumstellar material, which was ejected, as a stellar wind, from the progenitor prior to the explosion. This gas is nitrogen-rich and very similar spectroscopically to material observed in the putative pre-supernova object *eta* Carinae.

Neutrino events were detected simultaneously on February 23, within the errors of observational timing, by the Kamiokande II experiment team in Japan and the Irvine-Michigan-Brookhaven experiment team in Ohio. These neutrino detections, which preceded the visual brightening, are believed to be associated with the immense neutrino outbursts resulting from the iron core collapse in the supergiant star; this provides even more evidence that the supernova was caused by a core collapse.

From the neutrino observations, several workers estimated the upper limit of the rest mass of the electron neutrino. The estimates ranged from about 5 to 25 eV. Chiu, Chan, and Kondo at GSFC calculated the rest mass (not an upper limit) to be about 3 eV at a 97 percent confidence level. The putative mass of the neutrino has an important bearing on the problem of missing mass in galaxies and may also hold the key to the question of whether the universe is open or closed.

The results obtained thus far have already substantially improved our understanding of the supernova phenomenon. However, many questions remain to be answered. For instance, astronomers are puzzling over the nature of the bright spot found near the supernova in speckle-interferometer observations. It is not yet clear whether the bright companion is caused by reflection or fluorescence by an interstellar cloud; an explanation invoking neither mechanism may become necessary. Another important question is whether a neutron star or a black hole was formed at the time of the core collapse. Future radio, and possibly X-ray, observations made after the clutter of the catastrophic explosion has cleared away may provide a clue as to the nature of the object left behind.

Contact: Yoji Kondo
Code 680

Sponsor: Office of Space Science and Applications

Dr. Yoji Kondo is Project Scientist for the International Ultraviolet Explorer, as well as an Adjunct Professor of astronomy and astrophysics at the University of Pennsylvania. He specializes in interacting binary stars, the local interstellar medium, active galactic nuclei, supernovae and white dwarfs. Dr. Kondo, who received his PhD degree from the University of Pennsylvania, has been with Goddard for 13 years.

WILL DUST BLACK OUT SN 1987a?

On February 23, 1987, a type II supernova, designated SN 1987a, was detected in the Large Magellanic Clouds. The prospects for the formation and detection of dust in the cooling matter explosively ejected in the supernova event have been studied. The formation of dust will have immediate implications on the spectral analysis of the expanding ejecta, as the dust may obscure the visual and ultraviolet (UV) output of any pulsar that may have formed in the explosion (Gehrz and Ney, 1987).

Grains may form in the expanding ejecta as soon as they can survive the heating by the ambient radiation field, which may be as early as 3 to 8 months after the explosion. In practice, dust formation may be delayed. Typical densities of condensable elements at the time when dust is likely to form are between 10^{-18} and 10^{-17} g cm^{-3}. These values are comparable to those found in some novae or Wolf-Rayet stars, where dust formation has been observed to take place. However, for reasons that are still not well understood, some objects do not form dust even if it is thermodynamically feasible. Such a dust suppression mechanism may prevent the formation of dust in SN 1987a, as well. If dust forms, then a mass of 0.01 $M_\odot$ of dust in the envelope will obstruct the UV-visual luminosity of the pulsar for $\approx 3-20$ years, depending on dust composition. The supernova will be brightest in the infrared between the onset of dust formation and the time of maximum gamma-ray transparency (approximately day 600). If the dust shell is optically thick, the infrared luminosity will be larger than $\sim 10^{39}$ erg s^{-1}. Thereafter, all the infrared luminosity will be provided by the UV-visual output of the pulsar. If the pulsar has an initial luminosity and energy distribution like that of the Crab, then typical infrared luminosities will be $\sim 5 \times 10^{38}$ erg s^{-1}.

The formation of dust in the inner metal-rich layers of the ejecta may be suppressed for a few years by the presence of radioactively decaying matter. The mantle may, however, become Rayleigh-Taylor unstable and form high-density clumps in which dust may form as early as 1 year after the explosion. Since the clumps do not fill the entire volume of the ejecta, only a fraction of the visual, UV, and soft X-ray output of the pulsar will be reprocessed to infrared wavelengths. In this scenario, the formation and detection of dust in the mantle are closely linked to the early breakout of the UV and soft X-rays.

Theoretical models suggest that an ~ 25-$M_\odot$ progenitor can produce $\sim 1\ M_\odot$ of supernova condensates. Supernovae will then constitute a major source of dust, equaling the combined output of all other sources. The detection of this dust in SN 1987a will be a significant addition to the incomplete picture we now have of the presence of isotopic anomalies in the solar system and of the origin and evolution of dust in the interstellar medium.

Contact: Eli Dwek
Code 685

Sponsor: Office of Space Science and Applications

Dr. Eli Dwek received a PhD degree in astrophysics from Rice University. Dr. Dwek serves on the COBE project and is a member of NASA's Supernova 1987a Science Working Group. He has four years of experience with Goddard.

DETERMINATION OF NEUTRINO MASS AND PROPOSED METHOD TO DETERMINE COSMOLOGICAL DISTANCE

Evidence for a finite rest mass of the neutrino has been reported. A new method to determine the cosmological distance scales without using telescopes has been proposed based on a detailed analysis of Supernova 1987a neutrino data and recent progress in the experiment of ^{3}H (tritium) decay. By use of a new mathematical technique especially designed to analyze very small data sets, we showed that out of the 12 neutrinos detected in the Kamiokande II experiment in Japan, five were emitted within a very short period of time (around 0.2 seconds). By analyzing the dynamics and the time of arrival of this group of five neutrinos, we concluded that after the long travel from the Large Magellanic Cloud to the Earth (160,000 light years), the five neutrinos became separated. These neutrinos arrived at the Kamiokande II detectors according to a pattern that can be interpreted as due to a finite mass of the neutrino. From the differences in time of arrival (the so-called time dispersion), we concluded that the mass of the neutrino is 3.6 eV, around 1/150,000

of the mass of the electron, thus making the neutrino the least massive particle ever estimated from observed data.

The same method of data analysis can also be applied to the results of American neutrino detections, which are a joint effort of the University of California at Irvine, the University of Michigan, and the Brookhaven National Laboratory (also known as IMB). The results of the American experiment are consistent with those of the Kamiokande II data.

The time dispersion of the neutrinos can be likened to the race of an athletic track team. Suppose the weights of all athletes are the same (but not known). Further, each athlete's ability to run is related to his energy and the unknown weight via some precise law. At some moment, these athletes start to run from the same starting line toward some destination. The one with the highest energy will arrive at the destination first, and the one with the least energy will arrive last, with the rest in between. By relating the time of arrival to the energy of each athlete, the weight of the athletes can then be determined by comparing the differences in their times of arrival with the theoretically calculated differences of the times of arrival via the precise law. In a similar way the weight of the neutrino was determined.

For the method to work, there must be a sufficient number of neutrinos that were almost simultaneously emitted. The chief challenge in the analysis is in the smallness of both data sets. Sophisticated probability theory and extensive computer simulation were needed to show that the chance of five neutrinos arranging their times of arrival and energies in such a pattern to give rise to the interpretation proposed is less than two to three percent.

In addition, these results may soon be tested in laboratories. Terrestrial experiments to study the rest mass of the neutrino have been under way for some time. One American research group at Los Alamos, headed by J. F. Wilkerson, reported in May that they were close to pinning down the mass of the neutrino at the 10-eV level. Within the next decade the mass of the neutrino will probably be determined accurately in terrestrial experiments such as the one carried out by Wilkerson's group. If the conclusion of a nonzero rest mass for the neutrino is confirmed, then the terrestrial measurements of the neutrino mass may be used to recompute the distance to the Large Magellanic Cloud. The method proposed is different from conventional methods of determining distances in astronomy, which heavily depend on the use of telescopes and theoretical modelings. This new method does not call for the use of telescopes and is an independent way to measure astronomical distances wherever supernova neutrinos are detected in sufficient quantities to warrant the use of their methods of analysis.

Currently, our knowledge of the distance to remote galaxies is tied to the distance of the Large Magellanic Cloud: the Cepheid variables in the Large Magellanic Cloud are the primary distance indicators for galaxies as far away as 10 million light years. However, the distance to the Large Magellanic Cloud is currently known only through a series of complicated reasonings and measurements. The proposed method of distance determination to the Large Magellanic Cloud is direct and can provide a second opinion on this very important subject. It was proposed that, in addition to the neutrino observations such as the IMB experiment, experiments to determine the rest mass of the neutrino be given a high priority, since these experiments will provide an answer to the most fundamental question concerning our universe: how big is it?

The determination of the mass for the neutrino is considered significant because for the first time a quantitative method has been applied to observation data to obtain definite evidence of a nonzero rest mass for the neutrino, with an uncertainty level of less than three percent. Further, an experimental test of this finding may soon be available that, if verified, will provide an independent method to determine the distance to the Large Magellanic Cloud. This distance is the fundamental yardstick to measure the size of our universe.

Contacts: Hong-Yee Chiu, Yoji Kondo, and
Kwing L. Chan
Code 610

Sponsor: Office of Space Science and Applications

Dr. Hong-Yee Chiu, who has been with Goddard for 24 years, is involved with studies of solar radiation. His scientific specialties include neutrino astrophysics, stellar evolution, and supernovae. Dr. Chiu received a PhD degree from Cornell University, and he is a recipient of the Exceptional Scientific Achievement Award.

Dr. Yoji Kondo is Project Scientist for the International Ultraviolet Explorer, as well as an Adjunct Professor of astronomy and astrophysics at the University of Pennsylvania. He specializes in supernovae, interacting binary stars, the local interstellar medium, active galactic nuclei, and white dwarfs. Dr. Kondo, who received his PhD degree from the University of Pennsylvania, has been with Goddard for 14 years.

Dr. Kwing Chan, a computational astrophysicist with Applied Research Corporation, is involved with solar radiation and convection research. Dr. Chan, who received a PhD degree in physics from Princeton University, has almost eight years at Goddard.

PARTICLE ACCELERATION AND PRODUCTION OF ENERGETIC PHOTONS IN SN 1987a

Since its appearance in late February, SN 1987a in the Large Magellanic Cloud has created a great deal of excitement in the astronomical community. As the nearest supernova to be observed in the last few hundred years, it creates a unique opportunity to test theories of stellar evolution and core collapse, nucleosynthesis, and particle acceleration in young supernovae. The burst of MeV neutrinos observed a few hours before the appearance of the exploding star in optical light was expected on the basis of theory, and the general characteristics were in remarkable agreement with existing models for neutrino emission from a collapsing stellar core.

If a new pulsar was born in the collapse, its rapid spindown could release enough power to accelerate particles inside the remnant. High-energy electrons and protons would interact with the matter and magnetic fields in the expanding envelope to produce high-energy gamma rays and X rays. Detectors on satellites, balloons, and in ground-based arrays in the Southern Hemisphere have been monitoring the object since early spring. It is expected that the envelope of the collapsed star that was blown off in the explosion will absorb or scatter any radiation produced deep inside the remnant for at least several months after the collapse, until the expansion decreases the density enough to allow high-energy radiation to escape. The GINGA satellite recently reported the detection of 10–20-keV X rays, probably due at this time to scattered nuclear gamma-ray line emission. This earlier-than-expected appearance of the low-energy X rays indicates that the shell will soon become transparent to higher energy emission, whose detection could provide a first look at a newly born pulsar and the way in which it interacts with the surrounding remnant to accelerate particles.

Recently, A. K. Harding of Goddard's High Energy Astrophysics Theory Group and T. K. Gaisser and T. Stanev of the Bartol Research Institute (University of Delaware) have predicted the fluxes of X rays and gamma rays that would be expected if a young, rapidly spinning pulsar is responsible for accelerating particles deep inside SN 1987a. These predictions are based on a model for acceleration of particles in the shock that is produced when the relativistic wind carrying the spindown power of a pulsar interacts with the surrounding nebula. This model is able to account for the electron synchrotron radiation from the 1000-year-old Crab nebula as being powered by the 33-ms pulsar located near its center. When applied to SN 1987a, which may have a more powerful pulsar with a period as short as 1 ms, the model predicts that protons will be shock-accelerated up to energies of 10^{17} eV and electrons to energies of around 1 TeV. Interaction of these particles in the shell then leads to observable gamma rays for pulsar periods less than 10 ms, at energies from 100 MeV up to at least 1 TeV (the energies detectable by existing ground-based arrays in the Southern Hemisphere) from the protons and 1–10 MeV radiation from TeV electrons. Detection of unpulsed gamma rays at very high energies would therefore be the first direct evidence that protons are being accelerated in young supernova remnants.

Contact: Alice K. Harding
Code 665

Sponsor: Office of Space Science and Applications

Dr. Alice Harding is an astronomer who specializes in theoretical high-energy astrophysics. Her professional interests include pulsars, gamma-ray bursts, processes in strong magnetic fields, and UHE gamma-ray and neutrino sources. Dr. Harding holds a PhD degree from the University of Massachusetts, and she has been with Goddard for eight years. She is a recipient of a fellowship from the American Association of University Women.

GAMMA RAYS FROM SUPERNOVA 1987a

Supernova 1987a was discovered in the southern skies on February 23, 1987, causing great excitement for astrophysicists the world over. It is located in the Large Magellanic Cloud, our nearest neighbor galaxy, making it the closest observed supernova since Kepler's in 1604. It thus provides the first opportunity to study the explosion of a nearby star with modern astronomical instrumentation. Observations are being made in many wavelength bands by telescopes throughout the Southern Hemisphere and by detectors on NASA, Soviet, and Japanese satellites. Here we primarily discuss gamma-ray observations of the supernova.

All indications are that Supernova 1987a is a Type II supernova, which is caused by the core collapse of an evolved massive star. In a time scale of seconds, the core

contracted to densities higher than those of nuclear matter and rebounded, expelling the overlying envelope of the star. During the initial explosion, temperatures exceeded 10^9 °K in the inner regions, allowing the creation of new elements via explosive nucleosynthesis. This process, which is thought to produce most of the elements heavier than iron in the universe, has been studied extensively theoretically but never observationally. Supernova 1987a may give us the first opportunity to observe gamma rays emitted in the decay of radioactive nuclei produced by explosive nucleosynthesis and thereby directly test theoretical predictions.

The best prospects for gamma-ray detection are the gamma-ray lines from nuclear deexcitation in the $^{56}Ni \rightarrow {}^{56}Co \rightarrow {}^{56}Fe$ decay chain. The ^{56}Ni is thought to be produced in the inner layers of the envelope, which will attenuate the gamma rays to unobservable levels for approximately 1 year. The ^{56}Ni half-life is only 6 days, so the gamma rays from its decay will not escape at all. The ^{56}Co half-life, on the other hand, is 79 days, so the gamma-ray escape time is within the first few half-lives. There are several gamma-ray lines from this decay, the most prominent being at 0.847 MeV.

The Low Energy Gamma Ray Group in Goddard's Laboratory for High Energy Astrophysics is involved in several aspects of the quest for gamma-ray line observations from Supernova 1987a. We have participated in the balloon flight of a gamma-ray spectrometer from Alice Springs, Australia, in June 1987 and are planning to fly a more sensitive new-generation instrument in spring 1988. In addition, we have published model calculations of the expected gamma-ray emission to facilitate observation planning.

One of the results of the calculations is shown in the figure. The expected flux in the 0.847-MeV line is plotted as a function of time for two cases that we believe bracket the theoretical models. The upper curve is for a star that began life as a 25 $M_\odot$ main sequence star and then lost much of its envelope via a stellar wind, leaving a 10 $M_\odot$ evolved core and mantle. The lower curve is for a 15 $M_\odot$ star with envelope intact. Both cases assume that 0.1 $M_\odot$ of ^{56}Ni was produced, which is close to the amount (0.07 $M_\odot$) that has been recently estimated for Supernova 1987a based on the observed exponential decay phase of the optical light curve (Woosley, S. E., 1987). This same reference finds that the expected gamma-ray line flux is likely to be closer to the lower curve in the figure than the upper curve. Also shown by dashed lines in the figure are the sensitivities for the Phoenix and Gamma Ray Imaging Spectrometer (GRIS) instruments discussed below. It is seen that if the gamma-ray flux is indeed near the lower curve, only the new-generation GRIS instrument will be able to detect it. The arrows in the figure indicate the times of the NASA gamma-ray balloon campaigns. Another result of our calculations is the prediction that X-ray and gamma-ray continuum emission produced by Compton scattering of line photons should precede the gamma-ray line emission by several months. The recent detection of X-ray (Makino, F., 1987) and gamma-ray (Sunyaev, R., 1987) continuum from the supernova indicates that gamma-ray line emission may soon follow.

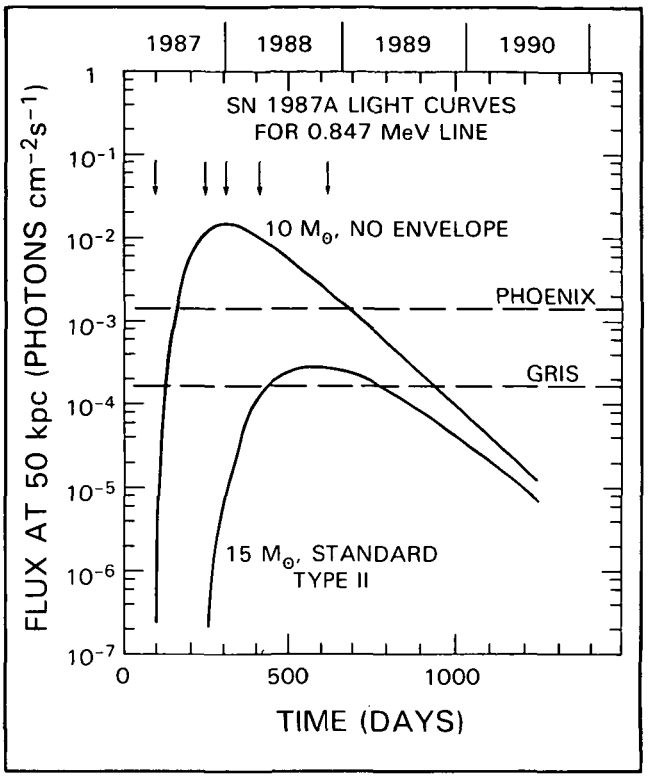

Gamma-ray light curves for ^{56}Co 0.847-MeV line for optimistic and pessimistic models. Dashed lines are the Phoenix and GRIS 3σ sensitivity limits. The arrows are times of NASA gamma-ray balloon campaigns.

NASA's first gamma-ray balloon campaign to observe Supernova 1987a was successfully undertaken in June 1987. We participated by collaborating in the flight of the Phoenix spectrometer, which was developed by colleagues at Bell Laboratories and Sandia National Laboratories Albuquerque. Four gamma-ray instruments were flown during the campaign, and measurements of the supernova were obtained. No gamma-ray emission was observed with limits of $\sim 10^{-3}$ photons/cm^2 – s

placed on the 0.847-MeV line flux. The result was not unexpected, as can be seen by comparing with the figure.

There will be NASA campaigns in fall 1987 and January 1988 in which our group will not participate. Our next flight will be in spring 1988 with the maiden launch of GRIS. This instrument is in the final stages of assembly and is a collaboration with the same colleagues mentioned above. It uses high-resolution germanium detectors and incorporates several new techniques for background reduction. We will be flying a major fraction of the world's largest n-type germanium detectors and will have the most sensitive high-resolution spectrometer observing the supernova. The sensitivity level indicated in the figure should be adequate to detect and study gamma-ray lines for even the lowest-flux models.

Contacts: Neil Gehrels and Bonnard Teegarden
Code 661

Sponsor: Office of Space Science and Applications

Dr. Neil Gehrels is the Project Scientist for Space Station Small Attached Payloads and is an Investigator on the GRIS, Galileo Heavy Ion Counter, and WIND TGRS projects. Dr. Gehrels has six years of experience at Goddard, and he holds a PhD degree in physics from the California Institute of Technology.

Dr. Bonnard Teegarden is Project Scientist for NASA's Supernova 1987a observation program and is an Investigator on the GRIS, RMT, and WIND TGRS projects. Dr. Teegarden, who holds a PhD degree from the University of Maryland, specializes in gamma-ray astronomy. He has been with Goddard for 23 years.

NEAR-INFRARED SPECTROSCOPY OF SN 1987a USING NASA'S KUIPER AIRBORNE OBSERVATORY

An infrared spectrum (1.5-3.0 μm) of the Supernova 1987a was obtained on UT 16.3 April 1987 with the University of Arizona's Fourier transform spectrometer on the NASA Kuiper Airborne Observatory, while based in Christchurch, New Zealand, for observations of Comet Wilson. The scientific team included H. P. Larson (University of Arizona), S. Drapatz (Max Planck Institute), M. J. Mumma (Goddard Space Flight Center), and H. A. Weaver (Space Telescope Science Institute). The dominant spectral features were a double-peaked emission line of atomic hydrogen and a sharp absorption edge in the continuum near 2.7 μm, both of which would have been obscured by strong telluric H_2O absorptions at ground-based observatories. These infrared features relate to models of the supernova shell and to the role of dust in supernovae.

The airborne infrared spectrum presented in the figure at medium resolution (15 cm^{-1}, or $\lambda/\Delta\lambda \approx 300$) reveals most clearly the fully resolved spectral features of the supernova. The signal-to-noise ratio (SNR) in the observed spectrum is very high (up to 4×10^2) across the K photometric band, but it decreases to less than 10 toward the short wavelength limit of the H photometric band because of reduced instrumental transmission. Our preliminary flux calibration indicated that the K magnitude of the supernova was $m_K = 0.85$, in reasonable agreement with ground-based measurements at the time of our observations.

Our airborne observations of SN 1987a included spectral regions that are highly obscured or completely inaccessible at ground-based observatories. As demonstrated in the figure, the dominant near-infrared spectral features of SN 1987a occur just in these obscured regions, including several atomic hydrogen lines (Brβ at 2.6 μm, Paα at 1.9 μm) and a continuum depression near 3 μm with a sharp absorption edge at 2.7 μm. In addition, the spectrum also exhibits many weak emission lines, some due to HI ($n > 7$ in the Brackett series). All line centers are shifted from their rest frequencies by approximately 300 km s^{-1}, the relative velocity of the Large Magellanic Cloud (LMC), where the supernova occurs.

The Paα ($n = 4 \rightarrow 3$) line connects the upper states of two important optical transitions: Hα ($n = 3 \rightarrow 2$) and Hβ ($n = 4 \rightarrow 2$). Observations of at least these three lines are

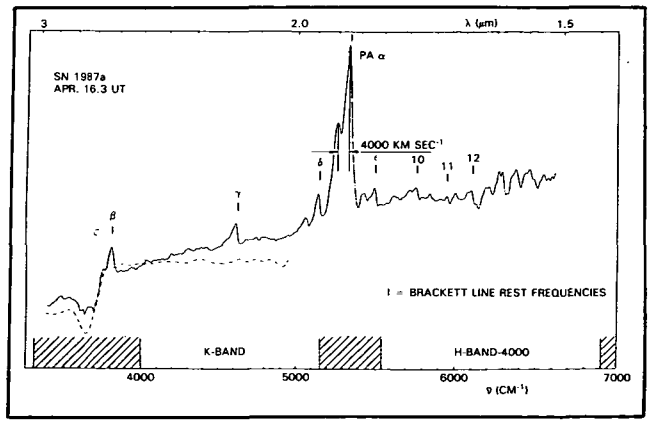

Near-infrared spectrum of SN 1987a obtained with the Kuiper Airborne Observatory.

therefore crucial for investigating different mechanisms (e.g., electron collisions and turbulence) that affect the shapes and intensities of hydrogen lines in supernovae. Our high resolution airborne observation of Paα in SN 1987a is apparently a unique measurement. We anticipate that its analysis will establish important constraints to supernova models based on hydrodynamic and non-equilibrium transfer calculations.

The observed Paα line profile in the figure is a blend of two components. The stronger component is Paα at its approximate rest frequency with respect to the LMC. The second component is redshifted by 4000 km s^{-1}. We cannot convincingly assign this companion to another species (e.g., helium). Rather, we suggest that the redshifted component is also Paα. The strong Brackett lines in our spectrum also indicate a double structure, although the relative intensities of the two components may be different than in Pα. In addition, optical observations of Hα lines at the time of our observations reveal line shapes similar to that in Paα, but the splitting is less pronounced. In general, such line profiles can be explained by geometric asymmetry, e.g., shells, clumps, and jets, or by asymmetries in other physical parameters. We are undertaking simultaneous modeling of Paα and Hα line profiles in SN 1987a to explore these possibilities. As an alternative explanation, we are examining the possibility that these lines represent light reflected from the nearby companion object.

The strong absorption feature found near 3 μm exhibits a sharp absorption edge at 2.7 μm and a depressed continuum that could extend beyond the long wavelength cutoff of our spectrometer at 3.0 μm. This structure was not anticipated, and we are exploring at least two possible interpretations: 1) an absorption band in material along the line-of-sight to SN 1987a; and 2) a photoionization threshold in the supernova atmosphere.

If the edge at 2.7 μm is a photoionization threshold, it cannot be due to hydrogen because the position is wrong. Moreover, no other prominent HI ionization edges are evident either in our spectrum or in observations at other wavelengths. The observed edge may be due to another species, and two other weak edges may be present near 2.2 μm and 1.5 μm, suggesting ionized helium.

As an alternative speculation, we are considering absorption in foreground material. The broad unresolved character of the feature implies that the substance is in the solid phase, and the position of the band suggests that H_2O or OH groups in minerals may be responsible. We therefore compared the spectrum of SN 1987a with laboratory spectra of two types of solids: H_2O frost and hydrated silicates. These materials are present in such diverse extraterrestrial environments as comets, meteorites, asteroid surfaces, and cold molecular clouds. The spectrum of H_2O frost does not match the supernova feature; however, certain samples of hydrated silicates provide very close matches to the spectrum of SN 1987a. One example, the reflection spectrum of montmorillonite, is included in the figure (dashed line). The general shape of its 2.7-μm band is due to bound H_2O, whereas the sharper edge at 2.7 μm is diagnostic of structural OH. Terrestrial assemblages other than montmorillonite could provide similar matches. Thus, the agreement in the figure may indicate the presence of clay-type minerals, such as are found in carbonaceous chondrite meteorites, but the identification of specific minerals may not be unique. Current thoughts for the origin of this feature include circumstellar dust associated with the progenitor of SN 1987a, dust produced by the supernova event itself, and interstellar dust. Detailed investigations of these possibilities are now in progress.

Contact: Michael J. Mumma
Code 693

Sponsor: Office of Space Science and Applications

Dr. Michael Mumma is the Head of the Planetary Systems Branch at Goddard. He has 17 years of experience at NASA and holds a PhD degree from the University of Pittsburgh. Dr. Mumma discovered and characterized natural laser emission on Mars and Venus, originated the theory of solar infrared fluorescence in comets, and detected water vapor in Comet Halley. In addition, he was the first to provide definitive definition and characterization of water in comets. Dr. Mumma also made definitive measurements of molecular dissociation excitation cross sections.

NUMERICAL MODELING OF THE CLASSICAL NOVA OUTBURST

Modeling the nova outburst with GSFC's IBM 3081 computer has been accomplished with accepted observational data. A 1-$M_\odot$ white dwarf, consisting of ^{12}C and ^{16}O, is allowed to accrete hydrogen-rich matter from a nearby companion star at a rate of 10^{-9} $M_\odot$/yr. The accreting matter arrives on the white dwarf with nearly Keplerian angular momentum, striking the star's surface horizontally at speeds of roughly 4000 km/s.

The resulting shear mixes the hydrogen-rich matter into the white dwarf, producing an accretion belt of mixed stellar and accreted matter. After approximately 10,000 years, the surface of the accretion belt rotates at nearly Keplerian velocity, and shear mixing between star and accreting matter ceases. Accretion continues for approximately another 240,000 years, when the nuclear reactions run away at a depth from the star's surface of 3×10^{-4} $M_{\odot}$.

Such runaways are by themselves insufficiently strong to cause nova-like mass ejection, mainly because too little mechanical confinement (i.e., tamping) of the burning regions exists. The reason for this insufficient confinement is primarily due to the centrifugal forces that support the rotating matter.

However, by recognizing that the convective motions caused by the nuclear runaway are able to transport angular momentum from the star's outer regions inward to the zone of peak burning, it is possible to overcome the problem of insufficient confinement. The inward flow of angular momentum creates a strong shear instability between the peak burning zone and its adjacent inner layers. This leads to rapid mixing of the matter in this region with three important consequences:

- The outer layers of the star lose some of their angular momentum and, hence, some of their centrifugal support. This increases the mechanical confinement of the burning regions.
- The strong shear mixing moves the peak burning zone deeper into the star, where gravitational confinement is greater.
- The mixing enriches the burning regions with additional ^{12}C and ^{16}O nuclei, which act as catalysts for the nuclear reactions.

The result is an explosive nuclear runaway and a nova outburst. Roughly 10^{-4} $M_{\odot}$ are ejected at speeds of between a few hundred to roughly 2000 km/s, in complete agreement with the observations of classical novae.

Contact: G. Siegfried Kutter
Code 681

Sponsor: Office of Space Science and Applications

Dr. G. Siegfried Kutter, who holds a PhD degree in physics from the University of Rochester, is currently on leave from The Evergreen State College in Olympia, Washington, to serve with Goddard for two years as a National Research Council Associate. Dr. Kutter's scientific field is stellar evolution, and his interests include the origin and evolution of life. He is the author of The Universe and Life: Origins and Evolution, *an interdisciplinary text for liberal arts majors.*

STARS AND SUN

GIANT GAS CLOUD FEEDS A GROWING GALAXY

Scientists have detected a giant gas cloud 50,000 light years in diameter surrounding the central galaxy in a cluster of galaxies. Material from the cloud is being swept up by the galaxy's gravitational field and condensed to form stars. As a result, this galaxy, unlike its companions, continues to grow. This discovery was made, in collaboration with Dr. W. Romanishin of Arizona State University, with the 4-m telescope at Kitt Peak National Observatory.

The scientists analyzed CCD images of the giant elliptical galaxy 0335 + 096. Previous X-ray observations with the Einstein Observatory satellite had shown that the surrounding cluster is filled with X-ray-emitting gas at a temperature of 100 million degrees. The denser gas in the inner regions of the cluster is cooling quickly and should become visible at optical wavelengths as it falls into the gravitational well of 0335 + 096.

Optical data were obtained in an effort to detect the accreting gas. The photograph is a pseudocolor composite

ORIGINAL PAGE
COLOR PHOTOGRAPH

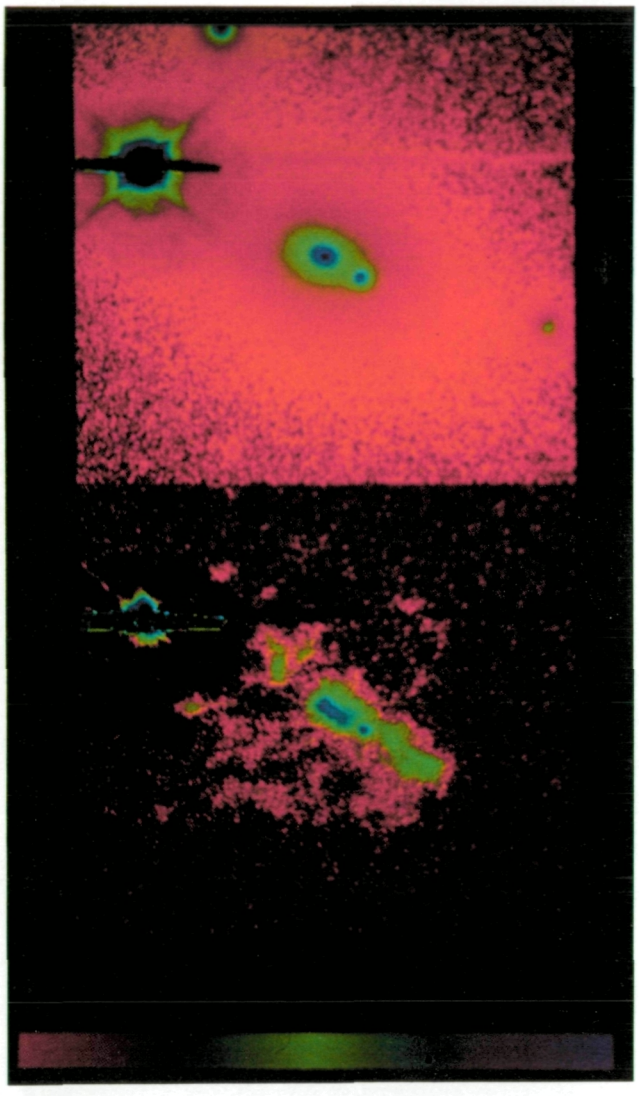

Galaxy 0335 + 096. Photos provided courtesy of the National Optical Astronomy Observatory.

containing two pictures: the color used indicates the brightness of the light in a given area. Black indicates no light, red indicates low light levels, green corresponds to intermediate illumination, and blue denotes the brightest areas in the field. The bright star in the corner of both photographs is a foreground star in our own galaxy and has nothing to do with 0335 + 096.

The top photograph, taken in red starlight, shows the smooth distribution of faint stars that forms the basic structure of the giant galaxy (this is the red area which almost fills the upper image). The green-and-blue ovals at the center are the double nucleus of the galaxy, a frequently seen phenomenon.

The lower photograph shows the same region of sky, but it was taken with a filter that excludes starlight, admitting only the light of atomic hydrogen gas. The resulting picture shows the irregular, filamentary distribution of the accreting gas that surrounds the galaxy. Each year enough gas collects to form 200 suns. As it flows into the galaxy's gravitational field, the cooling gas first collapses into thin filaments (shown in red), then collects in the enormous disk (the large green bar) that runs through the center of the galaxy. A portion of this gas is continuously forming new stars, and as a result the 0335 + 096 galaxy, unlike most other elliptical galaxies, continues to increase in size and luminosity.

Contact: Paul M. N. Hintzen
Code 681

Sponsor: Office of Space Science and Applications

Dr. Paul Hintzen is Liaison Scientist on the Faint Object Spectrograph for HST. Dr. Hintzen has a PhD degree in astronomy from the University of Arizona and has nine years of service with Goddard.

EVIDENCE FOR A RECURRENT NOVA IN THE SYMBIOTIC STAR SYSTEM R AQUARII

Stars evolve out of huge clouds of interstellar gas and dust, yielding roughly as many gravitationally bound double star systems as there are lone stars. Double star systems, if relatively close to Earth, can be studied in depth for the many interesting features they exhibit due to a multitude of physical processes. One of the most interesting classes of binary objects is the symbiotic star system, the closest of which is known as R Aquarii. These systems are typically comprised of a hot subdwarf companion star in orbit around a cool, voluminous, red giant star whose light output varies, in the case of R Aquarii, with a 387-day period. The surface temperature of the giant is ~2,500 °K, which is nearly half that measured at the Sun's surface, whereas the hot companion's temperature is ~25,000 °K. The companion star's presence is inferred spectroscopically from peculiar nebular line emission, but is hidden from direct view because it is dim relative to the giant star and may be occulted by a thick accretion disk. The orbital semi-major axis of the two stars is about the same as the distance from the Sun to midway between the orbits of Saturn and Uranus. However, at closest approach, some material from the cool

ORIGINAL PAGE
COLOR PHOTOGRAPH

star's atmosphere may flow toward the hot star, forming a surrounding accretion disk that can eject material parallel to the disk axis.

Indeed, at both optical and radio wavelengths, small-scale jet-like nebular features are seen extending ~6.5 arc seconds from the location of the red giant star. This supports the hypothesis that an accretion disk may be responsible for small-scale ejecta. International Ultraviolet Explorer (IUE) satellite observations of R Aquarii over the past 5 years have shown that the temperatures of the radio/optical jet-like features in the system fluctuate with an ~1.5-year period but are steadily increasing; this may portend a larger radiation outburst in the ultraviolet at some future date, so continued monitoring of the system with IUE is scheduled.

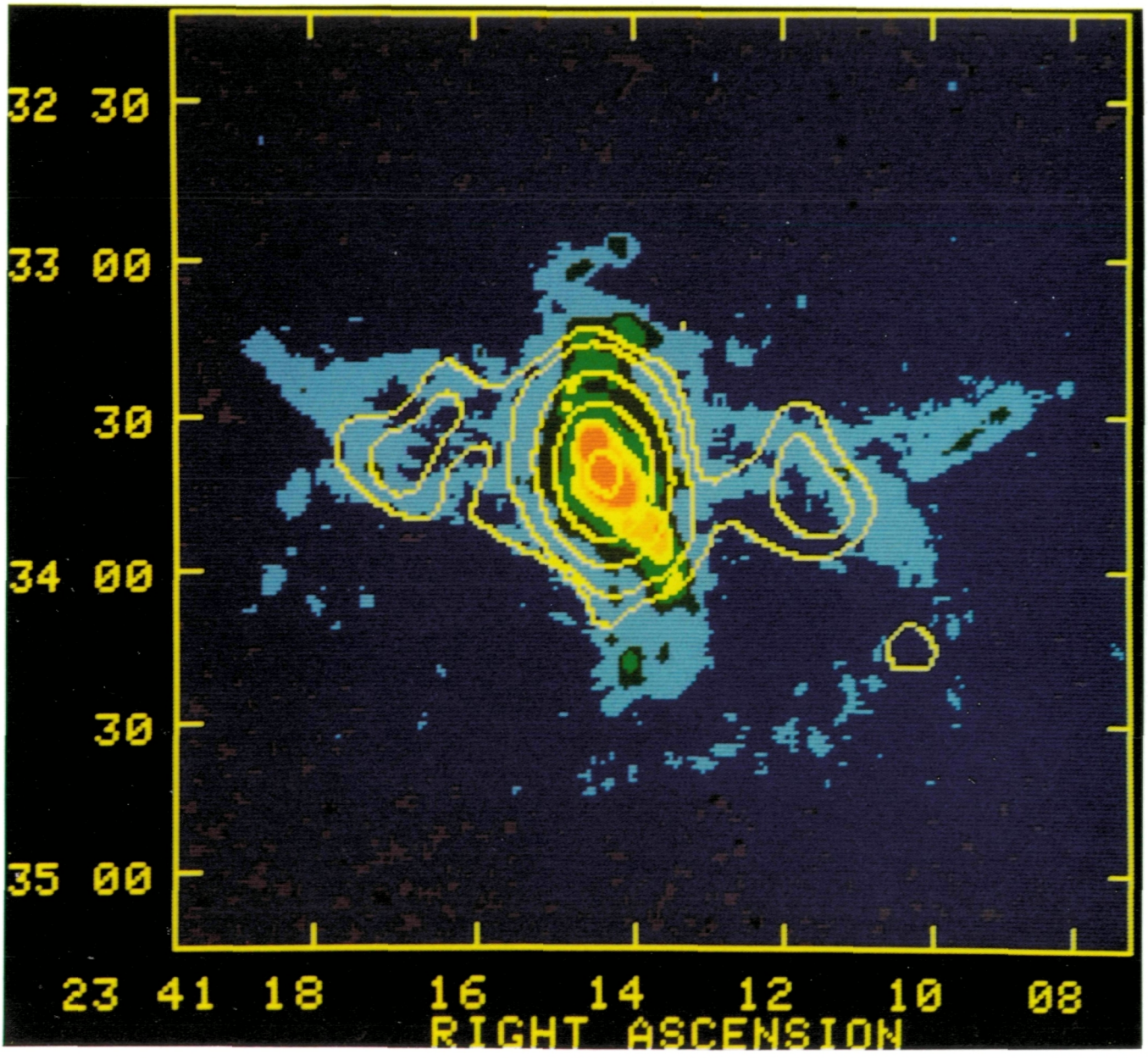

Large-scale radio and optical nebulae associated with R Aquarii. Contours display radio observations at 6-cm wavelength superimposed on an [O III] optical image at 5007 Å. The space between fiducial marks on the vertical axis is 30 arc seconds.

In addition, broad-band optical photographs of the R Aquarii complex have long been known to reveal a large symmetrical nebula whose origins are less certain than the aforementioned small-scale features attributed to the effects of an accretion disk ejection mechanism. Moreover, observations obtained with the Very Large Array radio telescope at Socorro, New Mexico, in April 1987 show a spectacular radio nebula centered on the R Aquarii red giant, extending ~120 arc seconds (1500 to 2500 times the orbital semi-major axis of the binary) in the east-west direction. This newly discovered radio nebula at the 6-cm wavelength is displayed as the yellow contour levels in the accompanying figure whose background is an optical atomic emission line spectrum of oxygen at 5007 Å, designated [O III].

The structure and extent of the [O III] nebula were reported by us in October 1986. There are obvious morphological similarities and differences between the optical and radio structures that can be explained by excitation effects and/or differences in formation mechanisms. Calculations indicate that the radio nebula possesses $\sim 4 \times 10^{42}$ ergs of kinetic energy typical of a recurrent nova outburst that, based on optical nebular expansion velocities, would have occurred about 600 to 1000 years ago. According to one recurrent nova theory, the mass that is transferred from the cool star to the hot companion just piles up and thus increases. Hence, the temperature increases until the hydrogen ignites like a nuclear bomb, blowing off the outer layer of accumulated matter. After the outburst, the hot star settles down, but the process eventually repeats since mass continues to flow from the extended, cool star to the hot companion. There may be some evidence for a previous eruption in the R Aquarii system.

Our observations also detected additional 6-cm radio sources in proximity to R Aquarii; most of them lie ~200 arc seconds away from R Aquarii and therefore are not shown in the figure. If this cluster of sources is associated with R Aquarii, it suggests a prehistoric eruption of the system's recurrent nova about 3300 to 5600 years ago. Since this is the first time a large-scale radio nebula and outlying discrete radio sources have been detected surrounding any symbiotic star system, similar observations will be conducted in the future to determine if R Aquarii is unique in this regard or is more of a prototype for other symbiotics that are suspected to contain recurrent novae.

Contact: Jan M. Hollis
Code 684

Sponsor: Office of Space Science and Applications

Dr. Jan M. Hollis, an astronomer with eight years of service with Goddard, is Head of the Science Operations Branch of the Laboratory for Astronomy and Solar Physics. Dr. Hollis, who received a PhD degree from the University of Virginia, is interested in the chemical and physical conditions within interstellar clouds and symbiotic star systems.

STELLAR ACTIVITY AND SMALL-SCALE STRUCTURES

Many stars, including the Sun, are observed to possess a hot corona of million-degree, X-ray-emitting gas. X-ray observations of the Sun have shown this coronal plasma not to be uniform, but to be confined within magnetic loops with heights of 10,000–100,000 km. This plasma cannot be heated by conduction from the stars' internal energy sources, since the photospheric gas below it is much cooler. It is now understood that the magnetic fields that confine the coronal plasma must also be involved in heating it. When these magnetic loops occur in active regions, containing sunspots (or starspots), they are sometimes observed to flare, rapidly heating gas to temperatures as high as 100 million degrees and accelerating particles to high, relativistic velocities. Both the hot coronal X-ray emission and flares are large-scale phenomena, involving large-scale magnetic structures. Recent research has indicated, however, that for magnetic energy to be dissipated as required for coronal heating and flares, smaller structures, with scales much smaller than the diameter of a single magnetic loop, are required.

One process by which wave energy is dissipated at small scales is resonance absorption. This process has been used to heat laboratory plasmas for some time; now it seems that it may be at least partially responsible for the heating of the plasma in stellar coronae as well. The fundamental concepts of the resonance absorption theory can be summarized as follows. A hot stellar corona is composed of discrete magnetic loops that act as high-quality resonance cavities for hydromagnetic waves. Each loop, driven by turbulent motions at its base, has a large-scale frequency response sharply peaked at the global resonant frequency of the loop. These large-scale motions are very nearly dissipationless, and therefore do not significantly heat the corona directly. However, they can resonantly excite small-scale waves in the loop whenever the global wave frequency equals the local Alfvén wave frequency. Dissipation of these small-scale waves then provides the energy necessary to heat the coronal plasma. The essential feature of the theory is the existence of the global mode and its subsequent coupling to the small-scale

dissipative waves. Since the bandwidth of the large-scale oscillation is narrow, the loop extracts power from the stochastic driving spectrum only in a narrow band of frequencies centered on the global resonance frequency. The loop can then be treated as a driven high-quality resonator, and the dissipation occurs in a very narrow, single resonance layer where the local Alfvén frequency is equal to the single frequency of the large-scale ideal magnetohydrodynamic oscillation. The heating rate is obtained by integrating the electromagnetic Poynting flux over the surface of the resonance layer to determine the energy dissipated in the loop. The heating rate derived in this way can be shown to be consistent with observations of the soft X-ray luminosity from active region loops. The scale of the dissipation region can be estimated from the theory. The actual dissipation region is expected to have a transverse scale much smaller than the width of the loop, with a width of 0.3–250 km. The wave amplitude in the resonance layer is expected to be a few hundred kilometers per second.

Resonance absorption is too steady a process to account for flares. Physical considerations indicate, however, that the energy release in flares must also occur in narrow layers. Flares are thought to result from instability within a magnetic structure or from the interaction of magnetic structures. This instability or interaction drives currents and electric fields within the magnetic structures, which result in heating and particle acceleration. These currents will most easily flow in one or more thin layers, or sheets. If we take into account the heating and particle acceleration requirements for solar flares and the observed magnetic field strengths in flaring regions, we are led to the conclusion that these sheets have thicknesses that typically range from 100 cm to 1 km. If most of the hard X-ray emission from the flare originates from electrons accelerated by the electric fields within these sheets, as may be the case for many flares, then 10,000 to over a million of these sheets are likely to have been present during the flare.

Stars of particular interest for studies of both coronal heating and flares are the M-dwarf flare stars. In addition to producing large flares, these stars are observed to emit coronal X-ray emission and a quiescent level of microwave emission that is not associated with discrete flares. The microwave emission might be cyclotron radiation from the same thermal coronal plasma responsible for the X-ray emission, but this interpretation has the problem that the required coronal radius is at least several times larger than the stellar radius, and the observed microwave spectra are not consistent with any simple model of this type. On the other hand, if the coronal plasma is heated in thin current sheets similar to those described above for solar flares, enough electrons can be accelerated to relativistic energies to explain the microwave emission as synchrotron radiation. This combined coronal heating-electron acceleration process may be fairly steady, or more likely, it may consist of many more rapid, transient events, similar to microflares that have been observed on the Sun. Hence, the M-dwarf flare stars may be showing a clear connection between coronal heating and flares. In any case, for both coronal heating and flares, small-scale structures play an important role in transferring energy to the coronal plasma.

Contacts: Joe Davila and Gordon Holman
Code 682

Sponsor: Office of Space Science and Applications

Dr. Joseph Davila, an astrophysicist with five years of experience with Goddard, holds a PhD degree in astronomy from the University of Arizona. Dr. Davila is studying the theory of solar phenomena, and he is particularly interested in the application of plasma physics theory to solar/stellar research.

Dr. Gordon Holman, an astrophysicist with four years of experience with Goddard, holds a PhD degree in astrophysics from the University of North Carolina, Chapel Hill. Dr. Holman's work is in the area of theoretical plasma astrophysics, with particular interest in solar and stellar phenomena.

OBSERVATIONS OF THE SOLAR CORONA WITH AN EUV IMAGING SPECTROGRAPH

The solar corona, the tenuous outer atmosphere of the Sun that extends into interplanetary space carrying the solar wind plasma and the Sun's magnetic field, continues to challenge solar physicists. Why is this region of the Sun's atmosphere so much hotter than the photosphere, the visible region of the Sun that lies beneath it? Furthermore, how is the solar wind then accelerated from this hot corona? Biermann proposed in 1947 that acoustic energy from the Sun's turbulent interior could propagate through the intervening atmosphere and be dissipated in the corona to provide the energy, but observations in space, such as those made by Orbiting Solar Observatory (OSO)-8, demonstrated conclusively that this hypothesis could not be correct. Recently, competing theories that propose that jiggling of the footpoints of coronal magnetic fields can produce traveling Alfvén waves that carry energy, or that the wandering of these footpoints

forces the magnetic fields closer together in the upper corona, resulting in ohmic heating, have received serious consideration. One approach to discriminate among these theories is to search for signatures of the presence of one physical process or the other. This can be done by studying the radiations from highly excited ions in the corona, which signal their motions by the broadening and/or spectral displacement of their emission lines.

To search for answers to these questions, our laboratory has developed and flown a specialized optical instrument, which uses a grazing incidence telescope produced by the GSFC Optics Branch (Code 717). The instrument, called an Extreme Ultraviolet (EUV) Imaging Spectrograph, disperses the solar spectrum while maintaining the spatial relations of the original solar sources so that spectral line intensities, which provide us with the density and temperature of the emitting plasma, and spectral line shapes that tell us about the motions of the emitting ions, can be recorded for many points in the solar corona simultaneously.

The EUV Imaging Spectrograph was flown on a Nike-Black Brant rocket from the White Sands Missile Range in October 1987 when solar activity and, hence, the level of coronal radiation were low. Nonetheless, the resulting observations between 280 and 370 Å provide data on the characteristics of coronal plasmas, both in the absence of solar activity and high above a small sunspot region. The observation shown in the figure was made with the optical entrance aperture of the instrument crossing the west limb of the Sun. In this way we simultaneously recorded radiation from the quiet corona against the solar disk (below the dashed line in the figure) as well as from the corona high (40,000-80,000 km) above a small sunspot region hidden from direct view behind the west limb of the Sun. The emission lines were observed to be broader than expected for a thermal plasma, the excess line widths being indicated in the figure by the spread between the heavy vertical lines. We conclude that excess ion velocities of up to 34 km/s along the line of sight are present to great heights above the solar surface. This could indicate the presence of energy-carrying Alfvén waves, produced by turbulent motion at the Sun's visible surface propagating to heights of possibly many solar radii above that surface and ultimately providing the source of energy to drive the solar wind into interplanetary space.

We plan a program of several rocket flights as the new solar cycle develops in which we will target different levels of solar activity to search for additional clues to the coronal heating/solar wind acceleration puzzles.

Contacts: Werner M. Neupert and Gabriel L. Epstein
Code 682

Sponsor: Office of Space Science and Applications

Dr. Werner M. Neupert, who holds a PhD degree from Cornell University, is Principal Investigator of the Solar EUV Rocket Telescope and Spectrograph and Mission Scientist for Spartan. Dr. Neupert studies the physics of the solar corona through observations of the corona's extreme ultraviolet and soft X-ray emissions. During his 26 years of service at Goddard, Dr. Neupert has received the John C. Lindsay Award, the NASA Exceptional Scientific Achievement Award, and the NASA Exceptional Service Medal.

Dr. Gabriel L. Epstein is Instrument Manager for the Solar Extreme Ultraviolet (EUV) Rocket Telescope and Spectrograph and Deputy Project Scientist for the High Resolution Solar Observatory. He is involved with the development of advanced electro-optical instrument systems for solar research on automated and manned space missions, and his professional interests include optical systems for ultraviolet and EUV wavelengths, excitation of the solar helium spectrum, and characterization of solar coronal plasmas from observation of their EUV radiations. Dr. Epstein, who earned his PhD degree in atomic physics at the University of California at Berkeley, has been with Goddard since 1970 and has received the NASA Special Achievement Award for Exceptional Service in the Performance of Official Duties.

SOLAR AND HELIOSPHERIC OBSERVATORY

The Solar and Heliospheric Observatory (SOHO) is a joint ESA/NASA project to address several basic questions regarding the Sun and the heliosphere. These questions can briefly be stated as: Why does the solar corona exist? What heats the solar corona? Where are the solar-wind streams, which carry the mass loss of the Sun, accelerated? What is the structure of the solar interior? These questions will be addressed in three distinct ways: 1) through spectroscopic studies of the outer layers of the Sun—the chromosphere, transition region, and corona—that use diagnostic techniques at high spectral resolution, and thus with high sensitivity to velocities; 2) by *in situ* measurements of fields and particles at the Lagrangian L1 point between Earth and the Sun; and 3) by monitoring the velocity and brightness oscillations of the solar surface that give indirect information about conditions throughout the Sun's interior (helioseismology).

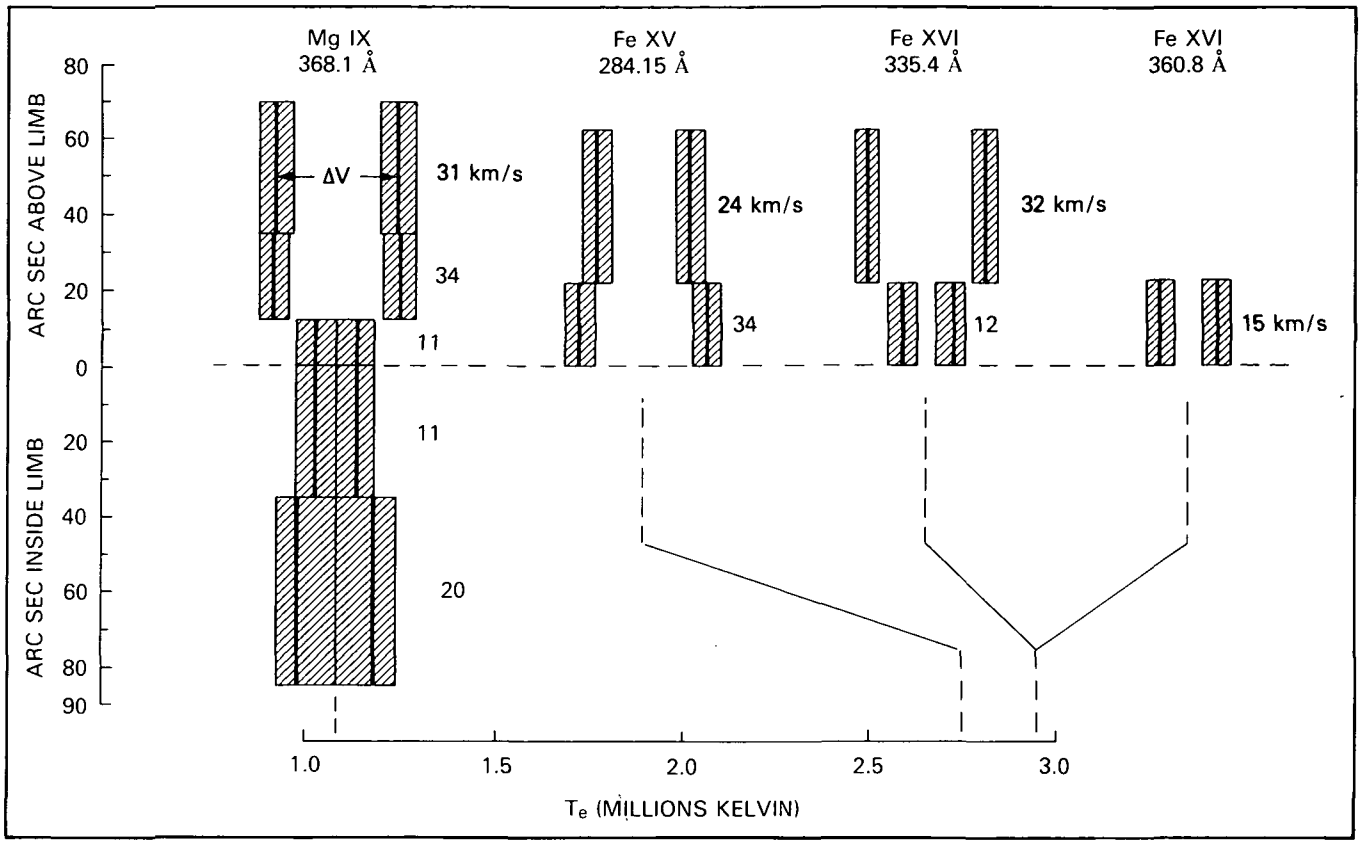

During a recent Nike-Black Brant rocket flight, a radial slice of the Sun's corona, beginning inside the edge of the visible solar disk and ending at about 120,000 km above the Sun's surface, was observed by an EUV Imaging Spectrograph developed at GSFC. The spatial ranges over which the four strongest coronal emission lines were recorded are shown by the vertical extents of the cross-hatched areas, with the horizontal dashed line indicating the solar limb. These spectral lines originate in plasmas at temperatures from one to three million Kelvin in the corona as indicated along the abscissa. The line widths were observed to be greater than would be expected from purely thermal plasmas. The "excess" widths, expressed as mean excess random velocities, ΔV, along the line of sight, are indicated by the spread between the heavy vertical lines. The width of cross-hatching is the probable error of the result. These results demonstrate that coronal plasmas, even at great heights, have a nonthermal component of motion that may be evidence of energy-carrying Alfvén waves produced by turbulent motions in the visible photosphere of the Sun.

The announcement of opportunity for this mission was released in February 1987, with proposals due in July 1987 and selection by December 1987. The spacecraft is to be built by ESA and launched by NASA in 1994. Approximately two-thirds of the payload is to be European and one-third American.

Members of the Laboratory for Astronomy and Solar Physics are co-investigators on four proposals that have been submitted for the SOHO mission:

1) Extreme Ultraviolet Imaging Telescope (EIT). This is an extreme ultraviolet (EUV) imaging telescope designed to provide full Sun images at the transition zone and coronal levels. It will obtain 5-arc second resolution images of the Sun in four spectral bands to observe a succession of iron lines that are formed in coronal plasma at temperatures between 9×10^5 and 2.5×10^6 °K and the HeII 304-Å emission line formed at ~50,000 °K. The data will be used to provide an understanding of the large-scale structure and evolution of the outer solar atmosphere. It will also provide a reference frame for the small-scale images obtained by the high-resolution spectrometers discussed below.

2) Coronal Diagnostic Spectrometer (CDS). This is a high spatial resolution EUV instrument with mod-

erate spectral resolution covering a wide range of wavelengths simultaneously. It uses a grazing incidence telescope to feed two spectrographs. The first is a grazing incidence system for observing between 150 and 300 Å, and the second is a normal incidence system for observing between 250 and 650 Å. Although the spectral resolution of this instrument is not adequate to obtain line profiles, it will provide some information on velocities. More important, it will simultaneously observe many spectral lines providing diagnostics for temperature and density from the upper transition region through the corona. The high spatial resolution, ~2 arc seconds, will provide information on the detailed topology of solar features. This instrument will also contribute to determining the energy balance in the outer solar atmosphere and measure the acceleration of the solar wind source region.

3) Solar Ultraviolet Measurements of Emitted Radiation (SUMER). This instrument is a high spatial and spectral resolution EUV spectrograph. It uses all normal incidence optics to observe in the spectral range from 500 to 1600 Å with a spatial resolution of ~1 arc second. The spectral resolution will be adequate to obtain line profiles for each line observed, but only over a limited wavelength range at any one time. This instrument will provide information on the structure and material velocities of the outer solar atmosphere. Thus, together with the data from the grazing incidence system described above, we will better understand the flow of energy, mass, and momentum through the outer solar atmosphere into the solar wind.

4) Solar Oscillations Imager (SOI). This instrument is designed to study the solar interior through the relatively new science of helioseismology. Oscillations trapped in the solar interior produce periodic Doppler shifts on the visible surface of the Sun with amplitudes from hundreds of meters per second down to perhaps as little as millimeters per second. Some of these oscillations, or modes, are concentrated in the deep radiative interior of the Sun, whereas others are concentrated in the convection zone just below the visible surface. So-called inverse methods can be used to determine the temperature, density, rotational velocity, and convective velocity as a function of depth, giving astronomers their first real probe of a stellar interior. Although many advances in helioseismology have been made with ground-based data, such observations are inherently limited by both atmospheric seeing (which prevents the analysis of high-degree modes, i.e., those on small spatial scales) and day-night cycling (which restricts our determination of mode lifetimes and internal rotation). This SOHO instrument will eliminate these ground-based limitations.

Thus, the joint NASA/ESA SOHO mission will provide a detailed view of our closest star from its interior, through its various atmospheric layers, and out to the solar wind that replenishes interstellar space. From this we should be able to greatly increase our understanding of the solar interior, its convective envelope, and the still-puzzling heating and dynamics of the outer atmosphere.

Contacts: Arthur I. Poland, Joseph B. Gurman, Stuart D. Jordan, and Roger J. Thomas
Code 682

Sponsor: Office of Space Science and Applications

Dr. Arthur Poland, an astrophysicist with seven years of experience at Goddard, is Deputy Project Scientist for SOHO (ISTP) and Co-Investigator on SMM. His professional interests include solar physics, energy transport, and computer modeling. Dr. Poland holds a PhD degree from Indiana University.

POLYCYCLIC AROMATIC HYDROCARBONS AS INTERSTELLAR GRAINS

It has been suggested that polycyclic aromatic hydrocarbons (PAHs) are the source of the interstellar unidentified infrared (UIR) continuum and emission features. In this scenario, infrared emission from interstellar PAHs occurs after absorption of an ultraviolet photon. Since energy transfer to the ground electronic state can be rapid for a species in which intersystem crossing is negligible, the emission spectrum may be viewed as resulting from an equilibrium vibrational temperature. This has been the basis for using infrared absorption spectra to calculate the corresponding emission spectra at various temperatures. These calculations have been made using room-temperature infrared absorption coefficients instead of those at the temperature of interest because of the latter's unavailability.

Proper assessment of the hypothesis that correlates PAHs with the UIR features requires additional experimental laboratory data. To address this need, the room-temperature absolute infrared cross sections for eight PAHs have

been obtained using a Fourier transform infrared (FT-IR) spectrometer. The structure for one such PAH-coronene is indicated at the top of the accompanying figure. The top trace is the room-temperature absorption coefficients for coronene. To acquire additional information that is complementary to the absorption data, a high-temperature cell has been designed and constructed. This cell can be attached to the emission port of the FT-IR spectrometer and is used to obtain thermal emission spectra for temperatures as high as 525 °C (~825 °K). Preliminary emission data for coronene at 425 °C appears as the lower trace in the figure. The spectrum is uncorrected for background emission and instrument response function; however, there are indications of thermal emissions from the molecule. As expected, some of the emissions coincide with absorption features; others do not. Of particular interest are the small spikes on the broad feature at ~500 cm^{-1} for which there are no corresponding absorption peaks.

The efforts described above yield information about ground electronic states. A series of ultraviolet-induced infrared fluorescence studies is planned that will provide corresponding data on infrared emissions from electronically excited states. These spectra will more realistically represent the proposed interstellar emission mechanism and will provide information on relative band intensities and peak positions not available from previous calculations. Comparison of that data with the UIR bands will permit a critical test of the PAH hypothesis because the interstellar features are known to better than 0.1 μm.

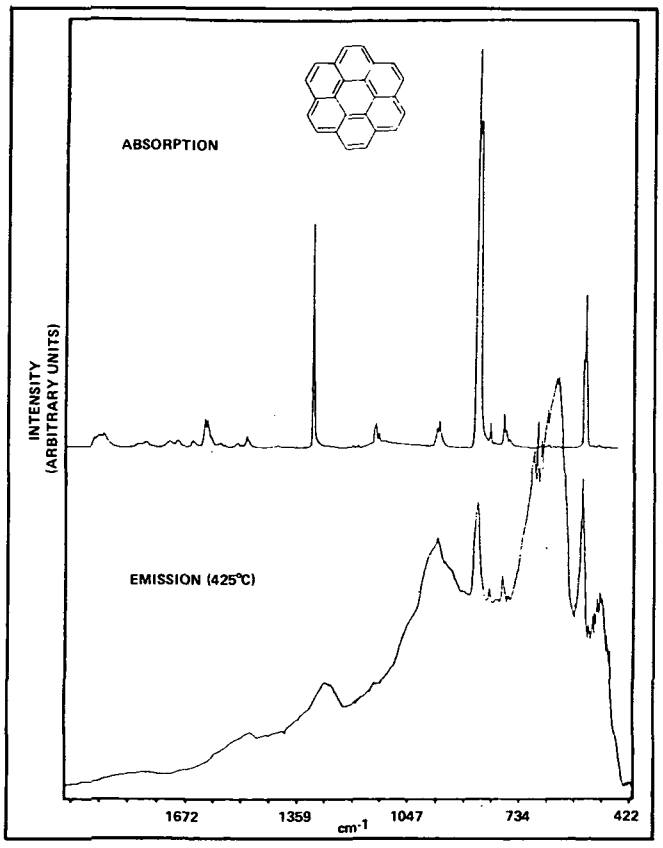

Room-temperature absorption spectrum and preliminary thermal emission spectrum of coronene.

The developmental nature of this program has provided opportunities for collaboration with Dr. R. Khanna at the University of Maryland through support of Mr. D. W. Salisbury, who is working at GSFC in the NASA Graduate Student Researchers Program, and with Dr. W. J. Moore of the Naval Research Laboratory, who has provided instrument time and support on a Bomem FT-IR spectrometer.

Contacts: John E. Allen, Jr., and Bertram Donn
Code 691

Sponsor: Office of Space Science and Applications

Dr. John Allen, Jr., is involved in research of interstellar grains, cometary and planetary atmospheres, and the upper atmosphere with the Astrochemistry Branch of the Laboratory for Extraterrestrial Physics. His professional interests include the application of optical techniques to chemical physics and the application of chemical physics to aeronomy and astrophysics. Dr. Allen received a PhD degree in applied physics from the University of Florida, and he has been with Goddard for nine years.

Dr. Bertram Donn is a senior scientist in the Laboratory for Extraterrestrial Physics with 28 years of experience at Goddard. He holds a PhD degree from Harvard University. His professional interests center about the formation of interstellar grains and the origin, structure, and composition of comets.

OBSERVATIONS OF 5-MICRON CARBON MONOXIDE IN LATE-TYPE STARS

Carbon monoxide is one of the most abundant molecules in cool giant stars. At stellar temperatures below 6000 °K, where carbon monoxide dissociates into its constituent carbon and oxygen atoms, infrared emission from a wide

range of vibration and rotation energy levels can be detected. Observations of this kind require the largest telescopes in combination with the most sensitive spectrometers in existence.

One goal of the astronomy program at Goddard is to establish carbon monoxide as a tool for investigating stellar atmospheres. By observing carbon monoxide at several infrared wavelengths near 5 microns, stellar atmospheres can be probed through a wide range in altitude. Weak lines are formed deeper in the atmosphere and are used to study characteristics of the photosphere. Strong lines arise in the upper photosphere and chromosphere.

Carbon monoxide moderates the temperature in the formation region through radiative cooling from line emission. In addition, lines of the isotopic variants of carbon monoxide can be detected in late-type stars. A high abundance of rare isotopes indicate the evolutionary stage of material exchange processes between the atmosphere and core of the star.

The Goddard program developed a cryogenic postdisperser for use in combination with the facility Fourier transform spectrometer at the 4-m Myall telescope of the National Optical Astronomy Observatories at Kitt Peak. The postdisperser is a liquid helium grating spectrometer that reduces thermal noise at the detector by narrowing the spectral bandpass. The spectra obtained with this approach is sufficient to resolve many narrow (2–3 km s^{-1}) carbon monoxide lines simultaneously with high signal-to-noise ratios. Carbon monoxide has been studied in 14 late-type giant stars.

This work was done in collaboration with G. Wiedemann (GSFC) and S. Saar and T. Ayres (University of Colorado).

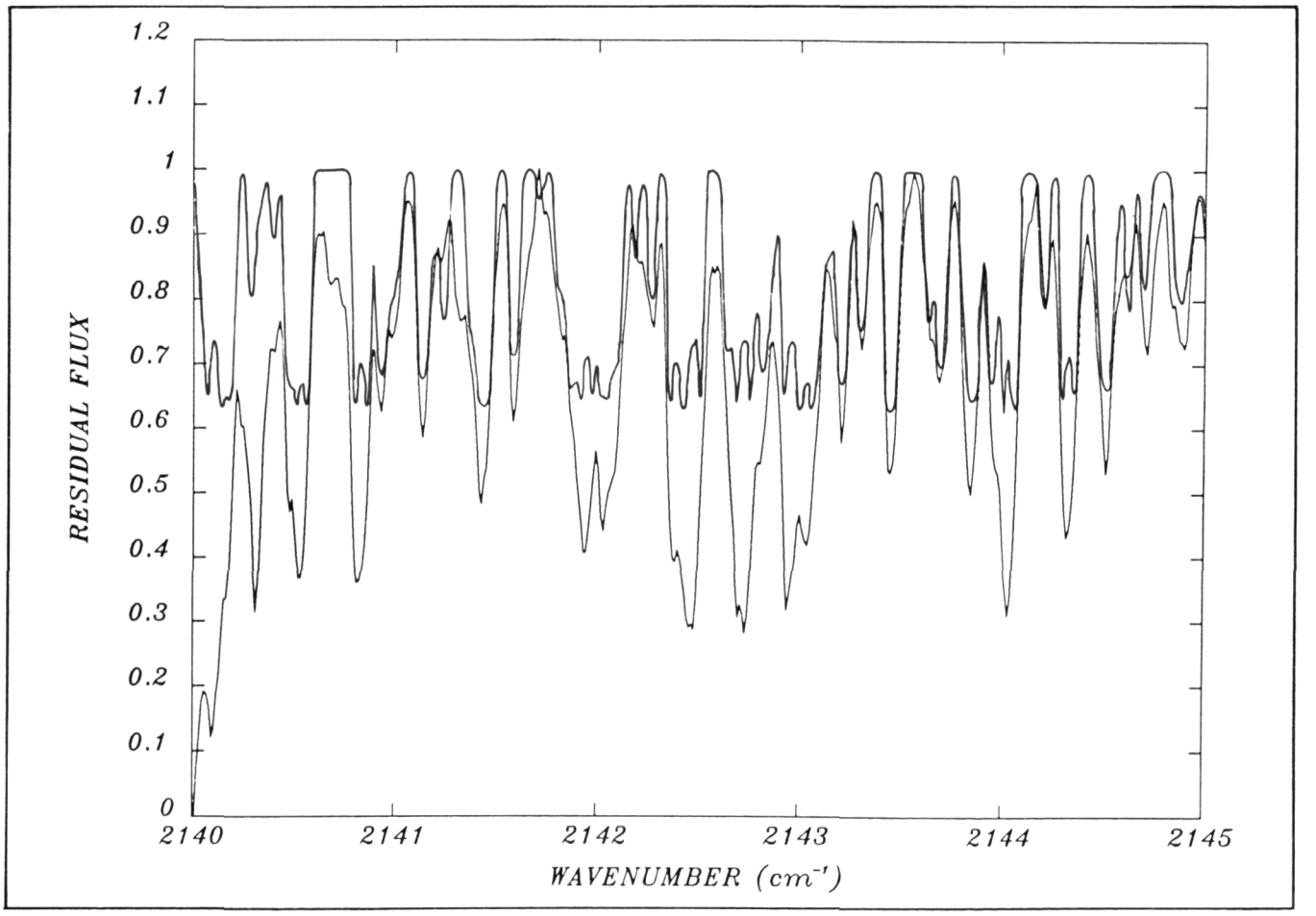

Observed spectra of carbon monoxide in Aldebaran (black line) compared with spectra calculated from a standard model.

ORIGINAL PAGE IS
OF POOR QUALITY

Contact: Donald Jennings
Code 693

Sponsor: Office of Space Science and Applications

Dr. Donald E. Jennings, who holds a PhD degree in physics from the University of Tennessee, has 10 years of experience as a space scientist with Goddard. Dr. Jennings is interested in infrared molecular astronomy and high-resolution laboratory molecular spectroscopy.

ISOTOPIC FRACTIONATION AND RARE GAS TRAPPING IN COSMIC DUST ANALOGS

For the last several years we have studied the physical, morphological, and spectral properties of simple refractory smokes condensed from vapors of Mg and SiO in a hydrogen buffer gas as analogs to more complex materials that condense in the outflowing shells of oxygen-rich stars. We have demonstrated that the spectral properties of our condensates bear a striking similarity to the infrared spectra of grains in circumstellar regions and to the infrared spectra of grains in the general interstellar medium. In addition, the morphology of a typical Mg-SiO condensate that has been annealed *in vacuo* at 1000 °K for 4 hours (Figure 1) is comparable to the morphology of a natural cosmic dust particle (Figure 2) collected in the stratosphere. We have begun to study the relationship of our cosmic dust analogs to grains in the primitive solar nebula because: 1) all solid material in our present-day solar system once resided in the interstellar medium as part of the interstellar grain population; and 2) several lines of meteoritic evidence unequivocally demonstrate that some circumstellar materials survive passage through the interstellar medium, processing in the primitive solar nebula, and incorporation into a meteorite parent body or a comet, remaining largely unchanged by these events. Here we briefly discuss two sets of experiments that were started within the last year-and-a-half specifically to study questions related to the oxygen isotopic composition and rare gas content of grains in the early solar system.

Preliminary measurements of the oxygen isotopic composition of the condensates from the reaction of various gas mixtures including $SiH_4 + O_2$, $Al(CH_3)_3 + O_2$, $Fe(CO)_5 + O_2$, $Fe(CO)_5 + SiH_4 + O_2$, and $Fe(CO)_5 + Al(CH_3)_3 + SiH_4 + O_2$ in a hydrogen flow gas at temperatures of up to 1000 °K have shown isotopic fractionations greater than ~1.5% per AMU with respect to the initial O_2 isotopic composition. This reported fractionation efficiency may be a lower limit to the extent of fractionation that actually occurs, since there is some evidence to indicate that the smoke sample may strongly chemisorb a significant amount of unreacted O_2 from the flow stream, thus diluting the measured fractionation effect.

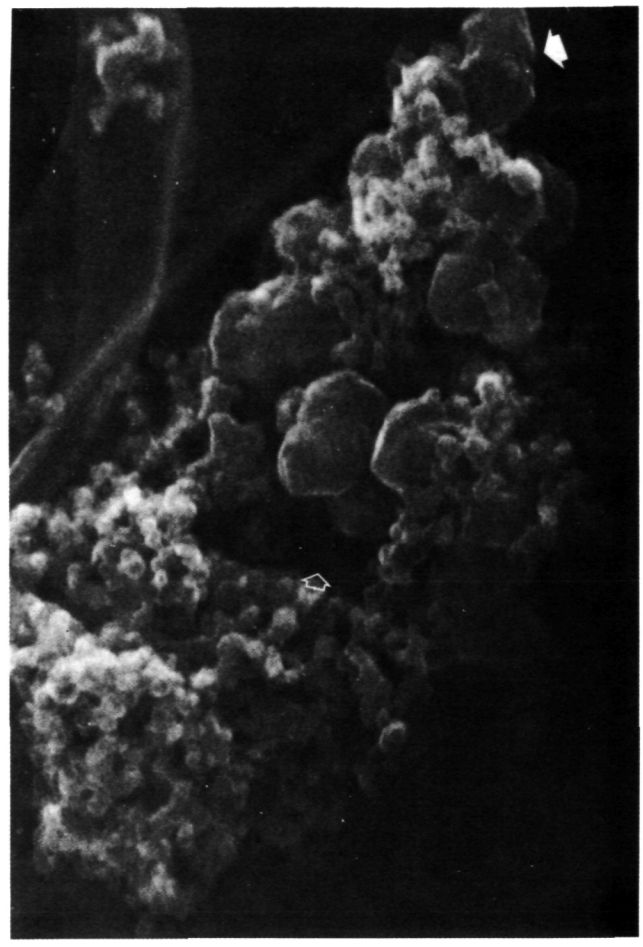

Figure 1. Scanning electron microscope image of Mg-SiO smoke produced in our laboratory and annealed in vacuo *at 1000 °K for 4 hours. Scale bar is 1 micron long. (Arrows indicate hexagonal silicon-rich plates.)*

The magnitude of the isotopic fractionation is much greater than would be expected for isotopic exchange and suggests that the process (or processes) which is responsible for the effect is kinetically controlled. If the effect occurs during the chemical reaction of simple radicals such as SiH with O or O_2, then our results would suggest that the oxygen isotopic composition of the grains in a circumstellar outflow might be several percent per AMU lighter than the composition of gas phase species

ORIGINAL PAGE IS
OF POOR QUALITY

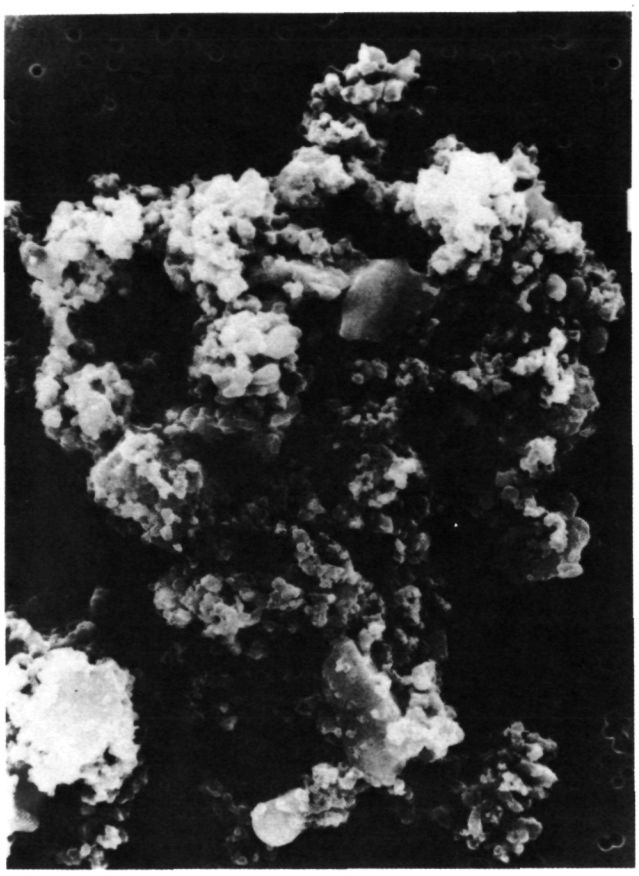

Figure 2. Scanning electron microscope image of an interplanetary dust particle (IDP) collected in the stratosphere; note 1 = micron scale bar. This particular IDP is classed as a chondritic porous aggregate and consists of relatively large grains of crystalline Fe, Mg silicates, and smaller, anhydrous grains of variable composition.

in the shell. This could therefore be a source of the oxygen isotopic variability observed in the meteorites. Experiments to determine the mechanisms by which this fractionation occurs are currently in progress, as are more carefully controlled experiments to measure the dependence of the degree of fractionation on such variables as the temperature at which the reaction occurs and the chemical composition of the initial gaseous mixture from which the grains condense.

In a second series of experiments, we condensed simple Si_2O_3 smokes at both low (<750 °K) and high (>1000 °K) temperatures in 35 torr of hydrogen gas to which variable amounts of a noble gas mixture containing Ne, Ar, Kr, and Xe had been added. Both Ne and Ar were very loosely bound in the smokes, as shown by the fact that the bulk of the adsorbed Ne and Ar is lost when the grains are heated to between 700 and 900 °K. However, Ar was found to be very efficiently chemisorbed from the atmosphere by the Si_2O_3 grains: concentrations of up to 3×10^{-4} ccSTP of Ar were contained in a gram of sample, and we do not yet know if equilibrium was attained. Higher concentrations may be possible for longer equilibration times. Both Kr and Xe were bound more strongly in the Si_2O_3 than was either Ne or Ar. In addition, both Kr and Xe showed distinct double release patterns in which one adsorbed component is increasingly lost from a grain's surface as the temperature increases, whereas a second component remains trapped. This trapped component is released in a pulse at ~1875 °K—presumably when the grains melt and the trapped gas can escape confinement within the crystal structure. Unfortunately, none of the noble gases trapped within the smokes as they grew were present in sufficient quantity to account for the concentrations of anomalous noble gases observed in meteoritic samples. The anomalous Ar adsorption efficiency of Si_2O_3 smokes will continue to be investigated, as will the possibility that Ne, Kr, or Xe may be efficiently adsorbed by other relatively abundant refractory metal oxide constituents present in the early solar nebula or in circumstellar outflows.

Contacts: Joseph Nuth and Bertram Donn
Code 691

Sponsor: Office of Space Science and Applications

Dr. Joseph Nuth, an astrochemist/geochemist with the Laboratory for Extraterrestrial Physics, performs laboratory studies of the formation and metamorphism of refractory silicates. Dr. Nuth received a PhD degree in chemistry from the University of Maryland, and he has worked with Goddard since 1975.

Dr. Bertram Donn is a senior scientist in the Laboratory for Extraterrestrial Physics with 28 years of experience at Goddard. He holds a PhD degree from Harvard University. His professional interests center about the formation of interstellar grains and the origin, structure, and composition of comets.

MAGNETIC SPLITTING OF LINES IN THE 12-MICRON SOLAR SPECTRUM

In recent years new spectral features have been discovered in the infrared spectrum of the Sun. Emission lines due

to high-Rydberg transitions in neutral magnesium and aluminum were discovered to occur near 12 μm wavelength. The lines appear as narrow emission features whose amplitude is approximately 10% greater than the solar infrared continuum. Why these lines appear in emission, whereas most lines in the solar spectrum appear in absorption, is not understood. However, this does not detract from the most important property of the lines: they are extremely sensitive to solar magnetic fields.

In the presence of a magnetic field, spectral lines split into several components due to perturbation of the atomic energy levels by interaction with the field. This is the Zeeman effect, and for visible region lines it is a very small amount. Even a 1000-Gauss magnetic field causes only a slight broadening of lines in the visible solar spectrum. Therefore, solar magnetographs use polarizing filters to separate the Zeeman-split components from Doppler broadening of the lines by thermal motions in the solar atmosphere. But polarization measurements alone are difficult to interpret, and information can be lost in the process. Instead, it is preferable to use lines where the Zeeman effect is very large. Fortunately, the Zeeman effect increases with wavelength; the 12-μm solar emission lines show Zeeman splitting eight times greater than visible-region lines, so they offer the possibility of studying solar magnetic fields with very great sensitivity.

The 12-μm lines, however, are not easy to observe. Thermal background emission from the terrestrial atmosphere and instrumental components produces a high noise level. However, an instrument has been developed at Goddard that makes it possible to obtain low-noise observations of these Zeeman-sensitive lines. This was done by using a blocked-impurity-band (BIB) detector together with a liquid-helium–cooled grating monochromator to construct a postdisperser for use at the output of Fourier transform spectrometers (FTS). The postdisperser was used with the FTS at the National Solar Observatory on Kitt Peak to investigate the magnetic field structure in sunspots. The figure shows the profile of an emission line at two locations in a sunspot penumbra. The sunspot magnetic field causes the splitting into three components; the upper profile reveals a greater magnetic field strength, as evidenced by the greater splitting. Observations of fully Zeeman-split lines such as these can reveal new aspects of the solar magnetic field. The vector geometry of the field can be derived, and mass flows can be seen to occur along the magnetic lines of force. Ultimately, it should be possible to use this type of data to reveal the occurrence and nature of instabilities in the magnetic field, which are believed to lead to solar flares and other releases of magnetic energy in the solar atmosphere.

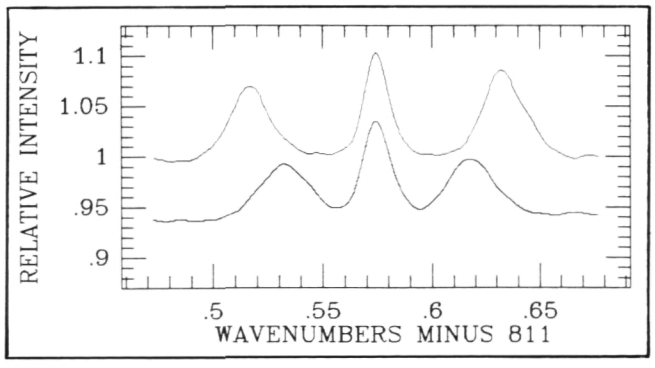

Zeeman-split emission line profiles observed at two locations in the penumbra of a sunspot. The sunspot magnetic field splits each line into three components. The greater splitting of the upper profile indicates a stronger magnetic field.

Contact: Drake Deming
Code 693

Sponsor: Office of Space Science and Applications

Dr. Drake Deming has seven years of experience as an astrophysicist with Goddard. He holds a PhD degree from the University of Illinois, and he is interested in the dynamics of stellar and planetary atmospheres.

FORECAST OF AN EXCEPTIONALLY LARGE SOLAR CYCLE

A dynamo theory method is used to predict long-term solar activity. The dynamo principle through which the Sun's main toroidal field is generated may be called Babcock's principle, and this is supported observationally by Hale's law of sunspot polarities.

This conventional dynamo transforms the Sun's poloidal field by differential rotation into a toroidal field; this toroidal field gives rise to subsequent spots and solar activity. Thus in a dynamo theory prediction of solar activity, the state of the Sun's poloidal field is monitored, either directly or indirectly. It is through these estimates of the polar field strength of the Sun at solar minimum that the next cycle's sunspot number is calculated. In 1978, we showed that a linear relation between four measures of polar field strength and future sunspot

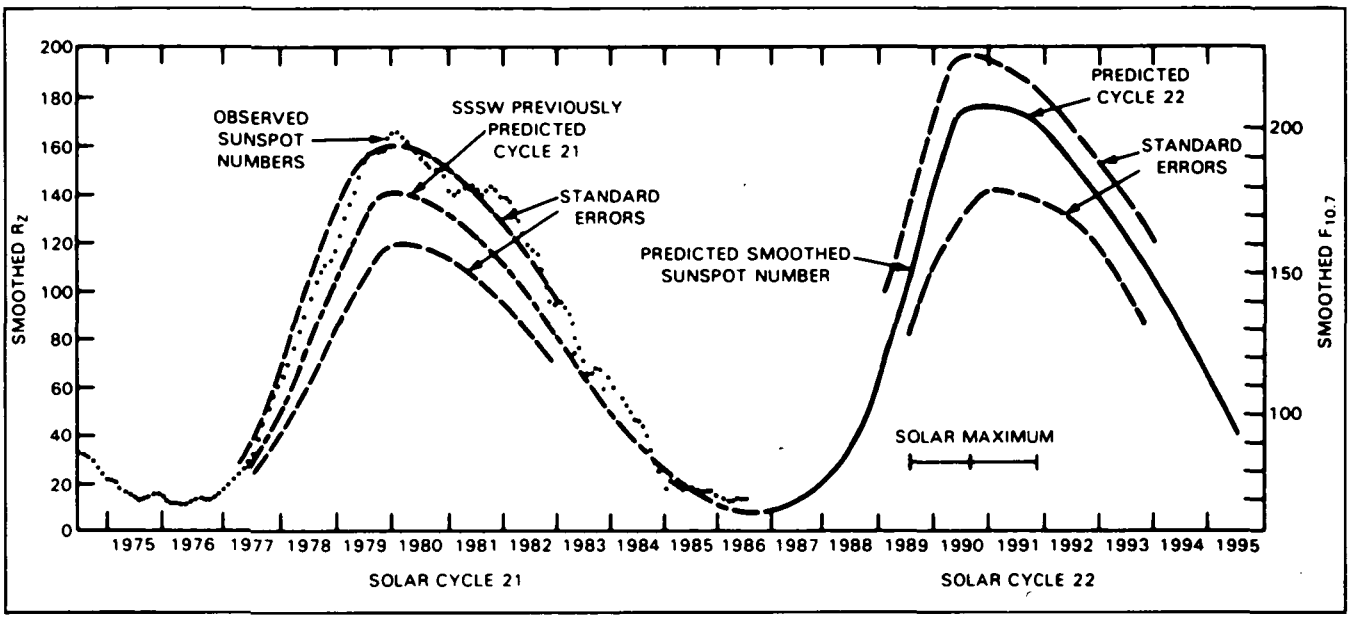

Predicted smoothed sunspot number and radio flux from 1984 to 1995 (solid curve). Estimated yearly average uncertainties (dashed curves) are smaller than in many other predictions. The previous prediction for solar cycle 21 compares well with the observed sunspot numbers (dots).

number held for eight solar cycles. On this basis, we predicted the strength of solar cycle 21 (see figure). The subsequent agreement provided additional support to the relation. There are no free parameters, and straightforward, repeatable methods are used. This is in contrast to other statistical, secular variations, or sunspot periodicity models, which utilize only sunspot number for the state of the Sun and attempt prediction by means of complex unphysical numerical algorithms.

Solar activity for solar cycle 22 has been predicted with the same technique. It is based upon direct and indirect indicators of the strength of the Sun's polar field near the present solar minimum. Several independent examinations of the polar field strength show it to be larger than even the last cycle's. This leads us to predict that the next solar cycle will be an exceptionally active one, somewhat larger than the last. A sunspot number, shown in the figure, of 170 ± 25 is predicted for September 1990 ± 1 year.

This large degree of solar activity affects the outer atmosphere of the Earth. The predicted ultraviolet heating will raise the density and temperature of the thermosphere to levels somewhat larger than those found in solar cycle 21. The predicted value of R_m of 170 ± 25 provides a value of the mean global exospheric temperature near 1200 ± 70 °K and a globally averaged density at 600 km near 5×10^{-16} gm cm^{-3} (Hedin, A., private communication, 1987). This will have an impact on the orbital lifetimes of low-altitude satellites. It was this same effect that brought the Skylab platform to its early demise.

There is concern that even-numbered cycles are historically small and that a large sunspot number for an even cycle is unlikely. Although recently even-numbered solar cycles have been smaller than the preceding odd ones, this relation was not generally obeyed before solar cycle 8 or for cycles 17 and 18.

Contact: Kenneth Schatten
Code 610

Sponsor: Office of Space Science and Applications

Dr. Kenneth Schatten, who holds a PhD degree from the University of California at Berkeley, is a solar physicist with the Solar Disk Sextant project. Dr. Schatten has been with Goddard since 1969 and has received several awards for his scientific achievements.

HIGH ENERGY ASTROPHYSICS

IMPLICATIONS OF A NEW SERIES OF SOFT GAMMA-RAY TRANSIENTS

Astronomy in the photon energy window of about 20 keV to about 20 MeV is a relatively undeveloped science. This energy band (which does not have a name of its own to distinguish it from the higher-energy gamma-ray astronomy in the fractional- to many-BeV region) studies the astrophysical origins of the fractional- to many-MeV photons that nuclear physicists usually call gamma rays: the products of annihilation, nuclear excitation, and decay processes. Specifically astrophysical phenomena such as cyclotron resonance features that involve energies too high for the X-ray label are also included. This discipline has been slow to develop compared with other areas of astronomy for reasons concerning signal-to-noise ratios. The background levels here are exceptionally high due to an accumulation of secondary effects, and the primary signal strengths are relatively ephemeral. Spectrometers to observe narrow nuclear lines promise entirely new harvests of information unavailable with other means, with unique insights into some of the most energetic processes in nature. One existing astronomical identification is the 0.511-MeV galactic center positron-electron annihilation line; observations of galactic nuclear lines are also beginning to appear, and one would hope to expect a great profusion from the Supernova 1987a (see the parallel report by Gehrels and Teegarden).

The phenomenology of astrophysical gamma-ray transients flowered during the previous decade, however, with studies of the unexpected but profuse gamma-ray bursts. In opposition to a program of steady-state source studies, observations of these enigmatic and intense transients have generally centered on their properties, given the absence of any northern hemisphere undisputed source location. In fact, as outlined below, their phenomenology may be too diverse for a source of one event to imply knowledge of other source populations. These studies have demonstrated the richness of the lower-energy gamma-ray avenue for information from dynamically changing, high-energy-density cosmic sources.

The recent discovery of a cluster of soft transients, buried within spacecraft data compiled in late 1983, adds a new aspect to the study of gamma-ray bursts. The characteristic energy of each of these events is geometrically between the X-ray burst and gamma-ray burst domains, complicating the understanding of the parent processes (as well as confusing the naming problem). The common source direction, inferred from the relative onset timing of each event of several space probes and satellites, is consistent with that of the galactic bulge. This property is not generally possessed by the isotropically arriving bursts, other than perhaps one in January 1979, also of an anomalously soft nature. These events were found first in Franco-Soviet data and confirmed, supported, and augmented with observations from Los Alamos Laboratory and Goddard Space Flight Center data from other space missions.

There have been only two other cases of repeating, soft transients found with gamma-ray burst instrumentation, including the one found as sequel to the unique March 5, 1979, event. All of these various event series of soft, ~25-keV, repeaters appear to differ considerably in phenomenology from the harder, generally 0.1- to tens-of-MeV, classical gamma-ray bursts that have not yet been found to repeat from any particular source direction: the repeater events are found to exhibit no spectral evolution and to have only uncomplicated time histories, unlike the classical events. It therefore appears that X-ray bursts, gamma-ray bursts, and this intermediate group form at least three differing transient classes, requiring at least three separate model envelopes. However, the transient of March 5, 1979, with its source direction exactly within the supernova remnant N49 in the Large Magellanic Cloud (LMC), remains as the parent of one nonclustering series, confusing any overall characterization.

We note that one distinction of this new intermediate class is the possible consistency of their source directions with a pattern of origin in the galactic disk and in the LMC (see figure) rather than with isotropy like the classical bursts. Such a source pattern is similar to those of X-ray binaries, infrared sources, and even visible dim stars. The size spectra of these repeaters, in fact, show a reasonable fit to this pattern, given an assumption of a standard brightness: that is, the maximum intensities found in each of the three series of events are, within a factor of two,

consistent with a proportionality to the inverse-squared distances of the three regions.

We contend that this phenomenology has at least two serious implications. First, it strengthens a previously maintained interpretation that soft repeaters and classical events are of dissimilar nature, implying that they may not even possess the same population of sources. At least, attributing to classical gamma-ray bursts the features established only for the repeaters may be entirely misleading. Similarly, the cyclotron resonance features found in the classical events do not necessarily tell much about the soft repeaters. With no sources yet identified for any transient event [the March 5, 1979, event source, superposed on the supernova remnant (SNR), contains no point object either associated with the SNR or more nearby], the assumption that one particular population of neutron stars, for example, may be the source of more than one variety of gamma-ray transients remains unproved.

Second, we maintain that this result may be regarded as supporting the identification of the N49 SNR region as the source of the March 5, 1979, event. The LMC source observation has often been taken to be controversial, due to the distance and to the anomalous intensity of the March 5 event, relative to its sequels and to classical events. Theoretical work on describing a possible emission process is independently under way, contrasting with the view that the source identification is not easily modeled and therefore only an unlikely accident. The collection of the sources illustrated is clearly not enough to establish a population distribution, but its embryonic beginnings could be confirmed with additional observations of other soft repeater series, if they were to be found with source directions also in the galactic disk. The only existing gamma-ray burst instruments are on Solar Maximum Mission and Pioneer Venus Orbiter, with incidental observations forthcoming from the Soviet Mir mission. Other European and Soviet experiments are expected to be launched in the near future. The Gamma Ray Observatory will be launched in a few years with a large dedicated instrument that should possess the sensitivity and measurement capabilities to confirm this prediction. Our group continues to pursue the studies of the observables of gamma-ray transients in this and other experimental programs.

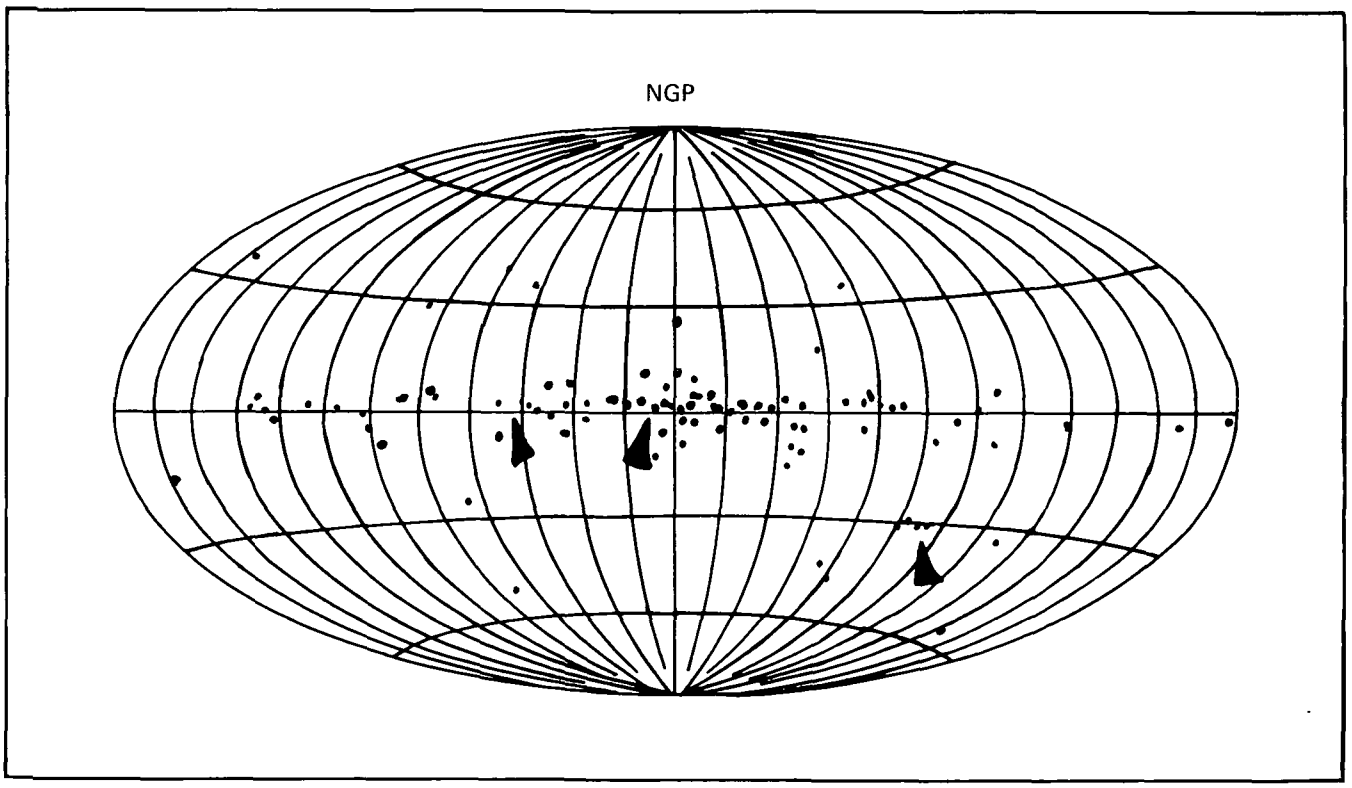

The source locations of the three known soft gamma-ray repeaters, plotted on a galactic map of the source distribution of X-ray binaries.

Contact: Thomas L. Cline
Code 661

Sponsor: Office of Space Science and Applications

Dr. Thomas Cline is a senior scientist with the Laboratory for High Energy Astrophysics. His professional specialties include gamma-ray astronomy and astrophysics, particularly gamma-ray bursts; cosmic rays; and solar particles. Dr. Cline, who received a PhD degree from the Massachusetts Institute of Technology, has been with Goddard since 1961. He is a recipient of the John Lindsay Award and the NASA Exceptional Scientific Achievement Award.

ANTIMATTER IN COSMIC RADIATION

Antimatter was found in cosmic rays nearly a decade ago (Golden, R., 1979) in the form of antiprotons. This was not unexpected since there are known processes that allow the creation of antiprotons by energetic collisions with ambient interstellar gas. However, the number of antiprotons relative to the other cosmic rays was surprising, nearly four times the amount anticipated from the accepted model for cosmic ray propagation. Subsequently, three experiments have measured antiproton cosmic ray fluxes, with all finding results higher than expected. One experiment (Buffington, A., 1981) reported an antiproton flux in the few hundred million-electron-volt (MeV) energy range, whereas the standard model predicts essentially zero flux.

Goddard Space Flight Center is engaged in a collaboration to make definitive measurements of antiprotons in the cosmic radiation over the interesting energy range from 200 MeV to 10 GeV. With colleagues Dr. Robert Golden at New Mexico State University and Dr. Ted Bowen at the University of Arizona, we have carried out a program of two successful balloon flights with a superconducting magnetic spectrometer augmented with various other detectors. The first of these, the Medium Energy Antiproton Experiment (MEAP), was flown in September 1986 and made measurements in the GeV range. The Low Energy Antiproton Experiment (LEAP) was flown in August 1987 and made measurements in the several hundred MeV range. Together, these flights have recorded over 20 million cosmic ray events.

The data from these flights contain other information in addition to the antiproton fluxes. In particular, the data can be used to set new limits on the presence of antihelium in the cosmic rays. This is of interest since the measured excesses of antiprotons have led to suggestions that the universe is baryon symmetric, containing equal amounts of matter and antimatter. The flight data should lead to a measured limit on the presence of antihelium that is at the low end of predictions from baryon symmetric cosmologies.

Other possibilities suggested to explain the previously measured antiproton excesses range from special sources to the decay of primordial black holes. Completion of data analysis on the MEAP and LEAP flights should help clarify both the experimental and theoretical situation with regard to antimatter in the cosmic radiation.

In addition to Drs. Golden and Bowen, collaborators in this work are Dr. J. Lloyd-Evans, (Los Alamos), Ms. Ann Moats (University of Arizona), Dr. J. F. Ormes (GSFC), and Mr. Steve Stochaj (GSFC and the University of Maryland).

Contact: Robert E. Streitmatter
Code 661

Sponsor: Office of Space Science and Applications

Dr. Robert Streitmatter, an astrophysicist with seven years of experience at Goddard, received a PhD degree in physics from the University of Chicago. He is interested in the experimental measurements of cosmic ray spectra and theoretical work on cosmic ray origins.

GAMMA-RAY INSTRUMENT DEVELOPMENT FOR FUTURE STUDIES OF HIGH-ENERGY SOURCES

High-energy gamma radiation is of special interest because its study will almost certainly provide direct evidence on the most energetic phenomena that occur in astrophysics. Observations of the intensity and energy distribution for the gamma-ray emission from compact objects such as neutron stars and black holes should provide valuable information about the physical nature, the energetics, and the evolution of these extraordinary objects, as well as about the related problem of the acceleration of high-energy particles.

The Energetic Gamma Ray Experiment Telescope (EGRET) instrument, when launched as part of the Gamma Ray Observatory mission in 1990, will provide the

ability to observe the gamma-ray spectrum for strong sources to somewhat above 10^{10} eV. Currently, ground-based detectors have a minimum energy threshold of about 2×10^{11} eV. Existing information on the few sources that have been seen by SAS-2 and COS-B at energies above about 100 MeV and also by ground-based detectors suggests breaks, or spectral features whose details would offer important clues as to the emission production mechanisms. Even when EGRET is able to observe these sources, a gap between its upper energy threshold and ground-based instrument data will exist, especially for the weaker sources. A new generation instrument with approximately an order of magnitude increase over the EGRET sensitivity will be desired to study point source emission in the energy domain of this gap.

An instrument of the size and sophistication anticipated for the future will require long lead times for technological developments as well as for design, fabrication, and testing. For this reason, it is important to define concepts that may have general application and which long-term developments are expected before they can be proposed responsibly for space application.

A research effort in our laboratory, supported by the SRT program, has been exploring general instrument concepts that potentially can provide a factor-of-six increase in area, reduce dead-time to nearly zero, and provide a factor-of-two improvement in angular resolution compared to EGRET. In addition, several key areas that require development, and at the same time do not depend greatly on a detailed instrument concept, have been identified and either are already being investigated or are proposed for work in the next several years.

The effort has focused on the use of large-area drift chambers with an aperture of 2 m $\times$ 2 m. One technical challenge for the use of drift chambers in space is the power consumption of its electronics. The total electrical power available to a detector with an extended life in space is perhaps several hundreds of watts. Circuits used in conventional drift chambers have been estimated to require several kilowatts for the type of instrument being studied. Power will have to be reduced by more than a factor of 10, but the speed and accuracy of current systems must be retained. The electronics associated with each of the approximately 4000 anodes of the detector must be able to locate a track in one dimension to an accuracy of 0.1 mm and be able to separate two tracks of an incident gamma-ray interaction to within 1 mm.

A small development chamber has been constructed that can readily be fitted with a variety of electronic circuits that have been developed for evaluation purposes. The output timing signals have been interfaced to a commercial microcomputer where a track reconstruction algorithm may be employed to evaluate the chamber. This work is currently in progress.

An investigation into fabrication methods is also in progress. A testing program has identified a material suitable for constructing the large frames made from a fiber-filled cement compound that has excellent strength and machining properties, and can be cast into wire support frames. A wrapping machine to place wires onto a supporting transfer frame has been tested for wire placement accuracy with encouraging results. A Kapton sheet with etched parallel conductors was fabricated and will be evaluated in the test chamber as a cheaper alternative to the cathode wire plane usually found in large-area drift chambers.

Future plans include first fabricating a 0.5 m $\times$ 0.5 m stack of eight modules that will incorporate the electronic designs now under study. These modules will be carefully aligned and used in an accelerator beam to verify the positional resolution. At the same time, construction of prototype 2-m modules will be investigated.

Contacts: D. Bertsch, C. Fichtel, S. Hunter, and
D. Thompson
Code 662

Sponsor: Office of Space Science and Applications

Dr. David L. Bertsch is an astrophysicist with the Gamma Ray Astrophysics Branch at Goddard. Dr. Bertsch, who has been with Goddard for 18 years, holds a PhD degree from Washington University at St. Louis. His significant responsibilities have included work as Assistant Project Scientist on the Gamma Ray Observatory, Co-Investigator on the Energetic Gamma Ray Experiment Telescope, and Principal Investigator on the Solar Particle Intensity and Composition Experiment.

Dr. David Thompson is an astrophysicist with the Gamma Ray Astrophysics Branch of the Laboratory for High Energy Astrophysics. He is Co-Investigator on the Energetic Gamma Ray Experiment Telescope on the Gamma Ray Observatory. Dr. Thompson received a PhD degree from the University of Maryland, and he has been with Goddard for 14 years.

COSMIC-RAY ANTIPROTONS, POSITRONS, AND GAMMA RAYS FROM DARK MATTER ANNIHILATION

It is known from studies of the motion of stars in the outer regions of galaxies that there must be missing, nonluminous matter in the galaxies themselves which far outweighs their stellar mass. This mass appears to be in the form of halos of gravitating matter, which probably extend far beyond the visible stellar disks of galaxies and make up approximately 90% of the mass associated with galaxies. There are various reasons for believing that the dark matter is not ordinary matter made up of protons, neutrons, and electrons but may be in the form of black holes or exotic new particles predicted by theoretical high-energy physicists. Furthermore, many cosmologists and particle physicists would like to have even more dark matter around in order to close the universe gravitationally as predicted by inflationary cosmologies.

Since there is a plethora of possible cold dark matter candidates to choose from, astrophysicists must look for experimental tests to determine the nature of the dark matter. Among the most popular cold dark matter candidates are a group of neutral weakly interacting particles with a mass at least several times that of the proton, sometimes referred to as weakly interacting massive particles (WIMPs). Such WIMPs are predicted by supersymmetry theory, a theory that may play a crucial role in our understanding of the unification of all the known forces. The heavy weakly interacting particles predicted by supersymmetry theory are supersymmetric counterparts of known particles, such as photons, and postulated particles, such as the so-called Higgs bosons, which play a crucial role in unifying the electromagnetic and weak interactions. The supersymmetric partners of these particles are known as photinos and higgsinos. They are their own antiparticles, i.e., they can annihilate with others of their kind. When such particles annihilate, they produce particles such as cosmic-ray antiprotons, positrons, and gamma-rays. Since antiprotons and positrons are relatively rare in the cosmic radiation, such cosmic radiation with the appropriate spectral characteristics can be searched for as the signature of annihilating WIMPs. Two important characteristics of the antiproton signature are a high energy cutoff in the spectrum at an energy of about Mc^2, where M is the mass of the WIMP; and a peak in the energy spectrum at an energy of approximately 1 GeV/c^2, regardless of the mass of the WIMP. Interstellar antiprotons with this energy are degraded to lower energies in the 100–300 MeV/c^2 range by fighting their way upstream against the solar plasma wind in reaching the Earth. Antiprotons have been observed by balloon-borne detectors to be puzzlingly abundant in the cosmic radiation. Their abundance and spectral characteristics are different than would be expected if they were simply produced by collisions of ordinary cosmic-ray nuclei with atoms of interstellar gas.

As reported in *Physical Review Letters*, Floyd Stecker of the Laboratory for High Energy Astrophysics together with S. Rudaz, and T. Walsh, of the University of Minnesota have found that the observed cosmic-ray antiprotons have the spectral energy characteristics that match the signature of the annihilation of WIMPs having a mass about 15 times that of the proton. The best type of particle for producing the antiprotons is found to be a higgsino or heavy neutrino weighing 15 proton masses. Therefore, these particles may currently be our best candidate for galactic dark matter. Stecker and Rudaz have shown that the cosmic-ray positrons and gamma rays from dark matter annihilation should have a continuous spectrum with the characteristic cutoff energy of about 15 GeV/c^2, which may have been seen in the antiproton spectrum. However, it may be difficult to distinguish them from those expected to be produced in similar quantities by competing astrophysical processes such as cosmic-ray collisions. Their results will be published in the *Astrophysical Journal*. Future space science experiments such as the Gamma Ray Observatory and the proposed Astromag experiment should greatly increase the quality of the cosmic-ray and gamma-ray data. It is hoped that observations made by using such facilities will definitively settle the question of the nature of the dark matter.

Contact: Floyd W. Stecker
Code 665

Sponsor: Office of Space Science and Applications

Dr. Floyd Stecker specializes in theoretical high-energy astrophysics and cosmology. He holds a PhD degree from Harvard University. Dr. Stecker, who has been with Goddard for 20 years, is a recipient of the NASA Medal for Exceptional Scientific Achievement.

FOREFRONT X-RAY SPECTROSCOPY

The use of calorimetry as a means for carrying out high-resolution spectroscopy has several advantages over previously used methods that involve charge collection or diffraction effects. First, the ultimate energy resolution of the calorimeter is limited by thermodynamic (statistical) power fluctuations, which can be made to be

as small as a few electron volts. Second, a calorimeter has a high intrinsic quantum efficiency over most of the X-ray band (0.1–100 keV), making it especially useful in X-ray astronomy. Third, a calorimeter is sensitive to both ionizing and non-ionizing forms of radiation. This is crucial for measurements in particle and nuclear physics where recoil energies are relevant. By using techniques that are readily available for micro-machining and in achieving low temperatures, it is now possible to produce devices that have an energy resolution of ~ 20 eV; in principle it should be possible to reach an energy resolution of <10 eV.

The X-ray astronomy group at Goddard has pioneered calorimetry for use in X-ray astronomy. Following the realization that Si or Ge bolometer-type detectors employed for infrared observations could be used to detect single X-ray photons or other particles (Moseley, Mather, and McCammon, 1984), a program of development was started in 1982 at Goddard with the purpose of demonstrating the technique for X-ray spectroscopy, with the goal of designing an experiment for the Advanced X-ray Astrophysics Facility (AXAF) mission. The early results showed enough promise that a Phase B study for AXAF was awarded in 1984 to the Goddard group (S. Holt, Principal Investigator) and their collaborators at the University of Wisconsin (D. McCammon, Co-Principal Investigator). During the early portion of the study phase, it was recognized that there are some processes involved in the thermalization of X rays and the heat-sensing mechanism (thermistor) that reduce sensitivity and contribute additional noise, thus degrading the energy resolution. However, there has been steady progress toward obtaining an understanding of some of these processes that has resulted in a calorimeter with a resolution of ~ 17 eV.

The X-ray calorimeter works by measuring the amount of heat deposited in a small, low-heat-capacity mass. An ideal calorimeter consists of three basic components: an X-ray–absorbing substrate medium, a thermometer, and a thermal link between the absorber and a cold reservoir. For the heat capacity to be made low enough to detect a single X-ray photon as a heat pulse, the device must be as small as possible, typically about $0.5 \times 0.5 \times 0.1$ mm, and must be cooled to a temperature of ~ 0.1 °K. Silicon is an ideal material for use in microcalorimetry because it has a relatively low specific heat at low temperatures and can be easily processed with chemical techniques to form microstructures.

The thermometer is made by implanting boron and phosphorous into the Si with a dose that yields a resistivity very close to the metal-insulator transition, which produces a very high temperature sensitivity.

The thermal conductivity of the connecting link determines the speed of the detector. For a large thermal conductivity, the calorimeter will cool quickly after the absorption of a photon and require a larger bandwidth amplifier to determine a pulse height, whereas for small conductivities, the pulses will have long time constants that may degrade the spectral resolution for sources with high counting rates. In principle, however, the signal-to-noise ratio is independent of the value of the thermal conductivity.

An ideal calorimeter, therefore, would produce a purely exponential pulse in response to absorbing a quantum of energy and would have an energy resolution determined by the base temperature and the heat capacity of the substrate, the ion implant, and a contribution from the thermal link. We have found, however, that there are several non-ideal effects that can limit the energy resolution unless several detector parameters are optimally chosen.

First, we have found that if X rays are absorbed directly in Si, a large fraction of the energy ($\sim 25\%$) is not converted to heat (phonons) but is apparently trapped onto ionized impurities in the forbidden band-gap of Si (even the purest Si available has $\sim 10^{12}$ impurity ions per cubic centimeter). This situation can be improved considerably by absorbing the X-ray in a material that has a very narrow band-gap or essentially no gap at all, such as a semimetal. Using this approach, we have been able to convert nearly all ($>95\%$) of the photon energy into phonons.

Second, we have found that when a large bias voltage is applied to the thermistor implant, the effective temperature coefficient of resistance is greatly reduced. This so-called electric field effect is not fully understood quantitatively, but its effects can be reduced by using a thermal link with lower conductivity so that the detector can operate with less bias power.

Third, we have observed 1/f noise in many of our calorimeters. The magnitude of the noise power seems to scale inversely with the implant concentration density, and so we have produced thermistor geometries that preserve the temperature sensitivity while using a higher ion-implant concentration.

Previously, we were able to produce a detector with a resolution of ~ 35 eV, which was already several times better than the best nondispersive spectrometers. Using

a calorimeter that was designed to at least partially compensate for some of the above mentioned non-ideal effects, we recently obtained an energy resolution of ~17 eV (see figure). This resolution performance, when placed at the focus of AXAF, will already achieve many of the scientific goals in X-ray spectroscopy planned for the AXAF mission.

Whereas microcalorimeters have the ability to accurately measure small amounts of energy with low noise and high efficiency, and are thus well suited for use in X-ray astronomy, they prove valuable in other fields of research as well. One possible application is in an experiment to measure the rest mass of the neutrino. Neutrinos exist in great numbers, and if they possess a finite rest mass, their collective mass could dominate the dynamics of the universe. Since very few of the weakly interacting neutrinos will stop in a detector, a calorimetric scheme can be employed where one constructs the spectrum of the residual energy as the neutrinos escape from atoms undergoing beta decay. Previously, the spectrum was obtained by implanting tritium into a solid-state spectrometer and inferring the energy of the emitted electron by correcting for the energy lost by the electrons that leave the sample, estimating the nuclear recoil energy, and the amount of energy stored in excited final states. By implanting the beta-decaying atoms directly into a calorimeter, one can collect all of the energy except for that carried away by the neutrino, and the rest-mass sensitivity should be extendable down to the level of <10 eV.

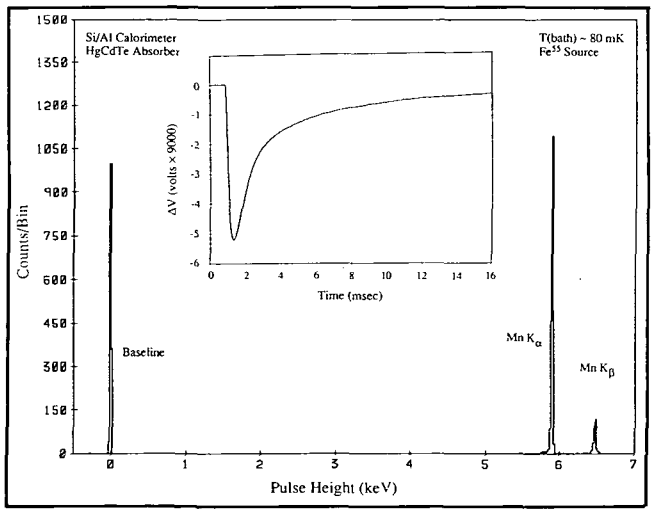

Spectrum of measured pulse heights from an Si calorimeter with an Al thermal link and an X-ray converter consisting of mercury-cadmium-telluride, which is a narrow-band-gap semiconductor. The two peaks at the right are from the 5.9 and 6.4 keV K_α and K_β X rays emitted by the decay of an Fe^{55} source. The width of the Mn peaks is 17 eV. The peak labeled "baseline" results from random samplings of the intervals between X rays and has a width equal to the total system noise. The inset shows the calorimeter response to a single X-ray photon.

In the realm of more exotic particles, experiments have been proposed to search for the weakly interacting massive particles that have been inferred from some particle theories that could make up some 90% of the mass of the universe. Experiments call for a kilogram mass of pure Si cooled to <0.1 °K and with many calorimeter devices attached to look for the infrequent signals expected from these particles.

There is also an increasing awareness of the importance of high-resolution microcalorimeters in nuclear physics. In nuclear processes that involve states that are weakly coupled to atomic electrons (thus having low rates) or that occur at low energy thresholds (<500 eV), it should be possible to look for weak X-ray signatures in a comparatively short amount of time and to measure line energies with less uncertainty due to recoil effects.

Thus, although the X-ray calorimeter was developed to dramatically increase our knowledge of the spectra of celestial X-ray sources, it may become an important new research tool in many other fields.

Contacts: Richard Kelley and Andrew Szymkowiak
Code 666

Sponsor: Office of Space Science and Applications

Dr. Richard Kelley works with the calorimeter X-ray spectrometer for the Advanced X-Ray Astrophysics Facility, as well as several other X-ray astronomy investigations being planned or developed in the Laboratory for High Energy Astrophysics. Dr. Kelley, who holds a PhD degree from the Massachusetts Institute of Technology, is interested in X-ray-emitting binary systems and the use of nondispersive X-ray spectrometers in astrophysics. He has been at Goddard for five years.

Dr. Andrew Szymkowiak, who has been with Goddard for 10 years, is working primarily on the development of the calorimeter for the Advanced X-ray Astrophysics Facility. He received a PhD degree in physics from the University of Maryland.

A HIGH-TECHNOLOGY SOUNDING ROCKET INSTRUMENT FOR X-RAY ASTRONOMY

The discovery on February 24, 1987, of the closest supernova to Earth in over 400 years (designated SN 1987a) has presented scientists the world over with a unique opportunity to observe the evolution of this spectacular celestial event.

The X-ray Astrophysics Branch has responded to this challenge with the rapid design and development of a high-technology sounding rocket payload to perform spectral measurement and accurate timing of X-ray emission from the supernova. The payload, 47.6 cm in diameter, 2.54 m long, and weighing 136 kg, will be launched by a Nike-Black Brant Rocket from Australia.

The central feature of this payload is a unique set of grazing incidence conical X-ray reflecting mirrors that were developed and built in-house at GSFC. The mirrors are fabricated from thin foils that allow the nesting of many foils to produce a large reflecting surface in a small volume (44 cm diameter). The primary and secondary reflector pairs each consist of 70 individual reflectors measuring 0.127 mm thick by 10.16 cm high. The mirrors have a total geometric area of 1050 cm^2, with 870 cm^2 of reflecting surface, and weigh 17 kg completely assembled. The individual reflectors are made from thin aluminum foil that has been overcoated with acrylic lacquer to enhance the surface smoothness, then vacuum deposited with gold to provide a reflecting surface for X rays in the 0.3- to 10-keV energy band.

At the focus of the mirror assembly, 2.1 m away, is a state-of-the-art Si(Li) solid-state detector. The detector has been segmented into five separate viewing areas to provide some spatial resolution. A central 4-mm-diameter pixel and four surrounding pixels give a total detecting area of 28.4 mm^2, with a field of view through the mirror assembly totaling 40 arc minutes. The noise-limited resolution of the central pixel, where most of the photons are collected, is 90 eV. The resolution in the important iron region of the spectrum, at 6 keV, is 150 eV full width half maximum (FWHM).

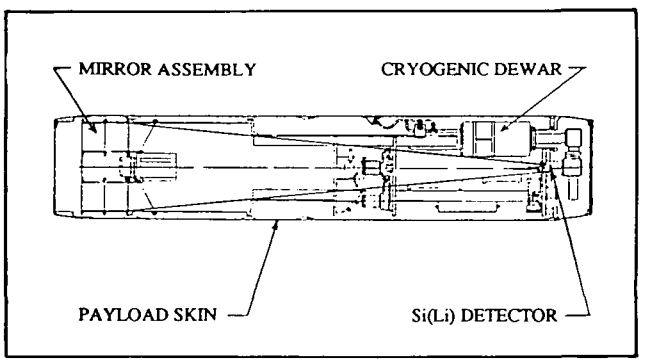

Rocket Payload Assembly.

In order to operate at such a low noise level, the Si(Li) detector must be kept near 100°K. To accomplish this, we have designed and built, at Goddard, a liquid nitrogen dewar system that will provide 2 hours of cooling capacity. The dewar, measuring 34 × 17 cm and weighing 10 kg, is vacuum jacketed and contains a unique interior baffle system to prevent sloshing of the liquid nitrogen.

Data from the payload are telemetered to the ground in real time, at 200 kbits/s. The telemetry stream includes spectral data from all five pixels, along with housekeeping data and event timing. Absolute timing of X-ray event arrival to within 50 μs is obtained by updating the onboard crystal oscillator with absolute time information obtained from signals received from orbiting satellites. This is believed to be the first time that direct satellite time transmission has been used for synchronizing a rocket payload telemetry clock. This absolute timing of X-ray data will allow other scientists to correlate measurements in different portions of the spectrum (e.g., ultraviolet, visible, and radio).

The rocket payload is scheduled for integration at the Wallops Flight Facility in late November so that it is ready for a January 1988 launch. Launch will be held in abeyance until orbiting satellites herald the awaited arrival of sufficiently intense X rays at the Earth.

Contact: Charles Glasser
Code 666

Sponsor: Office of Space Science and Applications

Mr. Charles Glasser is X-ray Experiments Manager of AXAF, BBXRT, SXO, SXS, and XTE. Mr. Glasser, who received a BS degree in electrical engineering from the University of Maryland, has been with Goddard for 23 years. He is a recipient of the NASA Exceptional Service Medal and the GSFC Exceptional Performance Award.

A HILLOCK MODEL FOR FACULAE

Faculae, Latin for torches, describe the area around sunspots marked by bright clouds. The brighter regions observed in monochromatic light are chromospheric

features, associated with faculae, and are called flocculi or plage. When the faculae are particularly dense near a sunspot and form a crinkle pattern, they are sometimes referred to as filigree. Together with sunspots, they are the only feature to affect the Sun's continuum energy for significant time periods. Thus they are very important in studies of the solar energy output.

The conventional astronomical wisdom is that brightness is associated with deeper solar layers. With this in mind, the classical facular models open a well that allows the deep solar layers to appear through a hole formed by the magnetic field. This geometry was considered common to both sunspots and faculae, since both features are associated with strong magnetic fields. In this view, sunspots appear most prominently at disk center where the dark bottom of the well is most visible, and faculae appear bright off disk center by augmenting the amount of hot wall seen when faculae are viewed obliquely. A fundamental problem with these models is the low facular contrasts observed near disk center. The angular emission of a radiating object is related very closely to the shape of that object. With both spots and faculae having the same well geometry, most models provide the greatest contrast at disk center. Only through careful adjustment of both heating and cooling parameters could well models obtain facular contrasts near zero at disk center. Importantly, in the well geometry, facular contrasts still tend toward zero near the limb, contrary to most facular observations. Thus the observations of faculae, showing opposite angular emission behavior to that of sunspots, suggest an opposite geometrical shape.

Thus to model faculae, we have examined a conical hillock geometry. This geometry is created by the expansion of material into the solar atmosphere. This expansion occurs through the process geophysicists refer to as isostasy, namely, buoyancy. Here it is associated with dynamical heating by an upwelling flow in vertical fibril flux tubes in the Sun's convection zone. Using the hillock geometry and radiative transfer theory, we have calculated the contrast for a hillock geometry. The figure shows the hillock model contrast agreeing closely with the observed facular contrast curves at various wavelengths. A small temperature enhancement in the hillock surface can result in the small vertical displacement of the observed curves above the hillock model curves. The well model contrast curves display an entirely different shape, roughly parabolic with a peak contrast near $\mu = 0.5$ and a near-zero contrast at the limb. Thus the contrast modeling appears to support the hillock geometry for faculae. We estimate their height to be roughly 100 km.

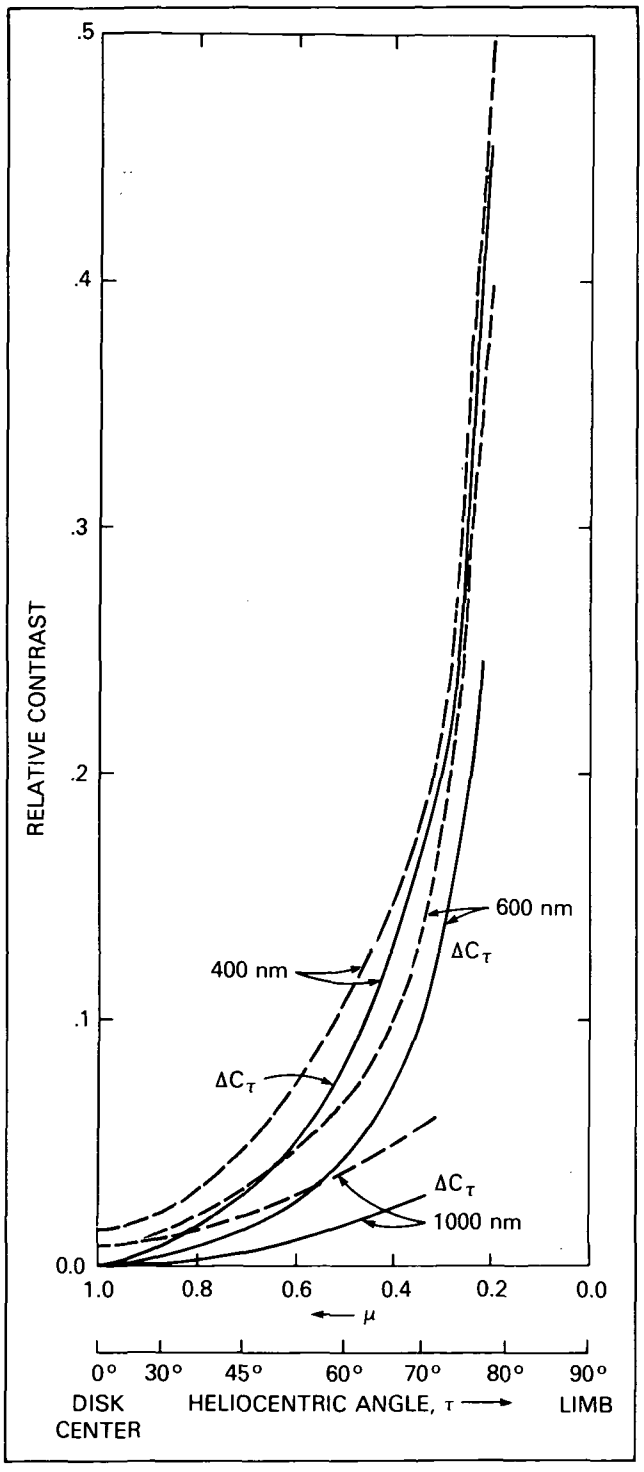

Facular contrast, ΔC_τ, for three different continuum wavelengths (red lines). Hillock model curves (black lines) agree closely. The best well model curves show an entirely different shape—parabolic with near-zero contrast values at 0° and 90°, unlike observed faculae.

This hillock model supports the view that faculae are an opposite photospheric feature to sunspots. In particular, aside from their opposite radiating characteristics, they shed the excess energy that is suppressed from reaching the sunspot umbra. This helps to explain the rough energy balance between sunspots and faculae, which has been observed in the solar constant observations from the Active Cavity Radiometer experiment on the Solar Maximum Mission.

Contacts: K. Schatten, E. Maier, and H. Mayr
Codes 610 and 614

Sponsor: Office of Space Science and Applications

Dr. Kenneth Schatten, who holds a PhD degree from the University of California at Berkeley, is a solar physicist with the Solar Disk Sextant project. Dr. Schatten has been with Goddard since 1969 and has received several awards for his scientific achievements.

Dr. Eugene Maier is a space scientist in the Solar Radiation Office of the Laboratory for Atmospheres. Dr. Maier, who holds a PhD degree from Carnegie-Mellon University, has been engaged in a variety of research topics since joining Goddard in 1962.

Dr. Hans Mayr is an atmospheric scientist with the Dynamics Explorer Pioneer Venus project. Dr. Mayr, who holds a DPhil from the University of Graz, has 19 years of experience with Goddard.

IMAGING SOLAR FLARES IN HARD X RAYS AND GAMMA RAYS FROM BALLOON-BORNE PLATFORMS

The solar activity cycle that is expected to peak in 1991 has already begun to produce flares. These events are relatively small and infrequent, as is usual during intervals between maxima in the Sun's 11-year cycle, but they serve as reminders of the opportunities soon to be available. Opportunities refers to the new technology now ready to address the outstanding questions in high-energy solar physics and the rich variety of high-energy phenomena to be observed. Major advances in the spatial and spectral resolutions of instrumentation required for high-energy solar physics have been achieved since the previous solar maximum. Now, for the first time, it is possible to observe processes associated with the fundamental acceleration of energetic particles on their intrinsic spatial, spectral, and temporal scales.

Vigorous efforts are under way for a coordinated, multiwavelength campaign during the next solar maximum. A prime thrust of these efforts for MAX '91 is to realize the potential of the new technology in imaging and spectroscopy for high-energy solar-flare research. The success of these efforts is challenged, however, by NASA's serious deficit in flight opportunities and the brief time interval in which development must be accomplished. Flexible and innovative approaches are required. High-altitude, long-duration, scientific ballooning offers just such an approach and also provides the heavy-lift capability that is needed for the high-energy payloads. Goddard is leading the team of investigators who are working toward the development of a hard X-ray and gamma-ray imaging instrument for balloon-flight applications. The instrument is known as the Gamma-Ray Imaging Device, or GRID, on a balloon.

Hard X rays and gamma rays cannot be reflected or focused by lenses or mirrors. Even grazing incidence reflection, used very effectively in soft X-ray astronomy, is impossible in the photon-energy domain above a few keV. What is required is some variation on a pinhole camera or collimator, consisting of material opaque to this radiation, interrupted with transparent apertures. The mask or collimator casts a shadow on a position-sensitive detector. The GRID telescope is based on a Fourier-transform imaging technique employing an array of subcollimators. One Fourier component of the angular distribution being imaged is measured with each subcollimator and its associated position-sensitive detector module. Each subcollimator consists of a pair of grids, one at the top and the other at the bottom of the telescope; each grid is formed from a uniformly spaced distribution of slits and slats. The array includes subcollimators with a variety of slit/slat orientations and a range of slit/slat spacings corresponding to the range of angular dimensions to be measured. In any subcollimator, the number of slits and slats in the top grid differs by one from the number of slits and slats in the corresponding bottom grid. The resulting X-ray transmission for each subcollimator forms a Moiré pattern with a single intensity contrast cycle extending over the width of the subcollimator, as illustrated in Figure 1.

Whereas fine slit/slat spacings are required for fine angular resolution, only modest spatial resolution (approximately 20% the width of any subcollimator) is required of the position-sensitive detector. This is particularly important because it is extremely difficult to make hard X-ray and gamma-ray detectors with spatial resolution much better than 1 cm. Displacements of one grid relative to the other by only a slit width cause shifts

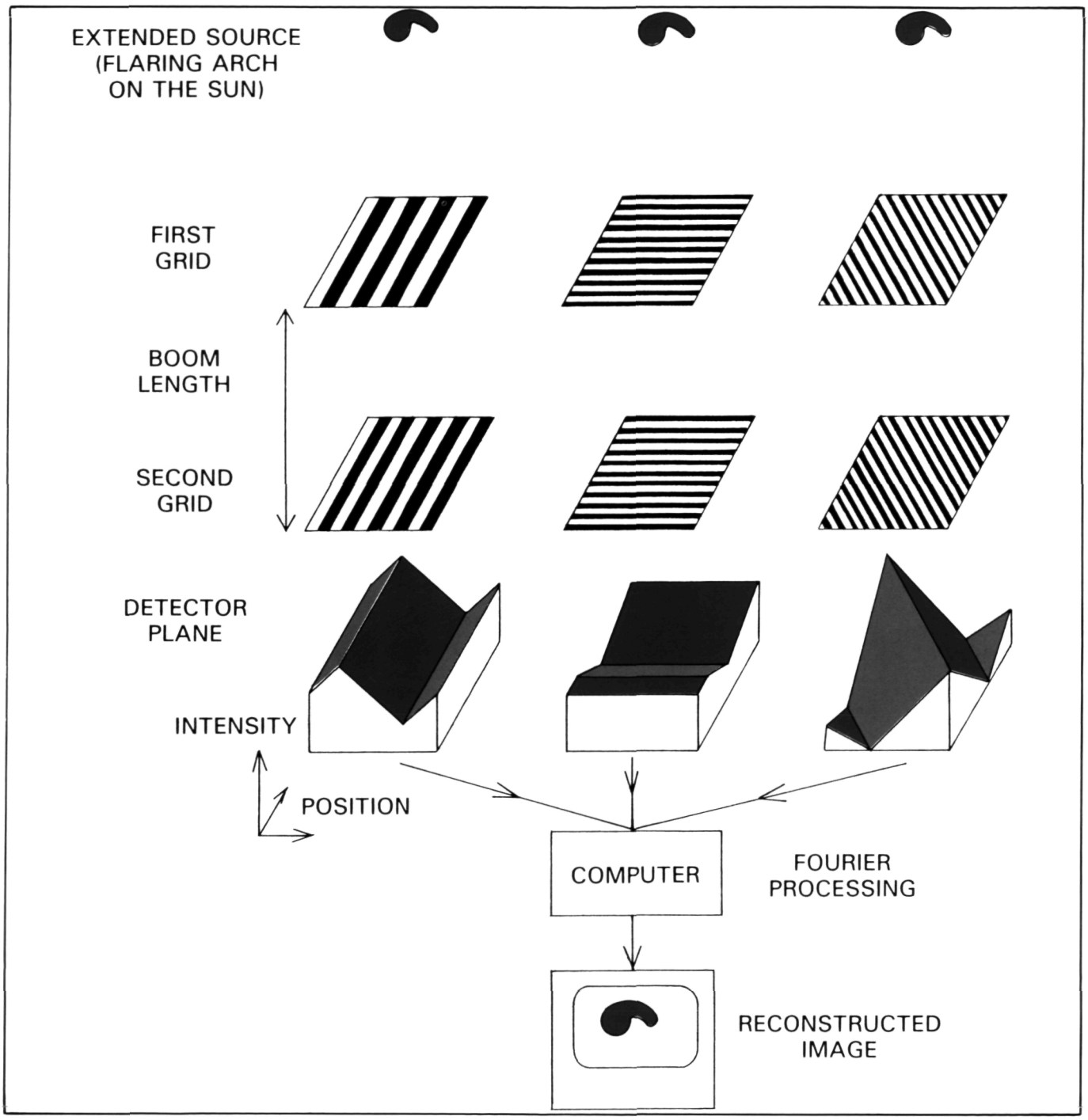

Figure 1. Schematic representation of the Fourier-transform imaging technique. (Courtesy of G. Hurford)

in the Moiré pattern of half a subcollimator width. This amplifier effect is readily demonstrated by following the suggestions accompanying Figure 2.

All of the information characterizing the angular distribution of a source is contained in the amplitudes of the intensity contrasts of the Moiré patterns and the spatial positions of their maxima. These are the amplitudes and phases of specific, well-chosen Fourier components of the X-ray image. This information is the exact mathematical analog of that provided by a pair of radio antennas in a radio interferometer. Because of this direct, one-to-one

correspondence, the analytic tools that have been developed and refined for radio interferometry can be used for analysis of the hard X-ray and gamma-ray observations obtained with GRID.

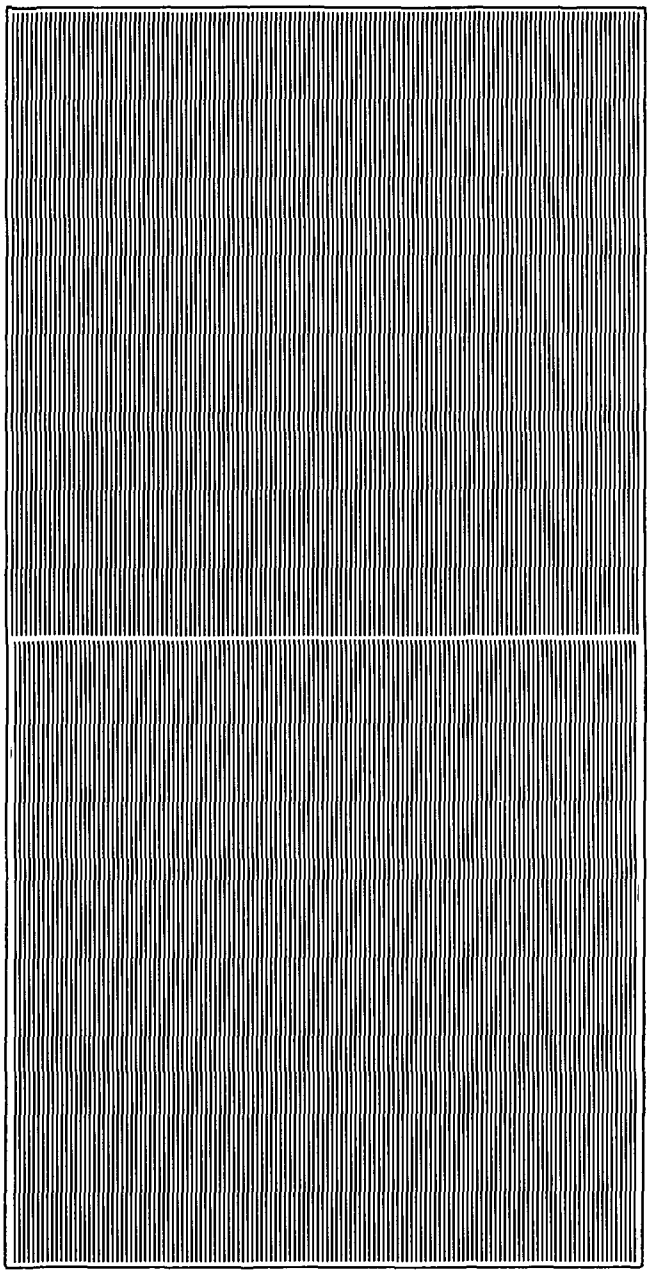

Figure 2. Schematic representation of a pair of grids. The reader is invited to make a copy of each grid on a transparency and then to superpose the two transparencies. The sensitivity of the Moiré pattern to small shifts of one grid relative to the other illustrates the amplifier effect that obviates the need for detectors with high spatial resolution.

GRID on a balloon is shown schematically in Figure 3. The aspect system, indicated by small circles in the telescope endplates, is, in reality, the Solar Disk Sextant (SDS), a sensitive instrument for measuring the Sun's diameter on very short time scales. For GRID, it provides the unique advantage of enabling a tradeoff of pointing stability requirements for fast data rates and *a posteriori* knowledge of precise pointing. The characteristics and capabilities of GRID are summarized in the table.

The investigative team members represent a number of institutions in addition to the Goddard Space Flight Center and bring their considerable expertise to this effort. These include the following institutions: the Marshall Space Flight Center, responsible for the balloon gondola and pointing system; Caltech, providing image-reconstruction analysis capability and expertise in position-sensitive detectors; Yale, responsible for development of the SDS; Delft University in The Netherlands, pioneering the development of new technology for fabrication of fine subcollimator grids; UCSD, liaison with the Pinhole/Occulter Facility Science Working Group that spawned the concepts on which GRID is based; the Naval Research Laboratory, providing design/performance analysis and contributing to grid technology; and the Los Alamos National Laboratory, providing expertise in image reconstruction for X-ray imagers and investigating grid fabrication technology. Goddard has fabricated the first prototype subcollimator grids and is currently constructing a test model of the position-sensitive detector.

MAX '91 holds great promise. New technology is ready to enable great advances in high-energy solar physics, and the GRID team is prepared to supply the effort necessary to realize these potentials.

Characteristics and Capabilities of GRID	
Detector type	Scintillation counters
Detector area	480 cm^2
Energy range	20 keV to 1 MeV
Subcollimator material	Tungsten and tantalum
Number of subcollimators	32
Sensitivity	~100 flares per week
Angular resolution	1 arc second
Field of view	Whole Sun
Pointing accuracy	3 arc minutes
Pointing stability	0.2 arc second per 10 milliseconds
Expected flight duration	15 days

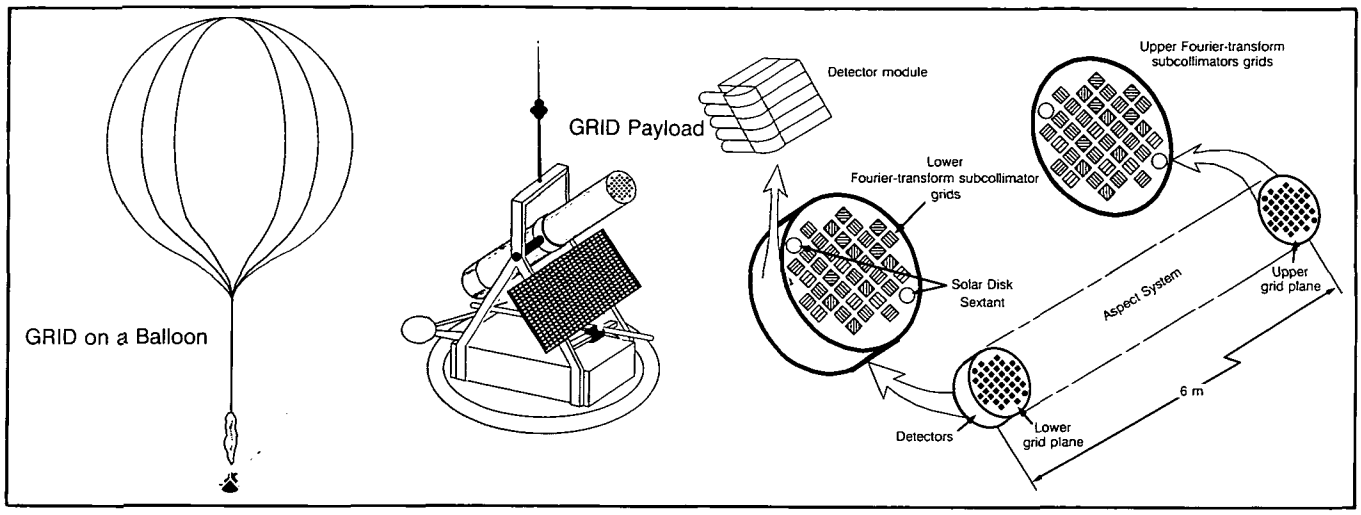

Figure 3. Schematic representation of GRID showing the telescope integrated into a balloon payload and an exploded view showing the end plates that hold the grid subcollimator pairs and the Solar Disk Sextant, and the canister housing the detector modules.

Contact: Carol Jo Crannell
Code 682

Sponsor: Office of Space Science and Applications

Dr. Carol Jo Crannell, who holds a PhD degree from Stanford University, is an astrophysicist with 18 years of experience with Goddard. Dr. Crannell is responsible for the Solar Physics Balloon Program of the Laboratory for Astronomy and Solar Physics. She serves in a number of elected and appointed positions of the American Astronomical Society and American Physical Society, and she is a popular speaker who has received Goddard's EEO and Silver Tongue awards.

PLANETARY AND INTERPLANETARY

THERMAL NOISE SPECTROSCOPY

During the encounter of the Interplanetary Cometary Explorer (ICE, formerly ISEE-3) with Comet Giacobini-Zinner, the radio astronomy team applied a novel technique to use radio measurements to obtain important plasma parameters in the cometary tail. The results in Figure 1 show simultaneous measurements of cometary plasma temperature and density with a time resolution of 18 seconds corresponding to a structure of 380 km. For some points, a 1.5-second time resolution was obtained.

These new results were made possible by the application of a technique not envisioned when the ISEE-3 radio astronomy experiment was designed. We call this new technique thermal noise spectroscopy because it utilizes the spectrum of the electric field fluctuations in a warm plasma to determine major bulk parameters of the plasma.

Thermal noise spectroscopy was developed by our team to understand the origin of the low-frequency spectral component observed by our instrument in the solar wind. Figure 2 shows a typical spectrum obtained by this instrument in the solar wind during times when solar radio

ORIGINAL PAGE IS
OF POOR QUALITY

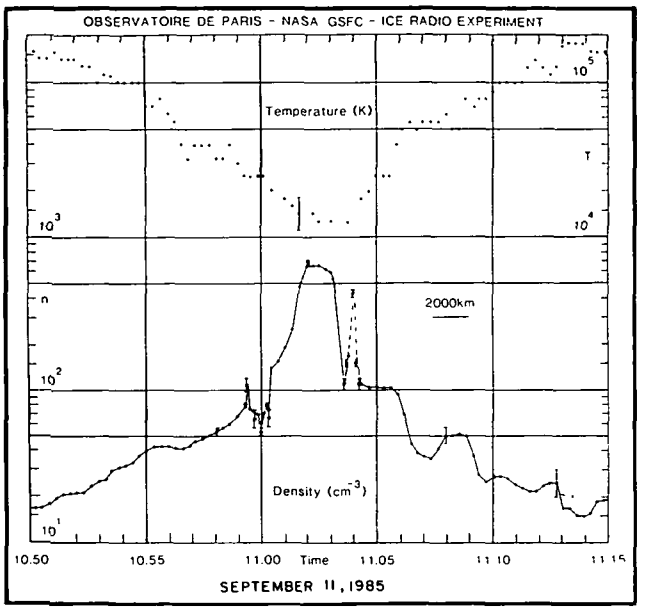

Figure 1. Plasma temperature (top) and density (bottom) along comet tail.

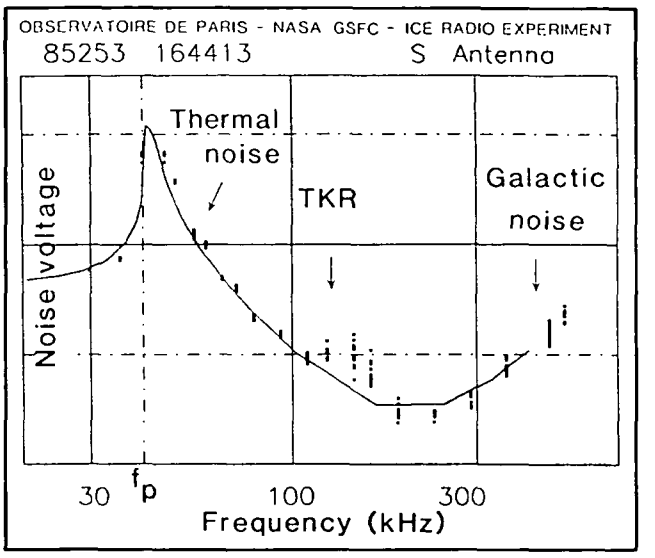

Figure 2. Noise spectrum recorded on ICE.

emission is not present. The noise component, terrestrial kilometric radiation (TKR), around 150 kHz is natural sporadic radiation from the auroral regions of Earth. Radio noise from the galaxy is visible above several hundred kilohertz. Both of these noise sources produce electromagnetic waves; using the information in spin modulation resulting from the spacecraft rotation (after an analysis first developed by us for IMP-6), we can measure the radiation arrival directions and identify its origin. At frequencies below several hundred kilohertz, there is a rising noise component that we have shown, after extensive analysis, is due to *in situ* fluctuating electric fields caused by the motion of the plasma electrons in the solar wind.

For a plasma in thermal equilibrium at temperature T, the noise spectrum voltage squared is given by the familiar Nyquest expression, 4KTR, where K is Boltzman's constant and R is the radiation resistance of the antenna in the plasma mode. This resistance is much larger than the well-known resistance for electromagnetic waves, and it depends on both the plasma temperature T and density n. For space plasmas that are generally not in thermal equilibrium, the result can be generalized. We have studied cases where the plasma electron population can be represented by one hot and one cold component, and we have shown that we can determine the four parameters of the plasma from the radio thermal noise measurements.

The importance of the thermal noise spectroscopy technique lies in its accuracy, time resolution, and insensitivity to spacecraft potential. With a stable well-calibrated receiver, radio measurements in the amplitude and frequency domains are inherently very accurate. In a properly designed instrument, the radio thermal noise spectrum can be determined in a fraction of a second, leading to the accurate determination of plasma parameters with very high time resolution.

Instruments optimized for these studies have been proposed by members of the ICE team for the WIND spacecraft and for the Cometary Rendezvous and Flyby mission.

The radio astronomy experiment on ICE is a joint project of the Paris Observatory and GSFC, and members of both teams participated in this analysis.

Contact: Joseph Fainberg
Code 622

Sponsor: Office of Space Science and Applications

Dr. Joseph Fainberg, who holds a PhD degree from the Johns Hopkins University, has been at Goddard for over 20 years. He has been working in low-frequency radio astronomy using space platforms and has participated in the design of spacecraft experiments, in the development of new data analysis techniques, and in the scientific analysis of returned data.

ORDINARY MODE RADIO EMISSION FROM URANUS

On January 24, 1986, during the inbound trajectory to Uranus, the Planetary Radio Astronomy instrument onboard Voyager 2 detected left-hand polarized emission for several hours at radio frequencies near 200 KHz. Unlike the dominant radio emission observed on the nightside of the planet, only a single episode of this inbound emission was seen, and the emission was observed to be extremely weak. Generating less than 500 kW, it is probably the weakest freely propagating planetary radio emission thus far observed by Voyager.

Goddard scientists have analyzed this emission component and have associated it with the planet's north (dayside) magnetic pole, where the field lines point approximately in the direction of the spacecraft when the emission is observed. The scientists have concluded that direct wave generation in the magnetoionic ordinary mode is most likely. This emission mode is consistent with the relatively high electron densities measured in this region if the generation mechanism is via the electron cyclotron maser. This mechanism is currently the favored theory for the generation of the Earth's auroral kilometer-wave radiation. Furthermore, the Uranus source location is consistent with a region magnetically conjugate to the dominant nightside source, which is located in the vicinity of the south magnetic pole. The situation at Uranus is nicely symmetric, then, from a radio standpoint, with extraordinary mode emission beamed from the nightside pole and ordinary mode emission from the dayside pole.

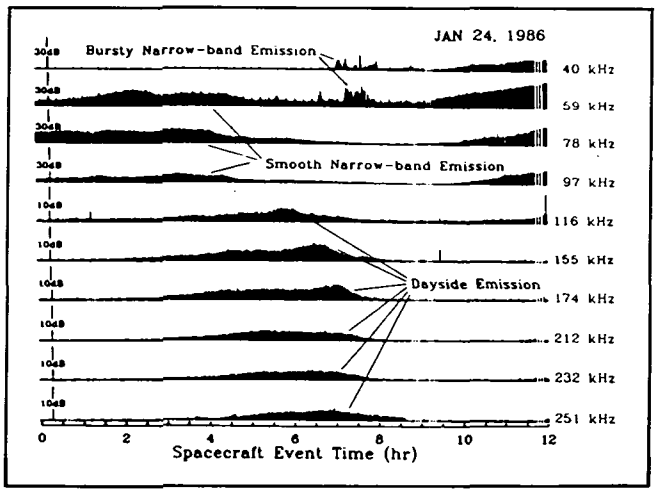

Intensity versus time plot of emission detected by Voyager during the first 12 hours on the day of closest approach to Uranus. The ordinary mode component from Uranus is identified here as the dayside emission.

Contacts: Michael D. Desch and M. L. Kaiser
Code 695

Sponsor: Office of Space Science and Applications

Dr. Michael Desch is involved in the analysis of Voyager spacecraft radio astronomy data of Jupiter, Saturn, and Uranus. Dr. Desch received a PhD degree in astronomy from the University of Florida, and he has been with Goddard for seven years.

Mr. M. L. Kaiser, who specializes in radio emissions of the planets, is ISTP Project Scientist for Data Systems. He holds an MS degree in astronomy from the University of Maryland. In his 18 years at Goddard, Mr. Kaiser has received an Exceptional Scientific Achievement Award and an award for saving Goddard over $1,000,000 in costs.

INTERNAL HEAT FLUX OF URANUS FROM VOYAGER MEASUREMENTS

One of the few remote sensing observations that provides information about the interior of the giant planets is that of the escaping internal energy and its distribution with latitude. Determination of this quantity requires measurement of both the total thermal emission and the total reflected sunlight; the escaping internal energy flux is the difference between the total thermal flux and the total absorbed solar flux. Since the amount of reflected light varies strongly with direction relative to that of incoming sunlight, measurements of reflected sunlight must be obtained at many different phase angles of the planet.

The Infrared Interferometer Spectrometer (IRIS) on the Voyager 2 spacecraft simultaneously observed the thermal and visible radiation from Uranus. As the spacecraft passed the planet, measurements at low and high phase angles were possible. Measurements made at great distances by the camera system on Voyager 1 helped to fill the gaps. From these measurements, it is found that Uranus reflects between 27 and 34 percent of the incident sunlight; from thermal measurements, the effective radiating temperature of the planet is 59.1 $\pm$ 0.3°K, showing very little variation with latitude.

A comparison of results for the planets visited by Voyager is shown in the table. Each is only moderately reflective. The Bond albedos (fraction of incident sunlight reflected)

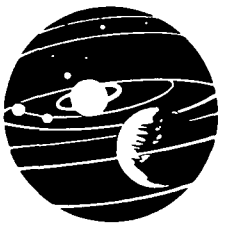

indicate that two-thirds or more of the incident solar energy is absorbed by the planets. The effective temperature (the equivalent temperature the planet assumes in order to radiate both the absorbed solar energy and the energy transported out from the interior) decreases with distance from the Sun, since the radiated flux of each planet is dominated by the absorbed sunlight. The energy balance (the ratio of total emitted to total absorbed energy) shows less regularity. Its behavior depends mainly on two factors: the planetary mass and whether separation of helium and hydrogen has begun on the outer portions of the planet. This separation can occur at intermediate pressures and temperatures, when helium becomes insoluble in molecular hydrogen, and forms drops that descend toward the core, giving up potential energy and leaving a depleted outer envelope. The helium mass fraction in the observable atmosphere, as determined from combined IRIS and radio occultation data, is shown in the last column of the table. For the Sun (and, by assumption, the overall composition of each of the outer planets), the helium mass fraction is ~0.23.

The large energy balance excess of massive Jupiter is due primarily to radiation of primordial accretional energy; a small contribution due to the early stages of helium separation may also be present. Saturn, three times less massive than Jupiter, has lost nearly all of its primordial heat; helium separation has advanced significantly, which provides its relatively large energy balance excess. Six times less massive than Saturn, Uranus has little or no radiative excess. It has long since lost its accretional energy, and separation of helium has not measurably advanced, due in part to a core structure that severely limits the region where immiscibility can occur.

An additional curiosity about these planets is that they all radiate their energy rather uniformly at all latitudes, even though the annually averaged absorption of sunlight has strong latitudinal dependence. For Jupiter, the equator receives substantially more solar input than the poles, whereas, due to its extreme axial tilt, the situation is reversed on Uranus. Present dynamical models suggest that if the energy balance exceeds ~1.27, then deep convection will be strong enough to distribute the absorbed solar energy uniformly with latitude. The small energy balance of Uranus may not permit this mechanism to work, so that very efficient transport of energy toward the equator apparently occurs in relatively higher parts of the atmosphere, although little cloud activity is seen.

Neptune's mass is similar to that of Uranus. However, ground-based measurements show that Neptune's stratosphere is warmer, its clouds are more prominent, and its energy balance excess is substantially greater than that of Uranus. The Voyager 2 encounter on August 25, 1989, will provide a definitive look at this puzzling fraternal twin of Uranus.

Contact: John Pearl
Code 693

Sponsor: Office of Space Science and Applications

Dr. John Pearl, who earned a PhD degree in physics from the University of Michigan, is Co-Investigator for the Voyager Infrared Spectrometer Experiment. Dr. Pearl has been with Goddard for 17 years and has received the NASA Exceptional Scientific Achievement Medal.

CONVECTION IN THE DEEP ATMOSPHERE OF URANUS

Within the atmospheres of the outer planets, in deep layers where the infrared opacity is too great for efficient radiative transfer, vertical heat transport occurs as the result of convective motion. This heat flux must exist because of the presence of internal energy sources and the deposition of solar energy at deep levels. Within the

Comparison Among the Outer Planets

Planet	Bond Albedo	Effective Temperature (°K)	Energy Balance	He Mass Fraction
Jupiter	0.34 ± 0.03	124.4 ± 0.3	1.67 ± 0.09	0.18 ± 0.04
Saturn	0.34 ± 0.03	95.0 ± 0.4	1.78 ± 0.09	0.06 ± 0.05
Uranus	0.31 ± 0.03	59.1 ± 0.3	<1.12	0.26 ± 0.08

convective region, the vertical temperature gradient is expected to assume a value approximately equal to what it would have if fluid parcels were displaced adiabatically. Thus, from measurements of the vertical temperature profile, it should be possible to establish the approximate pressure level where the convective zone begins.

The adiabatic temperature gradient is inversely proportional to the specific heat of the predominantly molecular hydrogen atmospheres of the outer planets. The appropriate value of the specific heat depends on the degree to which thermodynamic equilibrium is achieved between the ortho (parallel proton spins) and para (anti-parallel proton spins) states of molecular hydrogen. For pure hydrogen, the equilibration time can be as long as 10^9 seconds. If the time scale for the motion is sufficiently slow, then equilibration occurs, and the specific heat is relatively large, yielding a small equilibrium adiabatic temperature gradient. If, on the other hand, the motion is rapid, little equilibration will occur, resulting in a smaller specific heat and larger adiabatic gradient. The application of conventional mixing length theory to buoyancy convection in hydrogen atmospheres predicts a slow overturning with a vertical scale approximately equal to a pressure scale height. The temperature gradient should lie close to the equilibrium value, and the hydrogen ortho-para ratio should be approximately the thermodynamic equilibrium value at the local temperature at each level in the atmosphere. These were the conditions expected for the convective region of the atmosphere of Uranus; Voyager observations have provided a different picture, however.

The infrared spectrometer (IRIS) carried on the Voyager spacecraft obtained measurements of Uranus within the 200 to 400 cm^{-1} spectral region where the atmospheric opacity is dominated by a pressure-induced hydrogen absorption line. From these measurements it was possible to infer both the hydrogen ortho-para ratio and the vertical temperature profile in the upper troposphere. The ortho-para ratio was found to be near the equilibrium value as predicted, but the temperature gradient in the deeper levels substantially exceeded the equilibrium value as shown in the figure. The Voyager radio occultation measurements indicated that the equilibrium adiabatic gradient is exceeded at even deeper levels. The steep temperature gradient suggests that the true adiabatic gradient must result from a specific heat that is smaller than the equilibrium value, indicating that little or no ortho-para equilibration occurs during convective overturning. To reconcile the observed temperature gradient with the observed equilibrium ortho-para ratio, it is necessary to abandon the conventional model of overturning scales

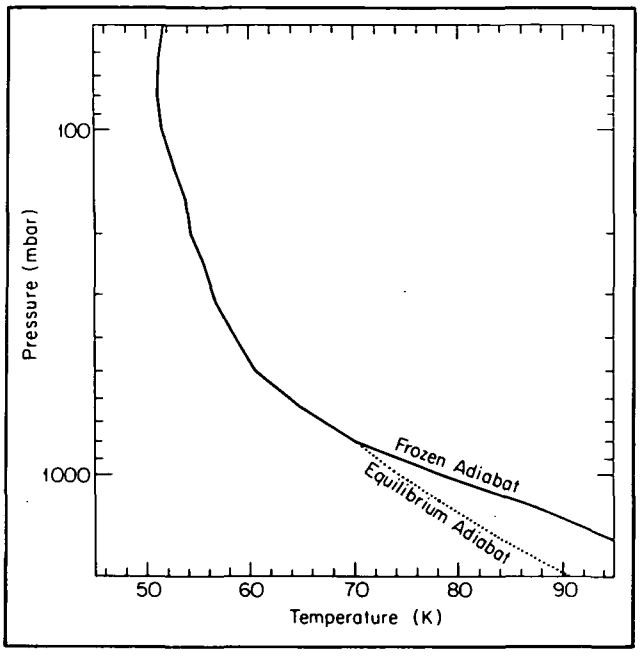

Temperature versus pressure level in the atmosphere of Uranus as determined from Voyager IRIS measurements. The broken curve shows the anticipated equilibrium adiabatic gradient. The measurements, indicated by the solid curve, follow instead an adiabatic gradient that occurs when convective overturning is rapid compared to the hydrogen ortho-para equilibration rate, and the hydrogen ortho-para ratio remains frozen.

comparable to the pressure scale height. Instead, overturning must occur rapidly within layers that are very thin compared with a scale height. In such a case, the overturning is sufficiently rapid to prevent significant ortho-para equilibration from occurring, resulting in a small specific heat and a large temperature gradient. However, if the residence time of the hydrogen in each layer is sufficiently long, the ortho-para ratio will be near the equilibrium value corresponding to the mean temperature within the layer in agreement with Voyager measurements.

The conclusion that convection is occurring in very thin layers represents a major departure from the conventional mixing length picture of slow overturning in layers approximately a scale height thick. It is possible that this situation exists in the upper convective regions of all four outer planets; however, of the three planets thus far encountered by Voyager, only Uranus is sufficiently cold so that an easily observable difference among the possible adiabatic gradients exists. The forthcoming Voyager

encounter with Neptune should provide another example of a cold atmosphere; comparisons with Uranus should be particularly interesting since the internal heat source and hence the convective flux are believed to be substantially larger on Neptune than Uranus.

Contact: B. J. Conrath
Code 693

Sponsor: Office of Space Science and Applications

Dr. Barney Conrath, a planetary astronomer, is the Principal Investigator for the Voyager Infrared Spectroscopy Experiment. The author, who holds a PhD degree from the University of New Hampshire, is interested in the structure and dynamics of planetary atmospheres. Dr. Conrath, a recipient of the NASA Medal for Exceptional Scientific Achievement, has been with Goddard for 27 years.

URANUS' CLOCK-LIKE RADIO EMISSIONS: UNIQUE PLANETARY MAGNETOSPHERE-IONOSPHERE-ATMOSPHERE INTERACTION

The existence of Uranian radio emissions has been known since the initial detection of the emissions by Voyager 2 just before encounter. After the Uranus encounter, Voyager 2 observations by the Planetary Radio Astronomy team have shown the dominant emissions to be located on the nightside of Uranus. More recently, two possible source regions have been identified: one for the smooth component of the emissions on closed field lines and one for the bursty component on open field lines.

Analysis of Voyager 2 observations has limited the nightside source region of the smooth emission component to a relatively small high magnetic latitude zone near the south pole centered at L $\approx$ 12 in a region containing mostly closed field lines.

From the location of the source field lines of the smooth nightside component of Uranus Kilometric Radiation (UKR), the most likely free energy source is the outer radiation belts. As the terminator sweeps over the magnetic north polar region (see Figure 1), precipitation of electrons produced by solar heating of the upper atmosphere and consequent submergence of the electron mirror points deeper in the atmosphere will create a back-scattered electron distribution with an enhanced population at large pitch angles. This distribution will propagate to the conjugate magnetic south pole of Uranus where the converging magnetic field lines will produce a mirroring electron distribution moving upward from the south pole that will drive a cyclotron maser instability. The upper frequency limit to the UKR emissions corresponds closely to the electron gyrofrequency of the mirror point of the weaker northern pole and is consistent with a back-scattered electron population originating from precipitation near the northern pole and hence mirroring at higher altitudes at the conjugate point in the southern magnetic hemisphere. The rise in emission intensity is shown to scale directly with the terminator's speed across the northern pole; the smooth emissions result from sunrise over the northern pole and collision-induced precipitation. Strong radio emissions are limited to the continually dark south pole, since only there is the electron plasma frequency to gyrofrequency ratio sufficiently small. The clock-like radio emission (see Figure 2) is a direct consequence of the terminator's control of the emission process. Hence, solar-driven upper atmospheric tides underlie the Uranian radio clock. Since the radiation belt population is most likely only weakly dependent on solar wind conditions, strong solar wind control of smooth UKR is not expected.

Contacts: Steven A. Curtis, Michael D. Desch, and Michael L. Kaiser
Code 695

Sponsor: NASA Program in Planetary Atmospheres Research

Dr. Steven Curtis, who holds a PhD degree from the University of Maryland, is a space plasma physicist with the Laboratory for Extraterrestrial Physics. He is particularly interested in the coupling of planetary atmospheres and magnetospheres. Dr. Curtis has 19 years of experience at Goddard, and he received an Exceptional Achievement Award for the correct prediction of Uranus' nonthermal radio emissions.

Dr. Michael Desch is involved in the analysis of Voyager spacecraft radio astronomy data of Jupiter, Saturn, and Uranus. Dr. Desch received a PhD degree in astronomy from the University of Florida, and he has been with Goddard for seven years.

Mr. M. L. Kaiser, who specializes in radio emissions of the planets, is ISTP Project Scientist for Data Systems. He holds an MS degree in astronomy from the University of Maryland. In his 18 years at Goddard, Mr. Kaiser has received an Exceptional Scientific Achievement Award and an award for saving Goddard over $1,000,000 in costs.

ORIGINAL PAGE IS
OF POOR QUALITY

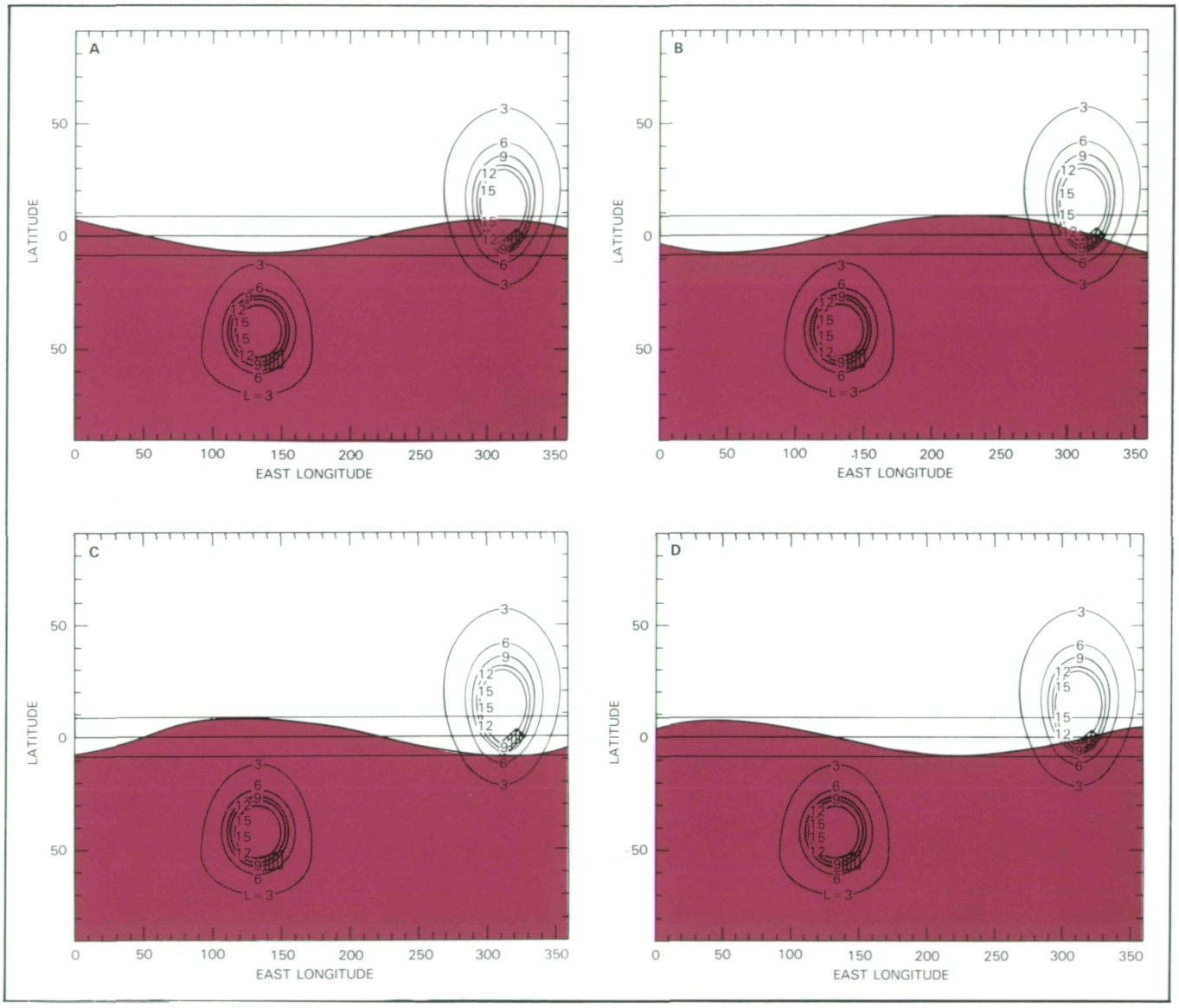

Figure 1. Position of the terminator as a function of time with respect to the north and south magnetic poles. The shaded region is the nightside and the hatched region near the south pole is the UKR source region. The hatched region near the north pole is magnetically conjugate to the UKR source region and is the energy source for the radio emissions. Electrons are scattered by the modification to the atmosphere upon exposure to sunlight, but they only emit radio waves at the nightside where the parameters are appropriate for cyclotron masing.

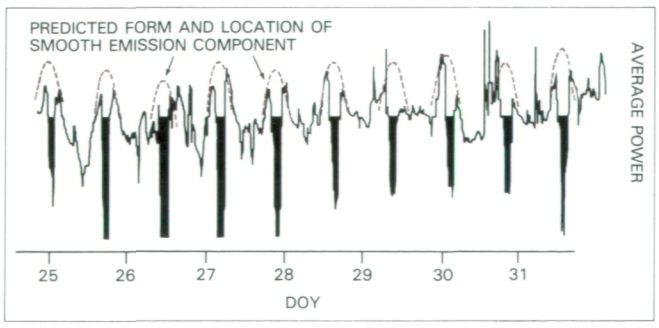

Figure 2. Clock-like radio emissions are shown as a function of time by the solid line. The blackened area represents signal dropout due to the hollow-cone nature of the emission process. The dashed lines represent the predicted shape and location of the radio emissions if viewed from an angle outside of the null in the emission cone.

ORIGINAL PAGE IS
OF POOR QUALITY

EROSION OF SATURN'S RINGS

The origin of Saturn's rings has been a subject of much debate for centuries, a debate that intensified after the Voyager 1 and 2 Saturn encounters of 1980 and 1981. The classical approach is to regard the rings as a relic of the circumplanetary accretion disk that formed out of the primitive Saturn nebula some 4.5 billion years ago. In this cosmogonic view, the rings represent a failed attempt at satellite building, a visible, perhaps highly evolved primordial accretion disk. An alternate approach is to regard the rings as the relatively youthful remains of a much more recent formation event, such as the catastrophic disruption of an inner satellite. In this view, the rings are evolving relatively quickly, victims of a plethora of erosional processes and dispersive effects.

A particularly effective electromagnetic erosion process, described by Northrop and Connerney (*Icarus, 70,* 124-137, 1987), can erode the rings on a time scale of tens of millions of years and accounts for some of the gross structure of the rings as well. In this mechanism, ring mass is removed by charged particles ranging in size from ions and/or ion clusters to submicron bits of ice. Such particles are constrained to move along magnetic field lines, propelled by the components of gravity and centrifugal force resolved along the magnetic field, in addition to electrostatic and the magnetic mirror forces. In Saturn's tenuous C-ring (see figure), once a small particle acquires a charge, it cannot be stably held in the ring plane. These particles accelerate along the magnetic field and are ultimately lost in Saturn's atmosphere. However, in the optically thick B-ring at greater radial distances from Saturn ($r > 1.525\ R_S$, $1\ R_S = 60{,}330$ km), such particles can be stably trapped in the ring plane. The net result is mass loss, or erosion of the rings inward of 1.525 R_S, and relative stability of the rings outward of 1.525 R_S. This explains the dearth of small particles in the C-ring as well as the sharp decrease in the optical thickness of the rings (or ring mass) inside of the boundary at 1.525 R_S, the inner edge of the B-ring.

Assuming that the small submicron ring particles are produced and/or charged by micrometeorite impacts on the larger ring objects, the present-day structure of the rings is consistent with a ring age of between 4.4 and 67 million years. The uncertainty is largely due to uncertainties in the micrometeorite influx. This is consistent with several other independent estimates of ring age: a 30-million-year estimate based on the photochemical properties of Saturn's ionosphere, a 4- to 20-million-year estimate based on the (radial) evolution of small imbedded ring moons, and a 10- to 100-million-year estimate based on atmospheric chemistry. Thus, it appears that Saturn's rings are relative newcomers in our 4.5-billion-year-old solar system.

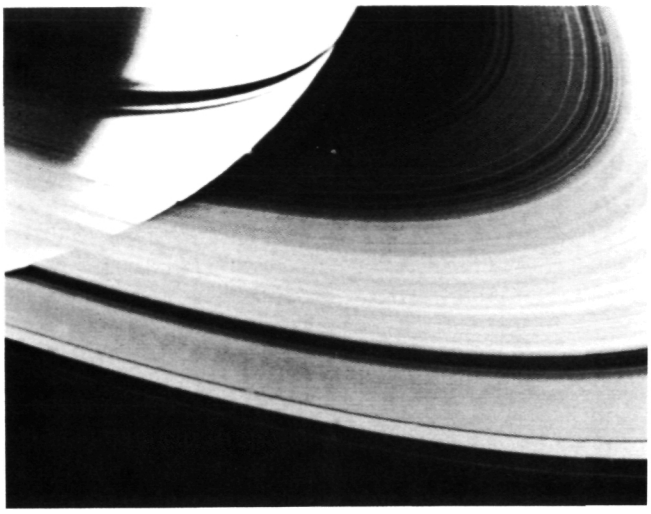

Computer-enhanced image of Saturn and the rings obtained by Voyager 1, looking back towards the planet a day after closest approach. The C-ring is the tenuous, slightly blue inner ring system which disappears when viewed against the illuminated limb of the planet. The optically thick B-ring extends from the C-ring outward to the wide dark gap (Cassini division) separating it from the A-ring. Just outward of the A-ring is the faint, narrow F-ring.

Contacts: J. E. P. Connerney and T. G. Northrop
Codes 695 and 665

Sponsor: Office of Space Science and Applications

Dr. J. E. P. Connerney is Co-Investigator for Voyagers 1 and 2, the Mars Observer, and the Tethered Satellite Magnetometer. He has been a part of Goddard for eight years and has received the NASA Medal for Exceptional Scientific Achievement. Dr. Connerney, who received a PhD degree in applied physics from Cornell University, specializes in magnetospheres, planetary magnetic fields, and geophysics.

CONDENSED C_4N_2 IN TITAN'S ATMOSPHERE

Titan's atmosphere contains a remarkable array of organic molecules in the vapor phase. Although composed mostly of molecular nitrogen, this atmosphere also

includes at least seven hydrocarbons (CH_4, C_2H_2, C_2H_4, C_2H_6, C_3H_4, C_3H_8, and C_4H_2) and three nitriles (HCN, HC_3N, and C_2N_2). Other gases observed spectroscopically include an isotope of methane (CH_3D) CO, CO_2, and molecular hydrogen, a by-product of the extensive photochemistry that occurs in the stratosphere and above.

In addition to emission and absorption features associated with these gases, spectra from the Voyager 1 infrared spectrometer (IRIS) include a few unidentified emission features in the vicinity of the north limb. Extensive investigations have ruled out additional organic gases as plausible sources. On the other hand, radiative transfer analyses have demonstrated that most of the identified organics are abundant enough to condense out in Titan's lower stratosphere. A laboratory investigation was undertaken to see if organics in the condensed phase could be associated with these unidentified emission features.

One outcome was the identification of a feature at 478 cm^{-1} as due to the condensed phase of the nitrile C_4N_2.

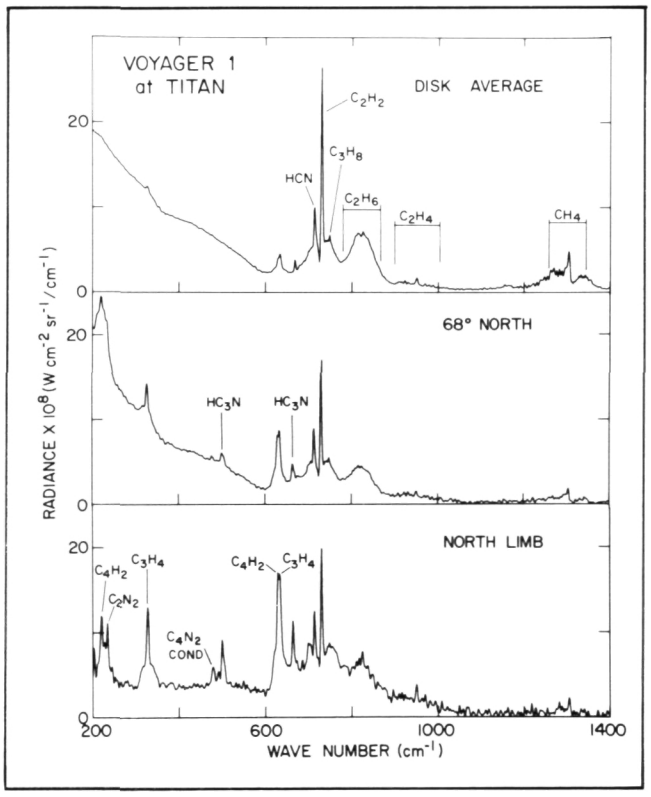

Voyager 1 IRIS spectra of Titan at three different locations. Emission features of various organic gases are identified, as well as one at 478 cm^{-1} attributed to the condensed phase of C_4N_2.

A vapor phase feature at 471 cm^{-1} is not found in the Voyager spectra, implying that C_4N_2 is almost fully condensed at the locations on Titan's limb where it is observed.

Radiative transfer analyses indicate that C_4N_2 is largely restricted to a cloud of condensed particles a few kilometers thick in Titan's lower stratosphere. The cloud appears to extend from the north pole to about 60° N latitude. The vapor phase abundance above the cloud averages less than required if the gas is uniformly mixed, implying that the cloud may be formed near the pole and dynamically advected southward between regions of atmosphere depleted in C_4N_2. This view is consistent with the rapid attenuation of other nitriles in the vapor phase as one moves south from the north polar region.

Contact: Robert Samuelson
Code 693

Sponsor: Office of Space Science and Applications

Dr. Samuelson, who holds a PhD degree from Georgetown University, has 25 years of experience at Goddard.

VARIABILITY IN STRATOSPHERIC ETHANE ON JUPITER

The composition of the upper atmosphere of Jupiter is determined by photochemical processes of constituent hydrocarbons. Hydrocarbon chemistry on Jupiter has been studied theoretically, and one-dimensional photochemical models have been developed. Ground-based and spacecraft measurements in the ultraviolet and infrared spectral region have also been made on molecular spectra of various hydrocarbons in the Jovian stratosphere. These allowed retrieval of molecular abundances and atmospheric temperatures and provided a test for the existing atmospheric models. The determination of altitude and spatial distributions as well as relative abundances of the constituent molecules is particularly important because it can permit the extension of these photochemical models to multiple dimensions. Spatial distributions of Jovian stratospheric emission can also reveal local physical phenomena such as ultraviolet auroral effects in the polar regions and infrared hot spots with enhanced molecular emission (e.g., CH_4 and C_2H_2).

Abundances and spatial distributions (vertical and horizontal) of C_2H_6 in Jupiter's stratosphere were obtained from ultra-high resolution ($\lambda/\Delta\lambda \sim 10^6$) spectra of individual ethane emission lines in the ν_9 band near 12 μm.

The measurements were made in 1982 and 1983 with the Goddard Space Flight Center infrared heterodyne spectrometer (Kostiuk and Mumma, 1983) at the McMath solar telescope at Kitt Peak National Observatory. The diffraction-limited spatial resolution of the heterodyne technique (~2 arc seconds FWHM) permitted spatial mapping of the planet and the study of a localized hotspot region near the north pole of Jupiter.

1. Spatial Distribution. The geometry for the observations as well as actual data obtained at various positions on the planet are presented in Figure 1. The 2-arc second diameter (FWHM) instrumental field of view is shown on a planetary disk of ~40-arc second diameter at the time of observation. Qualitatively, the data behave as expected for a stratospheric constituent. The C_2H_6 emission line is much more pronounced near the planetary limbs where a greater stratospheric column is observed along our line of sight. As the observations approach disk

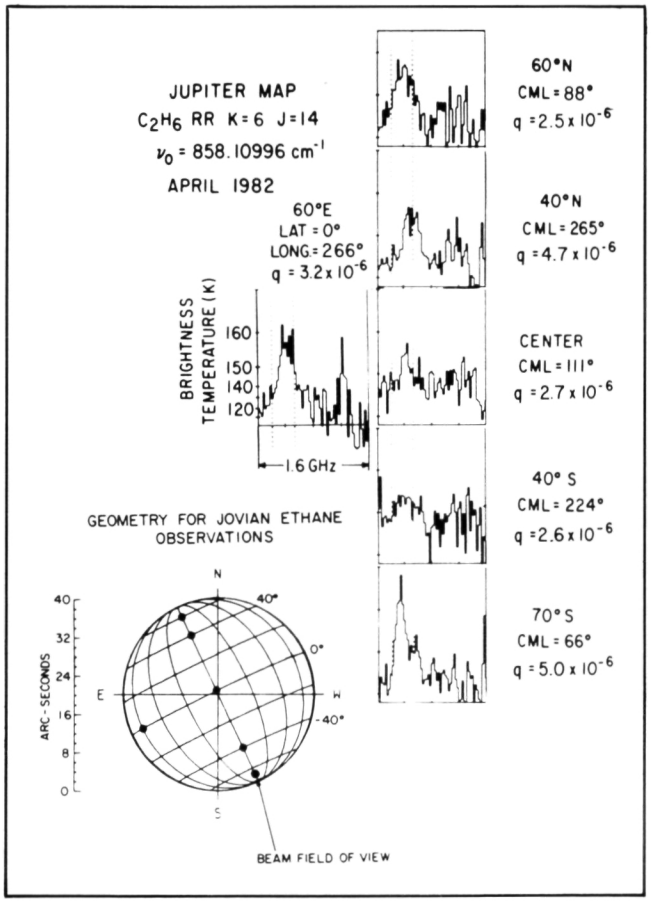

Figure 1. Spatial map of Jupiter in the C_2H_6 RR (6,14) line. The retrieved mole fractions at each latitude-longitude position are given.

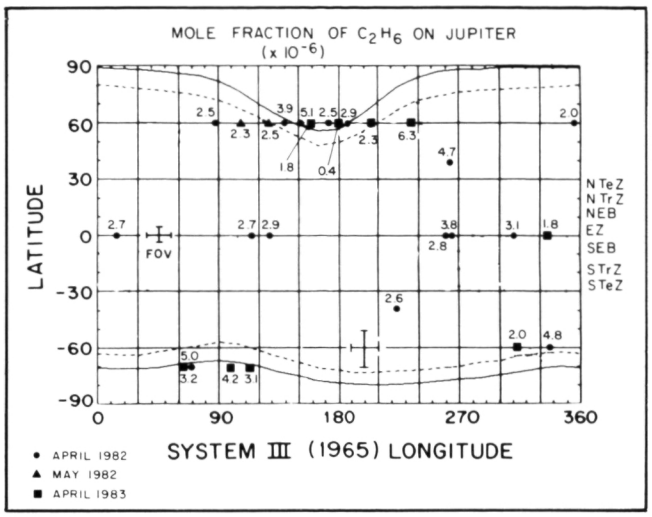

Figure 2. Summary of mole fractions obtained from measurements. The extent of the field of view covered by each measurement (~25 minutes integration) is shown by the error bars at the equator and at −60° latitude.

center, the measurement is of a thinner stratospheric layer, and thus, the emission line intensity is reduced. The measured continuum, however, increases, indicating that we are probing deeper into the atmosphere below the tropopause where it is hotter. These lines were fit to a calculated spectrum, modeled with existing molecular parameters and a Jovian model atmosphere (constant C_2H_6 mole fraction above the tropopause and Voyager-derived temperature profiles). The retrieved C_2H_6 mole fractions are given for each measurement.

A summary of the results obtained from measurements during three observing periods, April 1982, May 1982, and April 1983, is given in Figure 2. The coordinates of each observation are plotted on a latitude-longitude grid (System III, 1965). The retrieved mole fraction for the measurement is given at each plotted point. In the equatorial region, the retrieved mole fractions are relatively constant with an average value of $2.8 \pm 0.6 \times 10^{-6}$. One value was slightly higher (3.8×10^{-6}), whereas a lower result of 1.8×10^{-6} was obtained from measurements taken during a different observing run. The mole fractions retrieved from our total data set remain close to the average equatorial value everywhere on the planet outside the auroral oval (solid curve, Figure 2) and the footprint of Io's flux tube (broken line, Figure 2). Greater variability of the retrieved C_2H_6 mole fractions is observed at these boundaries and inside the auroral region. An increase in ethane emission and abundance is obtained near the south polar region.

Due to the resolved line measurements and improved molecular parameters used, our results are of higher quality than previous C_2H_6 abundance determinations that used lower resolution techniques. Our mole fraction retrievals have a precision of $\pm 20\%$, whereas the accuracy of the values depends on the input parameters. A two-fold uncertainty is possible in the absolute C_2H_6 mole fractions retrieved based on reasonable changes in the atmospheric temperature profile and altitude distribution of ethane. The retrieved mole fractions of ethane on Jupiter are consistent with recent photochemical models (Yung and Strobel, 1980; Gladstone, 1983; and Allen, 1986). They are also in agreement with recent observational determinations within given error bounds (Maguire et al., 1985; Kim et al., 1985; Noll et al., 1986; and Kostiuk et al., 1983).

2. North Polar Variability. Within the north auroral oval at 180° longitude (System III, 1965) and 60° latitude, no significant change in C_2H_6 emission was observed in April and May 1982 and in October 1986. In April 1983, a significant decrease in C_2H_6 emission (and thus mole fraction) was observed. This region coincides with the hot spot observed in 7.8 μm CH_4 emission (Caldwell et al., 1980) and 13.6 μm C_2H_2 emission (Drossart et al., 1986). Unlike the CH_4 emission, the behavior of ethane lines cannot be explained purely by a localized temperature increase. Such an increase would enhance the C_2H_6 emission as well. Since no such enhancements were observed, we suggest that a modification of stratospheric chemistry, forming more C_2H_2 at the expense of C_2H_6, is responsible for the observed effects in the northern "hot spot." Although dynamics may play a role in the lower stratosphere, ultraviolet hydrocarbon chemistry significantly modified by higher order effects of charged particles precipitating along the magnetic field lines may be the best candidate process for generating the observed phenomenon. Results of this investigation, "Variability of Ethane on Jupiter" by T. Kostiuk, F. Espenak, M. J. Mumma, D. Deming, and D. Zipoy, will be published in *Icarus* (1987).

Contact: Theodor Kostiuk
Code 693

Sponsor: Office of Space Science and Applications

Dr. Theodor Kostiuk is involved in high-resolution infrared studies of the composition, temperatures, and dynamics of planetary atmospheres with the Planetary Systems Branch. Dr. Kostiuk, who holds a PhD degree in physics from Syracuse University, has 13 years of experience at Goddard.

MESOSCALE WAVES AS A PROBE OF JUPITER'S DEEP ATMOSPHERE

Images of Jupiter's atmosphere at visible wavelengths show an atmosphere that is filled with a complex network of clouds. Time-lapsed tracking of discrete features in these clouds has indicated that the winds on Jupiter form an alternating pattern of eastward and westward jet streams. The clouds themselves are believed to be formed of frozen ammonia crystals, located at a barometric pressure of 700 mbar. Because of the cloud obscuration, we know little about the meteorological structure at greater depths. Remote sensing of Jupiter from the Voyager flyby spacecraft by the radio occultation experiment and by Goddard's infrared spectrometer (IRIS) has shown that the variation of temperature with depth at these levels is close to the dry adiabat, the same as that experienced by a parcel of atmosphere that is displaced downward without exchanging heat with its environment. In this situation, small departures of temperature from the dry adiabat can have profound consequences on the dynamical state of the deep atmosphere. Unfortunately, *in situ* temperature measurements, such as those to be made by the descent probe on the Galileo spacecraft, are ill-equipped to detect these small deviations, or even their sign.

The analysis of linear waves can be used to probe Jupiter's atmosphere. Waves are generally sensitive indicators of the properties of the medium through which they propagate, for instance, the spatial variation in temperatures and winds. Because waves typically propagate vertically as well as horizontally, they can sample the properties of the atmosphere below the level at which they are observed, for example, by a flyby spacecraft such as Voyager. This approach in many ways is reminiscent of that used in terrestrial seismology. A recent collaboration with P. J. Gierasch of Cornell University has led to the identification and cataloging of a remarkable class of linear wave patterns observed in the Voyager images. In general, the waves align themselves with the east-west winds on Jupiter, i.e., the orientation of the wavefronts is north-south. The horizontal wavelengths cluster about a mean of 300 km; the standard deviation about this mean is only 20 percent. Finally, the wavetrains are quite long, typically 20 or more crests in length.

These mesoscale waves have been interpreted as gravity, or buoyancy, waves that propagate vertically and horizontally. For these waves to oscillate, temperature must decrease with altitude more slowly than the dry adiabat. Then a parcel of atmosphere that is displaced upward is cooler and heavier than its environment, and it tends to

ORIGINAL PAGE IS
OF POOR QUALITY

An example of mesoscale waves observed near the equator by the Voyager 1 spacecraft. North is at the top, and the east-west dimensions of the photograph are approximately 28,000 km, or 23° of longitude. Wavetrains can be seen just to the left and right of the center of the mosaic. It is conceivable that they may correspond to one very long wavetrain. The contrast of the wave patterns is low; typically it is 4 units out of a dynamic range of 256.

sink back toward its original position. Likewise, a parcel that is pushed downward is warmer and lighter than its environment, and it goes back up. In either case, the parcel typically overshoots its initial position, and it oscillates about it. The long lengths of the observed wavetrains and their well-defined wavelengths suggest that the waves are resonant modes trapped in a waveguide at the base of the ammonia clouds. In order to have trapping, there must be a region above the waveguide in which the gravity waves cannot oscillate, and through which they cannot easily propagate into the atmosphere above. Convective mixing within the clouds themselves could produce such an environment. The waveguide evidently has only a single resonant mode, because the observed wavelengths cluster about a single value. Considering the propagation characteristics of gravity waves, this imposes a relationship between the vertical variation of wind speed and the small departure of temperature from the dry adiabat. The former can be measured with precision by Doppler tracking of a descent probe, such as Galileo's, thereby permitting a sensitive determination of the temperature variation in Jupiter's deep atmosphere.

Contact: F. Michael Flasar
Code 693

Sponsor: Office of Space Science and Applications

Dr. F. Michael Flasar is Co-Investigator for the infrared spectroscopy experiment on the Voyager spacecraft. His professional interests include theoretical modeling and interpretation of spacecraft data pertaining to the dynamics and meteorology of planetary atmospheres. Dr. Flasar, who received a PhD degree in physics from the Massachusetts Institute of Technology, has been with Goddard for 12 years.

DETERMINATION OF LOW-TEMPERATURE ETHANE LINE BROADENING IN A HYDROGEN ATMOSPHERE

Knowledge of collision-broadened spectral linewidths as functions of temperature is necessary for the accurate interpretation of remote sensing of planetary atmospheric gases. In particular, in the infrared region, laboratory measurements of H_2 collision half-widths of ethane ν_9 transitions at reduced temperatures are necessary for accurate modeling of high-resolution observations of stratospheric ethane in Jupiter's atmosphere. Resolved profiles of ethane lines in Jupiter's south polar stratosphere have been measured and were originally interpreted by T. Kostiuk, GSFC, on the assumption that the hydrogen-broadening coefficient was $\gamma(300\,°K) = 0.108$ $cm^{-1}/atm.$, and furthermore, that its temperature dependence was given by $\gamma(T) = \gamma(300\,°K)\,(T/300\,°K)^{-½}$. This temperature dependence is the expected kinetic-theory result for hard-sphere collisions.

We have experimentally determined the temperature dependence of the H_2-broadening coefficient for the ν_9 fundamental of ethane over the temperature range 95–300 °K with a novel low-temperature absorption cell used in conjunction with the GSFC Doppler-limited diode laser spectrometer. The GSFC scientific team included D. Jennings, G. Halsey, and S. Nadler.

Details of the low-temperature sample cell used in this work are shown schematically in Figure 1. The cell is our own design and has several unique features. The sample chamber is 30 cm long with a 2.5-cm bore to permit multiple-passing of a small laser beam, if desired. The windows (ZnSe was used in this work) are cooled along with the cell to avoid temperature gradients along the sample path. Maintaining a vacuum seal on windows in cold cells is generally very difficult at low temperatures; we have solved this problem by using spring-loaded Teflon O-rings (available commercially) that keep uniform sealing pressure on the window and cell surfaces. The cell has shown no hydrogen leakage at temperatures as low

as 45 °K. A single-stage closed-cycle helium refrigerator (Displex 102) provides cooling for the cell.

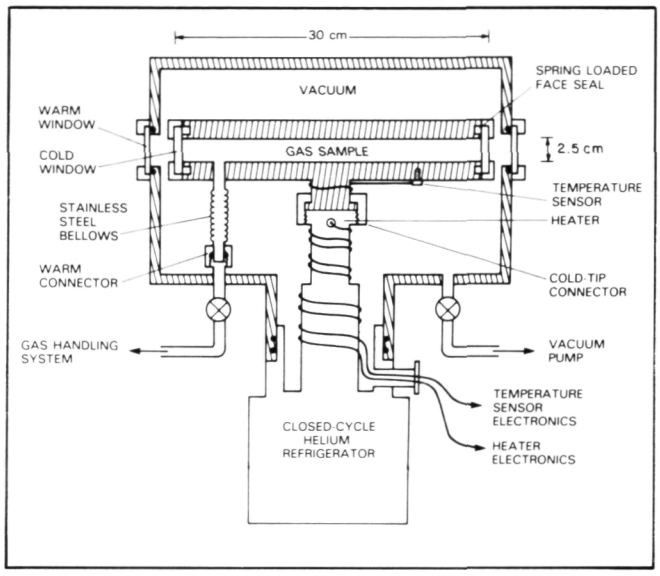

Figure 1. Low-temperature absorption cell. The cell is cooled with a closed-cycle helium refrigerator and operates over the range 50–300 °K. Optical path length, 30 cm; diameter, 2.54 cm. The cold windows are sealed with Teflon-covered, spring-loaded rings.

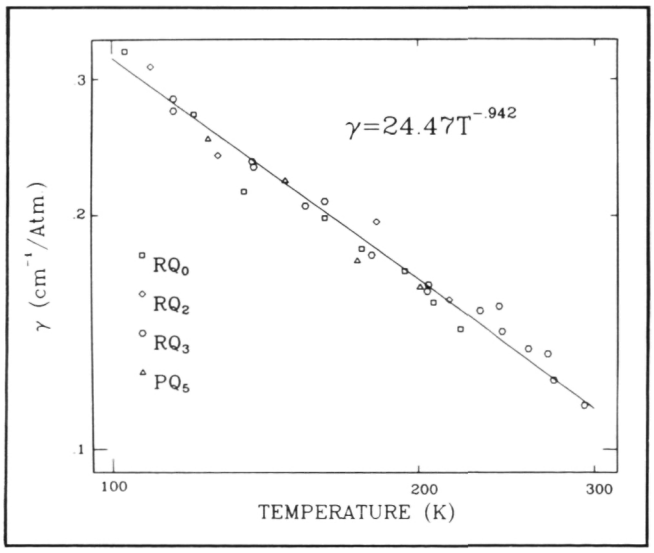

Figure 2. Results of the linear regression fit to the data. The fit is made to log γ = log γ_o + n log (T_o/T). The solid line represents the best fit.

The experimentally determined half-widths were assumed to follow a power-law dependence on temperature of $\gamma(T) = \gamma(T_o)\,(T_o/T)^n$ where $\gamma(T)$ is the hydrogen pressure broadening coefficient, and T_o is room temperature (296 °K). The room temperature broadening coefficient, $\gamma(T_o)$, and the temperature index n have been determined by linear regression analysis. These results are plotted graphically in Figure 2. A most striking observation is that $n = -0.942$, not -0.5, as was expected based on kinetic theory.

The kinetic-theory result $n = -0.5$ can be understood by considering the temperature dependence of the (broadening-) effective collision frequency given by $\omega = vN\sigma$. Here v is the relative velocity, N is the number density, and σ is the effective collision cross section. If one assumes an ideal-gas density dependence $N = P/kT$ and a Maxwellian velocity distribution $v = (8kT/\pi\mu)^{1/2}$, then the temperature dependence of the collision frequency is simply $T^{-0.5}$ times the temperature dependence of the collision cross section. If we further assume the temperature dependence of the collision-broadening process follows the same dependence as that of the collision frequency, one obtains the standard kinetic-theory prediction that $n = -0.5$ if the interaction potential is hard-sphere, i.e., if σ is independent of temperature.

The collision cross section may be temperature dependent if, for example, a different intermolecular force is involved. If any of the so-called van der Waals forces is assumed, where the potential varies as r^{-n}, $n \geq 3$, then the impulse derived from this force, i.e., the integral of this force over time, will result in a cross section that is inversely proportional to the relative velocity since t = distance/velocity, and therefore this cross section will depend on temperature, as $T^{-1/2}$. This impulse approximation results in an overall temperature dependence of T^{-1}, which is in essential agreement with our observations.

In summary, an improved temperature-dependent pressure-broadening coefficient has been experimentally determined over the temperature range 100–300 °K. A very reliable low-temperature absorption cell was employed for these measurements. A power-law dependence of $\gamma(T)$ is observed. Furthermore, it is observed that the temperature exponent n reveals no detectable rotational state (J,K) dependence in accordance with theoretical predictions.

These results have been applied directly to the interpretation of the recent observations by other members of our group of the abundance and spatial distributions of

ethane in Jupiter's stratosphere. Although other effects, notably planetary rotational broadening within the observational field-of-view, partially mask the effect of pressure broadening, application of our results has measurably improved their goodness of fit.

Contact: John J. Hillman
Code 690

Sponsors: Office of Space Science and Applications and Planetary Atmospheres Program

Dr. John J. Hillman is the Associate Chief of the Laboratory for Extraterrestrial Physics. His scientific specialties are molecular structure and spectroscopy, and his professional interests include remote sensing of Earth, planets, and stars, as well as the nature and evolution of planetary and stellar atmospheres. Dr. Hillman, who received his PhD degree in physics from American University, has been with Goddard for 18½ years.

OBSERVATIONS OF STRATOSPHERIC $ClONO_2$ WITH A BALLOON-BORNE FOURIER SPECTROMETER

The presence of chlorine nitrate ($ClONO_2$) in the Earth's stratosphere was first predicted by Rowland et al. (1976). Chlorine nitrate is an important temporary reservoir for reactive chlorine and nitrogen, and couples chlorine and nitrogen chemistry. $ClONO_2$ is produced by the reaction

$$ClO + NO_2 + M \rightarrow ClONO_2 + M \qquad (R1)$$

and is destroyed by photolysis

$$ClONO_2 + h\nu \rightarrow Cl + NO_3. \qquad (R2)$$

Current photochemical theory predicts that $ClONO_2$ increases between noon and early evening and decreases from sunrise to noon. Theoretical modeling shows that $ClONO_2$ exerts a strong influence on the diurnal variation of ClO in the present-day atmosphere. As chlorine levels in the Earth's stratosphere rise, chemistry involving $ClONO_2$ could lead to a nonlinear response of ozone to chlorine perturbations (Cicerone et al., 1983; Prather et al., 1984).

The difficulty in obtaining good data on the $ClONO_2$ distribution in the stratosphere has been one of the major uncertainties in the chemistry of ozone. Infrared spectroscopy has the potential to provide quantitative measurements of this important stratospheric reservoir gas. The first infrared emission observations of stratospheric $ClONO_2$ have been obtained with a high spectral resolution balloon-borne Fourier spectrometer, cooled to 100 °K, in November 1984 from Palestine, Texas. The ν_4 Q branch of $ClONO_2$ at 780.2 cm^{-1} was recorded with 0.04-cm^{-1} resolution for several angles on the Earth's limb. This feature is identified by the arrow in the observed infrared spectrum (dotted line) of the top panel of Figure 1. Theoretical computations of the limb spectrum are shown as a solid line, without and with the emission of $ClONO_2$, in the top and bottom panel, respectively.

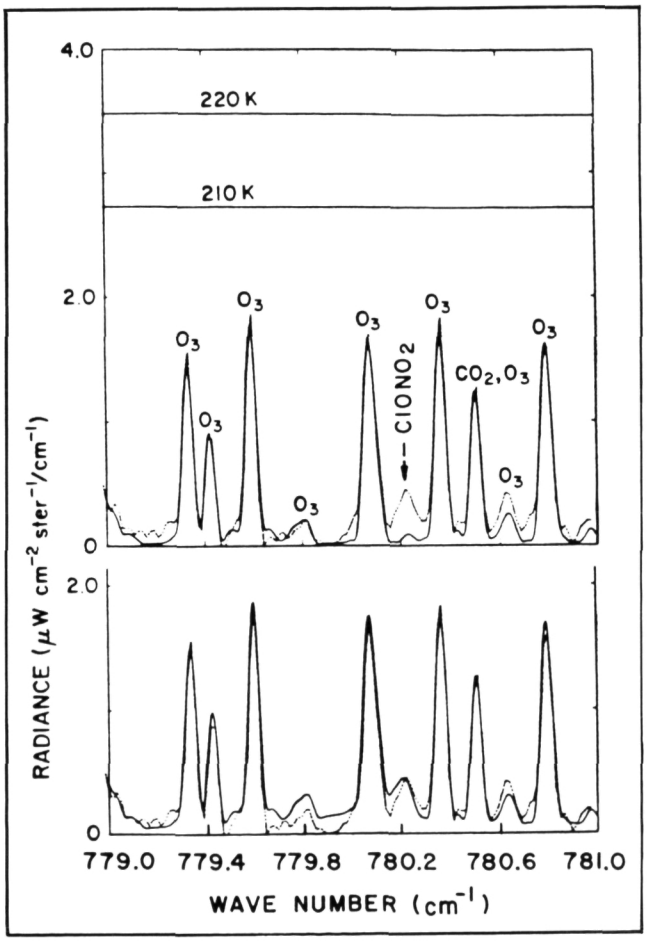

Figure 1. Observed and synthetic spectra for a tangent height of 23.2 km.

The derived mixing ratios for $ClONO_2$ are represented in Figure 2 by the open circles; the appropriate local time is 3 p.m. Also displayed are the values derived from solar absorption measurements by Rinsland et al. (1985), and

by Zander et al. (1986) from the Atmospheric Trace Molecule Spectroscopy (ATMOS) instrument operating from Spacelab 3. The ATMOS range of values is shown by the striped area. If one ignores the small potential seasonal and latitudinal differences, the data sets show overall agreement. To compare observation with theory, Figure 2 also displays a one-dimensional photochemical profile for $ClONO_2$ at 4 p.m. The agreement between theory and observation is good near the peak of the distribution. There is disagreement in the 22-km altitude range, with the observations showing higher $ClONO_2$ levels than predicted. Possible sources of error include one-dimensional model limitations, variability in HCl, extrapolation of rate constants to low temperatures, and photolysis rate of $ClONO_2$. Analysis of the midnight to sunrise time period is in progress for data from a September 1986 balloon flight.

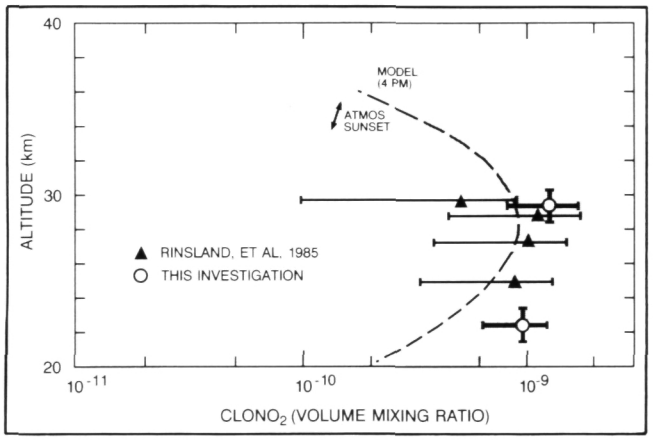

Figure 2. Observed and predicted distributions for $ClONO_2$ for 3–4 p.m. at mid-latitude sites.

Other collaborators on this research are J. Brasunas (GSFC), S. Massie (NCAR), and M. Abbas (MSFC).

Contact: Virgil Kunde
Code 693

Sponsor: Office of Space Science and Applications

Mr. Virgil Kunde, who specializes in planetary atmospheres and infrared spectroscopy, is Head of the Planetary Astrophysics Section. Mr. Kunde holds an MS degree in astronomy from the University of Maryland, and he has been with Goddard for 25 years.

TEMPERATURE STUDY OF THE KINETIC REACTION RATE OF ATOMIC OXYGEN WITH PHOSPHINE: IMPLICATION FOR MODELING PHOSPHINE PHOTOCHEMISTRY IN THE ATMOSPHERES OF GIANT PLANETS

The discovery of phosphine (PH_3) as a minor constituent in the atmospheres of Jupiter and Saturn has led to a great deal of speculation by planetary modelers concerning the role of PH_3 in the complex atmospheric chemistry of these planets. In particular, early interest centered on the roles that photochemical reactions of PH_3 played in models attempting to account for the origin and nature of the Great Red Spot (GRS) on Jupiter and the stability of ammonia (NH_3) in the atmospheres of Jupiter and Saturn. Following the quantitative observations by the Voyager infrared (IRIS) experiment, interest in the reactions of PH_3 has intensified regarding elucidation of the chromophoric source for the GRS and has expanded to include modeling of atmospheric aerosol science of Jupiter and Saturn (West, Strobel, and Tomasko, 1986).

Earlier work from this laboratory addressed some of these areas by having performed the first temperature dependence studies to determine the absolute kinetic rate constant for reactions of PH_3 with two atmospherically important species, namely, atomic hydrogen and the NH_2 free radical. To provide additional new kinetic data necessary for further refinement of atmospheric models involving reactions of PH_3 with other potentially relevant species, we have now completed a study that determined, for the first time, the reaction rate of oxygen atoms with PH_3 as a function of temperature and pressure. The major form in which oxygen exists in these atmospheric systems is as carbon monoxide (CO). Recent work by K. Noll and co-workers (1987), indicating a large reservoir of CO deep in Jupiter's atmosphere and rapid vertical mixing, sets an upper limit to the influx of free oxygen atoms from meteoroid or icy satellite sources. Thus, it is of interest to consider potential perturbations of PH_3 on oxygen chemistry. The laboratory method employed flash photolytic production of oxygen atoms, followed by time-resolved measurement of the resonance fluorescence signal of the oxygen atom as it decays by reaction with phosphine molecules. Results from the rate-constant data show the reaction of $O + PH_3$ to be moderately rapid (one in every few collisions leads to reaction) and independent of both temperature and pressure.

Implications for modeling the phosphine photochemistry in the atmospheres of the giant planets derived from this kinetic study are: 1) low-temperature data relevant for

the atmospheric conditions are provided; 2) the moderate rate of reaction supports mass spectrometric results (Hamilton and Murrells, 1985), which indicate that the O + PH_3 reaction proceeds via an addition mechanism yielding the H_3PO^* complex. This invites consideration of the potentially interesting atmospheric chemistry of O-P species; and 3) due to the temperature-independent nature of the O + PH_3 reaction and because other reactions of PH_3 have energy barriers, at temperatures appropriate to the planetary atmospheres, the O + PH_3 reaction is approximately 500 times faster than H atom and 25,000 times faster than NH_2 radical reactions with PH_3.

If adequate amounts of atomic oxygen were found to be present in the atmospheric systems of Jupiter and Saturn, the rate would be sufficiently rapid to consider the potential of the O + PH_3 reaction as a plausible reaction for perturbing other reactions of phosphine and/or oxygen-containing species in future modeling of these planetary atmospheres.

Contacts: David F. Nava and Walter A. Payne
Code 690

Sponsor: Office of Space Science and Applications

Dr. David Nava is an astrophysicist with the Laboratory for Extraterrestrial Physics. He is Co-Investigator for the Upper Atmosphere Research Program and for the Planetary Atmospheres Program, and he was Principal Investigator for NASA's Returned Lunar Sample Program. He also served on the editorial board of Chemical Geology. *Dr. Nava's scientific specialties are analytical geochemistry and chemical reaction studies, and he is interested in the application of chemical kinetic studies to atmospheric systems. Dr. Nava, who received a PhD degree in chemistry from Arizona State University, has worked at Goddard for 19 years and has received two NASA Special Achievement Awards and a NASA Exceptional Performance Award.*

Dr. Walter Allen Payne, Jr., an astrophysicist in the Astrochemistry Branch, is a Co-Investigator in the NASA Upper Atmospheres Program and in the NASA Planetary Atmospheres Program. His professional interests include chemical kinetics, photochemistry of small molecules, and laser-induced fluorescence. Dr. Payne, who earned a PhD degree from Howard University, has been with Goddard for 18 years.

THE HYDROXYMETHYL RADICAL: ITS ROLE IN ATMOSPHERIC CHEMISTRY AND THE TEMPERATURE DEPENDENCE OF ITS REACTION WITH O_2

The hydroxymethyl radical (CH_2OH) is one of the intermediates in the atmospheric oxidation of methane. In polluted atmospheres, hydroxymethyl radicals are produced by a series of reactions initiated by OH attack of ethylene. Studies from this laboratory have indicated that the reaction of chlorine atoms with methanol yields exclusively CH_2OH and HCl. Since there is the possibility of release of methanol into the atmosphere through its use as an alternative automotive fuel and with the continued release of chlorine atom precursors, i.e., chlorfluoromethane, methylhydroxy radicals may play an even greater role in atmospheric chemistry. It is therefore imperative that the chemistry of this radical is well understood.

The most likely fate of the hydroxymethyl radical in the atmosphere is reaction with molecular oxygen, i.e.,

$$CH_2OH + O_2 \rightarrow HO_2 + H_2CO \qquad (1).$$

There have been several previous investigations of the kinetics of reaction 1 at 298 °K. The three most recent studies, which include a study from this laboratory, report values for k_1 that are in excellent agreement; the mean of the three is $(9.5 \pm 2.0) \times 10^{-12}$ cm^3 s^{-1}. However, these results are in conflict with two earlier measurements that yielded values for k of 2×10^{-12} cm^3 s^{-1} and 1.4×10^{-12} cm^3 s^{-1} at 298 °K. These low values for k have been shown to be the results of secondary reactions stemming from the high radical concentrations employed in those studies.

Concerning the temperature dependence of k_1, the one previous study was in the range $1000 \leqslant T \leqslant 2000$ °K, and from that study an Arrhenius expression, $k_1 = 1.7 \times 10^{-10} \exp(-5000/RT)$ cm^3 s^{-1}, was deduced. At 300 °K, this expression predicts $k_1 = 4 \times 10^{-14}$ cm^3 s^{-1}. This value is more than two orders of magnitude smaller than the mean of the three recent determinations. Clearly, the high temperature Arrhenius expression does not predict the correct rate constant at lower temperatures.

We have recently undertaken a kinetic study of reaction 1 in the temperature range $215 \leqslant T \leqslant 373$ °K by use of the experimental technique of discharge flow-mass spectrometry. The results indicate that the rate constant k_1 increases from 2.5×10^{-12} cm^3 s^{-1} at 215 °K to a maximum of 9.0×10^{-12} cm^3 s^{-1} near 300 °K and then

decreases to 7.2×10^{-12} cm^3 s^{-1} at 373 °K. This complex temperature dependence cannot be described by a unique Arrhenius expression. The reaction has been previously suggested to occur via the formation of a vibrationally excited $HOCH_2O_2$ radical that can dissociate back to reactants or isomerize via H-atom transfer to OCH_2OOH. The OCH_2OOH readily dissociates to form the products H_2CO and HO_2. It may be speculated that the increase in k_1 in the range 215–300 °K is related to a barrier to rotation of the O-O group in the initially formed adduct about the carbon atom. The rotation is necessary to achieve H-atom transfer or isomerization. The decrease in k_1 from 300 to 373 °K indicates that the rate of dissociation of adduct back to reactants increases more rapidly than the rate of dissociation to products.

In summary, the temperature dependence of k_1 is complex, and model studies should use the appropriate rate constant for the region of the atmosphere being modeled.

This work was performed in collaboration with Dr. Fred Nesbitt, research associate at the Catholic University of America.

Contacts: Walter A. Payne and Louis J. Stief
Code 691

Sponsor: Office of Space Science and Applications

Dr. Walter Allen Payne, Jr., astrophysicist in the Astrochemistry Branch, is a Co-Investigator in the NASA Upper Atmosphere Program and in the NASA Planetary Atmospheres Program. His professional interests include chemical kinetics, photochemistry of small molecules, and laser-induced fluorescence. Dr. Payne, who earned a PhD degree from Howard University, has been at Goddard for 18 years.

Dr. Louis J. Stief, Head of the Astrochemistry Branch of the Laboratory for Extraterrestrial Physics, is involved with determining the rates and mechanisms of reactions occurring in the upper atmosphere of Earth. His scientific specialties are kinetics and photochemistry of atmospheric and astrophysical systems. Dr. Stief holds a PhD degree from the Catholic University of America, and he has 18 years of experience at Goddard.

MARS' MAGNETIC FIELD PAST AND PRESENT: EXAMPLE OF A TWO-STATE MAGNETOSTROPHICALLY LIMITED DYNAMO

Two sources of data exist from which the magnetic field of Mars may be quantitatively estimated. The first of these sources comes from the analysis of the interactions of the solar wind with Mars. These data have been extensively studied, and there exists general agreement that an upper-bound to Mars' current surface equatorial magnetic field is between 2 and 6×10^{-4} Gauss. The second source of information is the study of remanent magnetization in the SNC meteorites that are widely considered to have come from Mars. These meteorites closely resemble crystallized lava with an age of approximately 1.3×10^9 years. The inferred magnetic field in which the SNC meteorites solidified was 10^{-2}–10^{-1} Gauss. We have used these data and a scaling law based on the balance of Coriolis and Lorentz forces in a planet's core to show that when compared to other planetary magnetic fields, no Martian dynamo is currently operative. However, a fully developed dynamo is implied to have been operative when the SNC meteorites' assumed parent lava solidified on the surface of Mars approximately 1.3×10^9 years ago. The rare SNC meteorites were first found in Shergotty (India), Nakhla (Egypt), and Chassigny (France); the first letter in each location is used to form their name.

By applying our scaling law to Mars, we obtain a calculated field strength of ≈ 0.05 Gauss. The inferred SNC magnetizing field strength is thus consistent with the upper-bound computed from our scaling law. In the figure, we show the range of the normalized magnetic field inferred for Mars from the SNC meteorites by the vertical bracketed bar. The range of normalized magnetic field clearly indicates that the Martian dynamo was in the "on" state when the SNC meteorites were formed about 1.3×10^9 years ago. Currently, it is clearly in the "off" state. Thus, Mars can be considered to be an example of the two-state dynamo system: up to 1.3×10^9 years ago it operated near its magnetostrophic limit, whereas currently it is in the lower zero magnetic field state. Mars' solar wind interaction may be the first example of a hybrid obstacle to the solar wind composed of both an atmospheric obstacle, like that of Venus, and a weak magnetic obstacle formed by the remanent magnetism that would be the fossil of a once-robust global dynamo-generated magnetic field.

Contacts: Steven A. Curtis and N. F. Ness
Code 695

Sponsor: NASA Program in Planetary Atmospheres Research

Dr. Steven Curtis, who holds a PhD degree from the University of Maryland, is a space plasma physicist with the Laboratory for Extraterrestrial Physics. He is particularly interested in the coupling of planetary atmospheres and magnetospheres. Dr. Curtis has 19 years of experience at Goddard, and he received an Exceptional Achievement Award for the correct prediction of Uranus' nonthermal radio emissions.

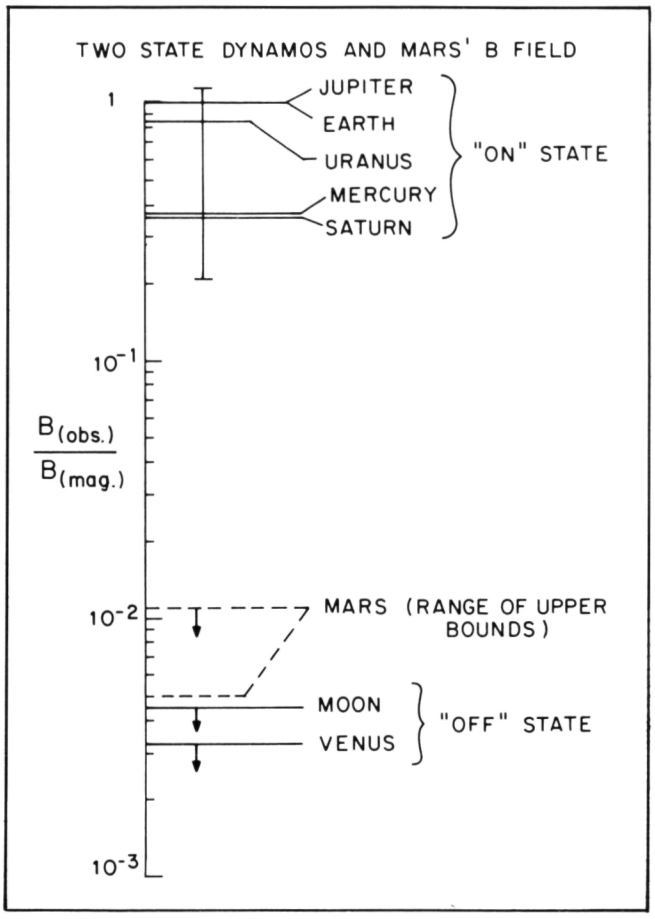

Comparison of observed magnetic field and that derived from magnetostrophic balance for the planets in the solar system for which data exist. The data fall into two groups: a magnetostrophically limited upper, or "on," state and a lower, or "off," state. From Mars' current position on this plot, we infer that Mars currently lacks any global dynamo and that any intrinsic magnetic field component to the solar wind interaction is due to remanent magnetism from an earlier active dynamo. From the inferred magnetic field from the SNC meteorites that are believed to be of Martian origin, the range of Mars' magnetic field approximately 1.3 B.Y. ago places it clearly in the range of active magnetostrophically limited dynamos, as illustrated by the vertical bar. Hence, the earlier robust magnetic field of Mars was the source for possible extensive remanent magnetism on the Martian surface.

MARS OBSERVER REMOTE SENSING GAMMA-RAY SPECTROMETER

Knowledge of the elemental composition of the surfaces of planets, comets, and asteroids is of fundamental importance for an understanding of such solar system bodies. The nature of this composition is related to the mechanisms of accretion and accumulation leading to planetary formation. The distribution of elements is related to the geological processes that were operative during planetary evolution. Measurements of discrete line X-ray and gamma-ray emission from condensed bodies in space can be used to obtain both qualitative and quantitative elemental compositions. Characteristic line emissions in this energy domain (0.2 keV to 10 MeV) can be attributed to several processes such as natural radioactivity, solar X-ray fluorescence, and cosmic ray primary and secondary induced activity. X-ray and gamma-ray spectrometers have been successfully flown on several planetary spaceflight missions, and geochemical maps were obtained. Such spectrometers were included on Apollo 15, Apollo 16, and Viking Landers of the United States spaceflight program; as well as the Luna Missions, Mars 4 and Mars 5, and several Venera missions of the Soviet Union.

The X-ray and Gamma-ray Remote Sensing (XGRS) spectrometers are being proposed for use on several future planetary missions. These missions are part of the program developed under the Solar System Exploration Committee Study. Because such instrument systems find use on a multitude of missions, the XGRS spectrometer was selected to be developed as a facility instrument to be flown where appropriate on the Planetary Observer and Mariner Mark II families of missions. The NASA has selected the Goddard Space Flight Center to have the responsibility of developing the XGRS facility instruments. The first of such missions, the Mars Observer mission, has been approved by the NASA for launch in September 1992. Because of the Martian atmosphere, only the gamma-ray portion of this facility instrument can be utilized. A Gamma-Ray Remote Sensing (GRS) spectrometer facility instrument has been chosen as part of the

Mars Observer payload. The GRS spectrometer also includes a neutron detection system.

An international group of scientists was chosen as the Flight Investigation Team (FIT) for the Mars Observer GRS facility instrument. The group consists of W. Boynton of the University of Arizona; J. Arnold, University of California, San Diego; P. Englert, University of Cologne and the University of California, Santa Cruz; W. Feldman, Los Alamos National Laboratory; A. Metzger, Jet Propulsion Laboratory; R. Reedy, Los Alamos National Laboratory; S. Squyres, Cornell University; J. Trombka, Goddard Space Flight Center; and H. Wanke, Max Planck Institute. The Goddard instrument manager is S. Floyd, and the Goddard instrument scientist is J. Trombka.

The Mars Observer mission poses several technological challenges for the design of the GRS instrument. First, a high-purity n-type Ge detector must be used to obtain the high-energy resolution and also radiation damage resistance required for mission operation. The mounting design of such a delicate crystal to ensure survival through the launch environment is a critical development effort. The design of an efficient but strong radiative cooler to operate the detector at cryogenic temperatures is a major engineering effort. Next, the Ge detector system must be able to be annealed to allow the detector to be recovered if there is extensive detector degradation due to radiation damage. Further, the construction materials for the GRS instrument must be selected so that they will cause minimum interference with the Martian gamma-ray characteristic line emission. These materials emit background gamma-radiation due to their natural radioactivity and cosmic ray–induced activity. Finally long-term spectrometer electronics stability is required to maintain the fine spectrometer continuous operation of over 2 years in Mars' polar orbit.

Extensive tests of the mounting and the mechanical system have been successfully carried out to develop a mechanical design that will survive the launch environment. Radiation damage studies utilizing high-energy protons are planned to verify the radiation hardness and annealing recovery capability of the system. All materials used for construction of the GRS are carefully screened to ensure that there will be a minimum gamma-ray radiation interference. Ultra-stable electronics are being designed and tested for use in the analog and digital portion of the electronics system. The figure shows a cutaway view of the GRS sensor head, as presently designed.

Contact: Jacob I. Trombka
Code 682

Sponsor: Office of Space Science and Applications

Dr. Jacob Trombka is Project Scientist for the Mars Observer Gamma-Ray Spectrometer and for the X-Ray/Gamma-Ray Remote Sensing Spectrometer for the Planetary Observer Missions. Dr. Trombka, who holds a PhD degree from the University of Michigan, is a recipient of the John Lindsay Award and the NASA Exceptional Scientific Achievement Medal, as well as several Group Achievement Awards. Dr. Trombka has been with Goddard for 24 years.

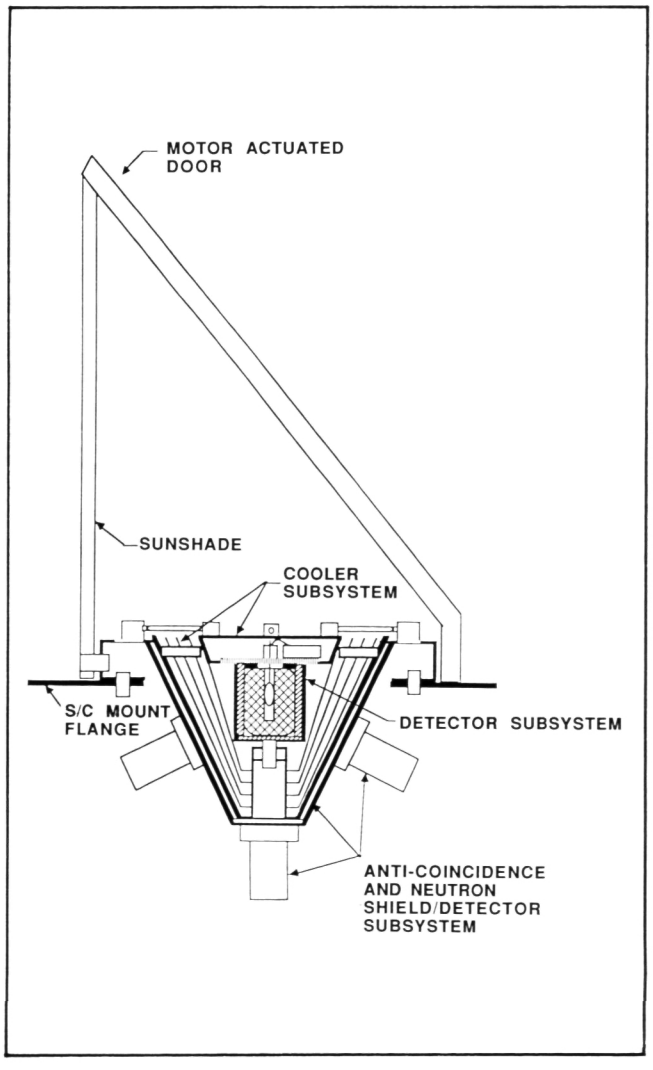

Cutaway view of the GRS sensor head.

ATMOSPHERES

STUDIES OF COMPARATIVE PLANETOLOGY

By popular perception, the environment of Venus is Dantesque, with extensive lightning and exploding volcanoes injecting large amounts of SO_2 high into the atmosphere. This view, portrayed in books, journal articles, and films, is largely based on plasma measurements made from the Pioneer Venus Orbiter (PVO). If valid, the lightning-volcanism scenario would have very significant implications for comparative planetology, involving the disciplines extending from plate tectonics and volcanism to the physics of the solar wind interaction with the ionosphere. Ongoing investigations of alternative explanations of the observations are being pursued at Goddard.

The lightning-volcanism scenario has been primarily encouraged by measurements from the PVO, which has been orbiting Venus since encounter in December 1978. Electric field noise at 100 Hz has been interpreted by F. Scarf and C. Russell (1983) as evidence of whistler mode waves stimulated from lightning discharges in the lower atmosphere. These authors also state that the noise appears most often when the PVO passes over mountainous regions, such as the Aphrodite highlands. Since it has been argued that the cloud physics of Venus is not conducive to natural lightning formation, Scarf and Russell argue that the mountainous regions must contain active volcanoes, whose explosive eruptions would supply the atmospheric perturbations necessary to induce lightning. In turn, these speculations were followed by the work of L. Esposito (1984), in which observed variations in the atmospheric SO_2 content were argued to result from massive volcanic eruptions, an order of magnitude larger than volcanoes experienced at Earth!

Through cooperative research between GSFC and Rice University, considerable evidence has been accumulated that discounts the asserted lightning-volcanism scenario. In particular, it has been shown that the 100 Hz noise in question is correlated with anomalous ionospheric troughs that are believed to be linked with the solar wind interaction with the nightside ionosphere. These plasma troughs, like their counterparts in the auroral regions of Earth, are the focus of solar wind–induced energetic processes that stimulate plasma instabilities, which in turn are believed to explain much of the observed electric field noise, negating the lightning interpretation.

However, evidence counter to the interpretation of lightning and volcanism has not been adequately addressed, and recently R. Singh and C. Russell (1986) asserted further evidence of lightning on Venus, which supported the previous work. Again through independent research, we have shown that the selection criteria and the data analyzed by Singh and Russell are incompatible with the work of Scarf and Russell. This is illustrated in the figure, where the electric and magnetic field data from PVO are shown, revealing that the types of noise independently interpreted as lightning by the two groups are totally different in nature and in time and space.

Lightning and explosive volcanism may or may not be presently occurring at Venus—the evidence is insufficient. Aside from the speculations on the PVO results, which we discount, we know of no evidence for or suggestions of present-day explosive volcanism on the planet. The independent observations of variations in SO_2 may be explained by changes in atmospheric circulation, and if so, there is no need to infer massive injections of this gas from volcanic sources.

Overall, investigations of PVO results have stimulated substantial interest and debate. The ongoing observations and research offer the potential for useful new insight into processes of common interest to the understanding of all planetary environments.

Contact: Harry A. Taylor, Jr.
Code 610

Sponsor: Office of Space Science and Applications

Mr. Harry Taylor, Jr., is a Principal Investigator for Pioneer Venus. His scientific specialties are ionospheric physics, aeronomy, and ion spectroscopy, and his professional interests include comparative planetology and scientific objectivity. Mr. Taylor, who received a BS degree from American University, has 29 years of experience at Goddard. He is a recipient of the Exceptional Scientific Achievement Award.

ORIGINAL PAGE IS
OF POOR QUALITY

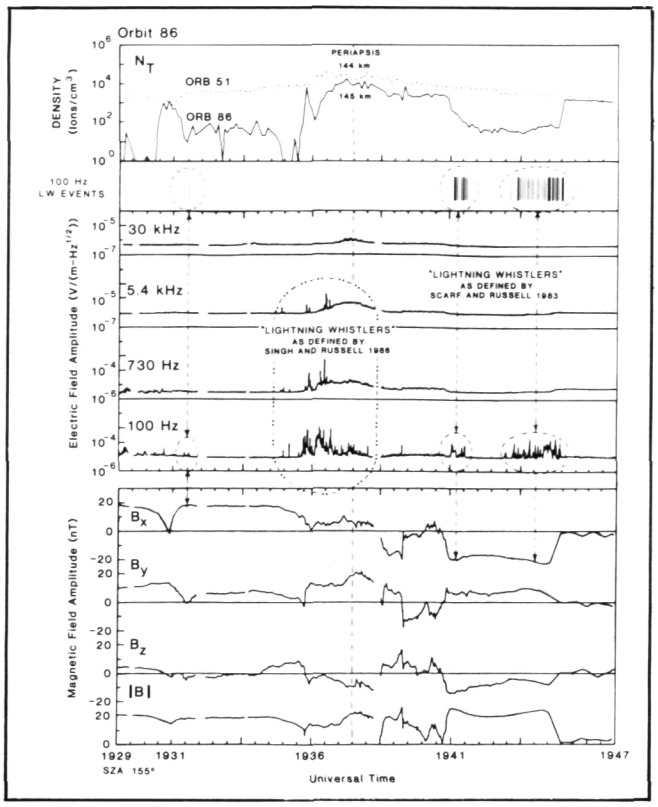

A composite of the contents of Figure 1 of Singh and Russell (1986) extended earlier and later in time, and with the addition of the time series of total ion density (N_T), for orbits 86 (with ion troughs) and 51 (no troughs). Specific 100 Hz noise bursts have been attributed to lightning-induced whistler waves by F. Scarf for orbit 86. We designate these bursts as LW events, and indicate each burst by a line segment at the corresponding time. No LW events were reported for orbit 51. These signals are exclusive to the 100 Hz channel and typically appear within ion troughs. Totally distinct from the LW activity, "lightning whistlers" as identified by Singh and Russell appear across the interval 1935–1938 as broadband impulsive noise, where the field is no longer radial. The smooth noise increase across periapsis has been attributed to impact-produced ion-acoustic noise by Curtis et al. (1985).

THERMAL AND MECHANICAL STRUCTURE OF THE CRUST AND UPPER MANTLE OF VENUS

Despite the relatively close proximity of Venus and the Earth, until recently little was known about the nature of the surface of Venus because it is obscured by an optically opaque atmosphere. To obtain a global view of the planet, images have been obtained using radar techniques. Radar images such as Figure 1 have revealed that Venus had an active geologic past exemplified by structural surface features that indicate broad-scale compression (folding and mountain-building) and extension (rifting). The forces responsible for the extensive deformation of the Venus surface are primarily a consequence of stresses associated with the loss of heat from the planet. The mechanism by which a planet loses heat determines the temporal and spatial extents of volcanic and tectonic activity, and knowledge of this mechanism is therefore crucial in understanding the manner in which a planet has evolved. Important insight into the mechanisms of heat transfer in a planet can be gained by understanding the thermal and mechanical structure of its crust and upper mantle.

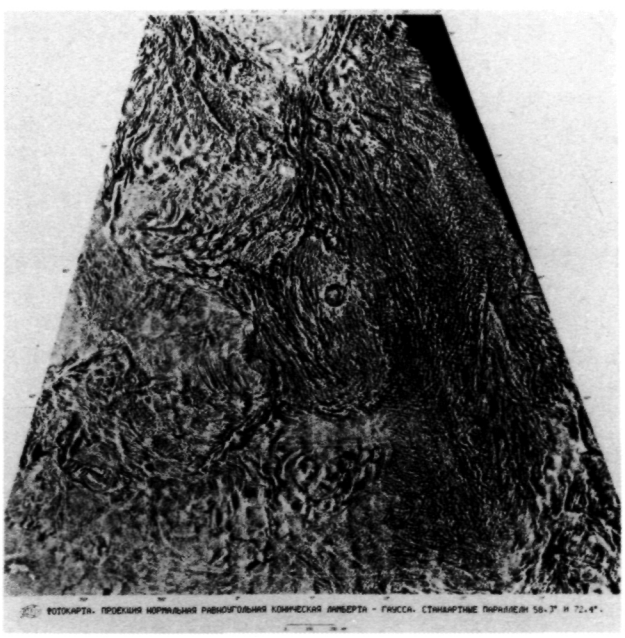

Figure 1. Radar image of surface deformational features in the northern hemisphere of Venus obtained by the Soviet Venera 15/16 spacecraft.

Fundamental knowledge of Earth's internal structure (e.g., density, temperature, and composition) is generally obtained from ground truth data such as earthquakes and gravity. On Venus, such data either does not exist or is not of high enough resolution to allow one to discern the structure of the shallow interior. Instead, the geometries of features observed in radar images can be used

to determine the subsurface structure. Many features of both compressional and extensional origin on Venus exhibit a very regular spacing. Two wavelengths of deformation have been recognized—a shorter one of 10–20 km and a longer one of 100–300 km. Theoretical models that describe the behavior of the outer shell of a planet in extension and compression have been developed and show that these wavelengths are primarily controlled by the thicknesses of strong or high viscosity layers in the crust and upper mantle. These layer thicknesses are governed by the thermal and compositional structure of the planet's outer shell. The structure of this outer shell can be constrained by combining theoretical models with observations of surface features and experimental data on the mechanical properties of rocks extrapolated to Venus' conditions.

Figure 2 shows possible ranges of the crustal thickness and near-surface thermal gradient of Venus as constrained by the geometries of two types of surface features: rift zones, which are extensional, and ridge belts, which are compressional. In both cases, the red boxes represent model results that are consistent with the geometries of the observed features. The results show that thermal gradients of <25 °K km^{-1} and crustal thicknesses <20 km are implied in areas where these features occur. The models also require that Venus' upper mantle is either stronger than or of comparable strength to the upper crust, which is consistent with experimental rock mechanics data.

The Earth loses heat primarily by solid-state convection in the mantle. This process is manifest as plate tectonics in which new seafloor is created at mid-ocean ridges over the hot, upwelling limbs of convection cells, and consumed at subduction zones that overlie cold, downwelling limbs of convection cells. The dominant mechanism of heat transport in a planet is related to its size and mass. Since Earth and Venus are similar in these regards, it might be expected that Venus also loses heat primarily by convection and therefore also should exhibit plate tectonics. Plate tectonics has not yet been positively identified on Venus; however, it cannot be ruled out given the resolution of current data. It has been suggested that plate tectonics does not occur on Venus because the crust is too thick everywhere to subduct. However, the modeling results described above suggest that the crust in many parts of Venus has a thickness similar to that of the Earth's ocean floor, where subduction is observed to occur. Therefore, if plate tectonics is not operating on Venus, alternative reasons, such as Venus' lack of water or high surface temperature, may need to be invoked. Further understanding of the dominant mechanism(s) of heat transport and the style of planetary evolution of

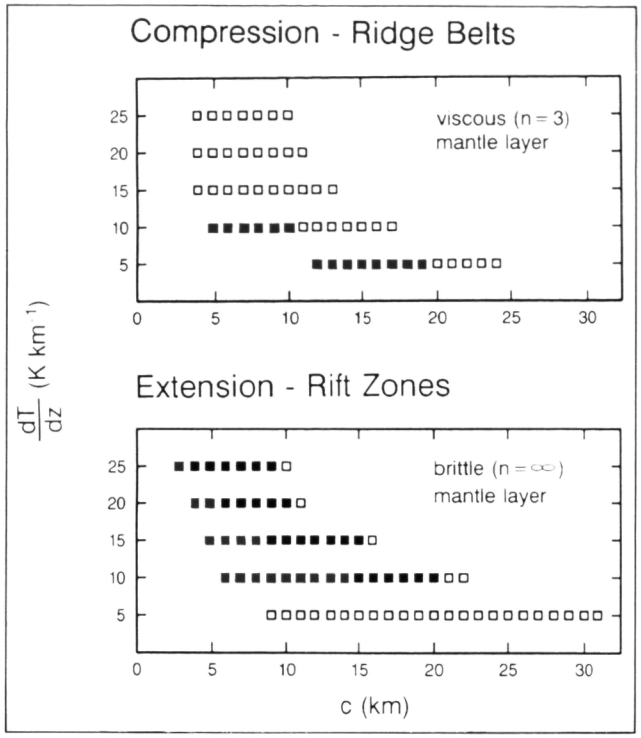

Figure 2. Thermal gradients and crustal thicknesses predicted by models of surface deformation on Venus. The red boxes are values that are consistent with the wavelengths of compressional and extensional surface features.

Venus will be possible through the development of more refined theoretical models and through the analysis of higher resolution radar images of the surface such as will be obtained in the upcoming Magellan mission.

Contact: Maria T. Zuber
Code 621

Sponsor: Office of Space Science and Applications

Dr. Maria Zuber, who received a PhD degree from Brown University, is a geophysicist whose professional interests include theoretical modeling of the structure and evolution of the solid planets. Dr. Zuber has been with Goddard for two years.

VENUS' FOUR-DAY SUPERROTATION, MIXING LENGTH THEORY AND EDDY DIFFUSION

Venus slowly rotates in the retrograde direction with a period of 243 days. At the same time, we know from

ground-based and spacecraft measurements that its atmosphere rotates much more rapidly. In the vicinity of the visible clouds, it spins with a period of about 4 days, in the direction of the planetary rotation (superrotation). This corresponds to a zonal velocity of about 100 m/s near the equator, 50 times larger than that of the surface—"one of the most surprising results to emerge from planetary exploration" (Covey et al., *Icarus*, 1986).

Actually one finds that in our solar system, every known atmosphere superrotates, including our own. Moreover, the observed maximum zonal velocities averaged over the globe are all typically between 25 and 150 m/s. This range is remarkably narrow considering the large differences in the physical properties of the planets and their varying distances from the Sun. Thus, the Venus 4-day superrotation may not be unusual. It may only appear unusual to the extent that the observed 100 m/s winds occur on a slowly rotating planet (with surface velocities of only 2 m/s). Apparently, nature is trying to tell us something.

In principle, atmospheric superrotation can be understood in terms of the so-called Hadley mechanism. An engine operates transforming some of the Sun's thermal energy into the meridional motions of a Hadley circulation, which redistributes energy and angular momentum, dissipated by eddy diffusion. The resulting pressure gradients are balanced by Coriolis and centrifugal forces to drive zonal winds in the direction of the planetary rotation (superrotation). Through surface friction, the angular momentum required for atmospheric superrotation is provided by the planet.

General circulation models of the Hadley mechanism have not been able to reproduce the observed magnitudes of the zonal circulation. In a recent analysis, computer experiments were carried out with different planetary rotation periods. For the longest period of 64 days, the computed zonal velocities were only 16 m/s, with a trend indicating that the magnitudes would be even smaller for the much longer rotation period of Venus.

The problem with the Hadley mechanism is that the transient eddies and Reynolds stresses interacting with the circulation are not understood. Since they must dissipate the expended energy, one may assume that their effects are diffusive; so parameterizations can be adopted in terms of eddy diffusion coefficients. These coefficients, however, are not known *a priori*. Unlike the coefficient of molecular diffusion, which depends only on the local properties of the medium, one may expect that the eddy diffusion coefficients are closely related to the circulation and ultimately to the forcing behind it, the absorbed solar radiation. But what is this relationship?

To address this question, we have assumed that the eddy diffusion coefficient and the meridional Hadley circulation are related through the mixing length hypothesis. Combining this constraint with the well-known meteorological concept of the Rossby radius of deformation yields zonal velocities around 100 m/s, qualitatively describing the trend observed in planetary atmospheres. In this view, the solar heating is both driving the superrotation through the meridional Hadley circulation and is dampening it through eddy diffusion. Thus, the heat source related to the planet-Sun distance does not appear explicitly.

In testing this hypothesis, we have developed a steady-state nonlinear one-layer model and performed parametric studies to find a relationship between the heat source (driving the motions), the meridional Hadley circulation, and the eddy diffusion coefficient, which would yield the large zonal velocities observed on Venus. This analysis leads to the following conclusions: 1) Proportional changes in the heat source and eddy diffusion coefficient do not significantly change the zonal velocities. 2) For a given heat source, the meridional velocities are virtually constant for large eddy diffusion coefficients. The zonal velocities then decrease with decreasing planetary rotation rates, consistent with the above-quoted results from a general circulation model (GCM). 3) Below a threshold in the diffusion rate, however, the meridional velocities decrease, commensurate with the mixing length hypothesis. Eddy heat transport then becomes important and shares with the Hadley cell advection in balancing the solar heating. The zonal velocities then reach large values near 100 m/s and are independent of the planetary rotation rate, reproducing the observed behavior.

Our analysis suggests that the computed zonal velocities depend sensitively on the eddy diffusion coefficients and heating rates adopted. The two cannot be chosen independently, any more than one can choose the surface gravity independently from the mass of a planet. This may be important for simulations with general circulation models that suffer from uncertainties in the parameterization of diffusion. Related to this is another problem: for the eddy diffusion coefficients chosen in these models, the integration times may have been much shorter than is needed to reach steady state. Short of performing parametric studies with present GCMs, prohibitive computationally, an alternative might be to choose artificially high eddy diffusion coefficients that shorten the integration times; to compensate for this, one could adopt larger heating rates. A scenario like this would not describe a known planet. But it may afford parametric

studies of an idealized fluid that shed light on the relationship between circulation and eddy diffusion, providing the basis for a self-consistent treatment of the problem.

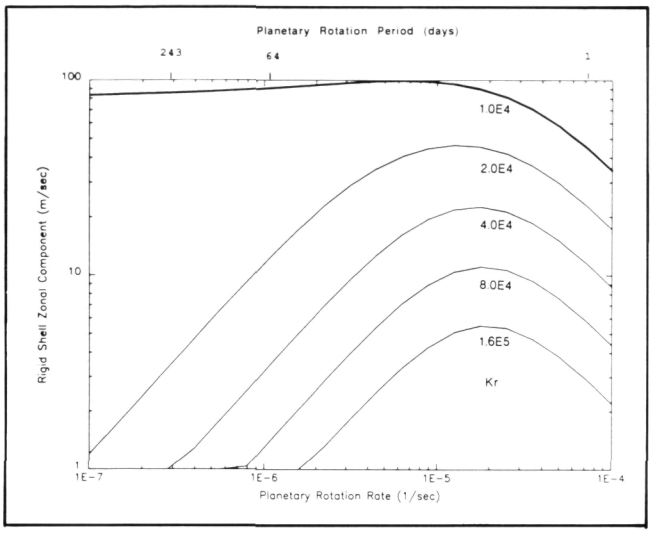

The rigid shell zonal component of superrotation at the equator, equivalent to the velocities quoted in the text, computed for different vertical eddy diffusion coefficients K_r (cm^2/s) and planetary rotation rates (or periods).

Contacts: Hans G. Mayr, Isadore Harris, and Kenneth Schatten
Code 614

Sponsor: Office of Space Science and Applications

Dr. Hans Mayr is an atmospheric scientist with the Dynamics Explorer and Pioneer Venus projects. Dr. Mayr, who holds a PhD degree from the University of Graz, has 19 years of experience with Goddard.

Dr. Isadore Harris, who received a PhD degree from Northwestern University, is a planetary aeronomist with 27 years of service with Goddard.

Dr. Kenneth Schatten, who holds a PhD degree from the University of California at Berkeley, is a solar physicist with the Solar Disk Sextant project. Dr. Schatten has been with Goddard since 1969 and has received several awards for his scientific achievements.

CLIMATOLOGY AND GENERAL TERRESTRIAL

CLOUD-CLIMATE STUDIES

One of the most difficult problems in climate dynamics is to determine the role of cloudiness in climate change. The clouds are a reflecting blanket; they can cool the planet by reflecting sunlight back to space, or they can warm it by trapping terrestrial radiation. It is not clear *a priori* whether cooling or warming wins out. Important new observational data sets that can shed light on this question are being produced through the International Satellite Cloud Climatology Project (ISCCP), the First ISCCP Regional Experiment, and Earth Radiation Budget Experiment.

To provide a framework for analysis and interpretation of these data, simulation studies of global cloudiness and its effects on climate have been carried out with the UCLA/Goddard Laboratory for Atmospheres' General Circulation Model (GCM). Results from the GCM are being analyzed to determine the simulated global distribution of cloudiness, the interactions of the clouds with large-scale circulations and the hydrologic cycle, and the sensitivity to aspects of the model's formulation. Data from ISCCP, High-resolution Infrared Sounder/Microwave Sounder Unit (HIRS2/MSU), Nimbus-7, and conventional sources have already been used for validation. Particular attention is being given to cloud radiative forcing (CRF), the interactions of cloudiness with cumulus

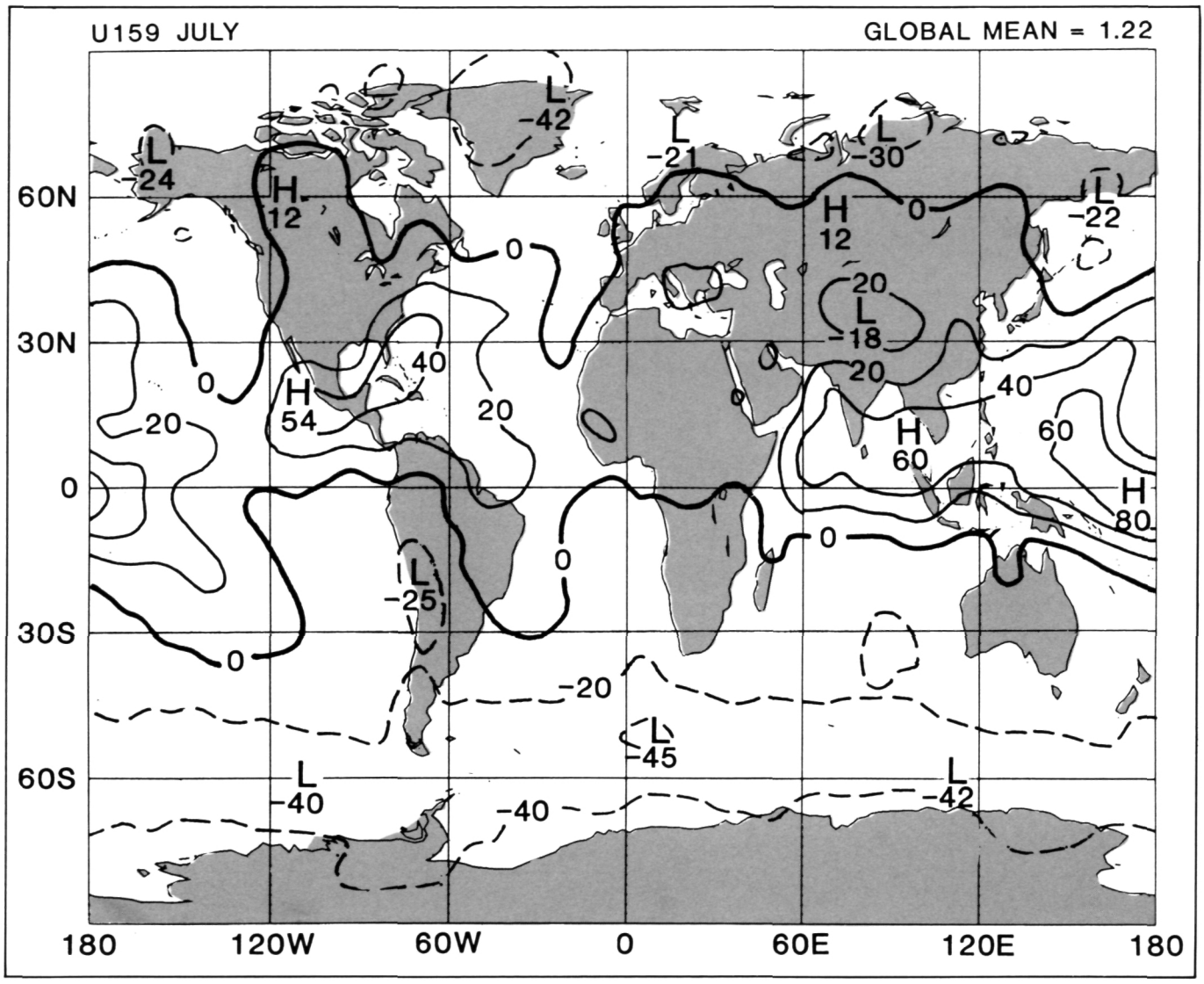

July atmospheric longwave cloud radiative forcing simulated by the UCLA/GLA general circulation model.

convection and boundary layer turbulence, and diurnal variability.

The CRF is defined as the difference between a radiation flux in the presence of clouds and that which would occur in the absence of clouds with all other fields unchanged. Here we briefly examine some CRF results from a July simulation with the GCM.

According to the model results, the net CRF is a cooling of -19.3 Wm^{-2} for the planet as a whole. The solar component of -47.6 Wm^{-2} thus dominates, although the longwave component of 28.3 Wm^{-2} is of comparable magnitude. These forcings are associated with a simulated planetary albedo of 29 percent and an outgoing longwave flux of 233 Wm^{-2}, which agree well with satellite observations. In a global sense, both the longwave and shortwave CRFs are felt almost entirely by the surface; the atmosphere is hardly affected. This is true even locally for the solar CRF, but, as shown in the figure, the terrestrial CRF has broad regions of intense positive and negative values, which nearly cancel in the global mean. In the Western Equational Pacific, the warming approaches 100 Wm^{-2}, whereas near the poles the cooling exceeds -40 Wm^{-2}. For comparison, a precipitation rate of 1 mm day^{-1} corresponds to a latent heating of 27 Wm^{-2}.

The clouds warm or cool the atmosphere depending on the altitude at which they occur. A high cold cloud tends to warm the atmosphere because it absorbs intense radiation from the Earth's surface, while emitting only weakly. In contrast, a low warm cloud tends to cool the atmosphere because it emits strongly both upward and downward, while absorbing mainly on its lower side. Since high clouds are common in the tropics, whereas low clouds occur frequently near the poles, the zonally averaged atmospheric CRF is a warming in the tropics and a cooling in higher latitudes, thus demanding a poleward heat transport by the atmosphere, in addition to that required by latent heating. The zonal structure of the atmospheric CRF is also very strong, with warming at longitudes of rising motion, where high clouds occur, and cooling at longitudes of sinking motion, where low clouds occur. The vertical motion field induced by the atmospheric CRF thus tends to feed back positively on the clouds. This tantalizing result suggests the possibility of radiative-dynamic instabilities.

Sensitivity tests with the GCM show that the high cloudiness associated with cumulus convection tends to suppress convection over land. This appears to be a result of cloud shadows, which reduce the surface evaporation. In this case, the surface CRF produces a negative feedback. A similar negative feedback, with a longer time scale, may operate over the oceans. A coupled ocean-atmosphere model is needed to investigate this.

Unlike some other climate models, the UCLA/GLA GCM includes the diurnal insolation cycle. The diurnal variability of cloudiness and precipitation simulated by the model is very pronounced, even over the oceans, and has an orderly geographical structure. Encouraging agreement with observed diurnal variations has been found.

These continuing cloud-climate studies are revealing not only the magnitudes of cloud effects on climate, but also the mechanisms through which these effects are produced.

Contact: David A. Randall
Code 611

Sponsor: Office of Space Science and Applications

Dr. David A. Randall, a meteorologist with the Global Modeling and Simulation Branch, joined Goddard in 1979. He holds a PhD degree in atmospheric sciences from the University of California at Los Angeles.

CLOUD CHEMISTRY ON THE GIANT PLANETS

The atmospheres of the giant planets are composed primarily of hydrogen and helium. In these atmospheres, the fully reduced forms of oxygen, carbon, nitrogen, and sulfur are water (H_2O), methane (CH_4), ammonia (NH_3), and hydrogen sulfide (H_2S); these compounds are expected to be the predominant forms of these elements in the upper tropospheres of the giant planets. The clouds are expected to be composed of liquid or crystalline phases of H_2O, CH_4, NH_3, H_2S, and NH_4SH (ammonium hydrosulfide). Remote sensing observations of the atmospheres of the giant planets are limited by cloud and gas opacities to the region well above the predicted base of the deepest cloud, that of water. We have used chemical equilibrium models, constrained by measurements of the composition of the visible atmosphere, to infer the cloud structure and to study the chemical reactions controlling the atmospheric composition throughout the cloud-forming regions. Since many of the trace gases are soluble in water, we have included the effects of aqueous chemistry on their vertical distribution and identified the factors influencing their abundance above the water cloud.

Vertical profiles of the mixing ratios are shown in the figure. Since methane remains well mixed (i.e., has a constant mixing ratio) throughout the cloud-forming region on Jupiter, it has been omitted from the figure. Observation of a solar NH_3/H_2 ratio at pressures less than 1 bar requires a bulk abundance of nitrogen that is at least 1.5–2 times solar to offset the effects of aqueous chemistry and the formation of NH_4SH. These results are based on the assumption that N/S remains solar. One analysis of Jupiter's microwave spectrum suggests that the NH_3 abundance is depleted by a factor of two in the region from 2 to 1.5 bar. Aqueous chemistry cannot be responsible for the observed depletion NH_3, since by the 2 bar level the solution cloud is already in the ice phase, and aqueous reactions no longer occur. A more likely explanation is the formation of NH_4SH with an enhanced (3 times solar) abundance of H_2S.

A similar situation is found to exist on Uranus. We find that 20–30 percent of the NH_3 is removed in solution by the cloud but that aqueous chemistry alone cannot account for the severe depletion in the 150–200 °K region of the atmosphere required to fit microwave observations. Again, a more likely explanation is the formation of NH_4SH clouds with an enhanced (4 times solar) abundance of H_2S.

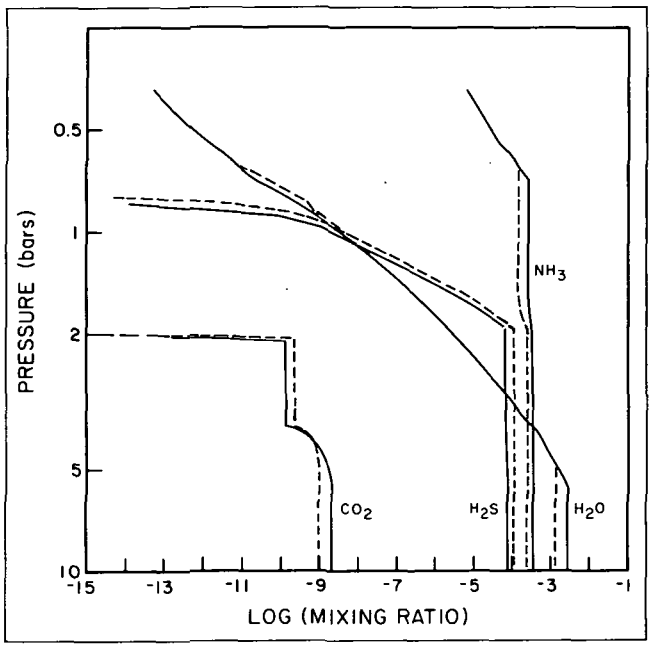

Vertical profiles of the mixing ratios predicted with a 2 times solar atmospheric composition (black lines). An alternative composition in which the NH_3 abundance is assumed to be 1.5 times solar, whereas the H_2S abundance is assumed to be 3 times solar, is also shown (red lines). Both of these assumed compositions fit the observations at pressures less than 1 bar.

This situation produces a delicate chemical balance between the abundances of NH_3 and H_2S above the water cloud. Perturbations to this balance, for example, by the general circulation on Uranus, would then produce regions with either NH_3 or H_2S clouds aloft.

The Voyager Radio Occultation experiment results suggest that methane comprises more than 2 percent of the atmosphere of Uranus, corresponding to a 28 times solar enhancement. The abundances of nitrogen, sulfur, and oxygen in the atmosphere of Uranus are not constrained by present measurements. Furthermore, our chemical equilibrium results suggest that the ratios of these elements present in the atmospheres of the giant planets are not solar. This has important implications for models of the composition and evolution of these atmospheres, as well as for models of the composition and conditions in the solar nebula at the time of their formation. *In situ* measurements, such as those that will be provided for Jupiter by the Galileo probe, combined with detailed chemical modeling are required to refine our understanding of these planets and the evolution of their atmospheres.

Contact: Barbara E. Carlson
Code 640

Sponsor: Office of Space Science and Applications

Dr. Barbara Carlson, who earned a PhD degree in mechanical engineering at the State University of New York at Stony Brook, specializes in planetary atmospheres at the Goddard Institute for Space Studies. Her professional interests include radiative transfer in cloudy atmospheres with an emphasis on remote sensing applications for planetary atmospheres, tropospheric chemistry in the atmospheres of the giant planets, and cloud physics. Dr. Carlson has been a part of Goddard since 1984.

HIGH-ENERGY ELECTRONS AS COUPLING MECHANISM BETWEEN THE MAGNETOSPHERE AND THE EARTH'S MIDDLE ATMOSPHERE

Only recently have instruments been flown to continuously monitor highly relativistic electron fluxes in Earth's magnetosphere. It has been observed that $\gtrsim 2$ MeV electrons increase dramatically for periods of a few days in the outer magnetosphere (at a geocentric radial distance of ~6.5 Earth radii; $1R_E$ = 6375 km), often with a recurrence period of ~27 days. This periodic enhancement in the relativistic electron flux is related to persistent solar wind stream structure in the middle and outer heliosphere, which in turn is controlled by the solar rotation. It is found that during a high-energy electron event period, the energy spectrum is very hard, with significant flux enhancements extending to >10 MeV. At present, the origin of the multi-MeV electron population in the outer magnetosphere is not clear. It is known that these electrons are not produced directly by substorms or major geomagnetic storms. One model of the electron source attributes the entire acceleration process, going from thermal energies all the way to several MeV, to physical processes such as radial diffusion and recirculation entirely interior to the terrestrial magnetosphere. A second model suggests that the initial and major acceleration occurs in Jupiter's magnetosphere. In this latter model, energetic Jovian electrons propagate to Earth and subsequently populate the terrestrial magnetosphere where they are further accelerated and confined.

Regardless of the ultimate source of the relativistic electrons, measurements clearly reveal their frequent presence

in the magnetosphere. Such electrons are very important from the standpoint of spacecraft operations, since multi-MeV electrons are known to cause satellite malfunctions and failures. When we consider the outer magnetosphere as a whole, the principal loss process is probably precipitation into the Earth's atmosphere.

Auroral electron precipitation is confined to a narrow latitudinal band (latitude ~68°–72°), i.e., the auroral oval itself, and auroral electrons penetrate only down to ~100 km altitude before stopping (see Figure 1). Unlike the auroral electrons, multi-MeV electrons are capable of penetrating down to the lower D-region and into the upper stratosphere over a broader latitudinal range. The bremsstrahlung X rays that such electrons produce when interacting with atmospheric constituents can penetrate even more deeply; thus both the primary electrons and the secondary photons can be significant ionization sources.

We have used a numerical transport code to study the interaction of relativistic electrons with the Earth's atmosphere. The code provides a realistic one-dimensional representation of vertical atmospheric densities and cross sections. We take actual electron spectra measured at 6.6 R_E for observed relativistic electron enhancements. The calculations (see Figure 2) show the large energy deposition rate in the 40–80 km altitude range, which is due to the ionization energy loss during the peak of an electron precipitation event. The secondary peak at ~25 km altitude is due to the bremsstrahlung deposition. Even this photon deposition is significant. For comparison, we have included the energy deposition rates for galactic cosmic rays (at solar maximum and solar minimum) at 50° geomagnetic latitude and for solar extreme ultraviolet. At mesospheric and upper stratospheric heights, the relativistic electron energy deposition is dominant when multi-MeV electrons are present. By use of the standard value of 35 eV per ion pair to estimate the ion production rate, we see in Figure 2 that the peak rate is 1000–3000 ions $(cm^3\text{-}s)^{-1}$ at ~50 km altitude.

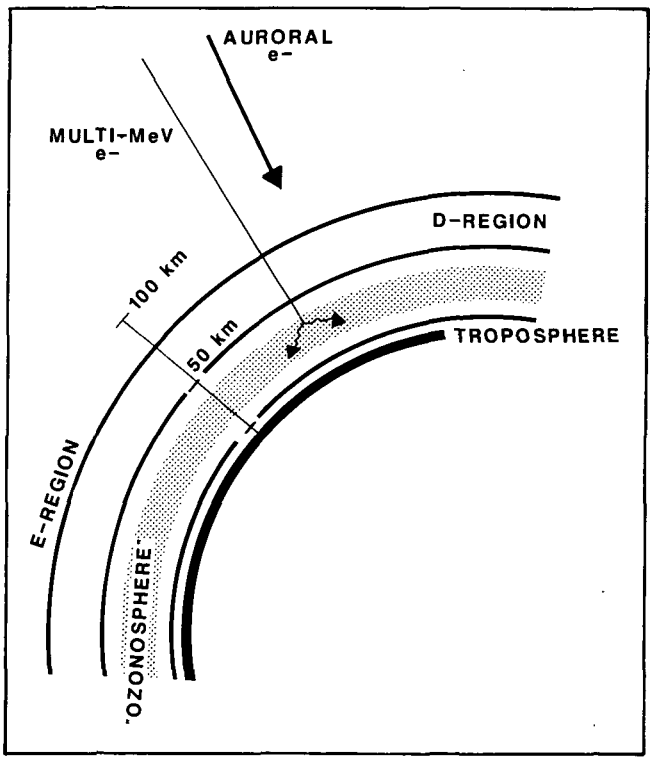

Figure 1. A cross-sectional view of the Earth's atmosphere and ionosphere showing the interactions due to energetic electron precipitation.

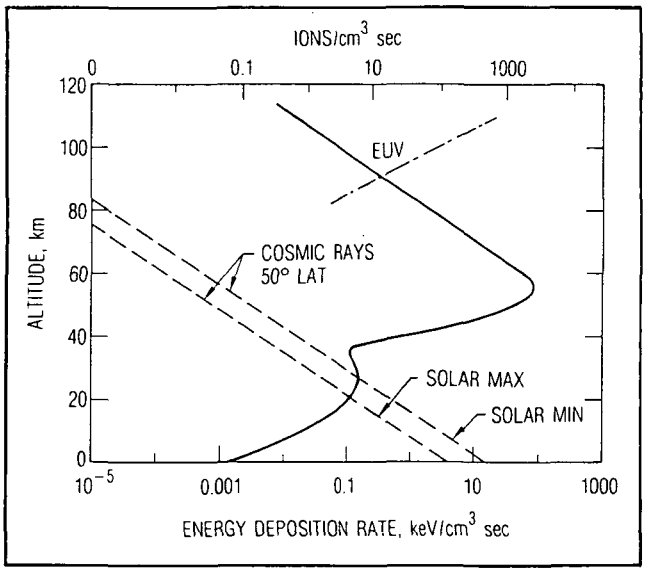

Figure 2. Results of a numerical transport code used to study the interaction of relativistic electrons with the Earth's atmosphere. The code provides a representation of vertical atmospheric densities and interaction cross sections throughout a complete vertical column of the neutral atmosphere and the ionosphere.

Relativistic electron precipitation (REP) events can be major sources of odd hydrogen and odd nitrogen in the atmosphere that, in turn, remove ozone (O_3) catalytically. Thus, enhanced relativistic electron precipitation events can lead to increased concentrations of odd-hydrogen compounds (H, OH, and HO_2) and odd-nitrogen compounds [N, $N(^2D)$, NO, and NO_2] in the 40

to 80 km altitude region of Earth's middle atmosphere. It follows from these models and from results as shown in Figure 2 that there may be a decrease in ozone concentrations caused by the increased concentrations of odd hydrogen (HO) and odd nitrogen (NO). It is conceivable that these chemical perturbations could lead to substantial temperature changes in the mesosphere and consequent changes in eddy mixing rates and gravity wave propagation. The NO increase would also lead to an increase in the daytime D-region electron density.

It has been previously speculated that a modulation of stratospheric ozone might affect the thermal structure and radiative damping properties of the middle atmosphere. Thus, it was suggested that this could influence the tropospheric energy budget and the atmospheric wave reflection characteristics involved in tropospheric weather system development. Our results support this general concept and extend the idea in several ways. First, the energies of electrons that we have measured are far greater than those in REP events, and as shown above, the energy deposition, ionization, and chemistry modification will extend much deeper into the atmosphere than previously suspected. Second, we find strong solar cycle variability in the multi-MeV electron component that will, in turn, impose a strong variability on ionization and chemistry effects on the middle atmosphere, possibly extending deep into the stratosphere. Third, we argue that relatively broad mid-latitudinal bands on the Earth's surface are involved.

A plausible scenario, therefore, may be the following. The Sun exhibits a strong 11- and 22-year activity cycle. A prominent aspect of this activity cycle is the occurrence of large, recurrent solar wind streams emanating from persistent coronal holes. They extend down to the solar equator and give rise to high-speed solar wind streams at $\gtrsim 1$ AU only during the approach to solar (sunspot) minimum. The high-speed streams, in turn, strongly control the presence or absence of multi-MeV electrons in Earth's outer magnetosphere. These relativistic electrons, when precipitated into the middle atmosphere, substantially modify O_3 concentrations, and thus leverage, and modify a much larger energy supply, i.e., solar ultraviolet radiation that may then affect tropospheric patterns as suggested above.

We cannot at present establish all elements of the above scenario, but we can say that the presence of multi-MeV electrons is soundly established by our *in situ* magnetosphere observations. The energy depositional and concomitant chemical effects in the middle atmosphere should follow. It remains to be seen how, or if, a true tropospheric connection can be established. Nonetheless, we would suggest that the effects of this previously unobserved magnetospheric electron component on the middle atmosphere could be profound.

Contact: Daniel N. Baker
Code 690

Sponsors: Office of Space Science and Applications and the U.S. Department of Energy

Dr. Daniel Baker recently joined Goddard as Chief of the Laboratory for Extraterrestrial Physics. His professional interests include solar-planetary relations, magnetospheric physics, plasma astrophysics, cosmic particle acceleration, and magnetosphere-atmosphere coupling. Dr. Baker, who received a PhD degree from the University of Iowa, is Associate Editor of Geophysical Research Letters *and is scientific representative to SCOSTEP. He has served on the National Academy of Sciences/Space Science Board's Committee on Data Management and Computing, and on the Panel on Long-Term Observations.*

INTERPLANETARY SHOCK AND DISCONTINUITY DRIVEN WAVES IN THE MAGNETOSPHERE: PROPAGATION DELAYS

This study, which combines theory and observational data, attempts to track an interplanetary (IP) signal and its resulting effects from the time it is detected at the Interplanetary Monitoring Platform-8 (IMP-8) spacecraft until it is seen as a sudden commencement signal in the Earth's magnetic field at various stations on the ground. This IP signal may be either a shock wave or a magnetic field directional discontinuity in the solar wind. Using data in the 1978 and early 1979 time frame, we have identified nine shock and five large directional discontinuities, the latter chosen because they possessed a large magnetic field magnitude change across the transition zone, in that sense resembling a shock. In both cases there is usually a large change of momentum across the transition zone. For some events, one or more spacecraft from among Geostationary Operational Environmental Satellite-2 (GOES-2) and GOES-3 and Synchronous Meteorological Satellite-2 (SMS-2) were located at synchronous orbit during the propagation of the resulting magnetohydrodynamic (MHD) wave in the magnetosphere, thus enabling them to observe this wave at 6.6 R_E altitude. In the case of an IP shock, the signal's path is envisaged to look like that shown in the figure.

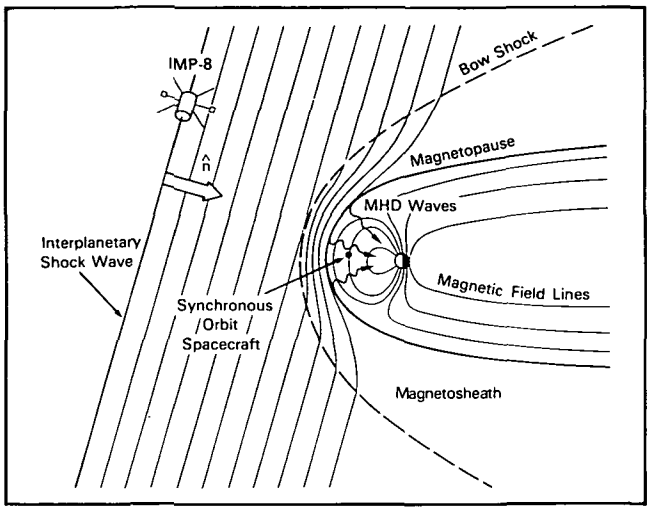

Sketch showing an interplanetary shock, observed first at IMP-8, which impinges on the Earth's magnetosphere and causes MHD waves to propagate within the magnetosphere.

The associated analytical path and assumptions used in the study are the following:

1) The detected IP shock front is assumed to be planar and to move in a straight line in IP space along the direction (**n**) normal to the shock surface at a speed reflecting the net effect of solar wind convection and shock wave propagation with respect to the solar wind. These speeds and the normal are determined from IMP-8 data with a highly accurate scheme recently developed at Goddard by A. F. Viñas and J. D. Scudder.

2) The IP shock surface strikes the Earth's bow shock at a point and time determined from knowledge of **n** and the detection time at IMP-8, as well as from assumptions of the shape of the bow shock and the state of the solar wind; the latter determines the size of the magnetosphere (primarily from the density and speed of the solar wind in front of the IP shock as measured by IMP-8). The shape of the bow shock is estimated with a formula developed by D. Fairfield.

3) The IP shock is modified by the bow shock and moves at a slower speed in the magnetosheath than in the solar wind. How much slower depends on the specific point of interest in the magnetosheath; for example, it moves slowest at the "nose."

4) This signal first strikes the magnetopause at a position, which we estimate, that is slightly downstream of an imagined point of first contact for an unimpeded (by the bow shock) IP shock.

5) Finally, the disturbed (fluctuating) magnetopause acts as a source of MHD waves throughout the magnetosphere. These are detected at synchronous orbit and on the ground. A primary goal of this study is to determine the time delay between the detection at IMP-8 and at synchronous orbit and those delays between synchronous orbit and at various positions on the ground and the total delay time (ΔT).

The scenario is almost the same for the case of the IP directional discontinuity, except that its normal is determined from minimum-variance analysis of the IP magnetic field, a well-known and usually accurate procedure. Of considerable interest will be differences noted between shock-produced waves and those produced by the directional discontinuities. These would include the associated time delays and the signatures at synchronous orbit and on the ground.

MHD wave propagation in the magnetosphere has been the subject of much theoretical work, such as time-delay calculations based on general properties of the magnetosphere. However, there has never been a sufficient number of spacecraft in appropriate positions (one of them necessarily located at the magnetopause) to properly track such waves from outer boundary to ground to confirm these theoretical studies. With the advent of accurate analysis schemes, such as the Viñas-Scudder shock-fitting computer code, we are able to accurately estimate the time and location of the first contact point between the IP shock and the bow shock (and, hence, between the modified IP shock and the magnetopause), making possible empirical estimates of the time delays of interest.

Preliminary results of the study show that the first point of contact with the bow shock for IP shocks is rarely in the region around the nose of the bow shock. These points are, in fact, extremely scattered, ranging in geocentric longitude from 41° to 89°, with respect to the Sun-Earth meridian plane, and in latitude from −53° to 42°, with respect to the ecliptic plane. The derived delay times, ΔT, also occur over a large range, 1.2 to 3.6 minutes, and surprisingly reveal no obvious relationship to the longitude of the first contact point on the bow shock. Also, we have determined that the average propagation speed from the first contact point to a spacecraft in synchronous orbit is about 1000 km/s.

This work comprises a combined effort of scientists at four institutions: Prof. A. Lazarus (MIT), who provided

the solar wind plasma data measured by IMP-8; Prof. M. Sugiura and Prof. A. Araki (University of Kyoto, Japan), who are providing ground-based data, synchronous orbit data, and theory to account for the MHD wave propagation in the magnetosphere; Prof. S. Kokubun (University of Tokyo, Japan), who is also providing synchronous orbit data; and the authors (Goddard) who have provided IMP-8 magnetic field data and who are coordinating the study. We hope that the results of this investigation will provide information useful to studies conducted during the International Solar Terrestrial Physics program, when simultaneous data from many more spacecraft may be utilized.

Contacts: Ronald P. Lepping and Adolfo F. Viñas
Codes 695 and 692

Sponsor: Office of Space Science and Applications

Dr. Ronald Lepping specializes in plasma physics and magnetospheric and interplanetary physics at the Laboratory for Extraterrestrial Physics. He performs magnetometer experiments on IMP-8 (Principal Investigator), Voyagers 1 and 2 (Co-Investigator), and ISTP-GEOTAIL and WIND (Co-Investigator). Dr. Lepping holds a PhD degree in physics from Rensselaer Polytechnic Institute, and he has 18 years of experience at Goddard.

Dr. Adolfo Viñas, a plasma physicist with the Interplanetary Physics Branch, is interested in plasma waves and instabilities in the solar wind and magnetosphere. Dr. Viñas holds a PhD degree in physics from the Massachusetts Institute of Technology, and he has seven years of service with Goddard.

INTRACAVITY DYE LASER DETECTION OF OZONE: ABSORPTION IN THE CHAPPUIS BANDS

Over the past decade considerable progress has been made in understanding the impact of natural and anthropogenic perturbations on the Earth's stratosphere. Of particular interest is the effect of the industrial release of chlorofluoromethanes, since photolysis of these compounds has been shown to produce chlorine atoms that catalytically destroy ozone (O_3). With the discovery of the Antarctic ozone hole, this problem has received increased attention. In one chemical explanation of this phenomenon, the reaction of chlorine oxide (ClO) and bromine oxide (BrO) plays a pivotal role. Such suggestions require accurate laboratory measurements of the appropriate photochemical and chemical kinetic processes, and this in turn frequently necessitates the development of new detection methods.

Intracavity laser detection is being developed as a complement to other methods for application to the detection of atmospheric species in laboratory experiments. In previous studies the technique was used to monitor trace quantities of nitrogen dioxide (NO_2), which represents a class of absorbers for which the transition linewidths are narrower than the laser bandwidth, so-called narrowband absorbers. Here laser mode competition produces dips in the laser spectral profile. The depth of such a dip was shown to correlate with NO_2 concentration, and it was demonstrated that for this situation, the intracavity technique is 10^5 times more sensitive than conventional absorption techniques. The method was then applied to a measurement of the rate of reaction of nitric oxide (NO) with oxygen (O_2) by detecting the NO_2 product, and agreement with previous measurements using conventional techniques was excellent.

The Chappuis bands of O_3 are a rather structureless, very weak absorption system in the visible portion of the spectrum. Here the absorption bandwidth is larger than the laser bandwidth; it is referred to as broadband absorption and represents the other extreme of intracavity absorption processes. Now each laser mode is affected by the absorber so that mode competition does not dominate, and no dips occur in the laser spectral profile. However, the area under the profile was shown to correlate with concentration and can therefore be used for detection. The accompanying figure shows the change in the laser spectral profile as the O_3 concentration was varied; the dye laser was centered at 630 nm. In (a) no absorber was present in the system, and in (b) through

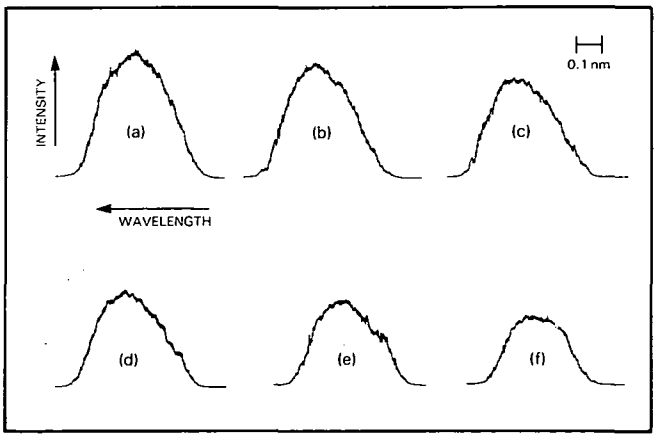

Intracavity absorption by O_3 in the Chappuis bands.

(f) the O_3 concentration varied from ~89 millitorr to ~372 millitorr. Although the technique is not as sensitive for broadband absorbers as it is for narrowband absorbers, it is ~10^2 to 10^3 times more sensitive than conventional absorption techniques under similar conditions. Experiments are in progress to understand the basic laser physics associated with intracavity absorption processes and to extend the method to ultraviolet and infrared wavelengths.

This program has benefitted from collaboration with the Johns Hopkins University through support of Dr. W. D. Brobst on the NASA Graduate Student Researchers Program. Dr. Brobst completed his doctoral research while working at GSFC on this project; he has continued his affiliation with GSFC as an NAS/NRC Resident Research Associate. Cooperative efforts with the University of Maryland continue through the support on the NASA Graduate Student Researchers Program of Mr. T. M. Lang.

Contact: John E. Allen, Jr.
Code 691

Sponsor: Office of Space Science and Applications

Dr. John Allen, Jr., is involved in research of interstellar grains, cometary and planetary atmospheres, and the upper atmosphere with the Astrochemistry Branch of the Laboratory for Extraterrestrial Physics. His professional interests include the application of optical techniques to chemical physics and the application of chemical physics to aeronomy and astrophysics. Dr. Allen received a PhD degree in applied physics from the University of Florida, and he has served with Goddard for nine years.

RESEARCH WITH NEAR REAL-TIME DATA FROM THE TOTAL OZONE MAPPING SPECTROMETER

The Nimbus-7 spacecraft has been in orbit since October 1978. Although designed for only 1 or 2 years of service, this satellite and its sensors still provide global coverage of some highly useful atmospheric parameters. Among the measurements, the Total Ozone Mapping Spectrometer (TOMS) instrument is providing high-resolution data on the nature and evolution of the atmosphere's ozone layer, particularly by the Antarctic ozone hole.

Over the intervening years, TOMS has had a highly successful record in obtaining crucial data for a variety of scientific experiments. For example, in the early part of this decade, NASA's TOMS team was called upon to provide near real-time ozone distributions in an effort to assess the presence of this gas in the cabins of high-flying jet aircraft. The cabin ozone experiment was only the first accomplishment in providing real-time ozone measurements.

When it was learned that the sulfur dioxide emissions from erupting volcanoes could be easily monitored with the TOMS instrument, many geological organizations requested access to the measurements in real time, as well.

In the winter of 1986, TOMS demonstrated its ability to provide real-time data for an extended scientific experiment. The Genesis of Atlantic Lows Experiment was a meteorological experiment that highlighted both the versatility and dependability of the instrument. During a 3-month period, TOMS provided continuous coverage of total columnar ozone and thus permitted studies of the relation of cyclogenesis to the ozone distribution. This show of reliability led to a subsequent, even more demanding real-time commitment for TOMS: the Antarctic Ozone Hole was discovered.

In 1985, a group of British scientists under the leadership of J. Farman discovered what appeared to be an unusually thin layer of ozone over their Halley Bay ozone station in Antarctica. Subsequent work confirmed that ozone concentrations over Antarctica were indeed being depleted year after year. When data from the TOMS instrument were inspected, a graphic depiction of the location and expanse of the ozone hole was found. The stage was set for another real-time TOMS experiment.

In the meantime, a team of scientists conducted surface-based measurements of the atmospheric chemical constituents from McMurdo base in Antarctica. This experiment, called the National Ozone Experiment, reflected the general concern of politicians and scientists alike that chlorine atoms released by ultraviolet sunlight falling on commercially produced chlorofluorocarbons may be having a deleterious effect on the ozone layer.

When NASA scientists examined the global TOMS data, they found that, although there was indeed a large area of ozone depletion in the Southern Hemisphere, it was also evident that the area surrounding the hole showed increased thickness of the ozone layer. From the figure it can also be discerned that the minimum ozone values decreased over 40 percent between October 1979 and October 1985.

ORIGINAL PAGE
COLOR PHOTOGRAPH

This led atmospheric dynamicists to suggest that perhaps the ozone was merely undergoing transport from one part of the hemisphere to the other and merely reflected a circulation change. So the two principal theories concerning formation of the ozone hole involved both chemistry and dynamics. Clearly, a definitive experiment that could measure not only the chemistry but the dynamics of the stratosphere was called for; hence, the Airborne Antarctic Ozone Experiment was designed.

The Airborne Antarctic Ozone Experiment was organized and managed by NASA personnel with substantial contributions from the NOAA, the National Science Foundation, the Chemical Manufacturers Association, various American universities, and European meteorological organizations. The experiment included flights of ER-2 and DC-8 aircraft, which were fully instrumented to measure ozone, aerosols, water vapor, ClO, BrO, HNO_3, NO, NO_2, CH_4, N_2O, air temperature, winds, and a host of trace species.

In support of the mission, Goddard's Atmospheric Chemistry and Dynamics Branch, the Nimbus Operations Center and the STX Corporation, Lanham, Maryland, provided near real-time TOMS data for the purpose of locating the ozone hole for use in flight planning. The author served as the Principal Investigator for this portion of the experiment.

Through a sophisticated communications network set up by Research and Data Systems, Inc., Greenbelt, Maryland, various near real-time data were assembled and transmitted to the aircraft operations center at Punta Arenas, Chile. Data sources included were Solar Backscatter Ultraviolet (SBUV) total ozone charts provided by R. McPeters (GSFC), SBUV/2 charts from R. Nagatani and A. Miller (NOAA), and total ozone charts derived from NOAA-10 High-resolution Infrared Sounder (HIRS) infrared radiance data from both J. Susskind (GSFC) and D. Cariolle (CNRM, Toulouse, France). Meteorological forecast charts came from the

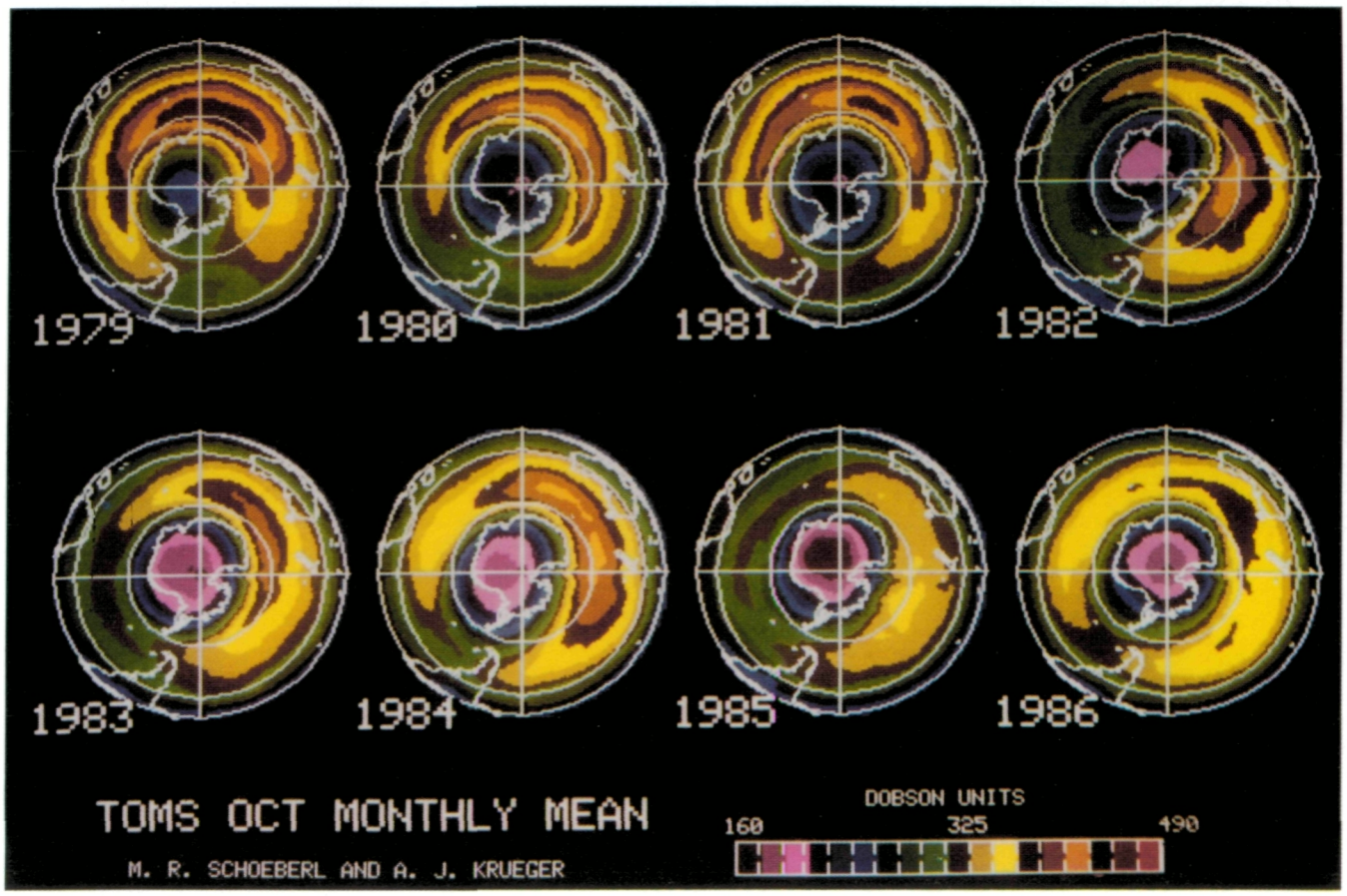

Global TOMS ozone data.

European Center for Medium Range Weather Forecasts (ECMWF) and the United Kingdom Meteorological Office (UKMO). The GSFC Global Modeling and Simulation Facility led by W. Baker also provided stratospheric analyses of temperature, winds, and potential vorticity to Punta Arenas.

Special radiosonde and ozonesonde observations were flown from Palmer Station on the Antarctic Peninsula by a team of NASA personnel from Wallops Island. These data were essential for providing weather data for the aircraft operation.

Aerosol profiles, gleaned from Nimbus-7 Stratospheric Aerosol Measurement (SAM) II measurements, were provided daily by P. McCormick of Langley Research Center. These data were useful for determining the possible presence of polar stratospheric clouds that have often been related to the ozone minima over the Antarctic continent.

Contact: Arlin J. Krueger
Code 616

Sponsor: Office of Space Science and Applications

Dr. Arlin Krueger, who received a PhD degree from Colorado State University, is Sensor Scientist for Nimbus-7 TOMS. His scientific specialties are atmospheric physics and chemistry, and his professional interests include volcanology and meteorological effects on the ozone. Dr. Krueger developed rocket and satellite instruments for measurements of the ozone. He has been with Goddard for 18 years, and he is a recipient of the Exceptional Achievement Award.

OBSERVATIONS FROM SPACE SHUTTLE ASSIST IN DETECTION OF A GLOBAL OZONE TREND

Stratospheric ozone depletion has become a major environmental concern because changes in ozone column amount will modify the amount of ultraviolet radiation reaching the Earth's surface, since ozone absorbs solar radiation in the wavelength region shorter than 300 nm. Changes in the vertical distribution of ozone can modify the radiative properties of the atmosphere and thereby alter the climate on a regional or global scale by modifying the atmospheric temperature structure. Ozone changes are being predicted as a result of certain man-made gases such as chlorofluorocarbons being released into the atmosphere.

There is now compelling observational evidence that atmospheric ozone is being altered on a global scale. The Antarctic ozone hole has been observed from both satellite and ground-based systems. To date, the cause of this hole during the austral spring has not been explained by models that employ our best understanding of the chemistry and dynamics of the atmosphere. In addition, observations from the Nimbus-7 Solar Backscatter Ultraviolet (SBUV) experiment have recently been interpreted as showing a nearly 6 percent decrease in the global total amount and a 16 percent decrease near 48 km. These changes far exceed those predicted by our best photochemical models.

These results are being thoroughly examined by large segments of the scientific community involved with atmospheric science. The difficulty in interpreting and believing the satellite data is due to the large correction to the Nimbus-7 SBUV instrument sensitivity required to remove its degradation after being in orbit for nearly 9 years. As a follow-on to the Nimbus-7 ozone observations, the National Oceanic and Atmospheric Administration (NOAA) has embarked on an ozone monitoring program with the SBUV/2 instrument, which is a refinement of the Nimbus-7 instrument. The first instrument began taking data from NOAA-9 in January 1985. SBUV/2 observations will continue from the NOAA series of satellites until 1996 with three additional instruments. Coping with instrument degradation and providing continuity from one instrument to the next remain major concerns in the plan for observing ozone over the next decade.

As part of the national plan for monitoring ozone, an SBUV instrument similar to that being flown on the NOAA series will be flown on the Space Shuttle on a regular basis. The data from the Shuttle instrument (the SSBUV) will be compared with nearly coincident data taken by the operational instruments on the NOAA satellites. Comparisons will be made of the observables from the two spacecrafts, thereby eliminating the atmospheric model or algorithm that converts the observables to atmospheric ozone. These comparisons are then used to evaluate the calibration stability of the NOAA instruments. The observations to be compared are the solar irradiance and the Earth backscattered radiance in the wavelength range from 250 to 340 nm. SSBUV will be carefully calibrated in the laboratory before and after each flight. In addition, its calibration will be monitored before, during, and after the flight with a unique in-flight

ORIGINAL PAGE
COLOR PHOTOGRAPH

calibration system. The SSBUV data can then be used as a transfer standard to correct the global data set derived from the NOAA instruments.

When combining the data sets from the two instruments, several variables must be considered to derive the true ozone trend. The requirement is that the statistical uncertainty in the observed trend after being corrected by SSBUV data must be less than the predicted ozone trend at the 95 percent confidence level. A statistical model was developed to establish flight requirements for SSBUV. The following variables are considered in the model. The magnitude of the ozone depletion is predicted to be 0.4 percent per year while the duration of the monitoring period is 10 years (1986–1996 for this study). The SSBUV and SBUV/2 measurement precision should be better than 1 percent, and the long-term repeatability of the SSBUV calibrations should be about 1 percent.

Laboratory tests at GSFC demonstrate that these high precisions are readily achievable. Atmospheric variability must also be considered, since the coincidences are not exact. Analyses of Nimbus-7 ozone data demonstrate that under the conditions of SSBUV and SBUV/2 coincidences, atmospheric variability will be about 1 percent. The frequency of Shuttle flights should be about every 8 months, and the number of coincidences per flight should be of the order 24. An orbital analysis as shown in Figure 1 indicates that a coincidence will occur once per orbit if an hour window is allowed. Given this 1-hour window, atmospheric variations will be about 1 percent at low latitudes.

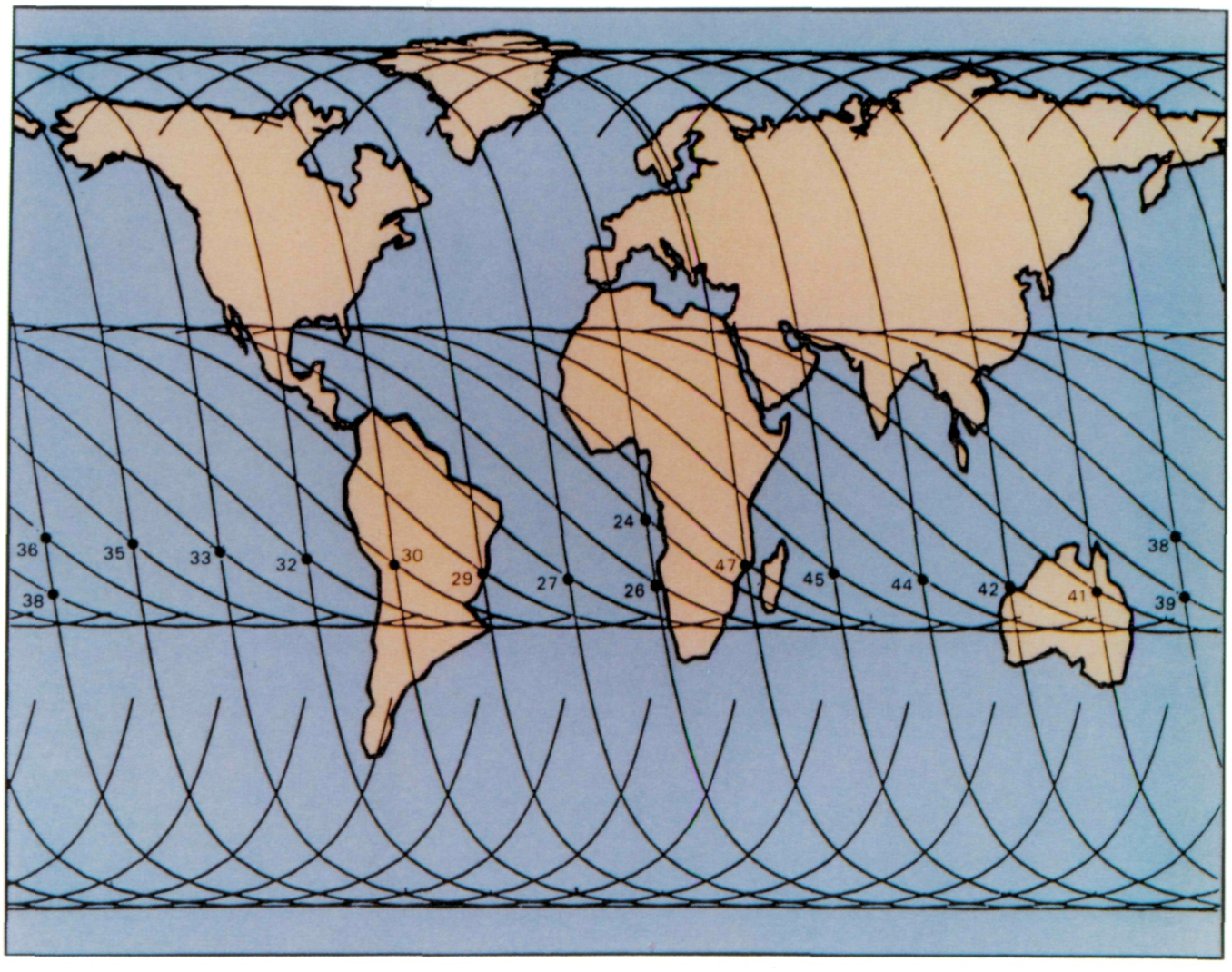

Figure 1. An analysis of Shuttle and TIROS satellite orbits demonstrates that 17 SSBUV and SBUV/2 coincidences (1-hour window) can be achieved per day.

ORIGINAL PAGE IS
OF POOR QUALITY

To ensure regular flights on the Shuttle, engineering interfaces need to be simplified and minimized. This has been accomplished through the use of Get-Away-Special (GAS) hardware developed at GSFC. Two GAS canisters are employed: the first, utilizing an opening lid, contains the SSBUV instrument; and the second contains the power, data, and command systems. This configuration is shown in Figure 2. This makes the SSBUV experiment a nearly stand-alone system. Most of the engineering

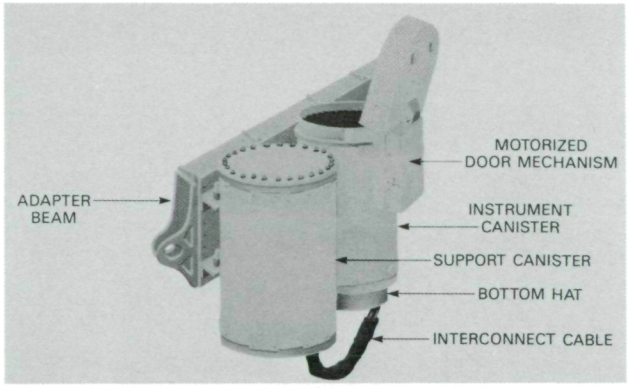

Figure 2. The SSBUV will be flown in two GAS canisters. These canisters are routinely flown on Shuttle. One canister contains an instrument nearly identical to that flown on the satellite. The second canister provides power, data, and command systems. This system minimizes Shuttle interfaces, ensuring regular flights.

developments to make the SBUV compatible with Shuttle are complete. Mission planning is at a fairly mature level, and the first flight will occur on STS-29 now scheduled for February 1989. Three flights are scheduled on 1-year intervals thereafter.

Contact: Ernest Hilsenrath
Code 616

Sponsor: Office of Space Science and Applications

Mr. Ernest Hilsenrath, Principal Investigator for the Shuttle SBUV, specializes in atmospheric sciences, experimental physics, and field observations. Mr. Hilsenrath received a BS degree in physics from George Washington University, and he has over 22 years of service with Goddard, where he received an award for innovative applications.

NON-LOCAL THERMODYNAMIC EQUILIBRIUM EFFECTS ON REMOTE SENSING OF STRATOSPHERIC GASES

The determination of concentrations of trace species in the stratosphere by measurement of infrared emission from vibrationally excited molecules constitutes an important part of our ability to remotely sense such concentrations. The Limb Infrared Monitor of the Stratosphere (LIMS) experiment on the Nimbus-7 satellite used this technique to measure concentrations of ozone (O_3), nitrogen dioxide (NO_2), water (H_2O), and nitric acid (HNO_3) over much of the stratosphere and some of the mesosphere, while the Stratosphere and Mesosphere Sounder measured nitrous oxide (N_2O) and methane (CH_4). GSFC's balloon-borne Stratospheric Infrared Interferometer Spectrometer (SIRIS) experiment uses this method to measure a variety of stratospheric trace species, including CO, O_3, $CFCl_3$, CF_2Cl_2, H_2O, CH_4, HNO_3, N_2O, NO_2, $ClONO_2$, and NO (Kunde, V., et al., 1987). This technique will also be used on two experiments on NASA's Upper Atmosphere Research Satellite (UARS), the Cryogenic Limb Array Etalon Spectrometer (CLAES), and Improved Stratosphere and Mesosphere Sounder (ISAMS). CLAES and ISAMS will together measure the same constituents as does SIRIS, along with HCl and N_2O_5.

Since these instruments all measure radiation emitted from excited states, the correct interpretation of the data requires that the ratio of the concentration of vibrationally excited molecules (the emitting species) to that of the ground state molecules (the desired quantity) be known. It is usually assumed that this ratio is determined by local thermodynamic equilibrium (LTE), which is given by a known function depending solely on the temperature of the atmosphere from which the emission originates. If LTE is assumed when it is not applicable, erroneous concentrations may be inferred.

In the past, it has been assumed that the LTE approximation is a valid one for the stratosphere and lower mesosphere because of the high molecular number densities there. Recent analysis of the LIMS data suggests that this may not be the case, however. Non-LTE effects have been found for O_3 (Solomon, S., et al., 1986), NO_2, and H_2O (Kerridge, B., and Remsberg, E., 1987) to result from the direct population by exothermic chemical reactions of vibrationally excited forms of either the emitting species (O_3, NO_2) or one that emits at the wavelength of another species (NO_2 for H_2O).

The importance of the remote measurement of infrared thermal emission in the SIRIS, CLAES, and ISAMS (and thus UARS) experiments suggests that possible non-LTE effects should be better understood prior to operation. Among the diatomic and triatomic species to be observed by infrared thermal emission, O_3, NO, NO_2, H_2O, CO, HCl, and ClO are produced in the stratosphere by exothermic chemical reactions and/or photolysis processes. They therefore have the potential for non-LTE effects associated with direct production of potentially emitting vibrationally excited states.

An assessment of the possible importance of non-LTE effects for these species has begun, and calculations demonstrate a potentially large effect (over 20 percent) for NO maximizing at approximately 30 km altitude. The major process producing NO in the stratosphere is photolysis of NO_2:

$$NO_2 + h\upsilon \rightarrow NO + O, \qquad (1)$$

which is known from a limited number of laboratory measurements to lead to preferential production of vibrationally excited NO at those wavelengths for which it is energetically possible. Another process producing NO that is important in the upper stratosphere is reaction of atomic oxygen (O) with NO_2:

$$O + NO_2 \rightarrow NO + O_2, \qquad (2)$$

for which nothing is known about the NO vibrational state distribution. Collisional excitation of ground state NO (the only mechanism producing vibrationally excited NO under LTE) is quite slow and at some altitudes is similar in magnitude to the rate of production of vibrationally excited NO by reactions 1 and 2.

We have carried out calculations of the relative importance of these various processes. Because of the scarcity of laboratory data, several assumptions needed to be made concerning the wavelength dependence of the vibrational state distribution of the NO produced in reaction 1 and the temperature dependence of that produced in reaction 2, as well as of the temperature dependence of the quenching of vibrationally excited NO by O_2. To make these assumptions, detailed considerations of experimental and theoretical results in chemical dynamics were required.

The results (non-LTE contribution of more than 10 percent of the population of vibrationally excited NO), summarized in the figure, indicate that non-LTE effects may be important over much of the middle stratosphere. Much larger non-LTE effects are predicted for higher vibrational levels of NO. The exact magnitude of these effects is open to some question, especially since there is uncertainty about the quenching rate of vibrationally excited NO by O_2 at stratospheric temperatures and about the vibrational state distribution of the NO produced in reaction 2. Nevertheless, the conclusions are sufficiently strong that they warrant further study.

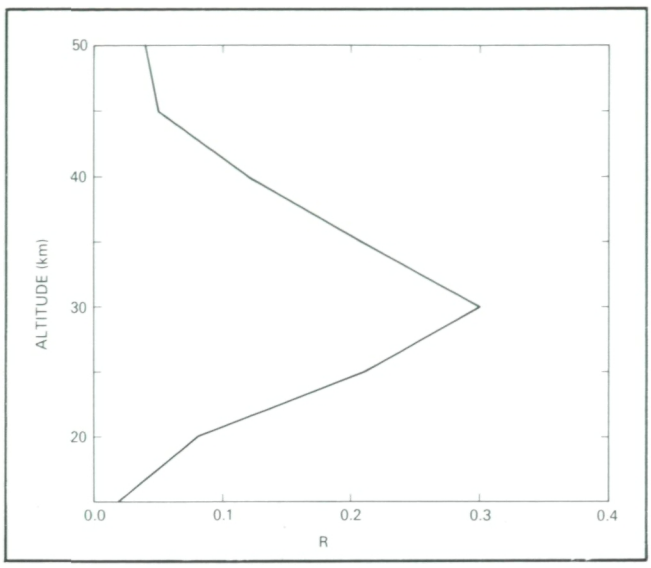

Plot of ratio R of NO(v = 1)/NO(v = 0) calculated with reactions 1 and 2 to that expected if LTE applies. Where R ≈ 0, non-LTE effects associated with direct photochemical production of vibrationally excited NO will be negligible; where R > 0, non-LTE effects make a contribution to the population of vibrationally excited NO.

Further assessment of similar non-LTE effects, which might affect other species to be studied by SIRIS, CLAES, and ISAMS, is under way. An important part of this work will be to highlight those photochemical processes for which additional laboratory data are needed if non-LTE effects are to be studied quantitatively.

Contact: Jack A. Kaye
Code 616

Sponsor: Office of Space Science and Applications

Dr. Jack Kaye is a space scientist assigned primarily to the Stratospheric General Circulation with the Chemistry Modeling Project. His professional interests include atmospheric chemistry, chemical kinetics and reaction dynamics, planetary atmospheres, and theoretical chemistry. Dr. Kaye, who holds a PhD degree from the California Institute of Technology, has almost four years of

experience at Goddard. He has also served as Vice Chairman and Chairman of the Younger Chemists Committee of the Chemical Society of Washington.

GLOBAL SURVEY OF THE IONOSPHERE AS OBSERVED ON AE-C AND DE-2 AND MODELED WITH THE IRI EMPIRICAL MODEL

A global scale survey of the electron temperature and density is made with data from the Atmosphere Explorer C (AE-C) and Dynamics Explorer 2 (DE-2) satellites and the International Reference Ionosphere (IRI) model. The IRI empirical model has been synthesized from a large data base comprising ground-based, rocket, and satellite measurements. It includes the electron temperature data from AE-C and none of the electron density data from AE-C and DE-2, yet there is good agreement between the combined AE-C and DE-2 data and the empirical IRI model. The global survey is made by plotting the electron temperature and density from averages in the altitude range 300 to 400 km versus invariant latitude, magnetic local time (MLT), and the solar activity index (10.7 cm radio flux F107).

Our survey is based on AE-C and DE-2 Langmuir probe measurements. Almost identical instruments were flown on AE-C (Brace, L., 1973) and on DE-2 (Krehbiel, J., 1981), covering a time period close to a solar cycle. The instrument provides measurements of electron density and temperature at the satellite altitude. AE-C was launched on December 16, 1973, into a highly elliptical orbit (perigee 149 km; apogee 4294 km) with an inclination of 68 degrees. In December 1974, the orbit was circularized at about 300 km where it was kept until February 1977, when it was placed in a circular orbit at about 400 km altitude until the end of its lifetime (re-entry in December 1978). AE-C was part of a satellite series that continued with AE-D and AE-E. Until now, AE-C was the longest and most data-intensive ionospheric satellite mission. DE-2 was launched on August 3, 1981, into an elliptical orbit (perigee 309 km; apogee 1012 km) with an inclination of 90 degrees.

The IRI is a joint project by the Union of Radio Science (URSI) and the Committee on Space Research (COSPAR) (Rawer, K., 1978; Bilitza, D., 1981). It was established by an international body of experts and has undergone more than a decade of improvement and critical review. IRI describes the global and temporal variation of electron density, electron and ion temperatures, and ion composition based on a large collection of ground-based, rocket, and satellite measurements. In the altitude range of interest for our study (300–400 km), the IRI electron density model is deduced from ground-based measurements, and the IRI electron temperature model is established with AE-C measurements (Bilitza, D., 1985).

We compare the average behavior as determined by the combined AE-C and DE-2 data base and by the IRI. For each satellite data point in the altitude range 300 to 400 km, the IRI model value is calculated, and average profiles in invariant latitude, MLT, and 10.7-cm solar radio flux (F107) are determined for the combined mission period (1974–1983). The resulting model and data average profiles for electron density and temperature are shown in Figures 1, 2, and 3. The standard deviations are between 15 and 25 percent for the data and the model. All the figures show excellent agreement between data and model averages.

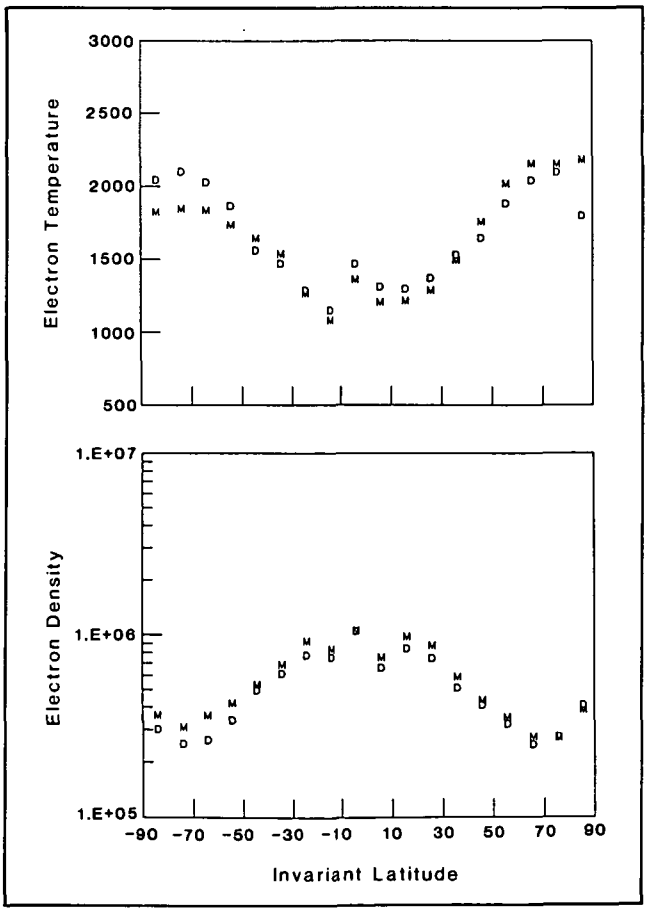

Figure 1. Latitudinal variation of electron density and temperature averaged over all longitudes, local times, seasons, and solar activity based on AE-C/DE-2 measurements (D) and on the IRI model (M).

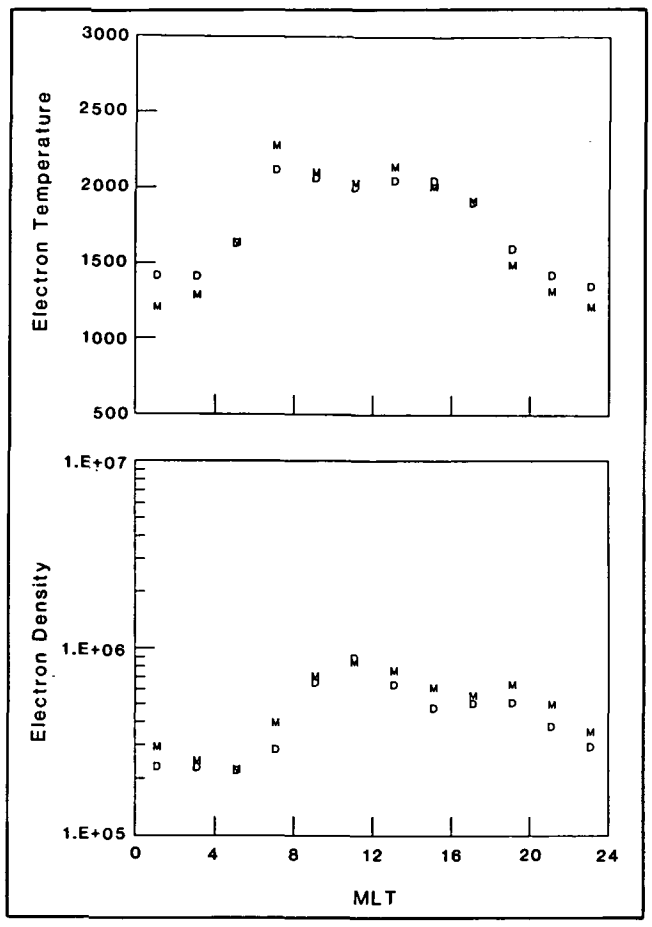

Figure 2. Diurnal variation of electron density and temperature averaged over all longitudes, latitudes, seasons, and solar activity based on AE-C/DE-2 measurements (D) and on the IRI model (M).

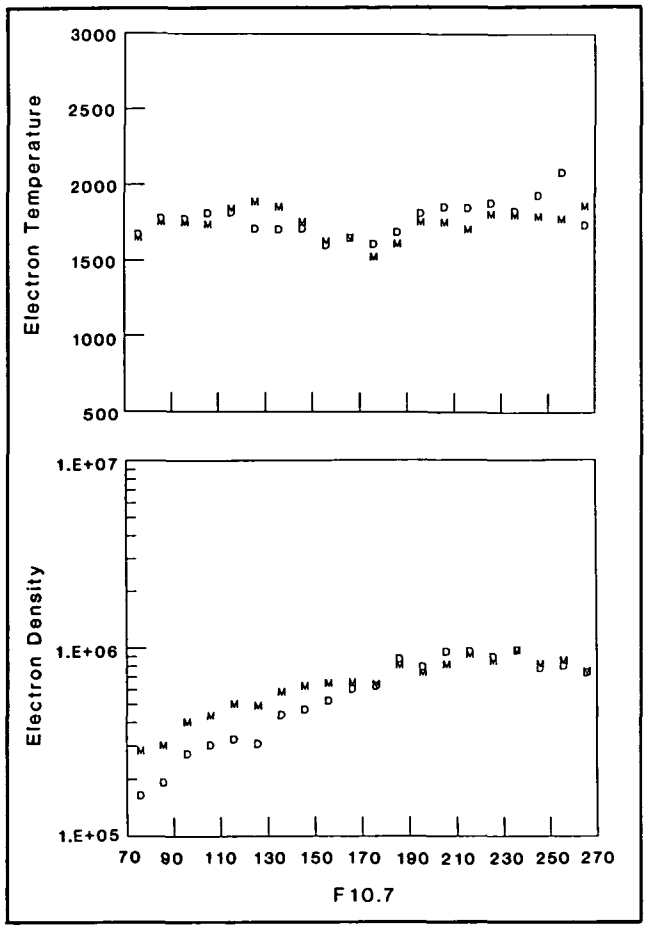

Figure 3. Electron density and temperature variation with the 10.7-cm solar radio flux averaged over all longitudes, latitudes, local times, and seasons based on AE-C/DE-2 measurements (D) and on the IRI model (M).

It should be noted that the characteristic features in all the figures represent fundamental variation patterns remaining after extensive averaging. Figure 1, for example, shows the typical latitudinal variation of electron density and temperature averaged over local time, season, and solar cycle. The figure shows the equatorial anomaly and the strong anti-correlation between electron density and temperature. The largest deviations between data and the model profile in Figure 1 are for latitudes poleward of 60°, where IRI has less density data due to a lack of ground stations.

Figure 2 shows the typical day-night variation averaged over all latitudes, seasons, and almost a whole solar cycle. The early morning and late afternoon peaks in electron temperature and the post-sunset increase in electron density remain as the most consistent features and are well reproduced by IRI.

Figure 3 shows that on average the electron density increases with solar activity, whereas the electron temperature remains at almost the same level. The good agreement between IRI and AE-C/DE-2 averages at low solar activity is expected because the IRI electron temperature model is based on AE-C data. The agreement of IRI and DE-2 at high solar activity is due to the small dependence of temperature on solar activity and to the latitudinal averaging used in this figure, which tends to mask the dependence. The average electron densities in Figure 3 indicate a saturation effect at very high solar activities in agreement with ground-based observations (Liu, R., 1983). The IRI represents this variation pattern correctly

but overestimates the data at low solar activity. The IRI electron density value in the altitude range of 300 to 400 km is strongly affected by the F2 peak density model, which is now the internationally recommended CCIR model.

This survey shows excellent agreement between the AE-C/DE-2 data and the IRI empirical model, and therefore it verifies the use of the model for global, averaged values of the ionospheric parameters: electron temperature and density. In contrast, a comparison using individual orbits (Hoegy, W., 1987, not shown) indicates the limitations of empirical models and also points out geographic regions where data in the IRI model is lacking.

Contact: W. R. Hoegy
Code 614

Sponsor: Office of Space Science and Applications

Dr. Walter Hoegy is a physicist who studies the ionosphere. He is also Co-Investigator for the Dynamics Explorer. Dr. Hoegy, who holds a PhD degree from the University of Michigan, has been a part of Goddard for 19 years.

ATMOSPHERIC ODD OXYGEN PRODUCTION DUE TO THE PHOTODISSOCIATION OF ORDINARY AND ISOTOPIC MOLECULAR OXYGEN

An outstanding unsolved problem in ozone determination in the stratosphere is the discrepancy that exists between the amount of ozone observed in the stratosphere and the amount that is predicted by various photochemical models in this layer. The observed ozone at certain altitudes is as much as 50 percent larger than the amount predicted by the photochemical models. The discrepancy indicates that either some sources of ozone production have been neglected or the capability of the ozone sinks has been overestimated.

Ozone is produced through the photodissociation of O_2 by the solar ultraviolet radiation. The resulting atomic oxygen produced through the photodissociation combines catalytically with O_2 to produce O_3.

A source of production of extra ozone in the stratosphere is the isotopic molecular oxygen, whose effect has so far been neglected in most calculations. Although the abundance in the atmosphere of the isotopic oxygen is minute compared to the ordinary oxygen, 0.408 percent for $^{16}O^{18}O$, and 0.082 percent for $^{16}O^{17}O$ compared to $^{16}O_2$, its spectroscopic properties are different from ordinary oxygen. Due to its small abundance, isotopic oxygen has a large optical path with respect to the solar ultraviolet radiation. As a result, the photodissociation of the isotopic oxygen takes place at lower altitudes where ozone production is important, resulting in a substantial contribution to the ozone production.

The main photodissociation of molecular oxygen occurs within particular bands of O_2 called Schumann Runge bands. The excitation lines within these bands are predissociative, i.e., the excitation leads to the molecular break up. As a result, the lines are broadened, and there are extensive overlaps not only among the lines of the same band, but among the lines of the various bands.

These overlaps constitute the main difficulties in estimating the amount of odd oxygen produced, since a proper calculation should take the effect of all of these overlaps into account. Similarly, in estimating the amount of the odd oxygen due to the isotopes, the overlaps between the ordinary and isotopic lines should be taken into account.

We at Goddard undertook a line-by-line calculation for the production of the odd oxygen, where the overlap of all of the lines has been taken into account. For simplicity, in the following we concentrate on the isotope $^{16}O^{18}O$. It is understood that the effect of $^{16}O^{17}O$ is one-fifth as great as $^{16}O^{18}O$.

Figure 1 shows the absorption cross section, equal to the photodissociation cross section, versus the solar radiation wave number in cm^{-1} for the ordinary oxygen, σ_{pcO}, and isotopic oxygen, σ_{pcI}. The subscript pc stands for the pseudocontinuum, indicating the predissociative nature of the lines.

The dashed line is for the ordinary oxygen, and the solid line is for the isotopic oxygen. The peaks of the lines are shown by vertical bars. On each peak, the digit before the comma is the vibrational quantum number. The rotational quantum number and whether the line is a P or an R branch are written after the comma. The figure shows the blending of various ordinary and isotopic lines belonging to different bands.

Due to the spin-orbit interaction, each line shown in Figure 1 splits into six lines: three main lines and three satellite lines. The splitting is not shown in this figure, although we have taken its effect into account in our

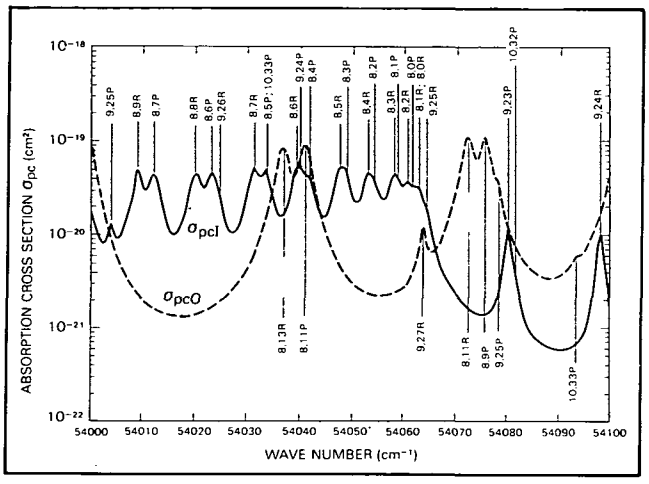

Figure 1. The absorption cross sections σ_{pcO} (dashed line) and σ_{pcI} (solid line) for a range of wave numbers 54,000 to 54,100 cm^{-1}.

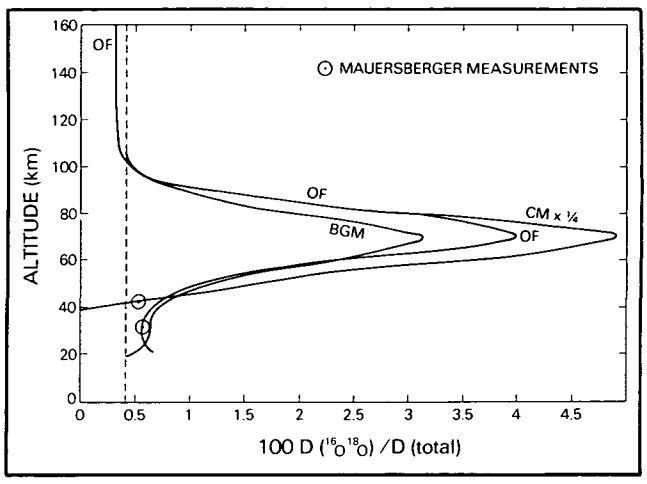

Figure 2. Ratio of the isotopic dissociation rate to the total dissociation rate multiplied by 100.

calculation. We have shown that due to the broadening of the lines, the contribution of the satellite lines can be neglected.

Similarly, we have studied the contribution of the initially excited vibrational bands of O_2, in addition to the main contribution that comes from the ground state. For the existing temperature profile of the stratosphere, this contribution has been shown to be negligible.

In summary, our calculation shows that due to its selective absorption, the isotopic oxygen $^{16}O^{18}O$ produces 10 times as much odd oxygen at 70 km as would be produced if the isotope did not have selective absorption. At this altitude 6 percent of the odd oxygen produced, and consequently 6 percent of the ozone produced, is due to this isotope. Also, our calculation indicates that 1.45 percent of the odd oxygen produced per second in an atmospheric column, and an equal amount of ozone produced per second, is due to $^{16}O^{18}O$. However, the excess odd oxygen produced is not enough to explain the excess amount of ozone observed in the stratosphere. We must then look for other ozone sources to resolve the discrepancy between observation and the photochemical models.

In Figure 2, the ratio of the isotopic dissociation rate to the total dissociation rate, multiplied by 100, is plotted as a function of altitude. The dashed vertical line represents this ratio if the isotopes had the same spectral properties as the ordinary oxygen. The three solid lines represent the works of three groups, as will be explained below, and represent the values of this ratio based on specific spectral properties of the isotopes.

"OF" refers to our work (1987), "CM" refers to the work of R. J. Cicerone and J. L. McCrumb (1980), and "BGM" refers to the work of A. J. Blake, S. T. Gibson, and D. G. McCoy (1984). CM results have been divided by four to fit the figure.

As can be seen, our work indicates that at 70 km, about 10 times as much odd oxygen is produced compared to the case in which the isotope did not have selective absorption. The work of BGM is similar to ours in that a line-by-line calculation has been performed, although the calculation has been done numerically without giving much detail, and the fine structure splittings and higher initial vibrational states have not been taken into account. The results of BGM agree with our results within 25 percent. In the work of CM, a line-by-line calculation is missing; their results are by a factor of five larger than our results, and the accuracy of their results is questionable.

Contacts: Kazem Omidvar and John E. Frederick
Code 614

Sponsor: Upper Atmosphere Research Program

Dr. Kazem Omidvar is the Principal Investigator on atmospheric temperature determination (Dynamic Explorer Project). He is also Principal Investigator on a study of excess ozone production due to the O_2 isotopes. His

professional interests include astrophysics, atmospheric physics, atomic and molecular physics, and recombination lines in planetary nebulae. Dr. Omidvar, who holds a PhD degree in theoretical physics from New York University, has 27 years of service with Goddard.

EARTH-ATMOSPHERE INTERACTION STUDIES

Numerical experiments with general circulation models (GCMs) under controlled conditions have shown that the surface fluxes of heat and moisture have a significant influence on the atmospheric circulation and rainfall. Our work at Goddard has focused mainly on deserts and desert-border regions. The primary motivation is to understand the biogeophysical processes of desertification, including the physical mechanisms responsible for the ongoing African droughts of the last 15 years (1971–86). Charney et al. (1977) and others have shown that an increase in surface albedo of desert border regions, which typically have very low evapotranspiration, produces lower tropospheric cooling along with sinking and drying aloft. Over the Sahel, its net effect is to move the Intertropical Convergence Zone (ITCZ) southward and reduce the local rainfall.

The influence of soil moisture, on the other hand, is much more model dependent. If soil moisture anomalies are regional, the increased warming of the planetary boundary layer (PBL), for the case of low evapotranspiration, produces thermally induced moisture convergence, which partially compensates for the lack of evapotranspiration. A new rain-evaporation parameterization by Sud and Molod (1987) that was included with the Arakawa-Schubert cloud parameterization and dry convective mixing calculation has been used recently to study the influence of surface albedo and soil moisture anomalies in the Sahara region. The results again show that surface evaporation has a strong influence on the amount of North African rainfall as well as on the northward migration of the ITCZ into the Sahel and/or southern Sahara (Figure 1).

In addition to surface albedo and soil moisture, the other important influence on desertification is that of surface roughness. On the scale of PBL turbulence (~ 50 m), the surface roughness is mostly determined by the height of tall vegetation (forests). GCM simulation experiments have been conducted on the influence of surface roughness of deserts on local circulation, the Indian subcontinent on the Indian Monsoon, and all land areas on global circulation and rainfall. The results show that the surface roughness and its dependent surface stress affect the convergence of water vapor flux transport in the frictionally interactive PBL. In the tropics, where the Coriolis parameter is small, even small changes in the curl of surface stress make a big difference in the water vapor and air mass convergence (Figure 2), whereas in the extratropics only large changes in the curl of surface stress can produce a significant change in the moisture convergence and rainfall. Because vegetation controls surface albedo, surface roughness, and evapotranspiration, our studies suggest that the deteriorating vegetation positively feeds back on the atmosphere to further reduce the local rainfall.

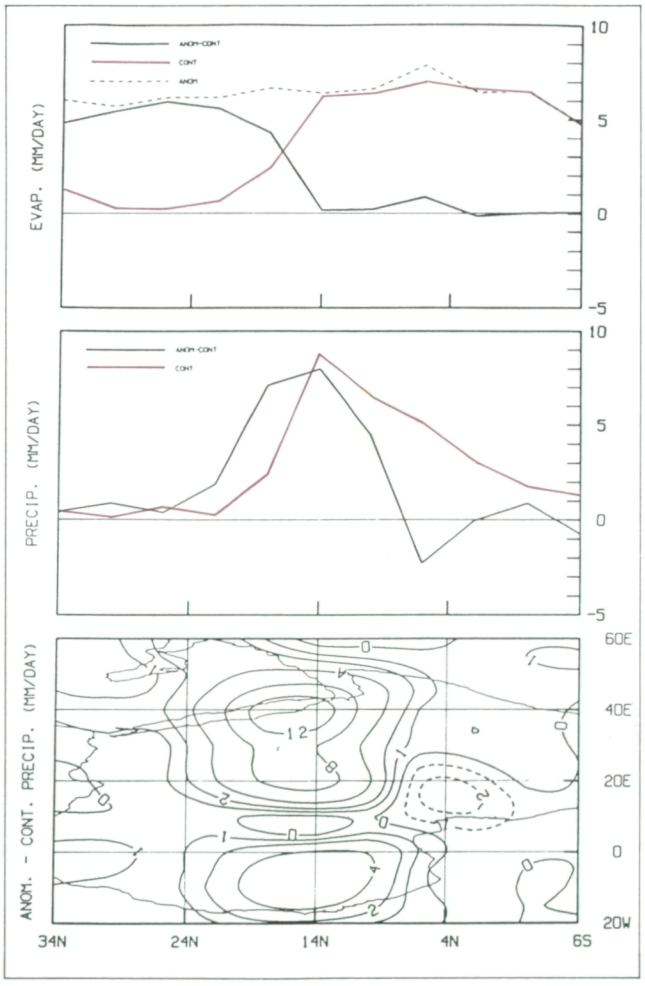

Figure 1. Top panel: Zonal average evaporation (mm/day) fields for control (solid red line), anomaly (dashed line), and anomaly minus control (solid black line). Center panel: Zonal average precipitation (mm/day) fields for control simulation (solid red line) and anomaly minus control (solid black line). Bottom panel: Rainfall (mm/day) differences: anomaly minus control.

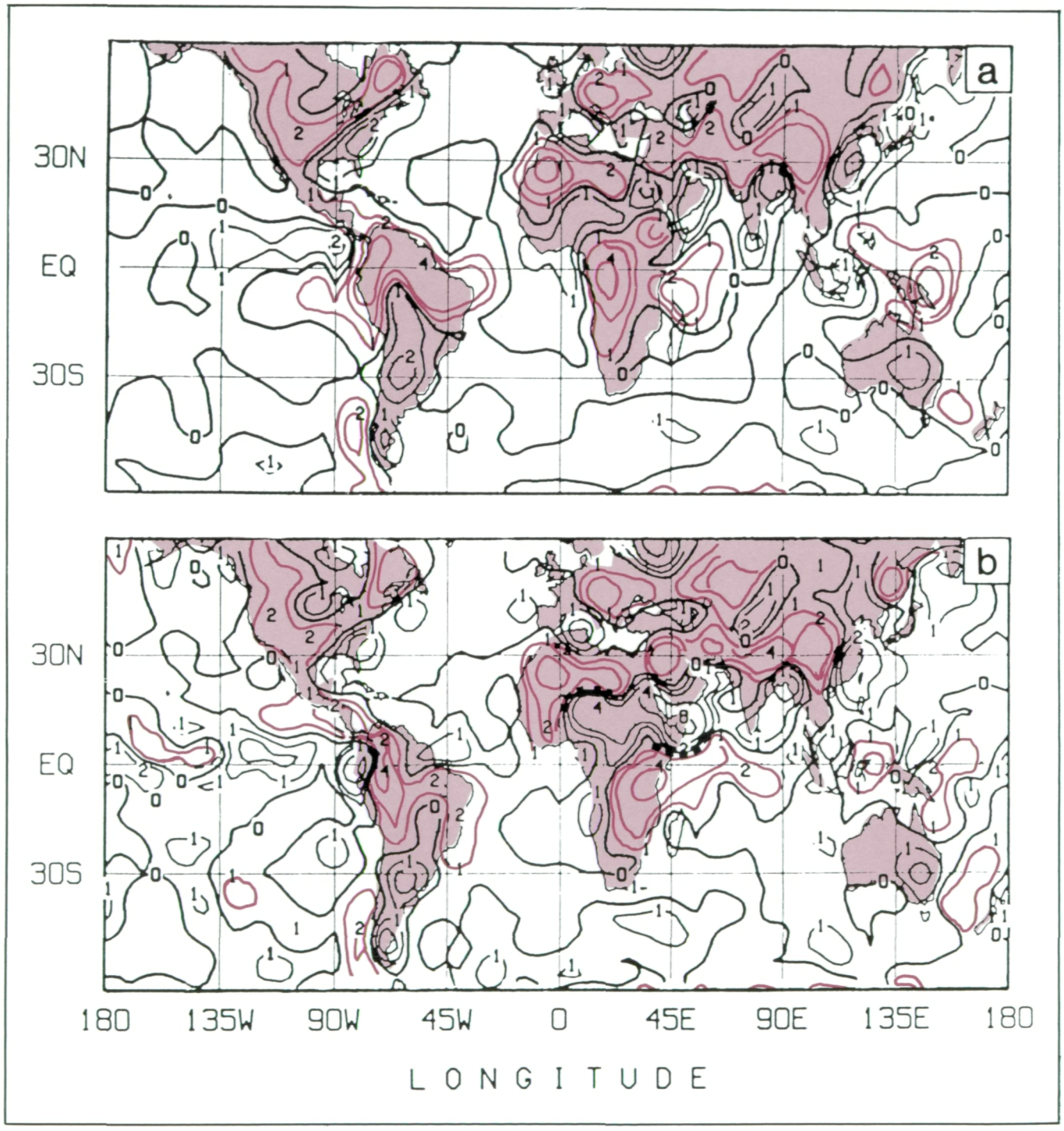

Figure 2: Influence of surface roughness of land on moisture convergence for simulated July. Panel a: Curl of surface stress divided by Coriolis parameter. Panel b: Moisture convergence in mm/day.

Because they lack a realistic parameterization of the biosphere is still unavailable, most of the modeling studies in the past, as well as those reported here, have employed bulk aerodynamic formulations of PBL fluxes for studying land-atmosphere interactions.

Such studies will lead to a better understanding of the influence of land surface processes on Sahelian circulation and rainfall; however, it is essential to explain the observed vacillation in Saharan rainfall (Figure 3).

Correlation studies between observed Sahelian rainfall and sea-surface temperature anomalies have also been conducted at Goddard. The results show a very significant positive correlation between the two. Corresponding GCM simulation experiments show that El Niño time-scale vacillations of the global sea-surface temperature force corresponding vacillations in the Hadley circulation (Figure 4). This finding provides an important insight into the mechanisms responsible for the vacillatory nature of African droughts. Similar studies by Folland (1986) and others have also suggested that sea-surface

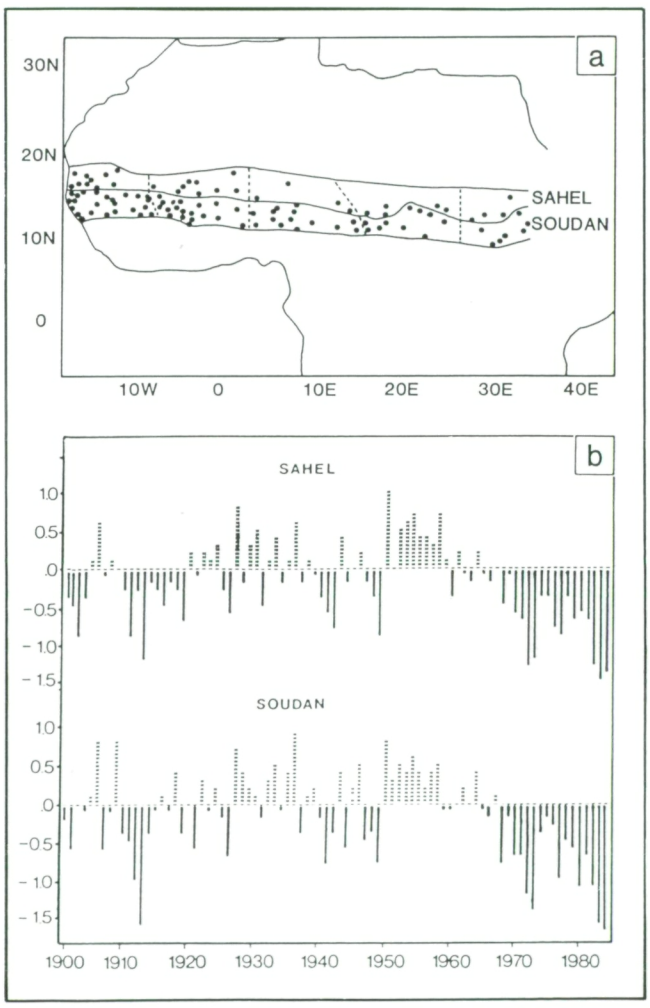

Figure 3: Annual Rainfall Index values in sub-Saharan Africa: Sudan and Sahel belts. Panel a: Station distribution. Panel b: Rainfall Index anomalies.

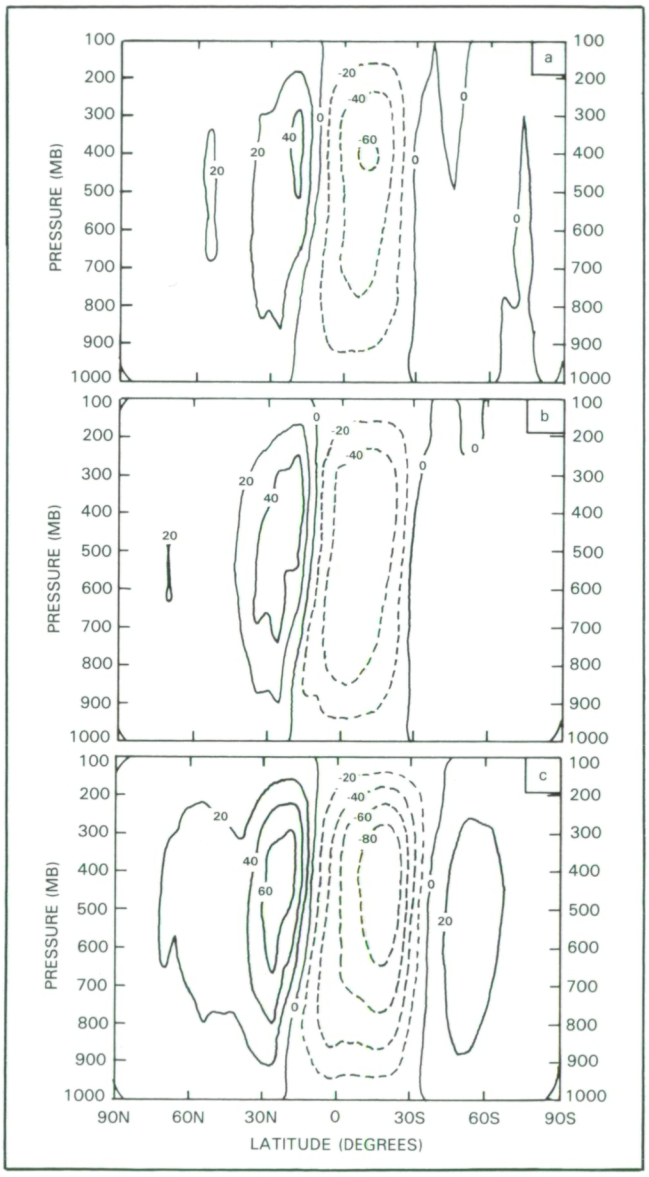

Figure 4: African Sector Hadley cell (10^9 kg s^{-1}) for July for the prescribed sea-surface temperature anomalies. Panel a: Warm phase El Niño scale anomalies from 40° S to 60° N observed in July 1983. Panel b: Climatological normals sea-surface temperatures, i.e., no anomalies. Panel c: Cold-phase El Niño scale sea-surface temperature anomalies as observed in July 1975.

temperature has a governing influence on the African droughts.

We plan to continue the research on the Earth-atmosphere interaction problem(s) with GCMs, employing better vegetation parameterization with the simple biosphere model developed by Sellers et al., as well as including realistic sea-surface temperature anomalies, preferably with coupled atmosphere-ocean models. We also hope to include Earth's surface data sets prepared from *in situ* and/or satellite derived, fields of vegetation phenology and morphology, soil moisture, sea-surface temperature, and snow and ice distributions. Currently, we are in the process of producing such global data sets from observations for a 20-month period (May 1981 through December 1982). These data sets will yield a much more realistic influence of Earth atmosphere interactions in the model simulations. We believe that studies of this type will serve as a useful precursors to future investigations employing EOS data sets.

Contact: Y. C. Sud
Code 611

Sponsor: Office of Space Science and Applications

Dr. Y. C. Sud is a physical scientist in the Global Modeling and Simulation Branch. He holds a PhD degree in mechanical engineering from Birmingham, England.

INTERACTIONS BETWEEN MESOSCALE GRAVITY WAVES, STRONG THUNDERSTORMS, AND THE JET STREAM

In the past few decades our ability to predict large- (synoptic-) scale circulation systems has increased considerably. However, accurate predictions of when, where, how much, and what type of precipitation will occur remain a formidable challenge because precipitation systems display highly complex, mesoscale structures (2- to 2000-km space scale, 0- to 24-hour time scale). It is widely recognized that inaccurate precipitation forecasts are largely the combined result of an incomplete understanding of mesoscale dynamics, the absence of quantitative mesoscale data useful as input to numerical weather prediction models, and inadequacies in model resolution and physics.

A large number of empirical and theoretical papers have suggested that the organization and morphology of cloud and precipitation fields can be partially explained by the presence of mesoscale buoyancy (gravity) waves and that such waves are even capable of triggering the development of violent thunderstorms. A review by L. Uccellini and S. Koch (1987) of published case studies of mesoscale gravity wave events reveals that such waves are excited within a similar synoptic flow pattern characterized by a jet stream approaching a stationary pressure ridge axis in the upper troposphere (see Figure 1). This configuration is conducive to gravity wave generation by a geostrophic adjustment process, which arises from an imbalance between the mass and momentum fields at the jet-stream level. Gravity-inertia wave generation by geostrophic adjustment processes has not been previously emphasized and has been customarily regarded as undesirable noise in numerical weather forecasting. Instead, these recent findings suggest the possibility of someday forecasting the occurrence of mesoscale gravity wave events.

In addition, there is also evidence that individual waves can be tracked (nowcast) with the help of conventional meteorological and geostationary satellite data. Analysis of detailed surface mesonetwork, radar, and rapid-scan (3-minute interval) stereoscopic Geostationary Operational Environmental Satellite (GOES) data collected during a mesoscale field program has permitted a very detailed study of a gravity wave event, its interactions with convective systems, and the wave source mechanisms.

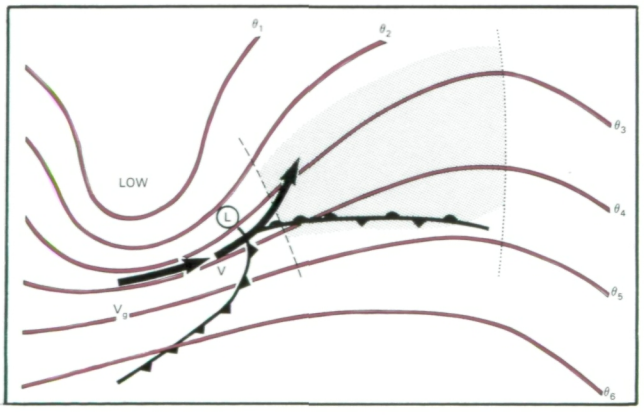

Figure 1. Subsynoptic region of mesoscale gravity wave activity is consistently observed to lie between the axis of inflection (dashed line) and the ridge axis (dotted line) in the 300-mb geopotential height field (red lines), and usually north of a stationary or warm front (suggesting wave energy may be ducted in statically stable lower troposphere). Waves also lie within right exit region of upper-level jet ($\underset{\sim}{V}$), which in unbalanced flow situation is displaced downstream of geostrophic wind maximum ($\underset{\sim}{V}_g$).

Mid-tropospheric winds near the wave crests derived by tracking clouds in the GOES imagery displayed a wave-induced divergence consistent with that in the surface mesoscale winds, thus also allowing for study of the wave vertical structure and mechanics. Coherent gravity waves diagnosed in the surface mesonet pressure and wind fields were either associated with propagating cloudbands or were made manifest by the transient enhancements of clouds as the waves passed through slower convective systems. An in-phase relationship between perturbation surface pressure (p′), wind (u′), and cloudiness was found (consistent with a gravity wave explanation). This phasing only became distorted in the *local* presence of strong thunderstorms triggered by the waves (Figure 2). Convection also enhanced the amplitude of the p′-u′ wave fields. Furthermore, the development of new convective cells at the storm's gust front caused a change in propagation velocity ($\underset{\sim}{C}$) of the gravity wave system, which resulted in an increasingly arc-shaped wave front and decreasing horizontal wavelength with time. These convective feedback effects on gravity wave structure and behavior have a bearing on any attempt to track waves with satellite imagery. It appears that, whereas the incipient wave mode appears to be altered significantly in the local presence of strong convection, it continues to provide organization to the convective system.

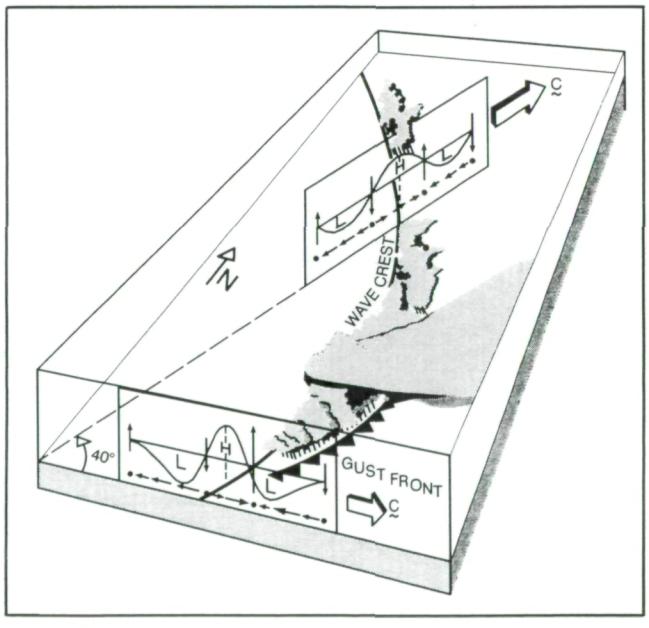

Figure 2. Schematic depiction of effects of strong convection on gravity wave structure and behavior. Notice differences between northern portion of wave (that part relatively unaffected by convective feedback effects) and that farther south, in terms of phase velocities ($\underset{\sim}{C}$), wavelengths, amplitudes, wave shapes, and p′-u′ phasing. Perturbation pressure (p′) wave is depicted, along with horizontal (u′) and vertical wind perturbations.

In the future, we want to explore means by which gravity waves generated through nonlinear physical interactions can be unambiguously differentiated from gravity waves resulting from numerical and initialization problems in numerical models. Work has also recently begun to determine the capability of the GOES Visible Infrared Spin-Scan Radiometer (VISSR) Atmospheric Sounder to detect mesoscale gravity waves sensed by ground-based systems, e.g., radiometric, microbarograph, and Raman lidar data (see Figure 3). These research efforts are being conducted in the hope that one day meteorologists may be able to both predict and monitor with acceptable accuracy these important weather-producing phenomena.

Contact: Steven E. Koch
Code 610

Sponsor: Office of Space Science and Applications

Dr. Steven Koch is a meteorologist whose professional interests include mesoscale dynamics, severe storm environments, satellite meteorology, and numerical weather prediction. He is a member of the NASA Weather Advisory Panel for Space Shuttle Support, and of the STORM-Central Network Designs Working Group. He is also an Associate Editor of the Journal of Atmospheric Sciences. *Dr. Koch, who holds a PhD degree from the University of Oklahoma, has seven years of experience at Goddard and has received the NASA Special Achievement Award and the NASA Outstanding Performance Award.*

CHARACTERISTICS OF MIDWEST SEVERE THUNDERSTORMS AND ANVILS

Meteorological satellites have been used to study severe thunderstorms in the Midwestern United States for about the past decade with the Geostationary Operational Environmental Satellite (GOES). Visible and infrared (IR) observations from these satellites have shown that individual severe thunderstorms having surface rain areas of only about 100 km^2 can have upper-tropospheric anvil outflows covering >10,000 km^2. Studies in the last several years have focused on the relation of the IR observations to the dynamics and microphysics of cloud tops and anvils. Improved understanding of interpretation of

ORIGINAL PAGE
COLOR PHOTOGRAPH

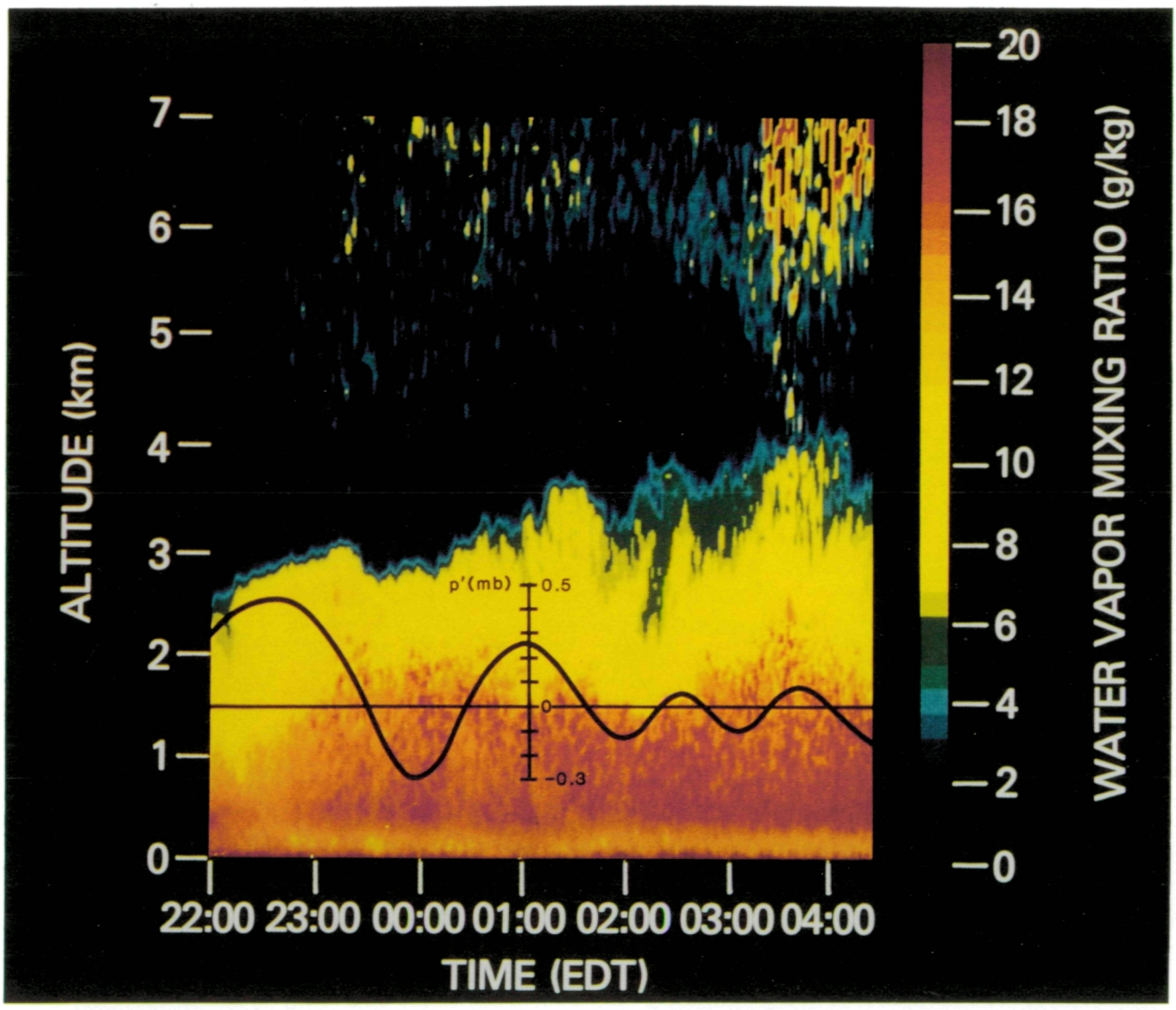

Figure 3. Fluctuations in Raman lidar water vapor mixing ratio in the 2 to 4 km layer correspond well with 1.5 to 2 hour oscillations in bandpass-filtered barograph data (black curve), indicating significant gravity wave amplitude over a deep layer.

satellite observations helps in the use of the data for detection of severe thunderstorms and nowcasting severe weather associated with thunderstorms. In the Severe Storms Branch, it has been possible with the Atmospheric and Oceanic Image Processing System to combine satellite measurements with those from ground-based Doppler radar, conventional upper-air soundings, and NASA-ER2 high-altitude aircraft measurements. In addition, one- and three-dimensional cloud models have been used in the interpretation of the satellite observations.

Vigorous thunderstorms often have cloud tops that penetrate several kilometers into the stratosphere. Cloud parcels in penetrating thunderstorm tops are usually colder than the environmental temperatures at the cloud-top altitude. A thunderstorm top penetrating the tropopause will appear in the IR measurements as a low temperature relative to the surrounding anvil. However, because of the strong vertical wind shears typical of Midwest thunderstorm environments, several severe thunderstorms have an IR cloud-top structure similar to that

ORIGINAL PAGE
COLOR PHOTOGRAPH

shown in Figure 1. Most notable is the V-shaped region of low temperatures with the vertex of the V pointed upwind. The region of coldest cloud-top temperatures (marked "C") is located upwind of the highest cloud tops. Also note two warm areas (marked "W") located downstream of the cloud top. Stereographic cloud heights derived from GOES-East and GOES-West satellites are superimposed on the image. The IR temperatures are radiometric measurements and thus may not represent the true air temperatures in the cloud and anvil tops. Comparisons of stereographic cloud-top heights and IR temperatures to aircraft analyses have shown that the overshooting cloud tops are nearly opaque at the 11-μm IR wavelength, and the surrounding anvil has emissivities less than unity and thus is more transparent.

Several hypotheses based on dynamics of the airflow above and within the cloud tops and radiometric characteristics of the anvil have been given for explaining the characteristics features in the IR observations. Because no *in situ* measurements have been obtained in severe storm tops, interpretations of the IR measurements have been based on detailed analyses of the remote measurements and various modeling results. Figure 2 shows a

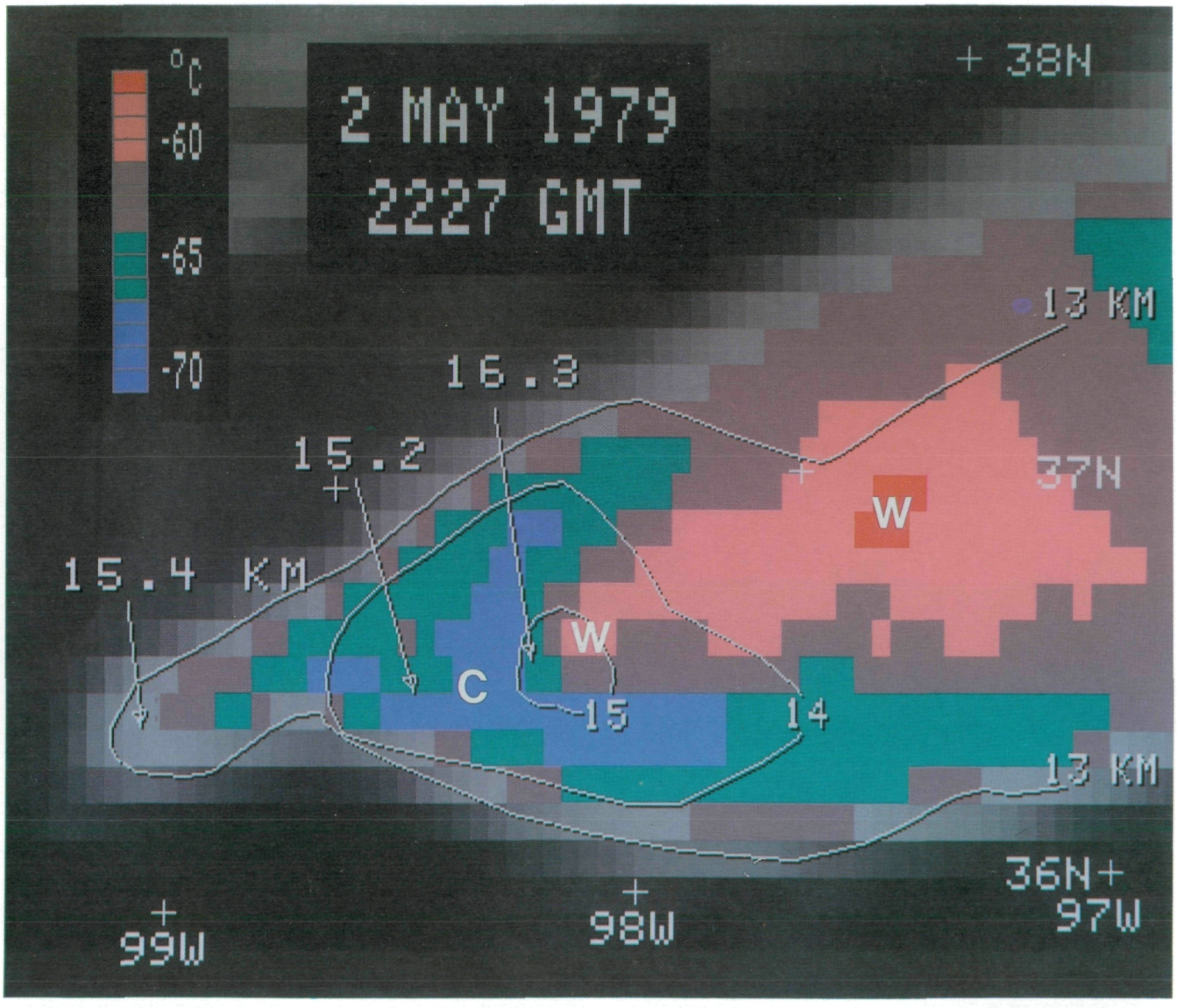

Figure 1. Color-enhanced infrared image from May 2, 1979. Stereographic cloud heights calculated from GOES-East and GOES-West are indicated by white contours. Peak cloud top heights are indicated by arrows.

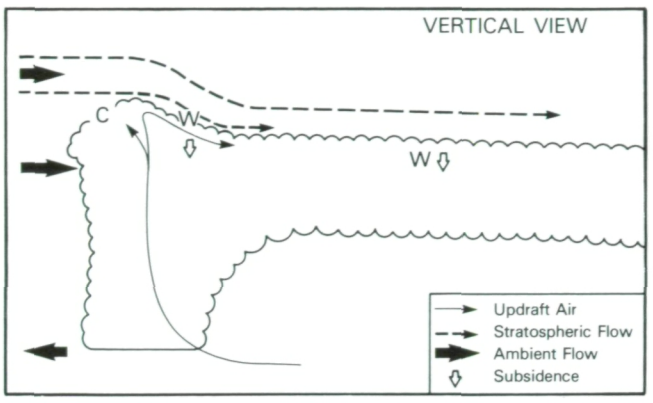

Figure 2. Schematic of cloud-top mechanisms.

schematic from more recent work explaining the cold and warm points in the cloud top. The cold point displacement has been inferred to be due to a combination of cloud-top mixing, strength of the updrafts, and strong temperature inversions in the lower stratosphere. The warm points appear to be due to subsidence produced by the negatively buoyant cloud air and stratospheric flow over and around the cloud top.

More recent studies have focused on measurements from the high-altitude ER-2 aircraft, which made overflights of intense Midwest thunderstorms in 1984 and 1986. The aircraft was equipped with visible, IR, and microwave radiometers and a cloud lidar system. In one thunderstorm event currently being studied, the aircraft flew over an intense thunderstorm similar to the one depicted in Figure 1. In the next few years, we plan to develop and fly a nadir-pointing Doppler radar on the ER-2, which will measure the vertical velocity structure over the entire storm depth. This will be helpful in addressing questions concerning the tops of clouds and the detailed internal structure of the clouds. In addition, GOES I–N series scheduled for launch in 1989 has nearly double the IR resolution of the current GOES (~ 4 km versus 8 km), and it will help resolve some of the cloud-top features.

Contact: Gerald Heymsfield
Code 612

Sponsor: Office of Space Science and Applications

Dr. Gerald Heymsfield, who holds a PhD degree from the University of Oklahoma, is a meteorologist with the Severe Storms Branch of the Laboratory for Atmospheres. Dr. Heymsfield is a recipient of the Laboratory for Atmospheric Sciences' Outstanding Paper Award (1982, 1984), and he has been a part of Goddard for eight years.

RAINFALL SIMULATIONS FOR SATELLITE SAMPLING STUDIES

Global monitoring of rainfall is important both for hydrological and climatological purposes, but the high variability of rainfall in space and time makes it one of the most difficult of physical quantities to measure. A stochastic model has been developed that is capable of generating two-dimensional rain fields with spatial and temporal correlations resembling those of tropical rainfall observed with radar during the Global-Atmosphere-Research-Program Atlantic Tropical Experiment period. The purpose of the model is two-fold: 1) to help in evaluating sampling problems for satellite-derived rainfall when the satellite observations are intermittent, as occurs with nongeostationary satellites; and 2) help in the investigation of the beam-filling problem, which occurs when the spatial inhomogeneity of rainfall cannot be resolved by a satellite instrument, and the relationship to rain rate of the radiation emitted by the rain is a nonlinear one.

The model generates rain fields with these characteristics. 1) The statistics are homogeneous and isotropic in space. 2) Rain occurs over a fraction of the area, a fraction that varies with time but whose average is determined by the average observed in the data. 3) Rain rate is log-normally distributed. 4) Spatial correlation of the rainfall can be arbitrarily prescribed. 5) Time stepping is carried out so that large-scale features persist longer than small-scale features. An example of the two-dimensional rain patterns generated by the model is shown in the accompanying figure.

Numerical code for the model has been developed for the Cyber 205 computer and is very efficient, allowing many Monte Carlo experiments with the model to be performed. The first use of the model will be in evaluating likely sampling errors in the rainfall climatology that would be obtained by the Tropical Rain Measuring Mission satellite currently being studied by NASA. Since the satellite will view a given area of the Earth only a few times per day, there is some concern about how accurately such a satellite will be able to estimate total rainfall within the area during a month. Moreover, sampling error tends to decrease with satellite altitude, whereas instrumental error generally increases with the altitude. By exploring the dependence of sampling error on orbital parameters with this model, it will be possible to choose an orbit for which the combined error is minimized.

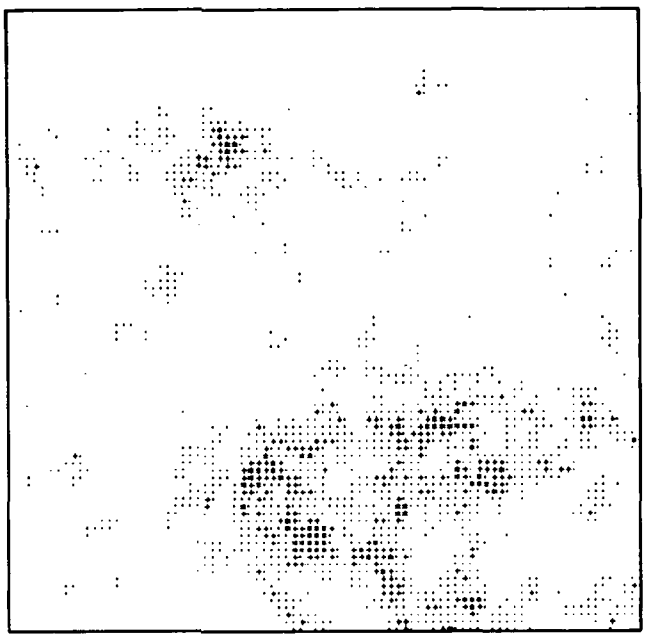

Model rainfield, 340 × 340 km portion from a 1024 × 1024 km simulation. Dots indicate rain rate $r < R_1 = 10$ mm/h, pluses indicate $R_1 < r < R_2 = 22$ mm/h, and asterisks indicate $r > R_2$. The divisions R_1 and R_2 are chosen such that 50% of the time-mean rain is due to rain rates less than R_1, and 25% is due to rain rates greater than R_2. Rain covers 20% of the area displayed.

Contact: Thomas L. Bell
Code 613

Sponsor: Office of Space Science and Applications

Dr. Thomas Bell, an atmospheric scientist, is interested in statistics, fluid dynamics and turbulence, radiative transfer, and the dynamics of climate change. Dr. Bell, who received a PhD degree in physics from the University of Chicago, has nine years of experience at Goddard.

NEW TECHNIQUES FOR MEASURING CLOUD HEIGHT FROM SATELLITES

Clouds play an important role in climate, with relatively small changes in the amount of clouds or their distribution causing climatic changes that are comparable in magnitude to that of doubling atmospheric CO_2. Yet, there is very little quantitative information on the Earth's cloud cover. This situation has led the World Climate Research Program, which was established in the late 1970s, to organize as its first major activity the International Satellite Cloud Climatology Project, whose objective is the development of a 5-year data set of global cloud cover parameters beginning July 1983. The source of information are the measurements of imaging radiometers on five geostationary and two polar orbiting meteorological satellites. However, those radiometers were not designed for quantitative measurement of cloud parameters and will consequently not yield all of the desired information or the necessary accuracy. Therefore, while this project forges ahead utilizing presently available data, research on remote sensing of cloud-cover parameters is leading to new sensors that could be deployed on future Earth-observing satellites.

The present effort to develop a climatology of cloud cover parameters is based upon measurements in two spectral channels that all of the meteorological satellites have in common: one channel in the visible spectrum (in the vicinity of 0.6 μm) and one in the thermal infrared window (around 11 μm). In the visible channel, reflectance is measured, from which the optical thickness of the cloud can be estimated. In the thermal infrared channel, the 11 μm brightness temperature is measured, which, along with the optical thickness, yields the cloud-top temperature. All of this would be fine if one could be sure that the scene is uniform within the field of view of each measurement, so that each pixel is cloud-filled or totally free of cloud. In that case, three important parameters for the cloud climatology can be determined: cloud cover fraction over a given area (by counting cloud-filled versus cloud-free pixels); cloud height (by using the atmospheric temperature profile to relate cloud-top temperature to height); and total liquid water in the cloud (by assuming a particle size distribution, a relationship between cloud optical thickness and cloud liquid water content is established).

One problem with this approach is the likely occurrence of partially filled pixels and pixels with mixed cloud properties. The present effort, which uses thresholds in one or both channels to determine whether a pixel is cloud filled or cloud free, does not allow for these occurrences, thereby subjecting the results to possibly appreciable errors.

Now that the Earth Observing System (EOS) is in the planning stage, thought is being given to the potential advantages of a variety of special cloud-sensing channels that could be used to determine the cloud fraction within each pixel. While the visible and 11-μm channels are used because the atmosphere, other than clouds, is transparent in those channels, additional information about the cloud

can be obtained by the additional use of channels for which the atmosphere is partially opaque. What can partially opaque channels tell us?

First, consider channels that are partially opaque to water vapor. Clouds consist of water particles surrounded by atmospheric gases. Since clouds are saturated (100 percent relative humidity), water vapor is among the gases that surround the particles and will absorb some of the radiation incident on the cloud, thereby reducing the cloud's reflectance (i.e., making the cloud darker). The amount of absorption (i.e., the degree of darkening of the cloud) depends upon two parameters: 1) temperature, which, under saturated conditions is uniquely related to the amount of water vapor; and 2) cloud particle density, which determines the depth of penetration of the cloud and the path length of the photon through the cloud before it is reflected back (Figure 1). There is also absorption in the atmosphere above the cloud due to the presence of water vapor. That effect, however, is not large because the air above the cloud is not saturated, and due to the decrease of temperature with height, the water vapor density decreases very rapidly above the cloud. Hence, the amount of water vapor encountered by the photon above the cloud is usually much less than the amount of water vapor encountered within the cloud. As a result, the darkening that occurs within a water vapor absorption channel is a measure of the temperature of the cloud, with some uncertainty associated with the range in cloud particle density. With information on the atmospheric temperature profile—that could come, for example, from satellite soundings of the atmosphere—cloud temperature can be converted to cloud height.

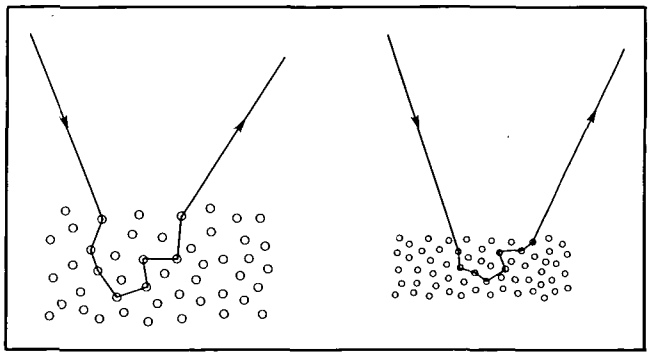

Figure 1. The effect of particle density on the photon path length within the cloud: keeping the total number of cloud particles constant, the more spread out the particles, the longer the photon path length and the greater the absorption by atmospheric gases that occupy the space between cloud particles.

Another possibility is the use of channels that are partially opaque to oxygen, which is well mixed in the atmosphere. In that case, most of the absorption occurs above the cloud, with the absorption within the cloud being appreciably less. The amount of absorption, in any event, depends upon two parameters: 1) cloud height, which determines the amount of oxygen above the cloud; and 2) cloud particle density, which determines the path length within the cloud. Consequently, the darkening that occurs within an oxygen absorption channel is a measure of the height of the cloud, with a range of uncertainty due to the range in cloud particle density.

Although these absorption channels do not pinpoint the cloud height, they provide additional information that greatly reduces the uncertainty in cloud height caused by using only the visible and infrared channels. An example based upon numerical simulation is shown in Figure 2. It assumes a reflectance of 0.4 in the visible channel and an 11-μm brightness temperature of 270 °K. With that information alone, the solution to the problem of determining cloud optical thickness and cloud temperature is bounded by the band that extends from the upper left to the lower right across the graph. The uncertainty in cloud temperature (between 210 and 270 °K) and in cloud optical thickness (from 5 of 200) is due to the uncertainty of the fraction of the field-of-view filled with cloud (ranging from less than 0.4 to 1.0, denoted by f in the figure). The uncertainty is indicated by span A in the figure. If the information from a water vapor or oxygen absorption channel is added, the uncertainty is reduced to span B. If the information from both oxygen and water vapor channels is combined, and a temperature/humidity sounding is used to determine the amount of water vapor above the cloud and the relationship between the cloud temperature and cloud height, the uncertainty is further reduced to span C.

With planning under way for the EOS in the mid-1990s, consideration is being given to incorporating oxygen and water vapor absorption channels into one of the EOS facility instruments, the Moderate-Resolution Imaging Spectrometer (MODIS), which will view Earth with as many as 40 channels, with ground resolution ranging from 0.5 to 1 km. The absorption channels that would be useful for cloud sensing are at 0.93 and 1.36 μm for water vapor and at 0.76 μm for oxygen. Adding these channels to those on the NOAA AVHRR now being used for cloud sensing would provide a very powerful tool for quantitative measurement of cloud cover parameters and help us understand both the effects of clouds on climate and their feedback role when climate is changing.

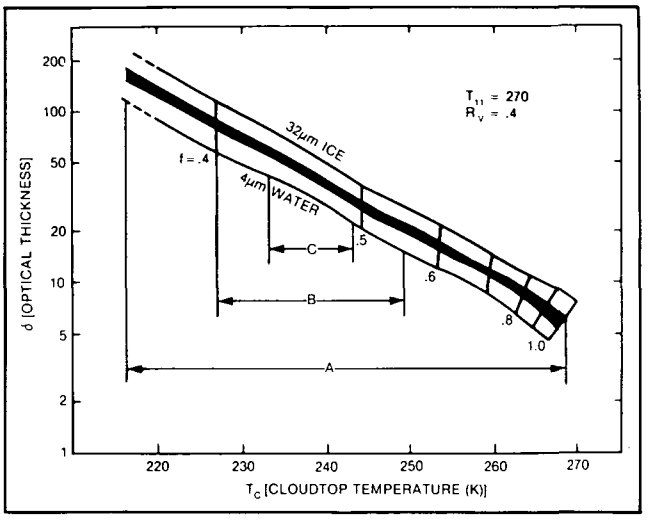

Figure 2. An illustration of the reduction in the uncertainty of the retrieval of cloud-top temperature and cloud optical thickness that could be achieved with O_2 and H_2O absorption channels in the near-infrared spectrum, in addition to the channels available on the AVHRR radiometer presently deployed on the NOAA polar orbiting meteorological satellites. This simulation was carried out for a measured visible reflectance R_v = 0.4, and 11-μm brightness temperature T_{11} = 270°K. Span A represents the range of uncertainty in the retrieved cloud-top temperature when the visible and infrared channels on the AVHRR are used. The uncertainty is caused by lack of information on the fraction of the field-of-view filled with cloud, denoted by f. Span B represents the improvement with the addition of an O_2 or H_2O absorption channel. Span C represents the further improvement when both absorption channels and information from a simultaneous measurement of the temperature/humidity profile are used. (Note that the width of the band of uncertainty is due to the uncertainty of the type of cloud particle, ranging from 4 μm water drops to 32 μm ice, but use of the 3.7 μm channel on the current AVHRR reduces the width of the uncertainty band to the darkened portion.)

Contact: Albert Arking
Code 613

Sponsor: Office of Space Science and Applications

Dr. Albert Arking, Head of the Climate and Radiation Branch, has 27 years of experience at Goddard. Dr. Arking, who holds a PhD from Cornell University, was TIROS Project Scientist (1973 and 1982) and VAS Project Scientist (1974 to 1979). He developed techniques for determining Earth Radiation Budget components from satellite measurements and also developed methods for extracting cloud-cover parameters from satellite imaging radiometer measurements.

LOW-FREQUENCY OSCILLATIONS IN THE TROPICAL OCEAN-ATMOSPHERE

Comprehensive data analyses and modeling studies of low-frequency oscillations (LFOs) in the tropics have been performed to better understand the role of tropical LFOs in global climate fluctuations. A unique feature of the present work is to study the many LFOs observed in the tropics as interrelated phenomena and to understand them within a common dynamical framework. The study includes an entire spectrum of LFOs: the 40–50 day (or 30–60 day) oscillation, the Southern Oscillation, El Niño, the Quasi-Biennial Oscillation, and others. The analyses are mainly based on data derived from space observations supplemented with conventional meteorological data. Examples are outgoing longwave radiation (OLR), sea-surface temperature, liquid water content, cloud properties and classifications, and many others. The OLR, in particular, is the most widely used parameter in meteorology as a measure of the relative intensity of tropical convection and a proxy measure for tropical rainfall.

For example, the following figure shows the time-longitude section of anomalous 5-day mean OLR along the equator for the period 1980 to 1984. Convective clusters (indicated by large negative OLR) can be seen propagating from the Indian Ocean to the central Pacific near the dateline. These convective clusters are associated with the 40–50-day waves in the tropics. A major 40–50-day convective pulse occurred over the Indian Ocean around May 1982 before the onset of the 1982–83 El Niño/Southern Oscillation (ENSO), which is indicated by the sudden appearance of strong convective activities over the central and eastern Pacific from June 1982 to July 1983. Thereafter, the fluctuations in convection appeared to go back to the normal condition, with the convective clusters confined over the climatological warm water of the eastern Pacific. These observations led us to believe that the 40–50-day oscillations and the onset of ENSO are closely related. At present, we are studying the above phenomena with cloud and thermal infrared data from the Nimbus-7 satellite.

Parallel to the data analyses, we have formulated a dynamical framework in which the 40–50-day waves and the ENSO can be collectively studied. This dynamical

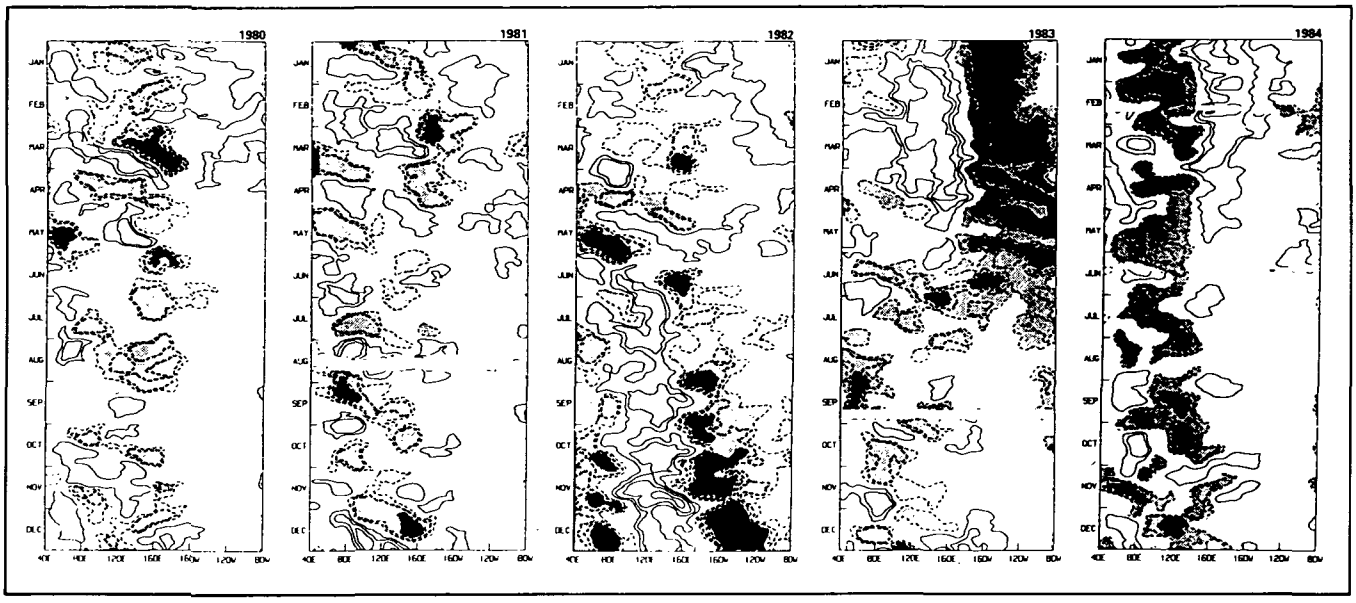

Time-longitude section of anomalous 5-day mean outgoing longwave radiation along the equator from the Indian Ocean (40° E) across the central Pacific to the eastern Pacific (80° W) from 1980–1984. Negative anomalies that indicate enhanced convection are shaded, with those exceeding 20 Wm^{-2} shaded darkly.

framework includes active moist processes in the atmosphere, and advection and upwelling in the ocean. It was found that, whereas the basic dynamic origin of the 40–50-day waves is in the atmosphere, through the interplay of dynamical moisture convergence, evaporation, upwelling, and advection in the ocean, these waves can exhibit low-frequency behavior that may be identified with the onset of ENSO. There is also evidence that the 40–50-day waves may be a partially coupled ocean-atmosphere phenomenon manifested as ultra-slow 60–90 day LFOs that are strongly modified by coupled air-sea interaction over the warm water (>28 °C). Results further suggest that a dynamical instability in the coupled ocean-atmosphere system is present as a result of explicitly including a moist hydrological cycle in the atmosphere-ocean system. This instability is not present in previous models of the coupled atmosphere system where moist processes are not included. As a result of the above and other results, it is hoped that a better theoretical understanding of LFOs can be obtained and that theory will lead to better guidance in the observational analyses and interpretations.

Contact: William K. M. Lau
Code 613

Sponsor: Office of Space Science and Applications

Dr. William Lau is Head of the Experimental Climate Forecasting Center and is a member of the Tropical Ocean Global Atmosphere Panel. His scientific specialties include monsoons, air and sea interactions, and climate dynamics. Dr. Lau, who holds a PhD degree in atmospheric sciences from the University of Washington, has seven years of service with Goddard. He recently received the John Lindsay Award for his work.

MOIST CONVECTION SIMULATIONS IN GLOBAL CLIMATE MODELS AND THEIR VALIDATION BY USING SATELLITE CLOUD CLIMATOLOGY DATA

Different global climate models (GCMs) disagree in their estimates of surface warming due to a doubling of CO_2 concentration. Cloud feedbacks are thought to be the principal cause of these differences in climate sensitivity. The parameterization of subgrid scale moist convective processes is central to any assessment of cloud feedback on climate. Cumulus convection is also an important forcing mechanism for the general circulation and its low-frequency variability, especially in the tropics.

The climate modeling group at the Goddard Institute for Space Studies is in the process of testing the response of

GCMs to various assumptions about the factors that determine cumulus mass flux. For example, it is well known that organized precipitating deep convection is favored by low-level convergence and lifting. Shallow fair-weather cumulus clouds are formed instead by turbulent surface fluxes of heat and moisture and often occur when the large-scale atmosphere is sinking.

We have compared GCM simulations that specify cumulus mass flux arbitrarily to experiments that predict the convective flux on the basis of low-level convergence and/or surface evaporation. The effects on cumulus heating rates are quite different in different convective regimes. In the highly convective equatorial West Pacific, convergence strengthens cumulus heating, whereas surface flux effects greatly weaken the heating. In central Africa, on the other hand, surface evaporation significantly increases deep convective heating, whereas convergence reduces convection strength. In subtropical shallow trade cumulus and marine stratocumulus regimes, convection is almost nonexistent when it depends only on lifting because of the subsidence that prevails in these regions. When surface flux effects are included, realistic heating rates result. A simple parameterization of saturated convective-scale downdrafts tends to reinforce the effects of low-level convergence, especially over the oceans.

Unfortunately, information on convective mass fluxes and heating rates is restricted to a few isolated regional field studies. Global information on the properties of convective clouds requires the use of satellite data. The International Satellite Cloud Climatology Project (ISCCP) is producing a 5-year climatology of cloud amounts and radiative properties with visible and infrared data from operational satellites. The primary ISCCP products involve large-scale clouds, but information on the geographical, vertical, and temporal distributions of deep convective clouds is also available.

Preliminary studies have already been conducted with a pilot version of the ISCCP data. The figure shows the diagnosed vertical distribution of deep convective cloud-top heights and its diurnal variation for oceanic and continental areas of the Intertropical Convergence Zone. Both regions exhibit deep convection that penetrates primarily to the 200-mb level, consistent with the predominant mode of deep convection in the GCM. The East African region, however, contains an additional mid-tropospheric peak in convection that is not simulated in the GCM. Whereas deep events in both regions increase in frequency from morning to afternoon, the mid-troposphere events are more common in the early morning, suggesting a different forcing mechanism. The GCM gives an afternoon maximum in precipitation in these locations when the cumulus parameterization includes the effects of surface evaporation but not when cumulus mass flux depends on large-scale lifting alone. This type of comparison, done on a global basis, promises to provide a stringent test of the physics of future GCM moist convection schemes.

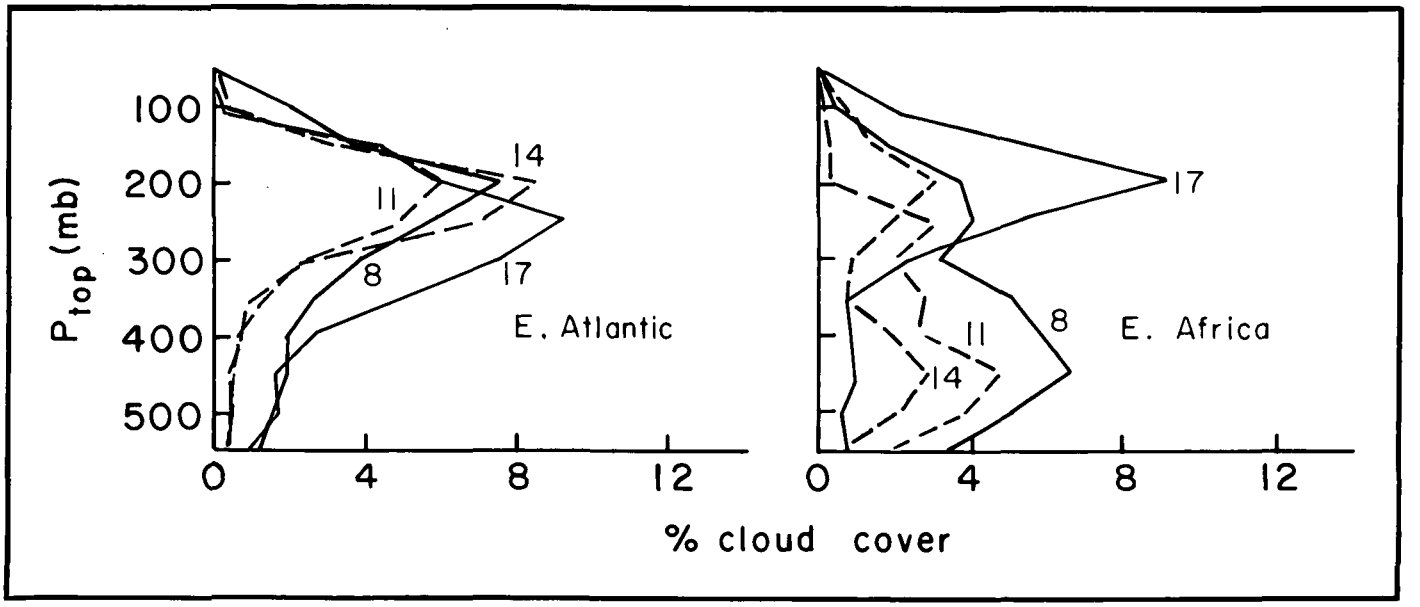

The vertical distribution of convective cloud-top heights and its diurnal variation for two tropical regions in July 1983 ISCCP data. Each curve is labeled by the local solar time in hours.

Contact: Anthony D. Del Genio
Code 640

Sponsor: Office of Space Science and Applications

Dr. Anthony Del Genio, a physical scientist with the Goddard Institute for Space Studies (GISS), is Coordinator of the GISS/Columbia Atmospheric and Planetary Science Program. Dr. Del Genio specializes in comparative dynamics of planetary atmospheres and in cumulus parameterization, and his professional interests include the modeling of superrotation on slowly rotating planets and the role of moist convection in tropical dynamics. Dr. Del Genio earned his PhD degree at the University of California at Los Angeles, and he has served with Goddard for eight years. He is a recipient of the NASA Special Achievement Award.

ANTARCTIC OZONE: HALOCARBONS AND METEORS?

The rapid decline in stratospheric ozone over Antarctica in the spring has been observed by several research groups. It has led, in turn, to several photochemical theories that relate the depletion of O_3 to the well-documented buildup of halocarbons in the stratosphere. These models require that a major fraction of the total chlorine liberated from halocarbons (Cl_x) is present in active forms, such as ClO, rather than in more photochemically passive reservoirs, such as HCl. The active forms of Cl_x participate in rapid catalytic destruction of O_3 when sunlight returns to the polar vortex in spring.

When a substantial fraction of NO_x ($NO + NO_2$) and HNO_3 is removed from photochemical participation in the lower stratosphere, partitioning of the Cl_x family shifts radically from HCl to ClO, and photochemical losses of ozone attributable to chlorine and bromine increase substantially. For Antarctic conditions, the currently proposed methods for maintaining low NO_x require either fast heterogeneous chemistry throughout the early spring or removal of NO_x and HNO_3 from the gas phase by formation and fallout of polar stratospheric clouds (PSCs) containing a substantial fraction of the stratospheric HNO_3.

Research presented here, in collaboration with Dr. J. M. Rodriguez (Atmospheric and Environmental Research), proposes that infall of meteoric material is a source of alkalinity and small particles that may control nitric acid vapor in the Antarctic stratosphere, providing one link in the chain of photochemical and heterogeneous processes that are responsible for the current decline in Antarctic ozone. Atmospheric circulation leads to an accumulation of debris from meteors in the Antarctic stratosphere at the beginning of austral spring. The major component of meteoric material is alkaline, comprised predominantly of the oxides of magnesium and iron. In the presence of PSCs, these metals may neutralize the natural acidity of stratospheric aerosols, remove nitric acid from the gas phase, and bond it as metal nitrates in the aerosol phase.

On a global average, meteoric metals are expected to be present in the middle stratosphere at concentrations much less than a part per billion, insufficient to neutralize the acidity of the natural Junge layer (H_2SO_4). Over polar regions, however, meteoric debris accumulates in winter and early spring as a result of the pole-to-pole mesospheric circulation illustrated in the figure in three-dimensional tracer simulations. Largest concentrations of meteoric material in the stratosphere occur in the Antarctic spring in amounts sufficient to neutralize parts per billion of acidic vapor (H_2SO_4, HNO_3) in the stratosphere.

If this mechanism is valid for Antarctica, what are the consequences? For one, the composition of aerosols in the springtime Antarctic stratosphere should have large abundances of the metals Mg and Fe plus NO_3^-, unlike

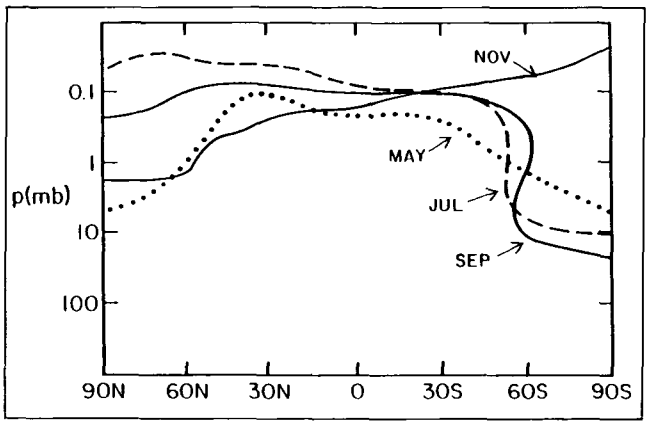

The distribution of meteoric metals as simulated with the GISS stratospheric general circulation model. Results for the months of May, July, September, and November show the zonally averaged extent of meteoric material and illustrate the buildup of high concentrations in the vernal Antarctic stratosphere. The region above each line represents that portion of the atmosphere with sufficient concentration of metals to neutralize 1 ppb of HNO_3.

ORIGINAL PAGE
COLOR PHOTOGRAPH

the trace detections of iron and nitrates found in the corresponding aerosols at mid-latitudes. For another, this phenomenon—the formation of metal nitrates—should also occur in the Arctic, but perhaps to a lesser degree since meteoric material is not predicted in the current simulations to extend as low in the stratosphere during the Arctic spring. Interannual variations in the springtime decline of O_3 could occur through changes in the acid-base balance in the Antarctic stratosphere, for example, by volcanic emissions or by meteor showers.

Contact: Michael Prather
Code 640

Sponsors: Office of Space Science and Applications and Upper Atmosphere Theory and Data Analysis Program

Dr. Michael Prather is a physical scientist with the Goddard Institute for Space Studies. Dr. Prather, who received a PhD degree in astronomy from Yale University, specializes in atmospheric chemistry and composition. He has two years of service with Goddard.

SIX-YEAR MEAN GLOBAL CLOUD CLIMATOLOGY

The Nimbus-7 cloud data processing team has accomplished its planned purpose of setting up a 6-year (April 1979–March 1985) global cloud data set. The data set was generated from Nimbus-7 Temperature Humidity Infrared Radiometer 11.5-micron radiances together with Total Ozone Mapping Spectrometer derived reflectivities, climatological atmospheric temperature lapse rates, and concurrent surface temperature and snow/ice information from the Air Force 3D-Nephanalysis archive.

In the fall of 1986, the data set was completed and placed in the National Space Science Data Center archive for distribution to interested scientists. In addition, in 1987 the data set was analyzed to yield a mean global cloud climatology. The climatology consists of monthly, seasonal, and annual means of the chief data-set parameters, which are: total, low, mid, high, cirrus, and deep convective clouds; 11.5-micron scene radiances; and Air Force surface temperatures. An interesting view of the cloud climatology can be seen by examining the annual mean total cloud field together with the annual amplitude of seasonal cloud changes. The two panels of the figure refer to ascending node (near noon) measurements of the total cloud cover. Descending node (near midnight) measurements are also present in the data set. The noon/midnight differences will be briefly discussed later. The heaviest cloud concentrations occur around the coast of Antarctica, in the equatorial rain zone on and just south of the equator, and near the Arctic Circle. In each of these three cloud belts there are major steady-state cloud fields with an annually averaged cloud cover of 70 percent or more. In the south this heavy cloud belt completely surrounds the coast of Antarctica. However, just off the tip of South America the mean cloud cover drops to a little under 70 percent. The equatorial rain zone has three major centers: the northern portion of South America with a maximum on the eastern slope of the Andes, the Congo

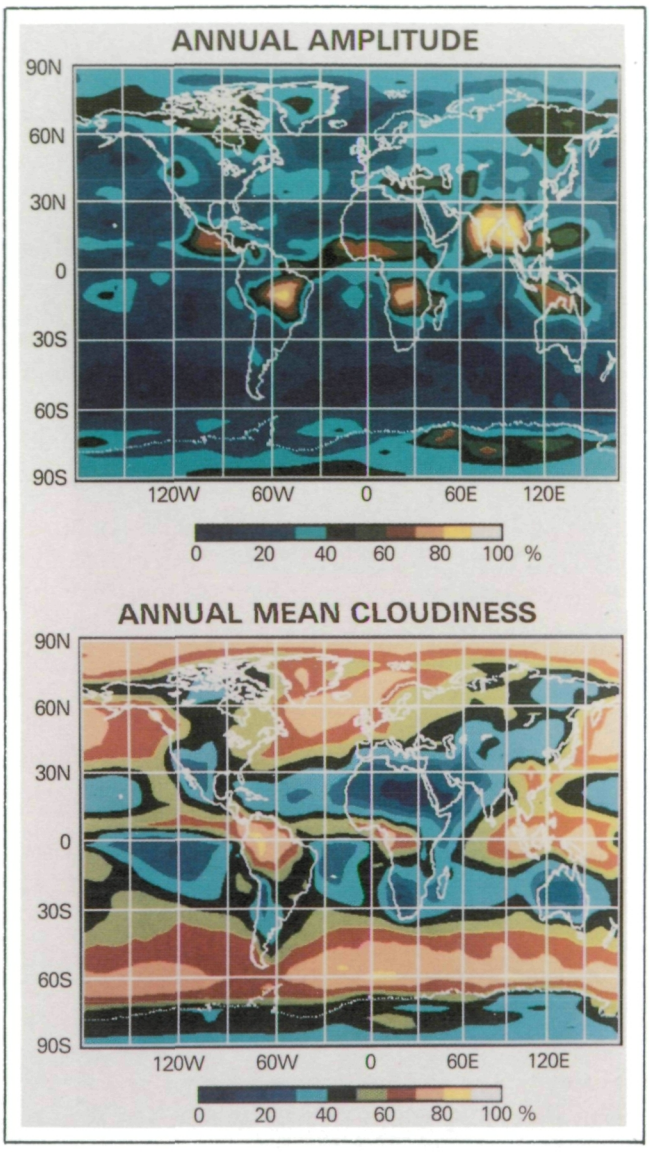

Top Panel. Annual amplitude in the monthly averaged cloud cover. Bottom Panel. Six-year mean annual global cloud cover observed near local noon.

River basin in Africa with a maximum on the coast, and around the Indonesian Island continent stretching along the equator from 90° E to 165° E longitude. The Arctic cloud belt has maxima in the north Atlantic, the north Pacific, and over the Arctic ocean.

Over land, the cloud-free arid regions are concentrated chiefly over the great desert regions of northern Africa and the Near East, southern Africa, Australia, southwestern North America, and in South America around the border of Chile and Peru. However, large dry regions also appear in the tropical southern oceans off both the Pacific and Atlantic coasts of South America. In fact, aside from the equatorial rain belt, the tropical oceans generally have a mean cloud cover of less than 40 percent.

The top panel of the figure shows the annual amplitude in the average monthly cloud cover. The northern and southern tropical monsoon areas are the most striking features. For instance, much of India and the Bay of Bengal go from nearly total overcast during the summer monsoons to nearly cloud free during the winter dry season. Driven by the seasonal changes in the incident solar insolation, the equatorial rain belt expands northward in June, July, and August, then retreats and expands southward in December, January, and February. Note that the northern and southern monsoon areas are closely tied to the three centers mentioned above in the equatorial rain belt.

The table shows the 6-year mean annual cloud cover, which was found to be 52 percent.

Percent Average Annual Cloud Cover			
	Land	Ocean	Global
Noon	43	53	50
Midnight	47	56	54
Mean	45	55	52

There are considerably more clouds over the ocean than over land, and clouds are slightly more plentiful at midnight than at noon.

The most popular Nimbus-7 cloud data set is called the CMATRIX. There is one CMATRIX tape per year that presents both daily and monthly averages for fixed (500 km)^2 regions. Finer details can be obtained from the weekly New Cloud/ERB (NCLE) tapes that contain orbital data averaged over (166 km)^2 regions. Both data products can be obtained from GSFC Code 633.4.

Contact: H. Lee Kyle
Code 636

Sponsor: Office of Space Science and Applications

Dr. H. Lee Kyle is Manager of Clouds and Earth Radiation Budget data sets preparation. Dr. Kyle, who received a PhD in atomic physics from the University of North Carolina, has been a part of Goddard for 28 years and has received a Certificate of Outstanding Performance for his work.

MOLECULAR RADIATIVE PROCESSES

Detailed knowledge of spectral line shapes as a function of pressure and temperature is required to understand how radiation is transmitted through an atmosphere. Besides controlling greenhouse effects by determining the amount of radiation absorbed by or transmitted through the atmosphere, these parameters are also required to interpret remote-sensing data. Examples of the latter include retrieval of atmospheric temperatures from satellite infrared radiometer soundings and analysis of extraterrestrial planetary atmospheres from rocket spectra.

The simplest and most widely used model for lineshapes, the Van Vleck-Weisskopf (VVW) theory, assumes a sum of independent Lorentzian lines. When the lines are broadened enough to overlap, however, which is commonly the case under atmospheric conditions, molecular collisions transfer intensity from one spectral line to another, vastly altering the lineshapes. For example, absorption in the "microwindows" between individual rotational lines in a vibrational band (which can be crucial for greenhouse effects) typically differs by an order of magnitude from VVW predictions. Another example of this effect is illustrated in the figure, which compares an experimental spectrum of the CO_2 Q-branch (used for satellite infrared temperature soundings) with VVW predictions; the latter are in error by a factor of two.

The correct theoretical description of such lineshapes is known in principle, but application has been hampered by the difficulty of properly treating the molecular collision processes that are involved. Recent attempts to improve on the VVW lineshape have used simplified models for the molecular collisions, but there is some question

C-2

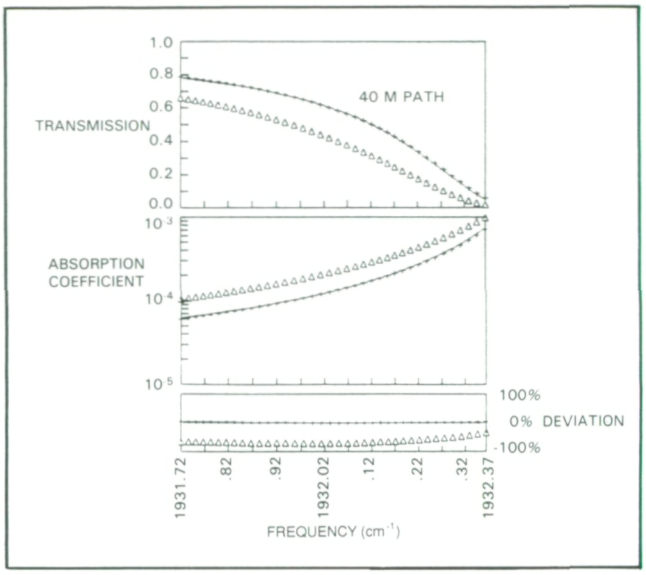

Comparison of experimental absorption with predictions of the traditional VVW theory of lineshapes for a Q-branch of carbon dioxide. Theoretical results (triangles) suggest that CO_2 absorbs much more radiation in this spectral region than is found experimentally (solid line through crosses).

about their validity. On the other hand, progress in numerical methods and computational capabilities has made an accurate description of some molecular collision processes possible, and work we have initiated at the Goddard Institute for Space Studies has, in fact, achieved solutions to the fully quantum mechanical description of molecular scattering for several systems of astrophysical interest. These studies are now being extended to lineshapes. Calculations have been completed for the fundamental band of CO in an atmosphere of He, and predictions agree well with experimental data available for this system at liquid nitrogen and room temperatures. More important, detailed results from this study suggest inadequacies in the simpler models of collision dynamics that have been proposed to treat lineshape problems. Although the line coupling terms are, in principle, complex quantities, all studies to date have ignored the imaginary parts, but these are not negligible in the accurate values for CO-He. Second, a sum rule that is generally used to relate diagonal and off-diagonal terms is found to be poorly satisfied. Finally, coupling between the P- and R-branches, which is also generally ignored, is found to be significant for the lower lines.

We hope to do calculations for other systems of interest for atmospheric studies, and we believe that results of such calculations will lead to improved models that might be applied routinely.

Contact: Sheldon Green
Code 640

Sponsor: Office of Space Science and Applications

Dr. Sheldon Green, who received a PhD degree from Harvard University, specializes in theoretical chemistry and molecular physics. He has seven years of service with Goddard.

GROUND-BASED BOUNDARY LAYER LIDAR

Knowledge of the planetary boundary layer (PBL) is important in the understanding of the exchange of heat and humidity between the Earth's surface and the atmosphere. To evaluate PBL-parameterizations in numerical prediction models it is necessary to capture the diurnal variation of the PBL-depth in great detail. To this end, a ground-based pulsed lidar system was developed at NASA's Optical Test Facility in Greenbelt, Maryland. This system (Nd:YAG at 532 nm) uses a 30-inch diameter telescope that can be scanned under computer control to rapidly probe large sections of the atmosphere. By repeating these scans over short time intervals, a highly detailed data set of atmospheric conditions can be gathered.

Starting at sunrise, the PBL-depth is of the order of 100 m. As the morning progresses, this layer will rise dramatically up to heights of 2.0–2.5 km in response to the surface heating. Large local variations in PBL-depth are indicative of the convective motions within the PBL.

The present system uses aerosols as tracers of atmospheric layer structures. Aerosols are injected into the atmosphere by natural sources and man-made pollution. Most of the aerosol is trapped in the PBL by means of a capping stable temperature inversion at its top.

The figure displays the backscatter inhomogeneities from one lidar scan in the lower atmosphere. The telescope was scanned in elevation while leaving the azimuth fixed. With the pulse repetition rate of 10 Hz, backscatter information is obtained with 0.1° angle resolution. The white area in the lower part of the picture corresponds to the PBL. The interface with the stable clear atmosphere (at approximately 900 m) shows a large undulation of the order of 200 m. The uniformly white area in the upper right of the picture is due to signal processing and does not reflect

ORIGINAL PAGE IS
OF POOR QUALITY

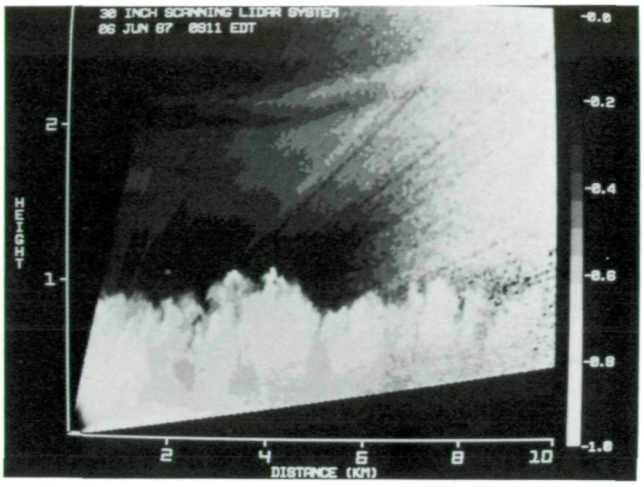

Lidar backscatter inhomogeneities in the lower atmosphere. The lower white area corresponds to the PBL. Note the large gravity wave at 2.2 km.

atmospheric conditions. At the time this scan was taken, the PBL was rising through an atmospheric layer of neutral stability. In such a situation, the PBL rise rate is proportional to the one-third-power of the surface heat flux, which was estimated to be 60 W/m^2.

At approximately 2.2 km in the picture, a large gravity wave is visible. Its amplitude is 200 m and its wavelength 10 km. In the absence of large-scale forcing, these waves are believed to be caused by the convective motions in the PBL; hence, they are called convection waves.

An experiment is under way in collaboration with researchers and students from the University of Maryland, which closely monitors the radiation and heat balance in the lower troposphere on a 24-hour basis. This data set will be used in combination with the lidar data to test PBL-models of the atmosphere.

Contact: Reinout Boers
Code 617

Sponsor: Office of Space Science and Applications

Dr. Reinout Boers has served as a visiting scientist in the Atmospheric Experiment Branch at Goddard for almost four years. Dr. Boers, who earned a PhD degree in meteorology from the University of Wisconsin, is interested in boundary layer meteorology and in lidar applications to atmospheric sciences.

CLOUD PARAMETERS FOR COMBINED REMOTE-SENSING AND IN SITU OBSERVATIONS

Over the past 4 years an experiment has been undertaken to develop and apply improved remote sensing of cloud physical parameters through the use of aircraft observations. Remote-sensing observations are made from the NASA ER-2 high-altitude aircraft. The primary instruments are a radiometer with channels specified for cloud sensing and a lidar system for cloud-top observations. Various other radiometers and microwave instruments have also been flown in some missions. A series of flight experiments has been performed which involves combined observations with several different *in situ* cloud physics aircraft. Two cloud types that have been studied are marine stratus, with a field experiment in 1983, and mid-latitude cirrus, with a field experiment in 1984. The stratus data have been analyzed to compare scales of convection derived from *in situ* and remote cloud-top observations. Cloud top liquid water and optical thickness from remote measurements have been derived with good comparison to direct measurements. Cloud radiation parameters have been derived for cirrus, and the results were compared to values inferred from *in situ* crystal observations. The combined analysis validates and supplements the results of the direct and remote measurements when considered separately.

An example of one application of the combined data analysis is shown in the accompanying figure. Marine stratus clouds were observed by the airborne lidar system simultaneously with *in situ* cloud physics measurements. An important measurement for stratus is the distribution of liquid water at the cloud top. The formation and structure of marine stratus clouds are maintained largely by radiative cooling at the cloud top, and models have shown that the interaction between radiative cooling and the cloud development are a function of the distribution of liquid water at the cloud top. A technique was developed by which the two-dimensional convective structure of the cloud top liquid water could be derived from lidar measurements. The figure shows a comparison between the lidar-derived liquid water along a flight line with the in-cloud measurement. Within the accuracy of the aircraft navigation, the direct in-cloud measurement validated the remote-sensing observation.

A much more extensive series of combined cloud observations was acquired in the last year during two regional field experiments that were carried out in support of the International Satellite Cloud Climatology Program. An analysis of results from these field experiments should

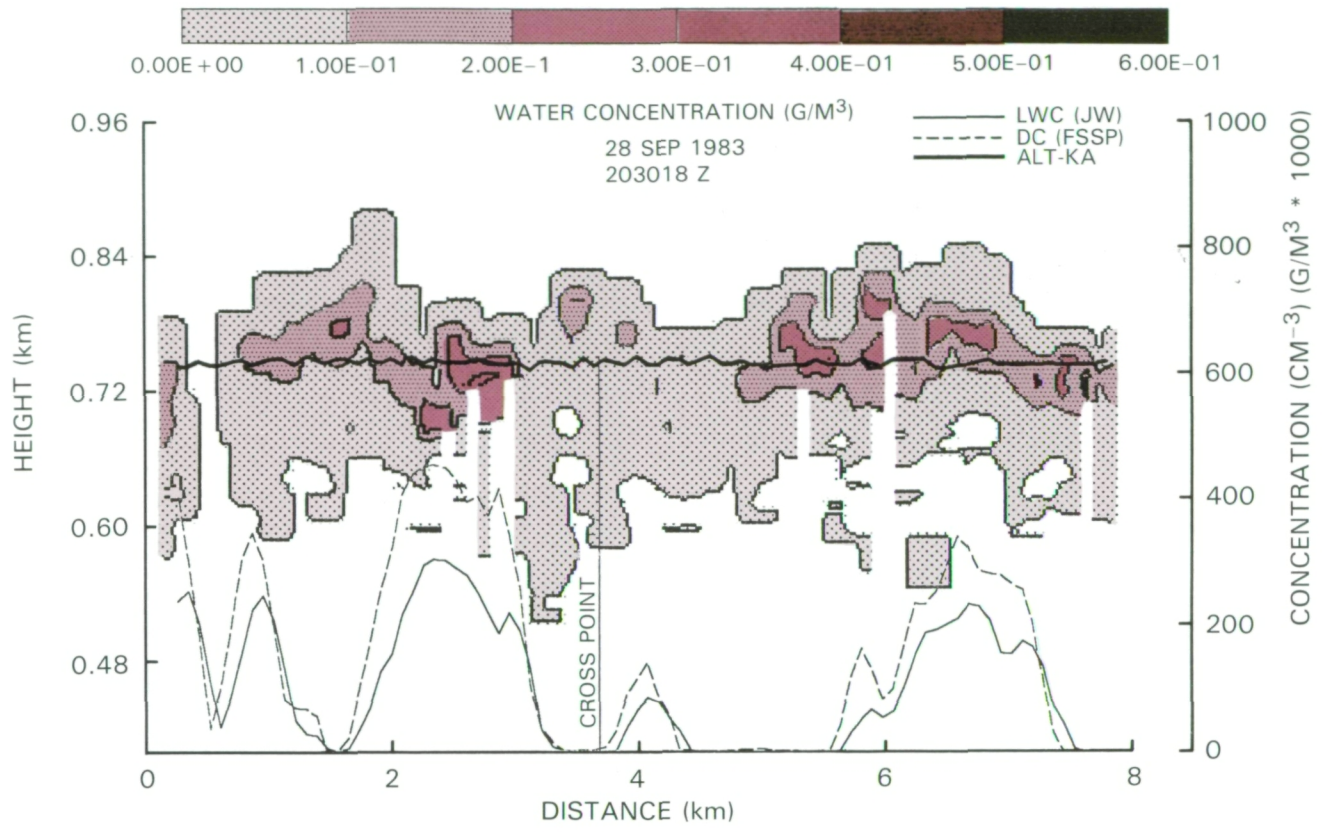

Liquid water distribution for a marine stratus cloud top as derived from lidar measurements. In comparison, the liquid water measured by simultaneous in-cloud measurements are also shown. The altitude track, droplet concentration, and liquid water for the in-cloud measurements are indicated.

improve understanding of cloud development and satellite retrievals of cloud parameters.

Contact: James Spinhirne
Code 617

Sponsors: Office of Climate Research and Office of Mesoscale Meteorological Research

Dr. James Spinhirne, who holds a PhD degree in atmospheric science from the University of Arizona, is Principal Investigator for the ER-2 cloud experiment. His scientific specialty is atmospheric remote sensing and instrumentation. Dr. Spinhirne has served with Goddard for eight years.

GLOBAL PRECIPITATION DERIVED FROM HIRS2/MSU SOUNDINGS

A new algorithm has been developed to estimate precipitation from space on a global scale. The algorithm uses difference fields of computed outgoing longwave radiation (OLR), i.e., the clear OLR minus the cloudy OLR together with the clear daytime OLR minus the clear nighttime OLR. All geophysical parameters used to compute the OLR fields are retrieved from analysis of the sounding data obtained from satellite radiometric measurements.

The geophysical parameters retrieved from analysis of the High Resolution Infrared Sounder 2/Microwave Sounder Unit (HIRS2/MSU) are used in conjunction with the radiative transfer code used in the Goddard Laboratory for Astrophysics' (GLA) General Circulation Model (GCM), to compute the total OLR. Its accuracy has been tested against two other independent determinations of OLR from satellite observations. The global mean difference is around 1 Wm^{-2} when compared with the National Oceanic and Atmospheric Administration's Advanced Very High Resolution Radiometer (11 μm) narrowband measurement of OLR and around 7 Wm^{-2} when compared with the Nimbus-7 Earth Radiation Budget (ERB)

broadband (from 5 to 50 μm) with standard deviations on the order of 7 Wm^{-2}.

The OLR computed from HIRS will be referred to as cloudy OLR because the cloud parameters, such as the cloud-top pressure and effective cloud fraction are included in the computation. Because we can compute OLR under actual conditions, we can also compute OLR fields under hypothetical conditions that have physical meaning but cannot be measured from space directly. One of these is the clear OLR, which is computed by assuming clear conditions.

The clear OLR represents a basic radiative state of the atmosphere that would occur if there were a laminar flow pattern with no clouds. Any changes in this basic circulation pattern that would produce clouds would perturb the OLR. The difference field of the hypothetical clear OLR and the actual cloudy OLR is a measure of the extent to which the basic state has been disturbed, which is referred to as the longwave cloud radiative forcing. It is found that this field is a good indicator of precipitation for most of the globe. However, precipitation is inhibited over land when the surface temperature is high during the day because heating from the ground raises the cloud base. An indicator of ground heating and possibly cloud base height, can be constructed by using the difference of clear daytime OLR and clear nighttime OLR.

We have shown that the global precipitation field is reasonably well depicted by a linear combination of the two difference fields, the clear OLR minus the cloudy OLR, and the clear daytime OLR minus the clear nighttime OLR. One set of global coefficients, applicable for the entire year, were derived by relating the global difference fields for each month of the First Global Atmosphere Research Program (GARP) Global Experiment (FGGE) year, 1979, to precipitation derived from rain-gauge measurements for the FGGE year, provided by Walker and Mintz (1987).

Figure 1a shows the field of precipitation derived in this manner using HIRS2/MSU soundings for July 1979. Precipitation measured by rain gauges for the same month is shown in Figure 1b. The agreement between these two fields is reasonable in general. The wet areas in eastern North America, north of the Mediterranean, in eastern Asia, in the southern tip of South America, and in the Intertropical Convergence Zone (ITCZ), and the dry areas over western North America, South America, North and South Africa, Saudi Arabia, and Australia show reasonable agreement in the two fields.

Over the oceans there is no ground truth measurements available. Nevertheless, the patterns shown are in good agreement with expectations based on atmospheric circulation. For example, in July the major ITCZ is in the Northern Hemisphere. The equatorial rain belt associated with the ITCZ, the monsoon rain band, the rain band associated with the winter storm tracks, and the polar front look reasonable. The oceanic dry zones associated with trade wind systems in both hemispheres are also reasonable.

The relative dry area over central China is a known phenomenon for July. The derived precipitation is closer to precipitation derived from rain-gauge measurements by Lau et al. (1986) than to the FGGE rain-gauge measurements that did not have many reports in this area. Lau used 11 years of rain-gauge data, which includes data provided by Academia Sinica of China.

When our method was applied by using Nimbus-7 ERB measurements of OLR in place of HIRS OLR (which is taken at 12 a.m., p.m. local time rather than 3 a.m., p.m. for HIRS), the precipitation over the Bangladesh area is closer to the rain-gauge measurement than that derived in Figure 1a. Therefore, the reason for the underestimation of precipitation over this area by the HIRS2 soundings may be due to diurnal variations.

Figure 2a shows the time-latitude cross section of the 10-day rainfall over east China. The two major monsoon rainfall onsets, the rainfall over the Yangtze river basin associated with the Mei-Yu front in late June, the northward propagation of the rain band, and the 20-day oscillation in the second monsoon rainfall period are all well depicted and show good agreement with the rain-gauge measurements of Lau et al. Figure 2a also shows that the 30 to 60-day oscillation around the equatorial region occurs throughout most of the year.

A similar latitude-time cross section has been plotted in Figure 2b for a region over India ranging from 10° S to 38° N and from 60° to 90° E. The 30 to 60-day oscillation around the equatorial region is clearly shown in Figure 2b. Other notable features are the Indian monsoon onset vortex in early June around the equatorial region, the heavy precipitation in late June, the short break in early July, and the heavy rain over India in late June and early August. The northward propagation of the rainfall in these two active periods is also revealed in this figure.

EOF (Empirical Orthosonal Function) analyses have been applied to the 10-day mean precipitation maps in different

ORIGINAL PAGE
COLOR PHOTOGRAPH

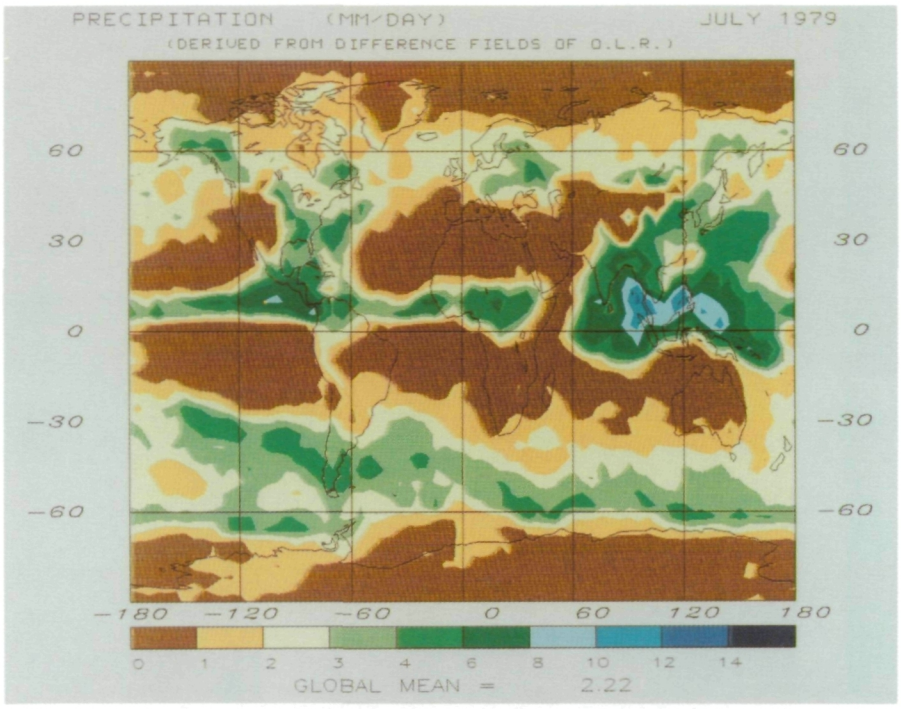

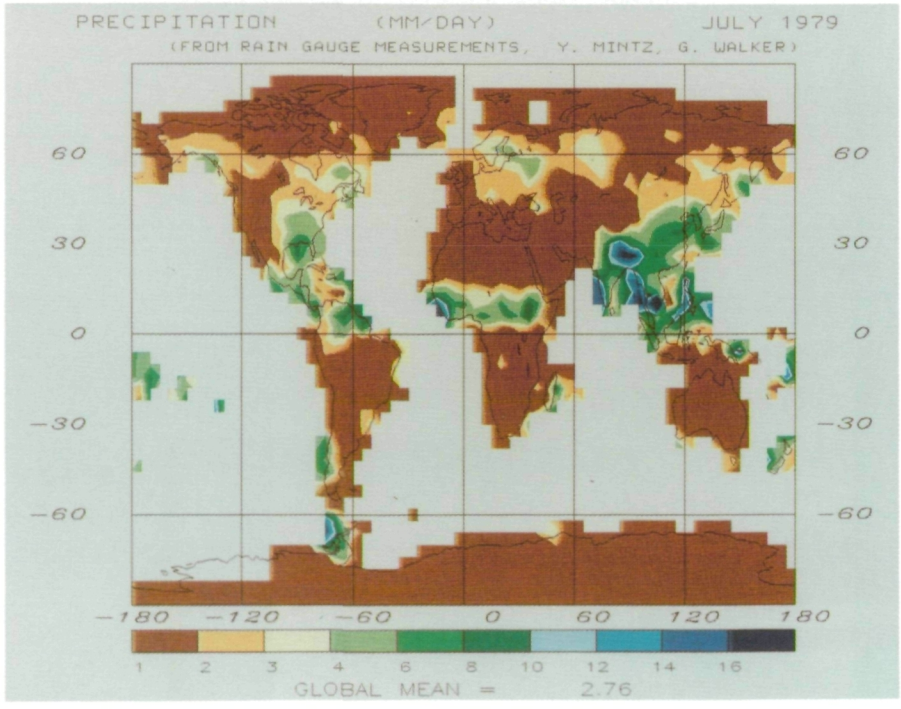

Figure 1a. Precipitation (mm day $^{-1}$) for July 1979, derived by using difference fields of OLR computed from HIRS2/MSU soundings.

Figure 1b. Precipitation (mm day $^{-1}$) for July 1979, derived from rain-gauge measurement (Courtesy of Walker and Mintz).

ORIGINAL PAGE
COLOR PHOTOGRAPH

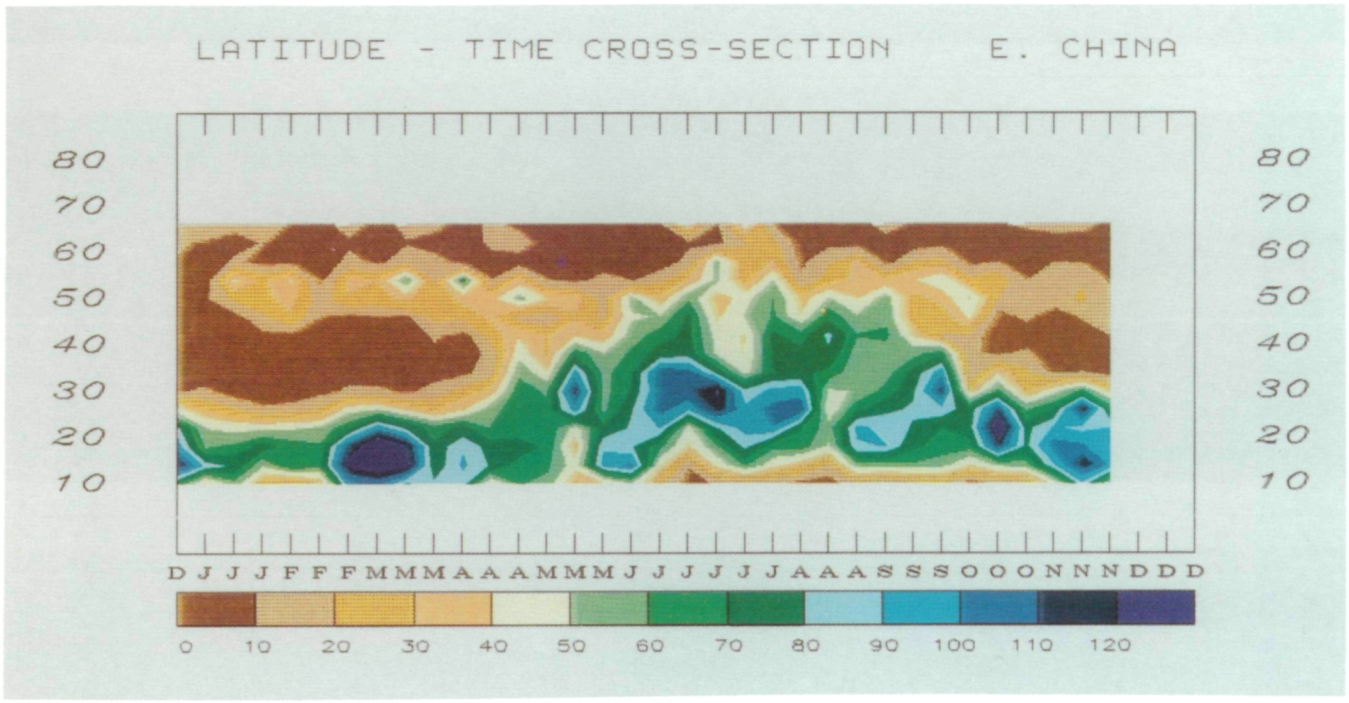

Figure 2a. Latitude-time cross section of 10-day precipitation over East China from December 21, 1978, to November 30, 1979.

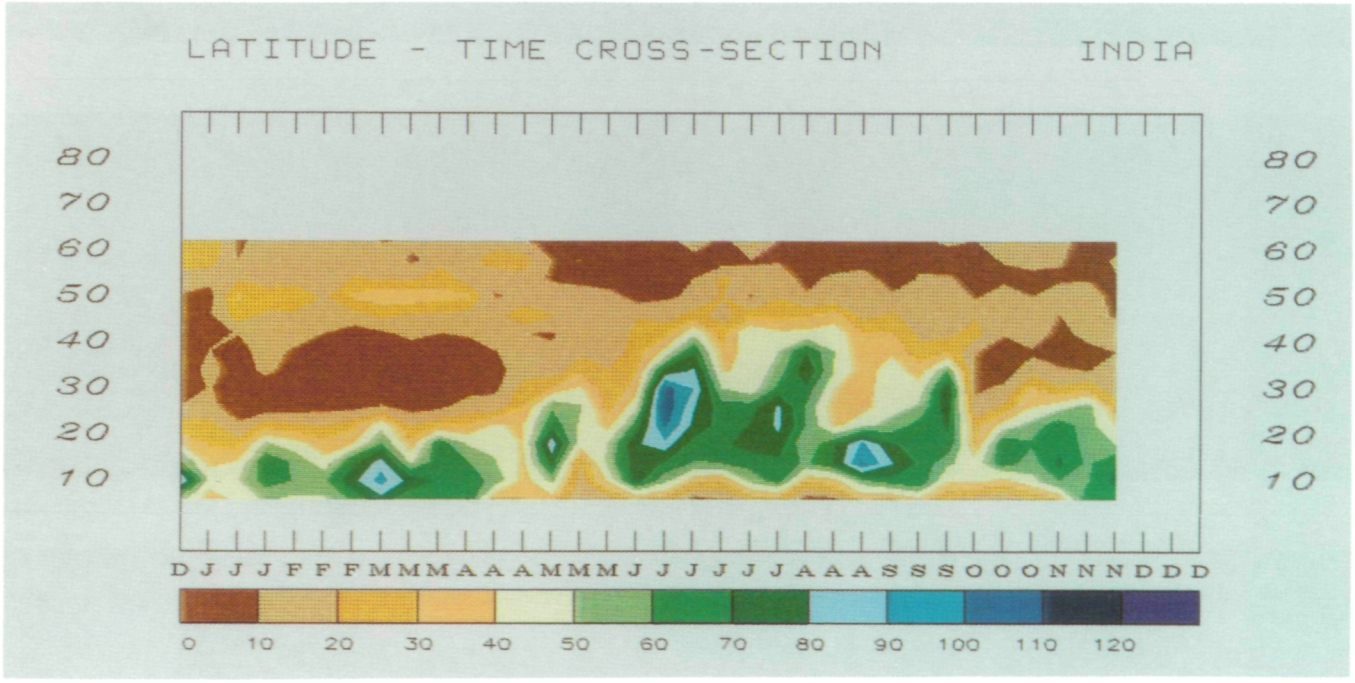

Figure 2b. Latitude-time cross section of 10-day precipitation over India from December 21, 1978, to November 30, 1979.

locations and seasons. The seasonal cycle, the 30 to 60-day oscillations, the monsoon trough over the Indian area, and the Mei-Yu and Bai-Yu fronts over east China and Japan are well depicted in the first three EOFs and their principal components.

This study indicates that precipitation is derivable from space on a global scale. This technique is flexible and can be applied to other satellite observations of OLR used together with HIRS2/MSU soundings. It is useful for studying intraseasonal variability and atmospheric oscillations. When a long-term record is available, it will be useful for studying intra-annual and interannual variability.

Contacts: Man-Li C. Wu and Joel Susskind
Code 611

Sponsor: Office of Space Science and Applications

Dr. Man-Li Wu is a physical scientist specializing in remote sensing, clouds and radiation, and climate and radiation. Dr. Wu, who received a PhD degree from the University of Chicago, has been with Goddard since 1979.

OCEAN

SIMULATION OF THE TROPICAL PACIFIC OCEAN

The tropical Pacific Ocean has a strong impact on weather and climate over the entire globe, particularly through perturbations in the sea-surface temperature that occur every few years in a phenomenon known as El Niño. Investigators at Goddard have identified long-period oscillators that act in simple models of the coupled ocean-atmosphere system and that demonstrate the importance of signal transmission through the ocean over distances in excess of 10,000 km, which take months to complete.

This theory for El Niño implies that 1) the large inertia of the ocean carries the system for many months; and 2) if properly initialized, a model for the coupled ocean-atmosphere system could possibly make use of this inertia to allow for extended range prediction of the tropical ocean, far longer than the 2- to 3-day predictability associated with atmospheric weather. If this is to happen, however, models that simulate the upper ocean in great detail must be constructed and coupled with highly accurate atmospheric models.

In the Oceans and Ice Branch of the Laboratory for Oceans, we have developed a new ocean model capable of such simulations and one that we are beginning to couple with a global atmospheric model. The model simulates the upper 500 m of the tropical Pacific Ocean by using the primitive equations of motion and by assuming that pressure variations below this depth are small. Wind stresses derived from climatological averages are applied at the surface to drive the currents, and a surface heat balance is maintained, based on heating proportional to air-sea temperature differences and solar radiation.

Figure 1 shows the elevation of the sea surface as simulated by the model. Many of the details of the field seen in climatological hydrographic studies are reproduced in the simulation: a 45-cm zonal tilt of height along the equator, the trough along 8–9° N, and the general character of the subtropical gyres. Figure 2 shows the temperature along 150° W as simulated and measured from the Hawaii-Tahiti Shuttle program.

Future work will include use of near-real-time wind stresses obtained from the National Meteorological Center to allow the reconstruction of the state of the ocean for rapid comparison with satellite and *in situ* data, the development of assimilation schemes for incorporating observations of surface height with the Geosat and TOPEX altimeters, and the inclusion of scatterometer wind-stress driving fields.

Contact: Paul S. Schopf
Code 671

Sponsor: Office of Space Science and Applications

ORIGINAL PAGE
COLOR PHOTOGRAPH

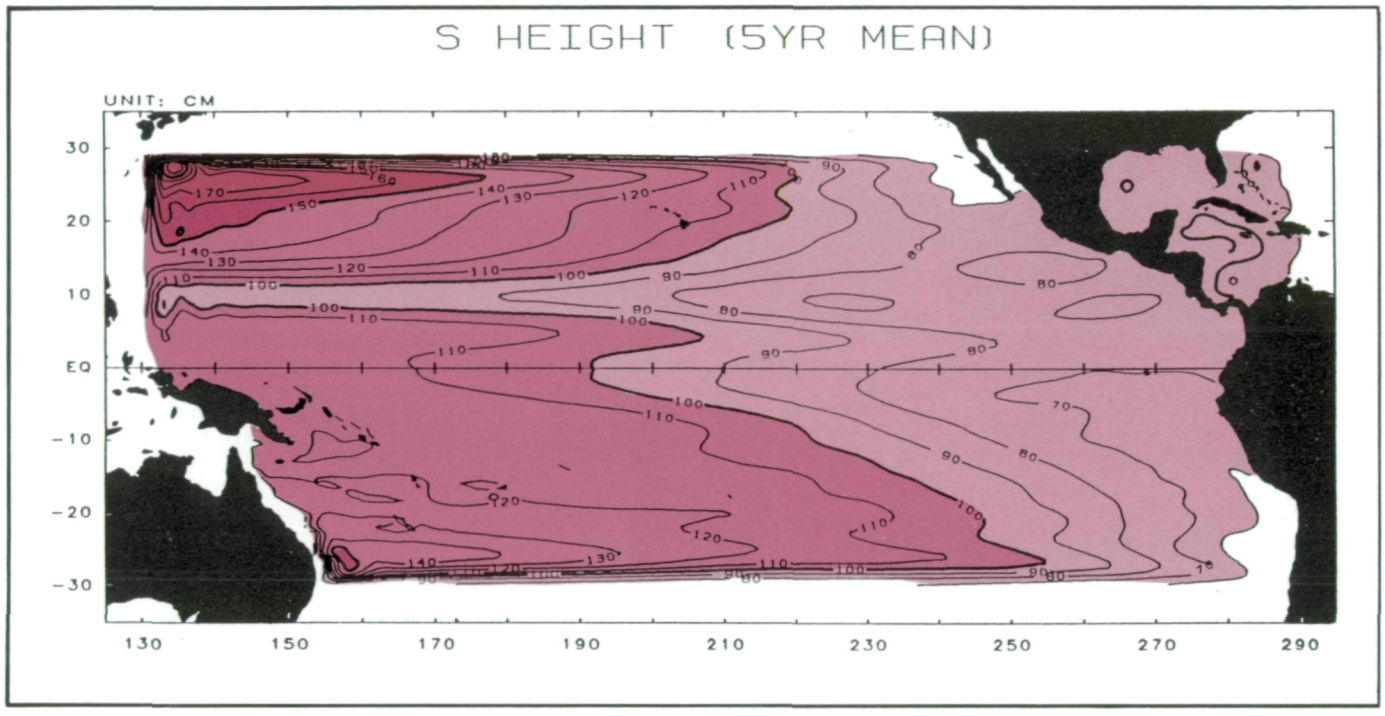

Figure 1. Elevation of the sea surface as simulated by new ocean model.

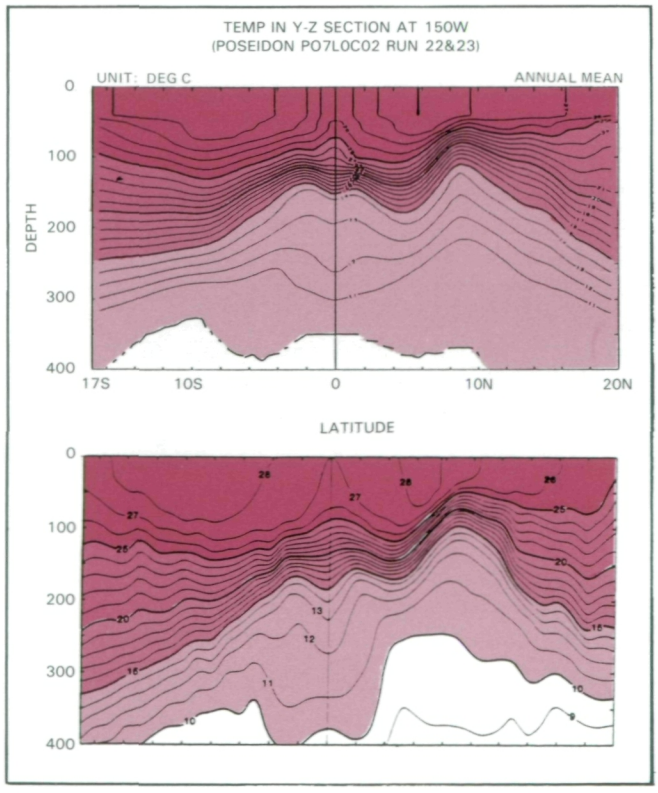

Figure 2. Temperature along 150° W as simulated and measured from Hawaii-Tahiti Shuttle program.

Dr. Paul Schopf is a research oceanographer specializing in geophysical fluid dynamics. His professional interests include coupled ocean-climate physics, tropical oceanography, and general ocean circulation. Dr. Schopf, who earned a PhD degree at Princeton, has been at Goddard for 10 years.

ESTIMATION OF WIND-WAVE INTERACTION SPECTRA BY MAXIMUM ENTROPY METHOD

The dynamics of wind-wave interaction has puzzled scientists for decades. Attempts to explain this complex behavior have not been very successful. An approach that is commonly used by experimentalists is to collect data and estimate the power spectrum. The power spectral estimation is normally obtained via sophisticated Fast Fourier Transform (FFT) periodogram techniques.

Power spectra, however, which are estimated by FFT by use of finite data windows, are known to suffer from distortion. This distortion consists of sidelobes associated with spectral lines. These sidelobes are reduced by applying some form of apodizing function to the data record (time series) before Fourier transformation. This reduces sidelobes but also reduces the effective spectral resolving power of the observation. Thus FFT spectra are

characterized by less-than-full resolution, and since the apodizing process is not complete, some residual distortion remains. In addition, a well-known limitation of Fourier techniques is that

$$\text{Resolution} \geq \frac{1}{T}$$

where T is the observation time spanned by N data samples.

The Principle of Maximum Entropy, originated in the work of Boltzman and Gibbs during the latter part of the 19th century, has to do with making inferences based on incomplete information. As such, it states that inferences should be drawn from that probability distribution that has the maximum entropy permitted by the given data. In 1957, Jaynes proposed that the Shannon information measure or entropy,

$$H = -\sum_i p_i \ln p_i \quad ,$$

be used to define the values for the probabilities, where the p_i are minimally prejudiced probability distributions. Thus, if data D concerning the outcome of an experiment are given, then predictions about the outcome should be based on that distribution p_i, which maximizes the Shannon information measure subject to the constraints imposed by the data. In the early 1900s, Gibb formulated and solved the problem in which the constraints represent mean values of various physical quantities. In 1967, Burg made his classical application of this principle to the field of signal processing, and in particular to the field of spectral analysis. He solved the problem in which time series information consists of measured values of the autocovariance function. He chose the spectrum that corresponds to the most random time series whose autocovariance coincides with the given set of values. The maximum entropy spectral density estimation found by Burg is given by

$$S(f) = \frac{\sigma_p^2 \, \Delta t}{\left| 1 + \sum_{K=1}^{p} a_{pk} \exp\left(-2\pi \, ifk \, \Delta t\right) \right|^2}$$

$$= \Delta t \sum_{n=-\infty}^{\infty} \Phi(n) \exp\left(-2\pi \, ifn \, \Delta t\right)$$

where the frequency f is constrained to be in the Nyquist interval $-\frac{1}{2}\Delta t \leq f \leq \frac{1}{2}\Delta t$, σ_p^2 is the output power of the p + 1 long prediction error filter, and the error filter coefficients are $(1, a_{p1}, a_{p2}, \ldots, a_{pp})$. In addition,

$$\Phi(n) = \begin{cases} \Psi(n), & |n| \leq p \\ -\sum_{K=1}^{p} a_{pK} \, \Phi(n-K), & |n| > p \end{cases}$$

where $\Psi(n)$ is the Blackman-Tukey spectral estimate up to lag p. For $n > p$, the Burg algorithm extrapolates $\Phi(n)$, and hence S(f). This has the effect of eliminating sidelobe leakage arising from windowing in the more conventional methods, and leads to higher resolution capability.

A version of the Burg algorithm has been applied to wave height data obtained from an experiment conducted at the NASA Wind/Wave and Current Interaction Facility at Wallops Island, Virginia. The purpose of this investigation was to examine the suitability of a power spectral analysis method derived from the Principle of Maximum Entropy for application to remotely sensed data, specifically remotely sensed oceanic data. The data provided by the experiment represent a time series of wave surface elevation measurements produced in a wave-generating tank by a mechanical plunger whose driving frequency was set at 2 Hz. The water depth is 0.76 m, and a wind-generating fan was allowed to run for half an hour at a maximum speed over the water surface of 20 m/s to ensure a steady-state condition within the channel. For the observed data record, the coefficients a_{pK} were compiled by the Burg-Anderson recursive technique in which the average output power of a (p + 1) long prediction error filter is calculated by running the filter over the data in the forward and backward directions. In this case, the one-dimensional MEM power spectral estimation has the same analytical form as an autoregressive model driven by white noise. In this study, the Final Prediction Error method of Akaike,

$$FPE = \frac{N + (M + 1)}{N - (M + 1)} P_M,$$

was used to select the appropriate value M, for the number of filter coefficients. Here N is the number of points in the time series, and P_M denotes the mean square residual for the solution of an M^{th} order fit to the error filter coefficients. When M has a value near six, it is found that the change in entropy caused by an incremental change in filter order decreases sharply for the first time, and consequently, this value was selected as optimal.

Results of the power spectral analysis, estimated from the Wallops Island wave height data were compared with those obtained from this same data by the classical periodogram approach. Some of the more important features resulting from this study may be summarized as follows:

- For large data records, the MEM and classical periodogram techniques give approximately the same power spectral density estimates.

- In computing the spectral estimate, the classical periodogram method utilized 64 samples, each of 1024 data points. On the other hand, a single data record of 128 points, sampled at a rate of 10 Hz, yielded a very good estimate with the Burg algorithm, with a high probability, while sacrificing only a small amount of resolution. Furthermore, the authors were able to show that the variance and resolution of a 5 × 1024-point MEM estimate as well as a single 1024-point MEM estimate at a 10-Hz sampling are the same as that for a 64 × 1024-point estimate at 100 Hz obtained from the classical periodogram calculation. This seems to indicate that the Burg algorithm is well suited and superior to the classical FFT approach for short data records. In addition, this implies that Burg-MEM yields the most consistent and unbiased estimates of the power spectral density when compared with the 100-Hz FFT estimate shown in the figure. This also suggests that for the same value of N, Burg-MEM should yield considerably higher spectral resolution than the FFT method.

- The stochastic wave height process, based on this time series, can be modeled by a small set of parameters (about 8 to 10, depending on the filter order M). From this, the performance of the MEM estimator exceeds that of the classical FFT spectral estimators. Since the number of modeling parameters is small, the time needed to compute the Burg-MEM spectrum is of the same order of magnitude as that of the classical methods.

- In general, there is a ubiquitous tradeoff between bias (resolution) and variance. Furthermore, when the Final Prediction Error (FPE) criterion is used, it is observed that for given records of length N, small values of filter order M yield spectral estimates with insufficient resolution. In this study, a small variance was maintained while utilizing the lowest FPE-based value of M (i.e., 6), which gave the same resolution as the 64K-point estimate obtained by the classical method.

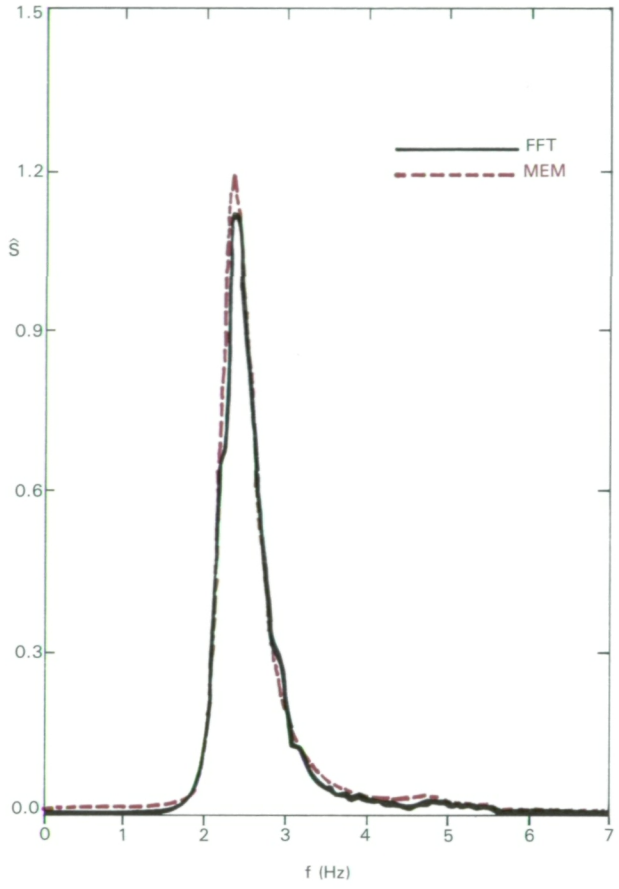

FFT power spectrum at a sampling rate of 100 Hz, and using 64 samples, each of 1024 data points (black curve). MEM power spectrum at a 10 Hz sampling rate, for 5 samples, each with 1024 data points (red dashed curve).

Contact: N. L. Bonavito
Code 636

Sponsor: Office of Space Science and Applications

Dr. N. L. Bonavito is a physicist with the Information Analysis Facility. Dr. Bonavito, who earned a PhD degree from the Catholic University of America, is interested in statistical physics and stochastic processes. He has been with Goddard for 26 years. During his military tour of duty, he served as a First Lieutenant of the U.S. Army's Guided Missile Center at Ft. Bliss, Texas.

DYNAMICS AND VARIABILITY OF ARCTIC SEA ICE

During late summer, approximately 5×10^6 km^2 of the Arctic Ocean remain covered with sea ice. Ice floes surviving the summer melt form multiyear ice, which becomes embedded in and surrounded by thinner first-year ice that grows from fall through early spring. The mass balance and long-term variability of the perennial (multiyear) sea ice pack are of particular interest in regard to climate change in polar regions. The distribution of thicker multiyear ice is of special interest because of its limiting effects on ocean-atmosphere heat and moisture exchanges. For example, various studies have focused on the possibility and consequences of significant decreases in the perennial ice pack, including a continued ice-free Arctic Ocean providing moisture for enhanced snowfall and continental ice sheet growth. Other concerns include the effects and changes in freshwater inflow from Siberian rivers and the practical limitations imposed by sea ice on offshore oil drilling and submarine operations in the Arctic Ocean.

The general features of the Arctic sea ice distribution and transport are well known. However, large-scale quantitative determinations of the amount of multiyear ice, the rate of new ice production, and the variability of the ice velocity field have been limited, particularly during winter. Although sea ice covers the entire Arctic Ocean each winter, the sea ice pack is in a continual state of motion, primarily in response to frictional forcing by winds. Divergent motion of the ice pack produces leads and polynyas partially covered by open water and newly formed thin ice. Convergent motion produces ice ridges and rafting. Large-scale advection of the ice pack causes export of ice from the Arctic Ocean, primarily between Greenland and Svalbard. Consequently, the multiyear ice distribution continually changes in response to changes in weather patterns, as well as interannual or 10-year changes in the atmosphere and ocean.

Recent research at GSFC has shown that multiyear ice distributions, derived from the Nimbus-7 Scanning Multichannel Microwave Radiometer (SMMR) passive microwave data, can be used to study the large-scale drift of the ice pack, convergence/divergence within the pack, and interannual variations in the multiyear ice coverage. In collaboration with Dr. John E. Walsh of the University of Illinois, ice drift and deformations are studied on daily, seasonal, and interannual time scales by use of the SMMR data and a numerical ice model. Daily maps of multiyear ice concentrations are analyzed to obtain the displacement of the multiyear ice edge and information on the convergence/divergence within the pack. A dynamic-thermodynamic sea ice model is run with daily timesteps and with forcing by varying fields of geostrophic winds (derived from observed pressure fields) and temperature-derived thermodynamic fluxes. Climatological values of the oceanic parameters are used. Therefore, the modeled variations in the ice velocity fields are a result of variations in the observed atmospheric forcing corresponding to changes in synoptic weather patterns and longer-term variations in the atmospheric circulation.

The sea ice velocity fluctuations deduced from SMMR data and the sea ice model are generally compatible, confirming that the SMMR-derived fluctuations are related to the atmospheric forcing. For example, both the model and the data-based drifts (Figure 1) for a 52-day period from November 25, 1978, to January 28, 1979, differ similarly from the classical pattern of ice velocities in the Arctic. The more typical pattern, consisting of an anticyclonic gyre in the Beaufort Sea north of Alaska and ice transport across the pole in the Transpolar Drift Stream, is shown the following year. In 1978–79, the transpolar drift dominates the entire Arctic Basin, resulting in an ice flux toward the Laptev Sea north of Siberia, in contrast to a modest outflow from the Laptev Sea in 1979–80. Overall, the model and the data exhibit the same patterns of ice movement with marked month-to-month and large interannual variations. Discrepancies occur near the edge of the total ice pack in the East Greenland Sea where the microwave characteristics of the sea ice are not consistent.

During the 1980–1981 winter, a region of very low multiyear concentration appeared around 80° N and 165° W. Examination of the daily SMMR maps showed that the low-concentration region formed within a two-day period around December 2, 1980, coinciding with the passage of an intense cyclone. The divergence of the ice pack implied by the changes in multiyear concentration is in qualitative agreement with the divergence computed from the modeled velocity fields. Both the microwave data and the model show similar spatial and temporal characteristics of pack ice response to the cyclone, demonstrating that major synoptic events can have long-lived impacts on the multiyear ice distribution in the central Arctic.

These results are providing new insights into the nature and causes of Arctic sea ice variability, as well as a means of monitoring changes in the perennial ice pack. Daily, monthly, and even seasonally averaged fields of sea ice motion are found to be highly variable, and departures

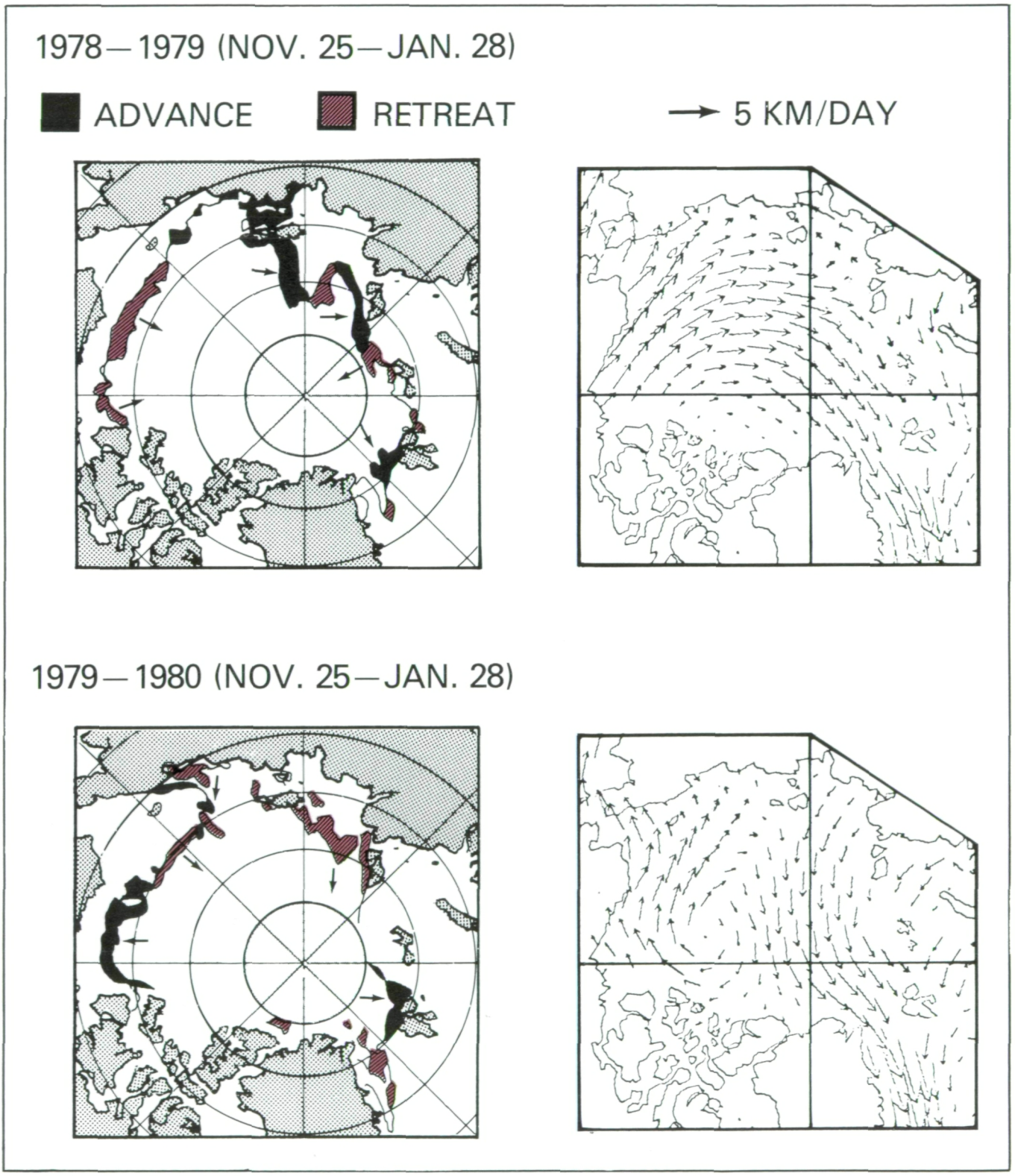

Figure 1. Motion of the edge of multiyear ice pack derived from passive microwave data from the Nimbus-7 SMMR and simulated ice drift vectors from numerical ice model for November 25 to January 28 of 1978–79 and 1979–80.

ORIGINAL PAGE
COLOR PHOTOGRAPH

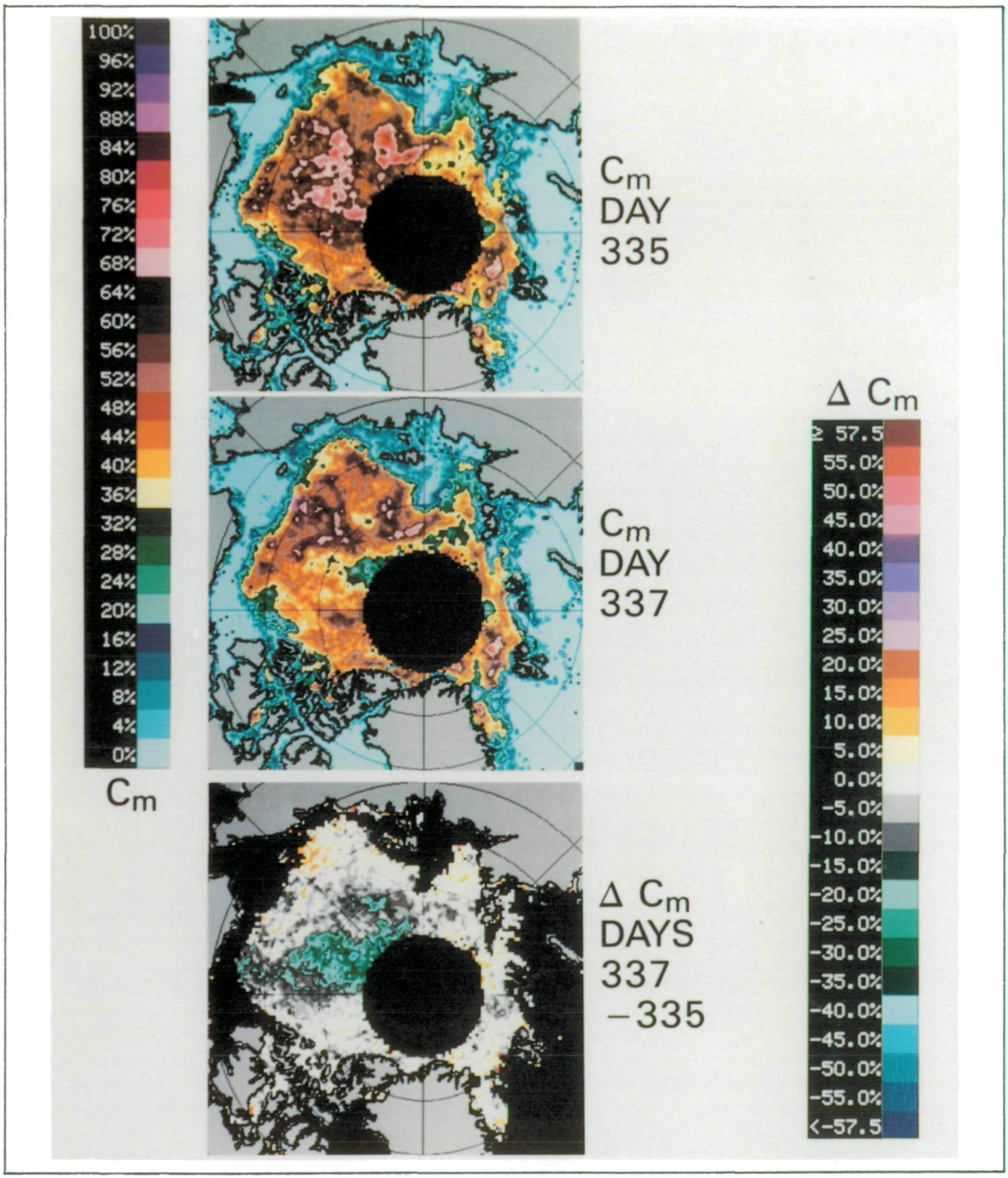

Figure 2. SMMR images of multiyear sea ice concentration for November 30 (day 335) and December 2 (day 337) of 1980. Field of change of multiyear concentration between November 30 and December 2 is associated with passage of a cyclonic atmospheric system that caused divergence of the ice pack.

from the climatological normal field can dominate the pattern for several days to several months.

Because variable air stress is the primary determinant of the modeled ice-drift fluctuations, the observed ice-drift variability is attributed primarily to the variations of the geostrophic wind or sea-level pressure. The SMMR data also present an excellent tool for studies of the mass balance of the Arctic pack ice. Since the total areal coverage of multiyear ice is approximately conserved during the winter months, estimates of the regional divergence of the multiyear ice can provide a measure of the area of new ice growth within the pack during winter, as well as the associated thermal and salinity fluxes to the atmosphere and ocean. For studies of overall mass balance, preliminary analysis of the 8-year times series of SMMR data indicate a significant temporary decrease in the multiyear ice coverage in the early 1980s. Through the use of the SMMR data and the ice model, the relative importance of interannual variations in the amount of ice divergence within the pack and variations in the large-scale ice advection is being assessed.

Contact: H. Jay Zwally
Code 671

Sponsor: Ocean Processes Program

Dr. H. Jay Zwally is a research scientist involved with observing and modeling the variability of polar sea and ice and continental ice sheets. He received a PhD degree in physics from the University of Maryland. During his 14 years of experience at Goddard, Dr. Zwally has received the NASA Group Achievement Award for his participation as an author of the Antarctic Sea Ice Atlas, *and the Goddard Exceptional Performance Award for his leadership in establishing a recognized cryospheric research program.*

SUB-TEN-CENTIMETER AIRCRAFT POSITIONING USING THE GLOBAL POSITIONING SYSTEM (GPS)

The long-term objectives of this investigation are to develop and apply technology and algorithms required to provide aircraft trajectories with an accuracy below 10 cm. This trajectory accuracy is relative to a fixed site, with separation distances of up to 200 km, or perhaps more.

The objective of this specific research task is to provide a precise reference position for airborne remote sensing systems, specifically laser and radar sensors. This technology will be applied to oceanographic measurements, including the possibility of detecting and measuring geostrophic currents, and for the collection of sea-surface condition data for calibrating satellite radar and laser altimeters. The capability will also be applied to the collection of measurements over ice and snow.

This project makes use of techniques developed for geodetic applications in which the phase of the GPS L-band carrier is tracked to provide very precise but ambiguous pseudo-ranges. The technique works very well for receivers at fixed locations but is somewhat more difficult for a mobile application.

A preliminary test was conducted in 1985 in which 10–12 cm results were demonstrated with receivers not designed to function in an aircraft. The project recently procured two receivers from Motorola that are intended for mobile operation and were used on a recent mission of the NASA P-3 to the North Pole. Data from this project are now being analyzed, and early indications are that performance of the GPS receivers was well within specifications.

Contact: William B. Krabill
Code 672

Sponsor: Office of Space Science and Applications

Mr. William Krabill specializes in the application of airborne lidar and precision navigation systems. Mr. Krabill, who holds a BS degree in mathematics from Salisbury State College, has been with Goddard for 19 years.

MULTIPROCESSOR AIRBORNE DATA SYSTEM

After extensive system analysis and benchmark comparisons, a new multiprocessor computer system has been designed and implemented in the Airborne Oceanographic Lidar (AOL). The system consists of five 68010 based microprocessors operating in parallel on a shared data bus. Each microprocessor is a complete computer system with private onboard input/output channels, bus interface for sharing information with other processors, random access memory, direct memory access capability, erasable programmable read-only memory, and a real-time operating system. A general purpose 4 megabyte universally accessible data queue (UDQ) is implemented for temporary data storage. Bus traffic is greatly reduced, resulting in increased system speed, since each processor has independent and local facilities that do not require access to the system bus. The increased bus bandwidth

is used for data transfers from the data source computers to the UDQ. All processors operate at full speed and in parallel. Up to eight processors can be accommodated on the commonly shared data bus.

The AOL real-time system utilizes UNIX and VRTX operating systems simultaneously. UNIX is utilized for program development, data analysis, and system control. VRTX processors execute real-time tasks such as data capture and instrument interfaces. The software system can be divided into three basic areas: data capture, instrument control, and data storage. Data capture is accomplished by the VRTX processors. Instrument control is a cooperative effort between each VRTX processor and a corresponding UNIX process or program. Data storage is accomplished directly by each of the VRTX processors. The writing of data to the physical device is controlled by a UNIX task.

Software development and data analysis are achieved under the UNIX System Five operating system executed on the primary microprocessor. All programs and related information are stored on Winchester hard disks in the UNIX environment. Near real-time data analyses are carried on as background tasks on the UNIX processor. Data may also be retrieved after a mission for analysis by the UNIX processor.

Three of the processors capture data from several laser-related sensors, as well as from aircraft navigation and flight data parameters. The data sources include the following CAMAC-based instruments: waveform digitizer, pulsed laser spectrometer, 36-channel passive spectrometer, several subnanosecond time interval counters and digital delay generators, and other interfaces supporting the lidar implementation. The two CAMAC crates are interfaced and controlled by a single microprocessor. Another processor controls three 256-channel charge coupled device spectrometers. A fourth processor displays real-time data providing immediate feedback for the operator. The fifth processor, the UNIX processor, communicates with the system operator and controls all of the other processors, as well as the storage of data on the selected media. Each processor, through a local I/O port, is interfaced to a particular portion of the AOL hardware. The captured data are stored in the UDQ and retained from 20 s to 20 min, depending upon data rate. The data stored in the UDQ are accessed by the real-time display portion of the system and UNIX-based near-real-time data processors.

Contacts: Charles W. Wright, Steven A. Bailey, and Charles R. Piazza
Code 672

Sponsor: Office of Space Science and Applications

Mr. Charles Wright is an engineer with the Airborne Oceanographic Lidar. Mr. Wright, who holds a BS degree in computer science from the University of Maryland, specializes in remote sensing systems and data systems. He has been at Goddard for eight years and has received the NASA Outstanding Service Award.

SHUTTLE LASER ALTIMETER

Laser altimetry offers the possibility of very high resolution measurements of Earth, lunar, and planetary surface topography from a space platform. As with conventional radar altimetry, the basis of the measurement is the timing of short pulses for round-trip propagation at the speed-of-light between the spacecraft and the surface to be measured. Vertical or height resolution of the altimetry measurement is determined primarily by laser pulsewidth and the timing precision of the altimeter electronics. With conventional gain-switched pulses from solid-state lasers and nanosecond-resolution timing electronics, meter or even submeter vertical range resolution is possible from orbital altitudes of several hundred kilometers. Horizontal resolution is determined by laser beam footprint size at the surface and the spacing between successive laser pulses. The most significant advantage of laser altimeters over existing radar altimetry devices is the orders-of-magnitude smaller footprint that results from the narrow laser beam of optical radiation. Laser footprints of tens-of-meters result from the submilliradian divergence angles possible with the optical frequency of laser beams.

A laser ranging instrument has been developed for altimetry measurements of the Earth's surface along the nadir track of the Space Shuttle. The Shuttle Laser Altimeter (SLA) is designed for transmission of a short laser pulse in the near-infrared at 1064-nm wavelength and reception of the backscattered laser radiation from the Earth's surface. Laser, telescope, detector, data processing and storage electronics, and battery power pack are packaged for spaceflight into two adjacent Get-Away-Special (GAS) canisters. The interface to the Shuttle in the form of GAS canisters is extremely important in

reducing payload costs one to two orders-of-magnitude from typical Shuttle experiments, but it also imposes severe design constraints on the SLA instrument to provide its own power, data acquisition and recording, and thermal control.

An assembly view of the SLA instrument appears in Figure 1. One canister, equipped with a motorized door assembly, contains the laser transmitter, receiver telescope, and detectors of the laser altimeter instrument. It also has a large-diameter glass window to maintain up to 1 atm. of pressure inside the canister and still provide the maximum clear aperture of 0.38 m for laser altimeter operation. The motorized door is closed during launch and landing and then opens on-orbit for experiment operation. The flashlamp-pumped Nd:YAG laser transmitter is a single-rod device capable of a 150-mjoule/pulse output in a 20-ns wide pulse at the 1064-nm wavelength. The second GAS canister contains the battery power supply, altimeter data acquisition electronics, flight computer, tape recorder, camera, and infrared (IR) radiometer. This canister is also sealed to provide up to 1 atm. of internal pressure. Its upper lid contains two 7-cm diameter windows for observations with the camera and IR radiometer. Both of these instruments provide data products for post-mission identification of altimetry targets. This support module is joined with the laser altimeter module by a power and data cable. Battery power from the support module is routed to the major power user, the laser, in the altimeter canister. Altimetry data pulses from the detectors are transferred by this cable to the support canister for processing.

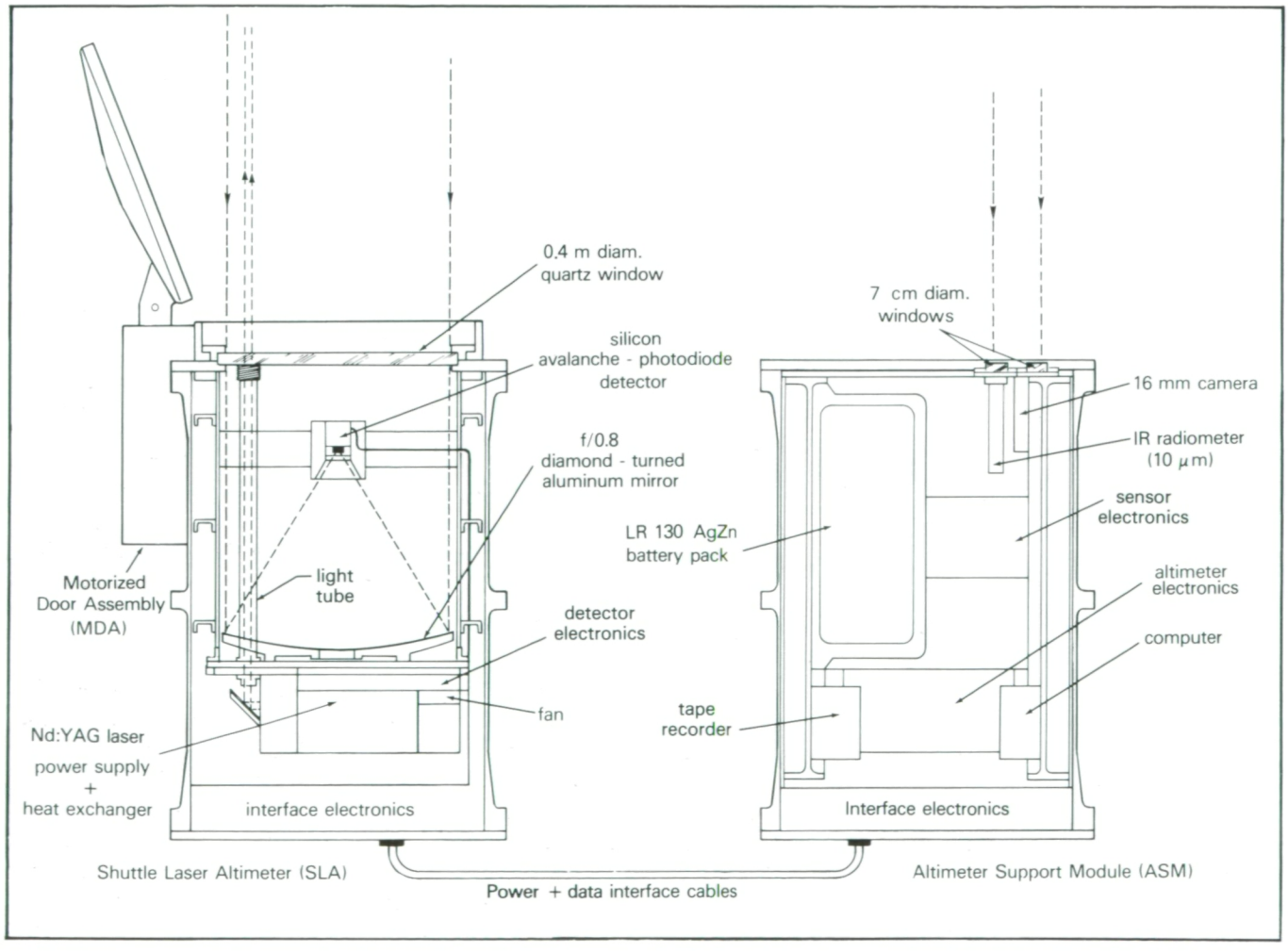

Figure 1. Shuttle Laser Altimeter dual-canister payload.

The basic data set for laser altimeter measurement is the laser pulse time-of-flight to the Earth's surface and return to the spacecraft. This is achieved by operation of a time-interval-unit (TIU) based on start and stop pulses derived from the transmitter and receiver pulse discriminators. A silicon photodiode detector for the transmitted pulse and a silicon avalanche photodiode for the received pulse produce current waveforms that are amplified and then processed for altimetry data. Both pulse waveforms are processed by electronic discriminators, with a simple threshold-crossing technique, to produce fast-risetime pulses of standard amplitude and width. These pulses are then used to start and stop the TIU with nanosecond-level timing precision, equivalent to a range resolution of 15 cm. Range-gating circuitry is included to discriminate against optical background noise, detector noise, and the presence of cloud backscatter. Ranging system TIU electronics are supplemented by high-speed waveform digitization to provide data on the surface-height distribution within the laser footprint. Twelve channels of digitization with 10-ns resolution are provided for each receiver pulse waveform. Altimetry output data also include transmitted and received pulse energy for each laser shot. These energy data points are acquired by integration over the entire pulse waveform. The ratio of received and transmitted energies as a function of time provides information on atmospheric transmission and target albedo vibrations. The TIU data, waveform-digitizer data, and pulse-energy data form the basic laser altimeter data set for each laser pulse. These data points are accumulated in a buffer in digital form, formatted into data blocks or files, and entered into the SLA data stream for recording. A compact tape recorder is used to store the altimetry data products.

While awaiting spaceflight opportunities, the SLA prototype has been tested from a high-altitude aircraft platform. The primary objectives of these tests were the verification of instrument performance, the acquisition of useful surface topography data sets, and the simulation of laser ranging from a spacecraft platform. For these tests the SLA instrument was positioned for nadir observations from the Wallops Flight Facility T-39 Sabreliner (NASA-431) high-altitude jet aircraft. Data were acquired on several flights at altitudes as high as 12 km above sea level. Altimetry results are available from flights over mountain-region terrain in the eastern United States, Atlantic Ocean coastal waters, various cloud layers, and a variety of volcanic, erosional, and impact-related landforms in the vicinity of Flagstaff, Arizona; Snake River Valley, Idaho; and Spring Lake Valley, Nevada. These data sets permit instrument performance to be assessed as a simulation of space-based laser altimeter measurements. Some measurements were made with laser pulse energies reduced to the sub-millijoule level to simulate the link losses of Shuttle-to-Earth propagation.

A very significant feature of the airborne laser altimeter operations is the use of the data to support NASA Land Processes science investigations in studies of volcanic, erosional, and impact landforms. Figure 2 is an example of topographic profile data acquired on a traverse through the center of Meteor Crater at Winslow, Arizona.

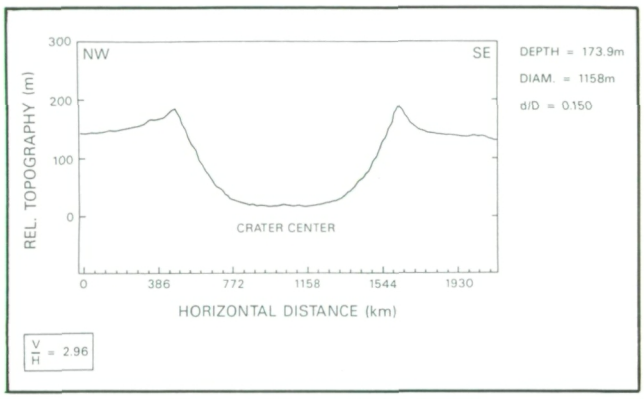

Figure 2. Shuttle Laser Altimeter profile of meteor crater: NW-SE traverse (through center).

This profile is composed of 1800 individual laser range measurements at a 3-m diameter footprint size with submeter vertical resolution. In addition, the waveform digitization data for this profile successfully identified a known effect of the smoothing of the near-rim ejecta blanket. Measured pulse spreading decreased from 3 m to 2.5 m just outside the crater rim. In the most recent profiling in Idaho and Nevada during July 1987, the satellite-based Global Positioning System (GPS) was used simultaneously with the SLA system for the first time. Preliminary data analysis shows GPS data to be extremely useful in removal of aircraft motion to the meter level for topographical profiles up to 25 km in horizontal extent. This has opened a new dimension of precision for airborne laser altimetry. The same GPS system can be used on the Space Shuttle. The result is a high-resolution laser profiling capability from airborne platforms that can be expanded to global coverage when spaceflight platforms become available.

Contact: Jack L. Bufton
Code 674

Sponsor: Director's Discretionary Fund

Dr. Jack L. Bufton is Head of the Experimental Instrumentation Branch in the Laboratory for Oceans. He has 21 years of experience in the design and engineering of laser and electro-optical instrument systems. He holds a PhD degree in electrical engineering from the University of Maryland.

TERRESTRIAL

SATELLITE DISCOVERY OF THERMAL ANOMALY: TM/AVHRR STUDY OF VOLCANIC ARABIAN HIGHLANDS

On June 22, 1984, data from the thermal band of the Landsat 5 Thematic Mapper (TM 6) recorded a large thermal anomaly around the southern flank of Jebel Chada, a geologically recent (1256 A.D.) volcanic cone. This currently inactive volcano is 19 km southeast of the city of al Madinah (Medina), Saudi Arabia. It is the largest area of high daytime emissivity reported to date by Landsat investigators.

Figure 1, a contrast-enhanced thermal image constructed with TM 6 data, shows this area of high thermal emissivity within the northern lobe of the Harrat Rahat flood basalts. Tonal variation from dark to light indicates increasingly higher temperature. This striking feature forms a 2-km wide apron about the base of the Jebel Chada volcano complex and appears as a thick U-shaped area that is 6 km across at its broadest extremity. The thermal profile A-A′ across this anomaly (Figure 2) shows thermal variations of up to 15 °C. Although the overall temperature values shown on the profile appear high for the hour of data acquisition, the general degree of difference between points is meaningful. These high recordings appear to have been caused by a systematic error in the instrument gain and could be reasonably well calibrated if appropriate underflight and/or ground data were available.

An isothermal map (Figure 3) constructed by density-slicing selected thermal intervals shows the highest temperatures (over 71.4 °C) to be concentrated irregularly within the northernmost 3 km of each limb of the thermal arc, and on the east-facing slopes of several of the most prominent volcanic cones. The temperatures within the arc trend irregularly lower toward the south. The northern margins are fairly well defined, having a transition boundary of only 200 to 300 m in width. Toward the south, the margin of the anomaly becomes progressively more difficult to map because the elevated values decrease gradually outward and grade into the thermal values for the surrounding basalt flows.

Small isolated thermal areas also frequently occur on the sunward-facing slopes of some of the higher volcanic cones that are concentrated along the north-northwesterly trending median axis of the Harrat Rahat. The mid-morning (09:16 local) solar rays (61 ° Sun elevation) striking terrestrial surfaces at 085 ° azimuth heat those surfaces normal to incidence (29 ° slope) to a greater degree than those rays striking at grazing incidence. The highest temperature recorded within the test area (77.9 °C uncalibrated) is on the east flank of Jebel Diba al Hurus. This volcanic dome is one of a group of trachyphonolite domes whose eruptions were accompanied by abundant pyroclastic activity that formed thick layers that have in part been eroded. The limited area of temperature elevation and contiguous shadow associated with Jebel Diba al Hurus suggest strongly that the elevated temperature is primarily a function of topography; the influence of lithology (pyroclastics), if any, is minimal. The steep-sloped areas affected by these combined warm and cool anomalies rarely exceed 1.0 km^2 in area.

Analysis of topography with overlapping 1:63,360 aerial photographs shows that only a small segment of the extensive Chada anomaly can be attributed to steep slopes and topographic orientation.

The Jebel Chada volcanic ridge includes a large cone to the north, flanked by several smaller subsidiary vents to the south-southeast. The thermal protrusion into the center from the southeast side of the U-shaped anomaly (Figure 1) parallels this ridge and appears to be the only

ORIGINAL PAGE IS
OF POOR QUALITY

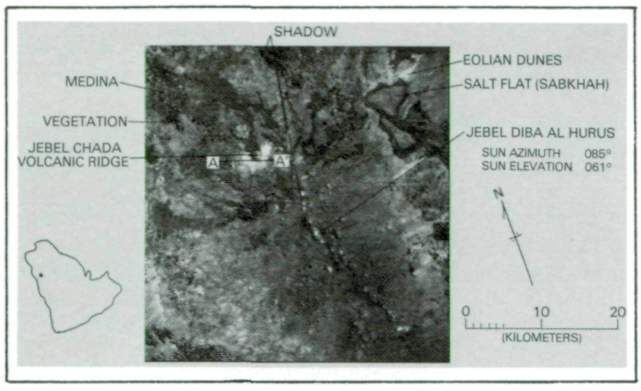

Figure 1. Contrast enhanced infrared (TM 6) image of Jebel Chada thermal anomaly, 19 km southeast of Medina, Saudi Arabia. (Landsat-5 Thematic Mapper Scene 50113 07164, June 22, 1984.)

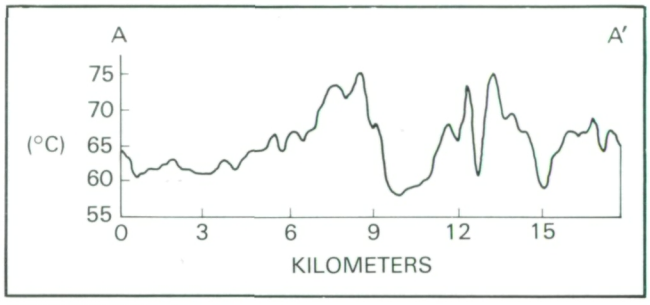

Figure 2. Thermal profile (uncalibrated) across Jebel Chada anomaly.

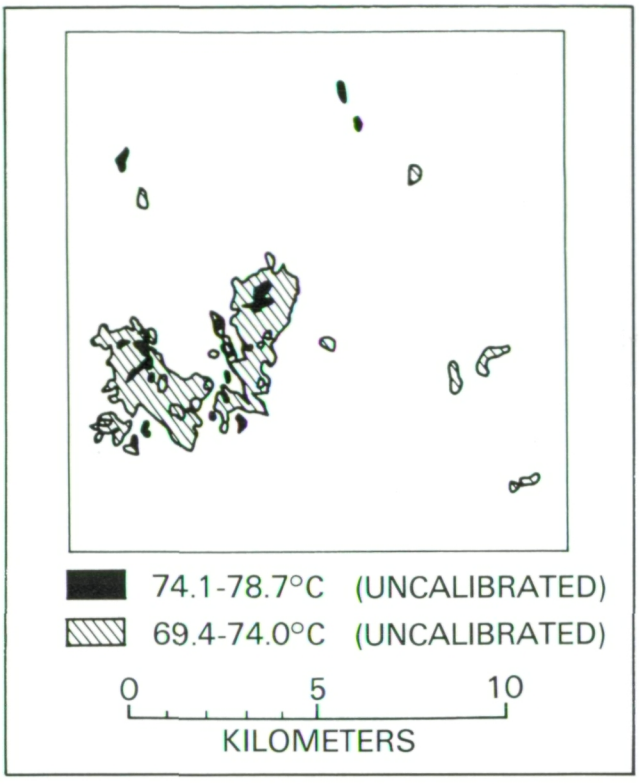

Figure 3. Isothermal map of Jebel Chada area, derived from Landsat-5, TM 6 data of June 22, 1984.

portion of the entire large anomaly that may be related to topographic relief, even though there is no well-defined complementary shadow along the northwestern slope of the ridge. The remainder of the large anomaly extends outward from the southernmost 2.5-km subcircular area depicting the most recent eruption center.

Areas of higher emissivity are also concentrated where eolian dunes developed locally on the flat, eroded Precambrian basement west of the harrat. These off-white unconsolidated quartz sands rapidly absorb solar heat and attain temperatures of up to 69°C (uncalibrated). A small dune field overlies the basement formations near the northeast corner of Figure 1. These thermal anomalies follow the outline of the dunes, suggesting that they are primarily related to lithology.

The anomalous TM thermal area was registered to and compared with each of the six simultaneously acquired visible and near-infrared TM bands. For each band within the anomaly outline, there are localized areas of intermediate reflectivity. These concentrations have a mottled appearance on each image and are concentrated within the northern extremities of the thermal arc. The zones of intermediate density distribution are not identical on each band image. None of the reflected spectra showed the intensity or aerial distribution displayed on the thermal data.

The Chada anomaly is large enough and strong enough to be recorded and identified on coarse resolution (1100 m) Advanced Very High Resolution Radiometer (AVHRR) data acquired by the NOAA 7 satellite. A day-night pair of AVHRR data were acquired on November 3 and 4, 1983, at 3 p.m. and 3 a.m., respectively. A 50 × 50 pixel subset of these data, selected to include Jebel Chada and its associated thermal anomaly, was extracted, and isothermal maps were prepared for each TIR band with digital number (DN) thermal values.

The area characterized by higher temperatures on the TM data are clearly displayed on the afternoon AVHRR thermal data. Channels 4 and 5, which include the emissivity range of the TM, show the anomaly to be well defined

geographically. AVHRR channels 1 and 2, recording in the visible and near infrared, respectively, show no unique irregularity in the vicinity of Jebel Chada.

The early morning AVHRR data record surface temperatures in equilibrium with the local environment. That is, the surfaces have not yet been affected by solar heating; the area of high daytime emissivity is not distinguishable.

Evidence for an internal heat source of either volcanic or hydrologic origin is poor. If the anomaly were caused by an internal heat source, pre-dawn data recorded by the AVHRR thermal channels should display a strong thermal high in comparison with other surfaces that had not yet been affected by solar heating.

Based on the data available, the following conclusions have been reached. Several small areas of the Harrat Rahat showing elevated temperatures are related to the topographic slope and attitude of the higher volcanic cones and ridges. Evidence for solar heating is supported by high thermal values being recorded on the sunward side of the cones and, conversely, by the presence of cooler than normal values on the opposite northwestern shaded slopes. These anomalies, however, are generally less than 1 km^2 in area. A small portion of the large thermal anomaly on the southern flank of Jebel Chada appears to be related to the south-southeast trending volcanic ridge that forms the higher topography of the jebel. The major portions of the large anomaly, however, form an apron about the base of the south-flank eruptives and transcend topography and mapped geological boundaries.

Based on the information available, the most probable explanation for the large Jebel Chada thermal anomaly is that its surfaces have a thin, irregular cover of pyroclastics erupted during one of the last active volcanic periods. These thin ejecta deposits have characteristic thermal properties but are indistinguishable from underlying basalts on the basis of relief. The slightly dark tonal areas seen in the reflected visual and near-infrared TM data are concentrated in the northern part of the anomaly where the highest temperatures are recorded, suggesting a thickening of deposits in these areas. Since they are associated with the most recently active volcano on the Arabian Peninsula, these deposits are assumed to be among the youngest ejecta in Arabia; they have been subjected to less compaction, erosion, and weathering than have older pyroclastic deposits, such as those reported in the vicinity of Jebel Diba al Hurus to the south, and thus they retain their original thermal properties. The high thermal values also recorded for eolian sand dunes would suggest that absorption of solar heat is more strongly related to density of material than to lithology.

Pyroclastic deposition was followed by a period of lava eruption that flowed predominantly northward. These youngest lavas flowed over the most recent ash deposits, completely covering those on the north flank of the volcanic vent, leaving a U-shaped apron around the southern base. This sequence of events accounts for the sharp interior margin of much of the anomaly and general decrease in temperature outward from the center of eruption, caused by a lessening of pyroclastic debris. The concentration of highest temperatures on the northern limbs of the anomaly would suggest that the southern areas had suffered more severe erosion.

Contact: Herbert W. Blodget
Code 622

Sponsor: Office of Space Science and Applications

Dr. Herbert Blodget, who holds a PhD degree from George Washington University, is a geologist with the Geophysics Branch. In his 21 years at Goddard, Dr. Blodget has received the NASA Special Achievement Award and two GSFC Group Achievement Awards for his work.

GEOMAGNETISM, SURFICIAL CORE MOTIONS, AND GEOPHYSICS OF THE CORE-MANTLE BOUNDARY

The origin, maintenance, and evolution of Earth's magnetic field presents one of the outstanding unsolved problems in physics. Geophysicists generally accept that solving this problem requires understanding the magneto-hydrodynamic geodynamo located in Earth's electrically conducting, liquid ferro-metallic outer core. Unfortunately, the use of satellite and surface observations of the slowly varying geomagnetic field to gain insight into such core processes is hampered by fundamental physical ambiguities, as well as by the intervening 2900 km of silicate crust and mantle. Researchers in the Geophysics Branch are at the forefront of efforts to not only gather, analyze, and model geomagnetic data—as evidenced by the Definitive Geomagnetic Reference Field models (DGRFs) now available at 5-year intervals from 1945 to 1980—but also to resolve these ambiguities and interpret the observations.

Such interpretations traditionally rely on the basic source-free mantle/frozen-flux core approximation, in which geomagnetic lines of force are frozen into the fluid core. The slow or secular variation of the geomagnetic field is attributed to the rearrangement of field line footpoints by the fluid motion at the top of the core. By adopting the working hypothesis of steady motion, the DGRFs can be used to estimate the large-scale fluid velocity at the top of the core. These estimates reveal a bulk westward drift that is complicated by superimposed jets, gyres, and regions of fluid upwelling and downwelling. The typical speed of the derived motions—10 km per year—is 100,000 times faster than the drift of the continents.

The fluid motion is estimated by using the CYBER 205 to implement an iterative, damped, and weighted least-squares inversion method capable of constraining the radial vorticity balance at the top of the core to be geostrophic. By use of this method, steady surficial core motions have been derived that fit the changes in the radial magnetic field at Earth's surface required by the DGRFs with root mean square errors of less than 10 percent. Such errors are one-third of those obtained in the past and are attributable to the simplicity of the underlying assumptions. Because these errors appear to be twice the accuracy of the DGRFs, the assumptions are being relaxed systematically. For example, allowance for steady magnetic flux diffusion at the top of the core introduces no formal ambiguity and is thus planned.

Furthermore, the dynamically plausible geostrophic radial vorticity constraint is being used to relax the hypothesis of steady flow and thus estimate a time-varying, surficially geostrophic flow. In cooperation with researchers elsewhere, this changing flow is combined with seismotomographic images of core-mantle boundary topography to estimate the changing mechanical torque exerted by the core on the mantle. This torque is, at least in part, responsible for decade fluctuations in Earth's angular velocity now observed using space-geodetic techniques. Evaluation of this effect, known as topographic core-mantle coupling, provides an important test of several geophysical hypotheses and paves the way for a merging of magnetic, Earth rotation, geoid, and seismic data via the joint inversion of geophysical data.

However, the possibilities of electromagnetic and viscous core-mantle coupling, as well as the likelihood of thermal and compositional core-mantle interactions via the D″ layer at the base of the mantle, ensure that even this project will provide but one objective for the Study of Earth's Deep Interior recently initiated by the International Union of Geodesy and Geophysics.

Contact: Coerte Voorhies
Code 622

Sponsor: Office of Space Science and Applications

Dr. Coerte V. Voorhies is a research geophysicist whose first year of service at Goddard follows a two-year post-doctoral associateship in the Geophysics Branch. Dr. Voorhies, who holds a PhD degree in astrophysical, planetary, and atmospheric sciences from the University of Colorado, is interested in geomagnetism, geophysical fluid dynamics, and geophysical inverse theory as applied to deep interior geophysics.

GEOMORPHOLOGY FROM SPACE

Geomorphology, the study of landforms and landscapes, is concerned with the description, classification, origin and process development, and history of planetary surfaces. Analysis and interpretation of imagery returned from space missions to the Moon, Mercury, Venus, and Mars and the Jovian, Saturnian, and Uranian satellites rely primarily on application of geomorphic principles to identify and map surface units and physiographic provinces on these planetary bodies. This approach to the exploration of these bodies is almost always regional to global in scope, taking advantage of the synoptic or broad-area coverage afforded by imaging sensors that survey the surfaces from varying distances. This perspective favors analysis of often complex and diverse landform assemblages developed from (and indicative of) crustal units at scales that best recognize and separate multiple geomorphic processes operating over wide areas.

The same approach can be applied to the study of terrestrial terrains and landforms by use of space imagery to portray at continental scales most of the larger landform classes that make up the Earth's land surface. With Landsat in particular, for the first time a capability exists for mapping major geomorphic units over vast areas. Yet, during the early years of Landsat when emphasis was placed on resources exploration, only a few studies of data returned from it, and later from the Heat Capacity Mapping Mission (HCMM), Seasat, the Shuttle Large Format Camera, and other orbiting systems, were concentrated principally on geomorphic topics.

Over the last 5 years, a growing awareness of the role of geomorphology in analyzing space-acquired imagery both for exploration and for examining fundamental geologic questions has led to an increasing number of

ORIGINAL PAGE IS
OF POOR QUALITY

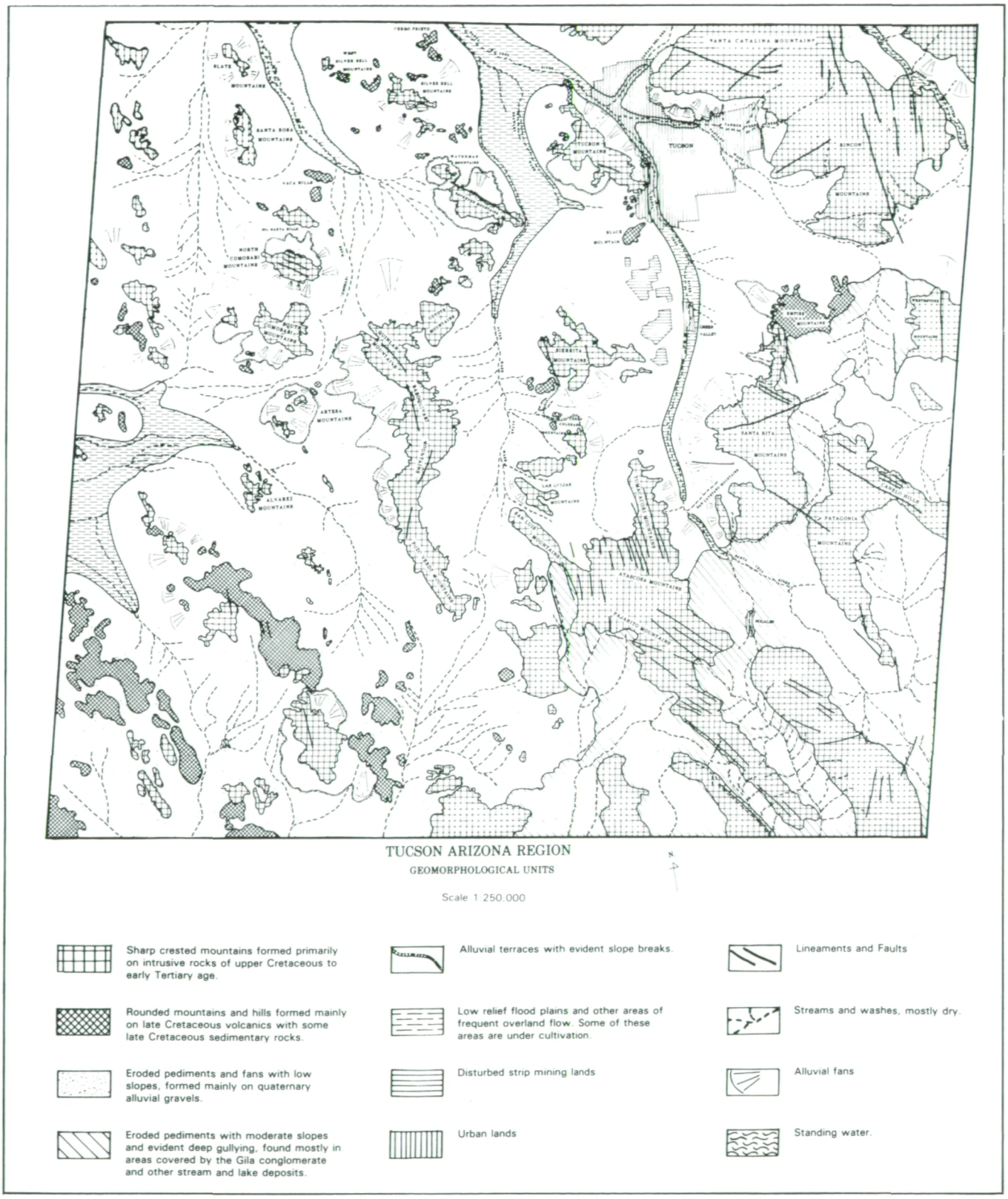

Figure 1. Geomorphic units map of the Tucson, Arizona, region, drawn from a Landsat MSS Band 7 image by Dr. Robert S. Hayden of George Mason University during his tenure at Goddard as an ASEE Fellow in 1984.

ORIGINAL PAGE IS
OF POOR QUALITY

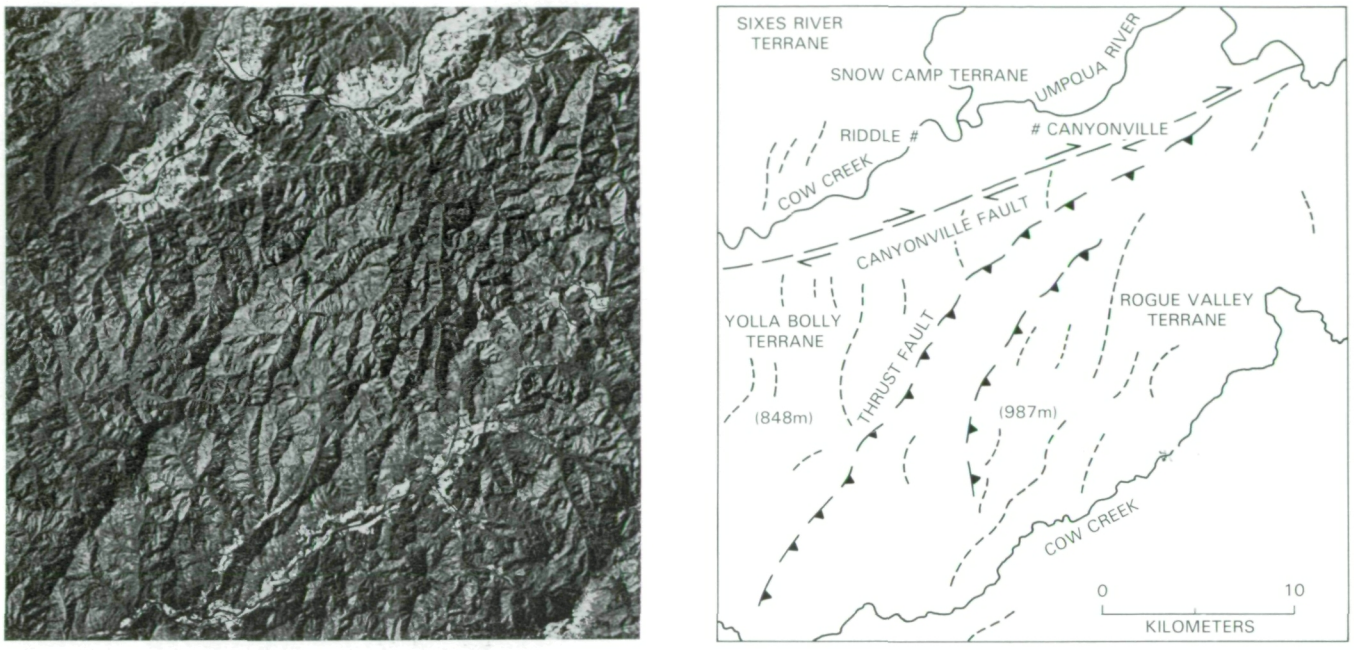

Figure 2. On the left, a Landsat Thematic Mapper subscene of the Klamath Mountains near Canyonville, Oregon, shows the characteristic terrains carved by stream erosion from four terrane blocks, each bounded and identified in the map in the right panel. Some of the major ridges (divides between adjacent streams), delineated by short-dashed lines on this map, are drawn as seen in Landsat imagery and topographic maps. The orientations of these divides, and the maximum elevations within each terrane (in parentheses), differ significantly between the Yolla Bolly and Rogue Valley terranes. Long-dashed lines mark the principal faults: the Canyonville Fault, a right-lateral strike-slip fault, and two thrust faults (solid triangles attached to lines).

geomorphology-centered projects within the remote-sensing and geoscience communities. Particular attention is being given to mapping geomorphic phenomena on large spatial scales, after a half century of neglect during which emphasis was placed mainly on quantitative measurements of landscape-modifying processes at local scales.

As part of an ongoing effort to document achievements in space-based geomorphic studies and to point the way for future uses of space systems in this field, a commission was received from the Land Processes Branch at NASA Headquarters to prepare a comprehensive book that summarizes the status and future potential of applying remote-sensing technology to regional geomorphic analysis. Begun in 1983, NASA Special Publication 486, *Geomorphology from Space: A Global Overview of Regional Landforms*, was published in March 1987. Co-edited by N. M. Short of Goddard and R. W. Blair, Jr., of Fort Lewis College in Colorado, the book was prepared by a group of NASA, university, and industry geoscientists to fulfill three purposes: first, to rekindle interest in descriptive geomorphology and in quantitative landform analysis at regional scales; second, to introduce geologists, geographers, and others in the general community to the practical value of space-acquired remotely sensed data in carrying out their research and applications; and third, to foster more scientific collaboration between terrestrial geomorphologists and astrogeologists, thereby strengthening the effective use of comparative planetology. Still another objective emerged as the book evolved, namely to utilize pictures and text to produce a compendium of continental surface geology over the entire globe in broad terms within a single sourcebook (a compilation lacking in today's literature).

This 717-page book contains 1178 photographs, nearly 100 in color. Many appear as individual plate images acquired by Landsat, Seasat, Synthetic Imaging Radar-A (SIR-A), and the HCMM sensors and with the Large Format Camera, together with two to four or more ancillary views from space platforms and from aerial or ground positions. The 237 plates in Chapters 2 through 10 encompass examples of geomorphic phenomena in 58 countries.

Chapter 11 presents several Landsat-derived large-scale geomorphic units maps, as exemplified in Figure 1 (generated at Goddard). Maps of this kind have been produced for only a small fraction of the whole world. (In contrast, maps of similar nature now cover nearly all of the Moon and Mars and large parts of other imaged planetary bodies.) Such maps should prove invaluable as a global data base for some projects being considered in the developing Earth System Science Program.

Participants at a Goddard-sponsored Workshop on Global Mega-Geomorphology held in Tucson in 1985 pinpointed some specific research problems in geomorphology that should be tractable to analysis with remote-sensing data. One responsive study of the geomorphic expression of *terranes* (large crustal blocks accreted to continental margins) as *terrains* (the lay of the land, particularly as incorporated in its topography) has been undertaken within the Geophysics Branch as part of a broader program to better understand continental evolution. The Klamath Mountains of southwestern Oregon–northwestern California are the type locality for the accretionary terrane concept, which in the last few years has gained wide acceptance as a major mechanism for continental growth and as an explanation for many (perhaps most) of the orogenic (mountain-building) events in the past, earlier attributed to other plate tectonic interactions. Figure 2 illustrates a typical example of results from this study, as described in its caption. It appears, at least from the Oregon Klamaths analysis, that some of their constituent terranes, commonly identified as such from disparities in rock types, life assemblages, and paleomagnetic pole plots, can likewise be recognized and separated on the basis of surface form and that real differences between terrane terrains, although largely due to compositional variability, also reveal the influence of underlying structural control.

Contact: Nicholas M. Short
Code 622

Sponsor: Office of Space Science and Applications

Dr. Nicholas Short, Sr., a research geologist with 20 years of experience at Goddard, is interested in geological remote sensing and in the effects of shock pressures on rocks. Dr. Short, who received a PhD degree from the Massachusetts Institute of Technology, is the author and editor of seven books on aspects of the space program.

MAGNETIC RECORDING IN CHONDRITE METEORITES

The magnetic record in the chondrite meteorites is the only direct source of information about the characteristics of magnetic fields during condensation and accretion of meteorite parent bodies. These magnetic fields are present during the early static metamorphism and are associated with the parent bodies. Additionally, the record associated with impact reworking is also present as an overprint. The carriers of the magnetic record in most chondrite meteorites are FeNi alloys for which there is little or no information about weak field recording characteristics. Therefore, obtaining the magnetic field record from the meteorites will require new experimental paradigms. Rock and paleomagnetism paradigms developed for the iron oxides in the terrestrial rocks cannot be applied to the meteorites. Although extensive physics and technology literature exists for the FeNi alloys, none of it is directly applicable to the meteorites. Cosmic time scale diffusion is responsible for magnetic phase relations that cannot be reproduced in the laboratory. Shock impact effects are superimposed on these phase relations and therefore can only be evaluated with the meteorites or in specially designed experiments that have not been performed to date.

A comprehensive meteorite magnetism research program is in progress in the Goddard Rock Magnetism Laboratory. The following points are the initial drivers of this program:

- Meteorites are precious materials, and therefore a credible context for magnetic analysis must be provided to wholly justify allocation of meteorite material for destructive magnetic analysis.
- The meteorite magnetic record is of obvious extraterrestrial origin and therefore embodies the recording of magnetic field information during the thermophysical history of the meteorite.
- Diffusional development of the magnetically hardest phases below respective Curie points and the overprinting by shock-induced effects render the meteorite magnetic record complex.
- Fundamental properties of the magnetic materials in meteorites are not known to any adequate degree.
- The existence of atomic ordering and other complexities in the M-shaped diffusion profile that we are

only now beginning to understand renders our present knowledge of meteorite magnetism quite inadequate.

The magnetic remanence in a chondrite meteorite can be easily shown to be of extraterrestrial origin. Contamination of the magnetic record during entry into the Earth's atmosphere is limited to the near surface even in the conductive iron meteorites, and a simple measure of the natural remanence (NRM) and the saturation remanence (SIRM) allows the ratio NRM/SIRM to be computed, enabling us to evaluate human contamination, such as with a hand-held magnet.

Dodd (1981) listed stages in the history of a chondrite meteorite that derive from consideration of petrologic and other data. Expressing a reservation about the sequence, he points out that it is a useful framework for discussion. If we are to establish the credibility of meteorite magnetism research, we must consider the magnetic record in some similar framework. We must consider when in the evolutionary sequence magnetic recording is possible and what the sources of record modification and contamination are, and we must devise experimental scenarios to maximize the information content. This work is in progress in the Goddard magnetic properties laboratory. The table below considers the stages in the

Magnetic Recording During the History of a Chondrite

• Nucleosynthesis	4.5 BY	• No magnetic record
• Condensation	~100 my duration	• Possible primordial record in metal would be associated with metal-silicate fractionation
• Chondrule Formation		• Chondrule magnetic recording during cooling
• Accretion		• Numerous scenarios might be recorded during accretion into parent bodies and then modifications
• Static Metamorphism	>950°C ~400°C	• Presence of magnetic fields during static metamorphism would be recorded in lower groups as an overprint and in higher groups as a reset
• Impact Reworking		• Magnetic modifications would result in alteration of the existent records and overprinting due to various levels of shock
• Ejection From Parent Body		• Parent body breakup effects would be elusive, but presumably an impact event is responsible
• Attrition in Space		
• Earth Impact		• Fusion crust and associated near-surface heating are easily evaluated; shock impact effects are important in some cases
• Recovery		• Possible contamination by hand-held magnet during collection or in passing from museum to magnetics laboratory
• Laboratory Study		

history of a chondrite meteorite and indicates the possible magnetic recording scenarios.

The first step in the analysis of the magnetic record in a chondrite meteorite is the examination of the polished surface of the meteorite that has been etched with NITAL (a dilute nitric acid in alcohol solution). This allows the microstructure to be observed. The microstructural record is a clear indication of the thermophysical history of the meteorite. Knowledge of the thermophysical history does not provide magnetic information, but it does provide the information for planning experiments that will maximize the magnetic record information content.

The model chondrite meteorite (see figure) illustrates the disposition of the different magnetic components in the meteorite. Each of the components may have different magnetic recording characteristics and response to a given level of shock impact. To perform an adequate analysis, the properties of the components must be understood, and these must be evaluated in terms of their contribution to the magnetic record of the bulk meteorite that has a distinctive history.

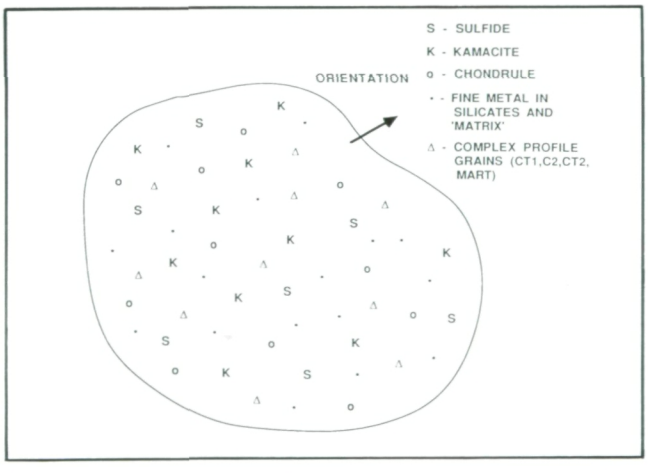

Model of a chondrite meteorite containing the magnetic components identified. Analysis of the vector record in each component will enable an evaluation of the makeup of the chondrite record.

It may be many years before a reliable method of paleofield estimation is forthcoming. There may never be a reliable method developed, but this question deserves to be addressed and answered. One important point should be obvious—the meteorite does contain a magnetic record, and the record is associated with the thermophysical history of the meteorite. If a reliable paleofield number cannot be had for a so-called primordial field, this would not negate the importance of the record. The different magnetic components in a chondrite meteorite have different magnetic recording characteristics and respond differently to shock impact. We need to know the vector makeup of the meteorite, the recording characteristics of the different magnetic phases, the role of atomic ordering, and the role of shock to be able to understand the magnetic record in the meteorites. Progress to date is promising.

Contact: Peter Wasilewski
Code 691

Sponsor: Office of Space Science and Applications

Dr. Peter Wasilewski specializes in magnetic properties of solar system solids, and his professional interests include the magnetic structure of Earth's crust and the meteorite magnetic record. Dr. Wasilewski participated in the 1987/88 Antarctic Meteorite Search Team, and he was a member of the 25th Japanese Antarctic Research Expedition. Mt. Wasilewski, a dacite volcano near the base of the Antarctic Peninsula, was named for the author. Dr. Wasilewski, who received a DSc degree from the University of Tokyo, has served with Goddard for 14 years.

BIOLOGY

LANDSCAPE PATTERN AND SUCCESSIONAL DYNAMICS IN THE BOREAL FOREST

Understanding and monitoring the dynamics of land-related vegetation is critical for several important scientific issues. One such issue is the effect of vegetation cover on regional and global climate, through energy exchange, water transport, and chemical cycling.

Vegetation dynamics are in turn affected by phenomena operating at many temporal and spatial scales. Temporally, for example, gradual warming since the last ice age

has resulted in a retreat northward of the southern boundary of the boreal, or cold northern, forests. Anthropogenic effects such as fire suppression during this century have been more immediate. Observing and quantifying these dynamics have been very limited at spatial scales beyond a few meters and at temporal scales beyond 2 or 3 years because of the labor-intensive nature of traditional data collection methods.

We have investigated the landscape-scale community dynamics of a boreal forest ecosystem by using the Landsat Multi-Spectral Scanner (MSS) data record from 1973 to 1983 to generate a stochastic description of the key life-cycle stages of the community landscape elements. Boreal forests were chosen for study because of their relative taxonomic simplicity (about eight species dominate the boreal forests of North America), their great extent, and their potential sensivity to climatic change. Our study area, the Superior National Forest (SNF) in northeastern Minnesota, is near the southern margin of the North American boreal forests and is particularly sensitive to climatic change. Fire, generally important in boreal forests, plays a critical role in determining landscape patterns in the SNF. Frequent fires (with an average return time of about 80 years), and abundant lakes and wetlands which serve as fire breaks, generate a complex mosaic of patches in all successional stages.

During the summers of 1983 and 1984 NASA, in cooperation with investigators from the University of California at Santa Barbara and Purdue University, conducted an intensive experiment in a portion of the SNF. Detailed vegetation data were collected over the test area by ground crews and aircraft for about 130 sample sites. The sample sites were selected to represent a range of stand density, age, and composition. Each site was characterized as a successional stage of the ecosystem based on species composition and age structure. Satellite-, aircraft-, and helicopter-mounted radiometer data were obtained, including a historical data base of Landsat MSS images from 1973 through 1984. Training pixels associated with the sample sites were then located in both the satellite and aircraft multispectral data.

Training pixels in the 1983 Landsat MSS data were analyzed by using a clustering algorithm. Spectrally distinct clusters were associated with ecological successional stages. The resulting stages (Table 1) include the major elements in generally recognized successional sequences that follow disturbance in this forest, for example, jack pine or aspen to upland spruce/fir. We have estimated lower bounds on the classification error rates between stages. All ecological stages were about equally separable—probabilities of correct classification ranged from 75 percent for mixed deciduous/conifer to 100 percent for conifers. Overall, the average probability of correct classification was 85 percent.

Table 1
Spectrally Distinct Ecological Stages
(in order of average age since disturbance)

Clearings	Sparse or low-density vegetation
Regeneration	Young aspen and jack pine
Aspen	Predominantly aspen/broadleaf species
Mixed	Mixtures of conifers and broadleafs
Conifer	Predominantly conifer species

We then used the cluster signatures to classify the MSS data and constructed ecological stage maps for two registered MSS acquisitions (July 3, 1973, and June 18, 1983) over a 2100 km^2 area covering the study area. By color coding the transitions from 1973 to 1983, we produced the ecological stage transition map shown in the figure. Here we have color-grouped ecologically similar transition events, e.g., transitions from vegetation cover in 1973 to clearing in 1983 are coded yellow, transitions from clearing in 1973 to vegetation in 1983 are coded red, and so forth. Areas that did not change (diagonals of the color matrix) are given unique colors to denote stable areas. The transition map of the figure emphasizes disturbance events (yellow) and regeneration (red).

Note that almost all of the yellow disturbance events occur in the managed area, where logging is common. Clearing to vegetation transitions (red) occurring in the upper right center of the image are associated with regrowth from the 1971 Little Sioux forest fire that consumed about 6000 hectares. This change image supports recent ecological theory that a naturally vegetated landscape is a rich mosaic of patches residing in a variety of succession stages.

Based on the pixel-by-pixel changes in the ecological stages, transition probabilities between ecological stages and areal proportions of each stage were computed. The matrix of transition probabilities (Table 2) between ecological stages is a primary indicator of ecosystem dynamics and stability, permitting prediction of steady-state conditions, transient behavior after disturbance, and

ORIGINAL PAGE
COLOR PHOTOGRAPH

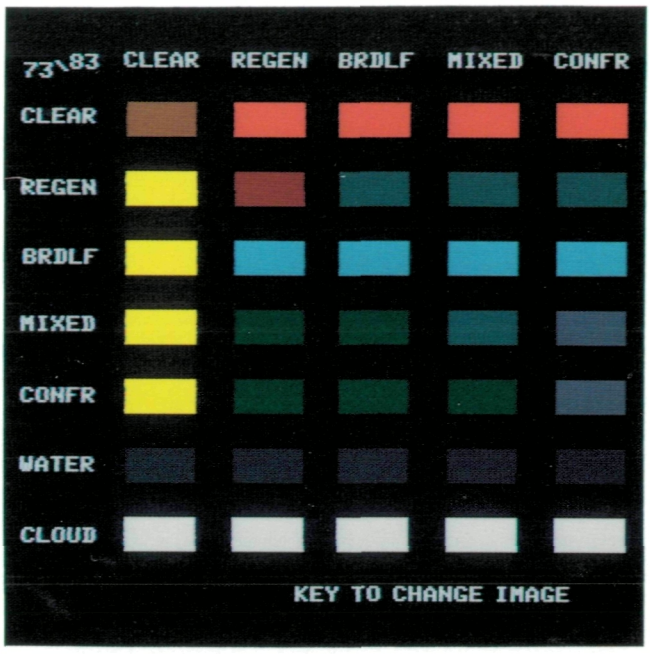

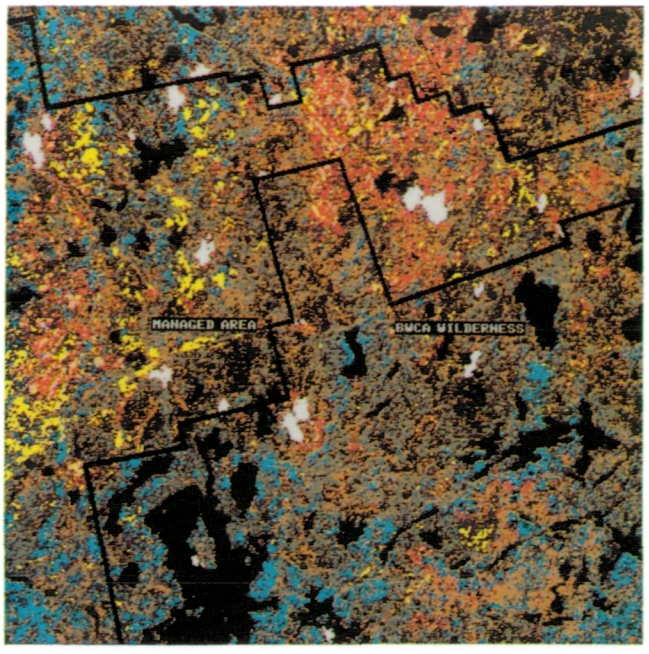

Panel 1. Color matrix. Panel 2. 1973–1983 ecological stage transition map of a 2100-km^2 area in the Superior National Forest, Minnesota.

characteristic response times. Each matrix element is the normalized frequency with which pixels observed to be in the *i*th stage in 1973 are observed to be in the *j*th stage in 1983. The diagonal elements of the matrices are simply the retention frequencies, i.e., the likelihood that a pixel will remain in the same successional stage, and the off-diagonal elements, the transition frequencies. The magnitude of the transition frequencies for a given stage indicates the relative importance of each possible transition path out of the stage.

As Table 2 shows, the magnitude of the retention frequencies calculated for the study area indicate a highly dynamic ecosystem at the landscape unit level. That is, in 10 years, over one-half of the landscape units changes state. For example, only 53 percent of the conifer landscape units remains unchanged. Clearly, any system that is in a high state of flux at the landscape unit level for a 10-year period can be highly dynamic over the course of a century. Perturbations to the system such as fire suppression, logging, and climate change could have very immediate implications for the character of the boreal forest biome. We can also note from the diagonal elements that the early successional classes, clearing and regeneration, have much lower retention frequencies than the older successional stages of aspen, mixed and conifers, indicating that much less time is spent in these early successional stages.

Table 3 gives the steady-state areal proportions of the classes in both the wilderness and managed areas as projected from the transition matrix, assuming a stationary Markov process.

The projected values are those that would be realized after undergoing many 10-year changes with the same transition probabilities as those observed in the 1973 to 1983 time period. From this analysis we see that the proportions in both the managed and wilderness areas are not projected to change much over current values, even though the forest is quite dynamic at the landscape unit level. Thus, both the wilderness and managed areas appear to be in a state of dynamic equilibrium.

In summary, we have used remote sensing to quantify the major parameters characterizing ecosystem dynamics and stability of a forested ecosystem. These parameters are the ecosystem succession class transition probabilities and relative abundances. Although our study utilized a boreal forest biome and a 10-year observation period with Landsat MSS data, the technique should be extendable to any ecosystem, satellite sensor, and observation frequency for which successional classes can be defined, resolved, and monitored. The techniques reported here also provide methods for linking ecological observations over a wide range of time and space scales. Through remote-sensing data and techniques, ground observations

Table 2
Transition Matrix for Total Study Area
(660,000 landscape elements)

1983	Clearings	Regeneration	Aspen	Mixed	Conifer	Water	Unclassified
1973							
Clearings	23.2	41.2	13.6	15.8	5.7	0.3	0.3
Regeneration	8.0	32.9	20.1	29.7	9.1	0.3	0.0
Aspen	3.0	19.1	51.7	22.2	3.7	0.2	0.0
Mixed	2.7	9.3	14.7	52.6	19.6	1.2	0.0
Conifer	3.0	6.5	3.4	29.7	52.6	4.9	0.1
Water	0.4	1.4	2.7	5.3	11.5	78.6	0.3
Cloud	4.4	20.4	26.5	29.2	16.8	2.6	0.0
Unclassified	8.1	21.1	23.8	28.1	13.5	4.3	0.5

Table 3
1983 Areal Proportions (%) and Markov Projections of Steady-State Proportions

Class	Wilderness		Managed	
	1983	Proj	1983	Proj
CLSD JP/BS	23.1	27.2	20.9	22.2
Mixed CON/BL	35.8	39.3	34.5	35.2
Regeneration	11.9	10.3	21.6	20.9
Aspen	15.8	13.2	13.2	10.6
Clearings	1.7	1.3	7.2	7.2
Water	11.6	8.6	2.6	1.2

of successional stage at meter scales and single dates were linked to regional scales and were used to establish the ecological stages 10 years earlier. We believe these same techniques can be extended to synoptic scales and periods far beyond the 10 years chosen for this initial study.

This study is part of a larger effort within the Earth Resources Branch (Code 623) to utilize remote sensing to improve our understanding of forest process and pattern dynamics as it relates to biospheric, atmospheric, and lithospheric processes. To achieve these aims, this larger effort seeks to combine forest pattern and process models, soil models, radiative transfer models, and ground-based and satellite observations over various temporal and spatial scales.

Contacts: Forrest G. Hall and Donald Strebel
Code 623

Sponsor: Office of Space Science and Applications

Dr. Forrest Hall is Science Coordinator of the First ISLSCP Field Experiment. In addition, as staff scientist with the Laboratory for Terrestrial Physics, he researches forested ecosystems. Dr. Hall, who holds a PhD degree in physics from the University of Houston, has two years of experience with Goddard. He has received the NASA Medal for Exceptional Scientific Achievement, as well as several NASA Achievement Awards for his work.

BIOSPHERIC STUDIES USING NIMBUS-7 37-GHz OBSERVATIONS

The difference of vertically and horizontally polarized brightness temperatures (ΔT) observed at 37 GHz frequency (wavelength about 8 mm) of the scanning multichannel microwave radiometer onboard the

ORIGINAL PAGE
COLOR PHOTOGRAPH

Nimbus-7 satellite has been processed as monthly composites of global observations from January 1979 to December 1985. (The data for 1986 will soon be added.) The spatial resolution of the digital data is 0.25° × 0.25° (latitude by longitude), and the monthly global data sets are stored on a Mercator projection. No spatial or temporal smoothing has been done to the data. A color-coded global image of the integrated average of 84 months of data is shown in Figure 1. A radiative transfer model for a soil-vegetation system provides an understanding of the spatial and temporal variations of the polarization difference. In essence, the vegetation emits largely depolarized microwave radiation and acts as a scattering/absorbing medium for polarized radiation emitted from the soil. The polarization difference has been found to be a nonlinear function of the green leaf area index, with observed ΔT values of about 30 °K over hot deserts (like Rub al Khali in Saudi Arabia) and 5 °K or a little lower over densely vegetated areas like the rainforests of Cameroon and Borneo. Temporal variations of ΔT for several locations are shown in Figure 2. The temporal variation is seen to be roughly sinusoidal, showing vegetation growth and decay; high ΔT values are observed during the period of low vegetation density (winter) and low ΔT values during the period of high vegetation density (summer). A major departure from the sinusoidal pattern for a particular year (as seen in Figure 2 for the Sahel zone of Mali during 1984) could be taken as an indicator of drought. Apart from vegetation, other surface signatures that could be seen in the ΔT data include open water

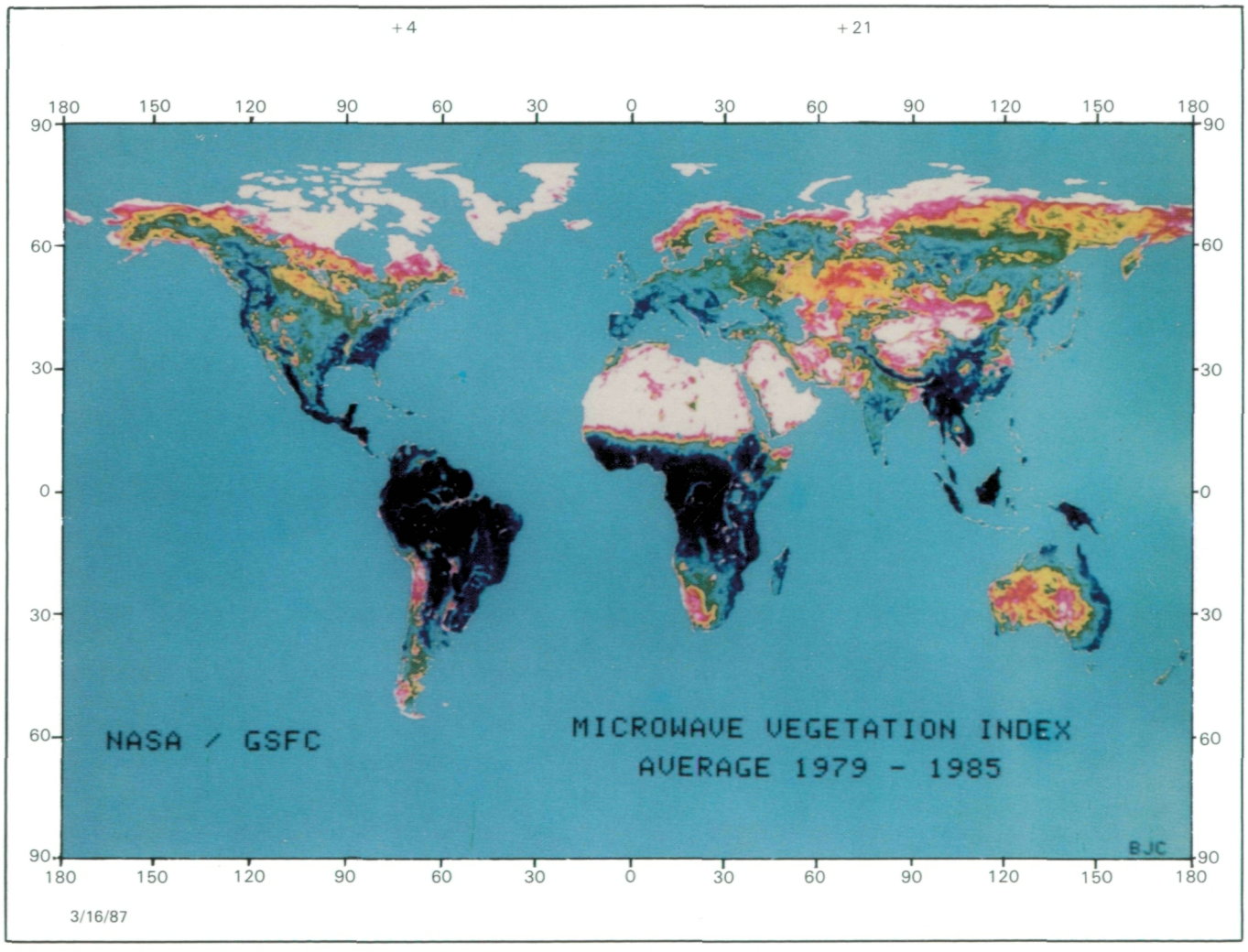

Figure 1. Color-coded global image of 37 GHz polarization difference brightness temperature averaged for 84 consecutive months of data (January 1979 to December 1985). The major factors determining the polarization difference are the spatial and temporal variations of vegetation, but other factors (for example, snow and open water) also have a noticeable effect on the difference.

(for major rivers and lakes), surface roughness, and snow. For example, in Figure 1 one could see the Amazon and the Congo rivers because of mixed land-water pixels. The high ΔT values over the water mix with the low ΔT values over the surrounding vegetation, causing the color anomalies in Figure 1.

The feasibility of indexing spatial and temporal variabilities of land-surface evaporation and biospheric primary productivity (which is the organic matter renewed and accumulated during a year by the terrestrial vegetation) with the ΔT data is being studied. Evaporation is recognized as an important component of the land-surface heat balance, whereas primary productivity determining the carrying capacity and its knowledge is of considerable importance in understanding the atmospheric CO_2 variations and in several biogeochemical cycles. Current global estimates of evaporation and primary productivity are based on spatial extrapolations of isolated field data.

The estimated evaporation and primary productivity values for 5° latitude bands from 75° N to 55° S are shown in Figures 3 and 4, respectively, together with the corresponding zonal averages of 84 months of ΔT data. In general, the zonal variations of ΔT data appear as a mirror image of both evaporation and primary productivity; high evaporation or primary productivity corresponds to a low ΔT value. It is recognized that the length of growing season and the density of vegetation are the major determinants of the annual evaporation and the

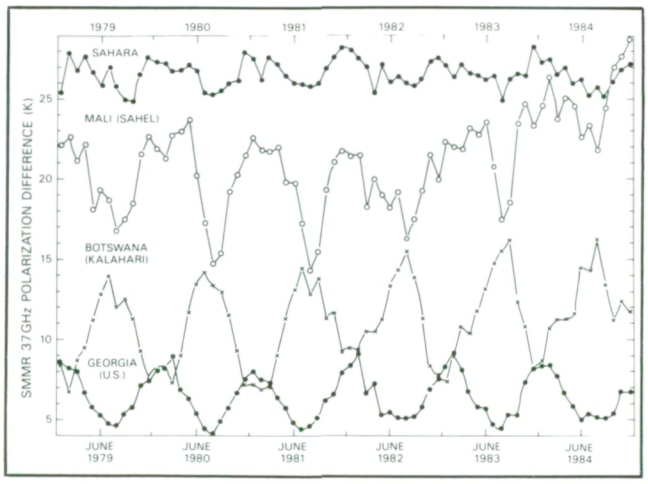

Figure 2. Time series of the observed polarization difference at several locations. This temporal variation is indicative of the phenology of vegetation in these locations.

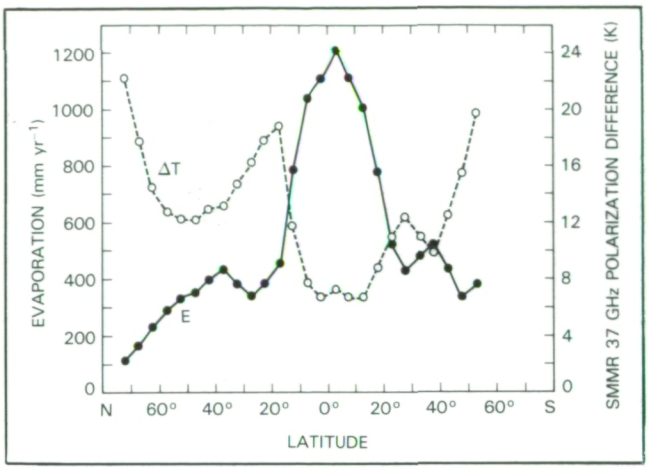

Figure 3. The zonal variation of the 7-year averaged polarization difference and the land-surface evaporation (calculated from a climatologic water balance method).

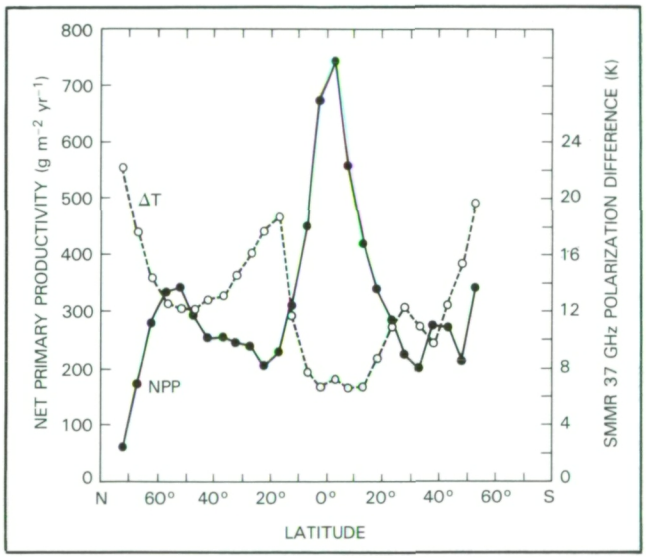

Figure 4. The zonal variation of the 7-year averaged polarization difference and the estimated net primary productivity of vegetation (which is an important parameter for understanding the atmospheric CO_2 variations and the carbon balance).

primary productivity, and as noted above, the ΔT values are correlated with the vegetation density. The results in Figures 3 and 4 are currently being studied.

Contact: Bhaskar J. Choudhury
Code 624

Sponsor: Office of Space Science and Applications

Dr. Bhaskar Choudhury is a solid-state physicist with the Hydrological Sciences Branch. Dr. Choudhury received a PhD degree from American University, and he has seven years of experience at Goddard.

AIRBORNE MULTISPECTRAL LASER IMAGING POLARIMETER

Polarized light reflected from the Earth's land surface, both the soil and plant cover, has the intensity ratio of its horizontal and vertical polarization states modified relative to the incident light. The degree of this change depends on both the observation and illumination angle and the wavelength of the light. It also depends on the nature of the surface and the physiological state of the plant cover. Atmospheric absorption and scattering blurs the variations in these orthogonal polarization components and makes interpretation of solar-illuminated, remotely sensed, wavelength-dependent, polarization data difficult. These problems are eliminated as significant factors when a controlled polarized light source is employed. By using a multispectral, polarized laser flown over known surface conditions, a data base of polarization phenomena can be built with which theoretical models can be developed, verified, and refined and from which predictions can be made. This is invaluable in refining current theories and opening up new areas of environmental remote sensing.

Most surfaces will selectively effect polarized light incident on them, a phenomenon well known to anyone who has used polarized sunglasses. Categorizing this effect, however, requires taking an ensemble of similar, although not identical, surfaces and observing them at various spectral wavelengths and polarization angles. Ratios of incident to reflected light as a function of these parameters can then be made. Data would need to be collected in a field environment rather than in a laboratory to produce the variety and scale of samples necessary for a complete data set. For this program, a laser capable of transmitting over a range of wavelengths will be aircraft mounted. Its pulsed, polarized light is transmitted through a cylindrical lens that, aimed at the Earth, results in a line of illumination on the Earth's surface. This line is oriented across the direction the aircraft travels and so moves along with the aircraft, illuminating a long, narrow strip of the surface. The reflected laser light is collected by four telescopes onboard the aircraft. Detectors at the focal plane of each telescope are high-resolution linear arrays consisting of hundreds of photosensitive elements. Three of the arrays will have polarization filters positioned at 0, 45, and 90° with respect to the laser polarization, thus enabling calculations of the degree and azimuth angle of the surface depolarization effects. The fourth detector is used to measure circular polarization by including a quarter-wave retardation plate with a 90° polarization filter. From aircraft altitudes of 300 m, swath widths up to 100 m across track are possible while still within eye safe limits. By employing a high-resolution linear array detector system, depolarization images of large surface areas can be generated. This gives the required ensemble information, as opposed to laboratory point measurements, which can then first be analyzed visually with special image pseudo colorization techniques. The data from the various scenes will then be analyzed for application to remote-sensing systems. Among other results, these analyses will determine if spaceborne passive radiometers for polarization measurement are feasible and, if not, whether the information is useful enough that development of a spaceborne laser polarimeter would be cost effective.

Contact: James E. Kalshoven, Jr.
Code 625

Sponsor: Office of Space Science and Applications

Dr. James Kalshoven, Jr., specializes in electro-optics, lasers, and sensors. He was recently named GSFC Inventor of the Year for a patent on measuring atmospheric pressure and temperature with a laser sensor system. Dr. Kalshoven, who received a PhD degree from the University of Tennessee, has been a part of Goddard for 13 years.

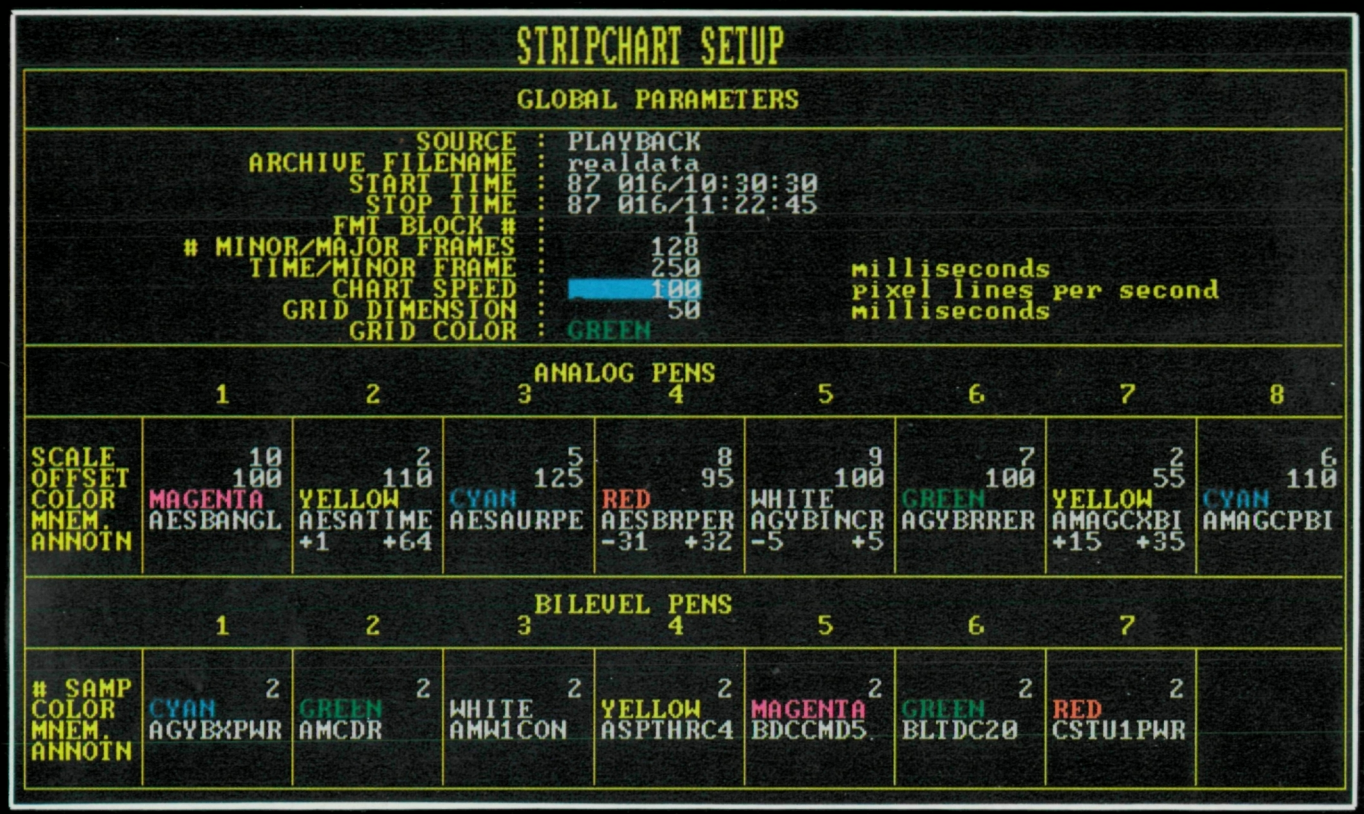
STRIPCHART SETUP
GLOBAL PARAMETERS
SOURCE : PLAYBACK
ARCHIVE FILENAME : realdata
START TIME : 87 016/10:30:30
STOP TIME : 87 016/11:22:45
FMT BLOCK # : 1
MINOR/MAJOR FRAMES : 128
TIME/MINOR FRAME : 250 milliseconds
CHART SPEED : 100 pixel lines per second
GRID DIMENSION : 50 milliseconds
GRID COLOR : GREEN
ANALOG PENS
1 2 3 4 5 6 7 8
SCALE 10 2 5 8 9 7 2 6
OFFSET 100 110 125 95 100 100 55 110
COLOR MAGENTA YELLOW CYAN RED WHITE GREEN YELLOW CYAN
MNEM. AESBANGL AESATIME AESAURPE AESBRPER AGYBINCR AGYBRRER AMAGCXBI AMAGCPBI
ANNOTN +1 +64 -31 +32 -5 +5 +15 +35
BILEVEL PENS
1 2 3 4 5 6 7
SAMP 2 2 2 2 2 2 2
COLOR CYAN GREEN WHITE YELLOW MAGENTA GREEN RED
MNEM. AGYBXPWR AMCDR AMW1CON ASPTHRC4 BDCCMD5. BLTDC20 CSTU1PWR
ANNOTN

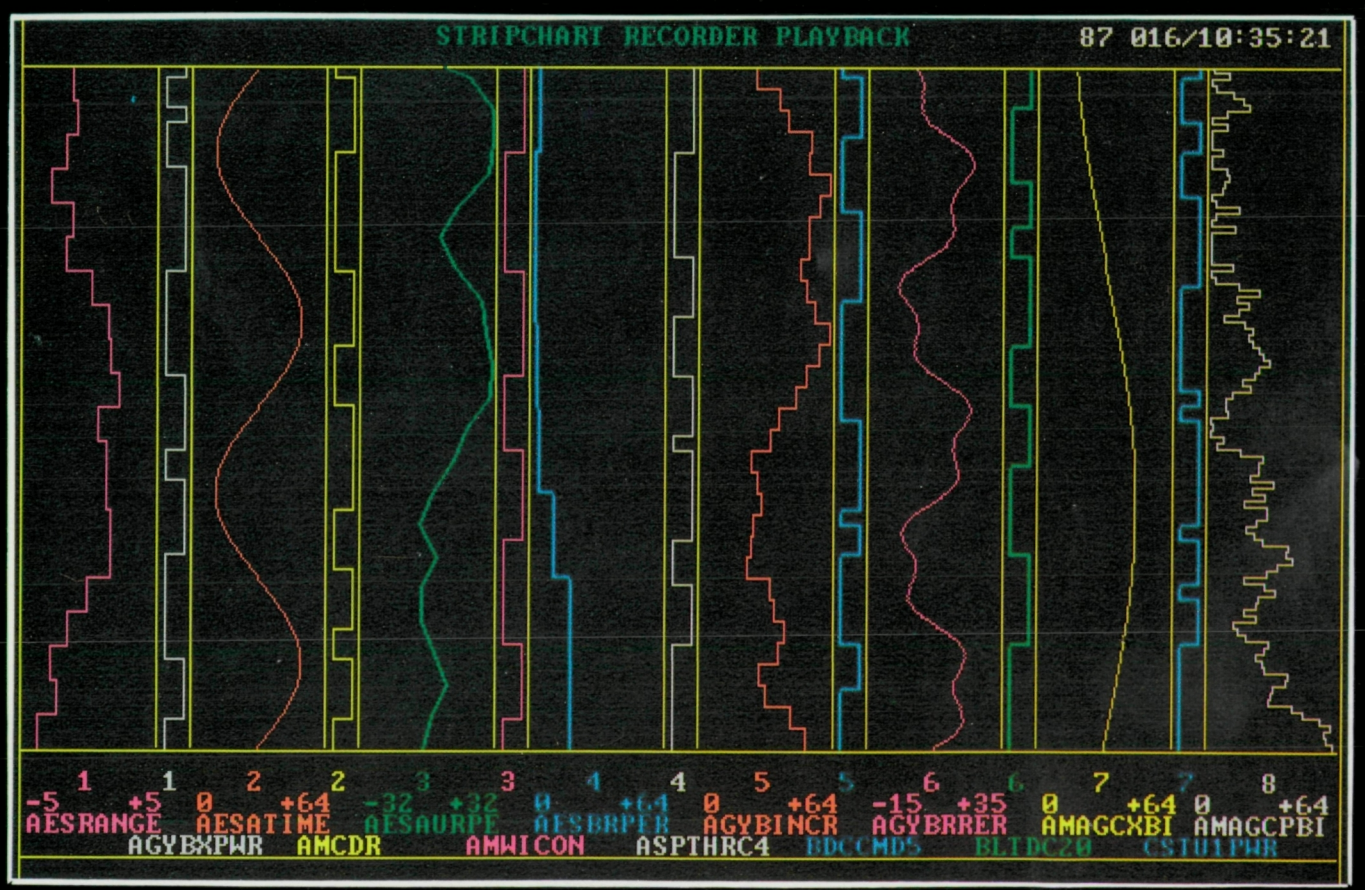
STRIPCHART RECORDER PLAYBACK
87 016/10:35:21
1 1 2 2 3 3 4 4 5 5 6 6 7 7 8
-5 +5 0 +64 -32 +32 0 +64 0 +64 -15 +35 0 +64 0 +64
AESRANGE AESATIME AESAURPE AESBRPER AGYBINCR AGYBRRER AMAGCXBI AMAGCPBI
AGYBXPWR AMCDR AMW1CON ASPTHRC4 BDCCMD5 BLTDC20 CSTU1PWR

PRECEDING PAGE BLANK NOT FILMED

With the new graphics stripchart systems, data can be received and plotted quickly, annotated, labeled, color coded, and archived.

SENSORS AND SPACE TECHNOLOGY

STRAIN MEASUREMENTS ON A THIN FILM BALLOON

In the wake of a period of scientific balloon failures, there has been a concerted effort to increase the engineering knowledge of balloon structural response and polyethylene material behavior. The extremely high success rate during the past year has shown the positive results of materials research and development. Because of the complexities of both the material behavior (polyethylene is a nonlinear, thermoviscoelastic plastic) and the structural geometry for a scientific balloon, the development of an accurate, advanced structural analysis tool is an arduous task. As a means of providing both general insight and useful engineering data, a test was performed to measure the strain field present in a small scientific balloon.

This test had two principal purposes. First, it initiated a series of tests with model balloons inflated and tethered at sea level. This type of test provides invaluable information without many of the costs and risks associated with in-flight testing. A major result included learning the problems and techniques associated with the implementation of this type of experimental test procedure. Second, the most significant product of the test was mapping the strain field of a balloon designed by the same general procedure used for full-scale vehicles. Variations in the circumferential and meridional strains were measured throughout a simulated ascent from launch to float.

The 17,500-ft^3 balloon (manufactured by Winzen International Inc.) was inflated with a mixture of helium and air to emulate the gas volume and differential pressure seen during an actual ascent. Strain data was gathered continuously from 36 strain sensors located at various gore positions on 6 of the 36 gores. Four of the sensors were located on load tapes. Additional data included temperature measurements, extensive photographic coverage, differential pressure measurement at the apex, zero differential pressure height, and forces in the load tapes.

Most of the strain sensors were arranged in pairs located along the gore center line. In each pair, one sensor measured strain in the meridional direction, the other in the circumferential direction. The results from three such pairs are shown in Figures 2, 3, and 4. (Note that the downward spike at approximately 14.8 hours on 2, 3, and

◀ *Stripchart set-up parameters (top) and resulting stripchart (bottom). Courtesy of Mike Maloney and Steve Lee (Bendix Corporation).*

ORIGINAL PAGE IS
OF POOR QUALITY

Figure 1. Test balloon partially inflated.

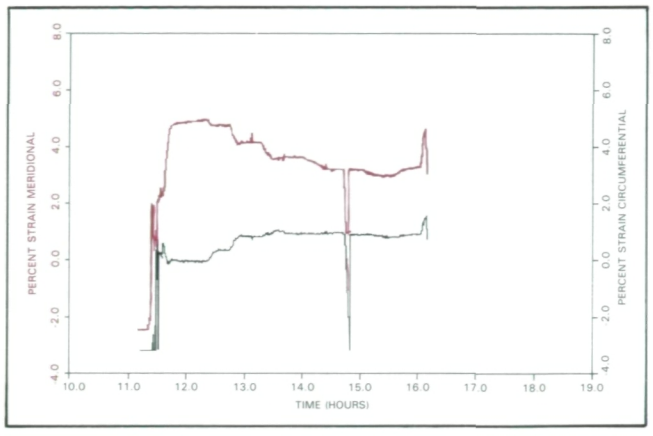

Figure 2. Strains for pair 19/20.

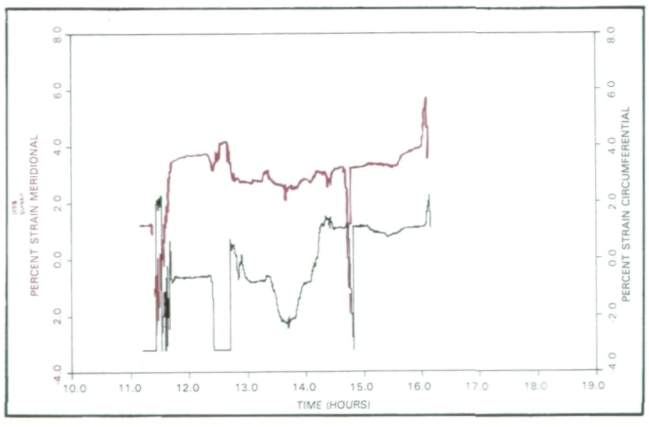

Figure 3. Strains for pair 37/38.

4 is a data dropout due to installation of a new magnetic tape.)

The introduction of gas occurred in discrete steps rather than continuously; in particular, the helium was injected between 11.38 and 11.75 hours. Subsequent inflations with air took place between 12.35 and 12.47, 12.73 and 12.9, 13.31 and 13.5, 14.02 and 14.54, 15.07 and 15.68 hours, and a superpressure period from 16.05 and 16.13 hours. Each inflation period was designed to simulate a 10,000-ft ascent to bring the balloon to its design float altitude of 52,000 ft. A gas analyzer was used to validate proper mixing of the inflation gases.

Figure 2 shows strain data throughout the test period for an orthogonal pair of sensors at 88 percent of the gore (measured from the base). At this gore position it can be seen that the meridional strains are significant soon

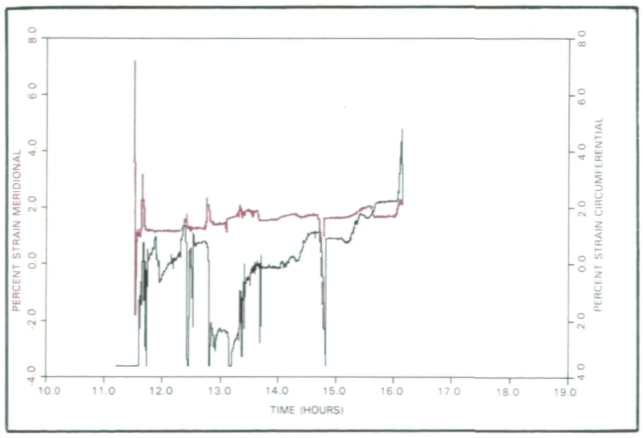

Figure 4. Strains for pair 25/26.

after the introduction of helium has begun. The meridional strain begins to decrease at approximately 12.4 hours in response to the addition of the first volume of air. Conversely, the circumferential strain increased in response to the same phenomenon. Note that because of the two-dimensional stress field, the strains are coupled due to Poisson's effect. Figures 3 and 4 show the same type of data for two different gore positions, namely 63 and 41 percent. In general, the lower the gore position, the longer it took for the strain response to become smooth. This is due to the sensors being captured in the folded, undeployed regions of the partially inflated balloon. From looking at the fully inflated case (15.68 hours) at 255 in. (Figure 4), it is evident that the strains in the circumferential direction have become larger than the meridional strains (Figure 4). Additional data provide insight into the strain distribution across the individual gore width, as well as tape/film load transfer phenomena.

Ultimately, the stresses in the balloon film will be determined with appropriate constitutive relationships that allow for the temperature, strain history, strain rate, and stress history dependency of the polyethylene film. Preliminary stress data have proven enlightening.

The data presented here are only a fraction of the gathered data. The complete data set answers some questions about balloon structural behavior while raising still more questions. At least as important, the testing procedure used has proved itself and brought forth possibilities of more efficient, less costly testing for future experimental analysis. This type of testing will become a crucial tool for validation of comprehensive structural analysis models for scientific balloons.

Contact: Joel Simpson
Code 842

Sponsor: Balloon Projects Branch

Mr. Joel Simpson holds a BS degree in aerospace engineering from the University of Maryland. He has worked with the Balloon Projects Branch at Wallops Island for two years. Mr. Simpson was Project Engineer and Project Coordinator for the model balloon experiment and will continue working in balloon structural analysis.

LABORATORY EXTRUDER FOR THE RESEARCH AND DEVELOPMENT OF ADVANCED BALLOON FILM

The Balloon Projects Branch has installed a laboratory-size blown film extruder at the Pennsylvania State University to develop advanced balloon films. Under a NASA grant, the Polymer Science Program at Penn State is processing several types of polyethylene to characterize the effect that extrusion parameters have on final material mechanical properties. This understanding will lead to the production of consistently reliable balloon film.

The extruder (manufactured by Killion Extruders, Inc.) fits easily into a small chemistry lab and can be operated by one person. With a 1-¼-in. barrel and a 2-in. diameter die, it can produce as much as 30 lb of film per hour. Since this throughput rate is a variable, it will be one of the parameters studied. Film lay-flat width, another variable, can be extruded as high as 15 in.

A balloon flight, though relatively slow, exposes the vehicle to high local dynamics. Additionally, the balloon soaks in the very low temperature tropopause region for a relatively long time during ascent. These extremes require that balloon films possess physical properties not normally found in polyethylene films. For example, both film strength and elongation must be high at warm launch conditions and cold ascent conditions. Another requirement of balloon film is that it retain good low temperature impact toughness, i.e., energy absorption capability. The optimization of this property is a principal focus of this study.

These mechanical properties are very much dependent on the structure, or morphology, of the material. Such things as the density and crystallinity of a film affect its strength; the toughness may be chiefly a function of the molecular branching in the film. Characterization of these properties and their effect on mechanical performance are additional objectives of this study.

The film properties discussed above can be traced back to the processing history of the material. This is the primary objective of this effort: to relate the conditions imposed during extrusion to the output morphological structure of the film and, finally, to the resulting mechanical behavior. Such extrusion parameters of interest include barrel zone temperatures, screw speed, take-off rate, frost line height, and blow-up ratio.

Although the film used in the manufacture of balloons is produced on much larger equipment, a lab-size unit

was selected for this research and development (R&D) effort because of several advantages it offers. The cost and amount of time to obtain a lab extruder are much smaller than that for the production model. More applicable to the program, however, is that the lab unit has a much faster response time to system changes and stabilizes much sooner after changes than does a large extruder—minutes versus hours. This is critical to an R&D program.

As a consequence of using a lab extruder, results will not be immediately transferrable to the production equipment. Extrusion scale-up models will be developed in this project to allow for the application of this new knowledge.

The work through this grant will provide valuable new information to the balloon community concerning the effect of extrusion parameters on film properties. Through scale-up models and morphological characterization, laboratory-produced film possessing excellent low-temperature toughness will lead to reliable, production balloon material.

Contact: Kirk M. Cantor
Code 842

Sponsor: Balloon Projects Branch

Mr. Kirk Cantor has been with the Balloon Projects Branch for five years. He obtained a BS degree in aerospace engineering from the University of Maryland. Mr. Cantor has received extrusion training and will be working closely with the Penn State laboratory.

THE NEUTRAL GAS AND ION MASS SPECTROMETER FOR THE COMET RENDEZVOUS ASTEROID FLYBY MISSION

An *in situ* study of the coma of a comet is considered essential for a detailed understanding of cometary chemistry, since many atomic and molecular species cannot be detected satisfactorily by remote sensing. A Neutral Gas and Ion Mass Spectrometer (NGIMS) is under development in the Atmospheric Experiment Branch for the Comet Rendezvous Asteroid Flyby Mission (CRAF). Plans call for a 1993 launch date of CRAF by using a Mariner Mark II spacecraft and a rendezvous with Comet Tempel II in 1996.

Interest in the study of the chemical and physical properties of comets arises, in part, from the hypothesis that comets, having never been extensively thermally processed, may provide the most accurate record available of early solar system conditions. In addition, the study of cometary chemistry is an important part of the effort to understand the details of the dynamical interactions of solar radiation with the cometary coma. Mass spectrometer data from the flyby missions to Comet Halley suggest the possible presence of polymerized formaldehyde (Heubner, W. F., *Science* 237: 628, 1987) or complex carbon/oxygen/nitrogen/hydrogen-containing compounds in dust particles (Kissel, J., et al., *Nature* 326: 755, 1987). Severe measurement constraints, however, were imposed on these experiments by the high flyby velocities ($\sim$70 km/s in the case of Giotto). The scientific instruments on CRAF will obtain images and measure properties of the nucleus, the coma, the dust jets, and the ion tail over a period of more than 3 years and will monitor the increasing level of activity as the comet approaches perihelion.

NGIMS measures neutral atomic and molecular species and low energy ions in the mass range 1–300 amu. As shown in the figure, the gas sampling system includes three ion sources: an open source, a closed source, and the secondary ion mass spectrometer (SIMS) source. Positive or negative ions from each source can be focused into a quadrupole filter and detected by a secondary electron multiplier. The open ion source is a beam source where gas flowing from the nucleus is collimated to form a beam to be ionized by electron impact ionization without any gas surface interaction. Reactive species such as radicals will most easily be detected by this source.

The closed ion source is designed to measure the flux of the nonreactive species with high sensitivity. The cometary gas thermally equilibrates with the walls of this ion source, and the conductance characteristics of the source are such that the gas density in the ionization region is enhanced relative to the density outside the instrument by a factor as high as 70, depending on the distance of the spacecraft from the nucleus. This distance is typically several tens of kilometers over much of the rendezvous phase of the mission.

The SIMS source will provide a sensitive test for the presence of complex, nonvolatile molecules that stick to surfaces. The SIMS collector is a cooled silver surface that is exposed to the gas and dust flow from the comet. After a typical collection period of several hours, an energetic cesium ion beam is focused onto the collector surface and the molecular species generated as secondary ions are mass analyzed. We anticipate that the extended set of measurements carried out by the NGIMS and other

ORIGINAL PAGE IS
OF POOR QUALITY

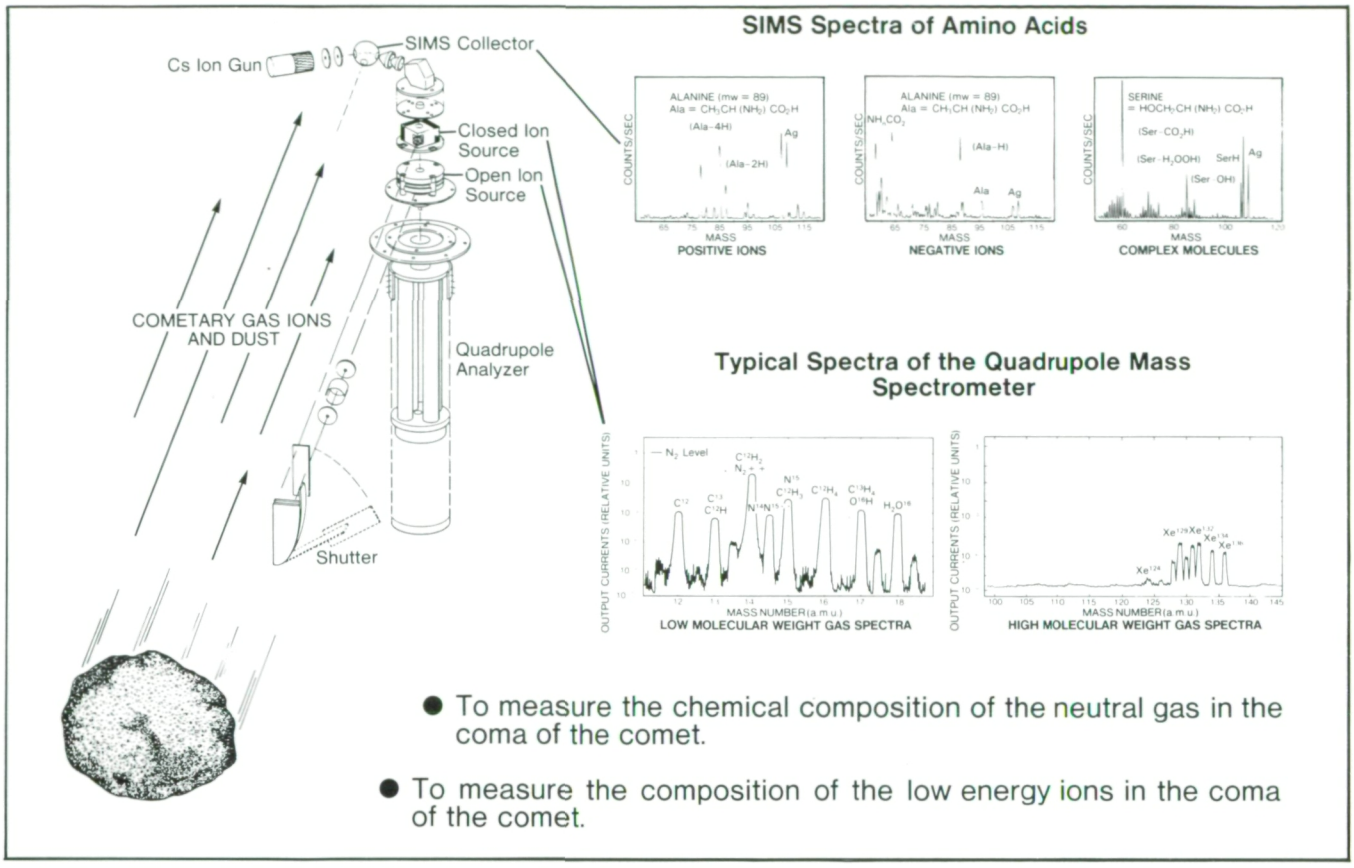

The Comet Rendezvous Asteroid Flyby Mission's Neutral Gas and Ion Mass Spectrometer.

instruments of CRAF will provide a more comprehensive understanding of the physical and chemical processes occurring in comets.

Contacts: H. B. Niemann, P. R. Mahaffy, and D. Harpold
Code 615

Sponsor: Office of Space Science and Applications

Dr. Hasso B. Niemann has participated in experimental atmospheric research for more than 20 years. Most recently, he served as Principal Investigator on the Pioneer Venus Orbiter Neutral Mass Spectrometer and the Galileo Probe Mass Spectrometer. Dr. Niemann obtained a PhD degree in 1969 from the University of Michigan, and he has been a part of Goddard for 17 years.

FLIGHTWORTHY INFRARED BOLOMETERS WITH HIGH THROUGHPUT AND LOW NEP

Two of the three experiments onboard the Cosmic Background Explorer (COBE) require bolometer detectors. All 4 detectors of the Far Infrared Absolute Spectrometer (FIRAS), and 2 of 10 Diffuse Infrared Background Experiment (DIRBE) detectors are bolometers. A bolometer is an infrared (IR) sensing device that consists of an IR absorber and a very sensitive temperature sensor. In monolithic bolometers, a single wafer serves both as the IR absorber and the temperature sensor (Downey, P. M., et al., 1984). In composite bolometers, a low heat capacity wafer is used as an IR absorbing substrate and a small doped silicon or germanium temperature sensing chip is glued on the substrate. The bolometers used in COBE had to meet very stringent

specifications. They had to be rugged enough to withstand vibrations experienced during launch and insensitive to microphonic inputs introduced primarily by the spacecraft momentum wheel. Yet they should exhibit exceptional performance characteristics. Our initial role was to test existing bolometers and determine whether they met the COBE specifications. None of the bolometers tested met the specifications, while at the same time proving to be flightworthy. It was, therefore, decided that we attempt to develop our own bolometers. Within a relatively short time, we were able to develop composite bolometers that met or surpassed all the COBE requirements.

The figure shows a schematic diagram of the GSFC bolometer. The temperature sensor is a silicon chip. Silicon crystals doped with Sb and compensated with Bn are obtained commercially and cut into wafers ~20 mils thick. These wafers are lapped to a thickness of 10–15 mils, implanted on each side with 2×10^{16} As ions/cm^2 at an energy of 150 keV to provide low-noise electrical contacts, coated with 1000 Å of gold to facilitate the attachment of leads, and diced into small chips. The chips were provided by H. Moseley and G. Lamb. We etched these chips to polish and reduce them to their final size of $\sim 12 \times 8 \times 8$ mils. Thermal leads are attached to the gold-coated ends of the chip with EpoTek HE20E silver epoxy. The physical time constant of a bolometer is the ratio of its heat capacity to the thermal conductance of the leads. For slow bolometers ($\tau \sim$ 40 ms), both leads are 10-mil lengths of 1/4-mil diameter PtWf wire. For fast bolometers ($\tau \sim 5$ ms), 0.3-mil brass wire is used for one of the two leads. In general, the composition, size, and length of the thermal leads can be used to adjust the time constant of a bolometer. The silicon chips are glued with stycast 2850-FT epoxy on the substrate. The FIRAS substrate is a 25-μm thick diamond octagon with an inscribed circle diameter of 7 mm. For DIRBE, 2.9-mm diameter diamond wafers 18 μm and 25 μm thick are used for IR radiation centered at wavelengths of 180 μm and 230 μm, respectively.

The substrate is suspended on a KEVLAR crosshair. Each span consists of two 6-μm fibers and is tensioned at 25 g. KEVLAR fibers were chosen because of their high tensile strength and the extremely low thermal conductivity that results in more than 99 percent of the heat being conducted through the thermal leads. The thermal expansion coefficient of KEVLAR, however, was found to be near zero. In the original design, aluminum was used for the support frame, and this resulted in a reduction of the bolometer resonant frequency by a factor of ~10, when it was cooled to LN_2 temperature. At the suggestion of J. Mather and H. Moseley, an INVAR frame was

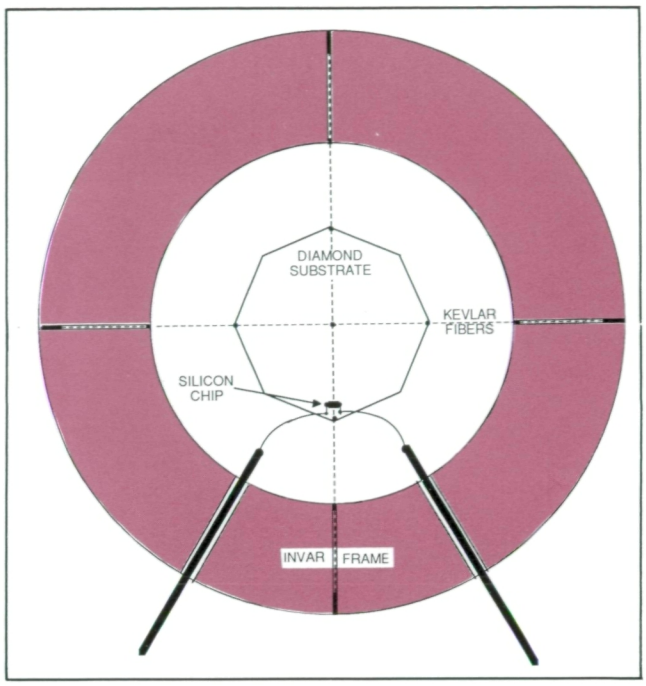

GSFC Composite Bolometer.

used, resulting in a resonant frequency reduction of only ~15 percent. A very small amount of stycast 2850-FT is used at four corners to secure the substrate on the suspension fibers. Two #30 stranded, Teflon-insulated copper leads are epoxied in the two grooves on the frame.

Finally, ½-mil gold wire is used to connect the thermal leads to the copper leads. Silver epoxy is used to make these connections. At this point, the bolometers are mounted in a dewar, and their electrical characteristics are measured. If everything is satisfactory, the back side of the substrate is coated with an IR absorbing metallic film. FIRAS requires flat absorptance in the wavelength range of 100 μm to 1 cm. John Mather calculated that for optimum absorptance, a film of surface impedance of 267 ohms per square is required. At first this was accomplished by evaporating ~40 Å of gold on the diamond. However, due to a concern about possible long-term instability of the gold film, it was decided to first coat the diamond with ~20 Å of chromium, then add ~5 Åof Cr-Au mixture, and finally add ~32 Å of gold. The surface impedance is monitored during the gold deposition, and the evaporation is stopped when the impedance reaches the desired value. The addition of chromium increases the overall heat capacity of the bolometer, resulting in a longer time constant. However, since there was not enough time to study the stability of

the pure gold film, we had to use chromium. Data obtained since then show that the pure gold film is quite stable; therefore, pure gold absorbing films may be used in the future.

The coating of the IR absorbing film on the flight COBE bolometers was done by C. Lisse. He also measured the IR absorptance of coated bolometers. The optimum absorptance is 50 percent, and his measurements consistently showed flat absorptances near 50 percent. For DIRBE, the thickness of the substrate was chosen such that internal reflections would enhance the IR absorptance at 180 μm and 230 μm, respectively. A film of ~65 ohms per square was deposited on the DIRBE bolometer substrates, resulting in a tuned absorptance of ~70 percent for each band. At this point, the bolometers were mounted again in a specially equipped dewar where, in addition to their electrical characteristics, their response to IR signal was measured and compared to the response of a control bolometer. It was thus possible to select the best performing bolometers to be used in the construction of the flight detectors for both FIRAS and DIRBE. The throughput of the FIRAS bolometers is 1.28 sr-cm^2, whereas for DIRBE it is 0.21 sr-cm^2. The time constants ranged from 3 to 40 ms, and their noise equivalent power (NEP) ranged from 4 to 13 $\times$ 10^{-15} W/Hz$^{1/2}$ at 1.6°K. The noise spectra of these bolometers are flat above 1–2 Hz.

Contact: Aristides T. Serlemitsos
Code 713

Sponsor: COBE Project

Dr. Aristides T. Serlemitsos is an aerospace engineer with 16 years of experience at Goddard. Dr. Serlemitsos, who received his PhD degree in physics from the University of Maryland, developed and built composite bolometers that are considered among the best in the world. He also designed and built the bolometer assemblies for COBE, and he was responsible for the IR sources used in the FIRAS internal calibrator. Dr. Serlemitsos also developed a computerized system for the complete testing of these detectors.

COBE BOLOMETER ASSEMBLIES

The Far Infrared Absolute Spectrometer (FIRAS), which is part of the Cosmic Background Explorer (COBE), requires four bolometer assemblies. Two of these detectors should be optimized for the frequency range from 1 to 20 Hz, and the other two for the range from 20 to 100 Hz. In addition to the very stringent performance requirements, the FIRAS detectors must provide adequate shielding against 100 MeV gamma radiation as well as against RF signals.

The figure shows a schematic diagram of a typical bolometer circuit. A load resistor is connected in series with the bolometer, and both are kept at the operating temperature (about 1.6°K). At the operating point, the bolometers developed for COBE have a resistance of about 25 MΩ. The load resistors consist of four commercially obtained 10-MΩ wire-wound resistors connected in series. To reduce the noise pick-up in the signal lead, a JFET source follower mounted near the bolometer is used to minimize the length of the signal lead. The gain of the JFET is 0.99, so its sole purpose is to reduce the output impedance from 25 MΩ to about 1500 Ω. Silicon JFETs become quite noisy below 60°K, and they stop conducting below about 20°K. Therefore, they had to be designed to operate at about 75°K. Two J230 JFET chips and a 375-KΩ chip resistor are mounted on a ceramic substrate. KEVLAR fibers were used to suspend this substrate inside an INVAR frame. When the temperature of the JFETs is below 20°K, the chip resistor, which dissipates about 100 μW, is sufficient to raise the temperature to above 20°K. At this point the JFETs start conducting, accelerating the elevation of their temperature. At the operating point the total dissipation is about 400 μW, which is sufficient power to keep the temperature of the JFETs at 75°K even though the temperature of the JFET case is at about 1.7°K.

To shield the bolometer from gamma radiation, a tantalum enclosure was used. The tantalum shield was designed such that with minimum weight, it provides at least 100 MeV gamma-ray protection in all directions except along the input aperture (1 in. long, 0.4 in. diameter). The use of tantalum provides an added benefit. Tantalum becomes superconducting at low temperatures, thereby

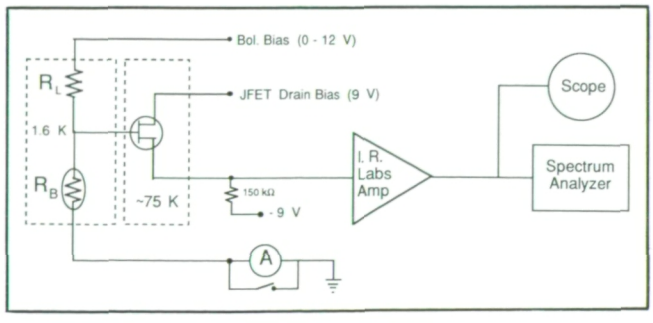

Schematic diagram of bolometer circuit.

COBE Bolometer Performance						
Bolometer Assembly	T (°K)	τ (ms)	NEP $\times 10^{15}$ (nV/Hz$^{1/2}$)	T (°K)	τ (ms)	NEP $\times 10^{15}$ (nV/Hz$^{1/2}$)
FIRAS Slow						
Specs	1.50	35.4	10.00	—	—	—
FA6	1.50	37.9	3.58	1.61	37.9	4.60
FA7	1.46	30.6	4.63	1.60	30.6	4.69
FA8	1.48	64.2	4.27	1.60	38.8	4.75
FIRAS Fast						
Specs	1.50	3.54	30.00	—	—	—
FA2	1.50	6.42	12.80	1.61	6.50	13.90
FA10	1.48	5.24	11.70	1.60	6.50	13.90
FA11	1.50	6.03	12.20	1.60	5.90	10.30
DIRBE						
Specs	—	—	—	1.60	<15	6.00
DA2	1.50	2.90	4.80	1.60	2.90	5.20
DA3	1.50	6.40	5.30	1.60	6.30	5.60
DA9	1.50	3.00	5.20	1.61	3.00	6.40
DA10	1.50	5.90	4.00	1.61	5.50	5.50

providing excellent electromagnetic shielding. To provide total RF shielding, each incoming lead is first shielded with a high iron content "spaghetti," and then it travels for about an inch in eccosorb CR124.

The shape and size of the Diffuse Infrared Background Experiment (DIRBE) bolometer assemblies are different. Also, they had to be much lighter than the FIRAS detectors. However, similar technics were used in the design and fabrication of these detectors.

All bolometer assemblies have been tested very thoroughly. The table gives some electrical characteristics at two temperatures. Note that for some assemblies, the time constant differs considerably from the one in the specs. The time constants in the specs correspond to 4.5 Hz for the FIRAS slow bolometers, 45 Hz for the FIRAS fast bolometers, and 32 Hz for the DIRBE bolometers. The time constant of a bolometer depends on the biasing current. The values given in the table correspond to biasing currents that provide optimum optical response of the bolometers respectively at the above frequencies. In addition to the electrical and optical measurements, all bolometer assemblies were successfully vibrated to levels expected during launch. Also, they did not exhibit excessive sensitivity to microphonic inputs. Recent tests show an overall reduction in the infrared absorptance of less than 5 percent in the course of a year.

Contact: Aristides T. Serlemitsos
Code 713

Sponsor: COBE Project

Dr. Aristides T. Serlemitsos is an aerospace engineer with 16 years of experience at Goddard. Dr. Serlemitsos, who received his PhD degree in physics from the University of Maryland, developed and built composite bolometers that are considered among the best in the world. He also designed and built the bolometer assemblies for COBE, and he was responsible for the IR sources used in the FIRAS internal calibrator. Dr. Serlemitsos also developed a computerized system for the complete testing of these detectors.

COBE-USO NAVIGATION EXPERIMENT

Currently, ground-based two-way tracking remains the primary technique for user spacecraft orbit determination (OD) via the Tracking and Data Relay Satellite System (TDRSS). This type of support requires the use of coherent forward and return TDRSS services and is oriented toward the use of large-scale computers for OD support. Future missions, however, are expected to require improvements in the speed, accuracy, and operational efficiency of current OD support. A need for onboard real-time navigation processing to derive orbit, time, and attitude data in support of mission operations is also anticipated.

TDRSS noncoherent scheduled tracking modes, one-way forward and one-way return, offer the potential to reduce the ground terminal requirements associated with routine two-way tracking and significantly increase the capability for real- or near-real-time navigation support. Realistic consideration of TDRSS one-way tracking modes as candidates for primary mission support, however, still awaits comprehensive demonstration to validate both hardware and software.

The Cosmic Background Explorer (COBE) mission provides an opportunity to demonstrate and space qualify one-way return Doppler tracking through TDRSS. COBE spacecraft state vectors will be estimated by use of a prototype one-way navigation processing system, with concurrent orbit determination by the Flight Dynamics Facility by use of both one- and two-way Doppler data to provide a means of evaluating one-way navigation performance. The COBE navigation experiment will thus foster the development and refinement of orbit determination algorithms for use in future onboard and ground-based one-way navigation applications, including frequency determination algorithms to model the user spacecraft oscillator. The COBE navigation experiment, however, is secondary to the COBE primary mission and

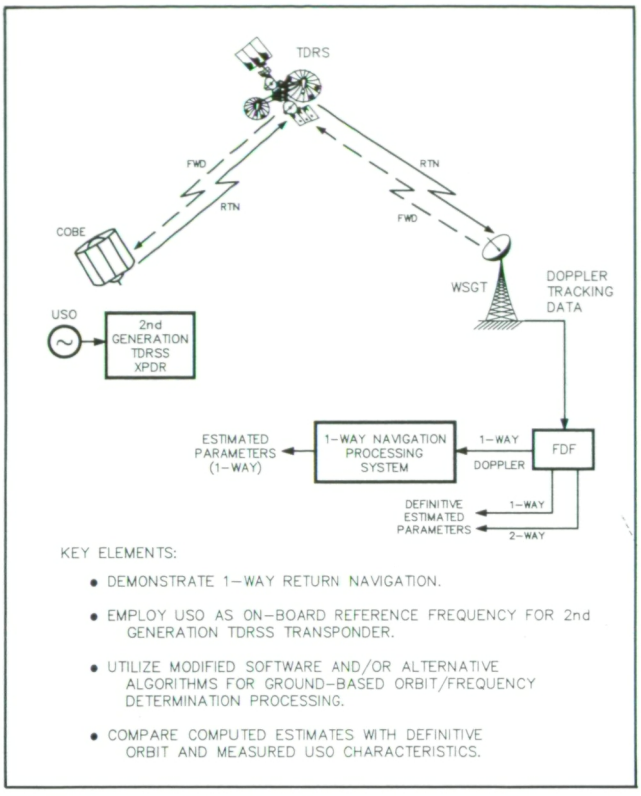

Overview of the COBE Navigation Experiment.

subject to constraints imposed by the primary mission objectives. TDRSS contact times, for example, will be limited to four or five 20-minute periods per day. One year after launch, though, the primary COBE mission will have concluded, and ideally, TDRSS contacts may be scheduled at will to allow investigation into the effect of alternative TDRSS contact options on one-way return navigation performance.

To provide the necessary frequency stability for one-way navigation, an Ultra-Stable Oscillator (USO) has been developed by the Johns Hopkins University Applied Physics Laboratory (APL) for use as frequency reference to the COBE spacecraft's second generation TDRSS user transponder. The COBE-USO thus provides an onboard frequency reference for communications support superior to the capabilities of prior NASA missions.

In-flight performance of the oven-regulated crystal USO has been predicted on the basis of testing in the NASA/GSFC RF Laboratory, including tests through the TDRSS network. Objectives of the RF Laboratory testing included the validation of the USO's performance as a stand-alone unit, determination of its performance in conjunction with the second generation TDRSS user transponder in both one-way forward and one-way return

modes, and a test trial of one-way return tracking through the TDRSS network.

Results of the RF Lab tests show that the COBE-USO fulfills the requirements of the COBE one-way navigation experiment. Linear frequency drift exhibited by the oscillator is less than 1 part in 10^{10} over 24 hours and has been successfully fit to linear drift models with 90 percent confidence intervals less than ± 5 parts in 10^{12} over 24 hours. The USO's phase noise spectral density has similarly been shown to be substantially better than specified. The USO's 19.056392 MHz output—required by the second generation transponder—makes definitive measurement of its short-term time domain frequency stability difficult; nonetheless, the USO's frequency stability as characterized by its Allan variance has been shown to be better than specified. Finally, testing of the USO transmitting through the TDRSS network in a simulation of COBE one-way return tracking has indicated that the one-way return range-rate noise level is comparable to that obtained with two-way coherent turnaround TDRS service. Such performance represents an order of magnitude improvement over one-way range-rate estimation with the transponder's internal frequency reference and strongly indicates the future success of the COBE navigation experiment.

COBE-USO Performance Characteristics

Quantity	Performance Characteristics	
	Specified	Measured
24-Hour Fractional Frequency Drift (After 10-day warm-up)	1×10^{-10}	$<1 \times 10^{-10}$
SSB Phase Noise $\mathcal{L}$ (f) (dBc/Hz) (19.056392 MHz output)		
1 Hz Offset from carrier	−70	−95
10 Hz Offset from carrier	−90	−115
100–10^7 Hz Offset from carrier	−110	≤ -115
Short-Term Frequency Stability $\sigma_y(\tau)$ (Square root of Allan variance)		
1-Second averaging time	5×10^{-12}	$\leq 4 \times 10^{-12}$
20-Second averaging time	1×10^{-12}	$\leq 1 \times 10^{-12}$
180-Second averaging time	1×10^{-12}	$\leq 5 \times 10^{-13}$
300-Second averaging time	1×10^{-12}	$\leq 4 \times 10^{-13}$

Characterization of the USO was done in collaboration with Mr. Alan Jacobsen of Stanford Telecommunications, Inc.

Contacts: Eddie M. Jones and David J. Zillig
Codes 550 and 530

Sponsor: Office of Space Operations

Mr. Eddie Jones, an aerospace engineer with 27 years of service with Goddard, is Flight Dynamics Engineer on the COBE Experiment. Mr. Jones holds a BS degree in engineering mathematics from North Carolina A&T State University.

Mr. David Zillig is Project Engineer for USO development and integration on the COBE Navigation Experiment Ultrastable Oscillator. The COBE Navigation Experiment is an application of one of the advanced communications capabilities of the Second Generation TDRSS User Transponder developed at GSFC by the Telecommunication Systems Branch. Mr. Zillig is interested in the development of a next-generation 5-band ranging system for mission orbit determination, and in the technology demonstration of onboard digital beamforming for possible use in a 5-band Multiple Access System aboard an advanced TDRSS. Mr. Zillig earned a BSEE degree from the Pennsylvania State University, and he has served with Goddard since 1966.

CONDENSATION AND EVAPORATION OF TWO-PHASE ANNULAR FLOW FOR SPACECRAFT THERMAL SYSTEMS

Future large space-based facilities, such as the Space Station, will require thermal energy management systems capable of transporting tens of kilowatts of heat over a hundred meters or more. This represents better than an order of magnitude improvement over current technology. Two-phase thermal systems, which rely upon the latent heat of vaporization/condensation of a refrigerant, are currently being developed to meet this challenge. Although there has been a significant amount of hardware development and testing over the past few years, relatively little basic theoretical work has been done. This is especially true for condensation. Our work is an initial attempt to address this lack of theoretical analysis.

The approach adopted in this effort begins with development of the basic equations for conservation of mass, momentum, and energy. Applying this approach to both the liquid film and vapor results in six separate equations. The next step involves nondimensionalization of these equations and application of the appropriate initial and boundary conditions. However, since the resulting expressions are nonlinear partial differential equations, an exact solution is not possible.

Two different techniques have been adopted in an effort to solve these complex equations. The first involves simplifying the expression for conservation of momentum into a linear partial differential equation. This expression can then be solved. The resulting solution demonstrates the presence of an inherent oscillation in such two-phase systems. This result agrees with experimental evidence from testing at Goddard and elsewhere. The solution also suggests that this inherent instability may be of greater magnitude in microgravity than in normal gravity. Although it has not yet been possible to perform the appropriate tests to confirm this prediction, if true it will be of significant concern in the design of two-phase thermal systems for spacecraft.

The second solution involves application of the method of finite differences. This numerical approach is workable, but it will require a major effort to define the six equations in appropriate computer format. The simplified two-dimensional case has been solved, and efforts to solve the more complex three-dimensional case are proceeding.

In addition to enhancing our understanding of the basic processes involved in two-phase thermal systems, a practical goal of this work will be to develop useful expressions for stability criteria. This will be of direct use in the design of actual spacecraft thermal systems.

Contacts: Theodore Swanson and Y. K. Hsu
Code 732

Sponsor: NASA-ASEE Summer Faculty Fellowship Program

Mr. Theodore D. Swanson is an aerospace engineer with three years of experience at Goddard. Mr. Swanson, who holds an MS degree from the University of Maryland, designed the first ammonia-based, operational two-phase heat transfer test bed along with two ground-based photovoltaic power stations.

Dr. Y. K. Hsu has been a senior math faculty member at the University of Maine for 16 years. He has been awarded summer faculty research awards in 1978 and 1980 and was also appointed Institute Guest by the Department of Aeronautics and Astronautics at the Massachusetts Institute of Technology. For the summer of 1987, Dr. Hsu was awarded a NASA/ASEE Summer Faculty Fellowship at GSFC.

SPACEWORTHY ADR AND LOW-CURRENT SUPERCONDUCTING MAGNET

The Cryogenics Technology Section at GSFC is developing a spaceworthy Adiabatic Demagnetization Refrigerator (ADR). The ADR will cool X-ray sensors in the Advanced X-ray Astrophysics Facility (AXAF). Cooling the sensors increases their sensitivity in two ways: by reducing the noise level and by reducing heat capacity. Cooling the sensors from 1.4 °K (the temperature of the space-pumped liquid helium coolant bath) to 0.1 °K (the temperature of the ADR) reduces the noise power by about 700 times, thus increasing the sensitivity. Cooling also reduces the heat capacity of the sensors, so that each X-ray photon that hits a sensor produces a bigger temperature change, and thus a bigger signal. Cooling the sensors, therefore, allows observations of a given sensitivity to be made more quickly, or allows a given observing time to produce observations of greater sensitivity.

The ADR cools cyclically, alternately cooling to 0.1 °K and exhausting at 1.4 °K. The heart of the ADR is the salt pill, a block of paramagnetic (weakly magnetic) salt. The salt pill absorbs heat energy during the cooling part of the cycle and stores it until the exhaust part of the cycle. The magnet produces a magnetic field that controls the absorption and exhaust of heat by the salt pill. The thermal bus allows heat to flow from the sensors to the salt pill and from the salt pill to the heat switch. The heat switch turns on to let the exhaust heat flow into the helium bath and turns off to stop heat from flowing back in. The helium bath (at 1.4 °K on AXAF) absorbs exhaust heat from the ADR, thus providing the first stage of cooling.

This will be the first ADR in space, though they have operated routinely on the ground for many years. To adapt the ADR for satellites, a tradeoff study was done to design an ADR with the greatest possible cooling power per weight. The study used a magnetic field calculation program adapted from one written at the University of

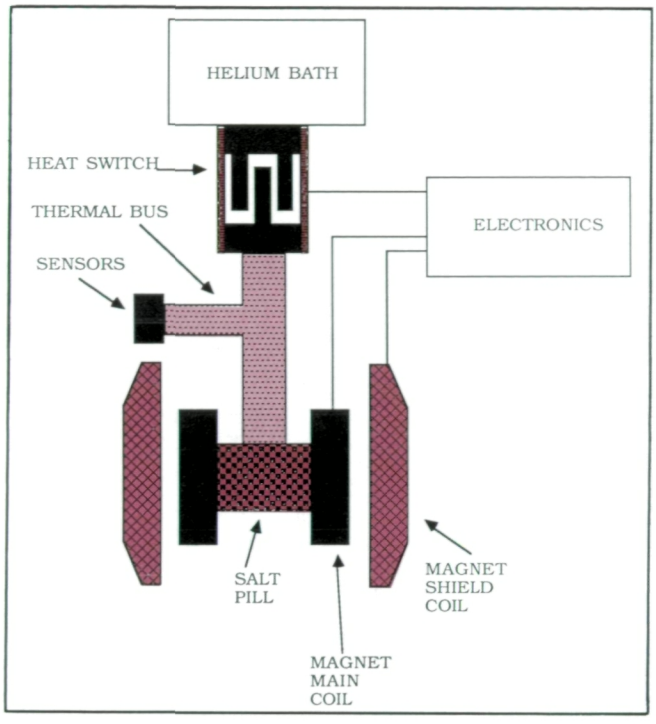

ADR schematic.

Southern California. The advantages of the ADR for spaceflight are its simplicity, lack of moving parts, and (except for the helium bath) lack of fluids.

To reduce heat loads to the helium bath, the ADR will use a low-current superconducting magnet. One of the largest sources of heat to the bath is the electrical leads that connect the power supply (which is outside the bath) with the magnet (which is inside the bath). This heating comes about in two ways: resistive, caused by electrical currents flowing in the leads; and conductive, caused by heat flowing along the wires. In general, changing the design of the leads to reduce one type of heating increases the other. For example, thickening the leads reduces the resistive heat load (by decreasing leads' resistance) but increases the conductive heat load. But the resistive heat load can also be cut by reducing the current. If the current is low enough, then leads designed for low conductive heating will also have low resistive heating, hence the use of the low-current magnet in this ADR.

Low-current magnets have other possible applications, both on Earth and in space, especially in situations that require low maintenance equipment. Leads for conventional high-current superconducting magnets are often designed to minimize resistive heating. Operators remove the leads when they are not in use, thus avoiding most of the conductive heating. Low-current magnets, however, have low conductive heating without using removable leads. Thus low-current magnets can be used on spacecraft (where removable leads are impractical). Low-current magnets can also be used on Earth, where avoiding the use of removable leads would simplify the design or reduce exposure of technicians to cryogenic fluids and equipment.

Code 713 procured a proof-of-concept low-current magnet. The magnet was successful, producing a central field of 3 Tesla with a current of 3 amps. GSFC recently awarded a contract for a low-current magnet for a breadboard model of the AXAF ADR. This new low-current magnet will include shielding coils to reduce the magnetic field outside the magnet bore. The shielding is needed to avoid interfering with the X-ray sensors and to meet electromagnetic interference requirements for AXAF.

Contacts: Brent Warner and Steve Volz
Code 713

Sponsor: Office of Space Science and Applications

Mr. Brent Warner joined Goddard's Cryogenics Technology Section in 1985. Mr. Warner has an MS degree in physics from the Ohio State University.

Dr. Stephen Volz joined Goddard's Cryogenics Technology Section in 1986. Dr. Volz has a PhD degree in physics from the University of Illinois.

MECHANICALLY PUMPED TWO-PHASE HEAT TRANSFER FLIGHT EXPERIMENT (MPTP)

The MPTP will test a small mechanically pumped two-phase thermal control system in both the 1-*G* and 0-*G* environments. The MPTP is a two-phase thermal control system that utilizes the latent heat of vaporization of its ammonia working fluid to transport large amounts of heat and yet maintain a nearly constant temperature at the mounting plate interface. This technology is required by the Space Station and its associated instruments and platforms, since current single-phase systems cannot efficiently meet the increased thermal control requirements of the Space Station.

Experiment operating characteristics such as evaporative and condensing heat transfer coefficients, two-phase pressure losses, temperature control, and flow stability will be evaluated. The experiment consists of two two-phase mounting plates (TPMPs), a reservoir, mechanical

ORIGINAL PAGE IS
OF POOR QUALITY

pumps, a flowmeter, boiling and pressure-drop experiments, a radiator, valves, and instrumentation (refer to Figures 1 and 2). The TPMP mounting plates were described by T. Swanson in the 1985 GSFC Research and Technology Report. The two TPMPs in this system are used to add heat to the ammonia working fluid in the evaporator mode and remove heat from it in the condenser mode, demonstrating the heating and cooling capabilities of this type of system. A two-phase reservoir controls the system temperature level and maintains the required liquid inventory. The reservoir temperature can be set to any required system operating temperature. Two pumps circulate the ammonia liquid, and the flowmeter is used to determine the mass flow rate. The boiling experiment is used to determine boiling heat transfer coefficients, and the pressure-drop experiment will measure two-phase pressure losses over a fixed length of tubing. The radiator provides the heat rejection for vapor condensation, and the valves direct the flow to either the condenser TPMP or the boiling and pressure-drop experiments. Various heaters, thermistors, pressure transducers, and control electronics are employed throughout the MPTP as well.

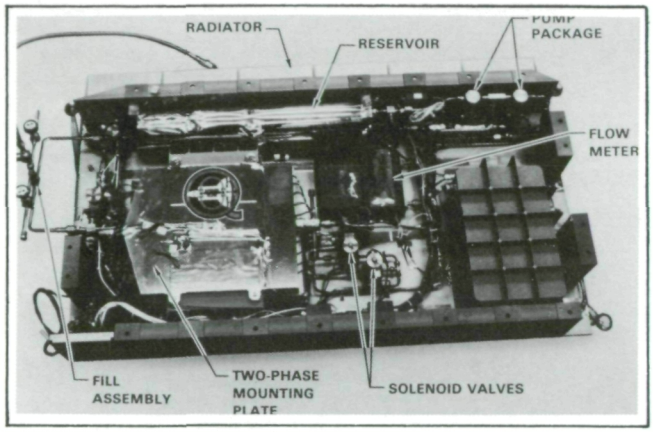

Figure 1. Mechanically pumped two-phase flight experiment.

Initial testing of the MPTP demonstrated excellent experiment performance. The tests included power levels ranging from 45 W to 1100 W, variable flow rates and temperature set points, subcool limit and transient cases, and condenser mode operations. Figure 3 shows a typical snapshot of temperatures for the 1100-W evaporator

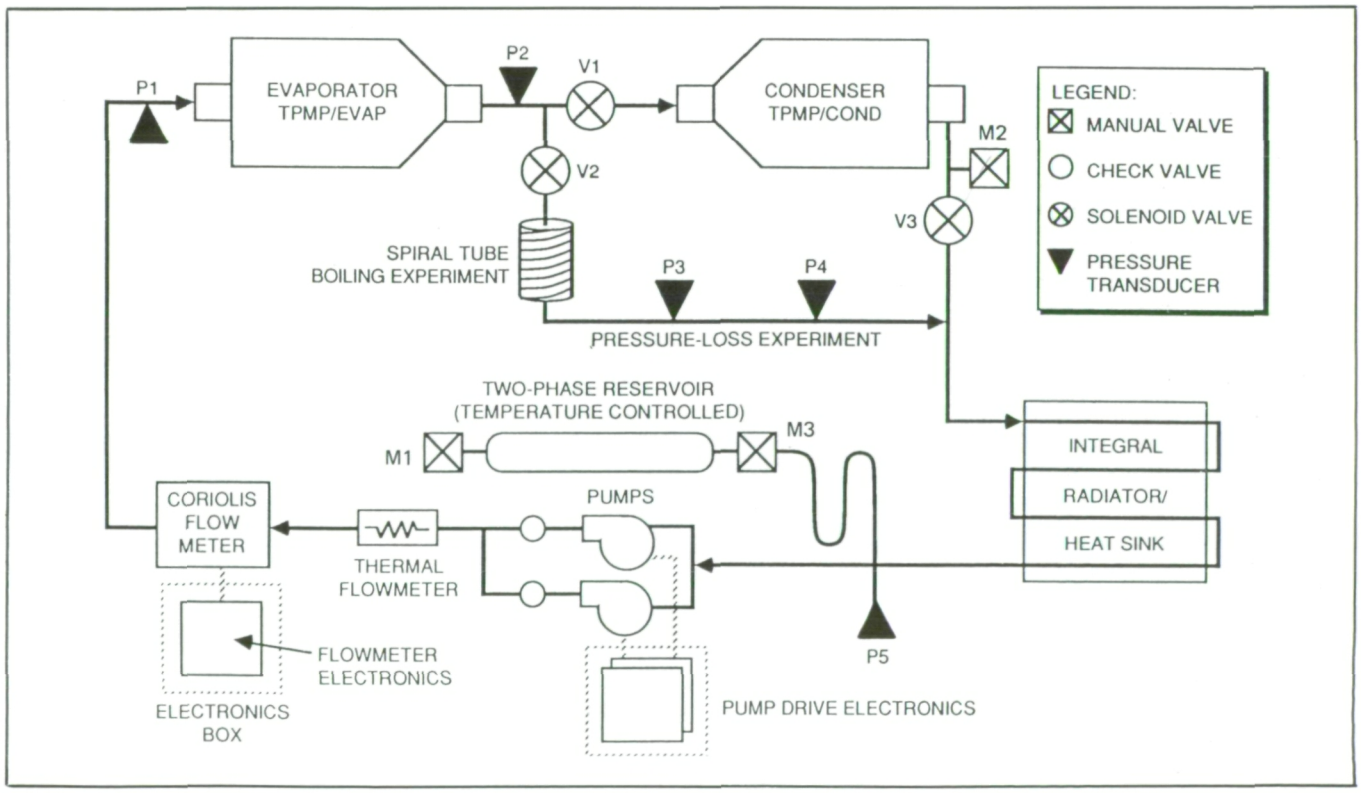

Figure 2. MPTP schematic diagram.

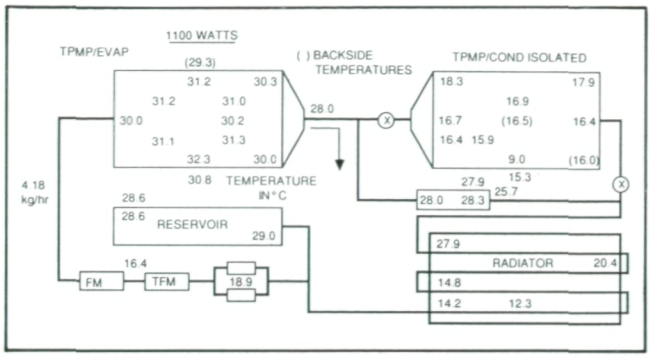

Figure 3. Evaporator mode test.

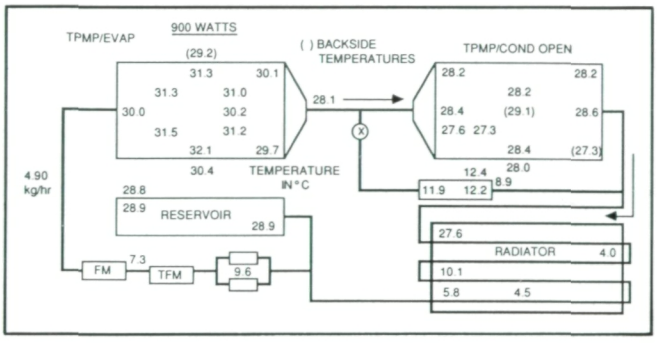

Figure 4. Condenser mode test.

mode test. Note the nearly uniform temperatures over the evaporator TPMP. (The condenser TPMP was valved off for this test.) Also, the TPMP temperature level was maintained within 2 to 3°C of the system set point temperature established at the reservoir. Furthermore, this temperature control can be maintained for power levels ranging as low as 45 W. Figure 4 is a temperature snapshot for the condenser mode test with the valves to the condenser TPMP open. Nine hundred watts were added to the system at the evaporator TPMP, with some of the heat removed at the condenser TPMP and the remainder at the radiator. Again note the nearly uniform temperature control maintained over both TPMPs, with temperatures close to the system temperature level established at the reservoir.

The MPTP is currently undergoing flight preparation and integration activities for flight on the Hitchhiker-G carrier system. It is also being considered for manifesting with JSC's Evaluation of Oxygen Interaction with Materials (EOIM-3) experiment. The MPTP is undergoing extensive testing and evaluation at the GSFC two-phase heat transfer laboratory as well.

The MPTP will be the first flight of a mechanically pumped two-phase thermal control system, and it is part of the Space Station Advanced Development Program. The experiment should be ready for flight early in 1988, and hopefully it will fly on an early Shuttle mission.

Contacts: Dan Butler and Roy McIntosh
Code 732

Sponsors: Office of Aeronautics and Space Technology and Office of Space Station

Mr. Dan Butler is a research and development engineer with the Thermal Engineering Branch with 10 years of experience at Goddard. He holds a BS degree in aerospace engineering from Virginia Polytechnic Institute. Mr. Butler currently serves as Program Manager for the Mechanically Pumped Two-Phase flight experiment.

Mr. Roy McIntosh, Section Head of Code 732.2, has 25 years of experience at Goddard. Mr. McIntosh, who received his education at Antioch College, has received two Exceptional Performance Awards and a NASA Exceptional Engineering Achievement Medal for work in two-phase heat transfer.

LONG-LIFETIME CRYOGENIC REFRIGERATOR

Many space instruments require ultralow temperature cooling to perform their measurements. Several Goddard technology programs are under way to fulfill this need. One such program is to develop an ultralow temperature (cryogenic) refrigerator that will operate in space for 3 to 5 years without maintenance.

The first unit of the new refrigerator, the Proof-of-Principle Model Stirling Cycle Cryogenic Cooler, successfully completed 3 years of operation in FY86. Running silently at an average speed of 25 cycles/s, it generates 5 W of cooling power at a temperature of 65 °K when its compression heat is rejected at 300 °K. Its reciprocating components work without conventional bearings, seals, or lubricants because they are levitated and centered by magnetic bearings. A closed-loop servo system controls the position of the free-floating pistons. Moving magnetic linear motors of a new design provide linear motion. The operating performance of the cooler has not changed during the 3 years of operations.

The second-generation cooler, the Technology Demonstration Model, is being fabricated; it is designed to survive Shuttle launch and operation in space. The launch

ORIGINAL PAGE IS
OF POOR QUALITY

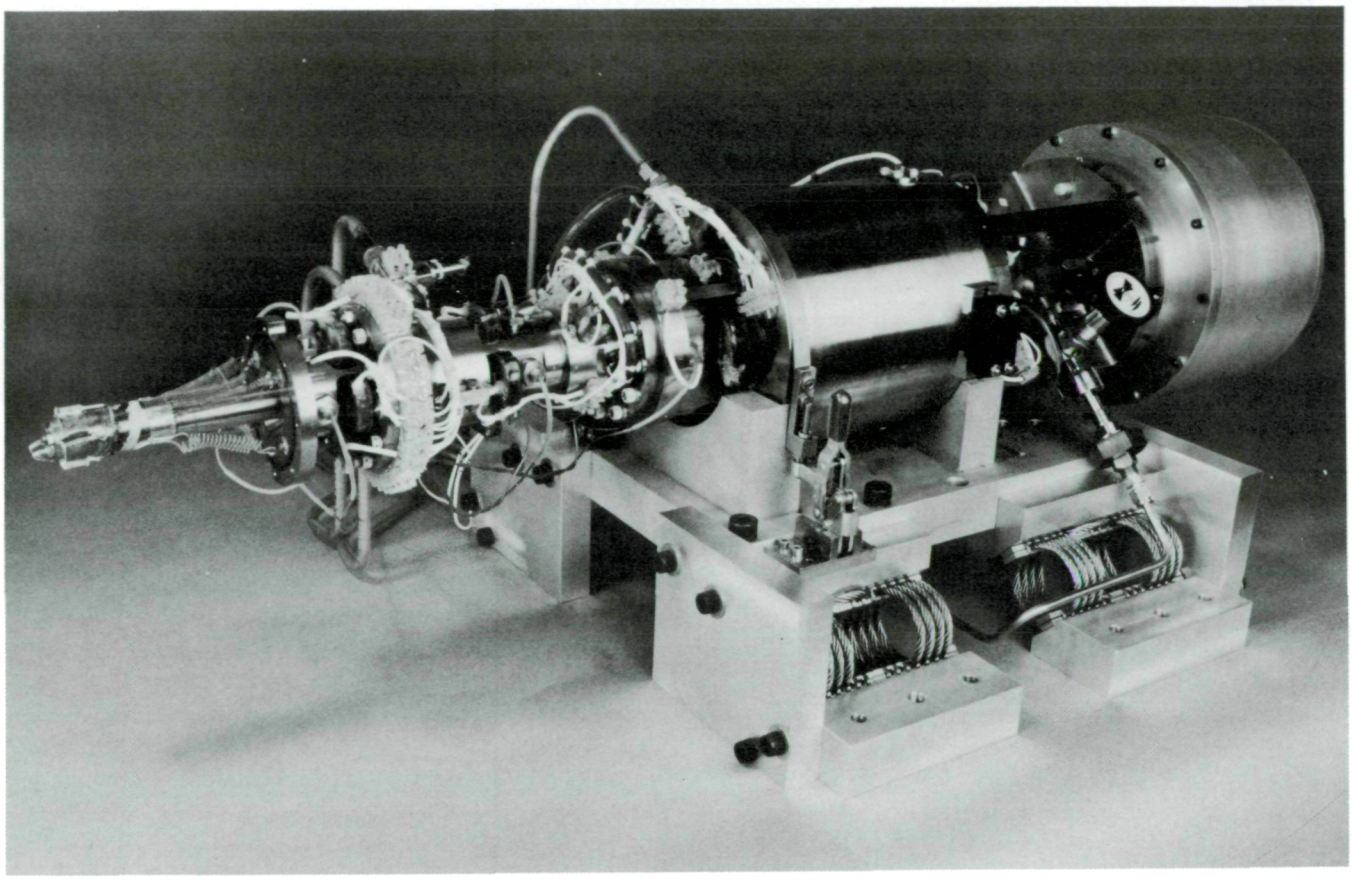

Proof-of principle model Stirling cycle cryogenic cooler.

specifications necessitated improvements in electromagnetic bearings, axial and radial position sensors, structural design of the moving elements, and the axial counterbalance. As in the first-generation refrigerator, organic contamination has been eliminated by the use of all metal and ceramic construction. Reductions in system input power result from an integral permanent magnetic displacer spring motor, and more efficient linear motors and drive electronics.

Improved Linear Variable Differential Transformers provide high-frequency capabilities to the axial control system. All clearance seal surfaces are specially treated with ion-plated titanium nitride to eliminate potential damage due to contact during launch and shipping. Transmitted vibrations are minimized by 6-degree-of-freedom spring mounts between the refrigerator and spacecraft. The counterbalance, a tuned spring mass system driven by a linear motor and supported radially by magnetic bearings, cancels the unbalanced axial force generated during operations.

This cooler development has won two IR-100 Invention-of-the-Year awards.

Contact: Max G. Gasser
Code 713

Sponsors: Office of Aeronautics and Space Technology and USAF Space Technology Center

Mr. Max Gasser is an aerospace engineer with 22 years of experience at Goddard. Mr. Gasser, who received his BS degree in chemical engineering from Virginia Polytechnic Institute, is involved with cryogenic cooler technology research and development for space applications. He received the IR-100 Award in 1983 and holds a patent on the Stirling cycle cryogenic cooler.

ALL-METAL COMPACT HEAT EXCHANGER FOR SPACEBORNE CRYOCOOLERS

The overall cycle efficiency (hence, input power requirements) of reverse-Brayton cryocoolers for space applications is highly sensitive to the thermal effectiveness of the heat exchangers. Applications for these cryocoolers in space dictate that these heat exchangers be as small and light as possible. To date, only heat exchangers employing organic materials have been able to achieve the high thermal effectiveness values required for these systems within the allowed size and weight limitations. However, heat exchangers with organic materials degrade cycle performance by leakage and system contamination. Therefore, a compact all-metal heat exchanger with high thermal effectiveness is required.

The GSFC has started a program to develop a high performance, all-metal heat exchanger. Two novel heat exchangers concepts were evaluated with respect to size, weight, and manufacturability with the aim of achieving a thermal effectiveness in excess of 0.98. Detailed thermal models of the heat exchangers were developed, and fabrication and assembly techniques of key exchanger elements were demonstrated.

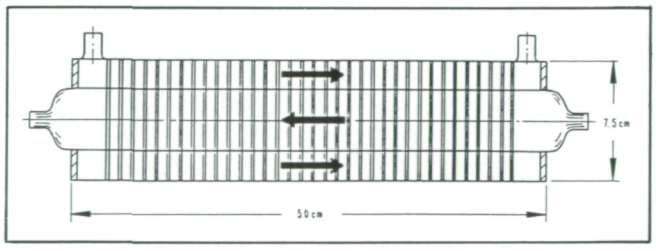

All-metal compact slotted plate heat exchanger for spaceborne cryocoolers.

The heat exchangers were sized to meet the specifications of a 5 W reverse-Brayton cycle cryocooler currently under development for the GSFC. The specifications are: 0.9 g/s balanced flow of neon: with 2.2 atm, 260 °K inlet conditions at the warm end; and 1.2 atm, 70 °K at the cold end. The thermal analyses of the heat exchangers showed that an overall effectiveness (effectiveness including pressure-drop penalty) as high as 0.985 to 0.995 could be achieved with modest heat exchanger weights (less than 3 kg). Fabrication of the heat exchangers also appears feasible but will require a special machine. The contractor has demonstrated the ability to design and build advanced machines for the manufacture of miniature turbomachinery, and the heat exchanger problem is much less demanding than very high speed turbomachinery or tilting pad gas bearings.

In addition to the specialized needs of spaceborne cryocoolers, this heat exchanger technology will have widespread application in commercial helium liquifiers and refrigerators.

Contact: Max G. Gasser
Code 713

Sponsor: Small Business Innovative Research Program

Mr. Max G. Gasser is an aerospace engineer with 22 years of experience at Goddard. Mr. Gasser, who received his BS degree in chemical engineering from Virginia Polytechnic Institute, is involved with cryogenic cooler technology research and development for space applications. He received the IR-100 Award in 1983 and holds a patent on the Stirling cycle cryogenic cooler.

A RELIABLE, LONG-LIFETIME CLOSED-CYCLE CRYOCOOLER FOR SPACE

Turbomachinery is used in large-scale gas liquification plants, but the components are much too large for NASA needs. Recent advances in miniaturization have made turboexpanders as small as 1/8 in. in diameter. These operate at very high speed when supported on self-acting (tilting pad) gas journal bearings with pressurized gas thrust bearings or magnetic thrust bearings.

A turbocompressor is being designed that will incorporate proven features in a new and patentable configuration. A double-sided impeller will limit axial thrust to an extent that an efficient permanent magnet thrust bearing can be used. In addition, the solid rotor motor has special features for heat removal.

A program is under way to design and build a reverse Brayton cycle system to produce 5 W of cooling of 70 °K with neon as the working fluid. When in operation, the moving parts are not in physical contact, so the system should have a very long lifetime. This system will use an all-metal heat exchanger and should be free of contamination. Because it is self-acting, the system is simpler than the magnetic bearing approach and requires only a compressor motor controller in place of complex electronics.

ORIGINAL PAGE IS
OF POOR QUALITY

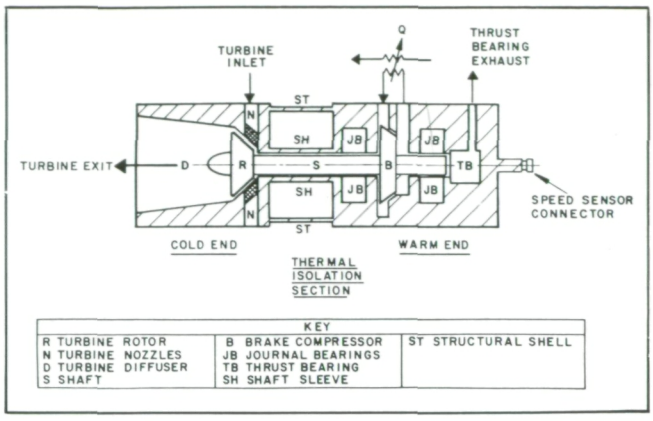

Diagram of turboexpander.

Unlike the Stirling cycle coolers, the gas bearing turbomachinery produces no noise or vibration. However, at the present time the magnetic bearing approach is much further ahead in its development.

When fully developed, the reverse Brayton cycle approach should be much less expensive to build than the magnetic Stirling and should have the same or greater efficiency for operating temperature above approximately 40 °K. The reliability would be greater due to the decreased electronics part count.

Contact: Max G. Gasser
Code 713

Sponsor: Small Business Innovative Research Program

Mr. Max Gasser is an aerospace engineer with 22 years of experience at Goddard. Mr. Gasser, who received his BS degree in chemical engineering from Virginia Polytechnic Institute, is involved with cryogenic cooler technology research and development for space applications. He received the IR-100 Award in 1983 and holds a patent on the Stirling cycle cryogenic cooler.

COMPONENT COOLING FOR A SOUNDING ROCKET PAYLOAD

At the request of an experimenter, who wanted to fly an experiment aboard a sounding rocket launched from Wallops Island, cooling was provided for photo tubes within a payload. The experimenter required bringing the photo tubes into a temperature range of 32 °F to 0 °F until launch using nitrogen gas at a limited flow rate.

Another controlling factor was the 125 ft from the payload, on the launcher, to an accessible location on the ground. After some testing it was discovered that there was a considerable temperature rise in long lines for nitrogen gas. Therefore, to limit the distance traveled by the chilled gas, a heat exchanger was placed on the boom of the launcher. The heat exchanger was built out of aluminum, brass, and copper tubing and was grounded to the launcher. It was filled with propylene glycol (antifreeze) that acted as a transfer medium.

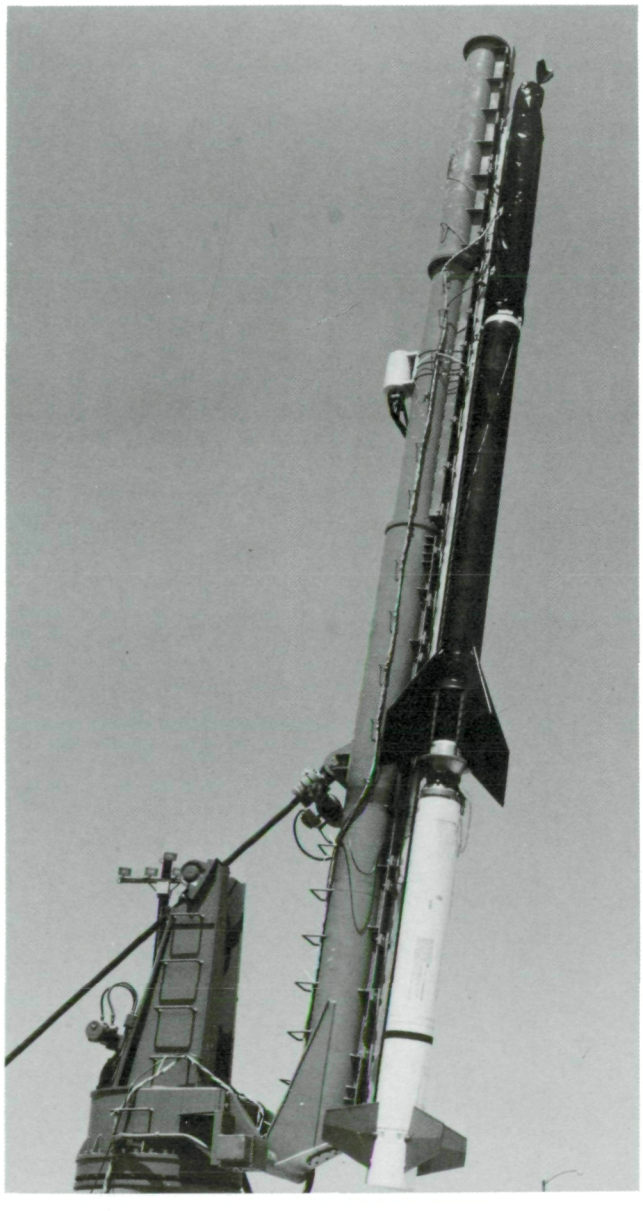

Sounding rocket payload with heat exchanger.

The heat exchanger was cooled by freon. Liquid freon came from a unit on the ground, via pressure rated nylon tubing, to an expansion valve mounted on the heat exchanger. The freon expanded through the valve into a coil of copper tubing within the heat exchanger. The temperature in the copper coil was cycling between $-20\,°F$ and $-40\,°F$, and the temperature of the glycol was approximately $-20\,°F$. The gaseous freon then returned to the ground through nylon tubing. On the ground, at the other end of the nylon tubing, was a compressor-condenser unit. The unit was 1.5 horsepower and could be turned on or off from the blockhouse. The nylon tubing was run through armaflex insulation, and the heat exchanger was insulated with the same material.

The nitrogen gas used to cool the experiment came from a trailer next to the pad. Its flow was regulated from the pad, and it could be turned on or off from the blockhouse. The nitrogen gas line, 125 ft of nylon tubing, ran to the heat exchanger in the same insulation as the returning freon for precooling. The nitrogen then entered a copper coil within the heat exchanger. From there it went through 5 ft of insulated nylon tubing and a pull-away umbilical connector, and entered the payload. In the payload, it was routed by stainless steel tubing into chambers containing the photo tubes and then back through the payload skin. The exhaust expelled into a purge bag covering the payload. The tubing and chambers were wrapped with foil insulation. The temperature within the chambers was controlled by the flow rate of the nitrogen. The temperature decreased with increasing flow. Minimum temperature was approximately $10\,°F$.

Contact: Theodore B. Gass
Code 822 detailed to 293

Sponsor: Instrument Engineering Branch

Mr. Theodore Gass, a mechanical engineer, has one year of service with the Wallops Flight Facility. He holds a BSME degree from The Georgia Institute of Technology.

THE SYSTEMS IMPROVED NUMERICAL FLUIDS ANALYSIS CODE

Currently, only a few computer programs exist that model fluid heat transport systems. Most of these have been written for the purpose of modeling the operation of a specific type of heat transport device or system. The Systems Improved Numerical Fluids Analysis Code (SINFAC) is a computer program being developed for modeling the steady-state and pseudo-steady-state performance of many sizes and types of single and two-phase heat transport systems.

The program utilizes the Systems Improved Numerical Differencing Analyzer (SINDA), which functions as the driver program from which modular routines are called. These routines determine the thermodynamic state of the working fluid in many types of thermal control components. The components that can be modeled include heat exchangers, radiators, mechanical pumps, capillary pumps, mechanically and thermally controlled reservoirs and pipe fittings. The program allows the user to simulate individual or combinations of components in addition to complete thermal loops. Thus, capillary pumped loops as well as mechanically pumped systems can be modeled. Even combinations of these two types of systems, known as hybrids, can be simulated.

The program requires that the user be familiar with the development of SINDA input files and the use of the fluid loop component routines. As with most general applications programs, SINFAC requires the user to spend some time applying the program to simple cases to become familiar with the methods with which the fluid modeling system is integrated into SINDA input files. This training will also help the user become familiar with all the available SINFAC options.

The fluid loop components are modeled with equations of state rather than with SINDA's lumped parameter finite differencing schemes. This allows for the fluid solution procedure to remain independent of the thermal analysis procedure of SINDA.

A single line in the input file characterizes each fluid system component. Thus, altering the analytic performance of a component is a relatively simple task. Consequently, one of the program's primary uses is as a design tool for performing component sizing and tradeoff studies.

Contact: Russell Schweickart
Code 732

Sponsor: Office of Aeronautics and Space Technology

Mr. Russell B. Schweickart is an aerospace engineer with the Thermal Engineering Branch. He developed and implemented the thermal design of the Spartan Halley spacecraft and has been involved in the development of capillary pumped loop heat transfer systems. Mr. Schweickart received an MS degree in mechanical engineering at Stanford University, and he has three years of experience at Goddard.

THE CAPILLARY PUMP LOOP MODELER

In an effort to significantly improve the thermal management of spacecraft with relatively large heat loads and long transport distances, many two-phase heat transport systems are currently under development. Two-phase heat transport systems offer the capability of transferring greater heat loads than conventional heat transport devices and require considerably less fluid for a given amount of heat than single-phase systems. The Capillary Pump Loop (CPL) is one such two-phase loop. The principal advantage of a CPL over other two-phase heat transport systems is its ability to circulate the working fluid through the loop without moving parts and with no external pumping power.

The CPL Modeler is a computer program developed for the purpose of simulating both steady-state and transient CPL operation. This modeler can predict temperatures and operating conditions for a wide variety of CPL configurations in most thermal environments. Brief descriptions of CPL systems and the CPL Modeler follow.

A CPL consists of multiple parallel capillary evaporators attached to a common vapor header, a vapor transport section, multiple parallel condensers, an optional subcooler section, a liquid return line, and a reservoir. The reservoir is required for fluid management and saturation temperature control. The unique features of CPLs are the capillary evaporator pumps. Each pump contains a porous polyethylene cylinder, or capillary wick, in which surface tension forces act to draw the working fluid to the heated evaporator surface.

The CPL Modeler predicts temperatures and pressures for the CPL system given CPL design parameters and a thermal description of the CPL environment. In addition, the modeler predicts system failure as a result of operating limits, including two high-power limitations. The first of these occurs when the power density at the heated evaporator surface is too large. The second happens when the pressure drop around the loop exceeds the maximum capillary pressure rise possible in the wicks. The modeler also predicts system failure as a result of inadequate heat dissipation in the CPL condenser.

The CPL Modeler program combines the functions of three different software packages to make modeling of CPLs a relatively simple task. These packages are the Systems Improved Numerical Differencing Analyzer (SINDA), a widely used thermal analysis program; the Transportable Application Executive (TAE), a user interface program developed at Goddard; and a set of operations and pressure analyzer routines. The modeler requires the input of a SINDA file that describes the CPL environment. This file is generally different for each system being modeled and must be created by someone with a knowledge of SINDA. Apart from this, no programming knowledge is required to run the modeler.

Once a SINDA file describing the CPL environment has been written and the CPL parameters (i.e., line sizes and diameters) are known, the modeler can be executed. TAE menus are used to enter the parameters describing the CPL. The definition of the CPL parameters are given not only in the CPL Modeler's User's Guide, but also in information screens that can be accessed while running the modeler. Many of the parameters have default values that suffice for some applications. Once the parameters are entered, a single command is used to convert this CPL data to SINDA input file format and combine this file with the SINDA input file developed earlier. This merged file is submitted to the SINDA thermal analyzer as the final step in the modeling process. The modeler returns two output files: one lists the CPL fluid and spacecraft temperatures, and the other lists the user-entered CPL parameters and the pressure of the fluid at each point in the fluid loop.

The program has been tested extensively by modeling currently operational CPLs and comparing modeler predictions with actual test results. Two operational CPLs have been modeled to date. The first is a CPL flight experiment flown on Space Shuttle Mission STS-61C in January 1986. The second is a CPL tested at GSFC that can pump 10 times more heat than the flight experiment. The comparisons have been used to verify the modeler and to determine a method for selecting a computational time increment that the user should apply to minimize the computational run time while still achieving a reasonable amount of accuracy.

Contact: Russell Schweickart
Code 732

Sponsors: Office of Space Station and Office of Aeronautics and Space Technology

Mr. Russell B. Schweickart is an aerospace engineer with three years of experience at Goddard with the Thermal Engineering Branch. While at Goddard, he has developed and implemented the thermal design of the Spartan Halley spacecraft and has been involved with the development of capillary pumped loop heat transfer systems. He received an MS degree in mechanical engineering at Stanford University.

SURFACE TENSION CONTAINED LIQUID CRYOGEN COOLER

Cooling on-orbit sensors and instruments to temperatures between 10 and 120 °K is often a technically difficult task. In many applications, a mechanical cryocooler requires too much power, is too bulky, is too expensive, or has other drawbacks. A passive cooler design that uses a cryogen to provide the cooling power is often preferable. However, this approach also has difficulties. The cryogen must be restrained in the tank to keep it from being expelled out the vent by its boil-off gases. Until now, the solution has been to use a Solid Cryogen Cooler (SCC), which freezes the cryogen in place, away from the vent line. Freezing is accomplished through the use of cooling coils or mechanical pumps on the ground, and the cryogen is kept frozen on-orbit by allowing space to pump on the cooler.

Recent NASA experience with the SCC has demonstrated several operational difficulties. The first is the requirement to keep the cryogen in a frozen state before launch, which has led to complicated support equipment and procedures for cooler servicing. Using a solid cryogen results in a decrease in the overall reliability of the system and raises numerous safety questions involving failures resulting in the cryogen melting before launch. Finally, the SCC would be nearly impossible to service on-orbit, an important consideration for the Space Station era.

A new approach is being developed to solve the problems of spaceflight cryogenic cooler complexity, ease of servicing, and on-orbit replenishment. This new concept is known as the Surface Tension Contained Liquid Cryogen Cooler (STCLCC). In this type of cooler, the cryogen remains in the liquid phase throughout the mission. Instead of being frozen in place, the cryogen is restrained to a known location in the cooler by being absorbed into a sponge. This sponge material must have several unusual properties, including insensitivity to cryogenic temperatures, small pores to increase the surface tension effect, large interstitial free volume to maximize the amount of cryogen carried, low density to minimize weight, and mechanical properties appropriate to surviving the Shuttle launch and landing environment.

Several sponge materials have been tested. The most promising candidate is a derivative of the amorphous silica material used for Shuttle thermal protection tiles. Principal characteristics of this material are insensitivity to low temperatures, an average pore size of 11 microns, a free volume of 96 percent, a density of 0.083 g/cm^3, and relatively good stiffness and strength. Calculations for the retention force of this material indicates that cryogen tank dimensions of over 1 m are attainable, given the requirement to restrain a full load of liquid nitrogen from moving under a worst-case on-orbit acceleration due to Shuttle maneuvers.

In translating this concept to a working design, several areas for further work have been identified. These include characterizing the wicking, dusting, and thermal transport properties of the sponge and developing a system for supporting the sponge within the cryogen tank. Procedures for maximizing fill volumes and providing pressure regulation on-orbit are also under study. A small STCLCC is under construction in support of the Supernova X-Ray Spectrometer series of sounding rocket launches out of Australia. Also, a larger generic STCLCC is in the conceptual design stage in anticipation of use with future Shuttle sortie class payloads.

Contacts: Michael E. Schein and Stephen H. Castles
Code 713

Sponsor: Director's Discretionary Fund

Mr. Mike Schein earned his BS degree in aerospace engineering from Virginia Tech and has been working in the Cryogenics Technology Section at Goddard for the last two years. He is now working on several spaceflight payloads that use cryogenics for cooling sensors in instruments or on-orbit technology development.

Dr. Stephen H. Castles, Head of the Cryogenics Technology Section, has nine years of experience at Goddard. Dr. Castles, who holds a PhD degree in physics, served as Technical Officer for the COBE Dewar and is the Goddard Program Manager for Liquid Helium Servicing. He has also designed a spaceworthy demagnetization refrigerator.

SUPERFLUID HELIUM ON-ORBIT TRANSFER FLIGHT EXPERIMENT

Many spaceflight experiments and facilities require liquid helium for cooling detectors, instruments, or entire facilities. Some of the major projects that currently use or may use liquid helium are the Infrared Astronomy Satellite, the Cosmic Background Explorer, the Space Infrared Telescope Facility, the Advanced X-Ray Astrophysics Facility, the Particle Astrophysics Magnet Facility, the Large Deployable Reflector, and the Gravity Probe-B. In most cases, the depletion of the liquid helium within the facility dictates the lifetime of the experiment. To extend this lifetime, the stored liquid helium must be replenished.

The Superfluid Helium On-Orbit Transfer Flight Experiment (SHOOT), an attached Shuttle payload, will demonstrate the core cryogenic technology required for liquid helium transfer in space. Critical components such as the superfluid pump, liquid-vapor phase separators, transfer lines, astronaut compatible transfer line couplers, motor-operated cryogenic valves, and fluid acquisition devices will be developed for the zero-gravity environment. The technology developed and demonstrated in flight by this experiment will be incorporated into the Superfluid Helium Tanker (SFHT) for the replenishment of liquid helium from the Shuttle and, ultimately, from the Space Station.

The SHOOT system consists of two dewars, an interconnecting transfer line, and both flight and ground electronics to perform the operations necessary to meet the objectives of the mission. The method to effect the transfer of helium is the thermomechanical pump, a simple electrically operated device that works because of the unique properties of superfluid helium. It is made up of a fine porous matrix and a heater. Laboratory tests conducted at the GSFC on a full-scale thermomechanical pump have demonstrated flow rates of up to 600 L/h and delivery pressures of up to 480 torr, controllable by the power applied to the heater. Transfer efficiencies between 90 and 99.9 percent, depending on the tank temperature and back pressure, were achieved. To determine the amount of helium transferred, another feature unique to superfluid helium will be used. Its extremely high thermal conductivity (much higher than that of pure copper, for instance) allows a simple heat capacity measurement to be made on the liquid within the tank. Coupled with the well-known specific heat of superfluid helium, this gives the mass remaining. GSFC has developed electronics to apply heat and accurately measure the temperature rise, allowing a mass gauging precision of 1 to 3 percent.

All of the other critical components are being developed and tested by the GSFC either in-house or under contract. These components include normal and superfluid helium phase separators, cryogenic valves, and fluid acquisition devices capable of supplying the superfluid helium to the pump at rates exceeding 500 L/h in the zero-gravity environment. With the exception of the superfluid helium phase separator, each of these components represents new cryogenic technology.

The SHOOT payload is scheduled for flight in mid-1991 on the Hitchhiker version of the Shuttle Payload of Opportunity Carrier. A schematic of the payload/carrier configuration is shown in the figure.

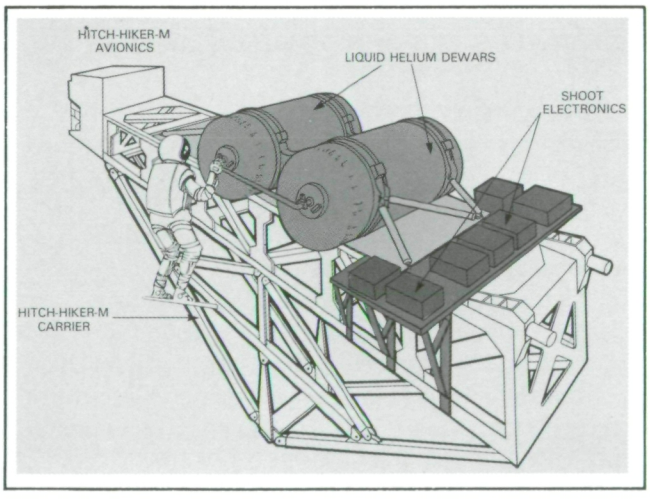

The SHOOT flight experiment on the Hitchhiker-M carrier.

Contacts: M. DiPirro, S. Castles, and O. Figueroa
Code 731

Sponsor: Office of Space Flight

Dr. Michael DiPirro, who joined Goddard in 1980, is Technical Investigator for the SHOOT program. He received a PhD degree in physics from the State University of New York at Buffalo. Dr. DiPirro developed analytical and experimental techniques for quantifying the operation of the superfluid phase separators used in IRAS, COBE, and future helium users in space.

Dr. Stephen H. Castles, Head of the Cryogenics Technology Section, has nine years of experience at Goddard. Dr. Castles, who holds a PhD degree in physics, served as Technical Officer for the COBE Dewar and is the Goddard Program Manager for Liquid Helium Servicing. He also designed a spaceworthy demagnetization refrigerator.

Mr. Orlando Figueroa, currently with the Cryogenics Technology Section, has 9½ years of experience at Goddard. Mr. Figueroa, who completed graduate studies in mechanical engineering at the University of Maryland, has supported balloon-borne and spaceflight programs including the Heat Capacity Mapping Mission and the Cosmic Background Explorer. He is currently the SHOOT Manager.

STAR★BUS TECHNOLOGY DEVELOPMENTS

The Star★Bus is a brassboard packet network that is fiber optic based and targeted for advanced flight data systems. Four major technologic achievements have been inserted into the Star★Bus. First, the International Standards Organization proposed protocols for the networking and transport layers of data management were added. These layers provide for the ensuring of end-to-end errorless data communications and for connection-oriented transmissions. Users of a connection-oriented data channel utilize the network such that all services are transparently performed, similar to a telephone voice connection. The second technology insertion was the Customer Interface Adapter (CIA). This unit provides for standard data interfaces (e.g., RS449/422, IEEE488, and RS170) to users of the network. Operating at a 10 mb/s throughput at full duplex, the CIA is flexible in configuration and performance incrementation due to its modular architecture. This modular design approach easily permits the addition of other standard data interfaces.

Third, a gallium arsenide enhancement-depletion mode gate array was developed and substituted for the high-speed emitter-coupled logic used in the receiver portion of the bus interface units of the Star★Bus. By employing 1-micron geometry and buffered field effect transistor logic on a 3000-gate array, improvements in power dissipation of about 75 percent and a three-fold increase in circuit speed have been realized. Fourth, an interface for the Fiber Distributed Data Interface has been developed. Termed a Network Gateway and operating at greater than 5 mb/s, this interface allows for data communications between heterogeneous packet networks.

The testing and integration of these technologies is now under way to deliver a working system to the JSC data management test bed. This system will be used by Space Station contractors for early identification of interface problems and to reduce risks in using evolving technologies by early testing.

Contacts: John Rende, Ken LaBel, and Glenn Unger
Code 735

Sponsor: Office of Space Station

Mr. John Rende is an electrical engineer responsible for the development of the Star★Bus for advanced data systems applications. Mr. Rende received an MSEE degree from Johns Hopkins University, and he has been with Goddard since 1963.

Mr. Kenneth A. LaBel is a graduate of the Johns Hopkins University with a BES degree in electrical engineering. Mr. LaBel has been at Goddard since 1983, working on both ground and flight data systems. He has also worked at the University of Maryland as a special student and is currently working on a Masters degree in electrical engineering at the Johns Hopkins University.

Mr. Glenn L. Unger obtained a BSEE degree from the University of Maryland in 1985. He worked at the GSFC as a co-op student from 1982–85, and he is now a full-time employee. Mr. Unger is currently working toward his Masters degree in electrical engineering at Johns Hopkins University.

SHUTTLE-BASED FREE-FLYING SCIENTIFIC CARRIER

The Spartan 300 is a study concept that is an upgraded version of the Spartan 200 series free-flying payload. The

Spartan 200 is a relatively small, low-cost payload designed for an approximately 2-day mission, being deployed from and retrieved by the Shuttle. The experiments it carries are, typically, astrophysics experiments of the type previously flown on sounding rockets.

Because of the limited manifest opportunities on the Shuttle, particularly in the wake of the Challenger disaster, the Spartan 300 carrier concept was developed. This allows the mounting of up to three multidiscipline standard-size Spartan instruments on a single Spartan 300 structure, thus taking advantage of a single manifest opportunity.

The figure shows an expanded view of the Spartan 300, which is the version that was used in the original study.

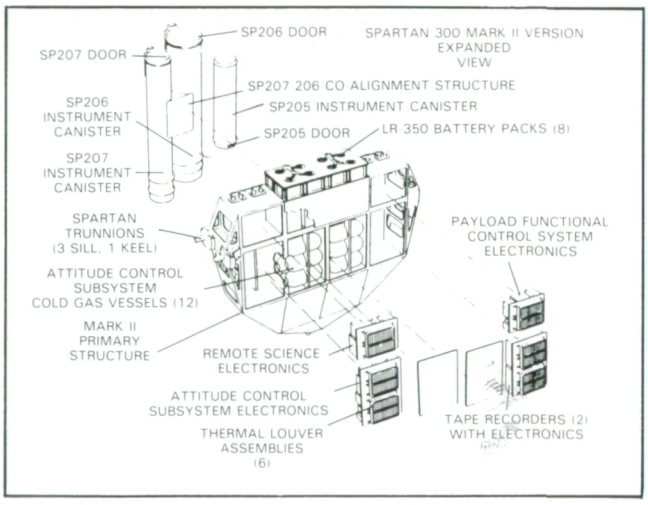

Spartan 300 Mark II version expanded view.

An important point to note is that, except for the structure, most of the subsystems are the same as those used on the Spartan 200 version. They need to be adapted for use in this new configuration, but essentially the Power System, Attitude Control System (ACS), Payload Functional Control System (PFCS), and Thermal Control System need no new developments to transfer from the 200 series to the 300 series. The power system is a series of LR-350 battery packs (up to eight can be contained in the 300 structure). The ACS is a cold gas system providing rotational attitude control only, no translational capability. In the 300 study concept, 12 gas bottles were baselined. As a result of the substantial increase in consumables allowed on the 300 carrier versus the 200 carrier, the nominal mission length can be extended to 4 days (instead of 2 for the 200 series Spartans).

All data are recorded on a tape recorder, as there is no RF link to the Shuttle or ground. The possibility of providing an RF link was examined, however, and it is a feasible option for a future enhancement.

The structure itself is a lightweight, across-the-bay structure of semimonocoque (stress skin) closed-box type construction. It provides a high stiffness and torsional rigidity-to-weight ratio with a high degree of redundancy. It is being designed to carry 2000 lbs of science payload. A major advantage of this structure is its light weight—estimated at about 1000 lbs.

The figure indicates the three strawman payloads used in the study, called SP205, SP206, and SP207. A shared-mission timeline approach was used in examining the feasibility of flying three instruments on a short-duration mission. Due to the extended mission duration of the Spartan 300 versus the Spartan 200, it was determined that the instruments could get nearly as much science time and sometimes more, depending on the assumptions used for experiment observations, as the 200 series currently provides—certainly enough to do a creditable science mission.

Adaptations of the Spartan 300 concept are currently being studied for use on the Space Station. This employs the same philosophy of a relatively low-cost, short-duration free-flyer providing a carrier for science missions in space. In this scenario, however, the carrier would be based on the Space Station and perhaps provide a unique capability to do science missions in the early phases of Space Station development.

Contact: Scott Lambros
Code 742

Sponsor: Office of Space Science and Applications

Mr. Scott Lambros, who holds a BS degree from Rutgers University, is an aerospace engineer. During most of his eight years at Goddard, Mr. Lambros has been involved with mission analysis.

TECHNIQUES

MULTILAYER INSULATION WITH MICROMETEOROID AND SPACE DEBRIS PROTECTION

The Energetic Gamma Ray Experiment Telescope (EGRET) for the Gamma Ray Observatory includes a large plastic scintillator as an outermost active detector. This scintillator must be covered by a light barrier and a multilayer thermal blanket. To minimize the production of background gamma rays by cosmic-ray interactions in this thermal blanket (through neutral pi meson production), the amount of material in the blanket must be kept small. At the same time, this blanket must offer protection against micrometeoroids and space debris, which could penetrate the material and leave a light path to the scintillator. Such a light leak could effectively render the scintillator useless under the full solar brightness. This problem has become more acute with the realization by groups at Goddard and the Johnson Space Center that the flux of man-made debris in space is now greater than the flux of natural micrometeoroids.

To offer more protection against these small, high-velocity particles without adding too much material to the outer layers of EGRET, the EGRET group decided to adapt the bumper concept used on other spacecraft. An outer layer of material is spaced about an inch away from the inner layers by a low-density space-qualified foam material. A particle hitting the outer layer will probably break up or vaporize. Any remains of the original particle that penetrate the outer layer will be dispersed in the separation layer, so that the inner layers can stop them more easily. Calculations based on models developed by the Johnson group indicate that the bumper design offers over 100 times better protection than the original multilayer thermal blanket.

Contact: David J. Thompson
Code 662

Sponsor: Office of Space Science and Applications

Dr. David Thompson is a Co-Investigator on EGRET. He received a PhD degree in physics from the University of Maryland and has been a part of Goddard since 1972.

TIME OF FLIGHT DIGITAL CONVERTER

A time-to-digital converter has been developed for space-flight application by using existing techniques, but with newer, faster hardware, and incorporating some new techniques (vernier ramp). This time of flight (TOF) unit measures the time period (0 to 500 ns) of the passage of an ion between two channel plate detectors. The method used for the time-to-digital conversion is a standard technique: logic is used to convert a start and stop pulse to obtain a pulse whose duration is the time between the start and stop pulses. This pulse is integrated with a high-speed linear integrator whose output is a linear voltage ramp. The maximum voltage of the ramp is then held with a track and hold circuit. Lastly, this is fed to a flash analog-to-digital converter.

The TOF unit is also to be used for a pulse height-to-digital conversion in conjunction with optical coupling across a high voltage. On the high voltage side of the optocoupler, a pulse height is converted to a digital pulse whose width is proportional to the amplitude of the pulse height. The pulse is then transmitted across an optocoupler to the time-to-digital converter. The advantage of this technique is that there is no degradation of pulse duration by aging or temperature characteristics of the optocoupler as there would be for an analog voltage transmitted across the optocoupler.

When the time-to-digital converter is used in the TOF mode, a seven-bit flash converter is used, which has a resolution of 1 part in 128. For a 500-ns range, this yields a 4-ns resolution. A modification has been incorporated into the converter, which subtracts a selectable time period from the start-stop time interval. In addition, the ramp slope of the integrator is also selectable so that the net effect is that a window has been created for a time of flight period; i.e., a delay and ramp slope is selected for a particular time range, rejecting other times and improving the resolution by the same factor as the increase in the ramp slope. If the ramp slope is increased by a factor of eight, the resolution is increased from 4 ns to 0.5 ns. The vernier modification provides a window capability that can look at portions of the time spectrum in high resolution. The TOF unit can do repeat conversions at a 1.5-μs interval. In-flight calibrations (automatic or by

command) are done with crystal-controlled preselected start-stop time intervals.

The integrator is the weak link in time resolution in the nanosecond range because of temperature drift problems. A vernier modification has the advantage of minimizing temperature stability problems in the same proportion as the reduction in window size. Using a finer resolution flash converter, i.e., an 11-bit converter with resolution of 1 part in 2048, yields results no better than the temperature stability of the integrator, which after temperature compensation, still had the integrator as the limiting factor of the converter. A variable width window and a variable delay one shot for delaying the integrator starting time are under design.

The vernier TOF will have the following options:

- Locking out redundant TOF data when looking for some infrequently occurring data of interest
- Sweeping the window across the TOF range in high resolution (0.25 ns) (window width 31.25 ns)
- Search in wide-open mode (500-ns window) followed by adaptively sweeping areas of high activity in high resolution (0.25 ns)
- Skipping around the TOF range in a high resolution (narrow window) mode in a (pre- or from the ground) programmed sequence
- Wide-open mode (window 500 ns) with 4-ns resolution
- Range of 5 in window widths covering 31.25, 62.5, 125, 250, and 500 ns
- Range of 16 in window start times in increments of 31.25 ns

Contact: Charles V. Moyer
Code 692

Sponsor: Office of Space Science and Applications

Mr. Charles Moyer is an electronics engineer with the Interplanetary Physics Branch of the Laboratory for Extraterrestrial Physics. Mr. Moyer, who has 20 years of experience at Goddard, holds an MSE degree from George Washington University.

DEVELOPING DESIGN GUIDELINES FOR ROBOTICALLY SERVICEABLE HARDWARE

Design guidelines for robotically serviceable hardware are being developed by the Mechanical Engineering Branch at Goddard. To demonstrate the guidelines, an existing spacecraft module was redesigned. A mock-up of the Hubble Space Telescope (HST) Scientific Instrument Command and Data Handling module was fabricated to verify the guidelines in tests with two force feedback controlled robots.

The design guidelines involve structural attachment and electrical connection methods. The HST module was chosen to demonstrate the guidelines because it contains both design elements, and its small size made robotic manipulation tests feasible. It consists of 17 electronic boxes attached to a plate, with an overall size of 3 × 2 × 1 ft high (Figure 1). The mock-up's design uses the module's original layout, physical dimensions, and Cannon and Deutsch electrical connectors. The design philosophy was that servicing requirements should follow the functional and spatial demands of a design.

A servicing operation consists of replacing an electronics box. During the operation, all parts must be constrained against rotational and translational motion. If two robot arms are used, then one arm can hold a box in place while the other arm removes its fasteners. If one robot arm is used, then one tool must simultaneously hold the box and remove its fasteners. The one-handed approach reacts fastener torques through the tool, rather than through the robot arm. However, the tool is more complex and requires a gripping point near every fastener. The two-handed approach simplifies tool design, since gripping and fastener removal functions are separated. Also, only one gripping point is required. Drawbacks of this approach are that the fastener removal torques may have to be resisted by the robot arm, and there may be possible interference between the two arms during module replacement.

The design guidelines that were applied to the mock-up are: 1) all parts must be constrained during a servicing operation; 2) fasteners and pins are the only allowable methods for constraining motion; and 3) two-handed servicing operations are allowed.

To replace electronic boxes, two problems must be solved: 1) the attachment of the box to the structure, and 2) the attachment of the electrical connectors to the boxes. The attachment problem consists of access to fasteners, manipulation of fasteners, and fastener storage. Electrical

ORIGINAL PAGE IS
OF POOR QUALITY

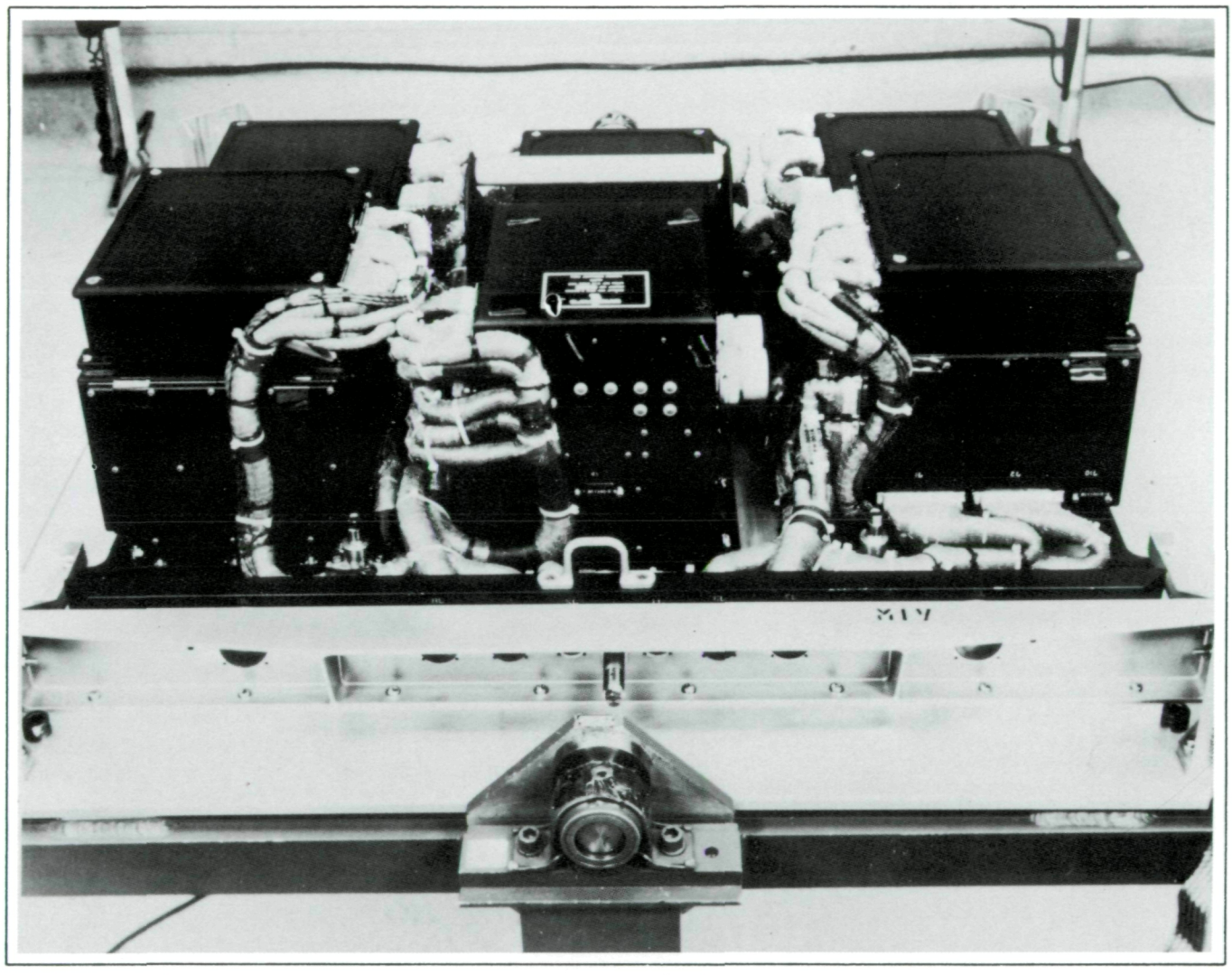

Figure 1. Hubble Space Telescope Scientific Instrument Command and Handling Module.

connectors pose problems of mating without pin damage and wiring harness manipulation. The harness spatially interferes with the box removal and is unconstrained when unplugged.

The boxes are attached to each other and to the structure by captive screws. All screws are accessible from above to facilitate their removal. Using captive screws provides for a simpler end effector because the robot needs only to turn the screw, not to grasp it. There is no need to put the screw in a temporary place while the box is being removed, thus reducing the number of steps in the servicing operation.

Three scenarios were developed to demonstrate solutions to the connector mating, wiring harness manipulation, and interference problems: rack method, mechanism method, and removable harness method. The rack method has the boxes plugging into a rack of fixed connectors (Figure 2). The mechanism method uses a worm gear and power screw to mate a movable gang of connectors to the boxes. The removable harness method has the harness designed to be removable in pieces.

The first two methods circumvent the harness by plugging the boxes into a bus. The connector shells were redesigned to facilitate insertion. The third method

ORIGINAL PAGE IS
OF POOR QUALITY

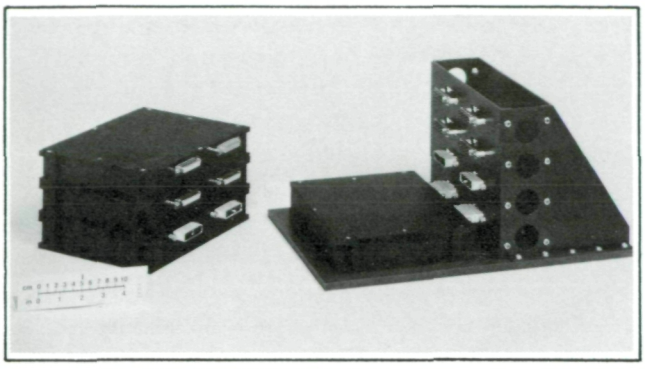

Figure 2. Mock-up demonstrating rack method.

removes the harness in pieces, solving the interference problems. One end of the harness is attached to the box, the other to an accessible location on the structure. The connectors are attached with clips, which the robot gripper releases when grasped. Removing the harness is a two-arm operation.

The mockup will be sent to the Jet Propulsion Laboratory for use in the telerobotics demonstrator, and a copy will be kept at the GSFC for use in testing autonomous robot control software and design guideline evaluation.

Contact: Timothy Premack
Code 731

Sponsor: Office of Aeronautics and Space Technology

Mr. Timothy Premack is a mechanical engineer in the Mechanical Engineering Branch with seven years of experience at Goddard. He holds an MSE degree in mechanical engineering from the Johns Hopkins University. Mr. Premack has been working on robotics projects for six years at Goddard and is currently Manager of the Automation and Robotics RTOP.

USER SPACE DATA SYSTEMS

MPP PARALLEL FORTH

The promise of massively parallel computers that provide easy access to computing power in the teraflop range (e.g., >1000 times a CRAY-1) depends on development of effective parallel high-level languages and the use of these languages to implement innovative parallel algorithms. Goddard is performing fundamental research in concurrent processing languages and algorithms with the goal of understanding and exploiting new parallel computational techniques to benefit very demanding NASA applications such as computational physics and structural mechanics, image understanding, new phenomena recognition, date compression, data base applications, graphics generation, expert systems, and robotic control.

The approach taken has been to implement a wide variety of applications on the highly parallel single-instrument-stream multiple-data-stream (SIMD) architecture of Goddard's Massively Parallel Processor (MPP) to understand the robustness of this type of computer. The MPP contains 16,384 processors, but it is the forerunner of machines with orders of magnitude more.

Last fall, the language FORTH was implemented on the MPP. A derivative of FORTH-83™, MPP Parallel FORTH incorporates serial and parallel processing, is interactive and extensible, and has low overhead, thus giving convenient access to the full processing power of the MPP.

During FY87, the MPP Parallel FORTH was used to implement and demonstrate three very different algorithms running in the MPP array unit: pure LISP, general ray tracing, and recursive function evaluation. All three are inherently irregular in nature, and none had previously been effectively mapped to the grid-like MPP architecture. The recursive function evaluation was able to take exceptional advantage of the bit-serial nature of the MPP processors.

The pure LISP interpreter evaluates the LISP functions CAR, CDR, CONS, EQ, ATOM, COND, APPLY, EVAL, EVLIST, and LAMBDA. The general ray tracing approach is based on an algorithm that finds the intersections of light rays and objects in a three-dimensional space. The computationally intensive recursive function,

ORIGINAL PAGE IS
OF POOR QUALITY

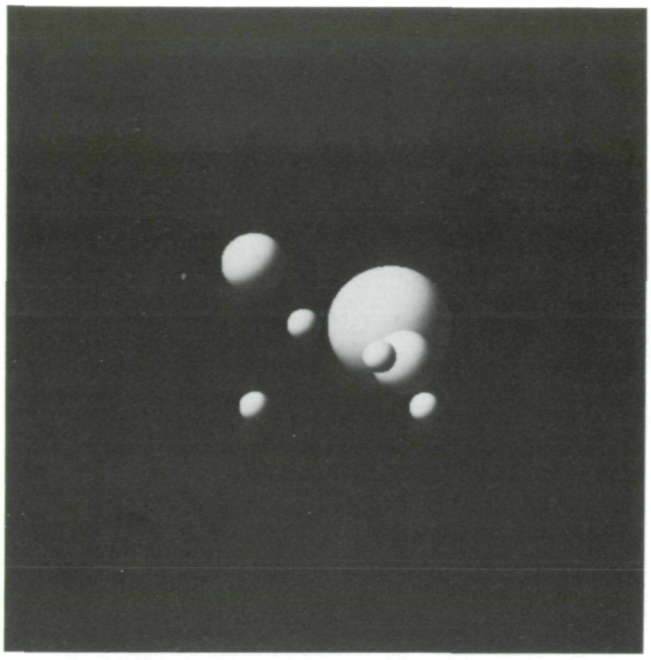

Figure 1. General ray tracing. The ray tracing algorithm finds the intersection of light rays and objects in a three-dimensional space.

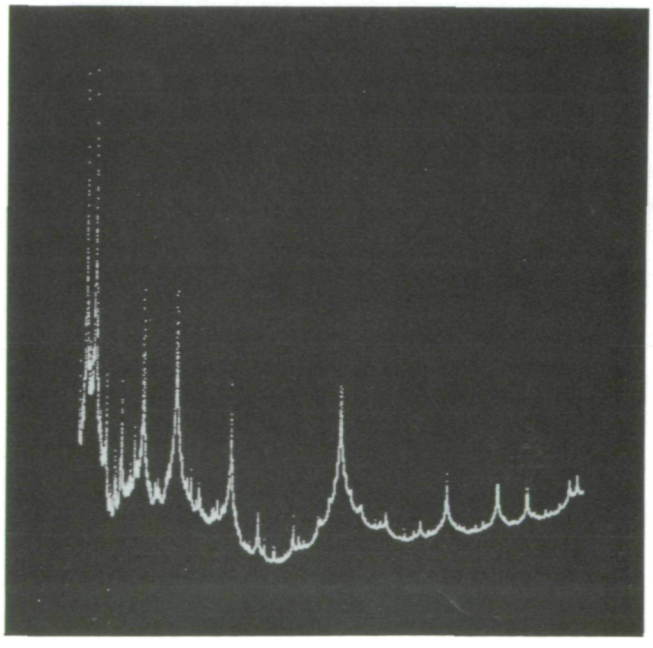

Figure 2. Recursive function evaluation. The computationally intensive recursive function, the standard deviation of j(t).

the standard deviation of j(t), was parallelized and executed on the MPP 4000 times faster than on a VAX-8650. Future plans include applying an enhanced version of the ray tracing to physical simulations such as foliage canopy modeling and to visualization of scientific data. In addition, we will develop a data base concept that takes advantage of the characteristics of highly parallel architectures.

MPP Parallel FORTH is easier to program in than MPP Pascal, the initial MPP high-level language. It takes far fewer words to write a program in MPP Parallel FORTH than it does to write the same program using MPP Pascal. Because a programmer can start subroutines as though they were the main program, it is easy to maintain and to debug both user programs and the FORTH compiler. To date, MPP Parallel FORTH users have encountered only a few minor bugs in the language, and these problems were easy to find and correct.

The SIMD parallelism that can be exploited on the MPP uses a single control unit and multiple arithmetic/logic units. The SIMD approach is very different from most of the multiprocessor systems that are multiple-instruction-stream multiple-data-stream. The control of a SIMD machine is much simpler because there is only one control program, and communication between processors is synchronous and simple. A standard serial FORTH system is implemented on the MPP control unit, and parallel extensions that execute simultaneously in all 16,384 arithmetic/logic units have been added under a new vocabulary called PARALLEL. Context switching between the serial and parallel vocabularies is accomplished by using the FORTH words '{' and '}'. This allows the user to redefine serial words as analogous parallel words, giving MPP Parallel FORTH the facility to treat parallel programming as though it were serial. For example, + normally means to add two scalar numbers located in the control unit, but in the parallel context '{+}', the + means to add two 128 by 128 arrays of numbers located in the MPP array unit.

Implementation of FORTH on the MPP was inspired by Dick Fahey, Arne Henden, Dan Klinglesmith, and Archie Warnock, astronomers from Goddard's Laboratory for Astronomy and Solar Physics, who convinced the author that FORTH would be a good language in which to program the MPP. The development of MPP Parallel FORTH has demonstrated how easy and straightforward it can be to extend a serial language (i.e., FORTH) to support parallel processing on a SIMD processor such as the MPP.

Contact: John E. Dorband
Code 635

Sponsor: Office of Aeronautics and Space Technology

Dr. John E. Dorband is a computer scientist with two years of experience at Goddard. He holds a PhD degree in computer science from Penn State University, and he is interested in concurrent processing, computer language, and artificial intelligence processing.

DISTRIBUTED ACCESS VIEW INTEGRATED DATABASE (DAVID) SYSTEM

It is extremely difficult for a space or earth scientist to perform research with multidisciplinary data sets, primarily for two reasons. First, the scientist who wants to access data from different facilities must learn several different access methods because of the diversity of computers (e.g., IBM, VAX, and SUN), operating systems [e.g., IBM OS, VAX/VMS, UNIX (Berkeley), and UNIX (AT&T)], data base management systems (e.g., ORACLE, INGRES, IMS, and RIM), communications options (e.g., ARPA Net, SPAN, Local Area Networks), and data distribution facilities (e.g., Infrared Processing and Analysis Center, National Space Science Data Center, and Space Telescope Science Institute). Second, even in an environment with a standard set of computers, operating systems, data base management systems, and communication options, there is often no on-line facility that helps the scientist locate which available data sets are relevant to a particular problem. Currently, the identification of data sets that are germane to the scientist's problem often comes to the scientist from either trial and error or word of mouth. As a result of these problems, much of the scientist's labor is spent away from actual scientific research.

Fundamental research is being conducted on the data base uniformization problem so that NASA space data users can access data independent of its physical distribution and specific organization. A system, called the Distributed Access View Integrated Database (DAVID), is being constructed on top of existing data bases/data base management systems. Below the DAVID system will be constructed interfaces to data bases/data base management systems that enable the DAVID system, and consequently the user, to communicate with the disparate data bases. On top of the DAVID system will be a library layer that will enable users to find and access data as though they were finding and accessing literature in a library.

This year's accomplishments have occurred in three parts. The first (and major) part involved the building and testing of the basic DAVID software. Some of this (C language) software runs on each of the computers partaking in the DAVID system. These modules are DAVID Generalized SQL Primitives, Host Language Interface, Generic Cluster Access, and File Access. Another portion of software runs primarily on an AT&T 3B/2, which has been designated as the "DAVID Machine" and which coordinates DAVID processing on each local area network. These modules include Terminal Interface, Generalized SQL Translation Package, Constraint Realization, View Integration Package, Scheduler, Installation, and Backup. In the coming year, we plan to develop Version 2 of many of these modules.

The second part involved building and testing interfaces between the DAVID system and underlying data bases and data base management systems. Some of these included some astrophysical source catalogues, as well as ORACLE and INGRES data base management systems. Each data set requires a corresponding DAVID definition together with fetch, insert, delete, and update commands. When interfacing a data base management system (e.g., ORACLE), one interface will work for all the data bases in the management system. Otherwise, an interface has to be built for each individual data set (e.g., IAPC Astrophysical catalogues). In this coming year, we also

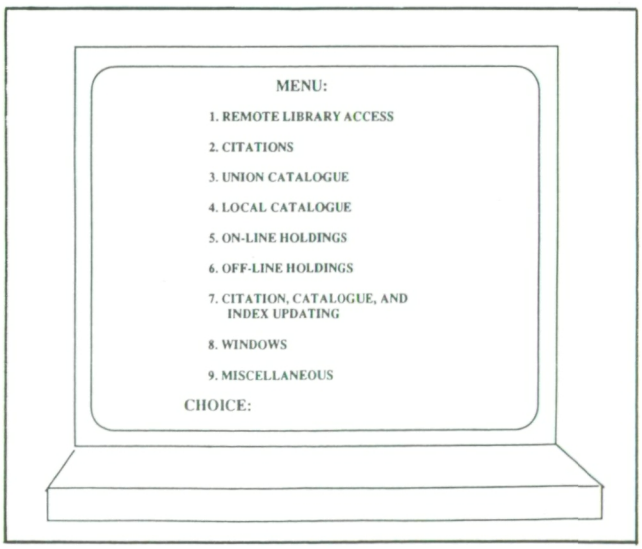

Distributed Access View Integrated Database (DAVID) system library concept.

plan to study the problem of semiautomating the construction of such interfaces.

The third part involved designing the detailed software specifications for a library layer on top of the DAVID system. In the design, each local area network becomes logically viewed as a library (see figure). The user normally begins in the "Citation" option (2) to locate data sets needed to solve a particular research problem. Next, the "Union Catalogue" option (3) tells the user which library has copies of the desired data. The user can also employ the Transfer function of the "Remote Library Access" option (1) that enables movement of the information obtained as the result of the union catalogue search to his local library.

At each local library, the "Local Catalogue" (4) option tells the user where each data set can be found in the local library (i.e., local area network). If the data is not on-line, then the "Off-Line Holdings" option (6) enables the user to borrow or loan the data system just as in an ordinary library. If the data is on-line, the user can use the "On-Line Holdings"(5) option to browse through a data set and build subsets of the data base in terms of pointers to the data records. The "Reproduction" option of the "On-Line Holdings" (5) option then converts the pointer subsets into other data sets for permanent storage or possible transfer over the network. The "Remote Library Access" option (1) allows users to either remotely logon, transfer data sets, send requests for off-line loans, or send requests for reproduction to other remote libraries. The "Citation, Cataloging, and Index Updating" option (7) allows the update of data in the citation and (local and union) cataloging options and adds new entries into the indexes of the individual data sets. Finally, the "Windows" option (8) allows the user to simultaneously access two libraries and pass information between the two.

Contact: Barry E. Jacobs
Code 634

Sponsor: Office of Aeronautics and Space Technology

Dr. Barry E. Jacobs is a senior research computer scientist with two years of service with Goddard. Dr. Jacobs, who holds a PhD degree from New York University, has published widely in the areas of data bases and mathematical logic.

CDAW-8: PROTOTYPE PROGRAM IN COLLABORATIVE DATA ANALYSIS

The Coordinated Data Analysis Workshop (CDAW) program sponsored by the National Space Science Data Center (NSSDC) is a unique experiment in enhancing a traditional workshop format of presentations and discussions by enabling participants to simultaneously access and interactively display relevant data.

The CDAW program began in the late 1970s as one approach to dealing with space science problems of large or global scale and complexity. The goal of the CDAW program has been to develop (and utilize) tools and techniques for the assembly and use of data from a multitude of sources and involving a wide cross section of the interested scientific community to attack such problems. Collaborative data analysis of this general nature is planned as an essential part of many of the new NASA programs for the 1990s. A prime example is the joint United States/Japan/Europe International Solar Terrestrial Physics (ISTP) program, where a veritable armada of spacecraft are to be deployed in a concerted attempt to piece together the continuing puzzle of dynamic processes and energy/plasma flow in the Earth's magnetosphere.

The latest in the CDAW series is CDAW-8. The first full meeting of the workshop was held in September 1986 at Goddard, with further meetings in January 1987 and September 1987. The scientific focus and data selections were initially defined around the periods of 1983 when ISEE-3 was traversing the deep magnetotail of the Earth. The major scientific questions for the workshop have centered on observational tests of the near-Earth neutral line model and the formation of plasmoids in the magnetotail (e.g., Baker, D., et al., 1987), with secondary emphasis on tests of the plasma sheet boundary layer model (e.g., Eastman, T., et al., 1985) and various models of energy flow in the magnetosphere. Data from 13 spacecraft positioned at various locations and numerous ground stations are included in the data base, which comprises some 60 data sets and more than 400 separate physical parameters.

Twelve papers derived from the CDAW-8 analyses were presented in a special session at the spring 1987 American Geophysical Union Meeting in Baltimore, Maryland, and 10 papers were presented at the joint International Union of Geodesy and Geophysics/International Aeronomy and Geomagnetism Association meeting in Vancouver. The workshop focus is now on the preparation of a set of manuscripts planned as a special section in a future *Journal of Geophysical Research* issue.

Key elements in the CDAW program that anticipate ISTP science analysis include:

- An emphasis on the coordinated analysis of simultaneous data from widely separated sites and diverse instruments, including both observations and models
- The use of a common format (the Common Data Format, or CDF) as the foundation for a common mode of access to these diverse data sets
- The development of powerful graphics and data manipulation software (the Network Assisted Coordinated Science, or NACS, system) keyed to this common format for interactive access to and display of the assembled data base
- The use of a widely accessible electronic network (the Space Physics Analysis Network, or SPAN) to allow remote access to the central data base and to facilitate the exchange of data.

The combination of these technical elements allows CDAW participants to interactively examine and correlate data as ideas occur during the workshop discussions. The participants can continue and extend these analyses from their home institutions between formal meetings of the workshop via SPAN.

The common format used for the data includes self-description of data set contents and the natural accommodation of multidimensional and gridded data (see Treinish, L., and Gough, M., 1987, for greater detail on the definition of CDF). The NACS analysis software allows a full range of selection, averaging, and computation on variables in the data base as well as device-independent graphics including histograms, two-dimensional X-Y plots, three panel plots with multiple traces/plot, mapped contour plots, spectrograms, and pseudocolor image plots. The NACS executive/user interface is built on the Goddard-developed Transportable Applications Executive (TAE) with commercial software packages running under TAE to realize data manipulation and display. Further evolution in user interfaces, data algorithms, modeling support through integrated access to advanced array processors, and an experimental distribution of the NACS system to remote user sites/workstations are all planned.

Advanced preparation has begun for a new CDAW series focused on data collected during the Polar Regions Outer Magnetosphere International Study period, to include conjugate imagery of the Earth's poles and simultaneous solar-wind and magnetotail measurements. Also, a high priority within NSSDC is to extend the CDAW concept beyond a traditional focus on solar-terrestrial physics into new and broader discipline areas, e.g., atmospheric sciences and astrophysics. Possible topics under consideration include the general problem of the Antarctic ozone, global cloud cover data collected under the First International Satellite Cloud Climatology Program Regional Experiment, and a coordinated analysis of data related to Supernova 1987a.

Contact: Robert E. McGuire
Code 633

Sponsor: Office of Space Science and Applications

Dr. Robert McGuire is a space physicist with the Central Data Services Facility of the National Space Science Data Center. He is interested in the physics of particle acceleration and propagation at the Sun and in interplanetary space. Dr. McGuire holds a PhD degree in physics from the University of California at Berkeley and has 11 years with Goddard.

AUTOMATED TRACKING OF ICE MOTION FROM SYNTHETIC APERTURE RADAR IMAGES

Studies of sea ice in the polar regions are important because they support both scientific and marine pursuits. Sea ice forms irregularly shaped objects called floes that move and/or deform (i.e., break up or join together) due to ocean currents and surface winds. Tracking the motion of ice floes is very helpful in studying ocean currents, surface winds, and ice morphology and in providing timely navigational information. Spaceborne Synthetic Aperture Radar (SAR) provides the potential for frequent, economical, wide-area coverage at a high resolution (e.g., 18 m) unconstrained by cloud cover or lack of daylight. Traditionally, the ice-floe tracking has been handled by manually identifying corresponding shapes in pairs of images obtained a few days apart and drawing vectors between them. The manual identification and vector plotting are aided by providing convenient display facilities. This is a highly labor-intensive and time-consuming procedure. The purpose of the present investigation is to develop techniques to automate this image correspondence problem.

The starting point for this development was the local cross-correlation algorithm used in the Hierarchical Warp

Stereo Analysis reported by Strong and Ramapriyan in last year's Research and Technology Report to determine elevation from stereo image pairs. There are several major differences between the image-matching problems for elevation determination and ice motion tracking. In this discussion, the combined effects of elevation and motion are not considered. The terms stereo image pairs and ice image pairs are used to imply, respectively, that only elevation and only motion effects are present. Stereo images are obtained from a pair of different incidence angles. Objects are stationary, and the elevation variations cause locally variable distortions between the images. On the other hand, the ice images are obtained with the same incidence angles in the different passes. Any differences due to elevation changes are negligible, and the locally variable distortions are primarily due to motion. In stereo image pairs, the disparity (the coordinate differences between corresponding pixels in the two images, also called parallax) is one-dimensional and relatively small (a few tens of pixels). The disparities in the ice image pairs are two-dimensional and can be quite large (a few hundred pixels), with the magnitude depending on the time lapse between the images. In addition, the ice images can have locally variable rotations and differences due to deformation of features.

Because of these differences, the algorithm used for ice motion tracking is a combination of global and local cross correlations. The two-dimensional correlation function computed between the entire reference and test images is called the Global Correlation Function (GCF). The GCF generally has several local peaks, each corresponding to a translation (without rotation) of one or more significant image features in the test image relative to the reference image. Therefore, if the test image is translated by the amount corresponding to the coordinates of a local peak in the GCF, then the corresponding significant image features will overlap in the two images. After this translation, a local correlation process is used wherein a small (e.g., 21 × 21) template neighborhood of each pixel in the reference image is correlated with corresponding neighborhoods in the test image within a slightly larger (e.g., 25 × 25) search neighborhood to generate a Local Correlation Function (LCF) at each pixel. A large magnitude of the peak of the LCF at a given pixel indicates that the pixel belongs to one of the significant image features. The displacement of the peak from the center of the search neighborhood provides a small correction to the translation obtained with the GCF. By repeating this process for each major local peak in the GCF, all the significant unrotated features are identified. Rotated image features are identified by first rotating the test image by a given amount and then evaluating the GCF and LCF. Since there is no *a priori* knowledge of the amount of rotation, and different features may have rotated by different amounts, the algorithm rotates the test image by small (e.g., 0.5°) increments between specified bounds and repeats the computations. Then, for each pixel, the best translation and rotation are determined and stored.

Due to the computationally intensive nature of this algorithm, it has been implemented on the Massively Parallel Processor (MPP) at GSFC's Space Data and Computing Division. The global correlation is implemented with two-dimensional Discrete Fourier Transforms of 512 × 512 arrays. An example of ice-floe matching is shown in the accompanying figures. The images used here were acquired by the Seasat SAR in 1978 and cover an approximately 65 × 65 km area near Banks Island in the Beaufort Sea. Figures A and B show the reference and test image, respectively, obtained approximately 3 days apart. The images are 512 × 512 pixels in size and are results of averaging 7 × 7 pixel neighborhoods of the full resolution data received from the Jet Propulsion Laboratory. Figure C shows the GCF with two major peaks for 0° rotation. Figure D shows the reference image highlighting the identified features obtained using the two major peaks in Figure C. Figure E shows the result of repeating the algorithm with rotation angles at 1/2° increments between −10 and 20°. The time required with the MPP was 10 minutes. Figure F shows the results of processing a subsection of the above images taken from the upper left hand corner of the reference image and the left center portion of the test image at a higher resolution (averaging over 3 × 3 pixel neighborhoods). More of the smaller ice floes are identified in Figure F. In a fully automated procedure, higher resolution subsections will be selected with the rotation and translation data provided from the low-resolution images.

Contacts: J. P. Strong and H. K. Ramapriyan
Code 636

Sponsors: Office of Naval Research and the National Oceanic and Atmospheric Administration

Dr. James P. Strong, who holds a PhD degree in electrical engineering and computer science from the University of Maryland, joined NASA in 1963. In 1972, along with D. H. Schaefer, he developed the concepts for TSE computers for which he and Mr. Schaefer received two patents. Dr. Strong is currently developing algorithms for image analysis and signal processing on the Massively Parallel Processor.

ORIGINAL PAGE IS
OF POOR QUALITY

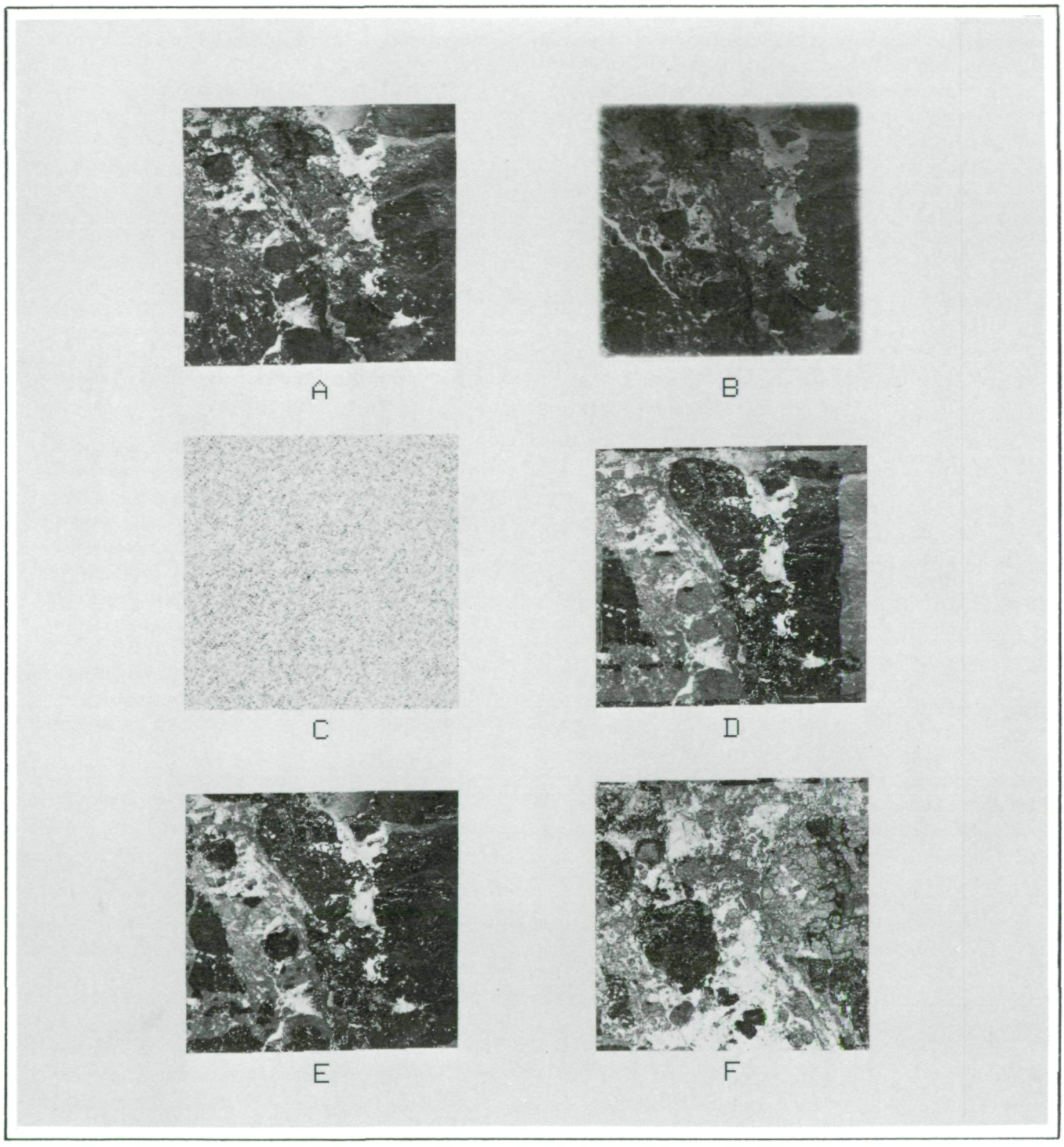

Figure A: Seasat SAR image of Banks Island in Beaufort Sea, Orbit No. R1396A. Figure B: Seasat SAR test image of Banks Island in Beaufort Sea, Orbit No. R1439D. Figure C: Global Correlation Function (GCF) from reference and test image for 0° rotation of test image. Figure D: Regions corresponding to highest two peaks in the GCF of Figure C. Figure E: Regions detected after applying algorithm to images with rotation of test image between −10° and 20° at 0.5° increments. Figure F: Regions detected after applying algorithm to higher resolution subimage with rotation of test image between −10° and 20° at 0.5° increments.

Dr. H. K. Ramapriyan, an electrical engineer with a PhD degree from the University of Minnesota, is Head of the Information Analysis Facility. He has also served on Flight Assurance Review committees for Landsat and GOES-IM. His professional interests include spaceborne remote sensor data processing, information extraction, image analysis, data compression, and parallel processing. Dr. Ramapriyan, who has nine years of experience at Goddard, has received several NASA awards for his work on remote sensing and image analysis.

PILOT CLIMATE DATA SYSTEM

The Pilot Climate Data System (PCDS)—as well as the system to which it is evolving, the NASA Climate Data System (NCDS)—is an interactive scientific information management system for locating, accessing, manipulating, and displaying climate research data. The Data Management Systems Facility of the GSFC's National Space Science Data Center developed this system and continues to enhance it to support NASA-sponsored scientists at universities and government agencies. The collection of data supported by the system continues to expand and currently consists of over 20 data sets. The size of the user community is also growing, with increased access being provided via new nodes on the Space Plasma Analysis Network.

The PCDS/NCDS provides functions that enable researchers to locate data of interest, preview data with graphical and statistical methods, and extract subsets for further analysis at their own sites. These functions are described below:

- Obtain comprehensive descriptions of several climate parameter data sets and the associated sensor measurements from which they were derived.
- Obtain detailed information about the temporal coverage and volume of data sets that are readily accessible via the PCDS/NCDS.
- Extract portions of a data set with criteria, such as time range and geographic location, and output the data to on-line disk files (in a special data set independent format), a user terminal, a system printer, or a tape.
- Access and manipulate the data in these data set independent files, and perform such functions as combining the data, creating a subset of the data, or averaging the data.
- Create various graphical representations of the data stored in the data set independent files.

The PCDS/NCDS provides these capabilities via the integration of several general purpose software packages—some commercially available, others developed by different groups within GSFC—with specialized software for reading the supported data sets. The result is a system that is both easy to use and flexible and that can easily be expanded to either provide support for additional data sets or provide additional functional capabilities.

Most of the development work during FY87 concentrated on completing the transition to the NCDS. Some of the accomplishments are listed below:

- A tutorial for university support personnel was held in October and was attended by representatives from the University of Maryland, the University of Michigan, and the Pennsylvania State University. The knowledge obtained by the attendees should allow them to assist students in using the system to complete homework assignments and term projects and to assist professors in using the PCDS for classroom demonstration of concepts. A memorandum of understanding was written with the University of Maryland to set up a program that increases the effectiveness of teaching meteorology by using the PCDS.
- A user support office was established, and several accounts were given to new users of the system. Several presentations and papers were prepared with data from the system:
  - John Dutton presented "Modeling the Future of Planet Earth" at the American Meteorological Society Conference on Climate Variations: Climate Dynamics Update in March 1987.
  - Paul Newman and Mark Schoeberl published "October Antarctic Temperature and Total Ozone Trends from 1979–1985" in *Geophysical Research Letters* (November 1986).
  - Richard Goldberg, Gilberto Tisnado, and Richard Schofield presented "Characteristics of Extreme Rainfall Events in Northwestern Peru during the 1982–83 El Niño Period" at the American Geophysical Union Chapman Conference on El Niño in Guayaquil, Ecuador, held October 27–31, 1986.

ORIGINAL PAGE
COLOR PHOTOGRAPH

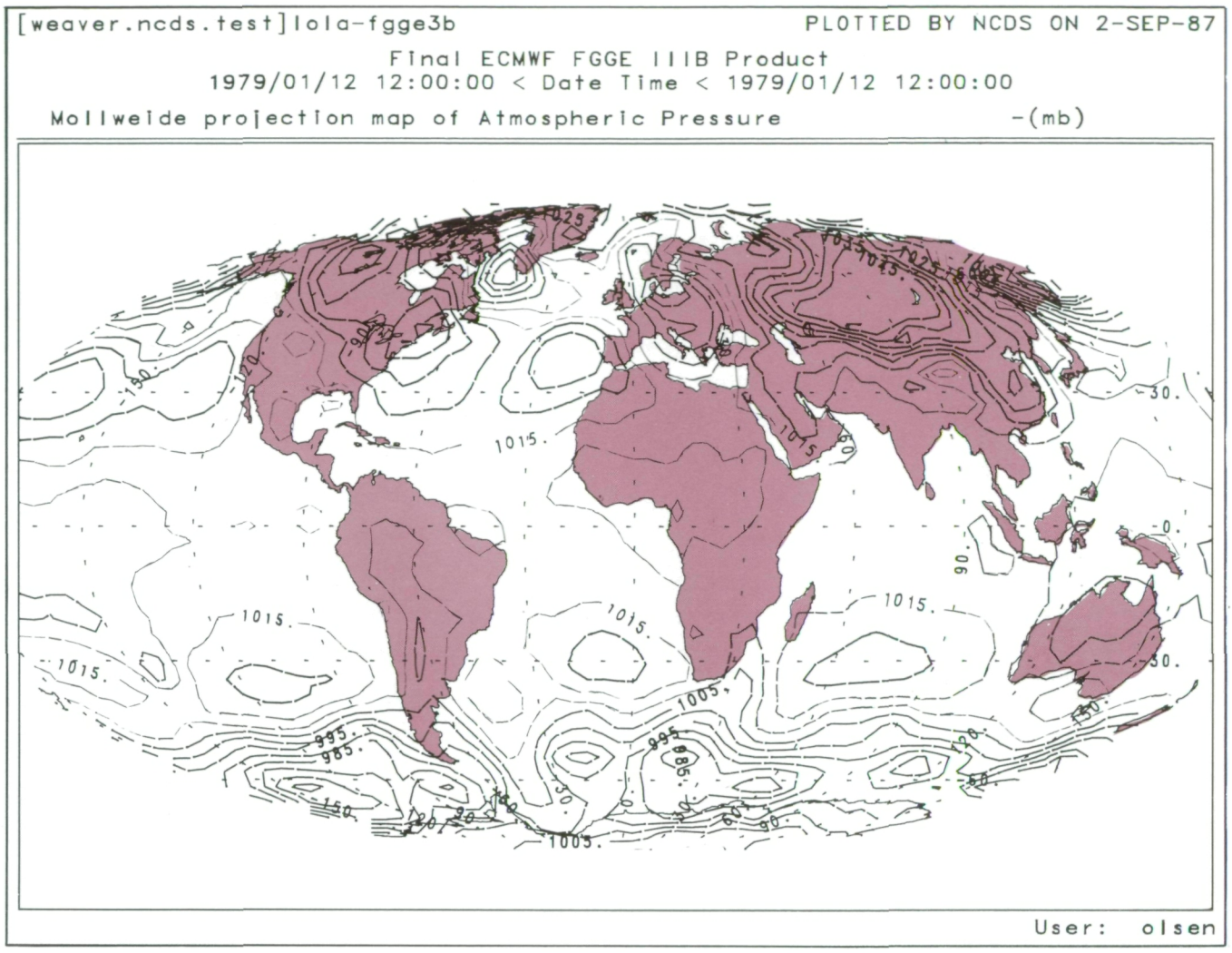

Surface pressure contour plot from PCDS's latest acquisition—reanalyzed First Global Atmospheric Research Program Global Experiment from European Center for Medium Range Weather Forecast data.

— Lola Olsen presented "The Pilot Climate Data System: A Powerful Research Tool" at the American Association of Geographers 83rd Annual Meeting in Portland, Oregon, held April 22–26, 1987.

- A primer has been written and widely distributed in draft form for comment.

- The entire on-line catalog was updated, and the data holdings were expanded. Over 300 additional tapes were made available to users.

- Support was provided for several additional data sets, such as the Nimbus-7 Earth Radiation Budget Solar Analysis Tape and Seasonal Averages, Solar Maximum Mission Active Cavity Radiometer Irradiance Monitor I Solar Irradiances, Solar Activity Data from the Geophysical Data Center, Nimbus-7 Solar Backscatter Ultraviolet, and Nimbus-4 Backscatter Ultraviolet Compressed Profiles.

- Plans were made for supporting the International Satellite Cloud Climatology Project (ISCCP) Stage C data, programs for reading preliminary data tapes were written, and feedback was given to the producer.

- Cooperative efforts established with First ISCCP Regional Experiment (FIRE) investigators led to a

refined standard data format that is to be used for the submission of data products to the PCDS, the designated FIRE central archive. PCDS provided sample tapes in this format, including software for generating required tape headers to the investigators.

- A new version of the system was released that included several simple enhancements and corrections. This also involved the incorporation of new versions of underlying software packages.

The PCDS provides several labor-saving utilities, allowing projects to perform significant research even with limited budgets. It also serves as a model for future information management systems in a variety of disciplines.

Contact: Mary G. Reph
Code 634

Sponsor: Office of Space Science and Applications

Ms. Mary Reph is NCDS Project Manager with the Data Management Systems Facility of the National Space Science Data Center. Ms. Reph, who received an MA degree from American University, has been with Goddard since 1978.

SNOW DATA SETS OVER THE COLORADO RIVER BASIN FROM THE NIMBUS-7 SMMR

Seven years (December 1978 through May 1985) of snow parameter data sets over the Colorado River Basin from the Nimbus-7 Scanning Multichannel Microwave Radiometer (SMMR) have been generated. Snow data have been computed only for the months December through May for each year. The snow parameter computed from SMMR data has been gridded onto a map with a spatial resolution of approximately 0.2° in latitude by 0.2° in longitude, and it covers an area of 32° to 46° north in latitude and 105° to 120° west in longitude. Each map contains 3 data days (6 calendar days) of daytime or nighttime data.

The snow parameter computed is called the Gradient Ratio (GR) and is defined as GR = (18V − 37V)/(18V + 37V), where 18V and 37V are brightness temperatures measured by 18 GHz and 37 GHz vertical polarization channels, respectively. The GR values are useful for determining spatial distribution of snow water equivalent in the area snowpack, and they may be used to predict the timing of the onset of snow melting. In the past, GR values have been provided in near real time to the U.S. Geological Survey's snow experiment teams to assist in the selection of pertinent sites for the special surface measurements.

Two forms of data sets are available: a digital data set generated by the IBM 3081 and stored on a 6250-bpi magnetic tape, and ASCII character maps stored on floppy diskettes (1 diskette for 1 year of data). These data sets can be obtained from GSFC Code 630.2.

Contact: Daesoo Han
Code 636

Sponsor: Office of Space Science and Applications

Dr. Daesoo Han is Manager of the SMMR Information Processing Team for the Nimbus project. Dr. Han, who holds a PhD degree from Yeshiva University, has been with Goddard for one year.

PRODUCING AND ARCHIVING A GLOBAL OCEAN BASIN CHLOROPHYLL DATA SET

The Nimbus-7 Coastal Zone Color Scanner (CZCS) acquired nearly 66,000 images between October 1978 and June 1986. This data set, which uses a consistent sampling strategy and single processing technique, represents the most comprehensive source of ocean color measurements to date. For most of the world's oceans, the changes in ocean color that can be measured from space are directly related to changes in near-surface phytoplankton pigment concentrations. Phytoplankton, the microscopic plants that grow in the upper, sunlit regions of the oceans, form the base of the marine food web, and knowledge of their distribution and abundance is critical for many branches of marine ecology and fisheries science. In addition, since the fixation of carbon in the ocean by photosynthesis is about equal in magnitude to that occurring on land, an understanding of the temporal and spatial distributions of phytoplankton biomass and primary production is necessary to better assess the role of the ocean in the global carbon cycle.

The Nimbus Project Office, in collaboration with the NASA/GSFC Laboratory for Oceans and the University of Miami/Rosenstiel School of Marine and Atmospheric Science, is processing all the CZCS imagery to produce a Global Ocean Basin Chlorophyll Data Set and to provide easy access to the data products by the oceanographic

ORIGINAL PAGE
COLOR PHOTOGRAPH

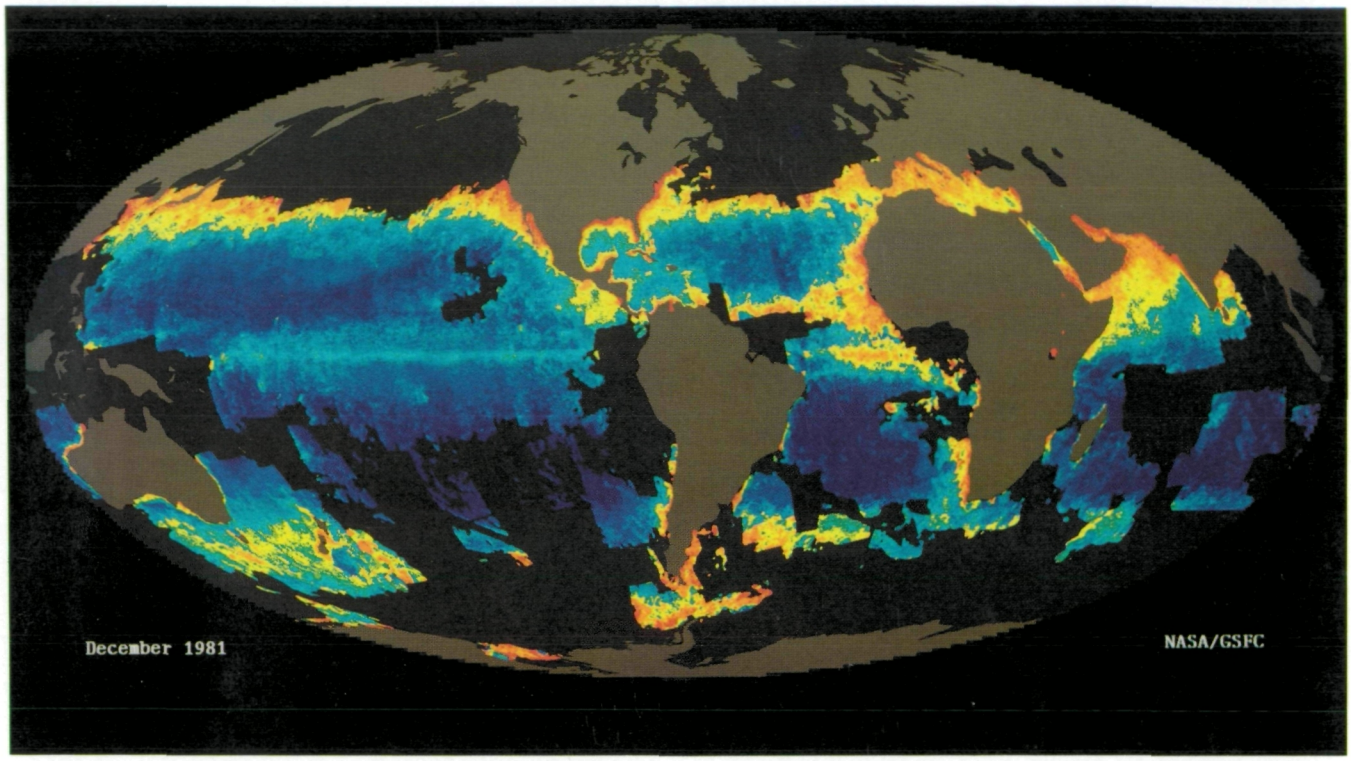

Synoptic picture of global distribution of phytoplankton.

community via NASA's National Space Science Data Center (NSSDC).

An image processing/analysis system utilizing recent advances in digital optical disk storage technology has been developed and is now operational in a full production mode. Approximately 3000–4000 CZCS images are being processed each month, and the data products are being archived on digital optical disks. The transfer to optical disk storage has several advantages. For instance, data storage media has been significantly reduced. Approximately 150–200 1600 bpi tapes containing the Level-I CZCS data can now be stored on a single 12-in. optical disk platter. With the incorporation of an optical disk autochanger (jukebox), the system will have on-line access to nearly 160 gigabytes of data, which will greatly facilitate the data flow through the system. At the current rate of production, the entire CZCS data set will be processed within 2½ years.

The data products will be archived by NSSDC in coordination with the NASA Ocean Data System (NODS) and the Pilot Climate Data System (PCDS). In addition to archiving the original Level-1 data, the NSSDC archive will also contain the Level-2 data products of the derived geophysical parameters in satellite swath coordinates and the Level-3 Earth-gridded products of these parameters. Composites of the key parameters (pigment concentration and diffuse attenuation coefficient) over weekly through annual time scales will also be archived along with the relevant compositing statistics. A catalog and inventory will be maintained on-line for remote access, search, and ordering of the data products. A portion of the data set, primarily the Level-3 composites, will be maintained on-line by the digital optical disks.

The accompanying figure represents the first truly synoptic picture of the global distribution of phytoplankton ever produced. The 928 individual CZCS scenes, each 800 × 1600 km, acquired during December 1981 were processed and averaged to produce this image. The colors represent the concentration of phytoplankton pigments (chlorophyll) in the near-surface waters, with deep blue to yellow to orange to red indicating higher concentrations. High phytoplankton abundance, or blooms, exists where nutrient-rich deeper waters have been mixed into the well-lit surface layer, such as along the continental shelves, in the northern Indian Ocean, and in the equatorial zones in both the Atlantic and Pacific Oceans. The apparent blooms in the Mediterranean and northern

Atlantic and Pacific seen in this image are suspect because the algorithms that were used to process this particular data set were not capable of dealing with the low Sun angles present during the northern winter. Recent algorithm developments, however, have greatly improved the accuracy of the data retrievals at low Sun elevations and have been incorporated into the processing system.

Contact: Gene Carl Feldman
Code 636

Sponsor: Office of Space Science and Applications

Dr. Gene Carl Feldman, who received a PhD degree in oceanography at the State University of New York at Stony Brook, has worked on the Nimbus project for 1½ years.

POLYNOMIAL REPRESENTATIONS OF GREY-LEVEL IMAGES

Grey-level images can be represented in a highly structured way through polynomials of two variables. Addition and multiplication among grey-level images can be defined such that these images become commutative semigroups under these operations.

An image A is composed of pixels, each shaded with a level of grey denoted by a real number between zero and one; the larger numbers represent darker grey levels. If Z denotes the integers, then an image A may be represented as

$$A = \{(x,y) \in Z \times Z \mid \mu_A \in [0,1]\}$$

where $\mu(x,y)$ denotes the grey-level of pixel (x,y).

Image addition can be defined as follows: let A and B be grey-level images.

Then

$$A \oplus B = \{(x,y) \in A \cup B \mid \mu_{A\oplus B}(x,y) = \min(\max(\mu_A(x,y),\mu_B(x,y)), \max(1-\mu_A(x,y),\ 1-\mu_B(x,y))\} \quad (1)$$

This operation is commutative and associative, thus making the set of all grey-level images a commutative semigroup under $\oplus$. Note that in the binary case (with μ = 0 or 1), the addition reduces to the "exclusive OR" addition. That is, in binary the set-theoretic addition of A and B can be represented as $A \oplus B = (A \cup B) \cap (\bar{A} \cup \bar{B})$ where $\bar{A}$ and $\bar{B}$ are the inversed images of A and B, respectively.

Multiplication grey-level images A and B can be defined by

$$A*B = \sum_{\substack{(x_1,y_1)\in A \\ (x_2,y_2)\in B}} (x_1 + x_2,\ y_1 + y_2) \mid \mu_{A*B}(x_1 + x_2,\ y_1 + y_2) = \min[\mu_A(x_1,y_1),\ \mu_B(x_2,\ y_2)] \quad (2)$$

where $\oplus$ denotes the addition in (1).

Multiplication is also commutative and associative, and it makes the set of all grey-level images a commutative semigroup.

To utilize both $\oplus$ and $*$ for polynomial formation, first consider the image consisting of one pixel $x = [1,0]$ with grey-level $\mu(1,0) = a$. Then $x * x = x^2 = [1 + 1, 0 + 0] = [2,0]$ with grey-level $\mu_{x^2}[2,0] = \min[\mu_x(1,0),\mu_x(1,0)] = \min[a,a] = a$.

Hence, $x^m = [m,0]$ represents a point on the x-axis with grey-level $\mu_x(1,0 = \mu_{x^2}(m,0) = a$ preserved. In a similar manner, an arbitrary point on the y-axis can be represented by $y^n = [0,n]$ with grey-level $\mu_y(0,1) = \mu_{y^n}$ preserved. Thus, in general if m and n are allowed to be any integer, A may be represented as the polynomial

$$A = \sum_{(m,n)\in A} \mu_{mn} x^m y^n \quad (3)$$

where coefficients μ_{mn} = grey-level of pixel (m,n) and summation is defined by (1). Note that the pixel cor-

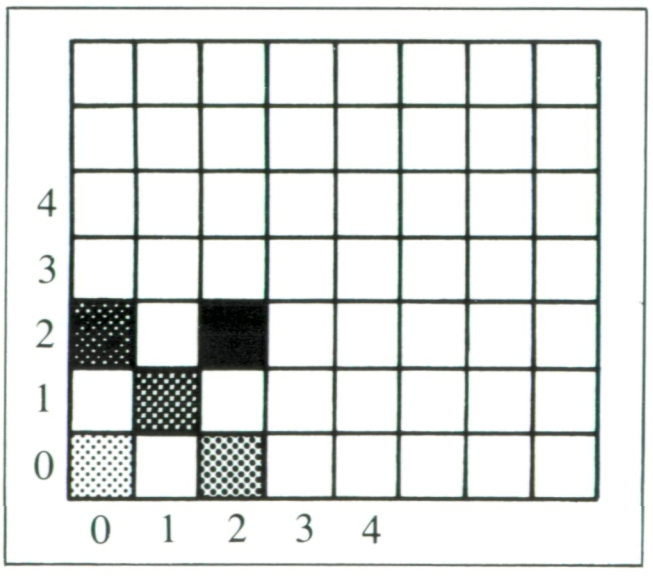

Figure 1. A = .2(1) $\oplus$ $.4X^2 \oplus .5XY \oplus .7Y^2 \oplus 9X^2Y^2$

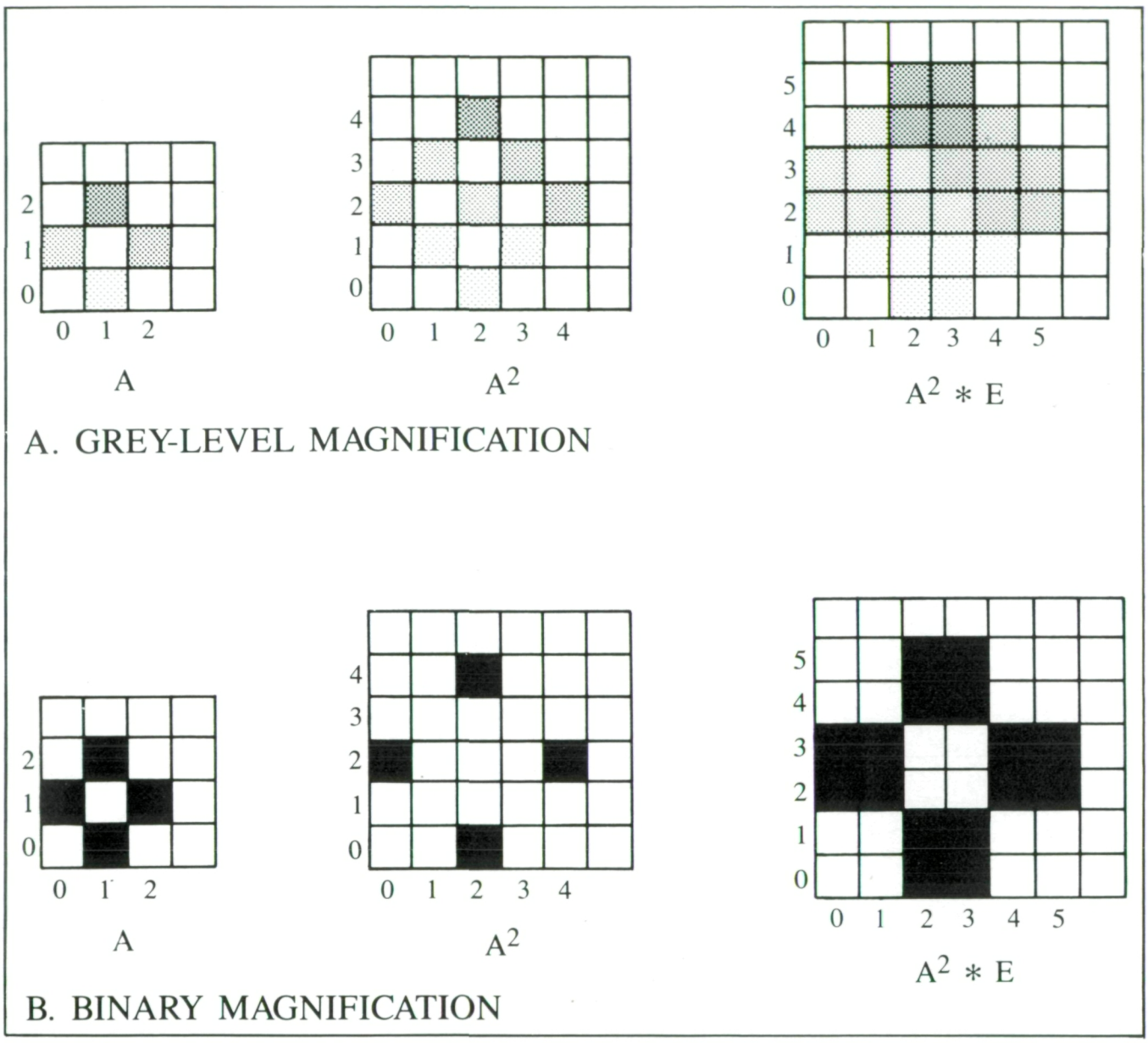

Figure 2. A = $.1X \oplus .2Y \oplus 3X^2\,Y \oplus 4XY^2$

responding to [0,0] in position can be designated as the polynomial constant 1.

Example: $A = \mu_{00}(1) \oplus \mu_{20}x^2 \oplus \mu_{11}x^1y^1 \oplus \mu_{02}y^2 \oplus \mu_{22}x^2y^2$

Figure 1 illustrates A with specific grey-level coefficients.

With the formulation of polynomials, ordered and randomized patterns of the same image can be represented in a structured way. Regular patterns or texture involving a grey-level image A can be obtained by the multiplication of A with a distributing polynomial consisting of geometric series. Randomized or irregular distributions of a grey-line image A can be achieved by the multiplication of A with a distributing polynomial consisting of a sum of monomials that describe simultaneous translations of A.

Another application area involves magnification. For example, a grey-level image A may be magnified twice by multiplying A by itself (forming A^2) and then multiplying by a binary enlarging polynomial $E = (1 \oplus X)(1 \oplus Y)$ to obtain a dense picture. This is illustrated by Figure 2.

Ongoing research is being conducted with the goal of applying these techniques to pattern recognition and contour extraction.

Contacts: Bao-Ting Lerner, Hans Thomas, and David Provost
Code 735

Sponsor: Office of Space Science and Technology

Dr. Bao-Ting Lerner is an Associate Professor of Mathematics at the U.S. Naval Academy. She was an ASEE Summer Faculty Fellow in 1987 assigned to the Robotics Laboratory at Goddard.

Mr. Hans Thomas, a student at Carnegie-Mellon University, has been a student intern and consultant at Goddard for the past three years. He is currently working with the Robotics Laboratory, developing autonomous vision algorithms.

OPTICAL DISK STANDARDS PROMOTED BY NSSDC

The Write-Once-Read-Many (WORM) optical disk technology has the potential to improve the storage and retrieval of data that is of archival quality or that is stable and frequently read. The current generation of 12 in. media holds 1 Gbyte of data (per side). The optical disks are desirable for many scientific digital data applications: interactive access to large volumes of scientific data, long-term archival, and data interchange of large volumes of data. For many of these activities, a significant impediment to the use of WORM disks is the lack of standards.

The National Space Science Data Center (NSSDC) is particularly interested in data archival and interchange via optical disks, as multi-gigabyte sets of data are due to be archived soon from the Dynamics Explorer experiments, and several other large data collections residing at research facilities need to be condensed, preserved, and archived. Existing collections of magnetic tapes have filled the space available at the NSSDC and sites of data originators. Many of these tapes are old and are susceptible to deterioration from environmental and operational causes. Thus a more compact and less error-prone media like optical disks is highly desirable. Currently, although there are national and international activities in the optical disk industry to develop standards, there is a lack of standards at all levels, and this adversely impacts data interchange.

A major interim solution to permit data interchange on optical disks between the NSSDC and research sites submitting or requesting data is the mass purchase of 40 optical disk drives initiated by the NSSDC. These drives will be distributed among the NSSDC; the Dynamics Explorer experimenters at diverse sites; and other participants at Marshall Space Flight Center, the Jet Propulsion Laboratory, and several universities. The optical drive selected is the Optimem 1000 optical drive. An Emulex host adapter provides the interface from the Small Computer System Interface (SCSI) standard protocol to Unibus or Q-bus on DEC computers. Along with this, the NSSDC is providing Software for Optical Archive and Retrieval to allow disks to be written and read with VAX/VMS Files 11 structure.

The use of the same physical equipment and the same files format permits experimenters to exchange optical platters with the NSSDC or among themselves. The use of VAX files format permits the optical platter to be read as a VAX/VMS logical device and avoids the need for rewriting the large base of extant applications software. Unfortunately, this is dependent upon a single operating system, even though the operating system is in wide usage.

The NSSDC is currently in the early phases of developing approaches and software to allow the interchange and usage of optical disks in a heterogeneous environment characterized by various vendors, disk drives, computers, and operating systems.

Contact: Barbara E. Lowrey
Code 633

Sponsor: Office of Space Science and Applications

Ms. Barbara Lowrey is Group Leader of Optical Disk Activities. Her professional interests include orbital mechanics, image processing, and astronomy. Ms. Lowrey holds a BS degree in physics from the University of New Hampshire. She has been with Goddard for 28 years and has received the NASA Special Achievement Award and a Group Achievement Award for Early Access to Landsat Thematic Mapper data.

NASA-WIDE CATALOG INTEROPERABILITY

In the past year, new emphasis has been placed on a project called Catalog Interoperability, which will provide

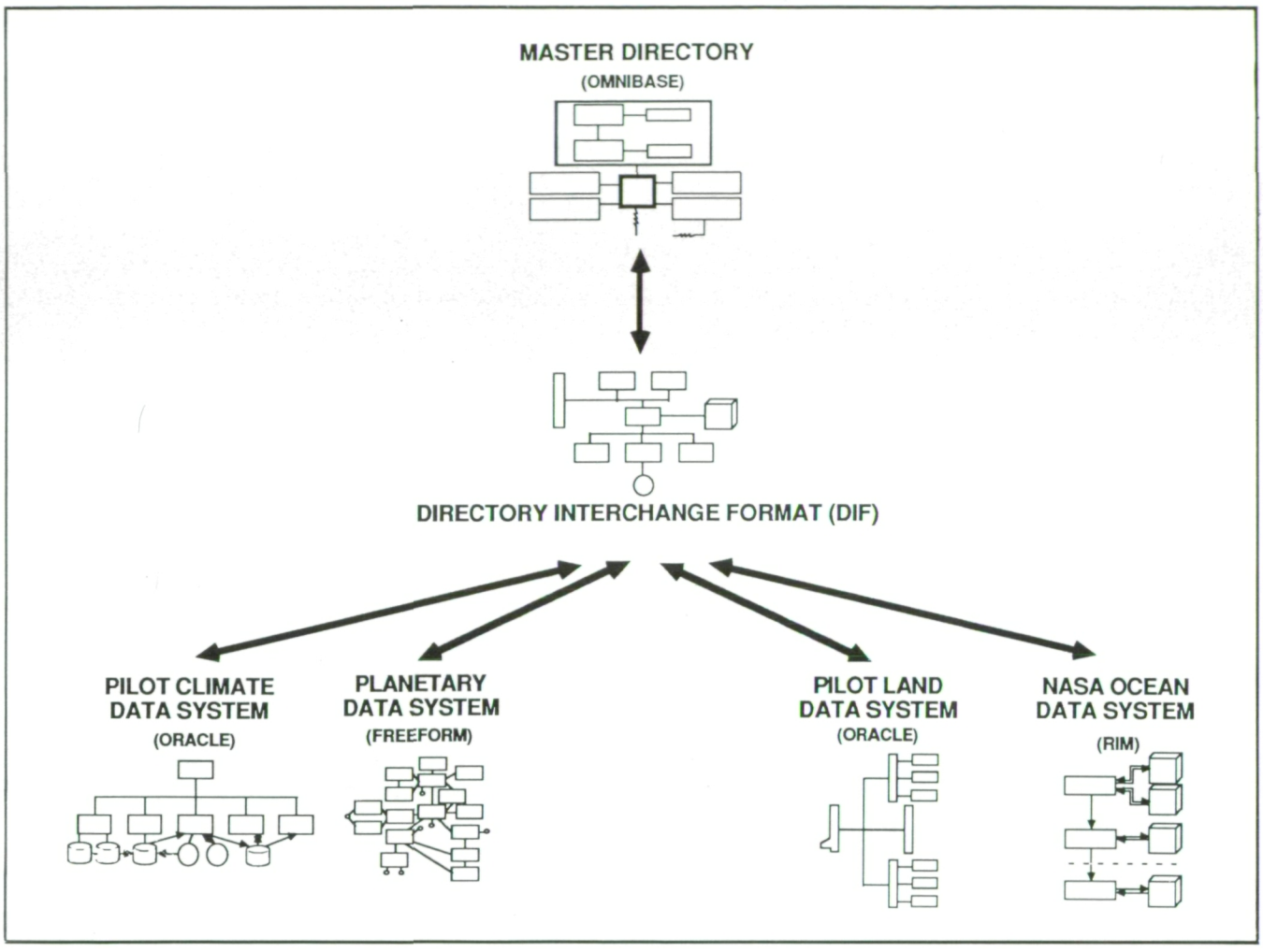

Catalog interoperability.

rapid online access to information about available data, especially NASA data, for science researchers. The goal is to enable a researcher to enter any of the interoperably connected master directory and data catalogs and efficiently find information about, and perhaps access to, useful data contained anywhere in the system. Movement toward this goal of an interoperable data information system is progressing in a step-by-step approach: taking existing data systems, linking them together, and gradually building a more uniform and unified whole that will provide the needed functionality. Three major steps are planned: creation of a master directory with brief high-level information about most of the important data sets and network links to the catalogs containing more detailed information; development of a method for passing directory-level information among the catalogs and directory to keep directory information up-to-date and to assist the user in searching multiple places efficiently; and modification to a more uniform appearance for the catalog environment to minimize the effort required of a user to use the system. The remainder of this article reports the initial achievement in this effort.

The first step, creating the master directory and links from it to the major data system catalogs, builds upon the work done previously in the creation of the Central Online Data Directory (CODD), and the National Space Science Data Center (NSSDC) Online Data Catalog System (NODCS). (See last year's report for a description of NODCS and CODD). The Master Directory, like CODD, is intended to be a directory to useful data sets across Earth or space science disciplines. The Master Directory does not contain as much information about the individual data sets as CODD, but it does allow faster expansion of the directory data base. The initial version of the Master Directory is currently available and can be

accessed via the Space Physics Analysis Network and dial-in lines. The Master Directory has links to two major discipline data systems (NASA Climate Data System and NASA Oceans Data System) as well as to several individual catalogs associated with individual data sets or a small group. This allows the user to search for more detailed information about a data set by invoking the link from the directory to the catalog and then by using the catalog software to continue a search.

The second step toward interoperability is more difficult. To keep the Master Directory up-to-date on the information about numerous data sets, it is necessary to develop an automated way of passing this information from the catalogs and data systems to the directory. This has been the first task of the Catalog Interoperability Working Group, which was formed last year from selected data system representatives to test solutions for interoperability among the participating systems. This group meets biweekly via teleconference and interacts on the many interoperability issues through electronic mail. The figure shows the present NASA participating data systems and the Directory Interchange Format (DIF) proposed to pass directory information among these systems.

The DIF is a data structure that has emerged from the discussions of the working group. It contains all of the directory information needed for a data set. When a data set is added or updated within one of the data systems, a DIF is created and passed across the network link. The DIF is then loaded into the directory data base and reviewed to assure correct and consistent content. A form of this DIF will also be used to make a directory user's search for information a little more automated. When a directory user decides on a data set(s) of interest and elects to continue a search within the lower level catalogs, the relevant search parameters used to select the data set(s) are passed to the catalog or data system through the DIF structure so that the user need not re-enter all of this information. This will improve the efficiency of the search and make the whole interconnected system a little more interoperable.

Because the Catalog Interoperability Working Group thought that additional input from potential users of an interoperable system was necessary, a Catalog Interoperability Advisory Group was established consisting of both NASA and non-NASA scientists in a variety of disciplines. The advisory group meets with the working group in semiannual workshops to discuss the progress of interoperability and make recommendations for the future.

The first workshop was held July 14–16, 1987. The requirements for the Master Directory were the main topic of discussion at that workshop. In addition, the DIF structure was discussed and plans made for its finalization. Some initial discussions were begun concerning the establishment of data system standards for the future. These standards represent the third and most difficult step toward interoperability. Once standards are established, however, the user should be able to transfer among data systems and see similarities in appearance and functionality, improving search efficiency. This may also permit automated multisystem searches to be performed wherein many data systems are searched in a single information request. The next workshop in January 1988 will discuss these plans for the future in greater detail.

Contact: James R. Thieman
Code 633

Sponsor: Office of Space Science and Applications

Dr. James Thieman, who holds a PhD degree from the University of Florida, is Manager of the Catalog Interoperability Project. His professional interests include astrophysics, specifically planetary radio astronomy and magnetospheric physic, and computer science. Dr. Thieman, a recipient of NASA's Special Achievement Award, has been with Goddard for 10 years.

SPACE COMMUNICATION SYSTEMS

TALKING TO SPACECRAFT: NASA'S NEW MULTIPROCESSING TELEMETRY AND COMMAND SYSTEM

To control and retrieve data for the next generation of orbiting spacecraft, data communication systems that meet the high-speed, compact, cost-effective requirements of the Space Station era must be built. To support this dialogue well into the future, the Data Systems Section has developed a new multiprocessor, VMEbus-based Telemetry and Command System (TAC). This system is comprised of a single card cage, utilizing application-specific very large scale integration (VLSI) components

and multiple commercially available processors, built around the widely supported VMEbus. The new system demonstrates not only a considerable reduction in size, but also a 100-fold increase in the performance/cost ratio over the existing system.

The TAC is not new to Goddard; it has supported communications between spacecraft and ground-control computers for more than a decade. The existing TACs, designed in the 1970s, support the transmission rates common during that time. Data rates in the Space Station era will far exceed the present TAC capabilities, calling for an advanced design to fill the void. The Data Systems Section completely redesigned the TAC system with advanced technologies and architecture to make it a viable system well into NASA's future, while at the same time making it smaller and less expensive.

A TAC serves as a front-end processor and interface between NASA's worldwide communications network (NASCOM) and ground Applications Processors (APs). The system links spacecraft communicating through NASA networks with Payload Operations Control Centers that house the APs. Spacecraft telemetry data and spacecraft commands are the major data flows through the TAC system, hence the name. APs generate spacecraft commands that are forwarded by the TAC to NASCOM and ultimately to the spacecraft. Spacecraft telemetry data returns to Earth via NASCOM and is preprocessed by a TAC, which formats and forwards the data to an AP.

The TAC hardware interfaces fall into four basic categories: 1) the A-Channel interfaces, which send and receive NASCOM data blocks; 2) B-Channel interfaces, which send preprocessed telemetry data to an AP; 3) the C-Channel interface, which receives spacecraft command data from an AP; and 4) the TAC operator interface from which all system setup and control information enter the system.

All data, which is external to the TAC, is transported in the standard NASCOM transfer block. When processing spacecraft telemetry data, the NASCOM interface cards (A-Channels) synchronize to the beginning of the blocks within the data stream and strip off the outer transport shell (the NASCOM header and trailer). Further processing is done on the contents of the blocks, again synchronizing to telemetry frames that are transported within the NASCOM blocks. The frames are packaged and handed to the APs by an AP interface card (B-Channel). When processing spacecraft commands, the C-Channel interface checks for errors and optionally reformats the data before routing it to the correct A-Channel for output to NASCOM.

The TAC system uses a multiprocessor architecture with two bus systems housed in a triple-height (9U) VME card cage (see Figure 1). One processor is dedicated to system control, and the other processors provide intelligence on the custom-designed channel cards. Commercially available VME cards are used whenever possible to minimize cost and engineering time. These include a Mizar 7120 containing a Motorola 68020 processor and 1 Mbyte of RAM; a 2-Mbyte DRAM card; a Winchester/Floppy Controller card to control the 20-Mbyte hard disk and 800-Kbyte microfloppy; a Communication Machinery Corporation Ethernet card and six Mizar 8115 cards, each containing a Motorola 68010 processor and 512 Kbytes of dual-ported RAM. The custom channel cards implement specific TAC functions in a unique triple-height (9U) configuration. Each channel card contains a Mizar 8115 single-height (3U) processor card connected to a double-height (6U) custom hardware card via a unique side connector (see Figure 2). All three connectors are used on the card cage backplane; the standard VMEbus on P1 and P2 and a custom data pipeline bus is on the P3 connector.

By using a dedicated data path (a custom design on the P3 connector) for transfer of data blocks and frames, separate from the VMEbus, much higher throughput is

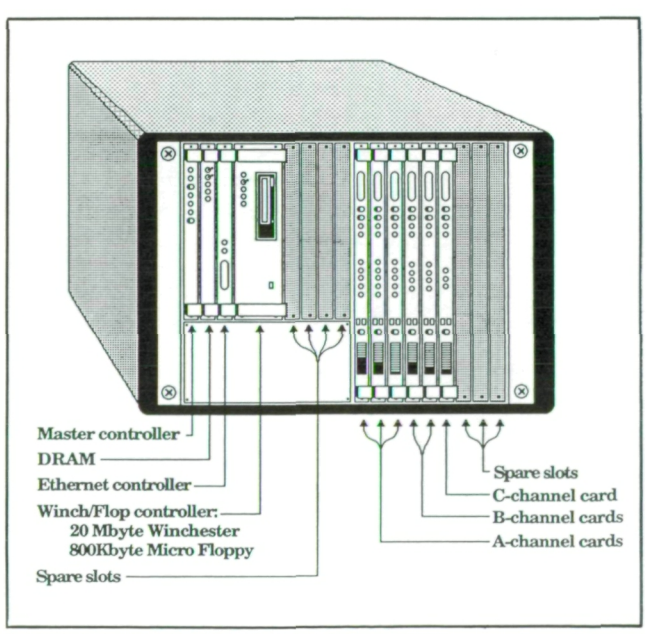

Figure 1. TAC system card cage.

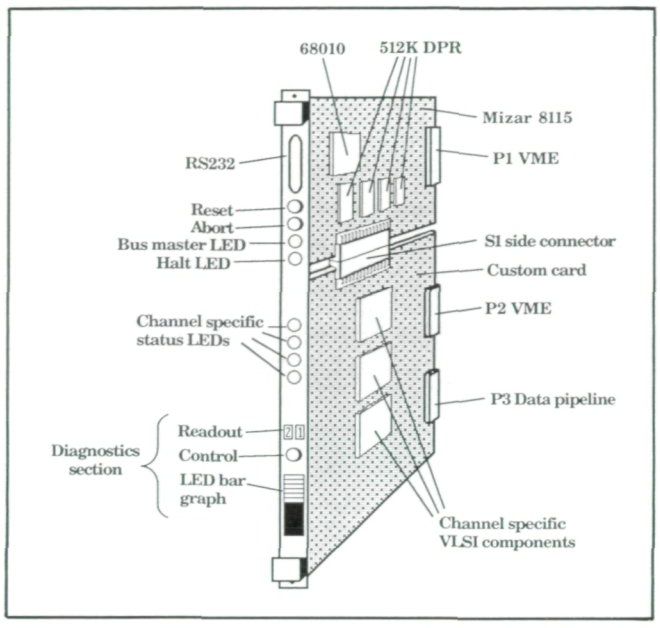

Figure 2. Typical channel card.

achieved. NASCOM data entering a channel card on the data pipeline is processed by custom-designed VLSI components onboard. The custom hardware generates interrupts to the local processor at key points in the data flow. Software onboard the channel controllers handle the interrupts, reformatting and moving data through the card.

To support information transfer between the channel and master controllers, part of the dual-ported RAM onboard each channel card serves as a gateway between the processors. The dual-ported RAM is addressable by both the channel controller locally and the master controller through the VMEbus. Both processors can simultaneously access the memory, leaving messages, without directly interfering with the other's processing. The memory area is the vehicle used by all interprocessor message passing software.

One advantage of a multiprocessor system is the ability to dedicate each processor to specific task(s). The hardware architecture partitions the software, at the top level, by processor. In the TAC system, the master controller is dedicated to system control, accounting, and status gathering. Each channel controller's software expands on the capabilities of the accompanying custom hardware; together they implement the channel's specific functions. Two considerations had to be made when designing the software at the system level. What information does each processor need to perform its tasks, and how will each processor get that information? Setup and control information entered by the operator must be transported to the associated channels; some form of information transfer between processors is necessary. Interprocessor communication software lies at the core of the TAC system software design as a resource to higher level, processor-specific software.

Because many of the Data Systems Section's future projects involve multiprocessing, VME-based designs, an important goal is to design control software that is modular, extensible, and reusable. The VLSI components are fully programmable, thereby enabling their use for other NASCOM or non-NASCOM telemetry handling projects. The multiprocessing hardware was built around the widely supported VMEbus, thereby allowing the system to be used either stand-alone or incorporated into a commercial VMEbus-based workstation like a SUN. In addition, since the VMEbus has over 3000 readily available products and more being introduced all the time, a straightforward maintenance and upgrade path will continue to exist many years into the future. The control software is implemented as a number of discrete tasks with consistent interfaces; these modules can be extracted from the TAC system and used in other systems. The software is extensible in that functions onboard custom cards can be easily added or changed. Also, entirely new cards can be accommodated by defining new commands and integrating the associated software modules into the channel controller's software.

A philosophy that includes total self-diagnosis is prevalent throughout the TAC system design. Each card performs extensive power-up self-diagnostics that include a checkout of the entire data pipeline and the components surrounding it. An in-house designed test pattern generator chip supports this testing by simulating a NASCOM data stream, which is routed through the data pipeline. This chip, which is fully programmable, once set up and started, runs autonomous of the local processor and requires no further intervention. Also, temperature, airflow, and voltage sensors monitor these critical parameters on each card. Software to support the diagnostics can be initiated and monitored through interprocessor commands.

Complete development of the new TAC system took roughly 2 years and was accomplished with an in-house manpower base. The design work in most areas was done in parallel. During the initial concept definition, the telemetry data pipeline was broken down into specific VLSI implementation blocks. These blocks were then translated into silicon gate arrays on a computer-aided-engineering workstation. Simultaneously, these same

blocks were used in the development of supporting electronics cards that control the gate arrays. The multiprocessing command and control software was designed, developed, and debugged during this period on the same commercial VMEbus processor cards that are used in the final TAC system. Most of the system software was fully developed and debugged before any hardware became available. Thus, by using this approach, most of the major system components became available at roughly the same time.

By taking advantage of current technological innovations and architectures, the new TAC is faster, more compact, and less expensive than the older designs. In the new TAC environment, processing power is increased, since many processors work simultaneously to accomplish the same job that was previously done by a single processor. The throughput of the system is further boosted by using a dedicated NASCOM data path separate from the control data path, as well as the use of VLSI gate array implementations of many NASCOM data processing functions. Memory is smaller and cheaper than it was a decade ago; this system has an abundance of memory, and thus all system and operational software can be memory resident. These same features yield nearly a factor of 10 reduction in size and cost. By designing the system in discrete, reusable modules of both hardware and software, the building blocks for future systems have been placed. The successful application of modern technologies and architecture have yielded a system that can support NASA's spacecraft communications well into the future.

Contacts: Ward Horner and Stephen Sabia
Code 521

Sponsor: Office of Space Tracking and Data Systems

Mr. Ward Horner, an AST electronic engineer with five years of experience at NASA, holds a BSEET degree from Capitol College. He specializes in the design of multiprocessing hardware and software implementations. Mr. Horner manages, coordinates, and designs a variety of sophisticated hardware- and software-oriented projects.

Mr. Stephen Sabia, a computer scientist with three years of experience at NASA, holds a BSCS degree from Towson State University. He specializes in the design and development of real-time software. Mr. Sabia does most of his work with the C programming language and works mainly in the hardware and software interface area.

AUTOMATED SIGNAL SYNCHRONIZATION FOR VIDEO MONITORS

We have designed an automated synchronization capability for a commercially available monitor. This monitor provides control rooms and ground stations with one monitor to work with many popular computer and video systems.

NASA facilities, such as control rooms and ground stations, require monitors that work at many video synchronizing rates. These facilities are supported by many types of computer and video systems that use different video synchronizing rates. The ability to use one monitor to display the output of each computer or video system is a very desirable feature, especially in multiuser environments. Commercially available RGB monitors that operate within a large range of sync rates require manual adjustments each time the video sync rates are changed. These adjustments must be made by removing the cover and using the service manual, an unacceptable time-consuming process in control rooms and ground stations. Since the operators in these control rooms are continuously switching between different computers, a monitor that makes the adjustments automatically was needed.

The Systems Research Laboratories' (SRL) 2143 19-in. high resolution RGB monitor was chosen to receive a board that automatically synchronizes (autosync) the monitor. Designed here at NASA, the autosync board is a microprocessor system that continuously checks the video synchronizing rates of the video signal. Based on the video sync rate, the processor examines a table in memory and adjusts the monitor to achieve the best picture in less than a second. The eight adjustments are the screen image height, width, horizontal centering, vertical centering, linearity, pincushioning, timing, and trapezoid. Most of these adjustments on the unmodified monitor are made with potentiometers. These were replaced by digital-to-analog converters to allow for control by a microprocessor. The timing and linearity were manual switches that have been converted to microprocessor-controlled analog switches. Also on the autosync board is an RS-232 interface to allow for the board to be trained.

Training refers to programming the autosync board to recognize the video rates to which it will have to synchronize the monitor. An untrained autosync board will not synchronize the monitor to any video signal. To train the board, a menu-driven program on an IBM personal computer or compatible is used to adjust the automated controls via RS-232. Once adjusted and a satisfactory picture is displayed, the parameters are saved in a table in

the battery back-up RAM on the autosync board. Retraining is not necessary every time the monitor is powered on, since the nonvolatile memory can last up to 10 years.

This SRL monitor with the autosync board provides NASA ground stations with adjustment-free displays. An autosync board for a video hard copier is currently being designed.

Contact: Andre Fortin
Code 532

Sponsor: None

Mr. Andre Fortin, who specializes in analog circuit design, is involved with NCC Augmentation. Mr. Fortin received a BSEE degree at the University of Dayton and is working toward an MSEE degree at Johns Hopkins. He has a year of experience at Goddard.

REMOTE PAYLOAD OPERATION CONTROL CENTER

Traditionally, the functions of a Payload Operation Control Center (POCC) are performed in a fixed location, usually a dedicated room, or rooms, of equipment. New technology permits this function to be performed on a workstation instead of a mini or mainframe computer as in the past. This concept of operating a satellite remote from Goddard is called teleoperations.

The University of Colorado has developed some generic software called the Operations and Science Instrument Support (OASIS) software package that can control instruments remotely. The software runs on a variety of computers and was demonstrated with a Digital Equipment Corporation (DEC) MicroVAX and a Heathkit robot. Presently, the University of Colorado is working to port OASIS to a SUN workstation. To demonstrate the remote POCC concept, the University of Colorado in conjunction with Code 511 developed the Remote Hitchhiker Instrument Support Environment (RHISE), which is the OASIS soft package running on a MicroVAX GPX workstation. The target project is the Ultraviolet Limb (UVLIM) experiment being conducted by the Naval Research Laboratory (NRL).

The UVLIM will be launched as an attached Shuttle payload (ASP) mission and will therefore reside in the bay of the Shuttle during the mission. Figure 1 depicts a generic ASP mission, which displays the basic lines of communication between the satellite and the experimenter. Note that in the figure, the customer ground support equipment (CGSE) is the RHISE in this case and is portable. In fact, the plan is to have the RHISE ultimately reside at the NRL with initial testing done at Goddard and the University of Colorado. An interesting fallout of this project is that testing thus far has been a distributed process with locations driven more by convenience than by the actual physical location of key equipment. That is, testing has been conducted with the RHISE at the University of Colorado and the RHISE at Goddard.

Figure 2 depicts the interface between the customer carrier ground support equipment (CCGSE), which is the basic link to the UVLIM via the ground segment, and the RHISE. Note that the RHISE can interface to the CCGSE from anywhere provided that a NASA communications (NASCOM) interface is available. Future enhancements include the possibility of interfacing to the CCGSE via other common interfaces such as telephone modems.

The RHISE, when in full operation, will send commands and receive low-rate telemetry data. It is a multiwindowed system that can be tailored easily to the particular experimenter. The OASIS system is written in Ada, and the graphics are driven by a graphics kernel system, which makes the software totally portable. The final support package will have graphics displays as specified by the experimenter and mouse selectable commanding.

As of September 1987, tests were conducted to verify the interface between the RHISE and the CCGSE, the RHISE and the UVLIM, and the NASCOM interface between Goddard and the University of Colorado. The tests remaining include testing of the NASCOM link between the RHISE located at the University of Colorado and the CCGSE located at Goddard, and the end-to-end testing of the complete link between the RHISE and the UVLIM via the CCGSE. These final two tests are expected to take place in late 1987. The only other remaining task is to finalize the user interface. The RHISE specific user interface will be done by the end of 1987. The UVLIM specific user interface will be completed when a launch date has been manifested for UVLIM and the design for UVLIM is complete.

An interface to the Mission Planning System is being planned for future enhancement. This will allow the experimenter to access mission planning. Flight dynamic information is already available via Shuttle ancillary data that the RHISE receives. Plans call for defining the data

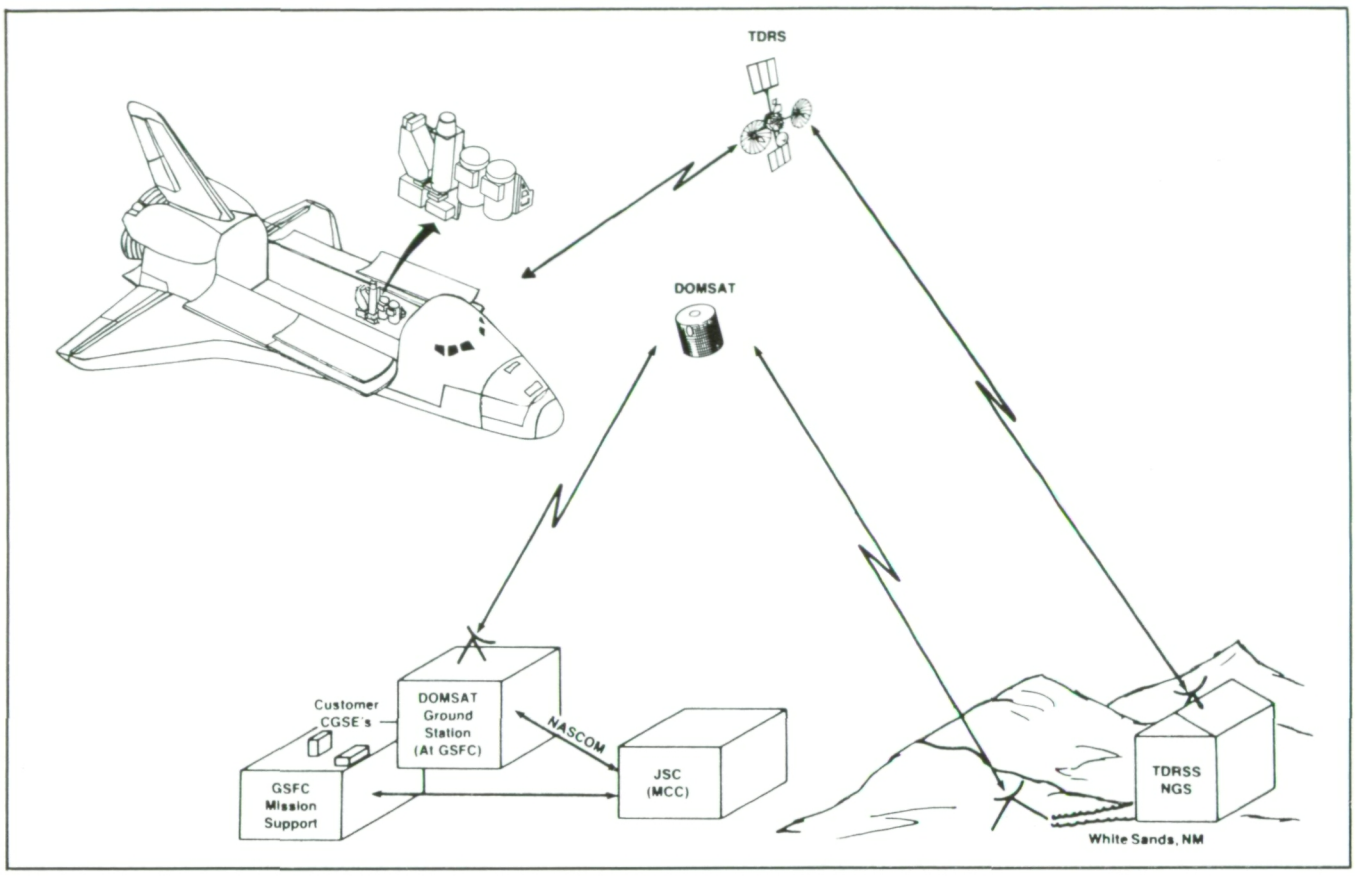

Figure 1. Basic configuration for an attached payload mission. Note that the customer ground support equipment is the RHISE.

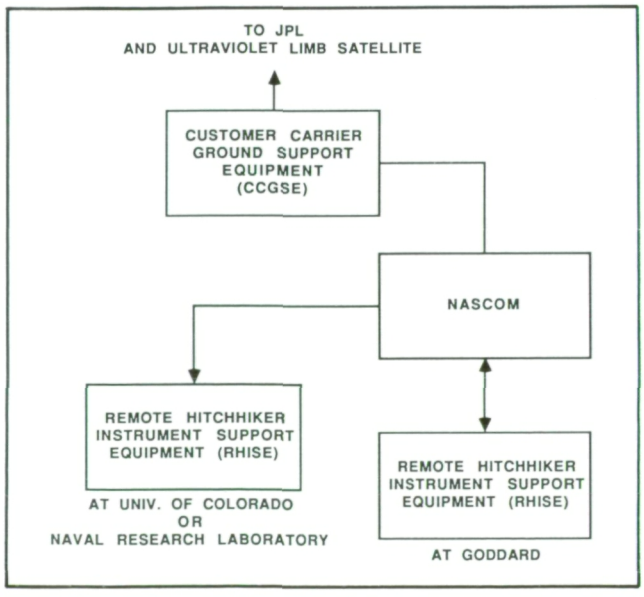

Figure 2. RHISE as customer ground support equipment.

that is available, thus allowing for future use of the data to create some flight dynamics related displays. By defining these additional interfaces, the RHISE prepares for the Space Station era in which the telescience/operations concept allows experimenters to have access to a wide range of information from many sources on one workstation.

Contact: Dan Mandl
Code 511

Sponsor: Office of Aeronautics and Space Technology

Mr. Dan Mandl works with the Control Center Systems Branch, and he is interested in computer graphics. Mr. Mandl, who holds a BSEE degree from the University of Maryland, has seven years of experience with Goddard.

LOW-COST, MICROCOMPUTER-BASED INTERACTIVE ANALYSIS SYSTEM FOR DIRECT-RECEPTION AND ARCHIVED REMOTE-SENSING DATA

A versatile hardware/software system has been developed based on the MicroVAX-II computer, the International Imaging Systems image processor, and numerous software packages developed recently for atmospheric, oceanic, and land remote data interpretation, as well as for disaster-warning-through-threat modeling. The system is a miniaturized version of a much larger system installed in Bangladesh for agro-climatic/environmental monitoring and resource management. It was developed in response to requests for a portable system of high capability that could be used in meteorological field experiments and by developing countries that needed distributed, remote-sensing data analysis capabilities at an affordable cost.

The current version of the system has the capability of directly receiving satellite transmissions of the Advanced Very High Resolution Radiometer, the TIROS Operational Vertical Sounder, and the ARGOS systems on the TIROS-N class of polar-orbiting spacecraft. The system receives these transmissions as well as by the Geostationary Operational Environmental Satellite (GOES), the Japanese Geostationary Meteorological Satellite (GMS), and METEOSAT with a low-cost, software-controlled, program-track antenna operated by the MicroVAX. The geosynchronous satellites require a larger but simpler antenna. Received data are ingested directly to the computer's disk storage, eliminating the normal requirement for a wideband analog tape drive.

The received data can be interpreted in terms of cloud imagery and cloud-top temperature, sea surface temperature, vegetation index, temperature/humidity profiles with overlays of geographic boundaries, latitude/longitude grids, and data collection platform measurements. These interpretations can be made for any portion of the globe, since also incorporated in the software is a world data base containing accurate outlines of all land features, including rivers, lakes, and islands. The computer system can also process computer tapes from Landsat, the multispectral satellite system (MSS), and the thematic mapper (TM).

Many image processing and enhancement functions are included, such as sectorizing, contrast stretching, color contouring, simultaneous black-and-white color enhancements, remapping, filtering, edge detection, bad line removal, movieloop sequences, and digital calibration according to selectable calibration curves. Other techniques include contour analysis and weather symbol plotting.

In addition to complete image handling and analysis functions, several numerical modeling capabilities are planned that use gridded data from satellites, data networks, or manual inputs. Examples of these are a tropical cyclone strike threat model, storm surge estimation models, and a Geographical Information System for disaster and emergency planning, flood modeling, coastal zone planning, and fisheries management.

The frame formatter has been designed to interface directly with the polar-orbiter MicroVAX, thereby allowing data from all weather satellites (GOES, GMS, TIROS, and METEOSAT) to be ingested in real time simply by modifying ingest software parameters. The figure is a block diagram of the system.

Contact: Fran Stetina
Code 670

Sponsor: Office of Space Science and Applications

Mr. Fran Stetina, who holds an MEA degree from George Washington University, is Manager of the Low Cost Real Time High Resolution Picture Transmission System. He specializes in physics as it relates to timing and frequency, data processing, and system engineering. Mr. Stetina has 21 years of experience with Goddard and has received two awards from the NOAA administrator for outstanding contributions to the Global Weather Experiment.

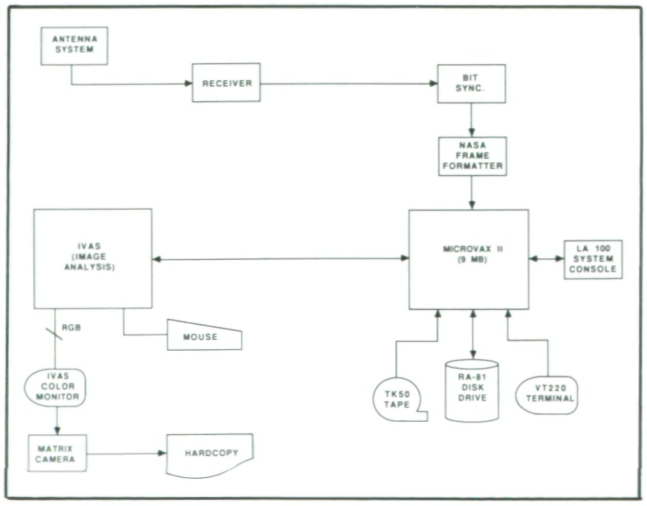

Real-time High-Resolution Picture Transmission analysis system.

ESTABLISHING A DISTRIBUTED SPACE STATION TEST BED

In conjunction with the Johnson Space Center (JSC) and the National Space Technology Lab (NSTL), Goddard's Data Systems Technology Lab has established the first end-to-end test bed for the Space Station Information System (SSIS). The proposed SSIS is a large heterogeneous computer network that will effect the distributed processing of all Space Station-related data. The SSIS will be composed of both ground and space networks that rely on state-of-the-art telecommunications hardware, software, and protocols. The SSIS will serve two main functions: the maintenance and operation of the Space Station itself and the support of the users of its orbiting facilities.

One innovative concept that has been proposed as a feature of SSIS user support is telescience. Telescience is the performance of all aspects of scientific investigation at a location remote from the NASA payload control centers. In this case, a scientist or principal investigator (PI) wants to perform experiments with the instruments of a payload that is attached to either the Space Station itself or to one of its co-orbiting platforms. Currently, the PI must schedule a payload activity far in advance with the NASA payload operations control center (POCC) for its payload. This activity often involves travel to a NASA facility. Once a request for a payload activity has been approved, the POCC is in charge of carrying it out; often it is weeks before the PI receives the data. In the telescience scenario, PIs would conduct these tasks from their home institution, usually

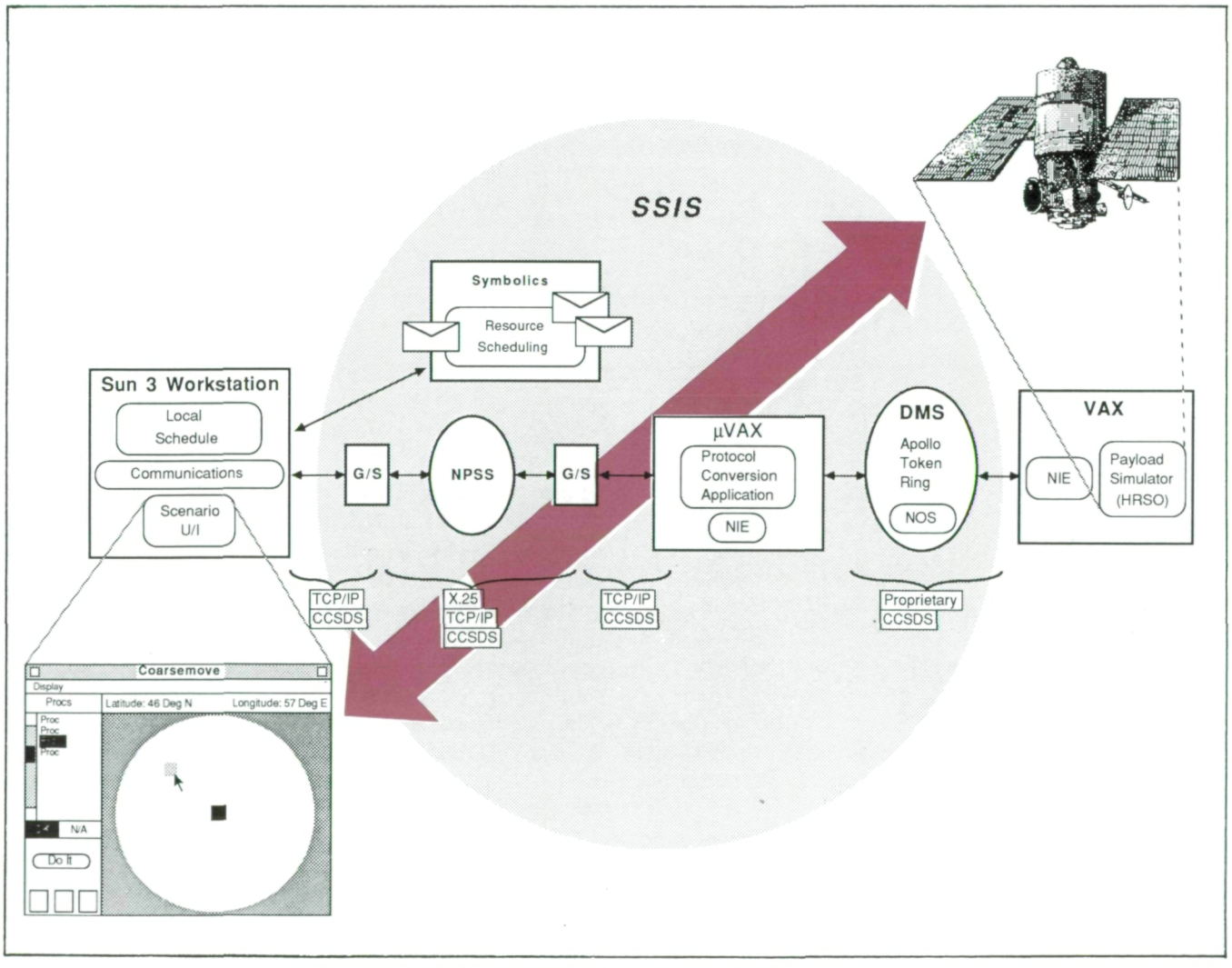

Space Station test bed.

a university or some other research center. The PI generates platform resource scheduling requests and submits them electronically to the main NASA scheduling system for approval. The PI also issues payload commands and receives payload status and data remotely. Thus telescience requires a certain amount of data processing at the site of the PI in addition to telecommunications capabilities.

The purpose of the test bed is to build, integrate, and exercise prototypes of the key systems in the SSIS. The JSC element is the Data Management System (DMS) test bed. The actual DMS will be a local area network that resides on the Space Station and coordinates the activity of and data transfer among various onboard subsystems, such as the environment control and life-support system and user payloads. The DMS test bed consists of a fiber-optic token ring of Apollo workstations and JSC proprietary software called the Network Operating System. Each Apollo node also has an interface unit that connects a given subsystem host to the DMS. Prototypes of several DMS subsystems have already been implemented, including a simulator for an attached Space Station payload, developed by NSTL.

The GSFC focus is on the ability of the system to support remote user access and the development of user interfaces to SSIS services. Code 520 has produced a prototype of a remote science user workstation for a Space Station attached payload, the High Resolution Solar Observatory (HRSO). The workstation, built on a SUN 3 workstation, allows the user to schedule payload resources and carry out real-time command and control of the simulated payload. The GSFC Transportable Applications Executive and the X Windows software package have been used to enhance the portability of the prototype software so that potential users may more readily evaluate it.

The payload, HRSO, is modeled by the payload simulator on the DMS test bed. The workstation initiates a connection from a local area network at GSFC through the NASA Packet Switching System to JSC, where the DMS test bed directs data to and from the payload simulator. Through the use of a bitmapped graphics user interface, the workstation allows the user to generate commands to the payload simulator and display status and science data that are received from the simulator over the network. In this way the end-to-end link has been realized, and the PI has the sense of remote manipulation of the payload instruments through the direct manipulation of graphical elements on the screen.

The user may also send scheduling requests to a local prototype of a Space Station scheduling system, which coordinates the use of on-orbit resources among the various attached payloads. The workstation provides another sophisticated graphical interface through which the user may browse through lists of predefined payload activities and place selections on a timeline. When the user is satisfied with the schedule request, it is transmitted to the scheduling prototype for approval. The current test bed, consisting of the user workstation, a scheduling system prototype, a communications link to JSC, the DMS network, and the HRSO payload simulator (see figure) is ready for end-to-end data flow exercises scheduled this fall.

Contacts: Clarence T. Ackerson and
Stephen G. Edwards
Code 522

Sponsor: Office of Space Station

Mr. Clarence T. Ackerson, who holds a Masters degree from the Catholic University of America, is an electrical engineer with 20 years of experience at Goddard.

Mr. Stephen Edwards recently graduated from the University of Pennsylvania with a BS degree in computer science and engineering. He has one year of experience at Goddard.

HIGH-ELECTRON MOBILITY TRANSISTORS

Future NASA and Department of Defense communication systems will utilize the millimeter-wave frequency bands around 60 GHz. Besides the wide available bandwidths that have been allocated for the space-to-space communications, these frequencies are within the absorption band of oxygen. Any interference to or from terrestrial sources will be attenuated by the atmosphere, resulting in secure, interference-free space communication channels. The solid-state technology under development is rapidly evolving into complete 60-GHz systems applicable for spaceflight use. One of the basic building blocks in millimeter-wave systems is the submicron field effect transistor (FET), utilizing Gallium Arsenide (GaAs) semiconductor material. A few years ago, the FET was considered the high-performance device for solid-state systems. However, conventional GaAs FET technology has reached the upper performance limitations due to transistor structures and material characteristics. Recently, a similar transistor called the high-electron mobility

transistor (HEMT) was developed. It exhibited superior experimental performance characteristics (gain and noise figure) over conventional FETs.

The first experimental demonstration of mobility enhancement was made by Bell Laboratories in 1978 but was not applied to millimeter-wave frequencies until 1983 by TRW laboratories, when there was a growing need for improved low-noise millimeter-wave devices. The design was based on improving noise figure parameters for existing FET devices. It was known from previous work by industry and universities that specific epitaxial layers of GaAs and Aluminum Gallium Arsenide (AlGaAs) in modulation-doped FETs produced devices with high transconductance and high-electron mobility. It was attractive to apply the concept to millimeter-wave devices, where improving noise parameters has not been a trivial task.

A cross-sectional comparison of conventional FET and HEMT devices reveal that they are basically the same device. The improved radio frequency (RF) performance of the HEMT is due to its epitaxial construction. A selectively doped heterojunction, when properly biased, allows for a two-dimensional electron gas layer to form between the AlGaAs and GaAs. The electrons from the AlGaAs diffuse into the undoped GaAs leading to the separation of the ionized donors from their electrons. Unlike the FET, the electrons flow through the undoped GaAs layer where there are fewer molecular impurities. They do not experience as much scattering, and therefore they exhibit high mobility through the transistor. In the past 2 years, considerable progress has been made in both optimizing the epitaxial layers and the parasitic elements of the HEMT device. To further improve RF performance, a thin Indium Gallium Arsenide (InGaAs) layer is inserted in between the GaAs and AlGaAs. The InGaAs' crystalline structure is unnaturally compressed to match the lattice structure of the GaAs and AlGaAs, and is termed the pseudomorphic layer. The resulting device is called a pseudomorphic HEMT.

Improved device understanding, modeling, and fabrication techniques have produced a transistor with a high yield, equal reliability, and superior performance compared to its metal semiconductor FET counterpart. Technology development has been progressing so quickly that complete multistage amplifiers have been qualified for spaceflight use at 60 GHz, as well as at many lower frequencies.

One of these multistage HEMT amplifiers was developed under a Goddard contract as part of a three-terminal device improvement program. The current 60-GHz communication equipment uses mixer front ends in receiver systems, and the system noise figure degrades as frequency is increased. The advantage of HEMT amplifiers is to incorporate it as a low-noise preamplifier to the mixer. System noise temperature is reduced drastically because the first stage of any receiver system contributes most of the noise to that system. This gives the receiver greater sensitivity, reducing the need for high power requirements on link transmitters and reducing antenna sizes on the spacecraft. In addition, with the improved sensitivity, the HEMTs are being used for modern radiometers.

A four-stage 60-GHz HEMT amplifier was demonstrated in 1987 with 5.6-dB noise figure with 15-dB associated gain. The HEMT transistors were grown on molecular-chemical-vapor-deposition materials, with two 0.25 × 30 micron gate fingers. Transmission lines consisting of 50-ohm microstrip circuits were fabricated on 4 mil thick quartz substrates with TiWAu metalization. Input and output matching circuits impedance match the waveguide-to-microstrip transitions and the next HEMT stage. Adjustable sliding backshorts provide mechanical tuning inside the waveguide channel. Each enhancement-mode HEMT requires two power supplies, one supply for the gate and another for the drain. The overall dimensions are 2 × 1.1 × 1.2 in.

The application of the HEMT in low-noise amplifier systems has been demonstrated. Once considered a high-risk technology, the HEMT has matured into the preferred low-noise millimeter-wave transistor.

Contacts: Robert W. Patschke and Michael T. Bukowski
Code 727

Sponsors: Office of Aeronautics and Space Technology and the U.S. Air Force (Space Division)

Mr. Robert Patschke is an electronics engineer in the Microwave Instrument and RF Technology Branch with three years of experience at Goddard. He is primarily involved with the development of millimeter-wave components for future satellite communication systems. Mr. Patschke holds a BEE degree from Pratt Institute.

Mr. Michael Bukowski is an electronics engineer in the Microwave Instrument and RF Technology Branch with four years of experience at Goddard. He is involved with

ORIGINAL PAGE IS
OF POOR QUALITY

the development of components for future communication systems. Mr. Bukowski holds a BSEE degree from Marquette University.

S-BAND TRACKING SYSTEM FOR KU-BAND RETURN LINK ANTENNA

An inexpensive method of tracking has been developed for a high data rate (up to 300 Mbps through TDRSS) Ku-band Tracking and Data Relay Satellite System (TDRSS) return link. A switched-beam S-band method of tracking uses a modified TDRSS user transponder, previously qualified flight-type gimbals developed for the Solar Maximum Mission, and Ku-band data and S-band tracking (KDST) antennas mounted on the same backing. By using components that already have been developed, this method provides an inexpensive alternative to a Ku-band monopulse tracking receiver.

Before the antenna is pointed within ±7 degree of the Ku beam peak, it is controlled by scanning step position commands to the gimbals provided from the ground through omnidirectional antennas. Once the forward link signal is found, the controller enters the acquisition mode.

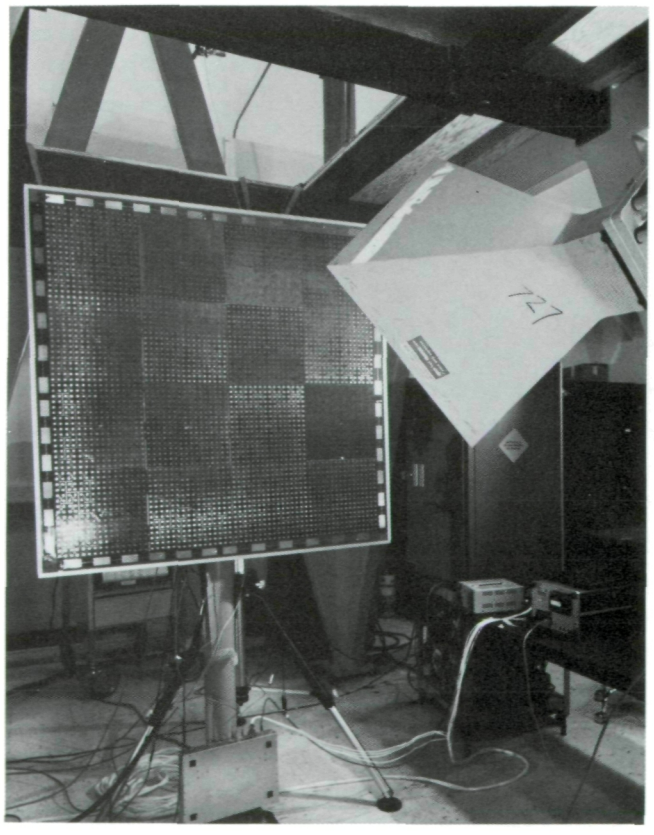

KDST antenna under test in Phoenix, Arizona, demonstrates amplitude and phase comparison tracking.

Due to the narrow beamwidth of the high-gain Ku-band antenna (−1 dB beamwidth approximately ±0.26°), precision pointing is required. Coarse acquisition of TDRS is accomplished with amplitude comparison of squinted beams in the plane along the length of the S-band antenna array, and fine acquisition and tracking is done by phase comparison in the plane transverse to the length of the S-band antenna array.

The coarse tracking S-band antennas are squinted so that their −5 dB crossover points are coincidental within ±1° of the peak of the Ku beam. Based on the difference in the received signal levels of four switched antennas, the controller rotates the gimbals until the Automatic Gain Control (AGC) values on each squinted antenna are nearly equal. When this condition is satisfied, the S-band boresight of the received signal is within 1°, and the controller enters the phase tracking mode. By utilizing unused pins on an existing D-type connector, which is normally used for the (optional) Doppler Processor Module (DPM), an NST tracker module supplies carrier AGC inputs to enable the second-generation TDRSS User Transponder to do wide-angle tracking.

For phase, the same antennas can be used in the transverse-unsquinted axis. During developmental tests, separate antenna sets were devoted to phase and amplitude tracking simply for convenience in measuring.

Four additional orthogonally pointed S-band antennas (peak of the beams coincident with Ku-band beam) were attached to the edges of the Ku antenna and fed to a separate 4PST switch for KDST phase tracking. The NST tracker module, a breadboard modification that will be designed into a direct physical replacement for the present DPM, enables the transponder to integrate the instantaneous frequency of signals that are controlled by lobe switching. A module component called the Numerically Controlled Oscillator (NCO) compensates for changes of phase between the four signals and outputs a digital word proportional to the integral of the phase jump error. Every 0.65 seconds the four antenna signals are sampled, the NCO word is integrated, and it updates the position command to force the phase error to zero for both azimuth and elevation planes. The phase tracking aligns the antenna to within 0.1° of the S-band boresight. The digital implementation of this method further reduces the risk of negative impact on the existing transponder design.

Azimuth axis tests of this concept were conducted May 1, 1987, in Phoenix, Arizona. It was verified by the upper and lower bounds of the azimuth angle versus time plot of 79 test runs that the measured angles were within $\pm 0.1°$ of the predicted TDRS azimuth values. A 10-Mbps data rate (transmitter limited) was achieved through the TDRS Ku-band return link to the White Sands Ground Terminal.

Further tests of NASA Data Link Module components and KDST antenna systems with data encoding equipment and distributed amplification will demonstrate data rates of 450 Mbps through TDRSS.

Contact: Lawrence M. Hilliard
Code 727

Sponsor: Office of Space Tracking and Data Systems

Mr. Lawrence M. Hilliard is an electronics engineer in the Antenna Technology Section of the Microwave and RF Technology Branch. Mr. Hilliard, who is a graduate of Michigan Technological University, has four years of experience at Goddard.

INTEGRATED RECEIVER CONCEPT USING PROGRAMMABLE CHARGE COUPLED SERVICES

The Network Division (Code 530) is currently involved in the design and development of a state-of-the-art integrated receiver that has both near-term and future applicability to the Tracking and Data Relay Satellite System (TDRSS) and its planned follow-on, Advanced TDRSS. This receiver uses programmable Charge Coupled Device (CCD) correlator technology as the basis for novel signal processing, which encompasses extremely rapid pseudo-noise (PN) acquisition, as well as PN tracking, and carrier/symbol synchronization. The PN acquisition portion of the receiver has been implemented and was demonstrated to Goddard in June 1987.

The programmable CCD analog-digital correlator being applied to this effort was developed by MIT Lincoln Laboratories and contains 256 stages, 128 of which are tapped. In addition, the digital tap weightings are externally controlled and updated in real time. As such, this CCD correlator can be used to implement a PN matched filter (PNMF) that can be matched to virtually any long or short PN code and can provide an effective parallel processing capability to a degree equal to the number of stages. It is precisely this PNMF flexibility, coupled with its high-level parallel processing capability, that makes this CCD correlator so attractive for TDRSS signal processing applications—especially for rapid acquisition of PN coded signals received from power-limited, low Earth orbiting spacecraft.

CCD correlator operation involves the voltage-to-charge transformation of input signals, followed by the propagation of these charge packets from one delay line stage to the next, at a rate controlled by an external clock. Accordingly, the CCD correlator is inherently an analog processing device, i.e., it introduces no amplitude quantization. In addition, current clocking capabilities exceed 10 MHz and should approach 100 MHz within the next few years. The PNMF property arises from the tapping, weighting, and summing of the charge packets at each clock cycle.

What is especially novel about the proposed CCD integrated receiver is its ability to apply the same circuitry, and the same signal information, to implement all key PN, carrier, and symbol synchronization functions. This is illustrated in Figure 1, where the analog CCD correlator outputs are A/D converted, and digital signal processing is used to implement all acquisition and tracking functions.

In June 1987, implementation of the rapid PN acquisition feature of the CCD integrated receiver was completed and demonstrated to GSFC. The principal capability demonstrated was the achievement of a one-second PN acquisition time, at 90 percent probability, under threshold TDRSS signal-to-noise ratio conditions. For comparable conditions, existing equipment at the TDRSS White Sands Ground Terminal requires more than one minute.

Figure 2 is a photograph of the equipment built to date and highlights the very compact Lincoln Labs CCD correlator chip. A production version of this receiver

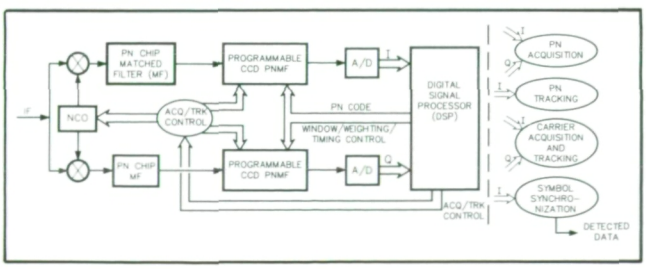

Figure 1. CCD PNMF implementation concept.

ORIGINAL PAGE IS
OF POOR QUALITY

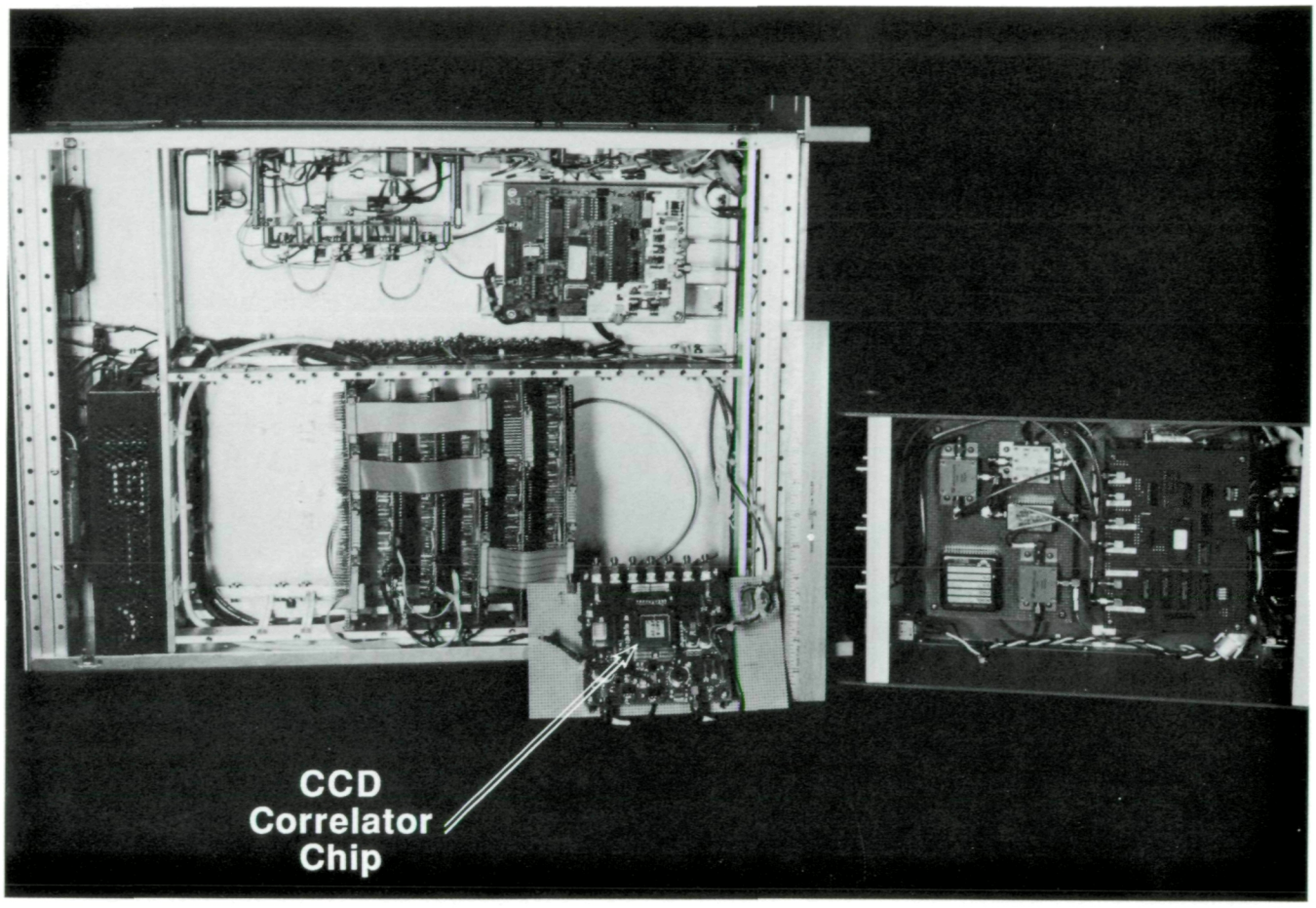

Figure 2. CCD PNMF acquisition receiver.

would probably require no more than 100–200 in^2 of electronics.

The remainder of this effort will focus on the other portions of the CCD integrated receiver and will include all PN, carrier and symbol tracking, and symbol detection functions. A final demonstration of the fully integrated CCD receiver will take place in March 1988 and will highlight not only tracking performance but also receiver operational flexibility, such as rapid reacquisition, and reconfigurations without RF-link interruptions.

Contact: Denver Herr
Code 530

Sponsor: NASA Small Business Innovative Research Program

Mr. Denver Herr, a staff engineer for the Telecommunication Systems Branch, is Deputy for Technical Management of the Second TDRSS Ground Terminal Project. His professional interests include advanced communications signal processing techniques. Mr. Herr holds an MS degree in telecommunications from George Washington University, and he has been at Goddard for 21½ years.

HIGH DATA RATE REED-SOLOMON DECODING WITH VLSI TECHNOLOGY

A new implementation for a Reed-Solomon (R-S) decoder that uses CMOS Very Large Scale Integration (VLSI) circuitry enables real-time operation to 80 Mb/s data rates. The R-S code is a powerful error correcting code standardized by NASA and ESA. The code is capable of correcting up to 16 8-bit symbol errors in a message of 255 8-bit symbols. Seven chips are needed for the decoding operation. Four of the seven decoding chips are customized VLSI devices implemented in CMOS 3-micron

technology. Approximately 1.65 billion Galois Field operations per second are achieved with the decoder chipset.

In this new implementation, the system is configured to perform in a pipeline manner where three messages are being processed simultaneously. The system clock is the symbol clock, which is an important feature. Therefore, the decoder can decode symbols at the same rate message symbols are received. Decoders that cannot use the symbol clock as the system clock must utilize a more complex clock system where the decoder operates at a higher clock rate than the symbol clock. Therefore, for a given technology, this decoder can operate faster than other designs that require a system clock that operates at a rate higher than the symbol clock.

The figure provides information regarding the four customized VLSI chips' complexity and operational speed. The general operation can be described as follows: the received polynomial is the input to both the first-in/first-out (FIFO) storage element and to the syndrome calculator module. Thirty-two syndrome values are determined and passed to the Euclid divide and multiply module that generates magnitude and error location polynomials. These magnitude and error location polynomials are passed to the Polynomial Solver Module (PSM) that evaluates both the error location and magnitude of the error and passes error magnitude and location information on to the Error Correction Module (ECM). The ECM receives signals from both the PSM and the FIFO. The signal from the FIFO is delayed original signal, which may contain errors. The ECM output is the corrected message that is passed on to the user.

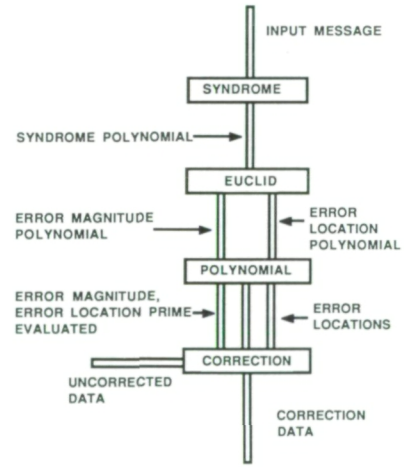

	TRANSISTORS	MOPS	CALCULATIONS
SYNDROME	19,400	640	16,320
EUCLID	66,000	122	3,110
POLYNOMIAL	33,000	840	20,910
CORRECTION	19,200	40	1,020
	137,600	1,642	41,360

Reed/Solomon (255,223) Decoder. (Eight-bit symbols, 16-symbol correction. Data rate 80 mbits/s; CMOS ¼ W/module.)

An R-S code is a cyclic symbol error correcting code that is useful in burst error channels. This code has potential application in communication systems and in digital systems where burst error condition exists. The Microelectronic Research Center at the University of Idaho has designed a chipset for NASA to implement a (255,223) R-S code. The chipset has been fabricated, is functional, and has been tested at 80 Mb/s data rate.

Contacts: James Morakis and Warner H. Miller
Codes 730 and 728

Sponsor: Office of Space Operations

Dr. James Morakis, an aerospace engineer with the Aerospace Data Standards Office, received a PhD degree from the University of Maryland. Dr. Morakis joined Goddard in 1964, where he has worked in telemetry, channel encoding, data processing, and communications.

Mr. Warner Miller, who received an MS degree in applied science from George Washington University, has been with Goddard since 1961. His interests include data processing, telemetry, channel encoding, and communications.

HIGH-SPEED PACKET PROCESSOR USING VLSI SYSTEMS APPROACH

The Mission Operations and Data Systems Directorate has begun an in-house project to develop a multichannel Data Capture Front End (DCFE), also referred to as Enhanced Front End Hardware. A DCFE channel will receive serial data in NASCOM block format, synchronize and extract telemetry transfer frames, correct errors in data, and reassemble source packets for processing in a Level Zero Processor. A Packet Processor utilizing semi-custom very large scale integration (VLSI) devices, microprocessors, and programmable gate arrays has been

designed to support the implementation of this system (see Figure 1).

The general requirement emphasized during the design of this capability was the adaptability to extract source data from various telemetry data formats, especially packetized data, at throughput rates up to 20 Mbps. Specific requirements for assembling packetized source data were derived from the *Goddard Space Data Packetization Standard (Standard 3.3)*, a subset of the *Consultative Committee for Space Data Systems (CCSDS) Packet Telemetry Recommendation*. This standard packet format includes the contiguous insertion of variable length source packets into telemetry transfer frames from up to eight multiplexed virtual channels. The locations of packets within the frame data fields are derived from a first header pointer in the frame header and packet lengths found in subsequent packet headers.

The Packet Processor design is outlined in Figure 2. The throughput capability of the Packet Processor is achieved by a data pipeline consisting of two separate RAM systems controlled by specially designed semi-custom VLSI logic. The first, the Tribuffer, triple buffers input telemetry transfer frames (up to 4 kbytes/frame) to allow a full frame period for extraction of frame and packet header data. The second and larger Reassembly RAM stores frame data separated by virtual channel (128 kbytes/channel) and provides the capability to reassemble packets by selective readout of packet pieces.

An adaptable format capability is provided by the programmability of the three microprocessors (MC68020s) labeled Header Processor, Quality Processor, and Output Processor. The Header Processor has interface connections to the Tribuffer Controller (VLSI) and a virtual channel selector connection to the Reassembly RAM Controller (VLSI). The Output Processor has interface

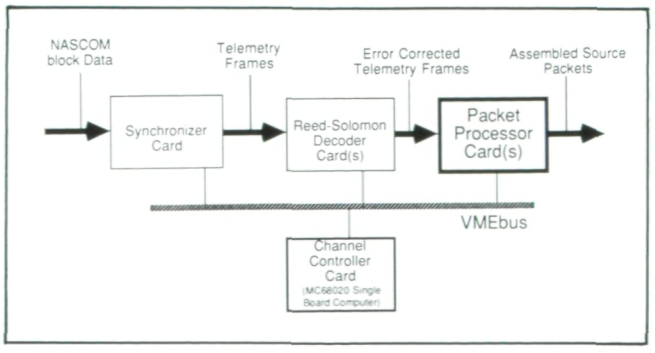

Figure 1. Data Capture Front End (single channel).

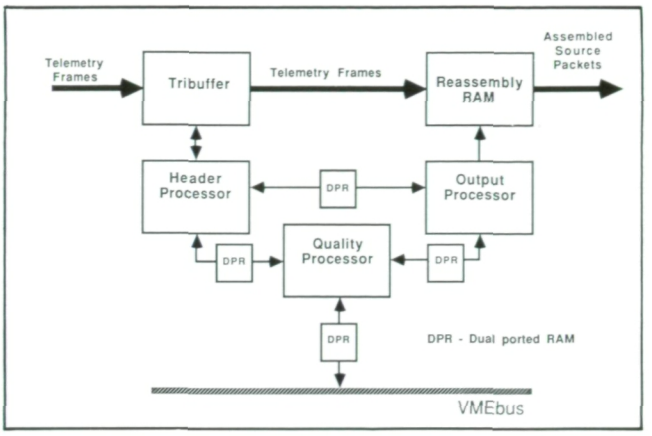

Figure 2. Packet Processor.

connections to the Reassembly RAM Controller. The Quality Processor does not interface with the data pipeline directly, but does communicate with the Header and Output Processors as well as the Channel Controller (VMEbus) via dual-ported RAM. In addition, the memory spaces of all three processors are accessible for read and write by the Channel Controller for loading software and/or session set-up parameters.

The Header Processor–VLSI Tribuffer Controller combination provides the following capabilities, with the processor generating the set-up controls to the VLSI device:

- set frame length for input data.
- set start and end addresses for reading output to Reassembly RAM.
- load start and end addresses for reading individual headers from a stored frame.
- read selected header data to Header Processor.
- the VLSI Tribuffer Controller automatically cycles memories when input, output, and header reading is complete and signals processors with an interrupt.

The Reassembly RAM is partitioned for eight virtual channels (128 kbytes/channel). The Output Processor–VLSI Reassembly RAM Controller combination provides the following capabilities, with the processor generating output instruction codes to the VLSI device:

- automatically stores frame data from Tribuffer Controller into contiguous RAM for virtual Channel identified by Header Processor.

- reads pieces of packet data identified by instruction codes from RAM to produce reassembled output source packet.
- inserts annotation passed with instruction code.
- inserts fill data passed with instruction code.
- RAM read and write operations can occur simultaneously since VLSI RAM Controller ping-pongs read/write between even and odd address spaces.

Dual-ported RAM interfaces are used for communication between each pair of processors. The Header Processor passes header data to the Quality Processor and passes packet piece locations within a frame to the Output Processor. The Output Processor maintains a directory of packet piece locations by use of the intra-frame locations provided by the Header Processor and a frame starting address from the RAM Controller. The Quality Processor performs analysis of header data to define the reassembly of source packets and generates quality and accounting information. A list of pieces and annotation for packet reassembly are passed from the Quality Processor to the Output Processor, and quality and accounting data are passed to the Channel Controller (DPR via VMEbus). The Output Processor generates instruction codes for the VLSI RAM controller by converting the piece list from the Quality Processor into instructions addresses with the piece location directory. Any fill or annotation defined by the Quality Processor is passed with an appropriate instruction code to the RAM Controller for output with the reassembled source packet.

The Tribuffer Controller and Reassembly RAM Controller VLSI designs were developed with the CAE/CAD capabilities available in the Code 521.1 laboratory. Completed designs have been submitted for VLSI chip production. The processor and VMEbus interface logic have been designed, implemented, and tested by use of RAM programmable gate arrays, and a prototype Packet Processor is being assembled on a (3-high, 2-deep) VMEbus compatible card. The Packet Processor development is scheduled to support full DCFE channel testing in early 1988.

Contacts: Gerry Grebowsky and Carol Dominy
Code 521

Sponsor: Office of Space Tracking and Data Systems

Mr. Gerald Grebowsky, who has been at Goddard for 21 years, is Code 521 Team Leader of the Data Capture Front End Development. He is interested in the system design of special purpose data processing systems. Mr. Grebowsky received an MS degree in physics from the Catholic University of America.

Ms. Carol Dominy is an electronics engineer with the Data Capture Front End Development. Ms. Dominy received a BS degree in electrical engineering from the University of Tennessee, and she has two years of experience at Goddard.

GRAPHICAL STRIPCHART RECORDERS

Traditional stripchart recorders have been the paper oscillograph type. These systems are and were heavily used in satellite missions to monitor the health and safety of the spacecraft. At the Multisatellite Operation Control Center (MSOCC), analysts for missions such as the Dynamic Explorer and Earth Radiation Budget Experiment make heavy use of the stripcharts.

The present stripcharts allow 15 parameters to be plotted, where 8 channels are values that can be scaled to 12 bits, and the other 7 are binary events, on or off, 1 or 0. Speeds of the paper can vary to change the time scale, and Greenwich Mean Time is plotted in the margin in a pulse code.

Code 511 has developed a graphic stripchart to replace these older stripcharts. The new systems consist of a Kandl Data Products AT, which is an 80386 CPU-based system compatible with the IBM AT, with a Dolen DC1-8 graphics card, a 130-megabyte disk, and a Seiko color printer.

These systems offer many new features over traditional stripcharts. Data can be received and plotted faster than with traditional stripchart recorders, and up to 4.5-megabytes of data can be archived for post pass analysis. Data channels can be annotated, labeled, and color coded.

One interesting feature is that the display can be distributed around MSOCC via the video distribution system. This feature is useful because during times when many people need to observe mission proceedings, the stripchart outputs can be viewed from outside the mission operation room. This can only be done now by putting a camera on the stripchart recorder and distributing that video.

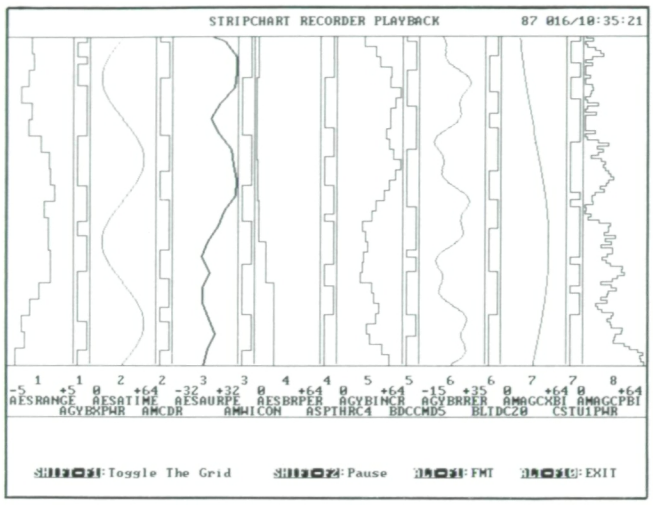

Figure 1. Typical graphic stripchart display.

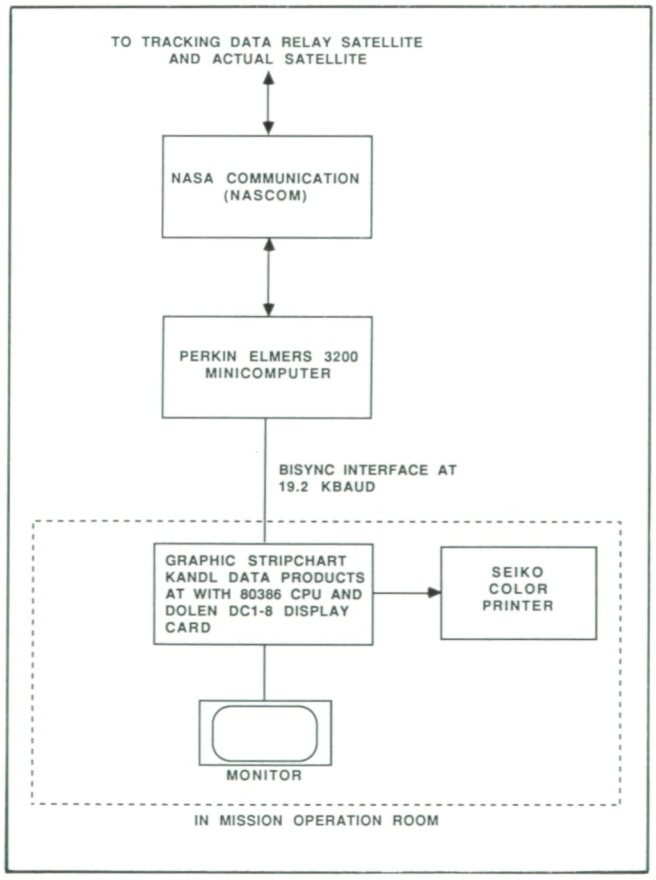

Figure 2. Configuration of the graphic stripchart.

The system's one drawback is that due to the MSOCC video compatibility requirement, the display only has a resolution of 640 × 480 pixels. This means that the actual viewing resolution is slightly less than traditional stripcharts. However, when required, these graphic stripcharts can be converted to higher resolution with minimal effort.

Although plotting on a graphics terminal has been done, stripcharting is an order of magnitude more difficult because of the sheer magnitude of data involved and the display scrolling required. Recent technology has made graphics fast enough to allow for enough performance to match the older oscillograph technology. These systems are targeted for support of the Cosmic Background Explorer and the Gamma Ray Observatory.

This project is being done in collaboration with Mike Maloney and Steve Lee of Bendix Field Engineering Corporation.

Contacts: Dan Mandl
Code 511

Sponsor: Office of Aeronautics and Space Technology

Mr. Dan Mandl works with the Control Center Systems Branch, and he is interested in computer graphics. Mr. Mandl, who holds a BSEE degree from the University of Maryland, has seven years of experience at Goddard.

NEW RAPID SINTERING PROCESS FOR CERAMIC MATERIALS

Ceramic materials are finding widespread use in NASA applications, from the skin of the Space Shuttle to microminiature electronic components. One of these applications is the dielectrically filled cavity resonator used in radio transmitters and receivers. These resonators are cascaded to form bandpass filters. When filled with a dielectric material, the linear dimensions of the cavities are reduced by the square root of the dielectric constant of the material. Ceramics are used because they have large dielectric constants, low loss, and are stable in various environments. Standard methods of sintering or firing ceramic materials are slow and energy intensive. Plasma sintering has been investigated as an alternative technique to speed production and as a method to reduce energy consumption.

Rapid sintering of isostatically pressed (pressure applied uniformly from all directions) pure and doped titania rods was performed in an induction coupled plasma furnace (see figure) operating at 5 MHz. The dopants used were

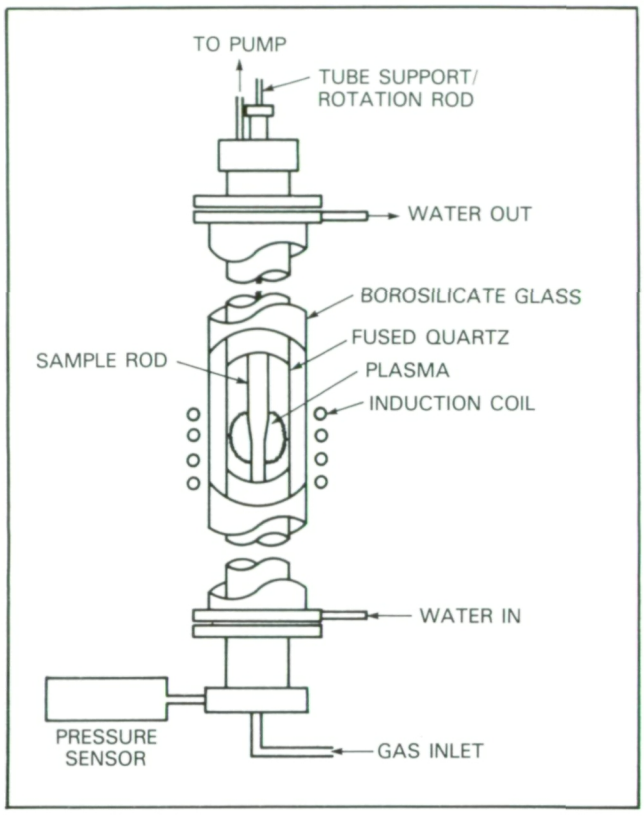

The radio frequency induction coupled plasma furnace reaction chamber.

tantalum and chromium. Oxygen was added to the argon in the plasma in various quantities from 1 to 10%, maintaining a constant system pressure of 45 torr. The oxygen was added for two purposes: 1) to increase the sample temperature and 2) to prevent reduction of the sample during sintering. By use of a translation rate of 2 cm/min, dense samples were obtained in 2 minutes of sintering time. Maximum theoretical densities obtained were 94.6% for the pure material, 93.6% for the 0.5 mol% tantalum-doped samples, and 96.8% for the 0.5 mol% chromium-doped samples.

The samples were characterized by a variety of analytical techniques. X-ray diffraction was used to determine the phase composition and crystal structure. The final density, as a function of oxygen content in the plasma, and sample translation rate were obtained. The electronic conductivity and dielectric constant of the material were obtained through measurements on a vector impedance meter. The effects of varying the oxygen content of the plasma on the microstructure were observed by scanning electron microscope (SEM) examination of fracture surfaces. The effects of the dopants on the microstructure were also observed by SEM examination. Etching of the sample surface by the plasma was evident in an SEM examination of the as-fired surface. Plasma species such as Ar^+ and O^+ were identified with an optical multichannel analyzer.

The density was found to have a strong dependence on the oxygen content of the plasma. Smaller dependencies were found on power and translation rate. Although the final densities were relatively low, less than 99%, good quality dielectric material (low loss) was obtained for the chromium-doped case. Pure or donor-doped material could be useful in oxygen sensor applications or the photoelectrolysis of water due to the large conductivity resulting from oxygen vacancies.

Contact: Carl Kotecki
Code 724

Sponsor: National Science Foundation

Mr. Carl Kotecki, an electronics engineer in the Instrument Microelectronics and Detectors Branch, joined Goddard in 1986. He holds an MS degree in materials science and engineering from Northwestern University.

PERFORMANCE CHARACTERISTICS OF THE GSFC LACN

The Goddard Space Flight Center is developing a campus-wide Hybrid Local Area Computer Communications Network (Hybrid-LACN) as a joint pilot activity among the NASA Communications Division (NASCOM) and several cooperating user organizations. NASCOM is involved in developing new approaches to solve the rapidly growing and varied communications requirements of the Agency and the Center. The diverse nature of data and computer communications often cannot be entirely satisfied by any single technology, standard, or networking scheme. As a result, two technologies may need to be combined in a hybrid network, which capitalize on the advantages of each technology. The glue that combines the two technologies is usually in the form of a black box acting as a network bridge, router, or gateway. At GSFC, the two technologies that make up the LACN are: 1) the very popular user interface standard, Ethernet (IEEE 802.3), and 2) the broadband CCTV medium with the capability to cover a much wider area. The bridge is embodied in the form of Applitek's NI10/E Ethernet Bridge, initially developed in response to the GSFC specification. As a result of overwhelming user acceptance, the Hybrid-LACN is now evolving into the institutional networking facility of the Center.

ORIGINAL PAGE IS
OF POOR QUALITY

The present study was undertaken to develop a deeper understanding of Hybrid LACN performance characteristics needed for the maintenance of intracenter computer communications services. Bridges and gateways are the focal points for characterizing and understanding hybrid networks and internetworks. Two approaches can be taken to characterize and quantify any system: empirical analysis (emulation) and mathematical analysis (simulation). Emulation usually gives results that are readily and directly applicable to the actual system, since they are real results. Goddard has the resources to build a test LACN and directly measure the data transmission characteristics of the system. The architecture of the GSFC Hybrid-LACN is illustrated in Figure 1, and the system employed to study it is depicted in Figure 2. Our approach was to implement a test hybrid LACN dedicated to measuring response to artificial workloads emulating various conditions. The results obtained from such emulations were then compared with actual traffic workloads observed on the institutional network, and loading projections were made.

The data gathered in this study allows us to characterize hybrid network performance in a more meaningful way and allows us to make some very useful assumptions applicable to network planning and configuration. The most meaningful quantity we found to describe bridge or gateway performance is throughput performance in terms of packets per second. This is because, although the physical layer interfaces operate at a very high rate, the higher layer procedures are not able to process the data fast enough to fully utilize that bandwidth. As a result of this bottleneck, the bandwidth available on the broadband backbone network is underutilized. However, measurements on the operational network indicate that most of the traffic on a typical Ethernet remains local and does not require bridging. A rule of thumb to follow when designing internets is that a backbone bandwidth of 0.1 of the aggregate of all the subnetworks' bandwidth is usually adequate.

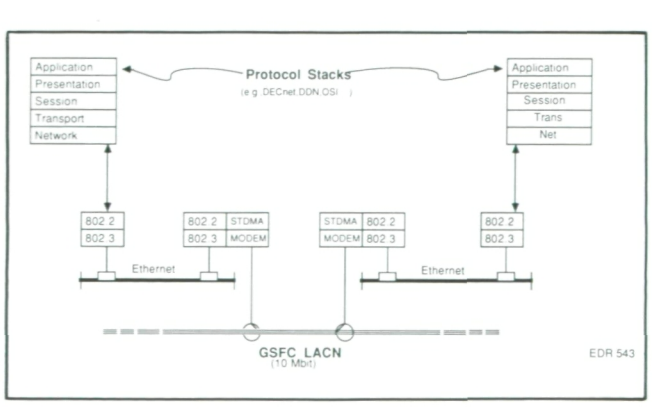

Figure 1. LACN architecture.

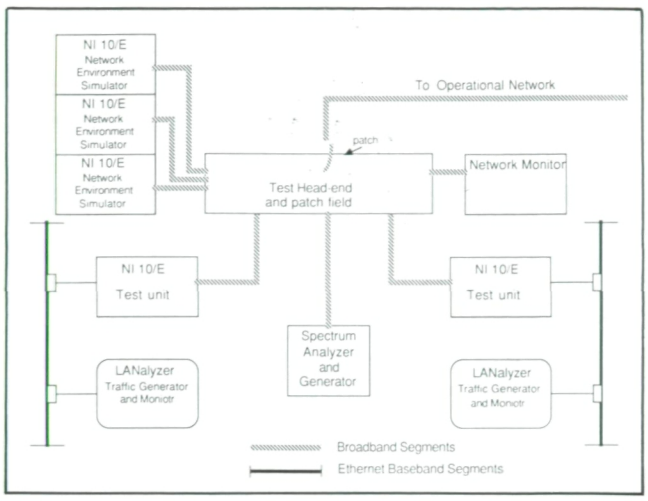

Figure 2. Test segments.

A slow growth trend in average network utilization has been observed, which indicates that workload demand will probably not saturate the capacity of the present system before the next 3 to 5 years.

Contacts: M. C. Spinolo and E. D. Rothe
Code 543

Sponsor: Telecommunications Branch

Mr. M. Chris Spinolo works with the Hybrid Local Area Computer Communications. He earned a BSEE degree at Memphis State University and has been at Goddard for two years.

Mr. Edward Rothe is involved with Hybrid Local Area Computer Communications. Mr. Rothe holds a BS degree in physics from the Illinois Institute of Technology, and he has been a part of Goddard for 28 years.

SPACE PHYSICS ANALYSIS NETWORK: A QUICK REACTION CAPABILITY

The Space Physics Analysis Network (SPAN) became operational in 1981 with three computer nodes and now provides computer-to-computer accessibility to well over 1600 nodes around the world. With its widespread connections to data centers, user facilities, and other networks, SPAN has become a very valuable research tool

to multidisciplinary scientists. It has proven to be an indispensable quick reaction capability for researchers as demonstrated during the Voyager and comet encounters, Coordinated Data Analysis Workshops (CDAWs), orbital debris studies, supernova research, and ozone hole investigation.

The International Cometary Explorer (ICE) encounter with the comet Giacobini-Zinner (G-Z) on September 11, 1986, provided SPAN with its first opportunity to exercise its quick reaction capability. ICE was originally called the International Sun Earth Explorer-3 (ISEE-3) and measured the solar wind phenomena. Its data processing and analysis had been controlled by the individual principal investigators (PIs) at their home institutions. When the decision was made to send the ICE spacecraft through the tail of the comet G-Z, a new data system that provided quick data analysis of the comet plasma and dust environment for spacecraft/instrument health was required (Green, J., and King, J., 1985).

Since no centralized data processing and analysis facility existed to support the ICE encounter and the millions of dollars necessary to develop such a system were not available, SPAN was used to connect remotely located facilities into a distributed processing system. These facilities included the University of Iowa, Los Alamos National Laboratory, Jet Propulsion Laboratory (JPL), and the European Space Research and Technology Centre. To accomplish this task, raw data tapes were generated and decommutated by the Information Processing Division, then carried by courier to the National Space Science Data Center (NSSDC) and the Laboratory for Extraterrestrial Physics for transfer of the data via SPAN to the PIs' home institutions where the analysis software resided. Processed data were returned to the PIs at GSFC for the encounter; thus, they could do real-time science analysis as well as support the remote science analysis team at the remote facility.

SPAN's success with the ICE encounter not only enabled the PIs to present their scientific results at a press conference on the same day of the encounter, it also demonstrated the feasibility of providing the same type of quick reaction with the reliable transfer of data between the United States and Europe. The direct result of this was the implementation of SPAN in Europe.

For the Voyager Uranus encounter, SPAN served in a slightly different role. It was used extensively by the Voyager investigation teams before, during, and after the encounter.

The scientific teams supporting the encounter were able to acquire the data much more quickly with SPAN than if they had waited for the data on tape—in some cases, within hours as opposed to 5 days. In addition to the quick turnaround, SPAN provided the co-investigators with an entirely different way of doing their research. For example, GSFC Planetary Radio Astronomy (PRA) scientists received 5 million bits of data per day over SPAN from JPL and communicated with PRA team members at JPL and in France via SPAN. The U.S. Geological Survey in Flagstaff, Arizona, used SPAN to access JPL's Navigation Ancillary Information Facility geometry files to accurately process and map project the Uranian satellite images. TRW transferred files and ran plots from the University of Iowa to JPL over SPAN, with the results produced on pen plotters or personal computers at TRW. The Photopolarimeter Subsystem (PPS) Team at JPL used SPAN to communicate with the rest of the PPS team at the University of Colorado to exchange instrument health information and science results.

SPAN also supported the Giotto encounter with Halley's comet. For the eagerly awaited comet, Halley, NASA did not have a spacecraft that participated in the encounter. However, SPAN played a key role in the encounter of Giotto, a European Space Agency mission, with the comet. Since comets are known for their rapid evolution and unexpected changes in structure and brightness when they are within the inner part of the solar system, the scientists involved in the Giotto mission needed up-to-date information on the comet throughout the encounter period. The best source of this information was obtained from the Table Mountain Observatory (TMO) in California.

Daily wide-angle views of the comet obtained at the TMO were sent over SPAN to the European Space Operations Centre (ESOC) in Darmstadt, Germany, before, during, and after the encounter and used to plan the Giotto instrument modes. Consequently, both wide-angle and near-nuclear views of the cometary process were made available to the scientists.

A dial-up X.25 connection between ESOC and the University College of London (UCL) was used to transfer large digital image files and input/output files from global thermospherical models between UCL, Rutherford Appleton Laboratory, and other major computing centers within the United Kingdom.

With the CDAW, the focus of SPAN's quick reaction capability is somewhat different. Scientists from around

the world gather at the NSSDC for an almost annual face-to-face workshop (Green, 1986) to research a predetermined scientific phenomenon with an assembly of on-line data sets. So far, CDAWs have concentrated on solar terrestrial research topics; however, the general format of the workshop could conceptually be used for any scientific discipline.

For a typical CDAW, the participating scientists meet and determine the phenomena to be studied and identify the data sets to be used. Then the data center collects and makes the data available on-line. By using the Network Assisted Coordinated Science (NACS) software, the scientists can do some analysis from their home institutions via SPAN before the workshop at the NSSDC. During the workshop, they use SPAN to access software at their home facility for further analysis and computational modeling. After the workshop, the scientists will access NACS over SPAN for performing follow-up analysis. CDAW-8, the first workshop to use the NACS software, attracted over 50 scientists from the United States, Europe, Japan, and Canada to study the magnetospheric substorm dynamics. The data used comprised 49 data sets from nearly 15 spacecraft and 5 ground-based instruments, with well over 400 geophysical parameters. It was the largest collection of correlative geophysical data assembled until that time (Green, 1986).

The orbital debris studies have benefitted from the existence of SPAN. The Space Sciences Branch of the Solar System Exploration Division at the Johnson Space Center (JSC) is studying orbital debris and its sources with its data base that contains element sets (ELSETs) on all artificial Earth satellites for which the United States Space Command makes available. Inputs for this data base are the modified North American Air Defense Command orbital element data sent to JSC by Code 513 three times per week in hardcopy form.

Because of JSC's unique requirements for quick access to the orbital elements, electronic transmission is preferred. Many fragments from collisions and explosions lie in unstable orbits, making frequent ELSET updates necessary. Also, when a "break-up" occurs, they must have the latest ELSETs quickly in order to schedule radar and electro-optical observations of the fragments soon after the event.

The unmodified orbital data are now put on tape and given to the NSSDC to transmit to JSC over SPAN. This quick reaction response to JSC's request has greatly improved the effectiveness of the debris study.

When Supernova 1987a was observed on February 24, 1987, it was only visible from ground-based observatories in the Southern Hemisphere, and the astronomers and astrophysicists in the Northern Hemisphere needed a way to quickly access data from this once-in-a-lifetime phenomenon. To satisfy the requirement for connecting the astronomers at the observatories to the rest of the astronomy and astrophysics community, SPAN was upgraded with 9.6 Kb/s tail circuits to the National Radio Astronomy Observatory in Charlottesville, Virginia, and the Smithsonian Astrophysics Observatory (SAO) at Harvard University. An X.25 connection was established to the Cerro Tololo Inter-American Observatory in Chile, and remote terminals were set up in Alice Springs, Australia, for the balloon launches, which looked at gamma rays from the supernova, and in Woomera, Australia, for the rocket launch campaign. In addition, SPAN had access to Starlink in the United Kingdom, Astronet in Italy, and the University of Otago in New Zealand.

As a result of the SPAN support, the latest information on the supernova from the observatories, balloon flights, and rocket launches were sent to SAO and published on the International Astronomical Union's "Circular," an on-line bulletin board. Thus, the information became readily available to the scientists around the world.

SPAN provided backup support for the ozone hole investigation. Data from the Total Ozone Mapping Spectrometer (TOMS) on the Nimbus-7 polar-orbiting satellite has indicated a significant local minimum in the amount of total ozone over the Antarctic region compared to the surrounding area during the Northern Hemisphere's early autumn months (RDS, 1987). During that time of the year, for 2 or 3 months, the amount of ozone in this area is lower than it is in any other area on the Earth at any time of the year. This occurrence is referred to as the ozone hole.

An ozone hole investigation was established to collect ozone data with an aircraft, based in Punta Arenas, Chile. The TOMS data were used to determine where the aircraft should be sent to collect the data.

To support this investigation, electronic communications among the systems in Punta Arenas, GSFC, and the European Meteorological Office were necessary. The primary means of electronic communications was analog. However, SPAN served as a backup for transmission of digital data. Systems in Chile and Europe supporting this investigation were accessible over SPAN for the ozone hole study.

Contact: Valerie L. Thomas
Code 633

Sponsor: Office of Space Science and Applications

Ms. Valerie Thomas, who holds an MS degree in engineering administration from George Washington University, is Project Manager of SPAN. Her professional specialties include wide-area network management, digital image processing, and development of real-time data systems. Ms. Thomas coordinated activities of Goddard's development and operations team for the Large Area Crop Inventory Experiment. She also managed the operations for Scrounge (Landsat-4 Early Access System). During her 23 years at Goddard, Ms. Thomas has received several awards for her scientific achievements.

NASCOM COMMUNICATIONS PROTOCOL CONVERTER

Design of new systems for real-time processing of NASA Communications (NASCOM) 4800-bit data blocks is often complicated by the unique nature of these circuits and the general unavailability of off-the-shelf interface hardware. When designing a new system, procuring computers that use the latest available technology is desirable. Chances are good that a new NASCOM interface would need to be designed either by the computer vendor or in-house after the equipment is delivered. Experience has shown vendor-designed interfaces to be expensive and to have limited success. In-house development can slow system implementation, since in many cases this effort cannot be started until the computer is delivered and designers are brought up to date on the vendor's unique bus interface.

As part of the Tracking and Data Relay Satellite System Network Control Center (NCC) Augmentation Project, new computers (VAX 8500) were procured to replace the current Digital Communications System. Rather than design new interfaces for these computers, a microprocessor-based interface device called an NCC Front End (NFE) is under development to provide the required interface to NASCOM. The interface into the VAX computers is provided by an industry standard Transmission Control Protocol/Internet Protocol (TCP/IP) Ethernet Local Area Network (LAN). The NFE acts as a bridge from NASCOM to TCP/IP Ethernet and thus provides a NASCOM interface into the VAX with commercially available VAX hardware.

An additional advantage to using a separate device for interfacing to NASCOM is the offloading of real-time response requirements from the main computer. The NFE firmware uses Ready Systems' Versatile Real-Time Executive Operating System and is better able to meet the stringent response times required when interfacing to several high-speed (56 kbits/s) communication lines. Data received by the NFE is forwarded to the VAX over a TCP communications channel. Since TCP provides flow control, data will be sent to the VAX at a rate that the VAX can control. A large amount of memory (1 megabyte) is used for buffering of input data during periods when the effective incoming data rate is higher than the rate allowed by the VAX.

The NFE was designed to make maximum use of off-the-shelf components to limit development costs and to minimize schedule impact. The system is based on the industry standard Multibus and includes a 68000-based microprocessor board as the main NFE processor, two memory boards (ROM and RAM), and two intelligent LAN Interface Controllers. The chassis is an off-the-shelf item vendor-modified for use with the NFE. A minimal amount of in-house work is required on the chassis to prepare it for operational use. A separate rack-mounted terminal is used for displaying status and for allowing configuration changes to be entered by an operator. The only custom-designed component in the NFE is the NASCOM Interface Controller.

Each NASCOM Interface Controller is capable of simultaneous communication with four full duplex communication circuits. Three controllers are used in the NFE to interface to a total of 12 circuits. Erasable Programmable Logic Devices are used to achieve the high circuit density required to fit four circuits on a single board. Direct Memory Access is used to increase system performance.

An important feature of the NFE is its software maintainability. Software (which resides in Read Only Memory) is written in a structured high-level language ("C"). Assembly language is used only when necessary. The development environment consists of a "C" cross-compiler and cross-debugger running on one of the VAX computers. The cross-debugger allows debugging of code at the high-level language source level. A 68000 in-circuit emulator is used in conjunction with the debugger and also allows the maximum amount of control over debugging of low-level hardware and software problems.

The NFE is not limited to use in the NCC as a Communications Front End. With the proper software the NFE may be adapted for use in such applications as

multiplexing/demultiplexing, data reformatting, protocol conversion, and data generation. Future plans include the development of an interface board for use in telemetry processing applications.

Contact: Thomas E. Sardella
Code 532

Sponsor: None

Mr. Thomas Sardella is an electronics engineer on the NCC Augmentation Project. Mr. Sardella, who has seven years of experience at Goddard, received a BS degree in electrical engineering from Worcester Polytechnic Institute, and he is currently working toward a Masters degree in computer science at Johns Hopkins University.

NETWORK SIMULATION MODEL OF NASCOM'S DDCS

The NASCOM Data Distribution and Command System (DDCS) allows for the efficient transfer of data between processing facilities and users. This system specifies X.25 interfaces between packet switching nodes and host/user Data Terminal Equipment (DTE) in the distribution network.

X.25 is a recommendation of the International Telephone and Telegraph Consultative Committee, which addresses how a user's DTE interfaces to Data Circuit Terminating Equipment (DCE) on packet switching networks, for exchanging data or control information.

A Network Simulation Model (NSM) was developed to help NASCOM evaluate the behavior of the DDCS under various operational scenarios and workload requirements. This effort includes assessing network performance under the data distribution requirements imposed on the DDCS by the Gamma Ray Observatory, Extreme Ultraviolet Experiment, Space Telescope, and Upper Atmospheric Research Satellite projects. The model output allows NASCOM to investigate the statistical relationship between various performance measures, such as amount of data transferred; message throughput; response time; link, CPU, and buffer utilization; error condition detection; network capacity; and bottleneck identification. Comparison of these output statistics provides the basis for optimization of the real system under various operating conditions.

The NSM is implemented in SIMSCRIPT II.5 in a VAX/VMS environment. Network system characteristics to be modeled, such as node connectivity, link data, and virtual circuit data, are input via four disk files. These four input files are labeled Unit 1, Unit 2, Unit 3, and Unit 4. Simulation parameters, such as run length, reporting intervals for intermediate statistics, and output options, are read in from another file. Unit 1 input includes network connectivity data, node addresses, and interconnecting link characteristics. Unit 1 contains the header, which includes the DCE name, node address, number of active ports, and number of packet processing modules. The input format for Unit 1 data items is as follows: node address, interface type, line speed (kbs), line bit error rate, and node name.

Unit 2 input provides the necessary information to construct permanent virtual circuits. A virtual circuit allows two DTEs to communicate as if they were using a real or dedicated circuit. User data flows may be either simplex or full duplex. The mean time between arrival of user data units (MTBA) defines the frequency at which user data arrives at the network layer to be transmitted on a virtual circuit. (An MTBA of 0 indicates that there is a constant supply of user data.) The MTBA defined in Unit 2 determines the mean of the exponential distribution from which interarrival times are derived. The input format for Unit 2 is: virtual circuit number, address of source DTE, addresses of all intervening DCEs, address of destination DTE, MTBA for source-to-destination traffic, MTBA for reverse traffic, and data packet size for each virtual circuit.

Unit 3 supplies the data link level node parameters for each link. Each link is uniquely identified by its source and destination addresses. Data must be provided for each direction of data flow on a link. The format for this file is: source node address, destination node address, acknowledgment option for data transmitted by the source node, acknowledgment timer timeout value, and source node T1 (retransmission) timer timeout value.

Unit 4 contains the network level parameters for each node. The input format for Unit 4 is: node address, source node information frame processing time, source node supervisory frame processing time, packet processing times (for both information and supervisory packets), and nodal buffer memory capacity for each node.

Once all input values have been established, in Units 1 through 4, the user is queried for a quit time (seconds), a reporting interval for the statistics, and desired run-mode (either interactive or batch-like). Low-level integrity checks have been incorporated that will flag illegal input values.

C-3

Data produced is output as a disk file through Unit 6. Unit 6 contains snapshot statistics of links, virtual circuits, and each DCE node, in addition to a summary of the input so that individual runs can be distinguished. Link level statistics provide information specific to each direction of data flow for a link. This output includes: source and destination node addresses, number of frames sent (information, supervisory, and number in error) for each direction, link utilization, and the number of timeouts (either retransmission or acknowledgment) that have occurred at the source node.

Virtual circuit statistics provide information for the virtual circuits at the time specified in the header in Unit 1. Information is given for both directions of data flow. This output specifies virtual circuit number and type (switched or permanent), source/destination node addresses, number of frames (information and supervisory) sent in each direction over each virtual circuit, number of timeouts at the source node, and number of resets for any specified virtual circuit.

Node level statistics provide information specific to each DCE node within the model. Node level output contains processor utilization and buffer utilization (given for both frame and packet levels at the nodes).

The NSM conforms with the International Standards Organization/Open Systems Interconnection layer specification of network architecture that facilitates investigation of other network protocols in addition to those currently being modeled.

Contact: Susan E. McGill
Code 541

Sponsor: Office of Space Operations

Ms. Susan McGill is Network Performance Evaluation Task Manager of the Network Simulation Model. Ms. McGill holds a BS degree from the U.S. Naval Academy, and she has been a part of Goddard for 2½ years.

REFERENCE SYSTEM AND NUISANCE PARAMETER CALIBRATION FOR SATELLITE TRACKING WITH GPS

Goddard has been investigating new techniques for very accurate orbit determination (<25 m uncertainty) of the geostationary Tracking and Data Relay Satellites (TDRSs). Accurate orbits are required for the TDRS because the geostationary platform provides user tracking data as well as communications services, and therefore, uncertainty in the TDRS position contributes to user spacecraft orbit errors. In addition, NASA wants to confine the TDRS-tracking ground terminals to the continental United States rather than extend to the current extra United States configuration. The combined requirements of tracking accuracy and restricted geometry greatly increase the importance of high-quality calibration of nuisance effects.

The most significant nuisance effects are unpredictable variations in the orientation of the Earth, troposphere propagation errors, station position errors, and (for one-way ranging systems) station clock synchronization errors. One-way ranging systems (differential one-way range or very long baseline interferometry) are of particular interest because the spacecraft tracking system payloads are highly simplified or eliminated altogether. Furthermore, the differential nature of these systems attenuates many of the systematic errors through common mode cancellation.

Novel techniques to calibrate satellite tracking networks have been investigated with the focus on the potential uses of the Global Positioning System (GPS) navigation satellites. These spacecraft are attractive radio reference objects for the following reasons: the full operational system will provide a constellation of 18 satellites with at least four visible at any given time; they transmit at two separate L-band frequencies that permit direct ionospheric determinations to be made easily; GPS transmissions permit on-site reduction or compression of the observation data. The GPS observations can be used to determine the orbits of those satellites and, as a by-product, simultaneously adjust model parameters for such effects as Earth orientation, tropospheric path delay, or interstation clock differences. Observations restricted only to geostationary spacecraft are far less robust for this sort of nuisance parameter estimation because of the nearly constant geometrical configuration. Note that the GPS satellites move in 12-hour orbits.

A detailed tracking scenario and error budget were developed and used with NASA's ORAN (orbital analysis) covariance analysis program to simulate tracking of the GPS constellation from several different continental United States networks. Both range and interferometric tracking of the GPS satellites were considered for near real-time calibration of an interferometric TDRS-tracking system. It was found that GPS calibration could be expected to produce geosynchronous orbits accurate to about 10 m or better by use of a small

network of three stations (baselines <1000 km) confined to the TDRS Ku-band downlink footprint. The figure compares the major error sources expected for GPS calibration with quasar calibration. In addition to the calibrated quantities, the effects of measurement noise and dynamical mismodeling of the solar radiation pressure on the TDRS orbit are also shown. The total orbit uncertainty is estimated to be 7.5 m for GPS calibration versus 10 m for quasar calibration.

The covariance analyses show that GPS calibration of satellite tracking networks can be as effective as observations of quasars. This is somewhat surprising given that the celestial radio sources form a very nearly inertial reference frame and therefore are not subject to the dynamical modeling errors that affect satellite calibrators. This result is very significant because quasars are faint and accordingly require large antennas and expensive observing systems. By contrast, GPS observing systems are relatively simple and inexpensive.

In addition to providing high-performance satellite orbit determination, a GPS-calibrated network could also be considered as a potentially valuable resource for rapid-turnaround Earth orientation determinations, tectonically significant geodetic measurements, time transfer, and ionospheric monitoring.

Contact: Philip E. Liebrecht
Code 531

Sponsor: Office of Space Tracking and Data Systems

Mr. Philip Liebrecht is Head of the RF Systems Section and Manager of Advanced Tracking Technologies. Mr. Liebrecht earned an MSEE degree from the University of Maryland, and his professional interests include communications and signal-processing theory. He has 10 years of experience at Goddard.

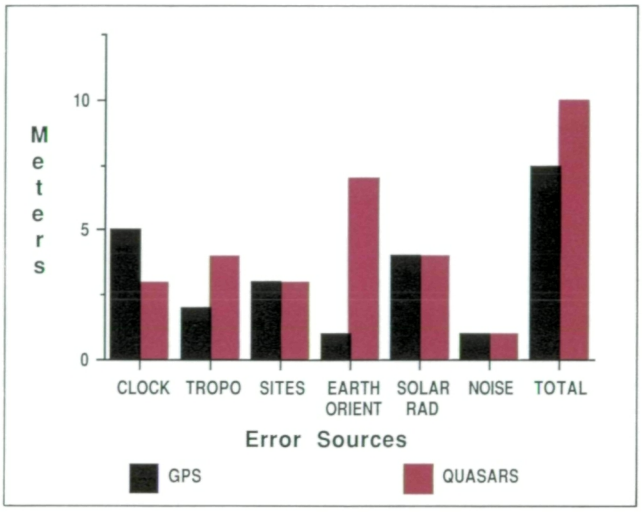

Error profile for interferometric tracking of TDRS-East (41° W longitude) by use of a small network calibrated by GPS or quasar observations. To minimize the calibration data volume, United States Naval Observatory predictions would be used for Earth orientation values with quasar calibration.

SYSTEM AND SOFTWARE ENGINEERING

DISPLAY MANAGEMENT SYSTEM

In the summer of 1986, Goddard's Space Data and Computing Division (SDCD) released Version 1 of the Display Management System (DMS). This multifunction subsystem of the Transportable Applications Executive (TAE), also originally developed by SDCD, is a generic image display system that supports both end users and developers of image analysis software. Like TAE, it minimizes the amount of recoding needed as the hardware environment changes. It is a unique solution to the development cost problem faced by most projects.

The number and variety of raster-based image display devices has been increasing significantly in recent years with increased interest in image processing in various space and Earth science disciplines. This has necessitated the development of tools to simplify programmer and

user interaction with such devices. It was in recognition of this need that the DMS development was started (Perkins, D., et al., 1984). The DMS separates features common to all display devices from those that are device dependent. Thus, by isolating the device-dependent software, DMS permits the users and applications programmers to interact with all display devices in the same manner without having to understand the specific display configuration. For example, with DMS, the user need not know the precise refresh memories in which an image resides. The system permits the use of image names rather than machine-dependent references. The applications programmer only needs to reference machine-independent functions.

As the figure (Parker, D., 1986) illustrates, whenever new display hardware is to be included in a system, only the DMS device dependent software needs to be recoded if it is not already available for the new machine. On a module basis, this represents about 10 percent of DMS code. DMS contains 503 device-independent and 52 to 69 device-dependent functions, depending on the display device. Device-dependent code has been developed for

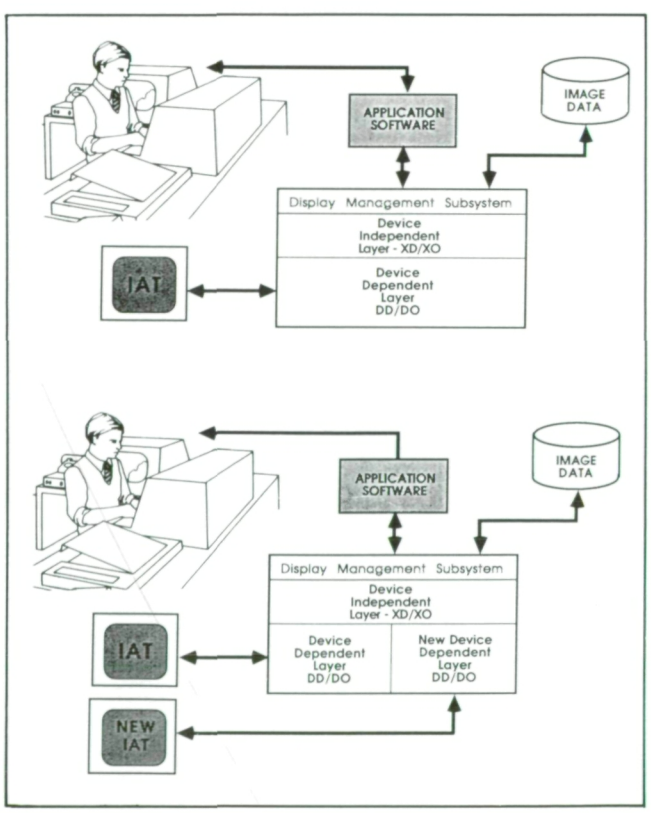

Display Management System. Top panel: a layered software design. Bottom panel: system upgrade with a new IAT added.

the International Imaging Systems (IIS), Rastertek, Deanza, and Adage machines. The percentage of code requiring conversion is even smaller than that (5 percent) if lines of code are considered. There are approximately 37,800 lines of executable source code in device-independent functions. The device-dependent code consists of approximately 1800 to 2550 executable lines.

In DMS there are three main packages of routines that can be called by applications programs. These packages perform the following functions:

- Track display device status during an interactive session.
- Transfer image, graphic, and look-up table data between the display device and disk resident files.
- Manipulate image and graphic data in the display device.

DMS also provides more than 30 application functions for use in device manipulation. These include allocating/deallocating/initializing a display device, basic disk-display image transfer, viewing/saving/deleting a display memory image and/or its configuration, image mapping, histogram creation, cursor definition/toggling, flickering between two images, zooming/panning/pivoting an image, applying mapping to an image, and site definition.

The system was developed in several stages under a Memorandum of Understanding with Earth Resources Observation System (EROS) Data Center in Sioux Falls, South Dakota. Development at Goddard initially worked with an IIS machine accessed through a VAX 11-780 under VMS. Version 1.1 of the code, which includes graphics capabilities, was released to Beta test sites in spring 1987. That code also runs under UNIX.

There are currently 13 user sites: Goddard (3 sites), the Arnold Air Force Station in Tennessee, EROS in South Dakota, the Computer Graphics Center in North Carolina, the Scripps Institute of Oceanography in California, Louisiana State University, the University of Colorado, the University of Washington, the Naval Ocean Research and Development Activity (NORDA), the United States Geological Survey, and the Naval Postgraduate School in California. Response from those users has been very positive. The Beta test sites have complemented the DMS for features such as:

- The ease with which system managers have been able to build and run the system for the first time.

- Its compatibility with TAE, which allows users to run Land Analysis System (LAS), TAE, Catalog Manager, and DMS functions alternately at will.
- The compatibility between DMS and LAS images.
- A well-designed and comprehensive system functionality.
- Thorough run-time error checking and extensive documentation.

Contacts: Marilyn J. P. Mack and Yun-chi Lu
Code 636

Sponsor: Office of Space Science and Applications

Ms. Marilyn Mack, who holds an MA degree in mathematics from Georgetown University, is Co-Investigator on the Distributed Image Analysis System. Her professional interests include programming, analysis image processing, and computer graphics. Ms. Mack has served with Goddard since 1970, and she received a Group Achievement Award as a member of the Project Development/Operations Team for Landsat Thematic Mapper Early Access System.

Dr. Yun-chi Lu, who received a PhD degree in plant physiology from Virginia Polytechnic Institute, is involved with the Pilot Land Data System and the Land Analysis System. Dr. Lu specializes in digital image processing and in renewable resource inventory. He has three years of service with Goddard.

GENERIC VISUALIZATION OF SCIENTIFIC PHENOMENA

Critical to the understanding of data is the ability to provide pictorial or visual representations of that data, particularly in support of correlative data investigations. This is a concept that the National Space Science Data Center (NSSDC) has recognized for several years and that has begun to grow in importance among the scientific community at large only recently. (Refer to the National Science Foundation's report, *Visualization in Scientific Computing*, July 1987, for a succinct discussion of this idea.) To implement this concept for the space and Earth science research community, the NSSDC has an ongoing program to develop new, generic (i.e., data-independent) techniques for the display of multidimensional data as well as associated information about these data or metadata. These techniques utilize the latest methods in computer graphics and imaging and state-of-the-art hardware. As part of these efforts, the NSSDC developed the NSSDC Graphics System (NGS), an interactive discipline-independent toolbox to support the visualization of data, on the NSSDC Computer Facility DEC VAX 8650 and VAX-11/780. To utilize the NGS, data of interest must be stored in terms of the NSSDC Common Data Format (CDF), a data-independent abstraction for multidimensional data structures. The CDF has been used to develop numerous generic data management, display, and analysis tools for a wide variety of disciplines at the NSSDC. The CDF development efforts are evolving into a standard method for storing space and Earth science data for a variety of applications. (Refer to L. Treinish and M. Gough, "A Software Package for the Data-Independent Management of Multidimensional Data," *EOS* 68: 633–635, 1987, for a description of CDF.)

The NGS supports the ability to display or visualize any arbitrary multidimensional subset or slice of any data set by providing a large variety of different representation schemes, all of which are supported by implicit animation. In other words, any field within one or more CDF-based data sets can be used for any axis, including sequencing for animation. In addition, the NGS places a strong emphasis on complete annotation of its graphical products and on extensive use of color. The NGS supports the following ways of displaying data:

- Two-dimensional histograms
- X-Y plots (including optional multiple axes, pseudocolor, and polar coordinates)
- Multiple panel displays
- Location maps
- Contour plots with and without maps
- Surface diagrams with and without maps (including optional pseudocolor)
- Pseudocolor images with and without maps
- Solid modeling without maps

In addition, the NGS will support these visualization techniques in the future:

- Solid modeling with maps

- X-Y-Z plots with and without maps
- Two-dimensional vector field plots with and without maps
- Three-dimensional vector field plots with and without maps
- Three-dimensional histograms with and without maps

The NGS also provides several options for each representation scheme, such as curve fitting, gridding, scaling, filtering, font selection, statistics, and graphics metafile generation. Specific options are associated with all representation schemes (e.g., controlling the range and increment of isolines on contour maps).

The NSSDC strongly emphasizes that the NGS develop very accurate, high-performance graphics tools for data visualization. For example, to support the visualization of large, geographic data sets, the NGS employs very flexible world mapping capabilities that are not only quick but also very precise to eliminate any distortion in mapped displays. Currently, 22 general projections are supported, and more can be easily added by user request. The user has complete control over the specification of the pole point and viewing window for any of the display techniques available with world maps, to support arbitrary reprojection of any data set. Both low and medium resolution world coastline data bases are supported, the latter with political boundaries. In the future, a very high resolution world coastline data base will be added as well as a world topographic data base.

The design of the NGS provides an open-ended framework for discipline-independent data visualization so that new capabilities can be added. New tools are being implemented as a result of NSSDC's research in several areas, which is an outgrowth of previous efforts supported by the GSFC Director's Discretionary Fund for interactive solid-modeling techniques employing NASA's Massively Parallel Processor (MPP). For example, the following specific new techniques have been recently developed:

- Advanced data structures supporting graphics as well as data analysis and management applications to assure rapid display and manipulation of large, complex data sets:
  - storage and sampling of three-dimensional data via generic oct-trees
  - polygon expansion via quadtree-based rectangular subdivision for pseudocolor imagery
- Rendering and manipulation algorithms with serial (e.g., VAX) and parallel (e.g., MPP) implementations that can operate on any data object or geometry:
  - n-dimensional gridding
  - ray-tracing via recursive spherical triangle subdivision

The NGS is designed to be portable so that copies eventually can be made available on computer systems outside of the NCF to promote the exchange of both software and data. In fact, it is expected that the NGS will be beta-tested at several sites on the Space Physics Analysis Network (SPAN) by late 1987 to evaluate it for potential use in future flight projects as well as to support specific scientific investigations. In addition, the NGS is currently available operationally to the users on SPAN of NSSDC's Network Assisted Coordinated Science system in support of the Coordinated Data Analysis Workshop. It will be available to users of NSSDC's NASA Climate Data System in the future. To properly support the diverse use of the NGS, the software is maintained with strict configuration control under NSSDC management.

In the future it is hoped that this work will be expanded to support the implementation of the NGS into low-cost graphics workstations (e.g., Apple Macintosh II) as well as high-performance graphics workstations (e.g., Silicon Graphics IRIS) and the support of production of presentation-quality animated visualizations. In such an operational environment, an analyst would use the various conventional NGS tools to examine data of interest at different levels of detail, and then interactively view a solid geometry model of the data in three dimensions on a graphics workstation, including the examination of sequences of such models. A user could optionally invoke the MPP or the NASA Space and Earth Sciences Computing Center CDC Cyber 205 to prepare the geometries or otherwise manipulate the data in a timely and straightforward manner. After such an examination, a user could visually choose an appropriate orientation for the geometries, and then request a ray-traced image(s) or animated sequence to be generated on the MPP or Cyber 205.

The figure is an example of the kind of data visualization that can be generated by the NGS. The montage

ORIGINAL PAGE
COLOR PHOTOGRAPH

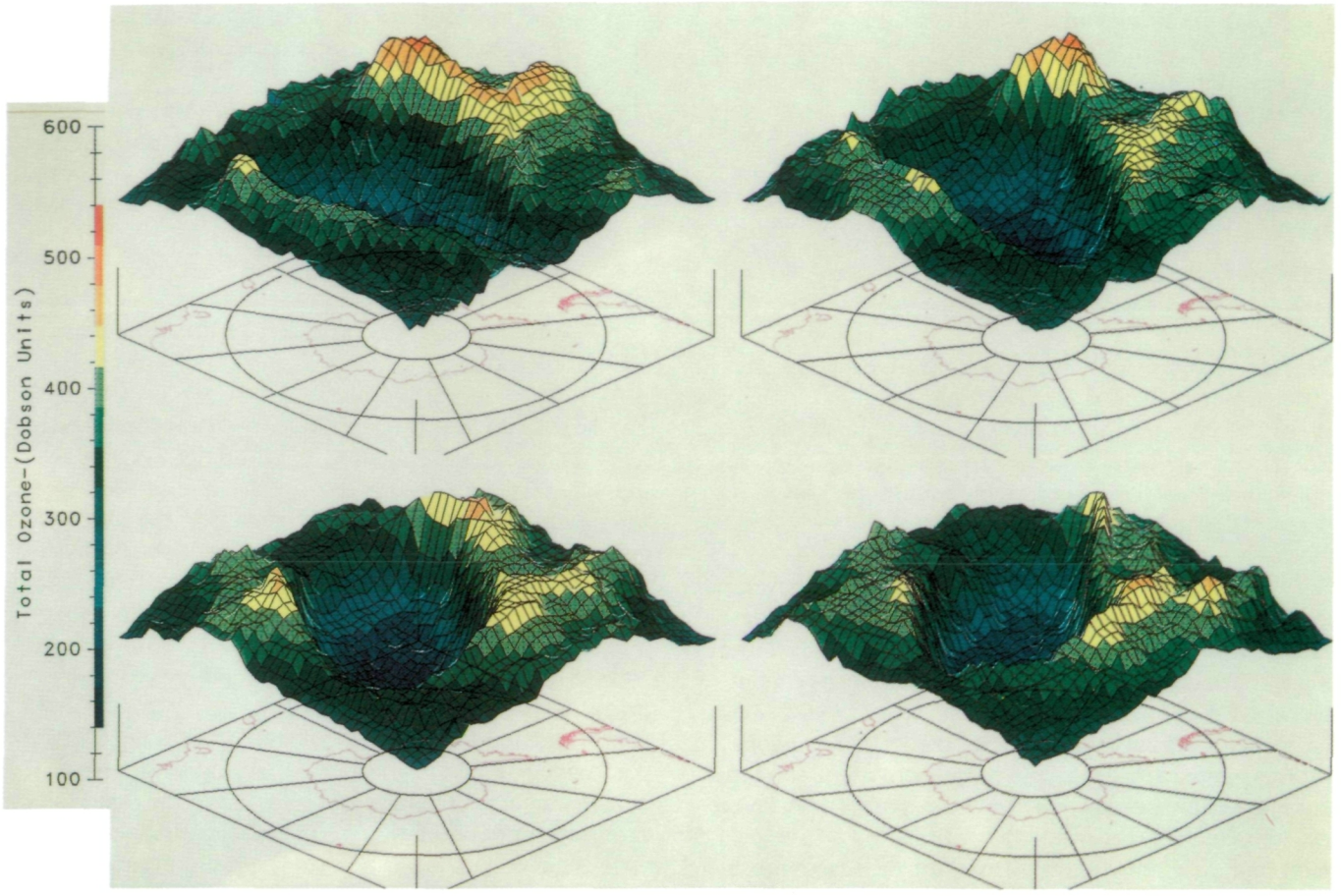

Data visualization generated by the NSSDC Graphics System of the results of the reduction in total ozone observed during the Antarctic spring last year (October 14, 15, 16, and 17 1986: upper left, upper right, lower left and lower right, respectively).

illustrates the results of the reduction in total ozone observed during the Antarctic spring last year. It shows daily ozone data on October 14, 15, 16, and 17, 1986, as an animated sequence (upper left, upper right, lower left, and lower right, respectively). Each day of data is visualized as a three-dimensional object centered over the South Pole in an azimuthal equidistant projection. The displays show total ozone in terms of Dobson Units, which is represented by both the pseudocolor spectrum and height. The height mapping dramatizes the concept of a hole in the ozone layer, while the color enhances this perception as terrain color would enhance a topographic map. Other visualization techniques (e.g., high-resolution pseudocolor imagery) might emphasize the detailed, quantitative evolution of the spatial structure instead. This technique emphasizes qualitative information and shows the temporal and coarse spatial evolution of the total ozone over the 4 days. The data used by the NGS to create these displays are derived from the Total Ozone Mapping Spectrometer onboard NASA's Nimbus-7 spacecraft. The data are available as daily world grids from late 1978 through the present and are archived at the NSSDC.

Contact: Lloyd A. Treinish
Code 634

Sponsors: Office of Space Science and Applications and the National Space Science Data Center

Mr. Lloyd A. Treinish is a data analysis mathematician with eight years of service at Goddard. He works on the development of advanced data systems for support of scientific applications, as well as studying space and atmospheric phenomena. Mr. Treinish developed the concept of using NASA's Massively Parallel Processor (MPP) as a computational geometry server, was the chief designer and developer of the Pilot Climate Data System

(PCDS), and conceived of the first, self-describing data abstraction for the storage and manipulation of multidimensional data, as the Common Data Format (CDF). Mr. Treinish received an S.M. degree in physics from the Massachusetts Institute of Technology and is the recipient of four NASA Certificates of Outstanding Performance.

GRO SPECIAL GRAPHICS

The Gamma Ray Observatory (GRO) special graphics is a third-generation research project that allows a spacecraft operator to monitor the status of a satellite via three-dimensional graphics. Selected satellites along with the Earth, Moon, Sun, and guide stars are modeled in three-dimensional graphics. The operator can then select any 4 of 12 preselected views to be displayed in the four viewpoint windows on a modified AT workstation. These points of view can be anywhere in the space surrounding the satellite, which includes looking from the inside of the satellite out, to model instrument fields-of-view, and looking from outside the satellite toward the satellite to see the attitude, position, and Sun impingement relative to the celestial bodies and other satellites such as the Tracking and Data Relay Satellite (TDRS). These displays allow the operator to visualize what is happening as opposed to having to translate pages of real-time telemetry data.

A good example of how these displays might be used is the case of modeling the Sun impingement on the GRO satellite. Certain parts of the satellite have to be kept in the shade. This is a function of the attitude and the position of the Earth, Moon, and Sun relative to GRO. A three-dimensional display of GRO with vectors depicting the Sun, Earth, and Moon angles and light source shading for the GRO satellite gets the information across to the operator much faster than having to read all the ASCII data from telemetry pages and integrate that information along with the position of the celestial bodies.

The original pilot project was performed on a Silicon Graphics (IRIS) workstation. Phase one of the pilot project involved modeling the Shuttle and the Cosmic Background Explorer (COBE) satellite in three dimensions, using both wireframe techniques and solid modeling techniques. The demonstration depicts COBE being deployed from the Shuttle bay. The four-windowed display can be arranged so that the user can select different eye points for each window, which includes simulated instrument fields-of-view. In addition, the user can select the option of displaying a mercator projection, a globe display, or an equidistant polar plot of the Earth in any of the windows. Finally, the user may decide that one of the windows should display simulated ASCII telemetry data. Selection of these options is made via the use of pop-up menus and a mouse. Selections can be made dynamically, that is, while the displays are operating. See Figure 1 for an example of a typical display.

Phase 2 of the pilot project was created in response to a request by the GRO project to examine the feasibility of implementing this system for GRO. For this phase of the pilot project, the GRO satellite was modeled with enhancements over the previous demonstration, again using the IRIS workstation. A methodology was developed and implemented that allowed for any object to be rapidly prototyped with a geometric solid model data base with hidden surface removal and light source shading. The demonstration with the Shuttle was an object specific hidden surface removal algorithm with no real light source shading. With the future addition of a digitizing tablet interface, the amount of time required to model a spacecraft will be reduced by 90 percent. Thus the task of modeling a satellite becomes a rapid prototype effort. In addition to the GRO solid model, a stripchart display and a propulsion subsystem display were added as options. See Figure 2 for an example of the GRO prototype. The demonstration for this prototype depicted GRO performing an attitude maneuver, while the other windows graphed attitude parameters and graphically showed the status of the propulsion subsystem.

The GRO project personnel reviewed the prototype in spring 1987 and decided that this would satisfy the needs of the projects. The next few months were spent developing requirements and a design for the real-time system that is called the GRO Graphical Monitoring System (GMS) and porting the demonstration onto a modified IBM AT compatible, a Kandl Data Products AT with a Weitek 7100 geometry engine.

The target hardware had to be ATs, since the Payload Operation Control Center (POCC) workstations are ATs. Tradeoffs were considered. In particular, performance is much slower on the POCC workstations than on the IRIS. In addition, the new IRIS systems have hidden surface removal and Gouraud shading built in. Another disadvantage is that the IRIS is a high-resolution, non-interlaced video display with up to 16 million different displayable colors, whereas the POCC workstation has medium resolution, interlaced video with 256 of 16 million colors displayable. For these reasons, the IRIS display has a more dynamic and pleasing appearance.

ORIGINAL PAGE
COLOR PHOTOGRAPH

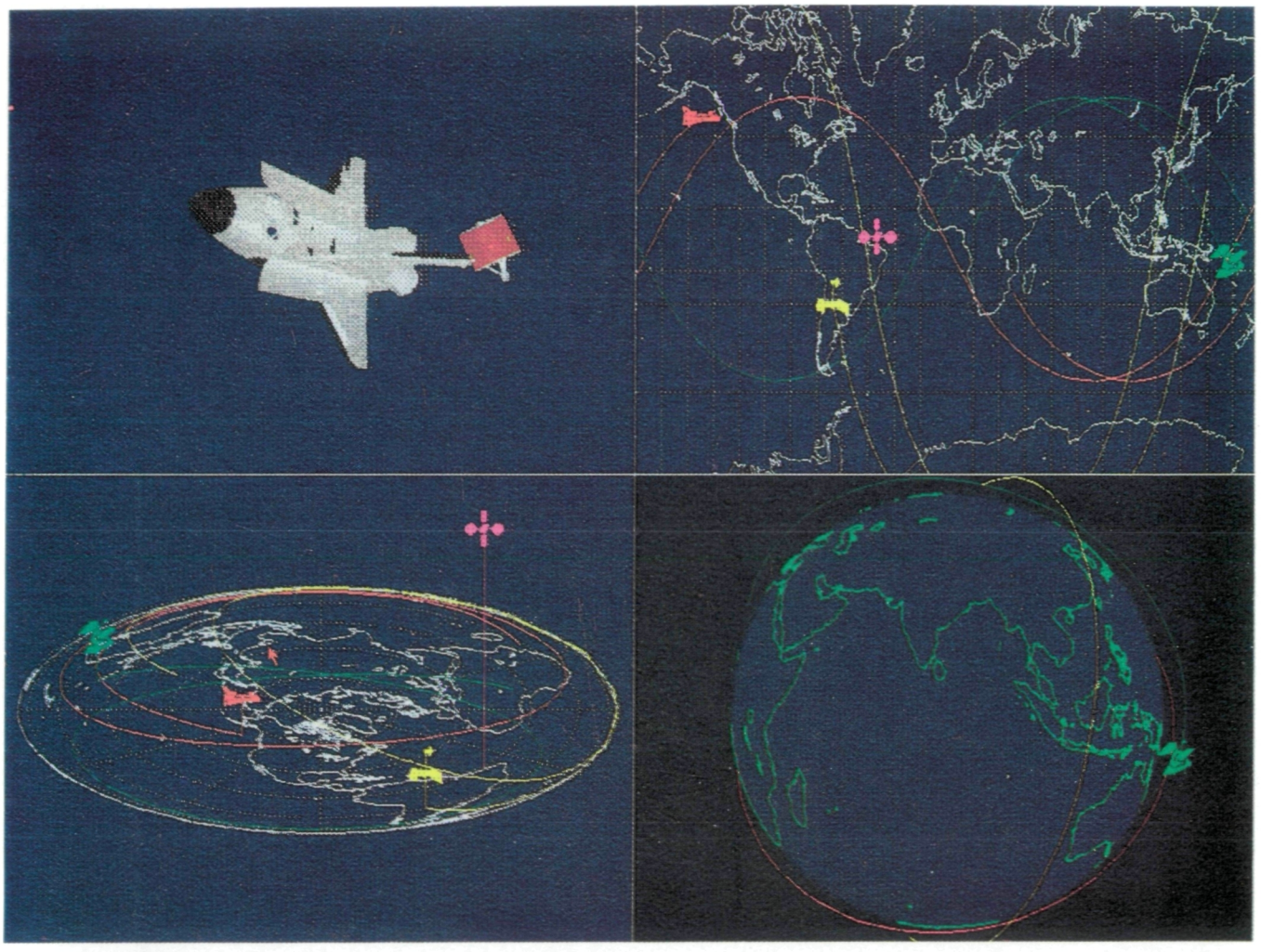

Figure 1. Original prototype on Silicon Graphics IRIS workstation, Cosmic Background Explorer being deployed out of the Shuttle (upper left window), mercator projection with icons for Shuttle, TDRS East and TDRS West (upper right window), equidistant polar plot of Earth with altitude depiction (lower left window), and globe (lower right window).

However, we could not use the IRIS because the Multisatellite Operation Control Center, where these systems will be operating, has a requirement for RS-170 RGB interlaced video because this video is distributed to other monitors. Also, the cost of the AT system is about one-fifth of the IRIS. Finally, since the telemetry display update rate is once every 4 seconds and this is the data used to update the GRO GMS displays, the performance of the AT workstation is fast enough.

The final prototype as presented in the design review in September 1987 to the flight operation team had 12 different displays. The displays include:

- Solid model of GRO with Gouraud shading to depict Sun impingement
- Depiction of GRO's position relative to Earth with the Zone of Exclusion, the Radio Frequency Interference zone, the South Atlantic Anomaly, and the day/night terminator indicated
  - — mercator projection
  - — three-dimensional Earth
- TDRS East and TDRS West fields-of-view with entry and exit times of the GRO satellite and indications as to which TDRS link is active
- GRO high gain antenna azimuth/elevation polar plots

ORIGINAL PAGE
COLOR PHOTOGRAPH

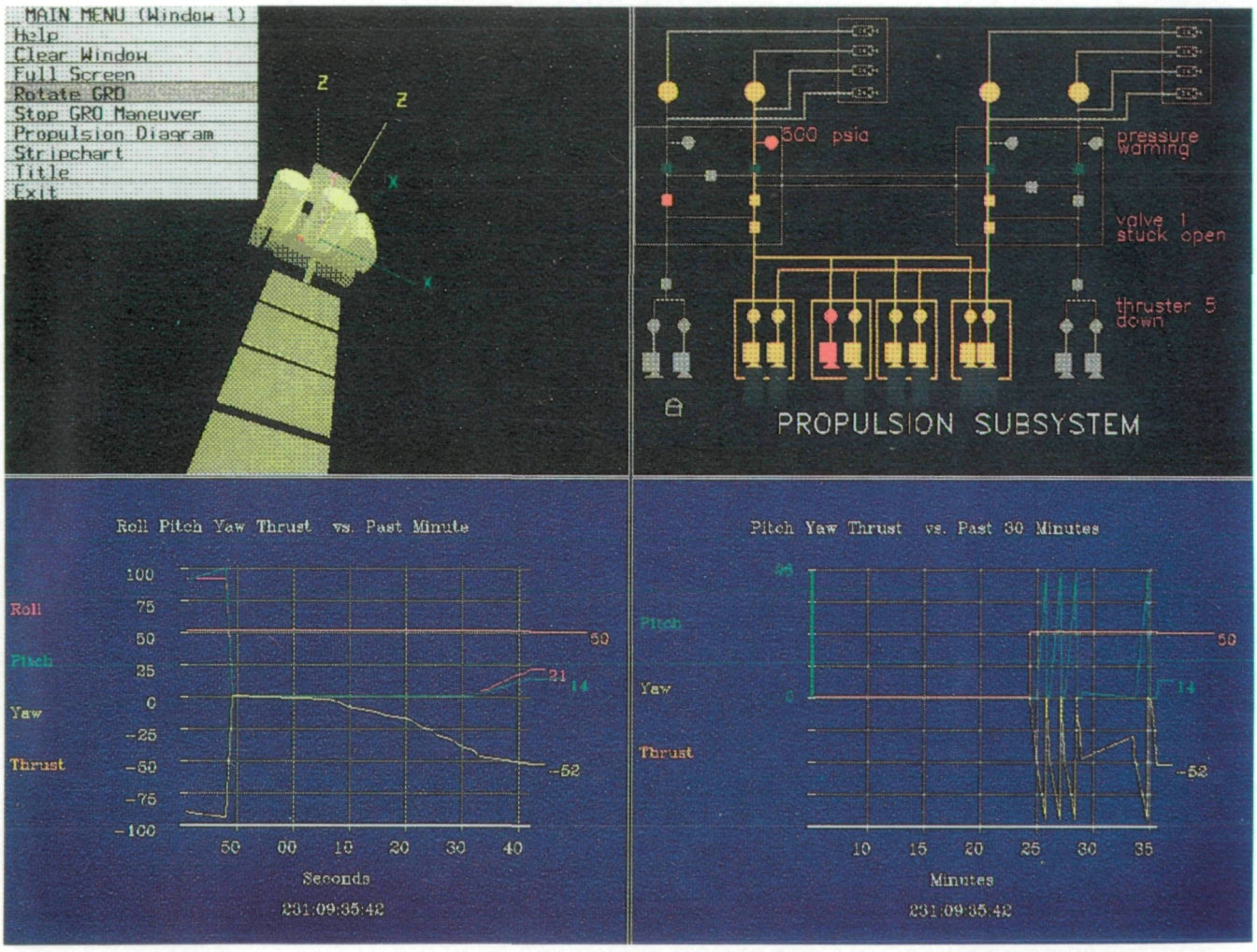

Figure 2. Gamma Ray Observatory performing attitude maneuver (upper left window), propulsion subsystem status (upper right window), and graph of pitch, yaw, roll, and thrust (lower windows).

- GRO field-of-view for the following:
  - — +X and -X axis
  - — bright object sensors 1 and 2
  - — fixed head star trackers 1 and 2
  - — fine Sun sensor assembly 1 and 2

This prototype will be integrated into real-time operations as outlined in the design review. The system will receive data in real time from a Standard Test and Operation Language telemetry display page and predict data from Flight Dynamics Facility via file transfer every week or two. See Figure 3 for a sample display of this final prototype and Figure 4 for a drawing of the hardware configuration that will be used in real-time operations.

The original prototype not only had this project as a real-time spin-off, but in addition, the Flight Dynamics Facility completed development of the original prototype to support Shuttle missions. They have supported the Shuttle High Energy Astrophysics Laboratory and are planning to support Space Telescope and GRO during the launch phases.

This project was done in collaboration with Doug Carlton, Ray Twiddy and David Vavles of Computer Sciences Corporation.

ORIGINAL PAGE
COLOR PHOTOGRAPH

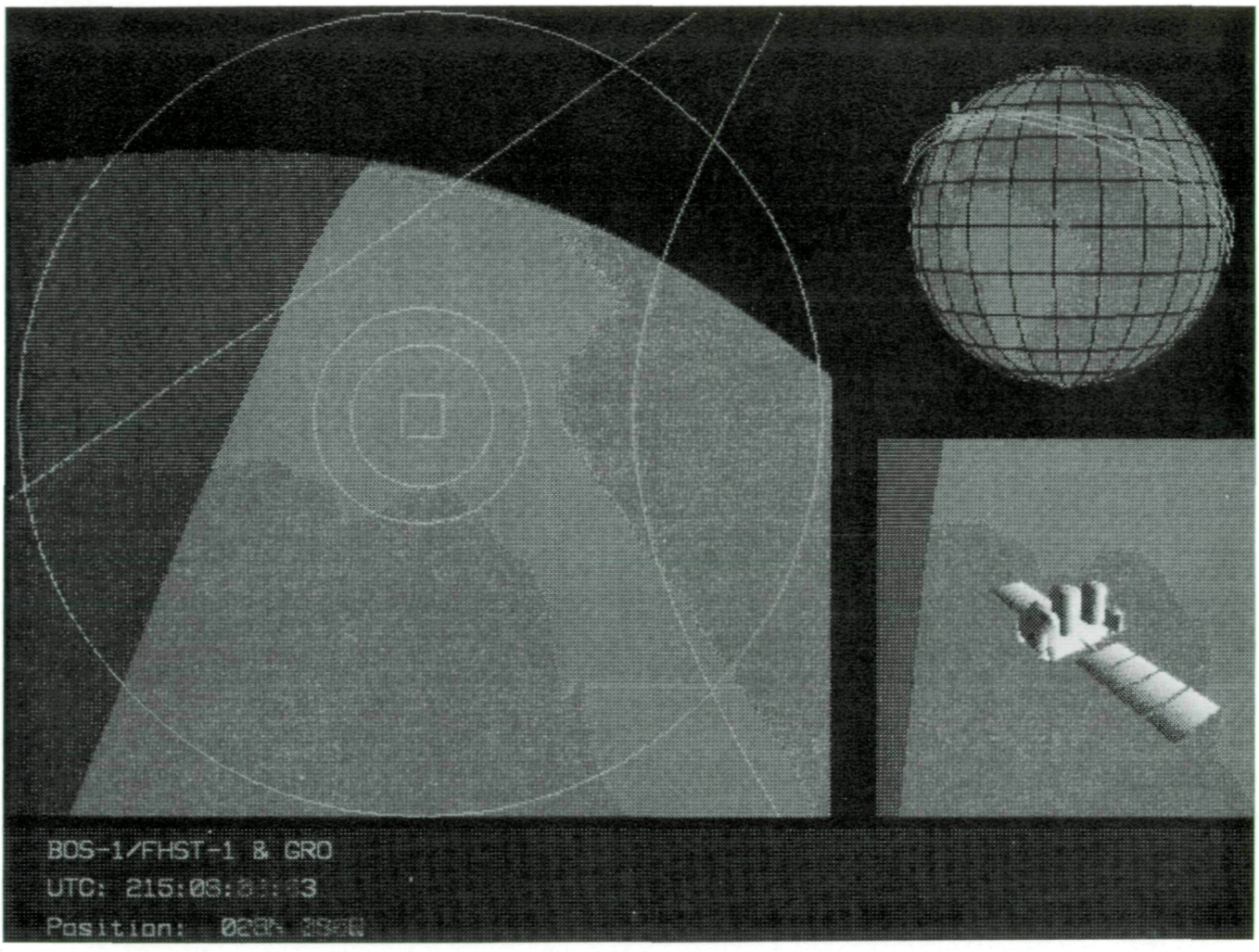

Figure 3. Bright Object Sensor (BOS) 1 in left window, Tracking Data Relay Satellite field-of-view in upper right window, Gamma Ray Observatory with Sun Impingement in lower right window.

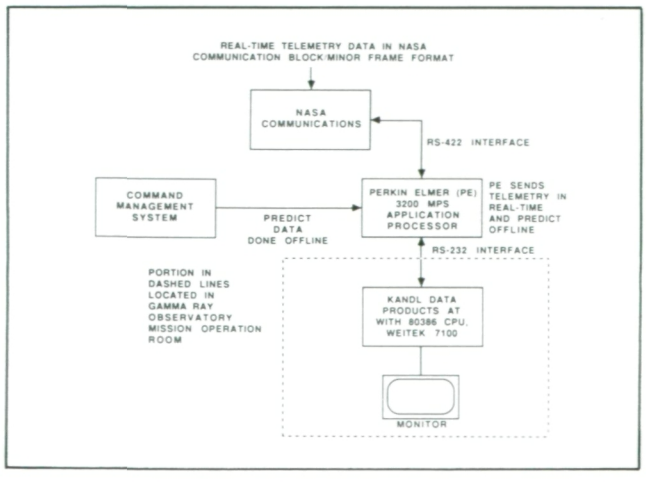

Figure 4. Configuration of Gamma Ray Observatory graphical monitoring system with interfaces.

Contacts: Dan Mandl and Ron Mahmot
Code 511

Sponsor: Office of Aeronautics and Space Technology

Mr. Dan Mandl works with the Control Center Systems Branch, and he is interested in computer graphics. Mr. Mandl, who holds a BSEE degree from the University of Maryland, has seven years of experience at Goddard.

Mr. Ron Mahmot serves with the Control Center Systems Branch. Mr. Mahmot received his Bachelors degree in computer science from the University of Maryland, and he has two years of experience at Goddard.

INTEGRATED TEXT AND GRAPHICS

The writing of scientific papers is one of the important activities performed by the scientists who use the NASA Space and Earth Science Computing Center (NSESCC). This writing process is cumbersome because the text, equations, and graphics must be generated separately and pasted together. To make the process more efficient, the NSESCC has provided its users with a means to generate a proof copy of an entire paper. To accomplish this goal, several things were required: an output device that could produce both text and graphics, the software to drive that hardware device, a flexible page layout program, a convenient equation formatter, and the software to create the graphics.

The output device chosen was one of the NSESCC system printers, an IBM 3800 Model 3 laser printer, because it had good resolution at 240 pixels/in., a rated speed of up to 215 pages/min, and the ability to address each pixel on a page. These features are the result of both hardware and software components. The printing engine itself is based on an electrophotographic process that is built around the properties of photoconductors.

When light strikes a photoconductive surface, the surface becomes more conductive. The printer has a drum wrapped with a photoconducting sheet that has a negative potential applied to it before each page is printed. A bitmapped image of the page is created, and two lasers scan the image onto the photoconductor, causing the negative surface charge to be neutralized anywhere the toner is to appear. The toner, a colored thermoplastic, is applied to the image, and the now-latent image is applied to the paper electrostatically. Finally, the toner is fused to the paper by heat and pressure.

The software component of the printing system is based on IBM's Advanced Function Printing Data Stream (AFPDS). The AFPDS is simply a set of commands that allows the 3800 to print bitmapped graphics, rules of varying thickness, up to 63 fonts on a page, information in different orientations, and data anywhere on a given page. The Print Services Facility (PSF) is the printer driver that interprets AFPDS for the 3800.

The scientist lays out a paper with IBM's Document Composition Facility (DCF) and the SCRIPT Mathematical Formula Formatter (SMFF). DCF is a text formatter that provides such features as pagination, index generation, footnotes, tables of contents, figures, tables, hyphenation, spell-checking, and macros. SMFF is an equation typesetter that reads formulas described in keywords and that closely follows the Bell Laboratories EQN program. For example, an equation is entered as:

```
s(x) = (1 + sigma) u sub 0 - q over 1%%
    left lb 1 + delta b + 2
    sum from <k = 1> to infinity of
    <a sub k + b tanh alpha sub k delta>
    over
    <alpha sub k (alpha sub k sub 2 + b alpha sub k
    tanh alpha sub k delta + 1) > %%
    cos alpha sub k x right rb
```

After the equation description is formatted, it looks like:

$$s(x) = (1 + \sigma)u_0 - \frac{q}{l}\left[1 + \delta b + 2\sum_{k=1}^{\infty} \frac{a_k + b \tanh \alpha_k \delta}{a_k(\alpha_k^2 + b\alpha_k \tanh \alpha_k \delta + 1)} \cos \alpha_k x\right]$$

The final part of any scientific paper is the graphics. The NSESCC provides its users with several device-independent graphics packages: DI-3000, NCAR, and

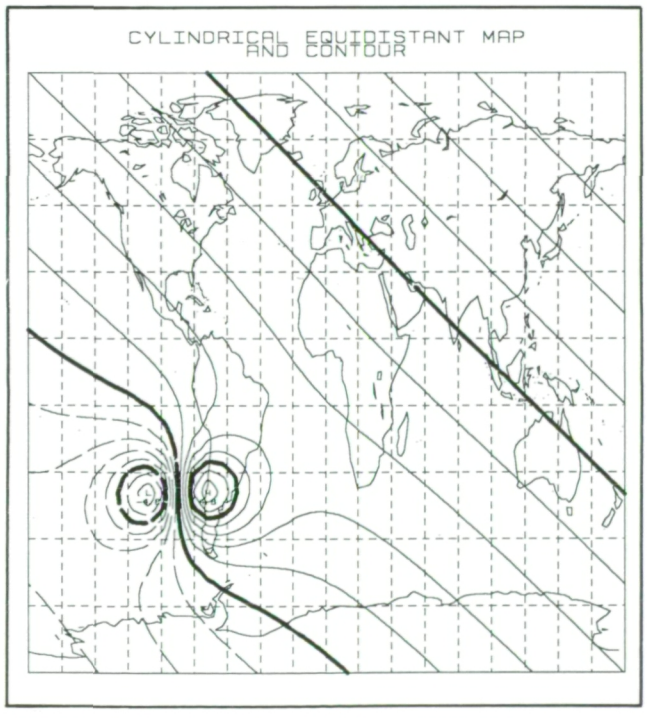

Example of NSESCC.

TEMPLATE. The device-independent nature of these products allows the users to generate plots on their graphic terminals, and when they are pleased with a particular plot, they can save it for inclusion in the paper on which they are working.

The project has been well received by the user community. Users are finding that they can quickly and conveniently produce graphics with text. The 3800 laser printer with the all-points-addressable feature is also proving to be very useful as a graphics output device to analyze results. Moreover, the new capabilities of DCF and SMFF are allowing more information to be put forth in a more readable manner. The NSESCC looks forward to improving these facilities as the software and hardware improve.

Contact: Thomas Schardt
Code 632

Sponsor: Office of Space Science and Applications

Mr. Thomas Schardt is a computer scientist with the Computational Methods and Analysis Facility. He is responsible for the implementation of integrated text and graphics at the NASA Space and Earth Science Computing Center. Mr. Schardt holds a BS degree from the College of William and Mary, and he has three years of experience at Goddard.

TRANSPORTABLE APPLICATIONS EXECUTIVE

The Transportable Applications Executive (TAE) is a software management system that binds a set of application programs into a single, easily operated system with a common user interface. TAE provides the application designer and programmer with a consistent screen layout for menus, parameter prompting, error and information messages, and help screens. TAE was originally developed in the early 1980s to support GSFC scientific interactive data analysis applications (e.g., General Meteorology Package, Atmospheric and Oceanographic Information Processing System, Land Analysis System, and Pilot Climate Data Systems). After 6 years of development, TAE is used for a variety of applications (i.e., image processing, planetology, CAD/CAM design, data-base management, prototyping, and operations/command consoles)—not only at GSFC but at all the NASA centers, other government agencies, universities, and private industries.

In FY87 TAE saw significant growth as its user community increased to 174 facilities, located at 110 sites—a fourfold increase from FY85. Each year the transportable element of TAE becomes more evident as the number of computers running TAE continues to grow. TAE is currently available for a variety of computers, under several operating systems including VMS, ULTRIX, UNIX 4.2 BSD, UNIX System V, and selected hybrid versions of UNIX. The current computer list includes: VAX/VMS, VAXStation II/GPX/VMS; VAX/UNIX; SUN/UNIX; Gould/UNIX; ISI/UNIX; Jupiter/UNIX; Apollo/UNIX; Macintosh with MacWorkStation; CDC/UNIX; HP9000/UNIX; AT&T/UNIX; and Altos/UNIX. TAE is also currently undergoing ports to other computer systems such as the IBM PC/AT under XENIX, the Perkin-Elmer, and the MAC II/UNIX.

New development work in FY87 has been concentrated on adding and extending TAE's user interface functions to support the latest interactive high-resolution graphic workstations and on building interactive tools for the application user interface designer. The sophisticated graphic and windowing capabilities of today's workstations provide system developers with the opportunity to rethink and redesign the user interfaces of NASA's next generation of software systems. For instance, in a command and control environment, many processes run simultaneously to monitor the state and status of the particular operation and its data. With modern graphic workstations, time-critical information on multiple events can be displayed concurrently on the same screen, organized into different windows, and displayed in a variety of graphical and textual presentations. Coupled with the need to prototype different user interfaces (as an effective means of defining and designing new systems), the challenge became to build an environment that provided sophisticated prototyping capabilities yet retained the TAE concept of portability, standard system services, and easy migration from prototype to operational interfaces.

To meet our needs, a rapid prototype of TAE Plus was implemented in FY87 to demonstrate the design-to-production concept. It provides services and tools needed to move from a mock-up of an application's user interface to a user interface supporting a fully operational application. A key component of the prototype TAE Plus is an interactive user interface designer's Work Bench, which allows an application designer or programmer to dynamically lay out application displays and define the static and dynamic areas of the screen. This tool kit also provides a set of interaction objects that have been predesigned and defined with TAE Plus. This eliminates the need for the developer to create objects from scratch. TAE Plus also provides an interactive method for tailoring and arranging the interaction objects. Figure 1 shows

ORIGINAL PAGE IS
OF POOR QUALITY

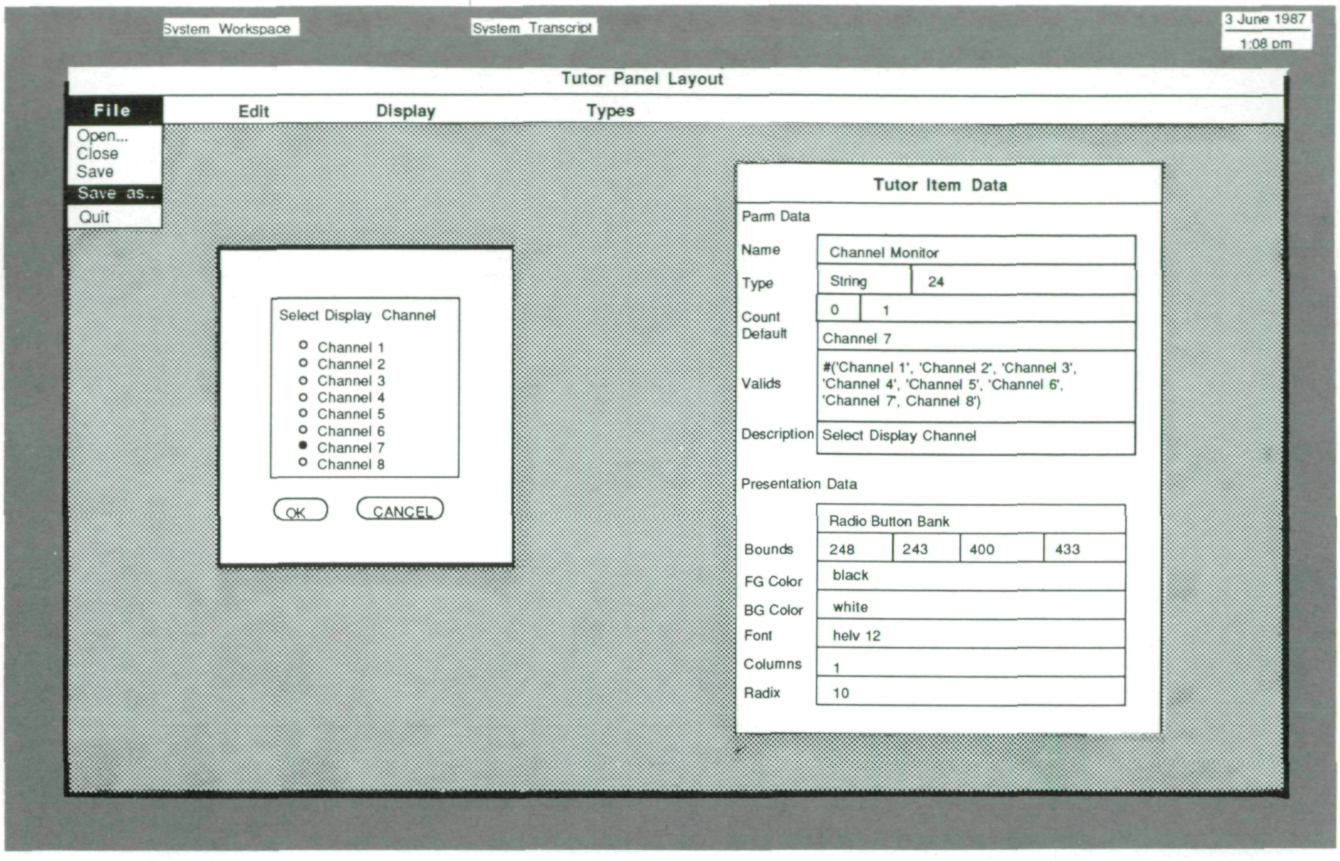

Figure 1. Interface designer uses the TAE Plus Work Bench to design a Radio Button Interaction Object.

a layout of a screen that has been designed in the Interactive Designer's Work Bench.

Once the application's screens have been designed, the Work Bench saves them in a data structure. The prototype includes runtime services used by the application program to display and control the previously defined screens. To change the interface or the screen layout, the designer goes back to the Work Bench, dynamically makes the modifications, and the data structures are updated automatically. The next time the application is run from TAE, the modifications will be in effect. Figure 2 shows an application's user interface during execution; the screen was designed with the Work Bench.

The TAE Plus prototype has validated our approach for an integrated application development environment. It also provides a test bed environment for:

- developing a powerful tool for supporting our current application prototyping tasks;
- building a model of an application-support environment that can be used for refining and validating requirements and human-computer interface techniques for the Space Station User Support Environment;
- using and analyzing X Windows as a window manager and determining if it solves our portability concerns and meets our stringent windowing support requirements; and
- employing the Smalltalk language for implementation of the interactive Work Bench to help understand the value and applicability of object-oriented programming to the user interface management environment.

In addition to the TAE Plus development, much work has been done to enhance TAE with new features requested by the user community. In FY87, major enhancements were made to TAE to provide support for Database

ORIGINAL PAGE IS
OF POOR QUALITY

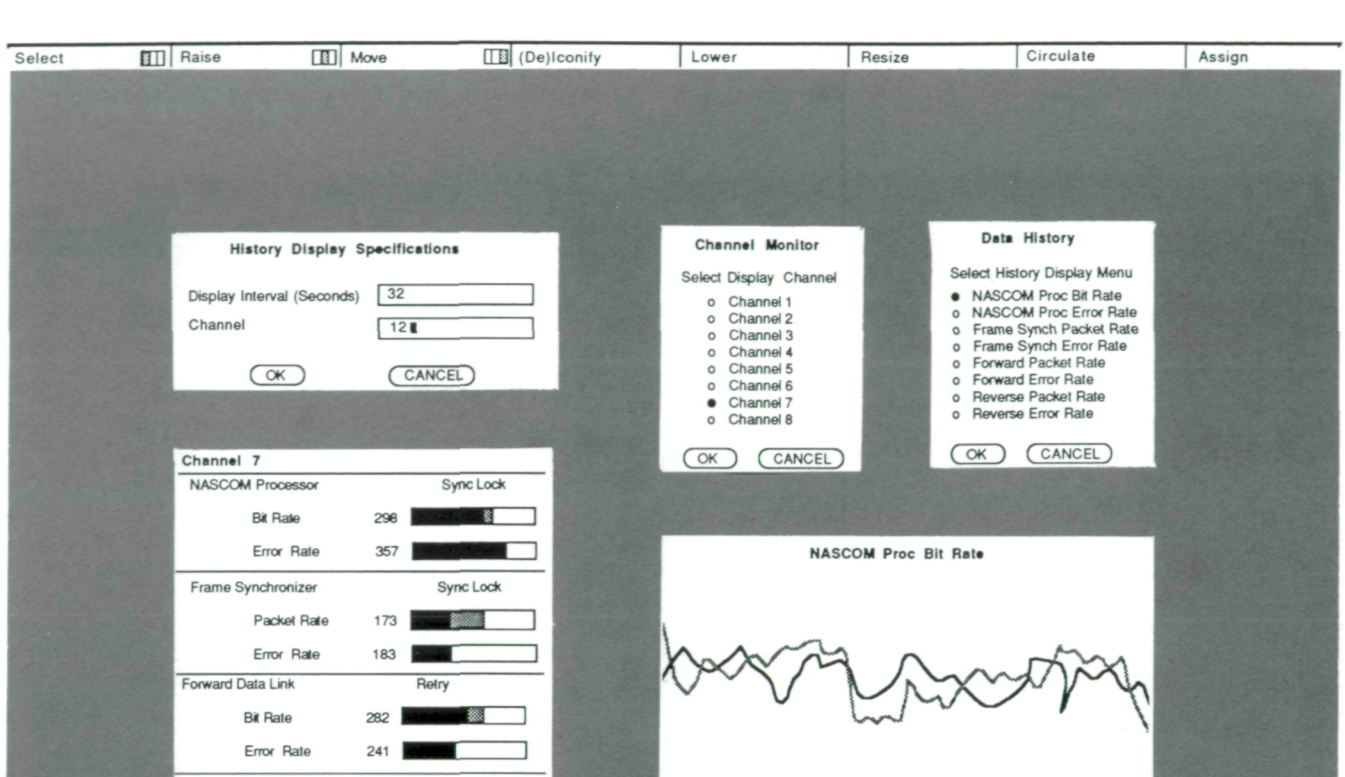

Figure 2. The end user's view of an active TAE application. The contents and layout of the screen were defined by use of the Work Bench.

Management System functions. These enhancements allow an application program to dynamically create TAE menu and parameter definition files based on end-user input. The National Space Science Data Center will be utilizing these enhancements in its data management environment.

An interesting new addition to the TAE family in FY87 is called MacTAE, which transforms a Macintosh computer into a graphics and windowing user interface to a VAX/VMS TAE environment. This allows a user to initiate a TAE application on a VAX from a Macintosh TAE-style user interface (see Figure 3). MacTAE combines the features of TAE, the power of a VAX, and the flexibility and ease of use of a graphical windowing environment at a cost much less than that of a high-resolution, graphics workstation.

Future TAE development efforts will include implementation of additional components and features to improve the overall capabilities of the TAE Plus prototype, as well as experimentation to improve the useability of the system. Evaluation of the prototype's features, architecture, and style will provide guidance in the development of an operational TAE Plus. In addition, porting the prototype

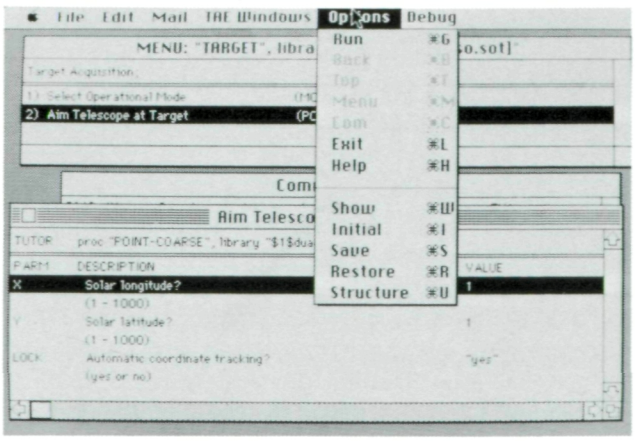

Figure 3. Screen from MacTAE.

from the SUN workstation to the VAXstation II and the MAC II is planned. With these developments, TAE Plus will be well on the way to providing a robust environment supporting an application's full development life cycle.

Contacts: Martha R. Szczur and Jay Costenbader
Codes 521 and 522

Sponsors: Office of Space Science and Applications and the Office of Space Tracking and Data Systems

Ms. Martha Szczur, who received a BS degree in mathematics from Converse College, is Manager of the Transportable Applications Executive Project. Her professional interests include human-factor elements of user interfaces; user interface designer support tools; and the common, standardized user interfaces. Ms. Szczur has been involved in design and development of interactive data analysis at Goddard for 18 years, and she has received several awards for her achievements.

THE SOFTWARE MANAGEMENT ENVIRONMENT

The Software Management Environment (SME) is an integrated set of software tools designed to assist a manager in monitoring, analyzing, and controlling an ongoing software project. Providing a set of capabilities that allow a manager to acquire pertinent, up-to-date information on the quality of a development project, the SME integrates much of the experience, results, and knowledge of major software engineering research that has been carried out at Goddard in studying software development projects over the past 12 years. The research analyzed characteristics of flight dynamics software projects ranging in size from 6000 to 150,000 lines of code. Through these efforts, research has provided a clearer understanding of the software development process within this one particular environment and the factors that lead to successful software projects.

The SME is an attempt to integrate this knowledge into an environment where the manager is better able to track the progress of new development efforts. A series of rules has been developed by studying the empirical data and interacting with software development managers in this environment. For example, a rule might be: "if the error rate of a project is above normal, and the project is early in the coding phase, then the possible reasons for this condition are 1) the problem is more complex than expected, or 2) the development team was less experienced than normal." Rules like this have been derived from the knowledge of the environment, and they will be used by SME to help the manager solve development problems.

The major functions of the SME include the ability to track software project parameters; to compare these factors to past projects; to analyze the differences between the current project's development patterns and the expected development pattern within the environment; to predict characteristics such as milestones, cost, and reliability; and to assess the overall quality of the project's development process. To provide these functions, the tool continually examines available development data from the project of interest including manpower, software changes, computer utilization, and completed milestones.

During 1987, the first demonstration version of the SME was completed. The major components of the system include human-computer interface; a rule base; a corporate memory of software development data; models of the software development parameters as they behave in this environment; and application software to interpret data, predict events, and assess project characteristics. The human-computer interface is the common access method for the manager to communicate with the SME. This interface is designed for ease of use and for maintaining a level of interest in the tool; it is the culmination of much research and comparison of differing types of interfaces. A second major component of the SME is the rule base, which contains the knowledge needed to assess and analyze projects. The rule base integrates the knowledge of the experienced software manager with the knowledge obtained by the software engineering studies to enable SME to determine the cause of deviations from the expected in the software project parameters and to assess the overall quality of the software project's development. The corporate memory is used to access the important software project parameters of both current and past development projects. These data are used not only for comparison and prediction purposes, but also for input for the analysis via software rules. A final component of the SME is the models of the software development parameters. These models would be used for such functions as predicting cost, reliability, and schedules for a project based on existing development data.

As an example of how the SME might look to the user, a sample of the monitor function that allows the manager to compare current projects with the model for that parameter is shown in the figure. This example shows the

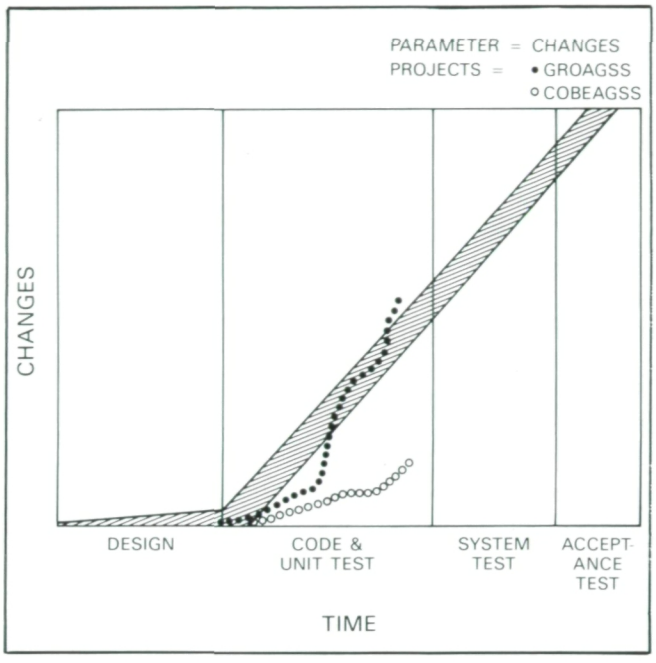

Software Management Environment Monitor.

relative number of changes for two projects, GROAGSS and COBEAGSS, over time. Both projects are in approximately the same stage of development, late code and unit test, but they have very different change histories. The GROAGSS started out below average in the number of changes reported and eventually goes above the normal amount of changes, whereas the COBEAGSS has consistently been below average in the number of changes. A graph like this will provide the manager with information on and insight into the current status of these two projects.

Contact: Jon D. Valett
Code 552

Sponsor: Office of Aeronautics and Space Technology

Mr. Jon Valett, who specializes in software engineering and artificial intelligence, is involved with the Software Management Environment. Mr. Valett received an MS degree in computer science at the University of Maryland, and he has four years of experience at Goddard.

GAMMA RAY OBSERVATORY DYNAMICS SIMULATOR

The Gamma Ray Observatory (GRO) Dynamics Simulator project was developed in parallel by using the FORTRAN and Ada programming languages to assess the advantages of using Ada for flight dynamics software. The project is a joint venture of Codes 520 and 550, the Computer Sciences Corporation, and the University of Maryland. The FORTRAN version of the simulator will be used to evaluate and test the attitude determination and control models to be used onboard GRO under conditions that simulate the expected in-flight environment. Data collected by the Software Engineering Lab from the developers of both versions will be studied and compared upon completion of the Ada version (GRODY), which is now undergoing system testing.

GRODY, one of the first large-scale Ada projects at Goddard (50,000 executable lines of code), has thus far produced or refined effective methods for Ada training, requirements analysis, and design. An Ada training course was developed, the Composite Specification Model (CSM) was refined and used for GRODY requirements analysis, and a General Object Oriented Design (GOOD) methodology was developed during the design phase of GRODY.

Ada is a complex language that incorporates many new concepts of software engineering, such as data abstraction, tasking, and generics. Managers of Ada projects must be certain that their software developers are learning to use Ada effectively as a software engineering tool. For this reason an Ada training course was developed by the GRODY team and outlined in *Ada Training Evaluation and Recommendation* (Murphy, R., and Stark, M., 1987). Students in this course attend two 1.5-hour lectures per week for 2 months. Time in between these lectures is allotted for completion of practice problems and exercises. Other important conclusions of the Ada training report were that there is a need for training software developers in design methodologies utilizing Ada features, for training project managers so that they will be able to understand the different notation of products such as those produced for design reviews, and for training managers in making schedules and staff planning estimations for large Ada projects.

CSM is a framework for expressing system requirements that are represented by three orthogonal views: the dynamic view that expresses the behavior of the system over time, the contextual view that captures the objects and relationships in the environment that is being modeled by the system, and the functional view that shows the data flow and transformations needed to accomplish the required functional processing (Agresti, W., et al., 1984). The GRODY team found the functional view to be the most useful, and the team refined some of its rules

and notation, which consist mainly of data flow diagrams and a data dictionary.

GOOD is a design methodology developed for use by the GRODY team as a result of studies of several existing design methods. It draws from the best features of object oriented and process abstraction methodologies. The notation of GOOD, called object diagrams, is a hierarchical structure in which objects can be decomposed into lower level objects. Arrows between objects indicate control flow or subprogram calls rather than data flows. The subprogram calls as well as their corresponding data flows are listed in the object description that accompanies the object diagram (Seidewitz, E., and Stark, M., 1986). GOOD is best suited for Ada projects; however, it is also applicable to projects implemented in other languages.

This project will continue to produce relevant results that will be used in assessing the benefits of Ada for flight dynamics and related software. On completion of GRODY acceptance testing, studies comparing the entire life cycles of the FORTRAN and Ada projects will be made.

Contact: Robert Murphy
Code 522

Sponsor: Office of Space Operations

Mr. Bob Murphy is a software engineer involved with software development for the Gamma Ray Observatory's Dynamics Simulator. Mr. Murphy earned a BA degree at La Salle College, and he has three years of experience at Goddard.

THE OPERATOR'S ASSOCIATE: AN OPERATOR FUNCTION MODEL EXPERT SYSTEM

Within the context of the ongoing human factors program, work is continuing on the further development of the Operator Function Model (OFM). The OFM provides a methodology for addressing the identification of system functions, allocation of functions to people and machines, and the decomposition of functions down to discrete realizable actions. The OFM is a normative model, i.e., it presents, in a clear descriptive form, a view of what should be done in various system contents to guide, control, or regulate proper and acceptable system behaviors. In the context of Payload Operations Control Centers, the OFM provides a mechanism for representing the interrelationships between dynamic control system states and operator functions.

After the successful application of the OFM in analyzing and developing a normative model of the subset of operator activities in the Multi-Satellite Operations Control Center, it became apparent that this modeling technique could be used to develop a knowledge base for an expert system whose function was to provide assistance to an operator. This expert system, named OFMspert, is an example of a type of intelligent system we call an Operator Associate. To date, an experimental version of OFMspert has been developed and demonstrated at the Center for Man-Machine Studies at Georgia Tech.

This line of research recognizes that the human operator is and will be a critical component in control systems. The goal of an Operator Associate is to enhance and amplify the skills of the human operator and to exploit the strengths of all system components, human or otherwise. The Operator Associate is designed to provide a dynamic symbiosis between the human operator and the rest of the control system.

The basis requirement for a viable Operator Associate is a normative model of the human operator behavior in various system contexts. For our system, this model is provided by the OFM. As a basis, the OFM provides information relative to the current operator state; predicted operator state; and an assessment/predictor of the operator's goals, functions, intuition, and performance.

In characterizing our version of Operator Associate, two broad classes of operational capabilities or properties emerge, namely, control and understanding. The control properties allow for the assumption, by the Associate, of varying levels of dynamic control of some part of the operational system. The level of control turned over to the Associate is determined by the human operator. The understanding properties provide the Associate with the capabilities of inferring current system goals and offering context-dependent assistance, advice, and reminders to the human operator.

Currently the focus of our development activity is on the understanding properties of the Associate. The level of understanding that can be supported by the Associate is, of course, a function of the application of the underlying operator model in explaining system operations.

Part of any understanding system are functions that we collectively call intent inferencing. Intent inferencing tries to provide plausible explanations for observed operator

actions given the current system state and past operator actions. Intent inferencing attempts to understand operator actions by interpreting them within the context of some normative model, which is the OFM in our case.

In providing information to support intent inferencing, the heterarchic-hierarchic structure of the OFM comes into play. Briefly, the heterarchic nodes correspond to the high-level functions in an operator's role. Each such high-level function has associated with it a three-level hierarchy that supports a decomposition of the function into subfunctions, tasks, and actions. Figure 1 addresses the OFM structure. In the current implementation of the Associate, this model information is manipulated by means of a blackboard system typical of those used in current artificial intelligence systems.

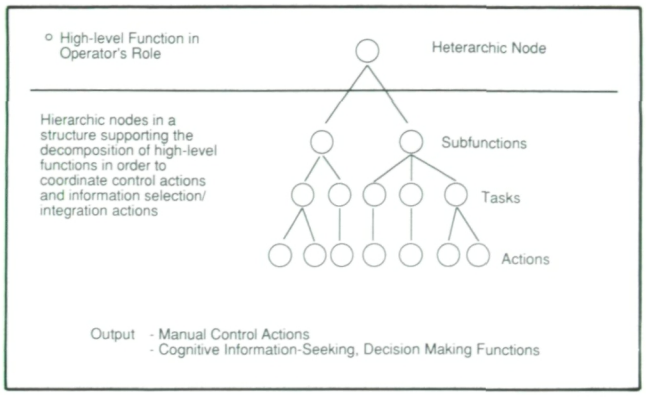

Figure 1. Heterarchic-hierarchic structure of OPM.

Figure 2 depicts the blackboard model used in OFMspert. This model uses a three-level hierarchy of knowledge sources (KS). The Strategy KS determines what type of event to focus on, the Activator KS selects a specialist KS appropriate for the selected event, and the Specialist KS provides the knowledge used to make modifications to the blackboard. The Enhanced Normative Model with its Goals, Plan and Task is based on the OFM.

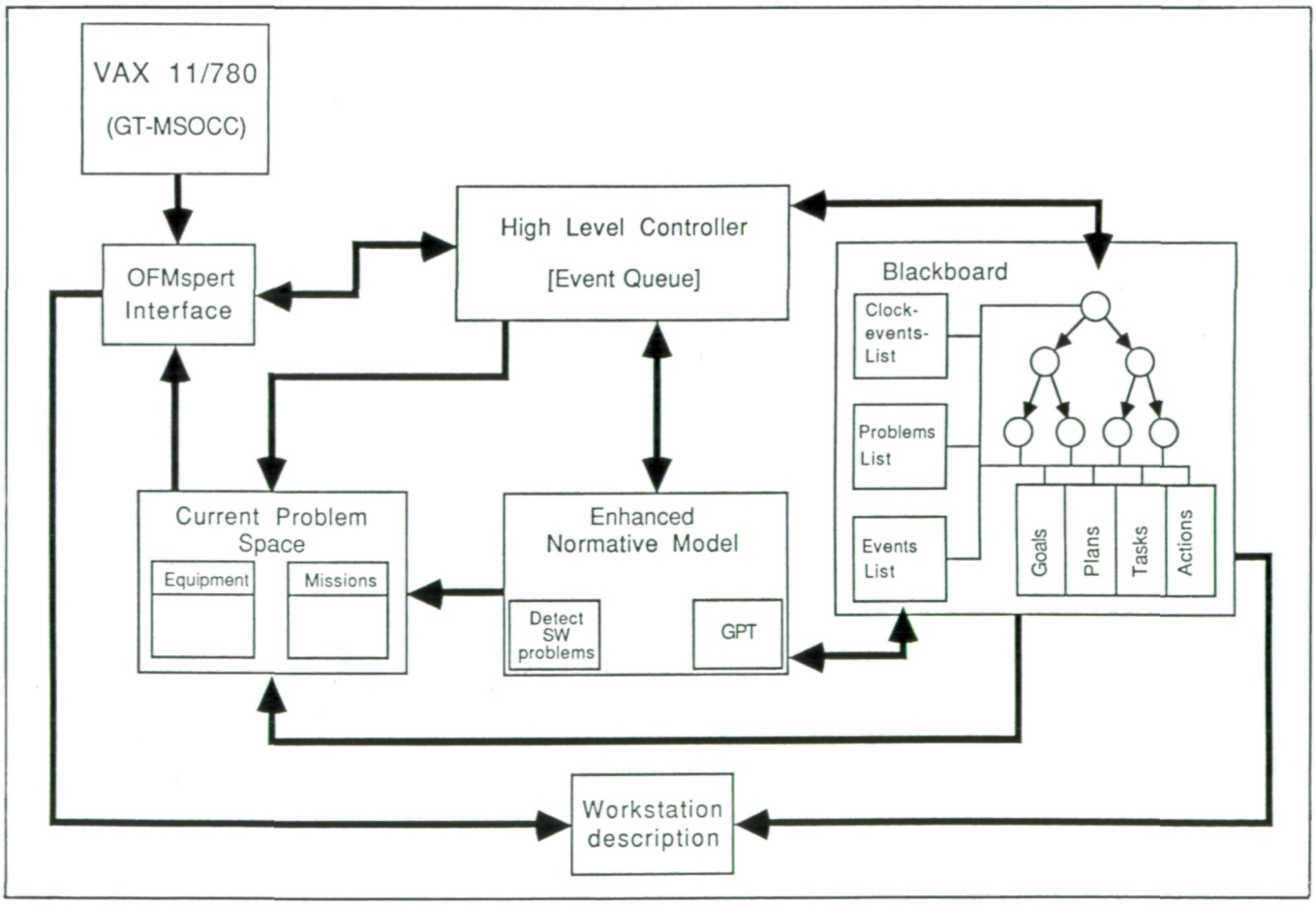

Figure 2. OFMspert architecture.

We believe that in the very complex operating environments that are now emerging, systems like the Operator Associate will become indispensable tools in helping to provide efficient and effective operation. The current OFMspert is being expanded to include the control functions and will be tested in the operational environments at Goddard in the near future.

Contact: Walt Truszkowski
Code 522

Sponsor: Office of Space Operations

Mr. Walt Truszkowski, a member of the Data Systems Technology Division, holds degrees in mathematics and computer science. His professional interests include the cognitive aspects of human/machine systems, artificial intelligence, and approaches to information exchange.

THE MISSION OPERATIONS PLANNING ASSISTANT

The Mission Operations Planning Assistant (MOPA) is a planning and scheduling system prototype developed to demonstrate the feasibility and utility of knowledge-based software support for spacecraft instrument activities. The prototype focuses on mission planning for a subset of the instruments to be carried by the Upper Atmospheric Research Satellite (UARS), a multi-instrument orbiting observatory scheduled to be launched by the Space Shuttle in 1991. Several important planning and scheduling concepts are demonstrated in the MOPA: activity abstraction hierarchies, multilevel planning, reverse plan maintenance, constraint representation and evaluation mechanisms, and contextual activity priorities. A significant feature of the MOPA is the use, and demonstrated effectiveness, of a frame-based knowledge representation.

Mission planning for a multi-instrument satellite is a complex, knowledge-intensive process. In the case of the UARS, there are 10 instruments whose activities must be defined, coordinated, integrated, and scheduled daily for the life of the mission. Further, since the UARS principal investigators will for the most part remain at their home institutions and not participate in the daily planning, the UARS mission planners will need to be cognizant of the functions and capabilities of each instrument as well as of the spacecraft itself. The problem addressed by the MOPA is to capture the principal investigators' knowledge of instrument operations to achieve scientific objectives and to utilize the knowledge to support the daily activities of the mission planners.

In the UARS instrument planning scenario, there are three phases of activity, each with its own plan. The strategic phase, before the launch of the spacecraft, results in a Long-Term Science Plan, which describes how each instrument will be utilized to achieve the scientific objectives of the mission. The tactical phase, a daily activity for the UARS mission planners, results in a Daily Science Plan, which specifies the operation of each instrument in terms of scientific objectives. The execution phase, also a daily activity for the mission planners, develops an Activity Plan, which specifies the operation of each instrument in terms of the detailed activities at a level of detail suitable for the generation of instrument and spacecraft commands by the UARS Command Management System.

The MOPA demonstrates knowledge-based software support for the UARS mission planners in the process of generating Daily Science Plans and Activity Plans. The specific knowledge acquired from the principal investigators fell into three general categories:

- Instrument operations to achieve scientific objectives. Generally, instruments have several modes for data collection, calibration, safing, and so forth. The specific knowledge concerns the conditions under and the order in which these modes are selected to achieve the scientific objectives of the mission.

- Instrument operational limitations and restrictions. Most instruments have operating constraints to prevent damage to themselves or another instrument or to avoid degradation of the captured data. The specific knowledge concerns the instrument restrictions and the operational limitations.

- Translation of objectives into command sequences. The process of creating an Activity Plan from a Daily Science Plan requires a decomposition of activities specified in terms of scientific objectives into detailed instrument activities. The specific knowledge concerns activities at the level of command generation and instrument execution.

In the MOPA, the principal investigators' knowledge of instrument operation to achieve scientific objectives is represented in frame-based Generic Plans, which capture much of the information present in the Long-Term Science Plan. For each instrument, a Generic Plan specifies the conditions under which an instrument operation

ORIGINAL PAGE IS
OF POOR QUALITY

should be performed. These operations are abstract functions, usually the scientific objectives to be accomplished by the instruments, and the level of abstraction is intended to be readily interpretable by the UARS principal investigators. The MOPA thus provides the mission planners with a collection of Generic Plans from which those that are appropriate for a particular planning day may be selected. Figure 1 presents the MOPA display of a sample Generic Plan.

The MOPA uses the selected Generic Plans together with environmental information, e.g., orbit and attitude data, and other events scheduled for the day to generate a Daily Science Plan. Although a text format is available, the plan is best displayed graphically in timeline format. Figure 2 shows the MOPA timeline display of a Daily Science Plan. The user interface provides the mission planners with the ability to quickly view and modify the Daily Science Plan. The MOPA will, at the option of the user, constraint check and report any violations or conflicts between instrument operations.

Once a Daily Science Plan has been generated, reviewed, and modified, the mission planners will normally request the MOPA to derive the Activity Plan. The MOPA can display the Activity Plan in either graphic (timeline) or text format, and the user may modify the plan in either format. Figure 3 illustrates the MOPA display of an Activity Plan in text format. As with the Daily Science Plan, the MOPA will, at the option of the user, constraint check and report any violations or conflicts between instrument operations.

Modification of the Activity Plan obviously results in a discrepancy between the detailed plan and the Daily Science Plan from which it was derived. Rather than require the mission planners to edit the higher level plan, the MOPA will reflect the lower level change back to the higher level plan for the day. Further, the MOPA will tailor a new Generic Plan based on either reflected or direct user modification to the Daily Science Plan, and the new plan may be added to the collection of Generic Plans for later use by mission planners. This reverse plan maintenance feature of the MOPA saves the user from performing multiple edits and regenerating one or both levels of plans.

The MOPA was developed on a Symbolics 3640 workstation in LISP and with the Automated Reasoning Tool,

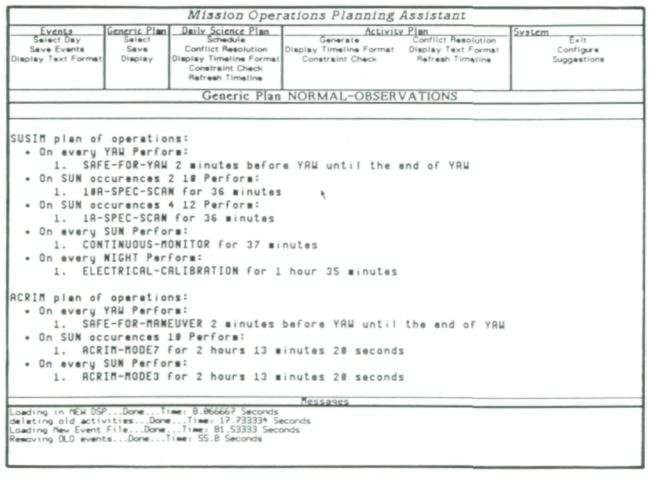

Figure 1. MOPA display of sample Generic Plan.

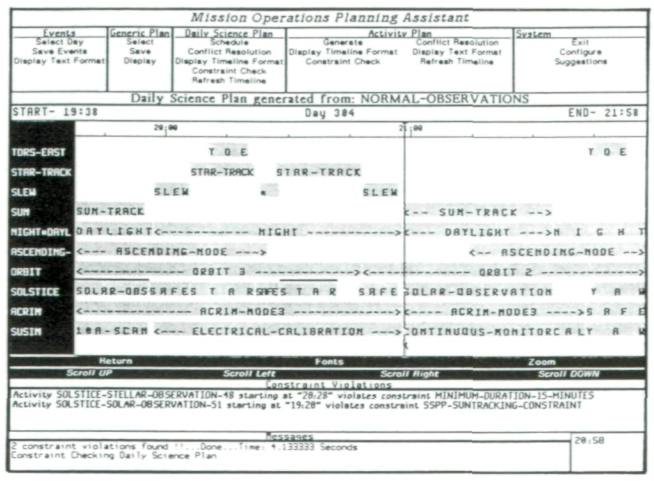

Figure 2. MOPA timeline display of Daily Science Plan.

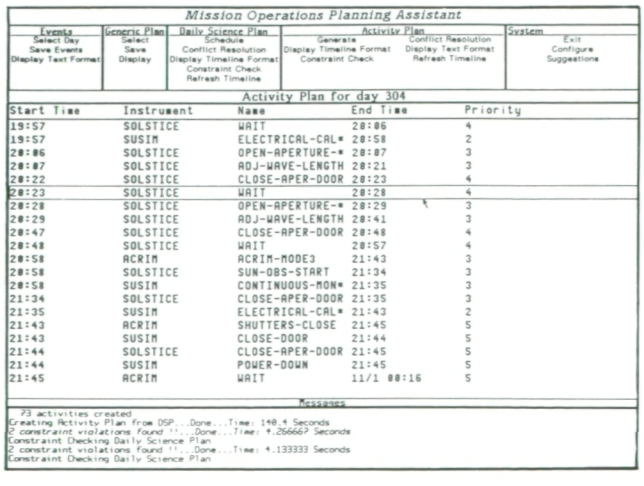

Figure 3. MOPA display of an Activity Plan in text format.

an expert system development product from Inference Corporation. The MOPA system features both textual and graphical displays for plan inspection and modification, recognition and reporting of instrument operation constraint violations during the planning process, and consistency maintenance between the different planning levels.

Contact: Larry G. Hull
Code 522

Sponsor: None

Mr. Larry G. Hull is a senior knowledge engineer with over 20 years of experience at Goddard in areas as diverse as real-time operational support for manned and unmanned spaceflight missions, computer performance and capacity management, discrete event simulation of computer and communications systems, and expert systems. He received his Engineering and MEA degrees from George Washington University, and he holds the Certificate of Data Processing. He is a member of ACM, IEEE, and AAAI. Mr. Hull's primary research interests focus on AI, activity scheduling, and discrete event simulation.

A GRAPHICS INTERFACE TO EXPERT SYSTEMS FOR SCIENTIFIC RESEARCH

The objective of this research was to develop a general capability that allows users to interact with a large operational scientific data base through the use of graphics, data, and knowledge and to be presented with useful spatial data as a result of an expert system consultation.

The approach for the development of graphics interface software for an expert system was 1) to design and implement graphic software tools that can be used to interface with an existing expert system (developed under the Intelligent Data Manager Project) that runs on a microcomputer workstation, and 2) to implement and demonstrate a system that allows intelligent interaction with an operational scientific data base. The data base chosen was the Crustal Dynamics Data Information System (DIS), which uses the ORACLE relational data base management system at the National Space Science Data Center Computer Facility (NCF).

The first year of research resulted in the development of a moderately capable rapid-prototyped expert system that allows users to graphically interact with spatial objects (i.e., crustal plates superimposed on the Earth) that are employed in the reasoning process of the expert system by translating the objects into language symbols. Once sufficient information is gained about a user's data needs, the expert system forms a data base query by constructing an English question based on language processing technologies. The English question is sent to Themis, a Natural Language Query Processor on the NCF VAX computer, where it is translated into SQL (a popular relational data base query language used by ORACLE) and then dispatched to the Crustal Dynamics DIS that runs under ORACLE. The query is then processed in ORACLE, and the resultant information is dispatched to an IBM PC/AT microcomputer, where the information can then be translated by the user.

Although the initial prototype provided for both limited access and expansion capabilities and showed a proof of concept, its inability to perform multitasking with processes that require virtual memory on the AT hindered both the software portability to other systems and the possibility for sophisticated expert systems and graphics interfaces. Because of these and other technical limitations, an alternative microcomputer workstation (SUN 3/260) was selected that contained a state-of-the-art expert system (Automatic Reasoning Tool, ART by Inference Corp.), three-dimensional graphics (Figaro by Template Graphics Software), and Unix operating system portability. Such portability allows for easy translation to the telescience operational workstation proposed for the Space Station era.

This advanced system is capable of demonstrating the use of spatial data in concert with an expert system that interacts with and reasons about operational data bases. This system allows spatial, data-base, and knowledge-base information to be effectively represented and processed in a graphical form, thereby allowing users to interact with the data base in the manner to which they are most accustomed. The significance of this research is that:

- It represents a data base in a form that maintains full data context that is unattainable in a PC environment.
- It contains graphical interfaces that use powerful multitasking software that can be linked to the expert system but function as separate processes.
- It contains expert systems that are able to understand spatial information and data in the context of a specific problem-solving domain.

Such a system can be expected to meet some of NASA's most critical long-term scientific research and operational needs because it will enable managers and scientists to access and utilize spatial data bases as if they were the data base experts. In addition, it will support the representation of knowledge, facts, and related data from a data base in a graphical form.

Contacts: William J. Campbell, Lloyd A. Treinish, and Carey E. Noll
Code 634

Sponsor: Director's Discretionary Fund

Mr. William Campbell was the Manager and chief designer of the National Space Science and Data Center's Applied Artificial Intelligence Laboratory and currently is Manager of the Advanced Planning Design Group. He is also the Deputy Project Manager and Systems Engineer and chief designer of the Pilot Land Data System. During his nine years with Goddard, Mr. Campbell has managed the Eastern Remote Sensing Training Program and served as leading professional in Geographic Information Systems. He was Principal Investigator for the integration of Geographic Information Systems and Remote Sensing Applications. Mr. Campbell holds an MS degree in geography from Southern Illinois University.

Mr. Lloyd Treinish is a data analysis mathematician with eight years of experience at Goddard. He works on the development of advanced data systems for support of scientific applications, as well as studying space and atmospheric phenomena. Mr. Treinish developed the concept of using the Massively Parallel Processor as a computational geometry server. He was the chief designer and developer of the Pilot Climate Data System, and he conceived of the first self-describing data abstraction for the storage and manipulation of multidimensional data, as the Common Data Format. Mr. Treinish has an SM degree in physics from the Massachusetts Institute of Technology and has received four NASA Certificates of Outstanding Performance.

Ms. Carey Noll is Data Base Administrator for the Crustal Dynamics Data Information System and the Pilot Land Data System ORACLE data bases. Ms. Noll, who holds a BA degree in mathematics from Western Maryland College, has 6½ years of experience at Goddard.

THE AUTOMATED REQUIREMENTS GENERATION TOOL (TARGET)

Today's data-driven philosophy has added complexity to the already difficult task of designing data management systems that meet user requirements without violating mission support constraints. This additional complexity clearly justifies the development of a tool that expedites data management system planning. TARGET is a personal-computer-based tool that provides: 1) an automated (via floppy disk or local area network) questionnaire/response link between the system design engineer and the system user, thus establishing an audit trail of user service requirements; 2) a data base of hardware cost/performance characteristics; and 3) a mathematical analyzer that evaluates the cost and performance of candidate system configurations based on user service requirements (workload).

TARGET supports system planning from end-to-end. The planning engineer first uses TARGET to design customized user service requirement questionnaires that can then be transmitted via floppy or two-way local area network links. This task is facilitated by TARGET's near-natural interface implemented in PROLOG. The engineer and user can then refine and clarify end user responses, thus improving early requirements definition. In the aggregate, user service questionnaires represent the system workload. With workload in hand, the system planner then selects candidate system configuration(s) from TARGET's data base of hardware subsystems. Driven by user-defined workload and schedule constraints, TARGET's mathematical analyzer is then used to generate performance statistics of each candidate configuration (model). Finally, based on cost, TARGET's optimizer will select the best configuration from among otherwise feasible systems.

Although still under development (completion expected in April 88), TARGET's mathematical analyzer is being used to support the Gamma Ray Observatory Applications Processor (GRO AP) Study task. In a matter of hours the GRO AP workload and system performance characteristics were simulated with TARGET. Results from TARGET agreed favorably with those generated manually with spreadsheets. Excessive central processing unit utilizations, identified by the spreadsheet model and verified by TARGET, were further analyzed with discrete event simulation. TARGET is being developed as a totally compatible component of a GSFC Space Station Data System Modeling Environment. This feature provides the TARGET user with on-line access to an extended range of modeling and simulation support services, including

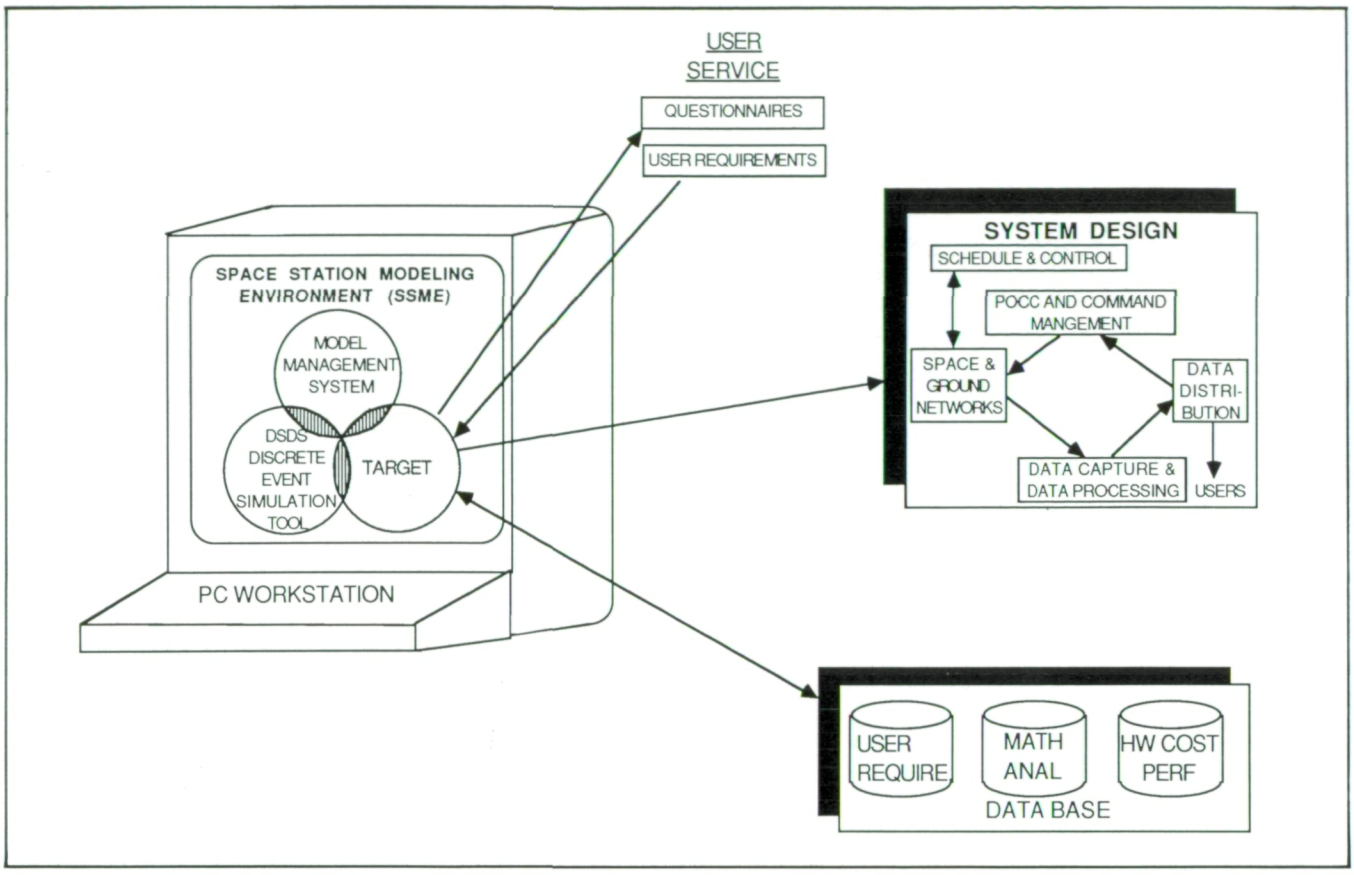

The Automated Requirements Generation Tool (TARGET).

the Data Systems Dynamic Simulator (DSDS), the discrete event modeling tool alluded to above.

Contact: William Davenport
Code 522

Sponsor: Office of Aeronautics and Space Technology

Mr. William Davenport is the chief developer of Goddard's Space Station Data System Modeling Environment. He specializes in modeling and simulation, and he is interested in promoting the use of models to pretest proposed data management systems. Mr. Davenport received an MS degree in physics from East Carolina University. He has 24 years of experience at Goddard.

EXPERT NIMBUS OPERATIONS SYSTEM

The expected performance and longevity of operations for the Nimbus-7 spacecraft have far exceeded design estimates. During the past few years, innovative methodologies have been applied to Nimbus operations and data processing that have both reduced costs and provided needed floor space for new mission control functions assigned to the Project Operations Branch. The first step, put into operation 3 years ago, related to scientific processing of data, and it freed about 2500 ft^2 of space and had operational savings of about $500,000 per year. The Expert Nimbus Operations System (ENOS) is the second phase of this plan.

The ENOS is a data-base driven software/hardware system that evaluates Nimbus-7 telemetry in real time for purposes of health, safety, and condition of the spacecraft. It is implemented on a modified IBM XT personal computer, and it functionally replaces over 2000 ft^2 of 1960s vintage computer systems. The ENOS is truly transportable, since it can provide on-pass visibility to the Nimbus-7 spacecraft anywhere that a NASCOM line is transferring Nimbus-7 data or where the Nimbus-7 clock and data are available. It is expert in the deterministic sense, in that over 50 years of Nimbus unique

experience is incorporated in the data bases, and computations and displays are implemented via generic software that operates on these data bases, although it is not expert in the sense of artificial intelligence. The software determines 200 spacecraft events, continuously performs over 1300 mode-dependent limit checks, and provides continual trilevel alarms for all spacecraft systems and experiments as well as displaying corrective operational procedures for alarmed states. Output displays can be called up within 2 to 3 seconds. They include spacecraft status, event changes, configuration displays, plots of any telemetry point from the beginning of the pass to the current time, and analysis pages for each subsystem and experiment. Several features in the ENOS are not present in other spacecraft ground systems.

Operations occur at the Nimbus-7 real-time input data rate of 4 kbits/s, although the system capability is of the order of 32 kbits/s. The ENOS captures full orbital playback data at a rate of 128 kbits/s, and after capture, ENOS analyzes the data by use of the real-time software with a variety of selection modes, such as every Nth frame.

Data bases are the source of expert knowledge for the system software. There are several data bases, all of which are related by a common telemetry function number (TFN). The telemetry data base contains information such as the TFN, row/column indexes for transmitted input data, calibration tables, function limits and dependent modes, and function names. The display data base contains the display coordinates for each page and a type code that identifies text, events, or TFNs.

Other data bases relate to corrective procedures and strip-chart functions. User-friendly software based on dBase III allows the data base to be changed quickly and accurately under formal configuration control.

The system hardware consists of a standard IBM XT personal computer augmented by two special cards and other performance devices, a 19-in. Conrac monitor for operational viewing as well as a 13-in. high-resolution monitor, and a graphic printer. In addition to commercially available cards and devices, e.g. a turbo card, streamer, software, and an EVA card, special purpose cards for ingesting the data from NASCOM and driving six eight-channel BRUSH charts are part of the system. The system in its current configuration, which includes expansion chassis, runs at the speed of an IBM AT.

The NASCOM ingest card is a combination of analog and digital methodology (firmware), and communication to this card can be made via the host XT. The card is generic in that all data required for signal detection such as spacecraft identification, source and destination codes, and data type are input by the operators via the XT. It decodes the NASCOM block header and provides data to the XT for an echo-checking feature. It can accept input data at a rate of up to 0.5 megabits and can output the data to the XT at any rate required by the system programs. Finally, the card is duplex in that it can output data from the XT in a NASCOM format, which also allows data transfer between machines.

The Strip Chart Recorder driver card is currently under design. In operation with the XT at downlink rates, it will have the capability of driving six eight-channel BRUSH chart recorders, each with eight analog and digital outputs as defined in the data base.

The ENOS has been used successfully in a prototype test mode for the real-time analysis of the Nimbus-7 spacecraft telemetry since early May 1987. In this mode, input data was provided by the serial data output from the PDP 11/55 front end telemetry and command (TAC) and accepted by a non-NASCOM ingest card that presents data to the XT in a synchronous major frame form. Data displays have operated flawlessly, and the Flight Operations Team relies upon the system in this mode. The NASCOM ingest card described above performs the TAC function of the PDP 11/55 and is currently under acceptance testing. In all configurations, ENOS is compatible with Deep Space Network, SUE, and DDPS formats. The real-time analysis portion of the ENOS became operational on October 1, 1987.

Use of this system for Nimbus operations has several benefits: 1) reduced maintenance costs (about $40K/mo), 2) reduced contractor staffing (8 positions), 3) reduced power needs (operating and environmental), and 4) release of 2000 ft^2 of operations space. The ENOS is adaptable to other spacecraft provided that the data bases conform to the ENOS structure, which should be an easier and less expensive task than designing new software to fit each data base. We are looking into applying the ENOS methodology to other spacecraft missions.

The author acknowledges the efforts of the GE/RCA government services personnel who developed this system, especially Richard Stephenson, John Sissala, Bernie Gonciarz, Rick Smith, Frank Demare, and Ed Rutkowski.

Contact: Michael Forman
Code 513

Sponsor: Office of Space Science and Applications

Mr. Michael Forman is the Operations Director of the Nimbus project. His professional specialties include Fourier spectroscopy, signal processing, and spacecraft operations. Mr. Forman received a Masters degree in physics and applied mathematics from the University of Lowell and an MEAd degree from George Washington University. He has 21 years of experience at Goddard and has received several awards in recognition of his work.

FORPS VERSION OF TRAPS

The Trajectory Preprocessing System (TRAPS) is a rule-based system developed to detect errors in spacecraft mission trajectory data supplied to the Communications Link Analysis and Simulation System (CLASS) located at Goddard. CLASS exists to provide a complete range of mission analysis and simulation products to spacecraft builders and mission planners. The purpose of the TRAPS application is to ensure that erroneous data is prevented from entering the CLASS processing stream and to aid CLASS users in pinpointing errors in their mission trajectory data.

TRAPS was originally developed on an IBM PC with the popular production system language OPS5, which is not available on the CLASS computer. FORPS, a new Forth-based production system, was selected as the tool for implementing the operational version of TRAPS on the CLASS computer (a Perkin-Elmer 3244). FORPS did not exist at the time of the original development of TRAPS. TRAPS has been converted from OPS5 to FORPS, and it is the first production system application to be implemented in CLASS. Other rule-based systems for CLASS are also expected to be developed in FORPS.

The main advantages of the FORPS version of TRAPS over the OPS5 version are that it executes about a third faster and it requires about one-fifth as much computer memory. In addition, the source code is somewhat more readable, and therefore more maintainable, in the FORPS version of TRAPS.

Future work will involve installing the FORPS version of TRAPS on the Silicon Composers PC-4000, a personal computer plug-in board built around the innovative Novix NC-4016 Forth engine. This approach will, at low cost, provide about 10 times the processing speed of an IBM PC/AT and will serve as the basis for building a coprocessor board for high-speed expert system processing in the CLASS computer.

Contact: James Rash
Code 531

Sponsor: None

Mr. James Rash is a mathematician with the Communications Link Analysis and Simulation System (CLASS) project. He is a member of the ANSI X3J14 Technical Committee that was organized to draft a proposed ANSI standard for the computer language FORTH, as well as a member of Goddard's Engineering Colloquium Committee. His professional interests include the development of expert systems for CLASS and the development of a new generation of powerful, multipurpose technical workstations for space applications. Mr. Rash earned a MA degree in mathematics at the University of Texas, and he has served with Goddard for 2½ years.

ECCO: MISSION PLANNING TOOL IN CLASS

An experimental system for optimizing user spacecraft communications configurations has proved the feasibility of a rule-based systems approach to provide software tools for mission planners utilizing the Communications Link Analysis and Simulation System (CLASS) at Goddard. Designated ECCO (Expert for Communications Configuration Optimization), this system supports mission planning for spacecraft that obtain telecommunications services through NASA's Tracking and Data Relay Satellite System (TDRSS). Implemented initially on a personal computer compatible with the IBM PC/AT in the OPS5 production system language, ECCO provides mission planners with information that allows them to make detailed adjustments to the mission plan for any TDRSS-compatible spacecraft to achieve the best possible communications performance during the mission. ECCO assumes that all characteristics of the user spacecraft communications system (e.g., frequency, data rate, and transmitter power) are compatible with TDRSS.

Given a user spacecraft and its mission constraints, and given a specific time point during the mission, the goal of communications configuration optimization is simply the selection of the best alternative from among all allowable communications configurations of the user spacecraft. A user spacecraft communications configuration is defined as a set of link combinations. Each link combination is specified by four controllable parameters together with a measure of communications performance

(signal margin). For the current design, the four controllable parameters are user antenna, supporting Tracking and Data Relay Satellite (TDRS), supporting TDRS antenna, and user communications link in use at the mission time point in question. Determination of the optimum spacecraft communications configuration is based on optimizing the combined signal margin.

Assuming that there exists at least one viable communications configuration of the user spacecraft at the given mission time point, ECCO finds the optimum configuration by means of an incremental optimization method described formally as follows:

a) Form the set K of all user spacecraft communications configurations that are allowable at the mission time point in question.

b) Incrementally apply all elimination steps (see accompanying figure), in the prescribed order, to the set K.

c) If the resultant set K contains more than one member (i.e., no way exists to discriminate between members to identify one as better than another), then select a member of K at random and designate it as the optimum configuration.

ECCO performs single-point optimization in which the discovered optimum configuration is independent of earlier or later events. The figure illustrates the flow of processing steps performed by ECCO for the selected mission time point. The actual optimization rules on which the design of ECCO is based are indicated in the box labeled "Elimination Sequence." Input data consist of characterizations of the predefined communications links for the spacecraft, and link margin values calculated by CLASS for all links that are viable (i.e., which have an acceptable margin). ECCO output is simply the communications configuration of the spacecraft which is the best.

Several tests based on telecommunication system specifications for a variety of missions have been performed, and ECCO has demonstrated performance consistent with the optimization rules around which it was designed. Exhaustive testing remains to be done, but results to date support the conclusion that the rule-based approach used in ECCO is valid.

Currently, ECCO is an experimental, personal computer-based system that can be demonstrated on request. Its operational version will be implemented on the CLASS computer when expert system development software becomes available in the near future.

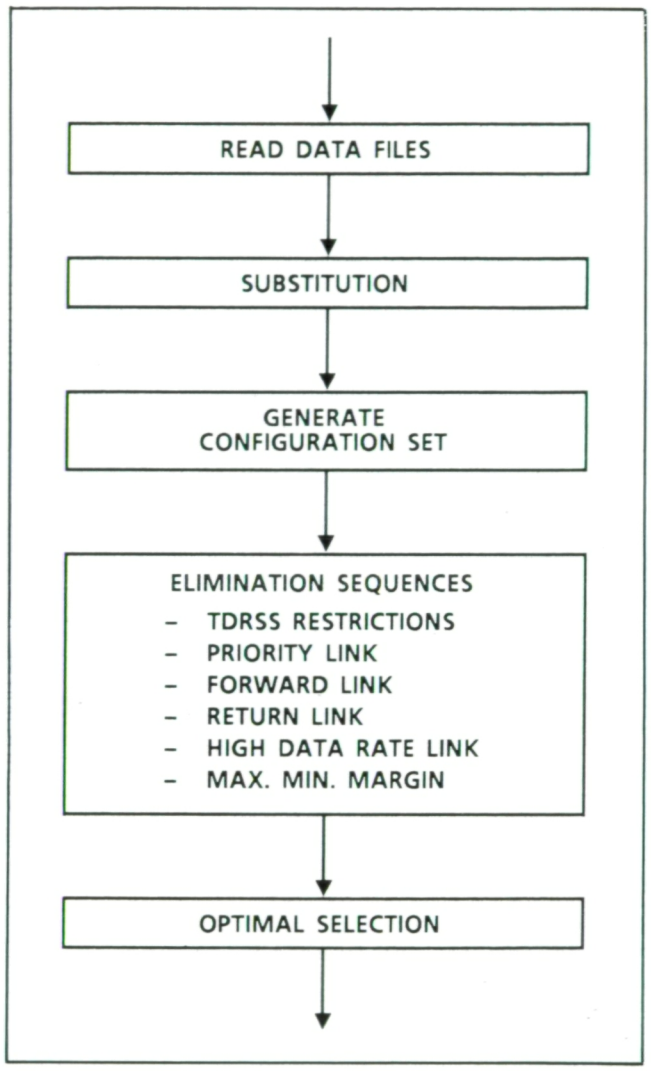

Processing steps in ECCO.

Future work will focus on the following areas: optimizing communications performance by means of spacecraft attitude adjustments, optimizing while precluding user antenna toggling, and multipoint optimization relative to mission phase. Optimum communications performance will also be extended to include stochastic losses (e.g., radio frequency interference and multipath) and synchronization (e.g., probability of loss of lock).

Contacts: James Rash, Yen Wong, and James Cieplak
Code 531

Sponsor: None

Mr. James Rash is a mathematician with the Communications Link Analysis and Simulation System (CLASS) project. He is a member of the ANSI X3J14 Technical Committee that was organized to draft a proposed ANSI standard for the computer language FORTH, as well as a member of Goddard's Engineering Colloquium Committee. His professional interests include the development of expert systems for CLASS and the development of a new generation of powerful, multipurpose technical workstations for space applications. Mr. Rash earned an MA degree in mathematics at the University of Texas, and he has served with Goddard for 2½ years.

Mr. Yen Wong is an electronics engineer for the Communications Link Analysis and Simulation System. His professional interests include digital-data satellite communications and signal-processing and computer-aided modeling and analysis of communication systems. Mr. Wong, who earned an MSEE degree from the City College of New York of the City University of New York, has almost three years of experience at Goddard.

Mr. James Cieplak, a co-op student with one year of experience at Goddard, is involved with Communications Link Analysis and Simulation. Mr. Cieplak is pursuing a BS degree in computer science, with an emphasis on artificial intelligence, at Embry-Riddle Aeronautical University, and he is interested in expert system design.

Flight Projects and Mission Definition Studies

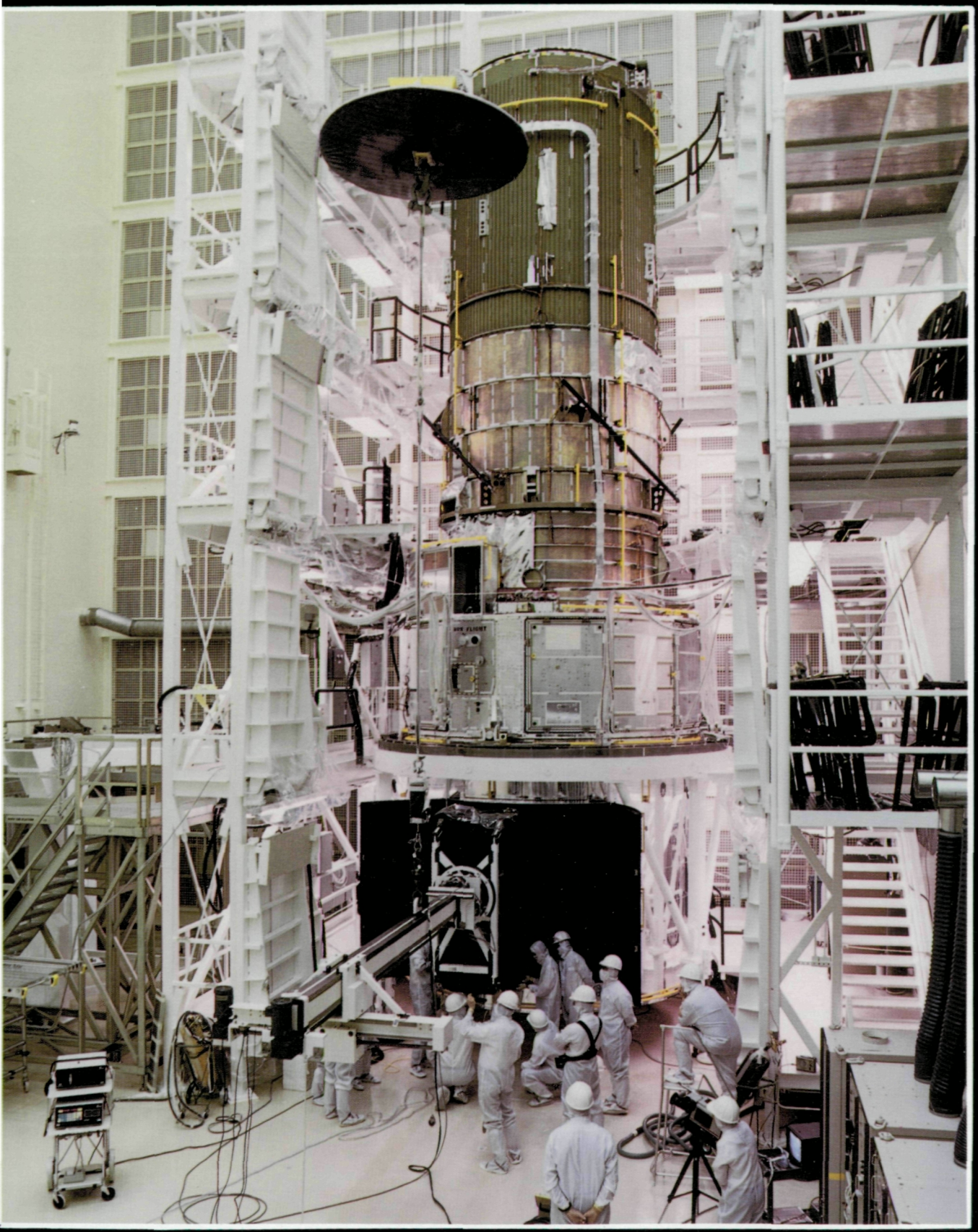

One of the rewards of working on flight projects is that we get to see state-of-the-art technological ideas and schemes become flightworthy space instruments. COBE, for example, will be operating at temperatures slightly above absolute zero to study the nature of the universe; and the Hubble Space Telescope will allow us to take a quantum jump in our ability to observe the celestial sphere. The marriage of science and engineering through research and technology makes these things possible.

FLIGHT PROJECTS

FLIGHT PROJECTS DIRECTORATE

The years 1986 and 1987 have been particularly challenging for the Flight Projects Directorate because of the unfortunate hiatus following the loss of the Space Shuttle Challenger, Flight 51-L. During this time some difficult decisions regarding certain spaceflight missions were made that have affected our research and technology. Considerable effort is going into new manifesting for spaceflight and into replanning our current missions, but research and technology has not stopped.

The Cosmic Background Explorer (COBE) was redesigned to fly on a Delta-II rocket. Originally, it was planned for a Shuttle launch, but the delay in Shuttle capability forced this important change. COBE must be launched in a polar orbit, which requires a West Coast launch site, but preparation work at this site has been postponed.

Another mission where the decision was made to switch from the Shuttle to a Delta-II rocket for launch is the Extreme Ultraviolet Explorer (EUVE). To change from a planned and studied method of performing a particular mission presents doable but, in some cases, difficult technological challenges. The objectives are to conduct sound, meaningful scientific investigations in the cases of both COBE and EUVE, while staying within tight budgetary restraints.

The X-Ray Timing Explorer (XTE) mission also has interesting technological challenges. This scientific payload is to be launched by the Shuttle on the Flight Support System (FSS) without a spacecraft bus. The XTE will utilize the Explorer Platform, which will have been launched as the spacecraft bus for the EUVE. The XTE and EUVE will be exchanged in space. The XTE will then remain in space for its scientific mission, and the EUVE will be returned to the Earth.

Major missions such as the Gamma Ray Observer (GRO) and the Upper Atmosphere Research Satellite continue in their development phases while responding to additional challenges imposed by new requirements resulting from the Shuttle accident. Some of these challenges have resulted from new safety requirements and the predicted ability of the Shuttle to perform optimally with a lesser payload than before. GRO, for example, has already been designed, and much of it is built, but the new loads for which it should be built and tested are different. Retesting the spacecraft at load levels for which it was not designed presents interesting and challenging decision points that affect research and technology.

Three activities are large, complex missions that have national and international ramifications: the Space Station, the ground operations and development of the Hubble Space Telescope (HST) flight instruments, and TDRSS. The Space Station work at GSFC has spun off a variety of activities in research and technology, especially in robotics and artificial intelligence. The replacement TDRSS spacecraft to replace the one lost in the Challenger accident has been readied, and we are looking forward to fully establishing the space segment of the

◀ *Installation of the Faint Object Spectrograph on the Hubble Space Telescope.*

TDRSS network in 1988. We are also looking into the future TDRSS spacecraft and ground system. Goddard will be responsible for the operation of the HST and continues the development of ground operations.

Thinking and planning for new spaceflight missions continue. Astromag, a particle astrophysics facility to be placed on the Space Station, is a project in the study phase that has a variety of very interesting and challenging technological hurdles.

Other missions under consideration are the Tropical Rainfall Measurement Mission (TRMM) and the Lyman/FUSE (Far Ultraviolet Spectroscopy Explorer) mission. The mission of the TRMM is somewhat stated in its name. The need to understand rainfall on our planet is obvious, especially as it affects global agriculture and climate. The Lyman/FUSE study mission will be a telescope that will search for ultraviolet targets in space as dim as 17th magnitude. Both of these missions push the state of the art in several technology areas.

Contact: Stephen J. Paddack
Code 402

Sponsor: Office of Space Science and Applications

Dr. Stephen J. Paddack, Chief of the Advanced Missions Analysis Office, is the editor of the Flight Projects and Mission Definition Studies section of this report. Dr. Paddack earned a PhD degree in engineering/physics from the Catholic University of America. He has been with Goddard since 1961 and is a recipient of the NASA Exceptional Service Medal.

HUBBLE SPACE TELESCOPE

THE HUBBLE SPACE TELESCOPE

The Hubble Space Telescope (HST) is a most ambitious undertaking from a scientific as well as an engineering viewpoint. It extends the state of technology in several dimensions simultaneously, and its successful construction presents an array of requirements for an operational ground system that are similarly ambitious, many being without precedent. The development of HST and its ground systems presents a significant management challenge in directing the efforts of nearly 2000 people distributed among several dozen organizations.

The HST has been under development for nearly 10 years and is now undergoing a system level test and verification program in preparation for launch and the subsequent operational phase. It is, therefore, timely to introduce this new scientific tool and describe the complexities of operating this new observatory.

The primary objective of the HST project is to construct and place into Earth orbit a high-quality optical telescope with appropriate scientific instrumentation that will provide substantial improvements in terms of sensitivity, resolving power, and spectral range beyond those which are presently achieved from ground-based observatories. A related objective is to provide an extended mission lifetime through on-orbit servicing to replace and improve scientific instruments and engineering subsystems.

Scientific Capabilities. The advantages of conducting astronomical observations from Earth orbit, above the obscuring and distorting effects of the Earth's atmosphere, have been well established by such pioneering missions as the Orbiting Astronomical Observatories, Astronomical Netherlands Satellite, and most recently by the highly productive International Ultraviolet Explorer. The HST will make similar gains in sensitivity and spectral range, but to a much greater degree by virtue of its large (relative to previous optical telescopes in orbit) primary aperture of 2.4 m diameter. This large, high-quality optical system will achieve a nearly 10-fold improvement in angular resolution compared with that achieved by conventional ground-based telescopes in operation today.

Optical System. The HST will extend the limiting magnitude by more than four magnitudes beyond that of the

Palomar 5.1-m telescope at visible wavelengths, while providing excellent optical performance from the ultraviolet well into the short infrared wavelength region of the spectrum. Table 1 provides quantitative performance parameters for the HST optical system.

Table 1
Hubble Space Telescope Optical Performance

Parameter	HST	Best Ground Performance
Angular Resolution (arc second)	0.1	0.5 to 1.0
Spectral Range (μm)	0.1 to 100	0.4 to 0.8
Limiting Magnitude (m_v)	+28	+24

The extraordinary performance of this optical system is a result of the high degree of precision with which its components are made. The primary mirror, which is 2.4 m in diameter, has been ground to its prescribed figure to within 0.25 μm to provide a total rms wavefront error of less than 1/20 of a wavelength of light (at 6328 Å). Figure 1 presents a sectional view of the telescope assembly. The metering truss supporting the secondary mirror relative to the primary mirror is constructed of a graphite-epoxy composite material to provide an extremely low coefficient of thermal expansion. The secondary mirror is mounted on a focusing mechanism, which can be commanded from the ground to move in minute steps in several degrees of freedom to achieve optimum image quality once in orbit. Electrical heaters maintain

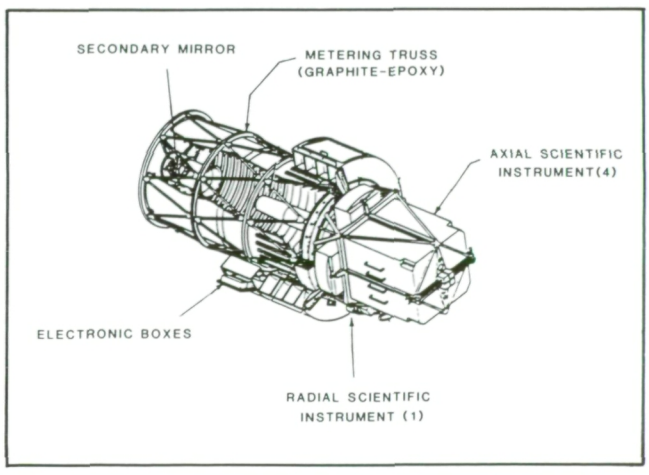

Figure 1. HST optical telescope.

the temperature of the primary mirror and other components at 21 °C. The Optical Telescope Assembly was designed and built by the Perkin-Elmer Corporation.

Instruments. The initial complement of five scientific instruments (SIs) aboard the HST will include two cameras, two spectrographs, and a high-speed photometer. Four of these instruments are designed to occupy a quadrant of the focal plane behind the primary mirror, with their longest axis parallel to the optical axis of the telescope, and hence they are referred to as axial instruments. The axial instruments share a common shape and mechanical and electrical interface such that any one can be installed in any of the four axial positions of the focal plane structure. This enables the on-orbit replacement of any axial instrument with a completely new instrument built to the same configuration. The fifth instrument is installed from a direction that is orthogonal to the optical axis of the telescope, and it has a mirror that extends into the central region of the focal plane. It can be interchanged with another instrument built in this radial configuration.

In addition to these SIs, the star-tracking instruments, used primarily by the guidance and control system, will provide an astrometric capability superior to that which is presently obtained from ground-based instruments. Moreover, the guidance system has special capabilities to enable the telescope to follow the apparent motions of nearby objects within the solar system with nearly the same degree of precision and stability that it provides for distant objects. This will enable spectroscopic studies of features of planets and their satellites, as well as comets, asteroids, and similar objects.

The Faint Object Camera (FOC), developed by the European Space Agency, is designed to exploit the full resolution capability of the HST on the very faintest objects detectable—expected to be about 28th magnitude. The FOC utilizes an image photon-counting system with a detector comprised of an image intensifier in conjunction with a vidicon vacuum tube. Integration is performed digitally in an electronic memory. This instrument is equipped with a coronographic facility so that very faint structures can be studied close to bright objects. It also provides a moderate-resolution spectrographic mode. The FOC was built by Dornier Systems, and the detector assemblies were built by British Aerospace Corporation.

The Faint Object Spectrograph (FOS) will obtain the spectra of astronomical objects to very faint magnitudes (down to 26th visual magnitude) in the ultraviolet and visible wavelengths, at moderate spectral resolution. The design is based on digicon detectors, which have been

applied to ground-based instruments for some time. The FOS also provides a capability for time-resolved spectral observations and for polarimetric studies. It was built by Martin Marietta Corporation.

The High Resolution Spectrograph (HRS) will measure spectra in the ultraviolet region between 105 and 320 nm of objects as faint as 17^{m} or 1000 times (7 magnitudes) fainter than those that could be detected by earlier space observatories. It employs digicon detectors similar to those used by the FOS. The HRS was built by Ball Aerospace Corporation.

The High Speed Photometer (HSP) contains four image dissectors, a photomultiplier, and a number of apertures with different filters and polarizers at the focal plane. The HSP enables short-time resolution (11 μs) in photometric observations of rapidly varying objects over wavelengths from 115 to 900 nm. An important HSP objective is to establish an accurate time correlation between observations made by ground-based and other space-based photometric systems with those made by the HST. The HSP was built by the University of Wisconsin.

The Wide Field/Planetary Camera (WF/PC) is the instrument that is built in the radial configuration so that its pick-off mirror will relay the best quality central focal plane images to its charge-coupled solid-state detectors. The Wide Field Camera captures a field of 2.7 arc-minutes diameter and images it onto the 1600 × 1600 element detector. The Planetary Camera captures a field of 1.1 arc-minutes by using a similar detector arrangement, and it will allow full-disk images of planets and their satellites to be obtained at a resolution approaching that of the Voyager at its encounters with Jupiter and Saturn. The WF/PC has a remarkable spectral range of from 115 to 1100 nm. It is the only current HST instrument with sensitivity in the near infrared region of the spectrum. The WF/PC was built by the Jet Propulsion Laboratory.

Each of these instruments is equipped with means to introduce a variety of filters and polarizers (in the case of the cameras and HSP) or different grating elements (in the case of the spectrographs) into their optical paths. While greatly extending the flexibility and utility of the basic detector systems, this diversity of operating modes requires individual calibration and the operational requirement of choosing appropriate modes for each observation.

Engineering Characteristics. Compared to presently operating scientific spacecraft, the HST is on a physical scale that is unprecedented. Technologically, it represents significant advances in the state of operational capability in areas such as optical quality, precision guidance and control systems, high-stability structures, and high-performance sensors. Table 2 summarizes a few technical characteristics of the HST flight system. One of the most significant engineering advances achieved for this spacecraft is the extraordinary pointing stability of 0.007 arc seconds, which is required to fully use the high angular resolution provided by the telescope.

Table 2
HST Technical Characteristics

Size	
Length	13.1 m
Width	4.3 m
Weight	11,600 kg
Power Consumed	2200 W
Pointing Stability	0.007 arc seconds
Science Data Rate	1.024 megabits/s
Average SI Weight	304 kg
Average SI Power	132 W

Maintenance and Servicing. The HST is NASA's first spacecraft that has been extensively designed to facilitate the on-orbit repair and replacement of its essential systems and instruments through periodic visits by astronaut teams aboard the Space Shuttle. This design will achieve a secondary program objective in that the remarkable performance of the HST will be available for at least 15 years after its launch. To some degree, the lifetime of a spacecraft can be extended by providing redundancy and operational switchover options in the flight equipment. This is now common practice in aerospace system design and has been employed in building the HST. Beyond these measures, the only way to ensure long-term operation of a space-based facility is to provide for the physical repair or replacement of failed equipment and renewal of expendables. Another factor driving the need to be able to replace components is the rapid evolution of detector performance, which is likely to cause the initial set of HST SIs to be approaching obsolescence after several years of operation in orbit.

How the HST Works. The HST will be launched aboard the Space Shuttle and released into a low Earth orbit with

an altitude of approximately 320 nautical miles and inclination of 28.5°. This altitude is the highest obtainable directly by the Shuttle for a cargo of this mass, and it provides the ability for revisit by the Shuttle for maintenance and repair of the HST. However, at this altitude the Earth occupies a large region of the sky that must be avoided in pointing the telescope at astronomical objects. Moreover, the short orbital period of 96 minutes limits the target integration time available for objects that are within the Earth occultation zone. The inclination of the orbit and its precession period of approximately 50 days will change the actual zone of the celestial sphere subject to Earth occultation with time; therefore, through careful scheduling, more targets can be made available for long exposures. Another solution to the Earth occultation problem is provided by the fact that four of the five instruments employ pulse-counting detectors (with little or no readout noise) so that long exposures can be made merely by adding together a number of short integrations.

Another difficulty is presented by the frequent passage of the HST through the South Atlantic Anomaly (SAA)—a region in near-Earth space that is characterized by a sharp increase in the density of energetic charged particles. The effects of this high-radiation environment range from increasing the background seen by some of the detectors to potentially damaging others. Therefore, another observation planning task is presented in predicting the SAA passages and avoiding certain operating functions and modes in that zone.

The externally imposed constraints discussed thus far establish the requirement that the HST be operated in a predominantly preplanned mode. This is in contrast with a previous mission, the International Ultraviolet Explorer, which is in a geosynchronous orbit and is operated exclusively in a real-time mode, since continuous direct communication with a ground station is possible. By carefully and completely specifying all spacecraft and instrument operations in advance, it is possible to optimize the use of the HST to maximize the science return. For example, one might order the sequence of targets to be visited in a way that imposes minimum slew times between the targets. Managing the use of limited resources such as electrical energy and onboard data and command storage is also possible and, in fact, is a necessity.

The extraordinary pointing stability of the HST could not be achieved through the use of gyroscopes alone—the HST is equipped with very accurate star-tracking instruments (fine guidance sensors) that share the field of view of the optical telescope.

The foregoing discussion of the sequence of operations will suggest that much detailed information is needed to direct the HST to perform its tasks. Moreover, since these operations are performed largely without the possibility of real-time intervention from the ground operations team, logical paths must be provided to handle situations when things do not work according to plan. An example of the latter would be the failure of the guidance sensors to find and acquire lock on one of the guide stars. There are several more levels of complexity to this process that cannot be adequately discussed within the scope of this paper. But the central point is that a large volume of commands and numerical information must be created daily and delivered to the HST for execution according to a precise timeline that properly accounts for orbitally induced geometries and events.

There are two separate digital computers onboard the HST that, among other functions, execute the stored command programs. One is responsible for engineering and spacecraft functions such as slewing, guidance, communications, and power management. The other computer performs SI and science data management functions.

Operations. Figure 2 shows a high-level view of the complete cycle of planning and conducting observations. It begins with the submission of research proposals by the scientific community in response to Announcements of Opportunity issued periodically by the HST Science Institute.

The proposals are reviewed by teams of scientific peers and selected on the basis of scientific merit and balance of the science program. The successful proposals enter a planning process that establishes a master observation calendar and develops the detailed instrumental configuration and guide star coordinates for each telescope pointing. This process operates on a 6-month time interval. Science scheduling involves expansion of the plan by providing specific instrument operations instructions and service requests such as telescope slews, new guide star acquisitions, and Tracking and Data Relay Satellite System (TDRSS) contacts. This step operates on a 1-month time horizon, incorporates more accurate orbital information, and results in a product called the Science Mission Specification. Mission scheduling adds engineering operations to the science program, including confirmed TDRSS support times. Final constraint checks are made to ensure that the integrated program is safe to execute, and command load segments are compiled for each of the spacecraft computers.

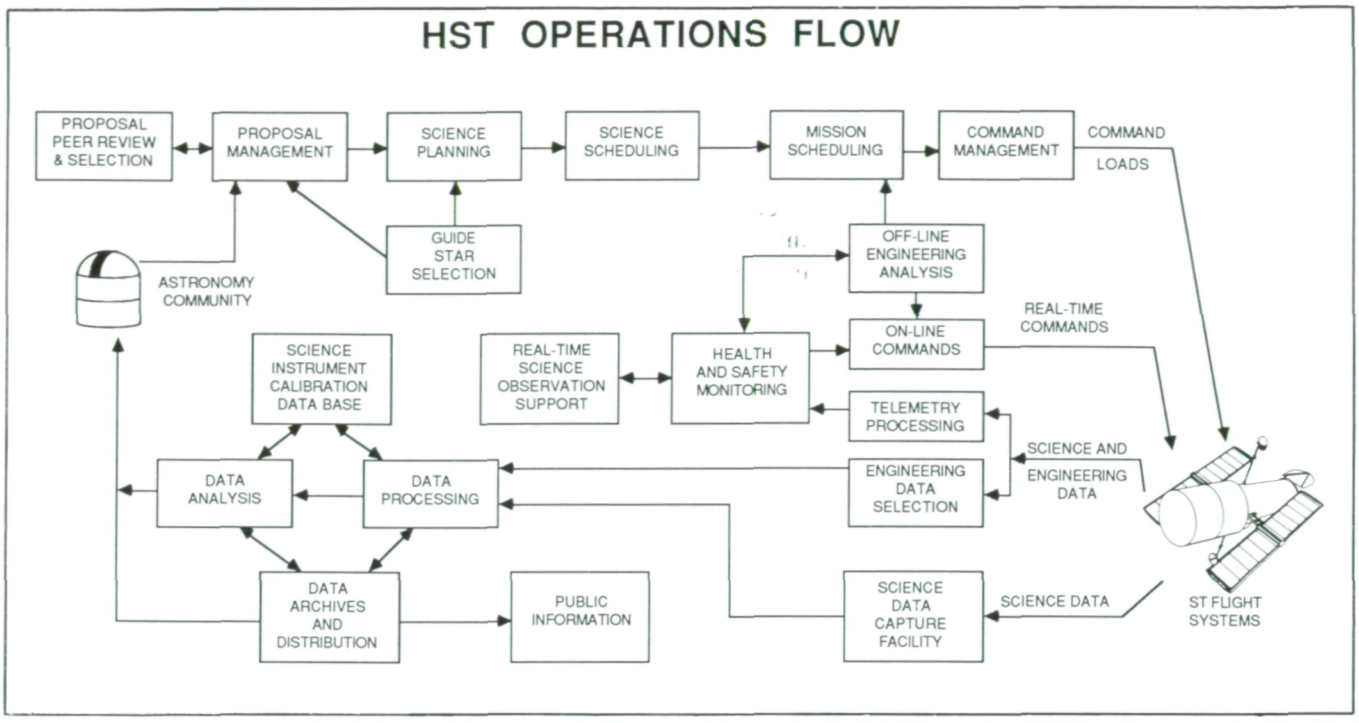

Figure 2. HST operations flow.

Several conventional operational functions are performed in the HST Operations Control Center. They include monitoring of onboard engineering systems, verifying execution of the science program, and taking actions to recover from failures or operational errors. Continuous engineering telemetry will usually be available via the TDRSS multiple access service. However, command capability will exist only at scheduled intervals.

Science data is received at the Data Capture Facility where the transmission packets and error protection coding are removed, and complete sensor data sets are assembled. These data sets, each with its unique identification code assigned during planning, are transmitted to the HST Science Institute for routine processing to remove the known instrument distortions and sensitivity functions. This processing is not interactive, but rather has been predefined for each observation during planning, and it proceeds without operator intervention. A data analysis system is available at the Science Institute for use by the observing scientists to operate on their processed data in an interactive way. It contains an extensive array of programs that can be used to compare and transform data sets to extract scientific information.

Operational Ground System Description. NASA has established the HST Science Institute to administer the HST science research program, which includes issuing the calls for proposals, review and selection of proposals, allocation of telescope time, and the detailed planning and conduct of the observing program. NASA provides only technical and policy guidance to the Science Institute in carrying out these functions. The Institute is operated by the Association of Universities for Research in Astronomy under contract to NASA.

A complex operational ground system has been developed to facilitate the planning and execution of scientific observations by the HST and to provide subsequent data processing and analysis services for its users. In aggregate, the system consists of 17 computers of the VAX 11/780 class, with over a million lines of specially developed program code. Table 3 summarizes the characteristics of each of the subsystems.

The Proposal Entry Processor (PEP) is a data base management system that accepts proposals submitted by scientists and supports the peer review process. The proposals as submitted define specific observations of targets and the scientific objectives for each. The PEP uses an expert system to transform these descriptions into specific SI modes and procedures needed to carry out the observations, and PEP builds the data base needed for the subsequent planning and scheduling process.

Table 3
HST Ground Subsystem Characteristics

Subsystem	Computers	Lines of Code
Proposal Entry Processor	1	115K
Science Planning and Scheduling	2	150K
Observation Support	2	100K
HST Operations Control Center	4	600K
Data Capture Facility	2	70K
Data Processing	2	100K
Science Data Analysis System	2	90K
Guide Star Selection System	2	160K
Ground System Totals	17	1,385K

The Science Planning and Scheduling System operates on a block of proposals and will automatically lay out a calendar of observations that satisfies the visibility and timing requirements of each observation while best serving to meet a table of objectives for the use of the observatory. It operates incrementally, that is, it begins with an empty calendar and selects the best candidate to add to it, and then it selects another candidate, and so forth. Ultimately, the process ends when no room is left for the addition of any of the remaining unscheduled observations. The objectives include such factors as minimizing slew distances between targets, minimizing changes of instrument states, conserving TDRSS and tape recorder usage, and ensuring adequate electrical energy reserves. It can also be used interactively by operators to manually schedule certain observations that have special needs that may not be characterized adequately in the planning data base.

HST promises to provide substantial gains in our knowledge of the universe, but it is impossible to predict what discoveries might actually be made. However, the temptation to speculate is at times irresistible, and here is my favorite: If the optical and instrumental performance of the HST lives up to expectations, it may be possible to perform direct imaging of a planetary system accompanying a distant star. Such an observation is very difficult because of the very small angular separation between the star and its planet and because the luminosity ratios would be quite large. Conditions for this observation would have to be just right—the planetary object would have to be of major size and well separated from its parent star, and the system could not be too distant. Such an observation cannot be accomplished from today's ground-based observatories.

Several other scientific objectives are planned for HST, which include:

- Improving the distance scale of the universe, which is presently uncertain, to about a factor of two. HST should be able to reduce the uncertainty to about 10 percent.
- Synoptic studies of solar system objects with image quality comparable to fly-by missions.
- Searches for black holes at centers of galaxies and elsewhere.
- Detailed studies of the life cycles of stars, particularly late stages of stellar evolution, including the nature of novae, supernovae, and neutron stars.
- Possible answers to mysteries of quasars. Where does their astonishing energy come from? What role did they play in the early history of the universe and in the formation of galaxies?

HST will be one of the first scientific missions to be launched when the Space Shuttle flights resume. At the present HST is scheduled for launch in June 1989, but this is subject to change as the Shuttle requalification program proceeds.

Contact: Charles F. Fuechsel
Code 400

Sponsor: Office of Space Science and Applications

Mr. Charles Fuechsel is Deputy Project Manager with the Hubble Space Telescope (HST) Project at Goddard. His primary duties are developing the HST operational ground system and preparing for the conduct of flight operations beginning at launch. Before this assignment Mr. Fuechsel was the Mission Operations Manager for the highly successful International Ultraviolet Explorer, and he served as Manager of the Data Systems Technology Program at NASA Headquarters. He holds a BSEE degree from the University of Virginia. Mr. Fuechsel is a recipient of the NASA Exceptional Service Medal.

COSMIC BACKGROUND EXPLORER MISSION

The Cosmic Background Explorer (COBE) has been specifically designed for studying the Big Bang, the primeval explosion that started the expansion of the Universe, and for measuring the diffuse infrared and microwave background radiation, which includes the primary remnant of the explosion. In addition, COBE instruments will determine the spectrum of the radiation and the variances between different points of the sky with far better sensitivities than can be achieved with other techniques.

The COBE was originally designed to be launched by the Space Shuttle. As a result of the Challenger accident, the COBE is being redesigned to be launched by a Delta Expendable Launch Vehicle. The COBE is being designed, integrated, and tested by engineers and scientists at the Goddard Space Flight Center; however, certain major subsystems have been procured from selected contractors. The planned lifetime for COBE is 1 year.

The COBE Observatory will carry three instruments: the Differential Microwave Radiometer (DMR), the Far Infrared Absolute Spectrophotometer (FIRAS), and the Diffuse Infrared Background Experiment (DIRBE). Using standard microwave receivers, the DMR will measure the anisotropy of the cosmic background radiation at wavelengths of 3.3, 5.7, and 9.6 mm, with an angular resolution of 7 degrees. The FIRAS will measure the spectrum (the intensity as a function of wavelength) over a wavelength range of 100 microns to 1 cm, with a 5-percent spectral resolution and a 7-degree angular resolution; it is a cryogenically cooled polarizing Michelson interferometer. The DIRBE will measure the brightness of the sky at wavelengths from 1 to 300 microns with a 1-degree angular resolution in 10 bands; it is a cryogenically cooled, off-axis, Gregorian telescope.

The three COBE instruments will be pointed away from the Earth to survey the cosmos-FIRAS along the spin axis, and the DMR and DIRBE will be pointed 30 degrees off the spin axis. These instruments are located inside a large deployable shield to protect against thermal and electromagnetic radiation from the Sun, the Earth, and the Observatory. Within the RF/thermal shield is a liquid helium dewar, similar to that flown onboard the Infrared Astronomical Satellite. To satisfy the requirements of two of the COBE experiments, the Observatory will rotate at approximately 1 rpm.

Science and ancillary data will be continuously stored onboard one of the two Observatory tape recorders, which will be played back once per day to the ground system. The Tracking and Data Relay Satellite System will be used to provide orbit tracking and telemetry and command for Observatory safety and health monitoring.

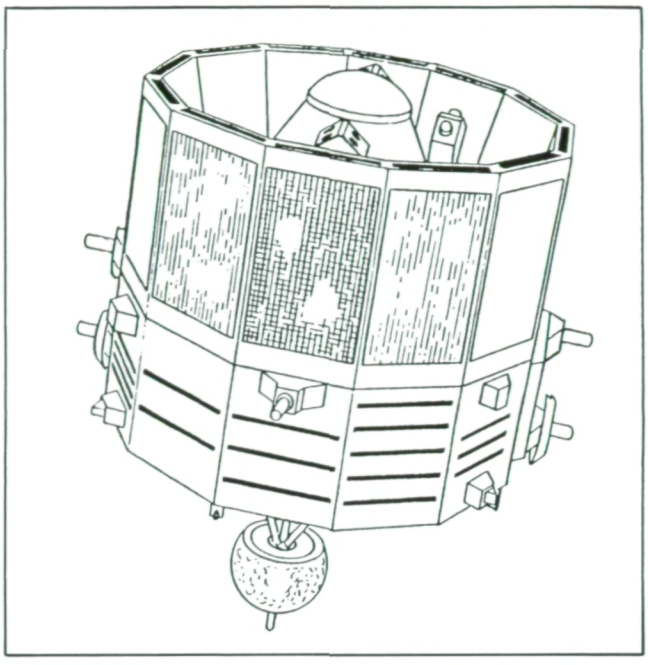

Figure 1. COBE designed for the Shuttle.

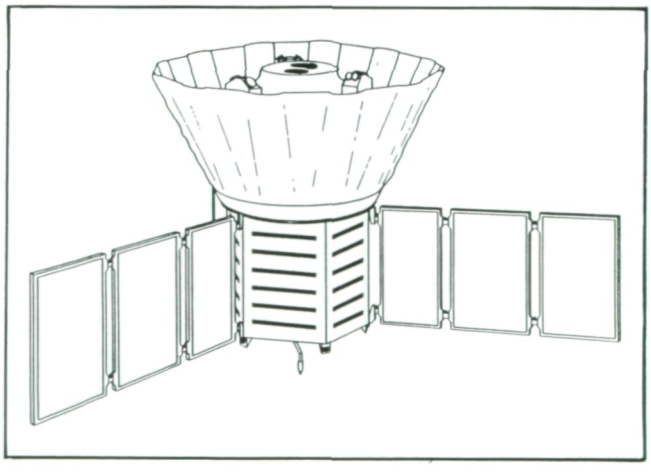

Figure 2. Current free-flyer COBE design.

Contact: Roger Mattson
Code 401

Sponsor: Office of Space Science and Applications

ORIGINAL PAGE IS
OF POOR QUALITY

Mr. Roger Mattson, COBE Project Manager, has been at Goddard for 24 years. Mr. Mattson, who holds a BS degree in chemical engineering, was Project Manager for the first successfully launched, commercially developed upper stage, and he was the first NASA employee to attend the National War College.

TROPICAL RAINFALL MEASURING MISSION

The National Aeronautics and Space Administration and the Radio Research Laboratory of Japan are studying the technological and programmatic features of the Tropical Rainfall Measuring Mission (TRMM).

The TRMM scientific objectives are to obtain a 3-year data set of monthly averaged rainfalls in grid boxes of 360,000 km^2 with an accuracy of better than 20 percent for the portion of the globe between the latitudes of 35° N to 35° S.

Present plans are for the TRMM satellite to be a free-flyer spacecraft in a nominal 300-km circular orbit at an inclination of 35°. With a launch by September 1994 and the planned mission lifetime of 3 years, the TRMM will operationally overlap the Tropical Oceans and Global Atmosphere program.

The anticipated joint venture between the United States and Japan includes the division of responsibility for the instruments, the spacecraft, the launch vehicle, and the scientific analysis. Present planning is that Japan will supply the Precipitation Radar, a Data Relay Tracking Satellite Terminal (DRTST), the launch vehicle (the H II), and the launch services. The United States will supply the spacecraft, the microwave radiometers, the visual and infrared sensor instrument, and the tracking and data communications services with NASA's Tracking and Data Relay Satellite System.

Contact: Thomas Keating
Code 402

Sponsor: Office of Space Science and Applications

Mr. Thomas Keating is Study Manager of the Tropical Rainfall Measuring Mission. He earned an MS degree in electrical engineering from the Catholic University of America. Mr. Keating has 27 years of experience at Goddard, where he has received two Special Achievement Awards.

ASTROMAG: PARTICLE ASTROPHYSICS MAGNET FACILITY

Particle astrophysics stands today at a critical juncture in its development. Observations over the past several years have given unexpected results on the elemental and isotopic composition of cosmic-ray nuclei and on the cosmic-ray abundances of antiprotons and positrons. Concurrently, theoretical developments have presented us with a new framework in which to understand the acceleration of these particles. These results have raised new

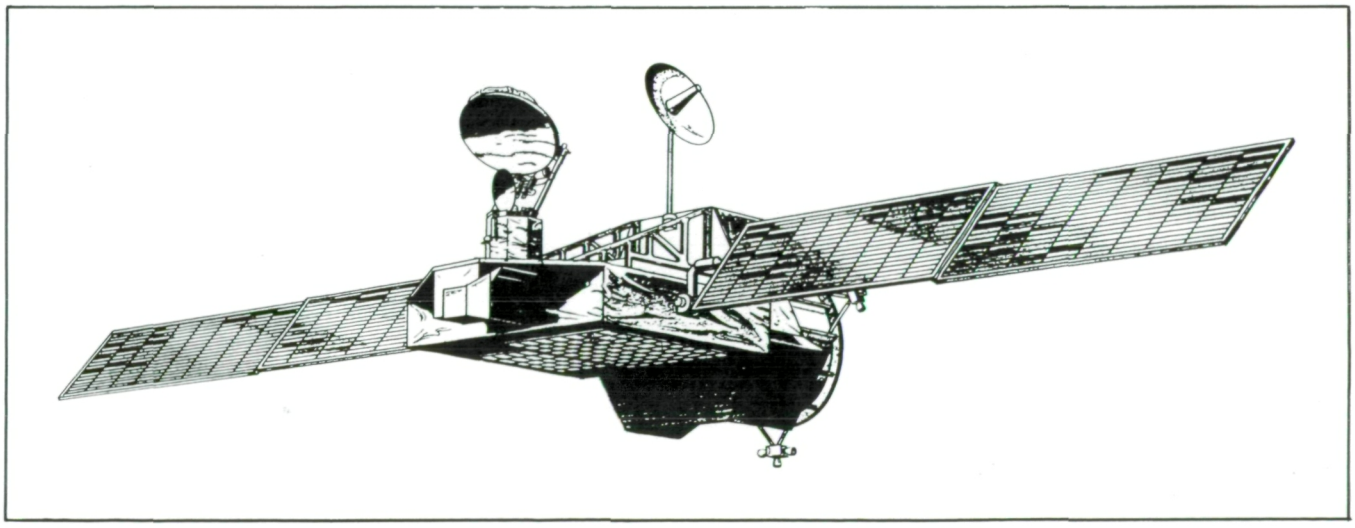

Tropical Rainfall Measuring Mission (H2 configuration).

questions about the origins of energetic particles in astrophysical settings, sometimes deeply related to fundamental questions of astrophysics, cosmology, and elementary particle physics. For example: What is the source of the large abundances of antiprotons observed in the cosmic radiation? Is there evidence for known or unknown particles that could account for missing mass in the universe? What is the nucleosynthetic history of this sample of non-solar system material? Answering these questions requires long space exposures of large instruments; the development of a permanently manned Space Station offers the opportunity to perform the needed experiments.

Over the past year the Particle Astrophysics Magnet Facility (Astromag) Definition Team has examined how a large magnetic spectrometer outside the Earth's atmosphere for an extended period of time could address these questions. A facility composed of a core magnet, dewar, and associated support equipment would be used to conduct a series of experiments with a variety of instrumentation. Several magnet and instrument configurations have been considered, and it appears feasible to construct and operate such a spectrometer facility on the Space Station. One of the configurations under consideration is shown in Figures 1 and 2. Different objectives would be achieved by changing and reconfiguring the instrument complement used in conjunction with the magnet. Plans for management and technical development of the Astromag facility were developed.

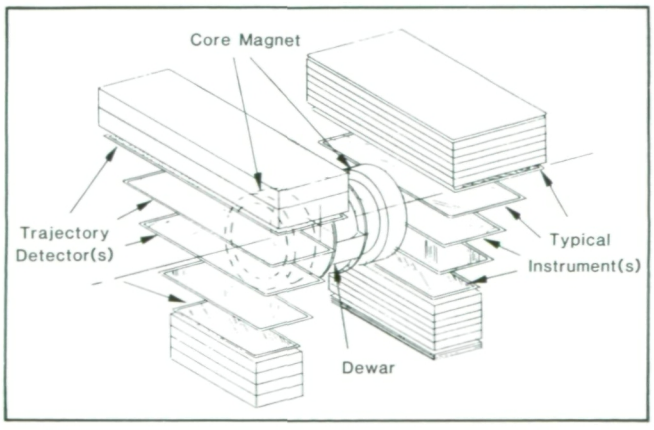

Figure 1. Conceptual design of the Astromag facility has opposing magnets to cancel the torque that a single magnet would apply to the Space Station and to permit two concurrent experiments with different instrumentation. Instruments can be replaced in orbit to conduct new experiments.

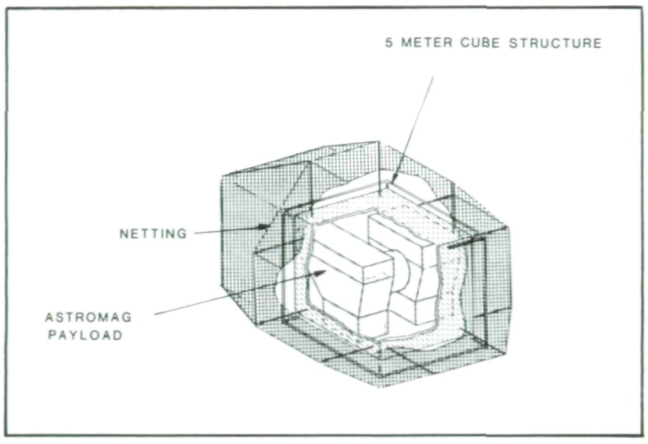

Figure 2. Astromag Space Station concept.

Most of the scientific objectives for Astromag require the long, on-orbit exposures possible on the Space Station, and most objectives can be met in its 28° orbit. On the other hand, some limited but important objectives not attainable in a low-inclination orbit could be met with 1-week exposures in a Shuttle-attached mode in high-inclination (>50°) orbit. If the Space Station were to be delayed significantly, an appropriate configuration of instruments could be flown with the magnet on a high-inclination Shuttle mission before placing Astromag on the Space Station.

Contact: Bill Hibbard
Code 402

Sponsor: Office of Space Science and Applications

Mr. William Hibbard is Study Manager of Astromag with the Advanced Missions Analysis Office. Mr. Hibbard, who earned a BSEE degree from Ohio University, has been with Goddard for 26 years.

SEARCH AND RESCUE SATELLITE-AIDED TRACKING MISSION

During FY87, the Search and Rescue (SAR) Satellite-Aided Tracking (SARSAT) Mission of the Metsat Project continued to improve the ground system to raise its operational state, and initiated activities leading to lower-cost, mass-produced 406-MHz beacons. Two system exercises demonstrated and confirmed the expected performance of the new 406-MHz system. One was an international exercise involving 26 beacons placed all

around the world, on both stationary and moving platforms. The other was a field test of two beacons placed in various regions of the Antarctic, including the South Pole. A facility designed to receive and process 406-MHz early alert distress data via the geosynchronous Geostationary Operational Environmental Satellite-H (GOES-H) satellite was completed. An international test plan for this geosynchronous experiment was developed, and joint tests with Canada and France were initiated.

The SAR Mission of the Metsat Project at the GSFC is responsible for the research and development activities of the SARSAT project, an international cooperative project involving the United States, Canada, France, and the Soviet Union. National Oceanic and Atmospheric Administration (NOAA) is the manager of the United States participation, which also includes NASA, Department of Transportation (DOT), and Department of Defense (DOD). Canada provides the spaceborne repeater for relay of the 121.5 and 243 MHz signals from Emergency Locator Transmitters (ELTs) carried by over 200,000 United States' aircraft and Emergency Position Indication Radio Beacons (EPIRB) carried by more than 2000 ships. Canada also provides a repeater for beacons operating at 406 MHz. France provides a spaceborne processor for the 406-MHz beacons. The United States integrates these two instruments onboard the Tiros Series of NOAA environmental satellites. Each country provides its own ground system. The location of the ELTs and EPIRBs is accomplished with the same Doppler location principle demonstrated by satellite data collection systems such as the Nimbus RAMS and the ARGOS system. The Soviet Union cooperates with the SARSAT partners by making its own SAR satellite system, COSPAS, interoperable with the SARSAT system. The SARSAT equipment will also be carried by NOAA-H,-I,-J,-K,-L, and -M to be launched during the next few years. GOES-H will perform 406-MHz SARSAT experiments from geosynchronous altitude.

The first spacecraft capability, the Soviet COSPAS-1 satellite, was launched in June 1982 and made available to the SARSAT project in September 1982. The first rescues with the help of this system also occurred during this month. The second Soviet satellite, COSPAS-2, and the United States, Canada, and France SARSAT systems onboard the NOAA-8 operational environmental satellite were launched in March 1983. COSPAS-3 was launched in June 1984; NOAA-8 failed in December 1985. NOAA-9 was launched in December 1984 and NOAA-10 in September 1986. The satellites were being used by the U.S. Air Force and the U.S. Coast Guard to assist in real-world rescue operations that use ELTs employed by the aeronautical community and the EPIRBs employed by the maritime community.

The 121.5/243-MHz beacons have no requirement for a stable frequency component and no unique identification. Therefore, satellite detection and location of these beacons present many problems, e.g., poor locations and poor image rejection occur in some cases; lack of unique identification causes inability of rescue personnel to relate detections to specific beacons. Also, coverage is restricted to regions in which the satellite can view a ground station and beacon simultaneously. These problems are eliminated with the 406-MHz system, which achieved initial operational status in 1985.

As of mid-1987, over 900 people were saved with the help of the COSPAS/SARSAT System.

Contact: Fred Flatow
Code 480

Sponsor: Office of Space Science and Applications

Mr. Fred Flatow is the SAR Mission Manager of the METSAT project. Mr. Flatow, who holds an MS degree in engineering from George Washington University, specializes in communications. He has been with Goddard for 21 years, and he recently received the Yuri Gagarin Award, Federation of Cosmonautics of the U.S.S.R.

EXTREME ULTRAVIOLET EXPLORER

Mission Description. The Extreme Ultraviolet Explorer (EUVE) is an Earth-orbiting, astronomical survey mission that will produce the first definitive sky map and catalog in the portion of the electromagnetic spectrum that extends from approximately 100 to 1000 Å. Scientifically, the mission includes three objectives: an all-sky survey, a deep survey, and spectroscopy observations of selected objects. The all-sky and deep surveys are done concurrently during the first 6 months of the year-long science mission. Spectroscopy will be added to the continuing survey studies in the remaining 6 months, with an optional mission extension of 6 more months.

The major elements for the EUVE mission flight systems are illustrated in the figure:

- The Multi-Mission Modular Spacecraft (MMS) is the spacecraft bus which serves as the explorer platform

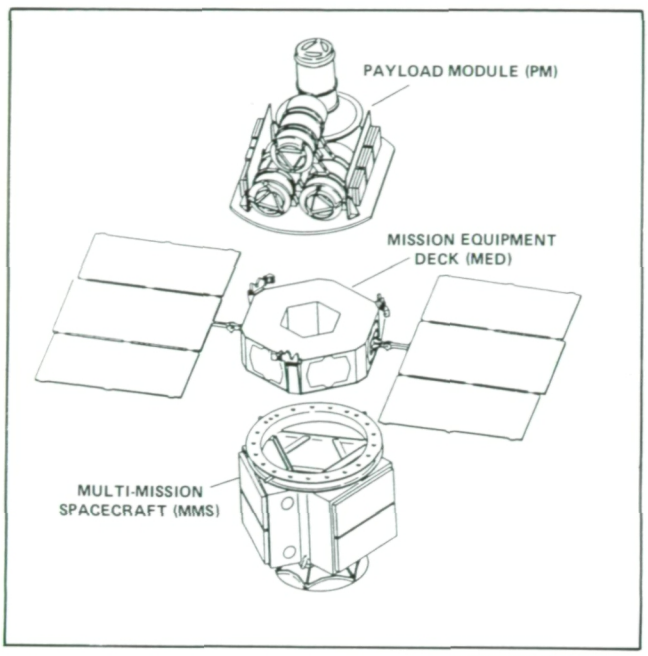

Extreme Ultraviolet Explorer.

for EUVE and which includes the Modular Power System, the Command and Data Handling module, the Modular Attitude Control System, the Signal Conditioning Unit, and the MMS structure.

- The Platform Equipment Deck (PED) provides mechanical, thermal, and electrical interfaces with the EUVE payload, as well as accommodation for the solar arrays and mission-unique equipment.

- The Payload Module (PM) is comprised of the EUVE instruments, support electronics, thermal control, and payload mounting structure.

Launch will occur from the Kennedy Space Center aboard a Delta II expendable launch vehicle. The Explorer Platform, or spacecraft bus, will consist of an MMS augmented with a PED. The EUVE PM will be mated with the Explorer Platform with motorized connectors to facilitate the PM exchange on subsequent missions.

After the EUVE has been launched into orbit, a checkout phase, lasting for about 30 days, is used to perform operational tests and to allow outgassing of volatile substances. The 6-month survey phase commences after it is determined that the observatory is operating satisfactorily.

The spacecraft spins about the roll axis at approximately three revolutions per orbit. Solar panels are mounted in a single plane perpendicular to the roll axis and facing the opposite direction as the Deep Survey/Spectrometer telescope. During the survey mission phase, the spin axis is pointed along the Earth-Sun line and is precessed by onboard magnetic torque rods by 1 degree per day to maintain that pointing. Thus, the solar panels always point directly at the Sun while the Deep Survey spacecraft rotates about the roll axis, the scanning telescopes would each scan a great circle lying in the plane perpendicular to the Sun-Earth line, and the Deep Survey instrument views a small area in the ecliptic plane. Data from the four telescopes are taken only during the nighttime portion of each orbit of the spacecraft when the Earth is blocking light from the Sun. A total data rate of 16 KB/s is shared by the four telescopes, combined with spacecraft engineering data, and the data is recorded at 32 KB/s on a 10E9 tape recorder. Subsequent transmission to the ground is via the Tracking and Data Relay Satellite System (TDRSS) at 512 KB/s.

Upon completion of its mission, the EUVE observatory will be retrieved by the STS, the EUVE PM will be exchanged for the new PM, and the EUVE PM will be returned to Earth.

Science Payload. The EUVE Science Payload consists of four telescope assemblies and five associated electronics boxes. Three of the instruments are used to make the all-sky survey and are called scanning telescopes; the fourth telescope is the Deep Survey/Spectrometer.

The scanning telescopes are approximately 22 in. in diameter by 35 in. long and weigh about 260 lbs each. The Deep Survey/Spectrometer is 64 in. long and weighs about 700 lbs. The electronics boxes weigh about 25 lbs each.

Mission Operations. Spacecraft telemetry data will be processed in the Project Operations Control Center (POCC) and displayed for analysis by the flight operations team. Stored and real-time commands will be formatted and generated by the POCC and Command Management System, respectively. All commands will be transmitted from the POCC to the Explorer Platform via NASCOM and TDRSS. The Explorer Platform (EP) real-time and playback telemetry data will be decommutated in the POCC and displayed for health and safety monitoring.

The Explorer Missions EUVE Science Operations Center (SOC), located at the University of California at Berkeley, will perform the following functions:

ORIGINAL PAGE IS
OF POOR QUALITY

- Science planning and iteration of the timeline with the Command Management System (CMS)
- Evaluating the real-time/quick-look data and payload health and safety
- Generating onboard microprocessor command loads and maintenance of onboard microprocessor software
- Building and maintaining the science data bases
- Analyzing data.

The SOC will be connected to the POCC/CMS via the NASCOM Switching Center at the GSFC and the CMS gateway. The SOC will also be connected to the Data Capture Facility via the NASCOM Switching Center to receive the data stream.

Contact: George Hogan
Code 410

Sponsor: Office of Space Science and Applications

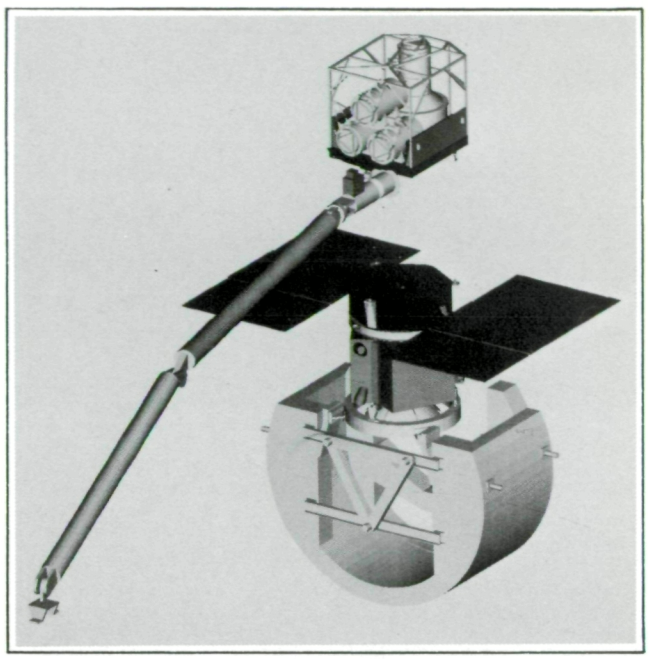

Figure 1. The EUVE payload module being removed from the Explorer Platform while in the orbiter bay.

Mr. George D. Hogan, the Explorer Mission Project Manager, has 26 years of experience at Goddard. He holds a BSEE degree from the University of Maryland.

X-RAY TIMING EXPLORER

Mission Overview. The X-Ray Timing Explorer (XTE) will be the first science payload to be exchanged on-orbit using the Explorer Platform concept described in the previous article on the Extreme Ultraviolet Explorer (EUVE). The XTE mission is designed to study a variety of X-ray sources including: white dwarfs; accreting neutron stars; black holes; and active galactic nuclei, making measurements over a wide range of photon energies from 2 to 200 keV.

The XTE instrument payload module will be carried into space mounted to the Explorer Platform Flight Support System (FSS), located in the Shuttle orbiter bay, where it will rendezvous with the EUVE satellite. After capture of the EUVE satellite, it will be brought into the orbiter bay, attached to the FSS tilt table where the XTE science payload module will be exchanged with the EUVE payload module (Figure 1). After a brief check-out in the orbiter bay, the XTE satellite will be placed into orbit using the Shuttle Remote Manipulator Arm, and the EUVE payload module will be stowed on the FSS for its return to Earth.

XTE Instruments. There are three instruments that make up the XTE science payload: the Proportional Counter Array (PCA); the All Sky Monitor (ASM); and the High Energy X-Ray Timing Experiment (HEXTE). An experiment data system provides data processing for both the ASM and PCA instruments. An artist's conception of the satellite is shown in Figure 2.

The PCA instrument consists of five identical sealed xenon-methane proportional counters having a total effective area of about 0.65 m^2 with a field of view of 1° × 1° (FWHM), covering an energy range of 2 to 30 keV. Each PCA detector element, which weighs about 250 lbs and measures 12 in. × 20 in. × 47 in., also houses the analog processing circuits and high- and low-voltage supplies.

The ASM consists of two scanning shadow camera (SSC) assemblies, each with two one-dimensional detectors mounted on a boom to clear its 7° × 90° (FWHM) field of view, and a resolution of 0.2°. The assembly rotates about the boom axis such that the two SSCs scan a large swath of the sky, 360° × 100°. The SSC detector is a

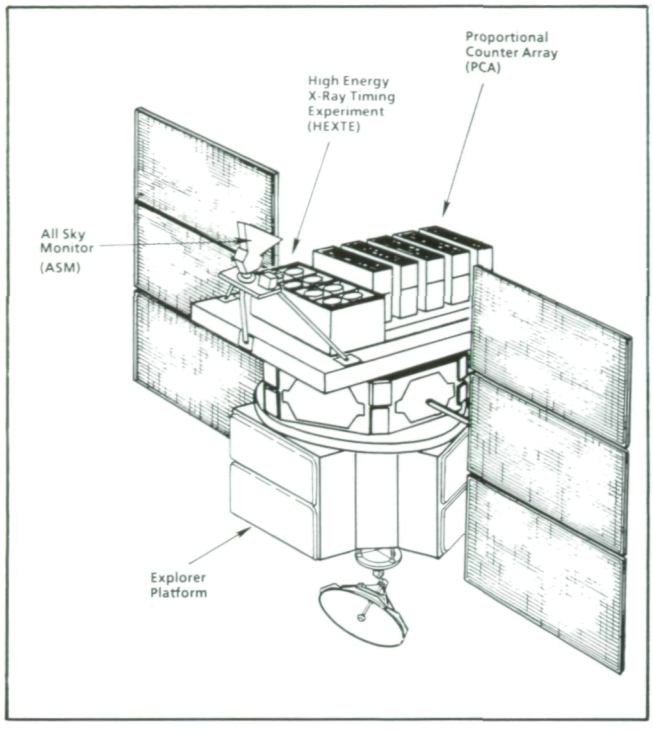

Figure 2. The XTE satellite after assembly and launch from the STS.

xenon-filled proportional counter with a sensitivity to 2–15 keV X rays. The imaged data can be deconvolved on the ground with fast Fourier transform techniques to give source intensity and position. Each SSC weighs 42 lbs and measures 30 in. × 15 in. × 20 in. exclusive of the mounting boom.

The data processing system for both the PCA and the ASM is provided by the EDS. To achieve a required data compression of as high as 50:1, the EDS uses six identical microprocessor-driven event analyzers that convert the event pulse height, time, and detector number to an energy, time, and bin address. The compressed data is transmitted on a common microprocessor data bus and transferred to the satellite communication and data handling system for onboard storage and transmission to the ground. The EDS weighs 44 lbs and measures 20 in. × 10 in. × 12 in.

The HEXTE consists of two clusters of sodium iodide/cesium iodide (NaI/CsI) scintillation detectors with a total effective area of about 1400 cm^2 and a spectral range of 15 to 200 keV. Each cluster is independently gimbaled so as to "chop" between source and background, thereby facilitating background calibration. The HEXTE detector field of view is 1° FWHM and is coaligned with the PCA detectors so that concurrent measurements from 2 to 200 keV can be made.

The HEXTE detector assembly weighs 418 lbs and measures 36 in. × 18 in. × 24 in. It has its own data system for onboard analysis and data compression, which measures 3 in. × 10 in. × 6 in. and weighs 17 lbs.

Mission Operations. Satellite telemetry data will be processed in the Project Operations Control Center (POCC) and displayed for analysis by the flight operations team. Stored and real-time commands will be formatted and generated by the POCC and Command Management System. All commands will be transmitted from the POCC to the XTE satellite via NASCOM and the Tracking and Data Relay Satellite System (TDRSS). The XTE satellite real-time and playback telemetry data will be decommutated in the POCC and displayed for health and safety monitoring.

The Explorer Missions XTE Science Operations Center (SOC), located at the GSFC with planning support and data analysis at the University of California at San Diego and the Massachusetts Institute of Technology, will perform the following functions:

- Science planning and iteration of the timeline with the Command Management System (CMS).
- Evaluating the real-time/quick-look data and payload health and safety.
- Generating onboard microprocessor command loads and maintenance of onboard microprocessor software.
- Building and maintaining the science data bases.
- Analyzing data.

The SOC will be connected to the POCC/CMS via the NASCOM Switching Center at the GSFC and the CMS gateway. The SOC will also be connected to the Data Capture Facility via the NASCOM Switching Center to receive the data stream.

Contact: George Hogan
Code 410

Sponsor: Office of Space Science and Applications

Mr. George D. Hogan, the Explorer Mission Project Manager, has 26 years of experience at Goddard. He holds a BSEE degree from the University of Maryland.

LYMAN/FAR ULTRAVIOLET SPECTROSCOPIC EXPLORER (FUSE)

The Lyman/FUSE mission has been in a study phase during 1987. It is competing with other astrophysics missions for selection as an approved and funded Explorer spaceflight mission. Despite that, there have been some significant technological advances stimulated by the needs of Lyman, which will have a beneficial effect on this mission as well as other astronomical missions.

The concept of this mission emphasizes high-resolution spectroscopy in the 900 to 1200 Å wavelength region. This region of the spectrum is referred to as far ultraviolet (FUV). The goal is to view and study FUV sources as dim as 16th visual magnitude. By comparison, Copernicus could only view stars brighter than 7th magnitude. The Hubble Space Telescope (HST), which is discussed elsewhere in this report, is designed to view stars in the ultraviolet, not the FUV region.

The major astrophysical problems that Lyman astronomers will address include cosmology, evolution of the intergalactic medium, the nature of the central engine in active galactic nuclei, the physical state and distribution of hot interstellar gas in the disks and halos of galaxies, cold gas in the interstellar medium, magnetic activity and winds in cool stars, the end stages of stellar evolution, and remote studies of the magnetospheres of the outer planets.

The telescope and spectrograph under consideration for the Lyman mission must have a very high throughput to achieve the required sensitivity for this kind of a spaceflight mission. Some interesting technological achievements have been made in this area.

Microchannel plates are to be used in the Lyman scientific instrument. The use of microchannel plates allows the counting of photons, which in turn permits the creation of images or spectra of celestial bodies. Until recently, the quantum efficiency of microchannel plates was in the 15 to 20 percent range. Developments at the Lawrence Berkeley Laboratories, stimulated by Lyman's requirements, have produced methods of making microchannel plates with efficiencies almost double what they had been. Quantum efficiencies of about 30 percent are now achievable.

In addition, technological achievements have also occurred in the area of reflective surfaces for FUV light. By using techniques developed and tested at the Lawrence Berkeley Laboratories, University of Colorado, and the GSFC (Code 717), again with the needs of Lyman in mind, silicon carbide overcoated gratings have been developed with efficiencies of about 18 percent up from about 11 percent.

New encoding schemes have been developed jointly at Stanford University and Ball Aerospace that allow the use of smaller pixels that would be produced by the multianode microchannel array. This, in turn, allows the use of a physically smaller spectrograph and therefore a smaller and less massive overall scientific payload. These technological efforts are being made for both the HST and the Lyman/FUSE mission.

The significance of these kinds of technological developments is that smaller, more efficient, and therefore less expensive, scientific instruments can be made. These are the kinds of technological advances that make missions possible. If Lyman/FUSE is selected for development, it would fly in the mid-1990s.

Contact: Stephen J. Paddack
Code 402

Sponsor: Office of Space Science and Applications

Dr. Stephen J. Paddack is Chief of the Advanced Missions Analysis Office, which studies, plans, and analyzes future spaceflight missions at Goddard. Dr. Paddack has been with Goddard since 1961. His professional experience includes aeronautical and aerospace engineering, astrodynamics, scientific research in geophysics and planetology, and the project management of scientific spaceflight missions. Dr. Paddack earned a PhD degree in engineering/physics from the Catholic University of America.

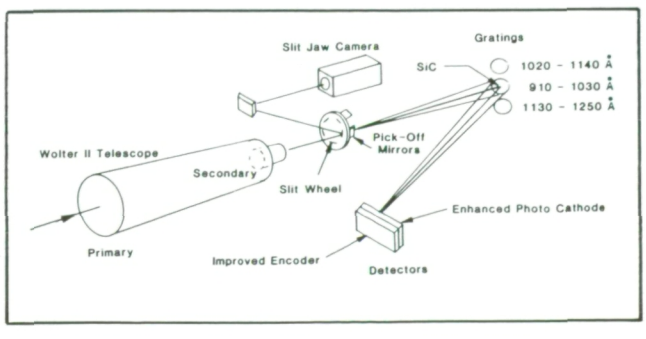

Lyman scientific instrument.

GAMMA RAY OBSERVATORY

The Gamma Ray Observatory (GRO) is one of the four great observatories being planned by NASA. Along with the Hubble Space Telescope, it will be launched in the next couple of years. The GRO is in the final stages of construction and should begin testing in early 1989 and be launched in the early part of the 1990s. GRO is designed to collect more and better gamma-ray data than was possible with earlier satellites. A full sky map of gamma-ray sources will be made. Particular information will be obtained on the distribution and nature of matter in the Milky Way Galaxy; on the formation of heavy elements; and on quasars, pulsars, and active galaxies.

Four scientific instruments will be flown on the Observatory: an Energetic Gamma-Ray Experiment Telescope, from GSFC; an Imaging Compton Telescope, from the Max Planck Institute; an Oriented Scintillation Spectrometer Experiment, from the Naval Research Laboratory; and a Burst and Transient Source Experiment, from the Marshall Space Flight Center. These instruments cover the gamma-ray range from 0.05 to 3 $\times$ 10 MeV. The first three instruments require extensive calibration, which is now in progress.

The low level of gamma radiation requires that the Observatory be pointed at a source for a period of 2 weeks to gain sufficient events for scientific analysis. The large-view angle of the instruments makes it possible to complete a full sky survey in approximately 1 year. Unlike most optical telescopes, data from the gamma-ray telescope takes considerable data analysis and understanding of the instrument to interpret. Guest investigators will be sought, but they will have to spend a great deal of time at one of the principal investigator's facilities to get a proper appreciation for the data. Special selected targets for study, except for supernovae or extraordinary solar events, will have to wait until after full sky map measurements are made.

Contact: Jeremiah J. Madden
Code 403

Sponsor: Office of Space Science and Applications

Mr. Jeremiah Madden, Project Manager of the Gamma Ray Observatory, has 28 years of experience with Goddard. Mr. Madden, who holds an MEA degree from George Washington University, was a recipient of the NASA Outstanding Leadership Medal.

SPACE STATION

SPACE STATION

The Goddard Space Flight Center is responsible for providing the following flight elements for Space Station:

- Customer Servicing and Assembly Facility
- Attached Payload Accommodation Equipment
- Platforms
- Flight Telerobotic Servicer (FTS).

GSFC is also providing several ground systems that will support the development and operation of the flight elements, and the operation of the WP-3 flight and ground systems; technical support for mission organizations; interaction with the user community; and technology development and transfer. A project has been established for each flight element and for the GSFC Space Station Advanced Development Program.

The GSFC Space Station Project sponsors research and technology development directed toward providing the technology required to support Goddard's Space Station

ORIGINAL PAGE IS
OF POOR QUALITY

role. The work to develop these technologies is performed by organizations throughout Goddard. Six of the technology areas sponsored by the Space Station Project are presented here.

Two-phase Thermal System Development. This research is led by Roy McIntosh, Ted Swanson, and Dan Butler of Code 732 and is directed toward producing data that can be used to design two-phase thermal systems for Attached Payloads and Platforms. This is accomplished through the design, fabrication, and test of prototype thermal instrument conditioning systems (i.e., both mechanical and capillary pump versions) to verify the two-phase thermal concepts for Space Station applications.

A second part of the thermal efforts involves the production of three flight experiments to test the operations of mechanically pumped and capillary pumped instrument conditioning systems in a zero-gravity environment. These experiments are to be performed in the Space Shuttle cargo bay.

Workstation, Remote Payload Command, and Control Technology. This research is performed by Karen Moe and Ted Ackerson of Code 522. A prototype workstation is being developed with commercial hardware elements to demonstrate and evaluate performance capability and limitations and to determine drivers of the user workstation interfaces to the SSIS. This research also includes the development and demonstration of remote

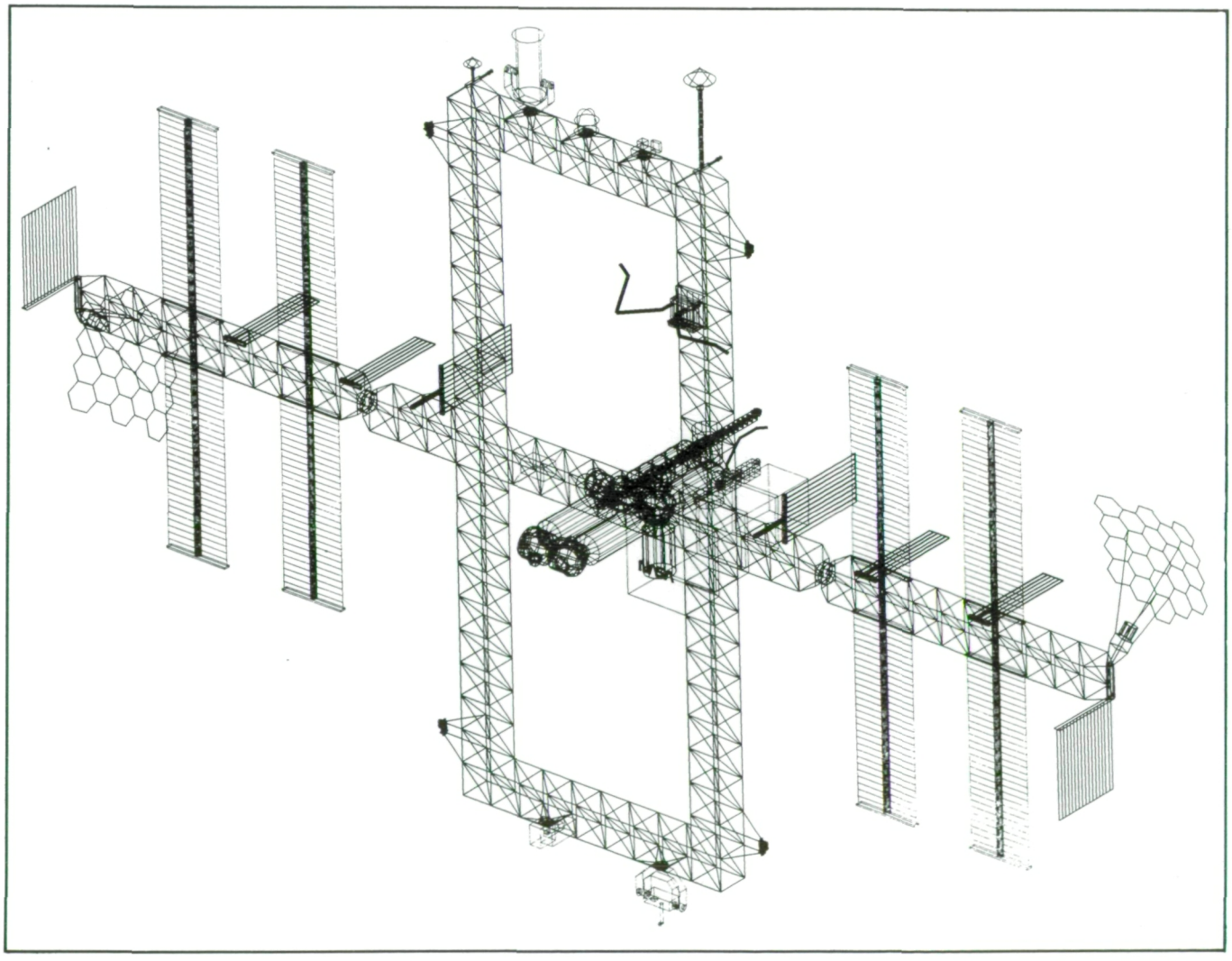

Revised baseline configuration.

user payload command and control (telescience), including planning/replanning in near real time, user-to-payload communications, interactive control, and the evaluation of health and safety issues.

Advanced Fiber-Optic-Based Data System. This research is led by John Rende of Code 735. This task is directed toward the development of a fiber-optic-based advanced data system for space flight application. This advanced data system uses the Star★Bus topology. The system uses a broadcast data bus of 100 Mb/s bandwidth, packetized data distribution, autonomous data transmissions, and hierarchically structured network communications protocols. The absence of a central data poller improves the reliability of the system over past data system designs and also reduces the complexity of testing and integration of payloads and other users interfaced to the data bus.

Also, network performance is being upgraded by replacing Emitter Coupled Logic (ECL) and Transistor-Transitor Logic (TTL) circuitry with modern GaAs and CMOS technology. Generous improvements in power and speed are accomplished.

Launch and Servicing of Polar Platforms. This study is led by James Watzin, Code 712. The objective of the study is to determine an optimum approach for the servicing and repair of Space Station Polar Platforms. The servicing approach emphasizes the use of ELVs and robotic technology. The study uses the Earth Observation Satellite payload as a baseline for the strawman instrument complement. Trades and analysis are performed to evaluate the feasibility and benefits of alternative servicing approaches. Robot and Platform accommodations needed for servicing are being identified. The results of this study will be compared with STS-based servicing approaches.

FTS Demonstration Test Flight. This task is led by James Watzin of Code 712. It provides the planning and analysis for a test flight demonstration of the FTS. The test flight demonstration will provide answers to some fundamental engineering uncertainties such as FTS dynamics and controls in zero gravity, operator restraint systems, FTS thermal system, and general performance and efficiency issues. The test flight will also demonstrate the prime contractor's manipulator system.

Telerobotics Laboratory. This effort is led by Stanley Ollendorf of Code 706. The Space Station Project supports the development of a Ground Telerobotics Laboratory, which provides for the test, evaluation, and development of ground and flight systems to support NASA's robotics efforts. This high bay facility will house robotics development and test equipment and personnel. The facility will provide a high degree of repeatability, accuracy, and versatility for evaluating robotic components, subsystems, and systems.

The functional capabilities that the ground laboratory provides to the Space Station robotics program are:

- A system architecture containing robot control software
- A computing facility to support development and evaluation of software for robot control systems
- A convenient means of robot control and observation
- Assessment of vision systems.

Contact: George Alcorn
Code 700

Sponsor: Space Station

Dr. George Alcorn, who holds a PhD degree in physics from Howard University, joined NASA in 1978. Before joining NASA, he served as Advisory Engineer/Scientist for IBM, Manassas, Virginia. He currently serves as Deputy Project Manager Space Station Advanced Development.

Institutional Technology

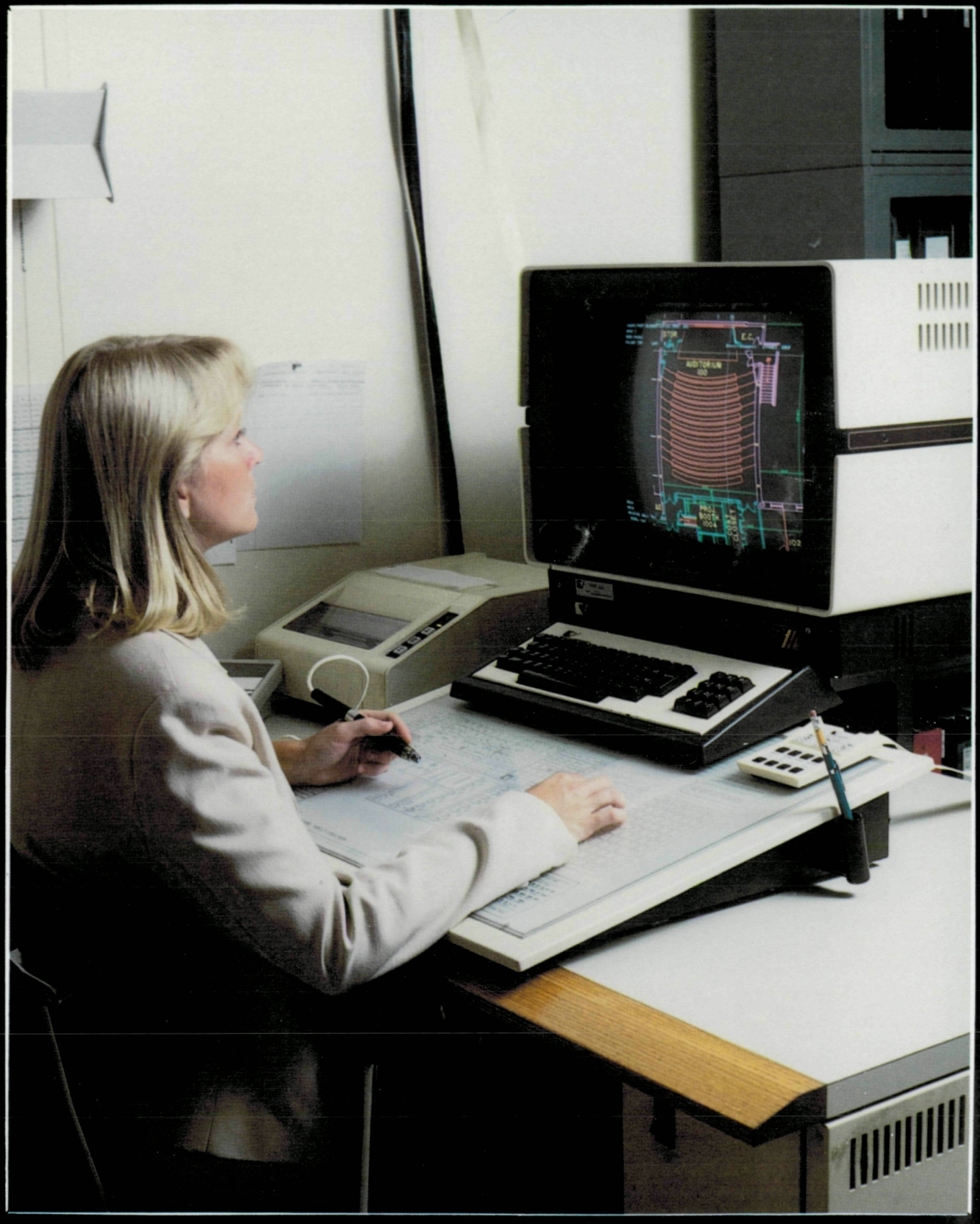

The objectives of the Procurement Management Technology Program are to increase procurement productivity and improve the quality of procurement documents and to provide accurate, on-line management information along with decreased procurement lead time and improved customer support.

INSTITUTIONAL TECHNOLOGY

COMPUTERIZATION AND PROCUREMENT

Not long ago, the computer was a mysterious machine that only a few people understood. Over the years we have associated computers with mathematicians, scientists, doctors, and a whole array of other professionals. Only recently have computers made an inroad into the procurement field. One reason for this is the development of personal computer software, such as the spreadsheet program. These programs have given the nonprogrammer the ability to design those what-if situations so often encountered in procurement. One example of a spreadsheet program is LOTUS 1-2-3, which alone has unlimited applications in procurement. Ordinarily, a person takes about 8 seconds to multiply two-digit numbers. During the same amount of time, a spreadsheet program can perform several thousand multiplications correctly.

One of the many possible applications of LOTUS 1-2-3 is automating the Structured Approach Profit/Fee objective, more precisely, placing the NASA Form 634 on a LOTUS program. Government agencies making noncompetitive contract awards over $100,000 use a structured approach for determining profit/fee. Before automating the calculation of profit/fee, a contract specialist performed all the calculations. Before negotiations, if any cost element increased or decreased, a recalculation in profit/fee was required. This became a cumbersome process subject to numerous errors.

In 1987, Goddard placed the profit/fee objective on the LOTUS 1-2-3 program. Now the negotiator needs only to include the recommended costs and assigned weights. The program performs all necessary calculations and transposes those figures onto the NASA Form 634. With a simple key stroke, the form is printed. The main advantage is that before or during negotiations, changes to any cost category or assigned weights are possible, and the profit/fee is automatically recalculated and printed within seconds.

This is only one example of how computers and procurement are working together. What about going into negotiations with a computer model that calculates over 160 different price ranges? Change a labor rate or decrease General and Administrative cost, and within seconds all 160 different price ranges are recalculated. We are only beginning to effectively use computers in procurement.

Contact: William K. Keller
Code 261

Sponsor: Management Operations Directorate

Mr. William Keller, who has a year of experience at Goddard, serves in the ADP Procurement Branch. Mr. Keller holds an MPA degree from the University of Baltimore, and he is currently earning a PhD degree in policy science at the University of Maryland.

◀ *We are only beginning to use computers effectively.*

PRECEDING PAGE BLANK NOT FILMED

PROCUREMENT AUTOMATION

Goddard is implementing the Procurement Management Technology Program (PMTP), which was established by NASA Headquarters for the purpose of automating certain procurement functions. The software for PMTP has been completed and is being provided to all NASA centers. Each center is responsible for providing the necessary computer hardware and for actual operational implementation. At Goddard, the Procurement Support Division is reponsible for implementation of PMTP. The objectives of PMTP are to increase procurement productivity, improve the quality of procurement documents, and provide accurate, on-line management information along with decreased procurement lead time and improved customer support.

The PMTP has three components:

- The Document Generation Subsystem, which is a personal computer–based system for the automation assisted preparation of solicitations, contracts, and modifications.

- The Procurement Regulation Subsystem, which is a personal computer–based system for the storage and retrieval of procurement regulations. The system includes key word search and other features.

- The Acquisition Management Subsystem, which is a mainframe-based system for preaward milestone tracking and postaward administration of small purchases, grants, and contracts. It permits on-line entry and retrieval of such information by both procurement and technical personnel.

PMTP has been developed over several years. The Acquisition Management Subsystem was initially developed by the Langley Research Center and was modified for NASA-wide application by Booz, Allen and Hamilton under contract to NASA Headquarters. The Document Generation Subsystem is a product of CRC, Inc., that has been adapted for NASA use. Most aspects of PMTP should be fully operational at Goddard during FY88.

Contact: Kent Cockerham
Code 260

Sponsor: Management Operations Directorate

Mr. Kent Cockerham came to Goddard in 1965 and has served as a Contract Specialist and Procurement Manager in support of several flight projects. Since 1983, he has been assigned to the Procurement Policy Branch, Procurement Support Division. Among his present responsibilities is the implementation of the Document Generation System at Goddard.

SMALL PURCHASES AUTOMATION PROJECT

A small purchase is an acquisition of supplies, equipment, or services valued at $25,000 or less. Nearly 80 percent of all procurement requests (PRs) processed by the Center are for small purchases, representing nearly 15,000 actions per year. Although the dollar values of these purchases are small, the items and services purchased are often crucial to the operation of the Center.

The process that exists to ensure the timely execution of these actions is both unique and complex. It is unique from most of our administrative functions, not only from the standpoint of the wide range of activities it must support, but also because of the many people who are directly involved in the process. Scrutiny of the process reveals that it has, in time, drifted from its fundamental objective of providing the Center with a quick, responsive, and simplified method of acquiring our small purchases to a more complex and unwieldy one.

The process encompasses all activities that occur from the time a need is identified until a contractor is paid for delivery of a satisfactory product or service. First, a PR is prepared and subject to programmatic and fiscal review and approval within the originating organization. The funds must then be certified and committed by the Accounting Operation Section. Once the funds are committed, the Property Disposal Management Section certifies that the desired product is not available from stock or other internal sources. The purchase order is then forwarded to Small Purchases for placement of the order. Quotations are solicited, and the purchase order is awarded to the firm that submits the most favorable quotation. The selected contractor is expected to adequately perform the service or deliver the product. Receipt, inspection, and internal delivery to the initiator occurs upon delivery to the Center. The user must accept or reject the delivered item or service. Upon acceptance, the contractor is paid.

How can this process be improved? We now recognize that the current process has fundamental problems that require fundamental changes. Changes are particularly necessary to accommodate the need to automate the process as much as practicable toward a paperless process

and to make appropriate changes to the organizational and physical structure within which the process works.

Toward this end, a committee of key persons from across the Center, representing every aspect of the process, has been formed to assist in developing the new system. Our first step has been to contract with Strategica, Inc., of Washington, D.C., for a feasibility study for automating the end-to-end small purchases processing system. A key feature of the analysis is the development of alternative conceptual designs, including an assessment of their impact upon existing systems and the overall organization. A second key feature is the development of a work plan that reflects the detailed design, development, testing, training, and implementation of an operable system.

We hope to maximize the capability for immediate file updates via on-line/interactive processes for funding verification, approvals, and updates. We require a system capable of accommodating simultaneous multiple user inquiries and updates. Anyone on Center with the appropriate equipment will be able to track the location and status of his PR. It will be fully interactive with existing systems. Ultimately, with the combination of electronic transmission of PRs into a single, highly automated processing Center, lead times for processing our small purchase actions should be reduced by as much as 3 weeks. We can make significant progress toward eliminating what appears to be an impenetrable maze of bureaucracy. Overall, this process is intended to be both user and processor friendly.

Due to both the complexity of our current process and the widespread impact to Center activities, adjusting the process through the changes listed above brings with it risk. Accordingly, we are going to proceed cautiously with each step of system design and development and rely heavily on the help of the user community. Having completed the feasibility study, we are now planning to contract for a detailed system design and implementation.

Contact: Michael Kelly
Code 247

Sponsor: Management Operations Directorate

Mr. Michael Kelly, Head of Construction/Purchasing Procurement, is involved in automating the End-to-End Small Purchases Acquisition Process. Mr. Kelly, who holds a BA degree in economics from the University of Pennsylvania, has 15 years of experience at Goddard and has received several awards for his work.

LOCATOR AND INFORMATION SERVICES TRACKING SYSTEM

Over the past two years employees in the Management Operations Directorate (MOD) have been developing and implementing a new locator system, the Locator and Information Services Tracking System (LISTS). LISTS has been in production at Goddard since March 1987. The reasons for retooling the old locator system were compelling. The programming that supported the system did not lend itself to easy and meaningful modification. This affected the accuracy and utility of the data base, which contained a high error rate.

These facts and others were revealed by a committee of MOD workers that was charged with reviewing the Locator and proposing a solution to improve it as a source for service and planning needs. Their recommendation was to scrap the old Locator and develop a radically different system—LISTS. LISTS emphasizes on-line data entry and retrieval. It therefore minimizes paperwork both in terms of submittal of locator forms and review of the information contained in the data base. It is built on Adabase/Natural, a fourth generation data base management software package. With LISTS we have an opportunity to improve services dependent on a sound locator-type data base (e.g., the mail operation, space utilization, the library, and others) and to establish a tool for better institutional planning.

The use of LISTS as an institutional planning tool is an important element in the success of the institutional component of the strategic planning work under way at Goddard. The unique ability of LISTS to highlight certain totals, sorts, comparisons, and trends over time establishes its planning aid feature. Some examples of this feature include:

- comparisons of civil servants and contractors by skill classification
- total number of contractors by contract, organization, building, and other sort fields
- comparisons of actual on-site contractor workers to authorized on-site levels
- changes in total work force over time through maintenance of a history file
- frequency of changes of our work force through maintenance of a transaction file.

ORIGINAL PAGE IS
OF POOR QUALITY

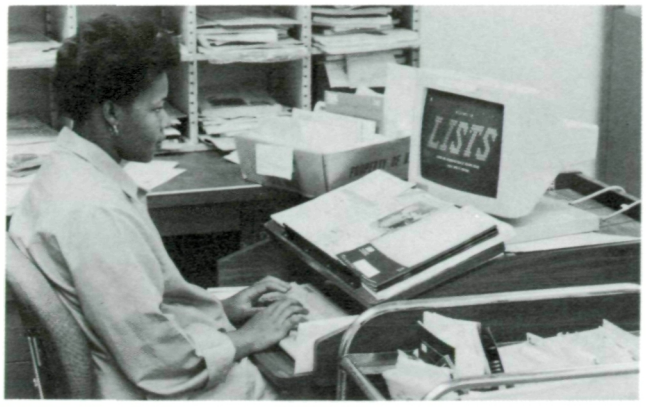

Locator and Information Services Tracking System.

The inclusion of accurate data about contractors and other workers (e.g., tenants, grantees, and visiting scientists) separates LISTS from the old Locator. To specifically define our contractor work force's responsibilities under LISTS, all on-site contracts were modified to insert a clause detailing their roles and responsibilities. Given their growing and major role in the accomplishment of Goddard's mission, it was essential that any modification to a locator system include improvements in the information we collect and maintain about our contractor work force.

A phrase used to describe LISTS is "another acronym, not just another system." During 1987, we put that claim to the test as we completed the initial data load of 11,000 records, made LISTS operational, and began using its data to better understand and manage Goddard's work force.

Contact: Mark E. Walther
Code 231

Sponsor: Management Operations Directorate

Mr. Mark Walther works with the Logistics Management Division's Locator and Information Services Tracking System (LISTS). He is a recipient of a Performance Award for Locator Study—Phase 1. Mr. Walther, who holds an MPA from Iowa State University, was a Presidential Management Intern, and he has been with Goddard for six years.

AUTOMATED CONSTRUCTION OF FACILITIES TRACKING SYSTEM

The NASA Construction of Facilities (CoF) Program is one of the longest and most complicated budget cycles of the Agency's institutional budgets. From initiation to completion of a major project can take 5 years or longer, with the average time of 4 years. It is the responsibility of the Planning Section to prepare this program and track it to the start of construction and even complete the preliminary engineering reports. At the beginning of the cycle, as many as 65 projects are eligible for consideration (Greenbelt and Wallops Flight Facility), but seldom will more than 15 or 16 be accomplished in the year they are presented because of the scarcity of funds and other factors. During the cycle, many status reports will be made to various levels of management at Goddard and NASA Headquarters. Keeping track of priorities, cost estimates, and status of projects on a real-time basis became a chore. In addition, keeping the appropriate organizations aware of the status of all the projects that they had submitted for the past 5 years became a problem.

During the course of the initial preparation of a CoF program, the status of projects is in constant flux, and there is a need for reporting on all aspects of the program on short notice. In the short time before several mandated milestone dates, there was a flurry of activity (e.g., projects withdrawn, added, and reprioritized).

When we acquired our AT&T 6300 Computer in 1985, we began using it immediately to reduce the effort involved in the preparing and tracking of the CoF programs. By using the dBase III+ Program as a base, we developed a data base and retrieval system that permits staff personnel to input and access data easily. Prioritization is easily accomplished, even within subcategories (e.g., directorate, type of construction, and location). Accurate reports are available on short notice.

Each potential project is given a number that it keeps throughout its lifetime. Because most projects that do not get funded are deferred until the following year, a complete history of all these projects is recorded. By the use of simple code letters and numbers for each project, all of the required information can be retrieved, formatted, and displayed in many different reporting formats. What formerly took hours of typing, prioritizing, and formatting is now done quickly and automatically.

The system has excellent graphics capabilities, and we are adapting these to produce material for the numerous presentations given during the CoF cycle.

Contact: Ralph L. Adams
Code 272

Sponsor: Management Operations Directorate

Mr. Ralph Adams, a mechanical engineer, is Head of the Planning Section of the Facilities Engineering Division. He is a graduate of the United States Merchant Marine Academy and has been a part of Goddard for 25 years.

NASA PROPERTY DISPOSAL MANAGEMENT SYSTEM (NPDMS)

At the 18th Annual Supply and Equipment Management Conference held in October 1985, the Goddard Space Flight Center was asked to take the lead in preparing a plan for development of a standardized automated property disposal management system. The details of the plan, cost estimate, and project schedule were presented at the Supply and Equipment Management Officers' meeting held at the Marshall Space Flight Center on April 22–25, 1986, and approved for implementation as an agency-wide system. GSFC has the only fully automated property disposal management system that interfaces with the NASA Equipment Management System (NEMS) and the General Services Administration (GSA). Therefore, this system was chosen to be the baseline for development of the standardized system.

The objective of the standardized disposal system, referred to as the NASA Property Disposal Management System (NPDMS), is to provide NASA with an agency-wide automated disposal management system to support operational requirements for the reutilization and disposal of excess personal property no longer required by the Center or contractor. The NPDMS will track NASA-owned property through the disposal process via an on-line system.

The NPDMS is a comprehensive automated information system to support information and operational requirements for the disposal function at all NASA field installations. The system will accommodate its user by providing the following features:

- Capability to: (a) record and track the reutilization/disposal of capitalized and noncapitalized controlled equipment, noncontrolled equipment, and materials inventory items; (b) screen procurement activities; and (c) conduct inventory of excess personal property.

- Report generation consisting of: (a) a basic set of batch and on-line reports; (b) generation of a daily report containing all transactions that update the NEMS Equipment File; (c) an option to generate the DD Form 1348-1, Single Line Item Release/Receipt Document, for reporting excess personal property to the Defense Reutilization and Marketing Office; and (d) an automatic generation of the Annual Report of Utilization and Disposal of Excess and Surplus Property (NASA 623 Report).

- Interfaces will be with the: (a) NASA Equipment Management System in direct update of the NEMS Equipment File for all recorded equipment items that are excessed; (b) GSFC supply system in an automatic update of the number of available units as disposition actions are processed on-line for supply items; and (c) General Services Administration Regional Office in an automated electronic reporting interface.

In addition, the system will provide an on-line update of the local installation data base, an on-line query and *ad hoc* report generation capability, and an automatic retirement of records regarding completed cases and concurrent update of the termination date.

The Critical Design Document (CDD) was prepared in August 1987 and distributed to Headquarters and to each Agency Project User Committee Member for review and comments. Headquarters believed the document could become an agency model for future agency-wide systems. The CDD Review was held August 25–27, 1987, hosted by Goddard.

The Goddard Development Team has submitted an Implementation/Maintenance Proposal to Headquarters for this project. If accepted, Goddard would assist each center in implementing this system and would maintain the system throughout its life cycle. NPDMS is scheduled for implementation in May 1988.

Contact: Connie Higgs
Code 235

Sponsors: Logistics Management Division and Property Disposal Management Section

Ms. Connie Higgs is the Center Development Project Manager of the NASA Property Disposal Management System (NPDMS). She and Property Disposal Specialist, Maureen Barber, are involved in the development, design, and implementation of a NASA-wide PDMS. Ms. Higgs has been with Goddard for almost 18 years and has received several awards for her work.

Index

Author	*Page*
Ackerson, Clarence T.	175
Adams, Ralph L.	242
Alcorn, Dr. George	234
Allen, Dr. John E., Jr.	17, 66
Arking, Dr. Albert	85
Bailey, Steven A.	106
Baker, Dr. Daniel N.	62
Bell, Dr. Thomas L.	84
Bertsch, Dr. David L.	26
Blodget, Dr. Herbert W.	110
Boers, Dr. Reinout	93
Bonavito, Dr. N. L.	100
Bufton, Dr. Jack L.	107
Bukowski, Michael T.	176
Butler, Dan	138
Campbell, William J.	211
Cantor, Kirk M.	129
Carlson, Dr. Barbara E.	61
Castles, Dr. Stephen H.	146, 147
Chan, Dr. Kwing L.	4
Chiu, Dr. Hong-Yee	4
Choudhury, Dr. Bhaskar J.	121
Cieplak, James	215
Cline, Dr. Thomas L.	24
Cockerham, Kent	240
Connerney, Dr. J. E. P.	43
Conrath, Dr. Barney J.	39
Costenbader, Jay	202
Crannell, Dr. Carol Jo	33
Curtis, Dr. Steven A.	41, 52
Davenport, William M.	212
Davila, Dr. Joseph	13
Del Genio, Dr. Anthony D.	88
Deming, Dr. Drake	21
Desch, Dr. Michael D.	38, 41
DiPirro, Dr. Michael	147
Dominy, Carol	181
Donn, Dr. Bertram	17, 20
Dorband, Dr. John E.	153
Dwek, Dr. Eli	4
Edwards, Stephen G.	175
Epstein, Dr. Gabriel L.	14
Fainberg, Dr. Joseph	36
Feldman, Dr. Gene Carl	162
Figueroa, Orlando	147
Fichtel, Dr. C.	26
Flasar, Dr. F. Michael	46
Flatow, Fred	228
Forman, Michael	213
Fortin, Andre	171
Frederick, Dr. John E.	75
Fueschsel, Dr. Charles	220
Gass, Theodore B.	143
Gasser, Max G.	140, 142
Gehrels, Dr. Neil	6
Glasser, Charles M.	31
Grebowsky, Gerry	181
Green, Dr. Sheldon	92
Gull, Dr. Theodore	1
Gurman, Dr. Joseph B.	15
Hall, Dr. Forrest G.	118
Han, Dr. Daesoo	162
Harding, Dr. Alice K.	6
Harpold, D.	130
Harris, Isadore	57
Herr, Denver	179
Heymsfield, Dr. Gerald	81
Hibbard, William	227
Higgs, Connie	243
Hilliard, Lawrence M.	178
Hillman, Dr. John J.	47
Hilsenrath, Dr. Ernest	69
Hintzen, Dr. Paul M. N.	10
Hoegy, Dr. Walter R.	73
Hogan, George D.	229, 231
Hollis, Dr. Jan M.	11
Holman, Dr. Gordon	13
Horner, Ward	168
Hsu, Dr. Y. K.	136
Hull, Larry G.	209
Hunter, Dr. S.	26
Jacobs, Dr. Barry E.	155
Jennings, Dr. Donald	18
Jones, Eddie M.	135
Jordan, Dr. Stuart D.	15
Kaiser, Michael Leroy	38, 41
Kalshoven, Dr. James E., Jr.	124
Kaye, Dr. Jack A.	71
Keating, Thomas	227
Keller, William K.	239
Kelley, Dr. Richard L.	28
Kelly, Michael	240
Koch, Dr. Steven E.	80

PRECEDING PAGE BLANK NOT FILMED

Index (continued)

Author	*Page*
Kondo, Dr. Yoji	2, 4
Kostiuk, Dr. Theodor	44
Kotecki, Carl	184
Krabill, Dr. William B.	106
Krueger, Dr. Arlin	67
Kunde, Dr. Virgil G.	49
Kutter, Dr. G. Siegfried	9
Kyle, Dr. H. Lee	91
LaBel, Ken	148
Lambros, Scott	148
Lau, Dr. William K. M.	87
Lepping, Dr. Ronald P.	64
Lerner, Dr. Bao-Ting	164
Liebrecht, Philip E.	191
Lowrey, Barbara E.	166
Lu, Dr. Yun-chi	192
Mack, Marilyn J. P.	192
Madden, Jeremiah J.	234
Mahaffy, Dr. P. R.	130
Maier, Dr. Eugene	31
Mahmot, Ron	197
Mandl, Dan	172, 183, 197
Mattson, Roger	226
Mayr, Dr. Hans G.	31, 57
McGill, Susan E.	190
McGuire, Dr. Robert E.	156
McIntosh, Roy	138
Miller, Warner	180
Morakis, Dr. James	180
Moyer, Charles V.	150
Mumma, Dr. Michael J.	8
Murphy, Robert	206
Nava, Dr. David F.	50
Ness, Dr. N. F.	52
Neupert, Dr. Werner M.	14
Niemann, Dr. Hasso B.	130
Noll, Carey E.	211
Northrop, Dr. T. G.	43
Nuth, Dr. Joseph	20
Omidvar, Dr. Kazem	75
Paddack, Dr. Stephen	219, 233
Patschke, Robert W.	176
Payne, Dr. Walter A.	50, 51
Pearl, Dr. John C.	38
Piazza, Charles R.	106
Poland, Dr. Arthur I.	15
Prather, Dr. Michael	90
Premack, Timothy	151
Provost, David	164
Ramapriyan, Dr. H. K.	157
Randall, Dr. David A.	59
Rash, James	215
Rende, John	148
Reph, Mary G.	160
Rothe, Edward D.	184
Sabia, Stephen	168
Samuelson, Dr. Robert E.	44
Sardella, Thomas E.	189
Schardt, Thomas D.	201
Schatten, Dr. Kenneth	22, 31, 57
Schein, Michael E.	146
Schopf, Dr. Paul	99
Schweickart, Russell B.	144, 145
Serlemitsos, Dr. Aristides T.	131, 133
Short, Dr. Nicholas M.	113
Simpson, Joel	127
Spinhirne, Dr. James	94
Spinolo, M. Chris	184
Stecker, Dr. Floyd W.	28
Stetina, Fran	174
Stief, Dr. Louis J.	51
Strebel, Dr. Donald	118
Streitmatter, Dr. Robert E.	26
Strong, Dr. J. P.	157
Sud, Dr. Y. C.	77
Susskind, Dr. Joel	95
Swanson, Theodore D.	136
Szczur, Martha R.	202
Szymkowiak, Dr. Andrew E.	28
Taylor, Dr. Harry A., Jr.	55
Teegarden, Dr. Bonnard	6
Thieman, James R.	166
Thomas, Hans	164
Thomas, Dr. Roger J.	15
Thomas, Valerie L.	186
Thompson, Dr. David J.	26, 150
Treinish, Lloyd A.	194, 211
Trombka, Dr. Jacob I.	53
Truszkowski, Walter	207
Unger, Glenn	148
Valett, Jon D.	205
Viñas, Dr. Adolfo F.	64

Author	*Page*	*Author*	*Page*
Volz, Dr. Stephen	137	Wright, Dr. Charles W.	106
Voorhies, Dr. Coerte V.	112	Wu, Dr. Man-Li C.	95
Walther, Mark E.	241	Zillig, David J.	135
Warner, Brent A.	137	Zuber, Dr. Maria T.	56
Wasilewski, Dr. Peter	116	Zwally, Dr. H. Jay	103
Wong, Yen	215		

Editors:

Gene Guerny
Karen Moe
Steven Paddack
Gerald Soffen
Walter Sullivan

Associate Editor:

Jan Ballard, Science
Systems and Applications, Inc.

prepared by Engineering and Economics Research, Inc.

National Aeronautics and
Space Administration

Goddard Space Flight Center
Greenbelt, Maryland 20771